Bone and Joint Disorders

Differential Diagnosis in Conventional Radiology

Francis A. Burgener
Martti Kormano
Tomi Pudas

2nd revised edition

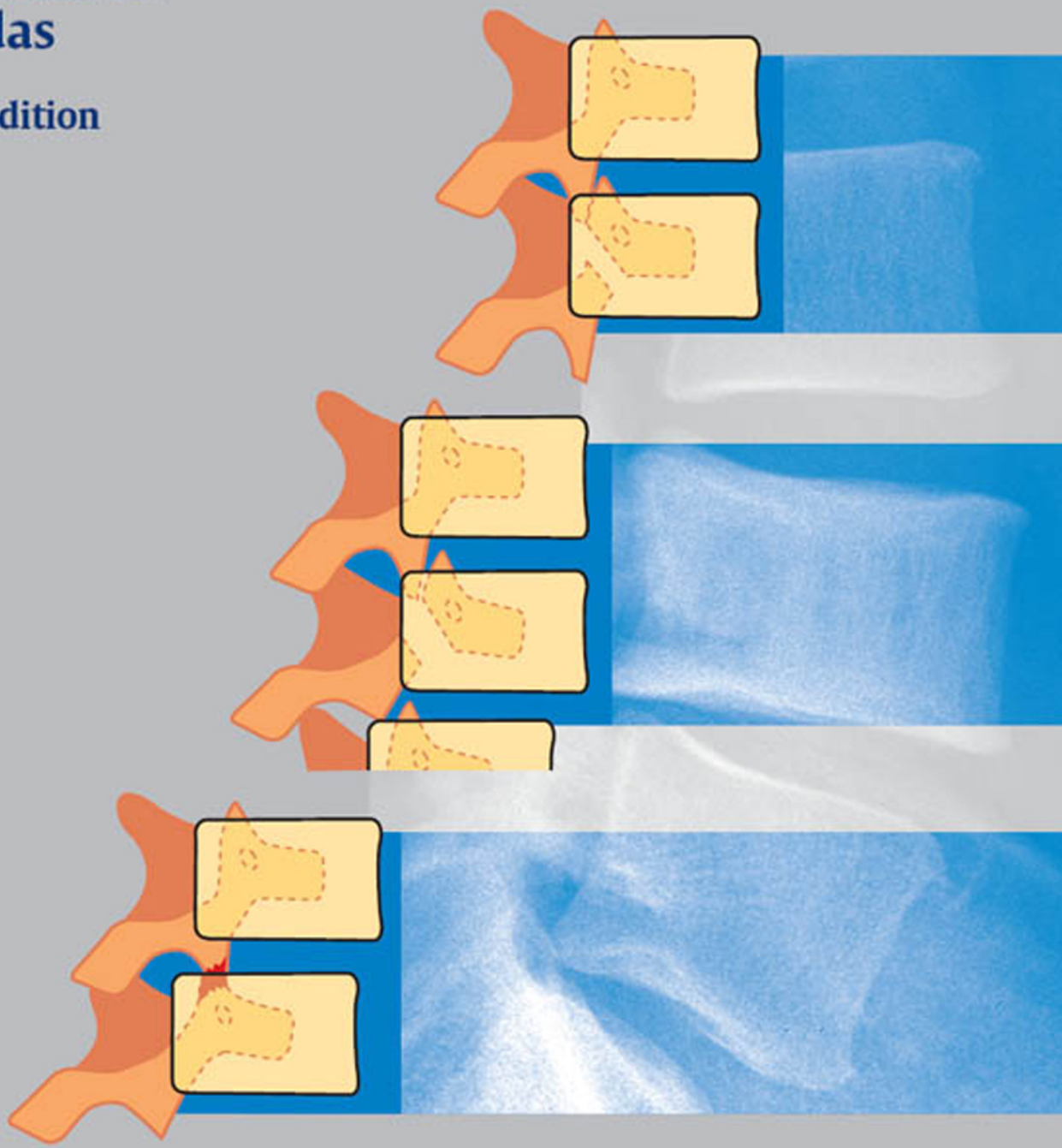

Thieme

Thieme

Bone and Joint Disorders

Differential Diagnosis in Conventional Radiology

Francis A. Burgener, M.D.
Professor of Radiology
University of Rochester
Medical Center
Rochester, N.Y., U.S.A.

Martti Kormano, M.D.
Formerly Professor and Chairman
Department of Radiology
University of Turku
Turku, Finland

Tomi Pudas, M.D.
Department of Radiology
University of Turku
Turku, Finland

2nd revised edition

1108 illustrations

Thieme
Stuttgart · New York

Library of Congress Cataloging-in-Publication Data
is available from the publisher.

Important Note: Medicine is an ever-changing science undergoing continual development. Research and clinical experience are continually expanding our knowledge, in particular our knowledge of proper treatment and drug therapy. Insofar as this book mentions any dosage or application, readers may rest assured that the authors, editors and publishers have made every effort to ensure that such references are in accordance **with the state of knowledge at the time of production of the book.**
Nevertheless this does not involve, imply, or express any guarantee or responsibility on the part of the publishers in respect of any dosage instructions and forms of application stated in the book. **Every user is requested to examine** carefully the manufacturers' leaflets accompanying each drug and to check, if necessary in consultation with a physician or specialist, whether the dosage schedules mentioned therein or the contraindications stated by the manufacturers differ from the statements made in the present book. Such examination is particularly important with drugs that are either rarely used or have been newly released on the market. **Every dosage schedule or every form of application used is entirely at the user's own risk and responsibility.** The authors and publishers request every user to report to the publishers any discrepancies or inaccuracies noticed.

© 2006 Georg Thieme Verlag,
Rüdigerstraße 14, D-70469 Stuttgart, Germany
http://www.thieme.de

Thieme New York, 333 Seventh Avenue,
New York, N.Y. 10001, U.S.A
http://www.thieme.de

Cover design: Martina Berge, Erbach
Typesetting by primustype Hurler GmbH,
D-73274 Notzingen
Printed in Germany by Grammlich, Pliezhausen

ISBN 3-13-107392-6 (GTV, Stuttgart)
ISBN 1-58890-445-8 (TMP, New York)

1 2 3 4 5

Some of the product names, patents and registered designs referred to in this book are in fact registered trademarks or proprietary names even though specific reference to this fact is not always made in the text. Therefore, the appearance of a name without designation as proprietary is not to be construed as a representation by the publisher that it is in the public domain.
This book, including all parts thereof, is legally protected by copyright. Any use, exploitation or commercialization outside the narrow limits set by copyright legislation, without the publisher's consent, is illegal and liable to prosecution. This applies in particular to photostat reproduction, copying, mimeographing or duplication of any kind, translating, preparation of microfilms, and electronic data processing and storage.

Preface

Conventional radiography remains the backbone of musculoskeletal radiology despite the advent of newer and more exciting imaging techniques such as computed tomography, magnetic resonance imaging, and, most recently, positron emission tomography. In contrast to many of these newer methods, conventional radiography is practiced not only by radiologists but also by a large number of clinicians and surgeons. With each examination, one is confronted with radiologic findings that require interpretation in order to arrive at a general diagnostic impression and a reasonable differential diagnosis. To assist the film reader in attaining this goal, this book is based upon radiographic findings unlike most other textbooks in radiology that are disease oriented. Since many diseases present radiographically in a variety of manifestations, some overlap in the text is unavoidable. To minimize repetition the differential diagnosis of a radiographic finding is presented in tabular form whenever feasible. Most tables do not only list the various diseases that my present radiologically in a a specific pattern, but also describe in succinct form other characteristically associated radiographic findings and pertinent clinical data. Radiographic illustrations and drawings are included to demonstrate visually the radiographic features under discussion.

The transition from film to digital radiography had the greatest impact on conventional radiology since the publication of the last edition. This change, however, did not affect the way radiologic diagnoses are ascertained. Since the publication of the last edition the name of a few disorders has changed (e. g., histiocytosis X to Langerhans cell histiocytosis) and a few disease are newly recognized (e. g., femoroacetabular impingement). These facts were taken into account in the new edition. The chapters "Localized Bone Lesions" and "Joint Diseases" were completely rewritten and newly illustrated, since I took them over from Dr. Kormano. The chapter "Trauma and Fractures" also under went a major overhaul by the inclusion of specific fracture sites. In the remaining chapters of the book the text was updated, many illustrations replaced, and large numbers of new illustrations added.

A changing of the guard has also taken place. Since Dr. Martti Kormano's professional endeavors do no longer include clinical radiology, he felt no longer up the task to update his original contributions to the text. He was however very fortunate to find in Dr. Tomi Pudas a very talented young radiologist to take over the revision of the chapters originally prepared by him.

I hope this new edition will be as well received as its predecessors in the past that were translated into five foreign languages. The concept of an imaging pattern approach in tabular form rather than a disease oriented text was introduced in 1985 with our original edition *Differential Diagnosis in Conventional Radiology* and has since been adopted by many authors. I feel complimented by the old cliché, "imitation is the sincerest form of flattery."

This book is meant for physicians with some experience in musculoskeletal radiology who wish to strengthen their diagnostic acumen. It is a comprehensive outline of radiographic findings and it should be particularity useful to radiology residents preparing for their specialist examination, especially since the exposure to conventional radiography during their training continuously decreased in the past in favor of newer imaging modalities. Any physician involved in the interpretation of conventional bone radiographic examinations should find this book helpful in direct proportion to his or her curiosity.

It is my hope that this new edition will be as well received as the previous ones by medical students, residents, radiologists, and physicians involved in the interpretation of conventional bone radiographs.

Francis A. Burgener, M. D.

Acknowledgements

It is impossible to thank individually all those who helped to prepare the third edition of this textbook. I wish to acknowledge the staff of our publisher Thieme, in particular Dr. Clifford Bergman and Mr. Gert A. Krüger.

I am deeply indebted to Dr. Gertrud Gollman, Steinach am Attersee, Austria, who translated the last edition of this text into German and suggested many alterations and corrections, which have been incorporated into this new edition.

My gratitude goes to all the radiologists whose cooperation made available illustrative cases to compliment the original collection or to replace older illustrations. I am indebted to Drs. Steven P. Meyers, Johnny U. V. Monu, and Gwy Suk Seo, all staff members of the University of Rochester Radiology Department, and to the former residents Drs. John M. Fitzgerald and Wael E. A. Saad for providing selected cases.

I wish to express also many thanks to Jeanette Griebel, Iona Mackey, and Marcella Maier for their assistance in preparing the references and to Shirley Cappiello for her general assistance. Last, but not least, I am most grateful to Alyce Norder who left the University and me after 30 years for the richness of the industry. She is the only person capable of deciphering my longhand and, as in the past, did a superb job in typing, editing, and proofreading the manuscript of the new edition of this text. Despite her heavy workload as executive assistant in her new endeavor. Alyce was kind enough to perform this task in her spare time, for which I am greatly appreciative.

Finally I appreciate the support of my wife Therese, who has generously given her precious family time for the preparation of this book.

Francis A. Burgener, M.D.

I would like to express my deepest gratitude to honorary professor Martti Kormano who invited me to carry on his work in this new edition. I continue to admire the massive work that he and Dr. Burgener originally put into the project in the early nineteen-eighties. The hundreds of hours which Dr. Kormano and I have spent together editing this edition have been a great pleasure. It was a fascinating time in my life.

I especially want to thank Drs. Kimmo Mattila and Seppo Koskinen for introducing me to musculoskeletal radiology, and for their extraordinary teaching and support. Many thanks also belong to Drs. Erkki Svedström, Risto Elo, and Peter B. Dean for encouraging me on my way in the field of radiology. The many fascinating discussions I have had with Drs. Seppo Kortelainen and Teemu Paavilainen brought me much delight, on non-radiological topics as much as on professional subjects.

I also express sincere thanks to the staff of the publishers, Thieme, especially to Dr. Clifford Bergman and Mr. Gert Krüger. Finally, much gratitude is due to Mr. Markku Livanaien for his valuable assistance with technical questions, and to Ms. Pirjo Helanko for all her help with general matters. Many other individuals helped in various ways with this project, and though I cannot name them all, I am grateful for their contributions.

Tomi Pudas, M.D.

Contents

1 Osteopenia 3
Francis A. Burgener

2 Osteosclerosis 15
Francis A. Burgener

3 Periosteal Reactions 41
Francis A. Burgener

4 Trauma and Fractures 53
Francis A. Burgener

5 Localized Bone Lesions 75
Francis A. Burgener

6 Joint Diseases 129
Francis A. Burgener

7 Joint and Soft-Tissue Calcification 189
Martti Kormano and Tomi Pudas

8 Skull 203
Francis A. Burgener

9 Orbits 233
Francis A. Burgener

10 Nasal Fossa and Paranasal Sinuses 237
Francis A. Burgener

11 Jaws and Teeth 245
Francis A. Burgener

12 Spine and Pelvis 255
Martti Kormano and Tomi Pudas

13 Clavicles, Ribs, and Sternum 305
Martti Kormano and Tomi Pudas

14 Extremities 313
Francis A. Burgener, Martti Kormano, and Tomi Pudas

15 Hands and Feet 353
Martti Kormano and Tomi Pudas

References 392

Index 393

Abbreviations

ABC	aneurysmal bone cyst
AC	acromioclavicular (joint)
ACTH	adrenocorticotropic hormone
AIDS	acquired immune deficiency syndrome
ALL	acute lymphoblastic leukemia
AML	acute myeloblastic leukemia
ANCA	antineutrophil cytoplasmotic autoantibodies
ANT	anterior
AP	anteroposterior
AV	arteriovenous
AVF	arteriovenous fistula
AVM	arteriovenous malformation
AVN	avascular necrosis
Bx	biopsy
Ca	calcium
CLL	chronic lymphatic leukemia
CNS	central nervous system
CPP	calcium pyrophosphate dihydrate crystals
CPPD	calcium pyrophosphate dihydrate deposition disease
CRMO	chronic recurrent multifocal osteomyelitis
CT	computed tomography
D	disease
DD	differential diagnosis
DDH	development dysplasia of the hip
DIP	distal interphalangeal (joint)
DISH	diffuse idiopathic skeletal hyperostosis
DISI	dorsal intercalated segmental instability
EAC	external auditory canal
EG	eosinophilic granuloma
F	female
HAD	calcium hydroxyapatite crystals
HADD	calcium hydroxyapatite crystal deposition disease
Hb	hemoglobin
HD	Hodgkin disease
HIV	human immunodeficiency virus
Hx	history
IAC	internal auditory canal
IM	intramuscular
IP	interphalangeal (joint)
IV	intravenous
L	left
LCH	Langerhans cell histiocytosis
LE	lupus erythematosus
M	male
MAI	Mycobacterium avium intracellulare
MCP	metacarpophalangeal (joint)
MFH	malignant fibrous histiocytoma
MPS	mucopolysaccharidosis
MR	magnetic resonance
MRI	magnetic resonance imaging
MS	multiple sclerosis
MTP	metatarsophalangeal (joint)
NHL	non-Hodgkin lymphoma
NUC	nuclear medicine
PA	posteroanterior
PATH	pathology
PET	positron emission tomography
PIP	proximal interphalangeal (joint)
PNET	primitive neuroectodermal tumor
PVNS	pigmented villonodular synovitis
RA	rheumatoid arthritis
RBC	red blood cell
RES	reticuloendothelial system
RSD	reflex sympathetic dystrophy
SC	sternoclavicular (joint)
SI	sacroiliac (joint)
SLAC	scapholunate advanced collapse
SLE	systemic lupus erythematosus
STT	scaphotrapeziotrapezoidal
TB	tuberculosis
TFC	triangular fibrocartilage
TFCC	triangular fibrocartilage complex
TMJ	temporomandibular joint
TNM	tumor-node-metastasis
VISI	volar intercalated segmental instability
WBC	white blood cells

1 Osteopenia

Osteopenia is defined as a decrease in bone density caused by reduced bone formation and/or increased bone resorption. Reduction in bone formation may result from either inadequate matrix formation (e.g., disuse osteoporosis and protein deficiency of any etiology) or inadequate matrix calcification (e. g., osteomalacia). Primary hyperparathyroidism is an example of too much resorption of both bone matrix and mineral. A combination of these causes results in the undermineralization present in the majority of osteopenic disorders. Furthermore replacement of bone matrix by benign or malignant bone proliferation (e.g. thalassemia, multiple myeloma and leukemia) or bone marrow disease (e.g. metastases, infections and storage diseases) may also result in osteopenia.

Approximately 30% of the bone mineral must be lost before a difference in the bone density can be detected by conventional radiography. More sensitive techniques useful for earlier detection and quantification of osteopenia include axial computed tomography and photon or x-ray absorptiometry. It should also be borne in mind that the normal bone density changes with age, increasing from infancy to age 35–40 and then progressively decreasing at the rate of 8% per decade in women and 3% in men.

The radiographic findings of osteopenia are loss of bone density and cortical thinning. Osteopenia may either be generalized or localized, and its differential diagnosis is discussed separately in Tables 1.**1** and 1.**2**.

In *osteoporosis,* a combination of loss of bone density and cortical thinning may result in an apparent increase in density of the cortex and vertebral endplates, that appear as thin, sharp lines (Figs. 1.**1** and 1.**2**). Bone resorption occurs preferentially in the transverse trabeculae, while the trabeculae along stress lines are accentuated. Resorption of all trabeculae in a vertebral body produces the "empty box" sign. As a result of compression fractures the vertebral body may depict a depressed endplate or become wedge-shaped, biconcave (fish vertebra) or uniformly compressed (pancake vertebral body). Cartilaginous (Schmorl's) nodes are caused by displacement of a portion of the intervertebral disc into the vertebral body. With the exception of osteogenesis imperfecta, bones do not bend in osteoporosis. A predisposition towards fractures, however, exists in the brittle bones, especially in the vertebral bodies, ribs, hips and wrists. Fracture healing is delayed and the callus formation poor. Abundant callus formation in osteopenic bones may occur, however, with exogenous (iatrogenic) or endogenous (Cushing's syndrome) hypercortisolism and osteogenesis imperfecta. In osteoporosis, serum calcium, phosphorus and alkaline phosphatase are normal.

In *osteomalacia,* a nonspecific loss of bone density is often the only radiographic sign. Blurring of both cortical margins and trabeculae results in a "ground glass" appearance of the involved bone and is more characteristic. This is often most obvious in the vertebral bodies. In the skull, a blurred mottled appearance similar to hyperparathyroidism is characteristic. Bones are softened and have a tendency to bend resulting in deformities commonly found in the thorax, vertebral column, pelvis and extremities. Pseudofractures (Looser's zones or Milkman's syndrome) occur frequently and represent infractions with incomplete healing. They are found in

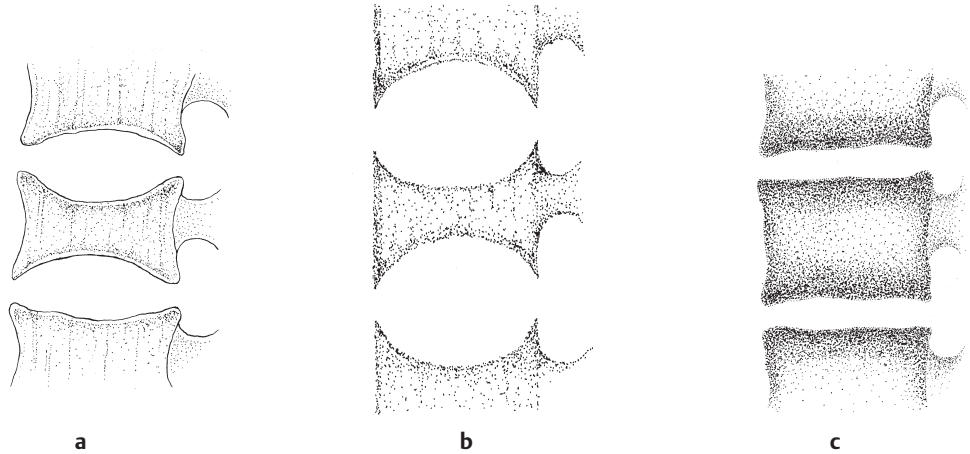

Fig. 1.**1** **Osteopenia. a** *Osteoporosis*: Deossified, biconcave vertebral bodies (fish vertebrae) with thin but dense-appearing endplates and prominent vertical trabeculae. The superior endplates typically are affected more severely. **b** *Osteomalacia*: Uniform deossification with loss of trabecular detail ("ground-glass appearance") and compression fractures. Fish vertebrae tend to be smoother than in osteoporosis and involve superior and inferior endplates with equal severity. **c** *Hyperparathyroidism*: A "rugger jersey spine" is usually only found in secondary hyperparathyroidism (renal osteodystrophy), whereas primary hyperparathyroidism depicts a bony texture similar to osteomalacia.

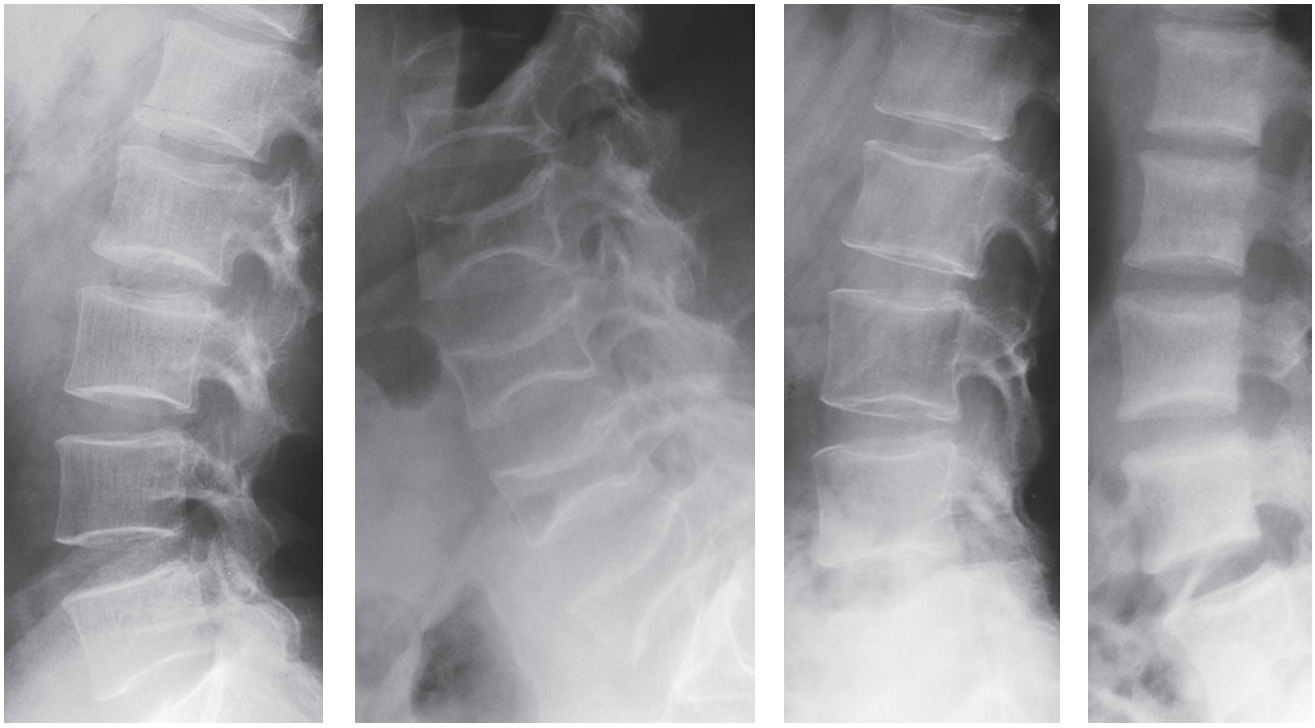

a b c d

Fig. 1.2 **Osteoporosis (a), osteomalacia (b) and hyperparathyroidism (c** and **d).** Osteoporosis (**a**): Thin sharply defined endplates with accentuation of the vertical trabeculae are seen. Osteomalacia (**b**): Uniformly biconcave vertebral bodies with poorly defined endplates and blurred trabeculae are seen. *Primary hyperparathyroidism* (**c**): Thin poorly defined endplates with blurring of the trabecular pattern in the vertebral bodies are seen. *Secondary hyperparathyroidism* (**d**): Blurring of the trabecular pattern in the vertebral bodies is associated with thickening and sclerosis of the superior and inferior endplates ("rugger jersey spine").

the scapula (lateral margin), ribs, clavicle, ischial and pubic rami, femur (especially medial aspect of the neck), and other long bones. Characteristic laboratory findings in osteomalacia include a slightly low to normal serum calcium, a low serum phosphorus and an elevated alkaline phosphatase.

Bony lesions are found in less than half of the patients with *hyperparathyroidism*. Subperiosteal resorption along the radial margin of the phalanges is virtually pathognomonic. These erosions occur most often in the proximal and middle phalanges of the index and middle finger (Fig. 1.3). Absorption of the terminal tufts and cortical striations ("tunneling of the cortex") are commonly associated with this condition. Endosteal resorption occurs in long bones. Resorption may also be evident in the acromial ends of the

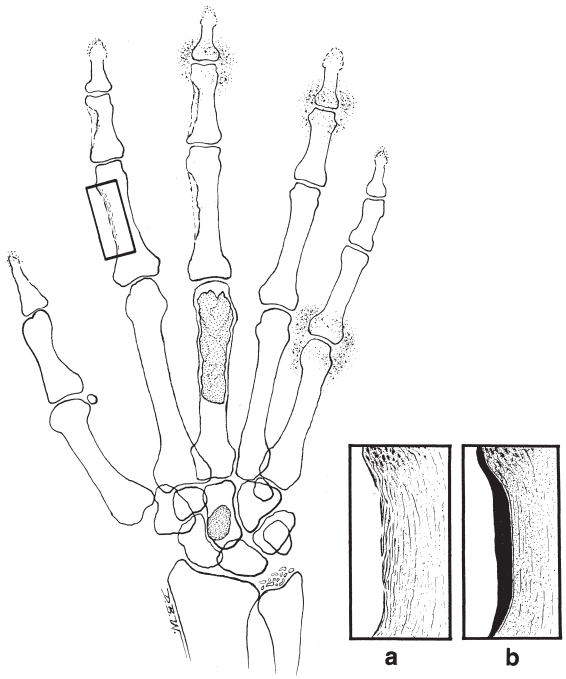

a b

Fig. 1.3 **Hyperparathyroidism** of the hand. Subperiosteal resorption and cortical striations, usually best seen on the radial margins of proximal and middle phalanges of second and third finger. A magnified view of these findings is demonstrated in insert a, whereas insert b shows a normal cortex for comparison. Additional findings include resorption of the tufts, periarticular soft-tissue calcifications, brown tumors (third metacarpal and capitatum), and joint cartilage calcification (often in the triangular fibrocartilage between ulna and corresponding part of the proximal carpal row).

clavicles, the sacroiliac joints, the symphysis, in the calcaneus at the insertion of the plantar fascia and in the ribs (usually in their upper borders). The bone is softened resulting in secondary deformities such as basilar impression in the skull and kyphoscoliosis. Cyst-like lesions and so-called brown tumors occur in tubular and flat bones. While brown tumors heal after removal of the parathyroid adenoma and may eventually even become sclerotic, cysts remain unchanged after treatment. Granular deossification of the skull results in a "salt and pepper" appearance. Resorption of the lamina dura around the teeth is commonly present. Soft tissue calcifications (especially arterial and para-articular), joint cartilage calcifications (especially menisci and the triangular fibrocartilage in the wrist), nephrocalcinosis, and nephroureterolithiasis are common features of hyperparathyroidism. Pancreatitis, peptic ulcer disease and gallstones may also be associated. Classic laboratory findings in primary hyperparathyroidism include a high serum calcium, a low serum phosphorus, and an elevated alkaline phosphatase in the presence of bone disease.

An increased bone density is often associated with secondary hyperparathyroidism (renal osteodystrophy). In these cases thickening of the superior and inferior endplates of the vertebral bodies can result in a "rugger jersey spine".

The skeletal changes in different forms of hyperparathyroidism are identical, although brown tumors are more common in primary hyperparathyroidism, whereas osteosclerosis and extensive soft-tissue calcifications are more often found in secondary hyperparathyroidism.

Table 1.1 Differential Diagnosis of Generalized Osteopenia

Etiology	Comments
Osteoporosis	Laboratory findings: serum calcium, phosphorus and alkaline phosphatase all normal.
Senile or postmenopausal	Most common form of osteoporosis. Females affected more often and more severely than males. Compression fractures typically spare the less weight-bearing cervical and upper thoracic spine.
Disuse atrophy	Prolonged immobilization from any cause (e.g., neuromuscular disorders, cast).
Protein deficiency (e.g., malnutrition, nephrosis) (Fig. 1.4)	Pure dietary protein deficiency is rare. In underdeveloped countries, extensive osteopenia is associated with *kwashiorkor*, a marasmic protein-calorie malnutrition affecting mostly children. Protein deficiency secondary to malabsorption is more common (see under osteomalacia). Abnormal protein metabolism is the underlying cause of osteoporosis in *scurvy* (vitamin C deficiency) and different *endocrinologic disorders*.
Juvenile (idiopathic)	Between ages 8 and 14, characterized by abrupt onset of bone pain. Rare, self-limiting disorder with commonly spontaneous healing.
Osteogenesis imperfecta (Fig. 1.5)	Osteogenesis imperfecta congenita (fractures present at birth) and tarda (fractures absent at birth). Deformities resulting from recurrent fractures in later life and bone bending characteristic. Both disorders inherited.
Homocystinuria	Inherited disorder that presents radiographically as combination of osteoporosis, Marfan-like changes (e.g., arachnodactyly), and metaphyseal and epiphyseal widening.
Anemia (Fig. 1.6)	Bone marrow hyperplasia causes widening of the medullary space, cortical thinning, and trabecular resorption by pressure atrophy. Occurs in severe *iron deficiency* and *sickle cell anemia*, but is more pronounced in *thalassemia*, where a generalized cystic appearance, particularly of the flat bones, is characteristic.
Bone marrow infiltration (e.g. multiple myeloma, carcinomatosis) (Fig. 1.7)	Deossification is caused by diffuse infiltration and proliferation of tumor cells in the bone marrow resulting in endosteal erosions, cortical thinning and trabecular resorption by both pressure atrophy and destruction. While osteopenia might be the only radiologic manifestation in multiple myeloma and diffuse skeletal bony metastases, patchy osteolytic areas are often present in these conditions. Bone marrow infiltration associated with cortical thinning and trabecular resorption can also be found in reticuloses (e.g. *Gaucher's* and *Nieman-Pick disease*), *histiocytoses* and *hyperlipoproteinemias*. In children, leukemia frequently causes osteopenia.
Connective tissue disease (especially rheumatoid arthritis)	Other more characteristic radiographic findings are often associated with the disease suggesting the correct diagnosis (see Chapter 6).

(continues on page 8)

a

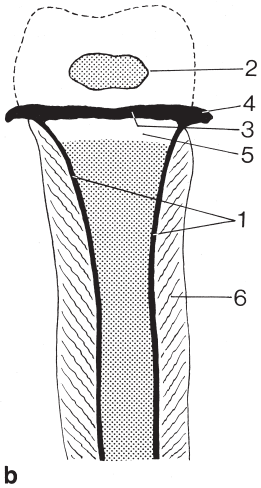

b

Fig. 1.4 a, b **Scurvy.** Characteristic findings include: (1) Osteopenia with markedly thinned cortex, (2) thin, dense, ring-like calcification around the epiphysis (Wimberger's line), (3) dense, linear calcifications in the distal metaphysis ("white line of Frankel"), (4) a small bone spur immediately adjoining the "white line of Frankel" (Pelkan's spur), (5) a radiolucent band proximal to the "white line of Frankel" (Trummerfeld zone), and (6) subperiosteal hemorrhage (calcifies only after therapy is instituted). Epiphyseal separation and/or fragmentation in the region of the metaphysis may also be associated.

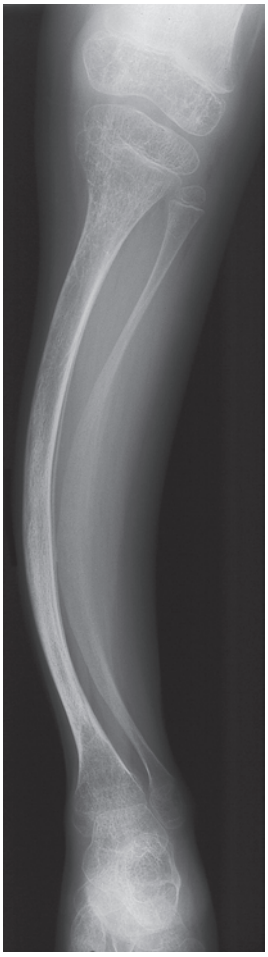

a

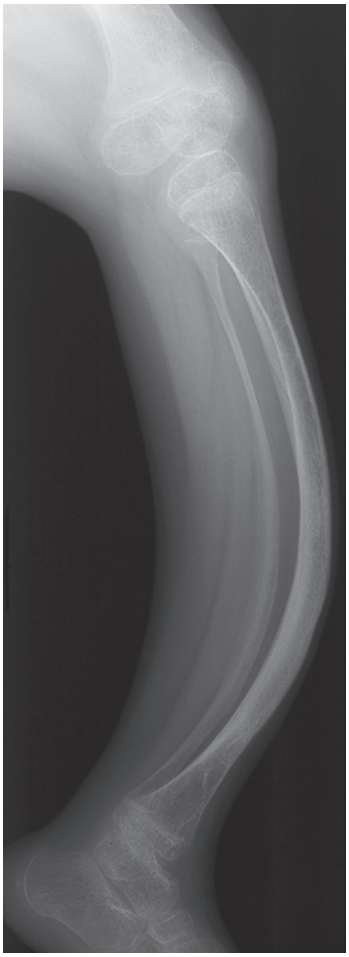

b

Fig. 1.5 a, b **Osteogenesis imperfecta.** Diffuse osteopenia with bowing deformities of the narrowed (overconstricted) tibia and fibula shafts with flaring of the metaphyses is seen in anteroposterior (**a**) and lateral (**b**) projections.

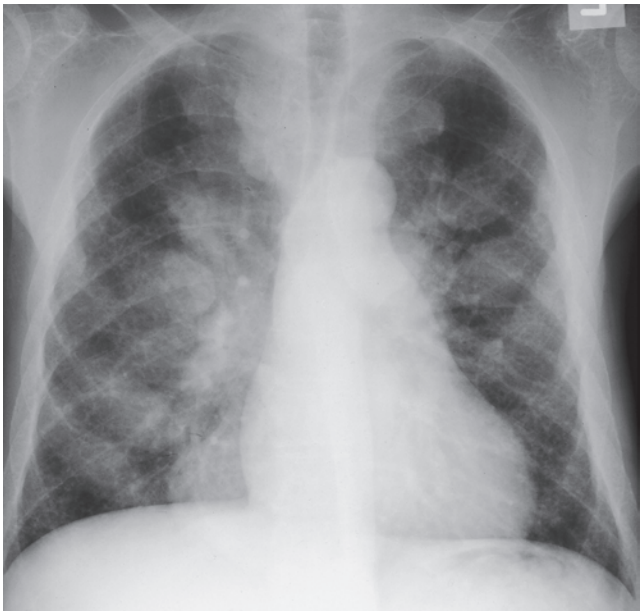

a

b

Fig. 1.6 **Thalassemia major.** Chest (**a**) and pelvis (**b**). Generalized, cystic-appearing osteopenia caused by red bone marrow hyperplasia, with main involvement of the central or flat bones characteristic. Note also the bulbous widening of the anterior ends of the ribs.

◁ Fig. 1.7 **Multiple myeloma** presenting as generalized osteopenia in the spine. In this case, however, extensive destruction of L1 and the destroyed left pedicle of L5 suggest the malignant process.

Table 1.1 (Cont.) Differential Diagnosis of Generalized Osteopenia

Etiology	Comments
Endocrine disorders	*Hypogonadism*: osteoporosis associated with delayed epiphyseal fusion (e.g., *Turner's syndrome*, *eunuchoidism*). *Cushing's syndrome*: chronic excess of glucocorticoids. *Addison's disease*: insufficiency of the adrenal cortex. *Diabetes mellitus*: osteopenia present in about 50 % of patients. *Hyperthyroidism*: often associated with cortical striations best seen in metacarpal bones. See also under hyperparathyroidism in this table.
Drug-induced (e.g., steroids, heparin) (Fig. 1.8)	Steroids: large dosages over several months. Heparin: 15,000 to 30,000 units for six months or longer.
***Osteomalacia* (Fig. 1.9)**	Laboratory findings in osteomalacia: serum calcium slightly low to normal; serum phosphorus low; alkaline phosphatase elevated.
Deficient absorption of calcium and/or phosphorus;	
1. vitamin D deficiency	Dietary causes, or lack of sunshine Adult: *osteomalacia*. Loss of bone density with blurring of both cortical margins and trabeculae characteristic. Bowing deformities and pseudofractures occur frequently. Children: *rickets* (Fig. 1.**10**). Most commonly found in premature infants. Develops most commonly between 6 and 12 months of age. Radiographic features include: indistinct, frayed and concave metaphyses ("cupping") with perpendicular trabeculae extending towards the epiphyseal areas. Delayed appearance of epiphyseal ossification centers with blurred margins (DD: Scurvy: sharply outlined epiphyses). Bulky growth plates in long bones result in swelling around the joints and a "rachitic rosary" at the costochondral junctions of the middle ribs.
2. Malabsorption	Diseases of the gastrointestinal tract, hepatobiliary system and pancreas associated with malabsorption are the most common cause of Vitamin D deficiency in developed countries. Rickets and osteomalacia is commonly associated with *sprue, celiac disease, Crohn's disease, scleroderma, small bowel fistulas, blind loop syndromes, small intestinal bypass surgery,* and *gastric* or *small bowel resection.*
3. Dietary calcium deficiency	Extremely rare.
Defects in renal tubular or intestinal calcium phosphate transport system:	
1. Vitamin D-resistant rickets (x-linked hypophosphatemia) and pseudo-vitamin D deficiency rickets (Figs. 1.11 and 1.12)	Proximal tubular resorption of phosphorus decreased. Inherited (X-linked dominant and autosomal recessive) disorders with similar clinical features (short stature, multiple fractures, varus or valgus deformities of the knees, bowing deformities of the long bones in the lower extremities and muscular weakness), but only the latter condition is commonly associated with convulsions. Enthesopathy in the spine may resemble ankylosing spondylitis but without erosions in the sacroiliac joints.

(continues on page 10)

Fig. 1.**8** **Steroid-induced osteoporosis.** Osteoporosis with thickening and sclerosis of the compressed end-plates is characteristic of exogenous or endogenous hypercortisolism.

Fig. 1.**9** **Osteomalacia.** Marked demineralization with blurring of the inner cortical margins and loss of trabeculations are characteristic. Several pseudofractures are seen, presenting as sclerotic transverse lines in the tibia.

Fig. 1.**10** **Rickets.** Characteristic changes include: (1) osteopenia, (2) poorly calcified and defined epiphyses, (3) widening of the epiphyseal cartilage plate, (4) widening, cupping, and fraying of the metaphyses, (5) periosteal reactions, and (6) bowing deformities. Greenstick fractures are also commonly associated, but not present in this case.

Fig. 1.**11** **Vitamin D-resistent rickets (x-linked hypophosphatemia).** Osteopenia with multiple fractures/pseudofractures and anterior bowing deformity of the tibia is seen.

Fig. 1.**12** **Vitamin D-resistent rickets (x-lilnked hypophosphatemia).** Mild osteopnia with bowing deformity and pseudofracture in the distal femur and genu varum is seen.

Table 1.1 (Cont.) Differential Diagnosis of Generalized Osteopenia

Etiology	Comments
2. Renal tubular acidosis (Fig. 1.13)	Metabolic acidosis attributed to renal loss of alkali. Pathogenesis of osteomalacia in this condition is unclear. Commonly associated with nephrocalcinosis and nephrourolithiasis.
3. Fanconi's syndrome (De Toni-Debré-Fanconi syndrome)	Idiopathic or acquired disorder characterized by hypophosphatemia, glucosuria and aminoaciduria. The idiopathic form is often associated with *cystinosis* (widespread tissue deposition of cystine crystals). The acquired form may be secondary to *Wilson's disease* (rare familial disorder with impaired hepatic excretion of copper and characteristic pigmentation of the cornea [Kayser-Fleischer ring], *multiple myeloma* and *lead* or *cadmium poisoning*.
Chronic anticonvulsant drug therapy	Anticonvulsants (e.g. Phenytoin) and many tranquilizers induce hepatic enzymes that accelerate degradation of biologically active vitamin D metabolites.
Fibrogenesis imperfecta ossium and axial osteomalacia	Fibrogenesis imperfecta ossium (axial and appendicular bone involved) and axial osteomalacia (only axial skeleton involved) are rare disorders found in middle-aged males. Loss of bone density with a few coarse trabeculae may produce a "fishnet appearance." Occasionally, the bone density may increase.
Hypophosphatasia (Fig. 1.14)	Autosomal recessive disorder with a wide spectrum of clinical severity. Generalized deficient bony mineralization is found radiographically. The most severe skeletal involvement is observed in neonates, in whom the disease is often fatal. In childhood the disorder resembles rickets, but associated irregular lucent extensions into the metaphyses representing uncalcified bone matrix are characteristic. The adult form is characterized by radiolucent bones, pseudofractures, and fractures occurring after minor trauma that show delayed healing with minimal callus formation. Biochemical hallmark; low alkaline phosphatase.
***Hyperparathyroidism* (Figs. 1.15 and 1.16)**	Laboratory findings of primary hyperparathyroidism: serum calcium high; serum phosphorus low; alkaline phosphatase elevated in the presence of bone disease.
Primary hyperparathyroidism	Found with parathyroid adenoma, primary chief cell or clear cell hyperplasia of all parathyroid glands, and parathyroid carcinoma.
Secondary hyperparathyroidism	Compensatory mechanism in any state of true hypocalcemia. Usually due to chronic renal failure, but may also be caused by hypovitaminosis D and malabsorption of calcium. In chronic renal disease, the skeletal changes are usually a combination of hyperparathyroidism, osteomalacia and osteosclerosis. This complex is best referred to as "*renal osteodystrophy* ."
Tertiary hyperparathyroidism	Development of an autonomous parathyroid adenoma in chronically overstimulated hyperplastic parathyroid glands (e.g., following renal transplantation).

Fig. 1.**13** **Renal tubular acidosis.** Increased bone density secondary to renal osteodystrophy is seen. Note also the extensive bilateral nephrocalcinosis.

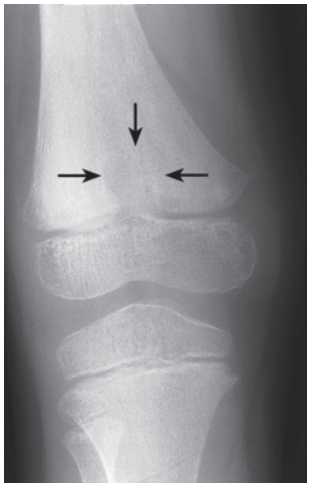

Fig. 1.**14** **Hypophosphatasia.** Osteopenia and a radiolucent lesion (arrows) extending from the growth plate into the distal femur metaphysis representing uncalcified bone matrix are seen.

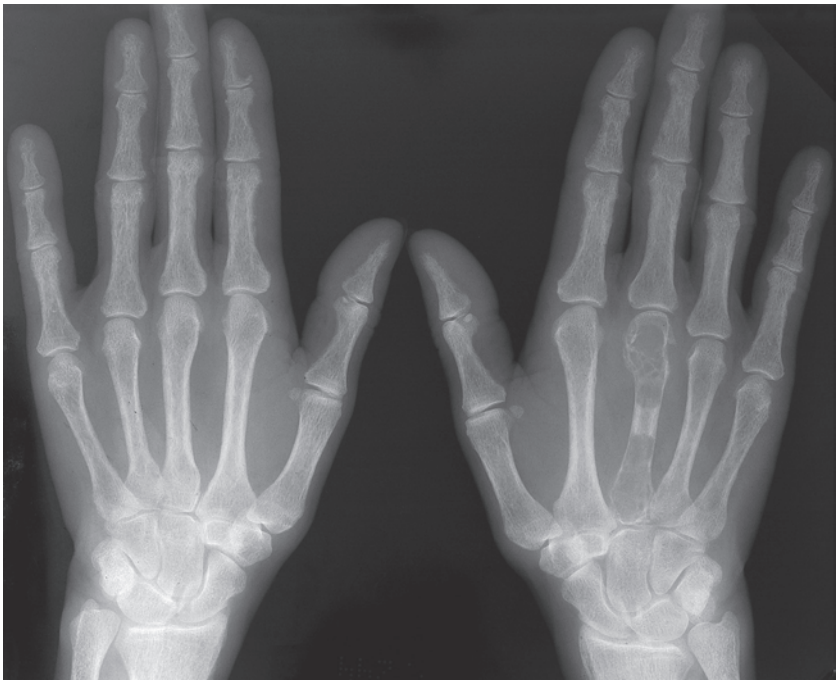

Fig. 1.**15** **Hyperparathyroidism.** Subperiosteal resorption best seen along the radial margin of the proximal phalanges of both index fingers. Brown tumors involving the distal phalanx of the left index finger and the entire right third metacarpal bone. Resorption of the tufts, especially in the thumbs. The cortex in the metacarpals and phalanges depicts fine striations.

Fig. 1.**16** **Hyperparathyroidism.** Subperiosteal resorptions seen along the radial margins of the proximal and middle phalanges of the second finger and the middle phalanx of the third finger are virtually diagnostic. Cortical striations are also evident.

Table 1.2 Differential Diagnosis of Localized Osteopenia

Etiology	Comments
Disuse atrophy (local immobilization): **1. fracture (more pronounced distal to the fracture site)** **2. cast** **3. neural paralysis** **4. muscular paralysis**	Besides identical radiographic features as in generalized osteopenia, the localized form may also have a patchy appearance due to spotty cortical thinning (e. g., reflex sympathetic dystrophy).
Reflex sympathetic dystrophy (RSD, Sudeck's atrophy) (Fig. 1.17)	Rapid development of often patchy osteoporosis associated with painful soft-tissue swelling following trivial trauma. Cerebrovascular disorders, cervical spondylosis, discal herniation, postinfectious states, calcific tendinitis, vasculitis, and neoplasm are other implicated conditions. Probably of neurovascular origin.
Regional transitory osteoporosis	A painful self-limited osteoporosis in middle-aged or elderly patients. Most often found in the hip ("transitory demineralization of the femoral head") , but may also involve any other major joint. Associated with disability lasting 2 to 4 months.
Shoulder-hand syndrome (Fig. 1.18)	Pain and stiffness in the shoulder combined with pain, swelling and vasomotor phenomena in the hand following an acute illness (e.g. myocardial infarction, in which condition it is usually located on the left side). Radiographically, it resembles reflex sympathetic dystrophy.
Burns and frostbites	Radiographic findings consist of osteoporosis, bone resorption, osteonecrosis, and dystrophic soft tissue calcifications (burns).
Inflammatory: **1. rheumatoid arthritis** **2. osteomyelitis** **3. tuberculosis**	Localized osteoporosis is usually the first, although nonspecific, radiographic manifestation of any inflammatory disease.
Bone infarct and hemorrhage	In their early stages, both bone infarcts and hemorrhages produce localized demineralization. With healing, lesions become calcified and eventually osteosclerotic.
Radiation osteonecrosis (Fig. 1.19)	Radiation changes are dose-related, with a threshold level of 30 Gy and cell death occurring at 50 Gy. Radiographic changes occur one year after radiotherapy at the earliest. They are initially often predominantly lytic, and progress with time to a mixed lytic and sclerotic stage.
Tumor (Fig. 1.20)	Osteolytic metastases and multiple myeloma must primarily be considered. Primary bone tumors (benign or malignant) may present as localized deossification, but only rarely.

(continues on page 14)

Fig. 1.**17** **Reflex sympathetic dystrophy.** Patchy demineralization most severe near the joints is quite characteristic.

a

b

Fig. 1.**18 a**, **b** Shoulder-hand syndrome. Deossification limited to the left shoulder (**a**) and hand (**b**) several weeks following myocardial infarction is characteristic.

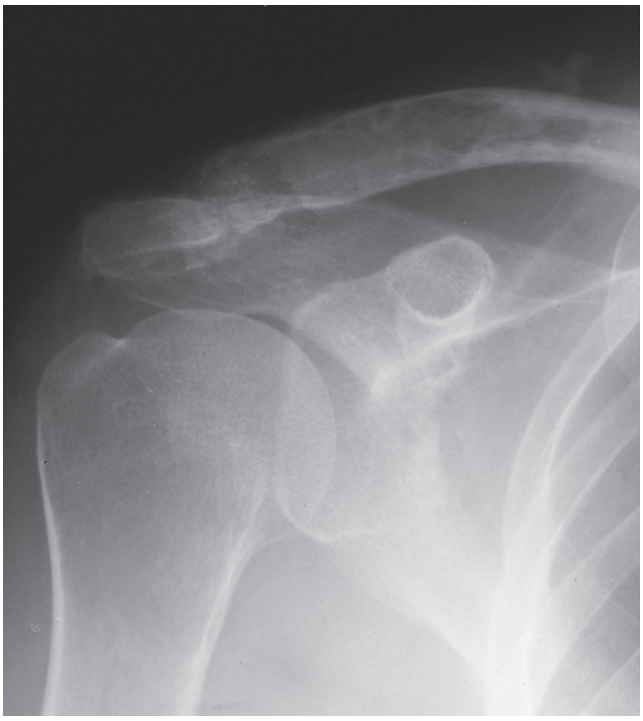

Fig. 1.**19** **Radiation osteonecrosis.** Deossification of the distal end of the clavicle with endosteal bone resorption is seen 4 years after irradiation for breast carcinoma.

Fig. 1.**20** **Multiple myeloma.** Demineralization is most pronounced near the joints, as in reflex sympathetic dystrophy in Fig. 1.**17**.

Table 1.2 (Cont.) Differential Diagnosis of Localized Osteopenia

Etiology	Comments
Paget's disease (lytic phase) (Fig. 1.21)	Skull: osteoporosis circumscripta. Long bones: usually a well-defined and V- or wedge-shaped area of deossification originating in the subchondral bone of an epiphysis.
Fibrous dysplasia (Fig. 1.22)	Both purely lytic lesions and a homogeneous, "ground glass" appearance occur, besides predominantly sclerotic manifestations. Cortical thinning and bony expansion is commonly associated with lytic lesions in tubular bones.

a

b

Fig. 1.**21 a, b** **Paget's disease.** The lytic phase in two different patients. Relatively well-defined V-or flame-shaped areas of deossification containing strands of increased bony densities in a slightly expanded shaft are characteristic (a: proximal tibia, b: distal tibia and fibula).

Fig. 1.**22** **Fibrous dysplasia.** Widening of the humerus, with a "ground glass" appearance and a few scattered patchy sclerotic areas, is evident.

2 Osteosclerosis

Osteosclerosis is defined as an increase in bone density caused by increased activity of osteoblasts or by osteogenic or chondrogenic tumor cells forming bone-like tissue. Calcification of tissue other than osteoid within bone is usually dystrophic in nature and may also increase the bone density radiographically.

Ossifications within the medullary cavity commonly present as homogeneous, fluffy, cotton-like or cloud-like densities. They most often are caused by bone islands or osteoblastic metastases (Figs. 2.**1** and 2.**2**). Calcifications within the medullary cavity typically present as punctate, annular, comma-shaped or shell-like densities and are commonly associated with chondroid matrix tumors and bone infarcts (Figs. 2.**3** and 2.**4**).

The increase in bone density may be scattered or diffuse. This distinction appears useful in the differential diagnosis of osteoblastic reactions, since certain diseases may exclusively present as scattered (solitary or multiple) sclerosis. Accordingly, the differential diagnosis of these entities will be discussed separately in Tables 2.**1** and 2.**2**. Table 2.**3** lists sites and commonly used eponyms for idiopathic avascular necrosis.

Fig. 2.**1** **Bone island**. A sclerotic focus is seen in the intertrochanteric area. The lesion depicts both tiny radiating bone spicules in its periphery and a central radiolucency, both radiographic features that help to differentiate it from an osteoblastic metastasis.

Fig. 2.**2** **Osteoblastic metastasis (breast carcinoma)**. An osteoblastic lesion is seen in the intertrochanteric area.

Fig. 2.**3** **Enchondroma**. An oblong lesion consisting of multiple irregular, often punctate calcifications is seen in the proximal tibia shaft.

Fig. 2.**4** **Bone infarct**. An oblong radiodense lesion with shell-like calcifications is seen in the distal femur shaft.

Table 2.1 Solitary or Multiple Scattered Osteosclerotic Lesions

Disease	Radiographic Findings	Comments
Bone island (enostosis) (Fig. 2.5)	Well-circumscribed isolated area of increased density rarely exceeding 1 cm in diameter. A very slow growth in size is occasionally observed. Margins demonstrate characteristically tiny spiculations or a "brush" border. A central radiolucency is occasionally observed. Occur at any location but pelvis and upper femora appear to be most common locations.	Radionuclide bone imaging is normal. (DD: Osteoblastic metastases are invariably associated with a markedly increased radionuclide uptake.) A large, very dense and structureless bone island within the medullary cavity is often called *enostoma* (Fig. 2.**6**). Without proper clinical history such a lesion is often indistinguishable from a surgically excised and *methylmethacrylate cemented bone lesion* (Fig. 2.**7**).
Osteopoikilosis (Fig. 2.8)	Multiple round or ovoid bone densities ranging in size from 2 mm to 2 cm. May demonstrate a radiolucent center. Can be found in all bones, but skull, mandible, ribs, sternum, and vertebrae are only rarely involved. In long bones they are characteristically located in metaphyses and epiphyses, whereas in the scapula and pelvis they are typically found around the glenoid fossa and acetabulum, respectively.	Rare familial disorder not associated with clinical symptoms and therefore incidentally discovered at any age. No increased radionuclide uptake is found in bone scans.
Osteopathia striata (Fig. 2.9)	Dense longitudinal striations that involve the metaphyses and may extend into the epiphyses and diaphyses. In the ilium, the linear densities radiate from the acetabulum. Vertebral bodies and skull may also be involved.	Rare and usually asymptomatic bone disorder. Occasionally associated with focal dermal hypoplasia *(Goltz's syndrome)*
Chondrodysplasia punctata (congenital stippled epiphyses) (Fig. 2.10)	Multiple punctate calcifications occurring in the epiphyses before the normal time of appearance of the epiphyseal ossification centers. DD: *Zellweger's cerebrohepatorenal syndrome*, where the stippling is limited to the patella.	Rare genetically heterogeneous epiphyseal dysplasia associated with a broad spectrum of clinical symptoms. Affected bones may be shortened, or the disorder may regress and leave no deformities. The epiphyseal calcifications may disappear by the age of 3, or may gradually increase in size and coalesce to form a normal-appearing single ossification center.
Multiple epiphyseal dysplasia (Fairbank's disease)	Irregular mottled calcifications of the epiphyses diagnosed in children and adolescents. Sequelae in the adult consist of epiphyseal irregularities, degenerative joint changes, and rarely, asymmetrical shortening of tubular bones.	Can be considered to be the tarda form of chondrodysplasia punctata. *Cretinism* with delayed appearance of stippled and fragmented epiphyseal ossification centers and sclerotic metaphyseal bands must be differentiated.

(continues on page 18)

Fig. 2.**5** **Bone island**. Well-circumscribed focus of increased density with tiny spiculations in its periphery ("brush" border) is seen in the ilium.

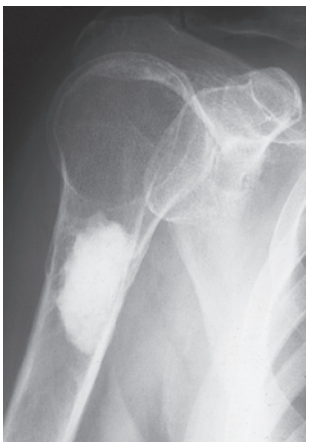

Fig. 2.**6** **Large bone island (enostoma)**. A large, very dense and structureless lesion is seen in the proximal humerus.

Fig. 2.**7** **Methylmethacrylate bone cement**. Sequelae of excision with subsequent cementing of a giant cell tumor are seen in the distal femur.

Fig. 2.**8** **Osteopoikilosis**. Multiple round to ovoid sclerotic lesions measuring a few millimeters in diameter are seen. In the tubular bones they are characteristically located in the metaphyses and epiphyses

a

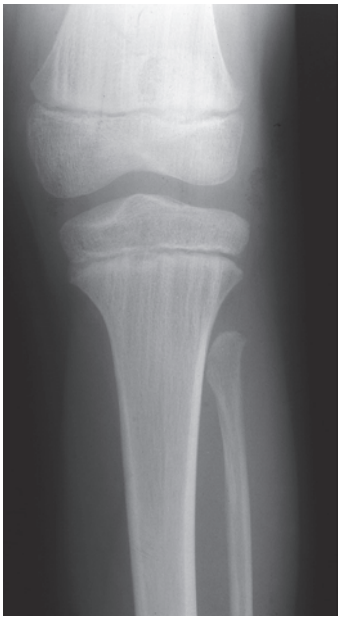

b

Fig. 2.**9** **Osteopathia striata**. Longitudinal striations involving the pelvis (**a**) and mainly the metaphyses of the femur and tibia (**b**) are seen.

Fig. 2.**10** **Chondrodysplasia punctata**. Punctate calcifications are seen in the epiphyses. Note also the widened and irregular metaphyses

Table 2.1 (Cont.) Solitary or Multiple Scattered Osteosclerotic Lesions

Disease	Radiographic Findings	Comments
Melorheostosis (Fig. 2.11)	Presents in early stage as linear hyperostosis beginning at one end of a tubular bone, progresses with time towards the diaphyses, and results finally in cortical thickening involving either one side or the entire cortex. The lesion may simulate wax flowing down the side of a candle. Osteoma-like protrusions and soft tissue ossifications may be associated.	Often limited to a single limb, in which one or more bones may be affected. At an advanced stage it is part of the differential diagnosis of diffuse osteosclerosis and will be discussed in Table 2.**2**.
Osteoma (Fig. 2.12)	Protruding mass lesion composed of abnormally dense bone with structureless appearance. It rarely exceeds 2 cm in diameter, and is usually confined to bone that is produced by the periosteal membrane. It arises from the outer or inner table of the skull, the paranasal sinuses (especially frontal and ethmoid), from the mandible, maxilla, and rarely from the tubular bones of the extremities.	Benign hamartomatous lesion consisting exclusively of osseous tissue. *Gardner's syndrome*: Multiple osteomas associated with soft tissue tumors and pre-malignant polyposis, mainly of the colon.
Benign and malignant bone tumors (Figs. 2.13, 2.14 and 2.15)	Predominantly sclerotic lesions, either as a solitary focus (enchondroma, osteochondroma, chondrosarcoma, osteoid osteoma, osteoblastoma, osteosarcoma, and Ewing's sarcoma) or as multiple foci (enchondromatosis or Ollier's disease, hereditary multiple exostoses or diaphyseal aclasis, and osteosarcomatosis).	Differential diagnosis of bone tumors is discussed in detail in Chapter 5.

(continues on page 20)

Fig. 2.**11** **Melorheostosis**. Sclerosis of several metacarpals and phalanges caused by cortical thickening, often with involvement of only one side of a bone. The presentation of the disorder has been compared with the "flowing of wax down a burning candle." Note also the involvement of the small osteoma-like protrusions from the proximal phalanx of the third finger (ulnar side) and the middle phalanx of the fourth finger (radial side).

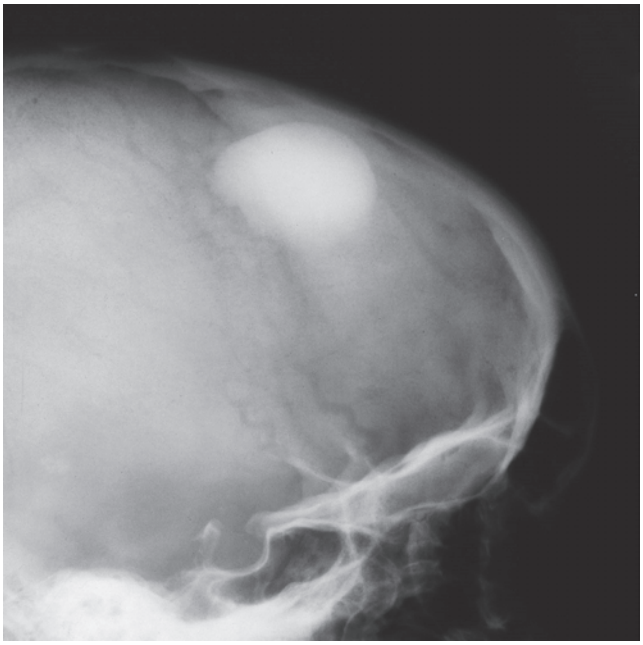

Fig. 2.**12** **Osteoma**. An abnormally dense lesion with structureless appearance is characteristic. In this case, the osteoma originated from the outer table and could easily be palpated.

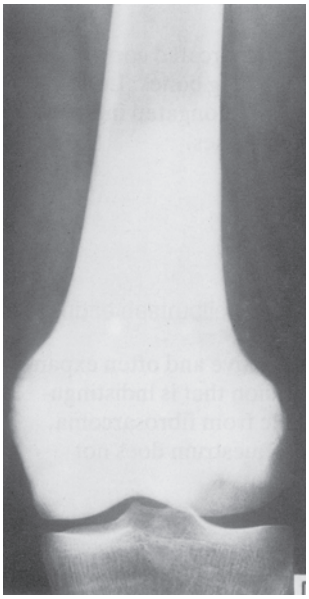

Fig. 2.**13** **Osteosarcoma.** A rather homogeneous sclerosis of the distal femur sparing only a small portion of the subchondral bone in the lateral femur condyle is seen.

Fig. 2.**14** **Parosteal sarcoma**. This posterior cortical tumor of the distal femur diaphysis presents as an irregularly defined sclerotic lesion in this anteroposterior projection (viewed face-on). The lateral projection of this sarcoma is shown in Fig. 4.**49**.

Fig. 2.**15** **Ewing's sarcoma**. A relatively poorly defined sclerotic lesion is seen in L3 involving the posterior two-thirds of the vertebral body and pedicles.

Table 2.1 (Cont.) Solitary or Multiple Scattered Osteosclerotic Lesions

Disease	Radiographic Findings	Comments
Osteoblastic metastases (Fig. 2.16)	Poorly defined areas of increased density with indistinct or lost trabecular structure. With increase in size, adjacent metastases may coalesce, resulting finally in most diffuse sclerosis. With the exception of renal and most thyroid carcinomas which produce invariably lytic and often expansile metastases, osteoblastic metastases may originate from virtually every carcinoma, but *carcinoma of the prostate* and *breast* are the most common sources. Other primary tumors include osteosarcomas, carcinoids, and carcinomas originating in the lung, nasopharynx, gastrointestinal tract and urinary bladder. Of the lymphomas, *Hodgkin's disease* and *histiocytic lymphoma* (reticulum cell sarcoma) are most likely to produce osteoblastic bone lesions.	In *children*, leukemia, neuroblastoma, and Ewing's sarcoma metastases must be considered, although these lesions are more commonly lytic before treatment is instituted.
Multiple myeloma	Focal sclerotic lesions are a rare initial manifestation.	Characteristic lytic lesions may become sclerotic with proper therapy.
Plasma cell granuloma (Fig, 2.17)	Solitary or scattered osteoblastic foci that are only slowly growing.	Consists histologically of a dense infiltrate of normal plasma cells. In contrast to multiple myeloma and plasmacytoma, all laboratory findings are normal. Nowadays considered to be a variant of *chronic recurrent multifocal osteomyelitis* (CRMO) or SAPHO (synovitis, *a*cne, *p*ustulosis, *h*yperostosis, *o*steitis), respectively
POEMS syndrome	Solitary or multiple osteosclerotic lesions and fluffy spiculated hyperostotic areas preferentially at sites of ligamentous attachment in axial and para-axial locations.	POEMS is the acronym for *p*olyneuropathy, *o*rganomegaly, *e*ndocrinopathy, *M* protein, and *s*kin changes.
Chronic or healed osteomyelitis (Fig. 2.18)	May present as localized, thickened sclerotic bone usually containing radiolucent areas.	Bacterial, tuberculous, and fungal organisms may all cause a chronic sclerosing-type osteomyelitis. *Sclerosing osteomyelitis of Garré* is a low-grade chronic infection not associated with bone destruction or sequestration.
Brodie's abscess (Fig. 2.19)	Central lucency surrounded by a slight to extensive reactive sclerosis. Located typically in the metaphysis and, less commonly in the epiphysis or diaphysis of tubular bones. Cortical thickening, periosteal new bone and sequestrum formation may be found with Brodie's abscess, but are not typical.	Chronic, often painful lesion.
Tropical ulcer	Often expansile lesion involving preferentially the lower half of the tibia. Associated with periostitis, resulting in localized fusiform periosteal and cortical thickening or even broad-based excrescences resembling osteomas.	In patients of all ages in Central and East Africa.
Callus formation (Fig. 2.20)	Healed fractures result in a localized increase in bone density.	Commonly in ribs or metatarsals following a fatigue fracture.
Stress fracture (Fig. 2.21)	Findings dependent on both location and time. A fracture line (cortical or complete) is not always evident. In the shaft of tubular bones, localized cortical thickening and periosteal reaction are characteristic. At the end of tubular bones (e.g. femoral neck, tibia plateau) and in cancellous bone, a band-like focal sclerosis without appreciable periosteal reaction is usually found.	Presents clinically with activity-related pain that is relieved by rest. Radionuclide examination and magnetic resonance imaging are both much more sensitive for early detection and diagnosis. A stress fracture occurring in normal bone under abnormal (increased) stress is referred to as a *fatigue fracture*, whereas a stress fracture occurring in abnormal (osteopenic) bone with normal stress is referred to as an *insufficiency fracture*.
Healed bone lesion (Fig. 2.22)	Spontaneously or under appropriate treatment, healed lytic lesion may become sclerotic.	Benign bone lesions such as fibrous cortical defects and nonossifying fibromas may spontaneously regress and persist as sclerotic foci. Lytic metastases (e.g., from bronchogenic carcinoma, breast carcinoma, lymphoma) and multiple myeloma manifestations may respond to local irradiation, chemotherapy, and/or hormone therapy by becoming osteosclerotic. Brown tumors in primary hyperparathyroidism become sclerotic after removal of the parathyroid adenoma.

(continues on page 23)

a

b

Fig. 2.**16** **Osteoblastic metastases** from prostatic carcinoma (**a**) involving the spine and pelvis and from Hodgkin's disease (**b**) involving only the left fourth and fifth rib. The involvement of different vertebral bodies varies from barely visible, poorly defined areas of increased densities in some vertebrae to almost complete sclerosis ("ivory vertebra") in L4.

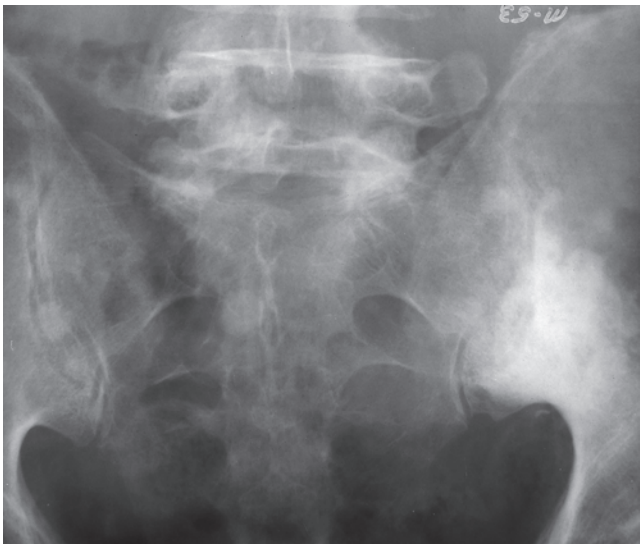

Fig. 2.**17** **Plasma cell granuloma**. Scattered osteoblastic lesions and a larger osteoblastic area in the left ilium adjacent to the sacroiliac joint are seen.

Fig. 2.**18** **Sclerosing osteomyelitis of Garré**. A homogeneous sclerosis of the proximal spindle-shaped tibia shaft is seen.

Fig. 2.**19** **Brodie's abscess**. Radiolucent lesion with surrounding reactive sclerosis in the distal tibia metaphysis is characteristic

Fig. 2.**20** **Healed fracture**. Irregular widening of the shaft, cortical thickening and sclerosis is seen in this healed comminuted fracture of the proximal femur.

Fig. 2.**21** **Insufficiency fracture**. A poorly defined osteosclerotic zone is seen in the lateral aspect of the proximal tibia.

a

b

Fig. 2.**22** **Brown tumor** in primary hyperparathyroidism, **a** before and **b** five years after removal of a parathyroid adenoma, Healing of the brown tumor resulted in a persistent sclerotic focus.

Table 2.1 (Cont.) Solitary or Multiple Scattered Osteosclerotic Lesions

Disease	Radiographic Findings	Comments
Bone infarcts (old) (Figs. 2.23 and 2.24)	Most often found in the proximal or distal ends of long tubular bones. Healed infarcts present as irregularly calcified areas in the medullary cavity, demarcated from the normal bone by a dense serpiginous contour or irregular streaks. The calcifications may eventually progress to ossification.	Infarcts are often associated with other diseases such as occlusive vascular disease, sickle cell anemia, pancreatitis, connective tissue disease, caisson disease, Gaucher's disease, and radiation therapy. A similar calcification in the medulla of long bones can occasionally be seen after *removal* of an *intramedullary rod*. Enchondromas can simulate bone infarcts (Fig. 2.**25**).

(continues on page 24)

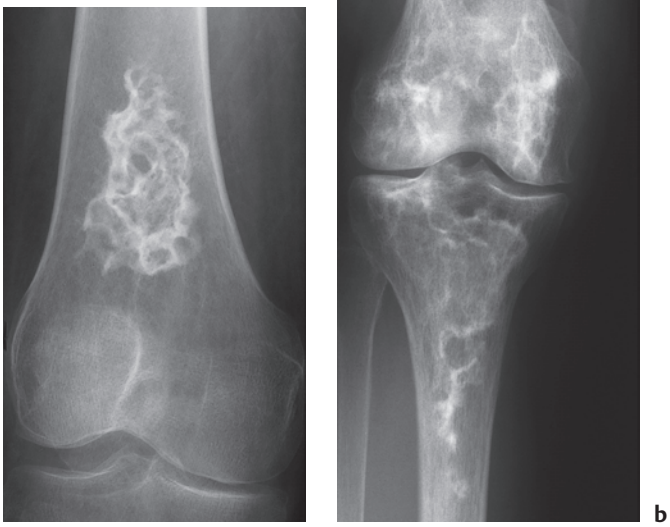

a b

Fig. 2.**23 a**, **b** **Bone infarcts**. Irregular peripheral rim calcifications are seen in the distal femur (**a**) and more extensive in both the distal femur and proximal tibia (**b**) in these patients with sickle cell anemia.

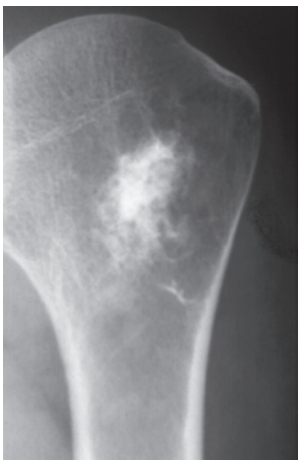

Fig. 2.**25** **Enchondroma**. An irregular calcification is seen that is most dense in its center.

a

b

Fig. 2.**24 a**, **b** **Bone infarcts**. In an attempt to heal the originally calcified infarct becomes ossified from its periphery towards the center and eventually presents as an irregular sclerotic lesion as seen in the proximal femur shaft in **a** and about the knee in **b**.

Table 2.1 (Cont.) Solitary or Multiple Scattered Osteosclerotic Lesions

Disease	Radiographic Findings	Comments
Radiation osteonecrosis (Fig. 2.26)	May present years after therapy as a mixture of sclerotic and lytic lesions even when no infarcts have occurred.	This condition can be differentiated from a local tumor recurrence with bone involvement by a normal or even depressed uptake on a bone scan.
Avascular (epiphyseal) necrosis (AVN) (Fig. 2.27)	Sequelae of avascular necrosis in epiphyses consist of sclerotic and cystic areas of flattened and irregular joint surfaces, which lead to early secondary degenerative changes, particularly in the weight-bearing joints. Most idiopathic avascular necroses occur during childhood and adolescence. Idiopathic avascular necroses occurring in adulthood are found in the medial femur condyle (*Ahlbäck's disease*, also reffered to as *spontaneous osteonecrosis about the knee* or *SONC*) and in the lunate (*Kienböck's disease*). Ahlbäck's disease typically occurs in the elderly with female predominance and occasionally affect the lateral femoral ar the tibial condyles. New evidence suggest it represents a stress (insufficiency) fracture rather than a spontaneous osteonecrosis. Kienböck's disease is usually found in young adults. In an advanced stage, the lunate shows increased bone density, fragmentation, and compression.	May be found in any disorder associated with medullary bone infarcts. Avascular necrosis is caused by interruption of the blood supply to the epiphyses with subsequent death of the hematopoetic cells in 6–12 hours, osteocytes in 12–48 hours, and lipocytes in 2–5 days. The etiology may be traumatic (e. g., femoral neck fracture), thromboembolic (e. g., sickle cell disease), vasculitic (e. g., systemic lupus erythematosus), stereoidal, marrow-infiltrative (e. g., Gaucher's disease) or idiopathic (e. g., Legg-Calvé-Perthes disease). An idiopathic genesis of this abnormality is commonly associated with an eponym (see Table 2.**3**).
Paget's disease (Fig. 2.28)	Can cause uniform areas of increased bone density in the sclerotic phase. In the reparative (mixed lytic and sclerotic) stage, the disease is characteristically associated with cortical thickening resulting in enlargement of the affected bone. Any bone can be affected; "cotton wool" appearance of the skull and "ivory vertebral body" are representative examples of the sclerotic phase of the disease.	Purely sclerotic phase is less common than the combined destructive and reparative stage virtually pathognomonic for the disease.
Fibrous dysplasia	Besides having a cyst-like or "ground glass" appearance, it can also present as purely sclerotic lesions. Manifestations are usually associated with bone expansion, particularly in tubular bones. With more extensive involvement, bone deformities almost invariably occur.	Occurs in monostotic and polyostotic forms. An *ossifying fibroma* of the skull, face and mandible cannot be histologically differentiated from fibrous dysplasia, and can be considered radiographically as a localized manifestation of this disease. Ossifying fibromas occuring in long bones, especially in the tibia and to a lesser extend fibula are referred to as *osteofibrous dysplasia* (Fig. 2.**29**)
Mastocytosis (Fig. 2.30)	Can present with focal or diffuse bone involvement. Focal form is characterized by scattered, well-defined sclerotic foci often alternating with areas of bone rarefaction. Skull, spine, ribs, pelvis, humerus, and femur are preferred sites of involvement.	Majority of patients develop skin lesions containing mast cells during the first year of life. Hepatosplenomegaly, lymphadenopathy, and pancytopenia may be associated.

(continues on page 26)

Fig. 2.**26** **Radiation osteonecrosis**. Mixed osteolytic and osteoblastic lesions are seen in both pubic bones with several pathologic fractures 7 years after irradiation for bladder carcinoma.

Fig. 2.**27** **Avascular necrosis of the lunate** (Kienbock's disease). Increased sclerosis of the lunate, which is compressed and shows early fragmentation. A shortening of the ulna (negative ulnar variance) as present in this case has been implicated as predisposing to Kienbock's disease through increased pressure on the lunate from the medial corner of the distal radius.

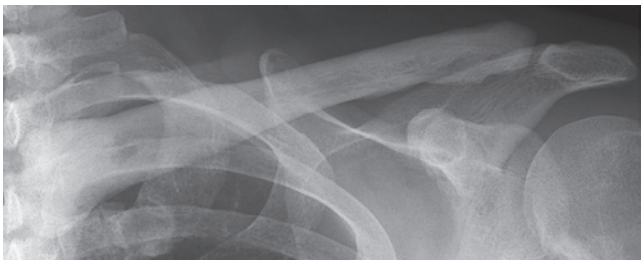

Fig. 2.**28** **Paget's disease**. A slightly thickened and uniformly sclerotic clavicle is seen.

Fig. 2.**30** **Mastocytosis**. Multiple sclerotic foci are evident.

Fig. 2.**29** **Osteo fibrous dysplasia**. Anterior bowing of the sclerotic and slightly widened tibia shaft with a thickened irregular posterior cortex and several lytic lesions in the anterior cortex are seen. Similar but less severe changes are also present in the fibula.

Table 2.1 (Cont.) Solitary or Multiple Scattered Osteosclerotic Lesions

Disease	Radiographic Findings	Comments
Tuberous sclerosis (Fig. 2.31)	Often presenting with scattered intracerebral calcifications, renal hamartomas, and bone lesions. Characteristic skeletal changes are patches of osteosclerosis ranging from a few millimeters to several centimeters in diameter. The lesions are not associated with any bone enlargement, and are most commonly found in skull, lumbar spine (especially pedicles), and pelvis, although all bones may be involved. Cyst like lesions may be seen in the hands and feet.	Rare familial disorder with defect in developing ectodermal structures. Present clinically with adenoma sebaceum of the face, with epilepsy, and with mental deficiency.
Sarcoidosis (Fig. 2.32)	Focal or generalized osteosclerosis is a rare manifestation involving spine, pelvis, skull, ribs, proximal long bones and terminal phalanges (acro-osteosclerosis).	A more characteristic presentation that is found especially in the bones of the hand consists of osteopenia with a coarsened, reticulated or lacework trabecular pattern and localized cystic ("punched-out") lesions.

Fig. 2.**31** **Tuberous sclerosis**. Irregular sclerotic areas are interspersed with small cyst-like lesions.

Fig. 2.**32** **Sarcoidosis**. Poorly defined patchy sclerotic areas are noted throughout the spine.

Table 2.2 Generalized Diffuse Osteosclerosis

Disease	Radiographic Findings	Comments
Physiologic osteosclerosis of newborn	Cortical thickening and abundant spongiosa formation can result in considerable osteosclerosis, mainly affecting the long tubular bones.	Sclerotic changes disappear gradually during the first weeks of life and have no pathologic significance. Can be found in more than half of all premature infants.
Congenital syphilis (Fig. 2.33)	Symmetrical involvement of metaphyses and diaphyses, with the epiphyseal ossification centers being spared. Metaphyseal involvement varies from transverse striping to destructive lesions originating in the corners adjacent to the cartilage plate and a frayed appearance of the metaphyseal ends similar to rickets. Particularly characteristic is a destructive lesion adjacent to the medial metaphyseal growth plate of the proximal tibia (Wimberger's sign). In the diaphyses, subperiosteal cortical thickening and periosteal reactions may be associated with focal destructive lesions.	Changes in congenital syphilis caused by a combination of luetic osteomyelitis and nonspecific trophic disturbances in enchondral bone formation. Radiographic changes may be present at birth or develop subsequently.
Rubella embryopathy (Fig. 2.34)	Predilection for distal femoral and proximal tibial metaphyses and adjacent diaphyses where irregular longitudinal lytic and sclerotic densities are found, giving a "celery-stick" appearance. Metaphyseal ends are irregular but not cupped.	Caused by maternal rubella infection in the first trimester of pregnancy. Associated clinical findings may include congenital heart disease, hepatosplenomegaly, cataracts, chorioretinitis, and thrombocytopenic purpura. *Toxoplasmosis* and *cytomegalic inclusion disease* may result in similar bony changes.
Erythroblastosis fetalis	Transverse metaphyseal bands and diffuse sclerosis of the diaphyses may be present.	Congenital hemolytic anemia caused by Rh factor incompatibility. Clinically, severe prolonged jaundice (icterus gravis neonatorum) and generalized edema (hydrops fetalis) are associated.

(continues on page 28)

Fig. 2.**33** **Congenital syphilis**. Sclerosis of the diaphysis is caused by cortical thickening and periosteal reactions. Destructive lesions are no longer recognizable in this healing phase.

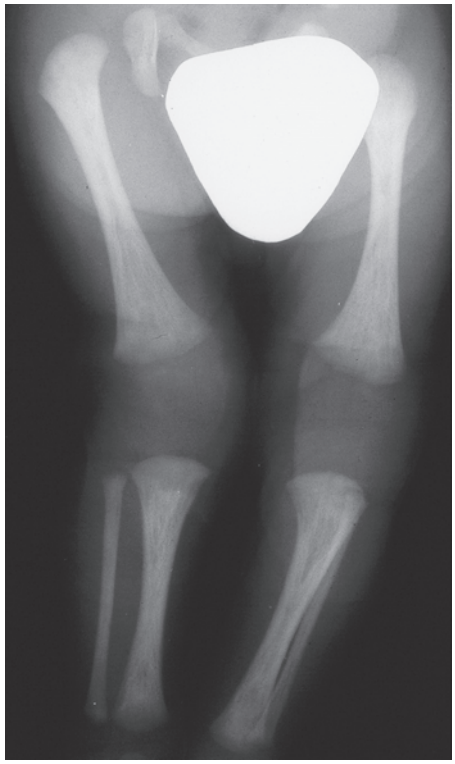

Fig. 2.**34** **Rubella embryopathy**. Irregular longitudinal lytic and sclerotic densities in the distal femur and proximal tibia ("celery-stick" appearance) are characteristic. Metaphyses are slightly irregular, but not cupped.

Table 2.2 (Cont.) Generalized Diffuse Osteosclerosis

Disease	Radiographic Findings	Comments
Infantile cortical hyperostosis (Caffey's disease) (Fig. 2.35)	Cortical thickening, sometimes with asymmetrical distribution. Mandible clavicles, long bones (especially ulnae), ribs, skull, scapula and pelvis are involved, in that order of frequency. Tubular bones may have a spindle-shape appearance since only the diaphyses are involved. A laminated periosteal reaction is only associated in the healing phase.	Uncommon disease of unknown etiology with onset in the first 5 months. Clinically, the affected bones are associated with tender soft tissue swellings and fever. Recovery occurs over a period of a few weeks to several months. Roentgen changes regress within a year.
Ribbing's disease	Solitary or multiple, often asymmetric involvement of the diaphyses of long bones (especially femur and tibia) with sclerosis and hyperostosis.	Usually asymptomatic and often considered as forme fruste of Engelmann-Camurati disease. When a solitary bone is involved the differential diagnosis includes chronic *sclerosing osteomyelitis of Garré*.
Progressive diaphyseal dysplasia (Engelmann-Camurati disease) (Fig. 2.36)	Cortical thickening of the long bones beginning in the midshaft and progressing peripherally, resulting in a spindle-shape appearance with relatively abrupt transition to normal bone. Involvement of other bones with sclerosis is less common.	This autosomal dominant transmitted neuromuscular disease is usually diagnosed between 4 and 12 years of age. Characteristic clinical features include a peculiar wide-based, waddling gait, muscular weakness, and malnutrition.
Generalized cortical hyperostosis (van Buchem's disease) (Fig. 2.37)	Diffuse symmetrical sclerosis and cortical thickening, predominantly of the diaphyses of all tubular bones. Sclerosis and thickening occurs also in the vault and base of the skull, mandible, clavicles, ribs and spine (particularly affecting the spinous processes).	Rare autosomal recessive disorder occurring in adulthood with male predominance. *Worth's syndrome*: Autosomal dominant form, with similar but less severe radiographic findings, is often detected incidentally on radiographs obtained for unrelated reasons.
Hereditary hyperphosphatasia (Juvenile Paget's disease)	Marked cortical thickening can be found in all bones. In the long tubular bones the process involves the entire bone rather than only the diaphyses and bowing deformities occur, especially in the femora. Pseudofractures and "splitting" of the cortex may also be seen.	Rare autosomal recessive disease developing usually in the second or third year of life with striking, predilection for those of Puerto Rican descent. Radiographic features resemble Paget's disease. Alkaline phosphatase is elevated. Pseudoxanthoma elasticum may be associated.
Craniometaphyseal dysplasia	Osteosclerosis of the diaphyses of the tubular bones is only found in infancy, and is subsequently replaced by widened diaphyses with cortical thinning and metaphyseal expansion (Erlenmeyer flask deformity). Sclerosis of the skull (calvarium and base) occurs. Lack of aeration of the paranasal sinuses and mastoids is present. The mandible can be markedly thickened and sclerotic, with defective dentition.	Rare autosomal dominant or recessive disorders characterized by failure of normal tubulation of bone and skull abnormalities. Clinically, hypertelorism and a broad flat nose are characteristic, and cranial nerve deficits (progressive hearing and vision loss and facial paralysis) occur. In *craniodiaphyseal dysplasia* (autosomal recessive) massive and progressive hyperostosis of the skull and facial bones are associated with cortical thickening and lack of normal modeling of the long and short tubular bones (Fig. 2.**37 A**).
Hypoparathyroidism	Osteosclerosis, particularly of the axial skeleton, is the most common bony abnormality, but may be subtle and defy detection. Transverse sclerotic bands in the metaphyses of the long bones, increased density of the iliac crest, and marginal sclerosis of vertebral bodies can also be found. Ossification of muscle insertion and ligaments and subcutaneous calcifications occur. Enthesopathy in the spine resembles diffuse idiopathic skeletal hyperostosis (DISH). In the skull calvarial thickening, basal ganglion calcification and defective dentition are characteristic.	Hypocalcemia induces neuromuscular excitability, resulting eventually in tetany in both primary and the more common secondary hypoparathyroidism. The latter is most often caused by accidental removal of the parathyroid glands during thyroid surgery. *Pseudohypoparathyroidism* differs from the primary form by the presence of short metacarpal and metatarsal bones and the lack of response to parathyroid hormone substitution therapy. *Pseudopseudohypoparathyroidism* has similar radiographic features, but no blood chemical changes.

(continues on page 30)

Fig. 2.**35** **Infantile cortical hyperostosis (Caffey's disease)**. Periosteal reactions with subsequent cortical thickening result in widened and relatively dense diaphyses of the long bones in the upper extremity.

Fig. 2.**36** **Progressive diaphyseal dysplasia (Engelmann-Camurati disease)**. Cortical thickening of different severity in both femurs of the same patient produced spindle-shaped, sclerotic diaphyses with a relatively abrupt transition to normal bone.

a

b

Fig. 2.**37 A** **Craniodiaphyseal dysplasia.** Marked cortical thickening of the short tubular bones of the hand in seen.

◁ Fig. 2.**37** **Generalized cortical hyperostosis (van Buchem's disease)**. Symmetrical sclerosis and cortical thickening predominantly of the diaphyses of the femur (**a**) and the tibia and fibula (**b**), is seen.

Table 2.2 (Cont.) Generalized Diffuse Osteosclerosis

Disease	Radiographic Findings	Comments
Osteopetrosis (marble bones, Albers-Schönberg disease) (Fig. 2.38)	Symmetrical increase in bone density ranging from minimal to extreme may be found. All bones may be involved with no predilection for a specific location within one bone. Tubular bones lack modeling, often causing flaring of the ends (Erlenmeyer flask deformity). Longitudinal and transverse striations as well as "bone-within-bone" appearance occur.	Rare hereditary bone disorder with usually normal serum calcium, phosphorus, and alkaline phosphatase levels. At least four different types are differentiated, one of which is associated with tubular acidosis.
Pyknodysostosis	Diffuse Osteosclerosis occurs but differs from osteopetrosis by the absence of both Erlenmeyer flask deformities and "bone-within-bone" appearance. Hypoplasia of the mandible and short bones of the hands and feet with osteolysis of the distal phalanges are characteristic.	Rare autosomal recessive disorder consisting of osteosclerosis, short stature, frontal and occipital bossing, small face with receding chin, short broad hands, and hypoplasia of the nails.
Dysosteosclerosis	Sclerosis of skull, ribs, clavicles and tubular bones similar to osteopetrosis. However, platyspondylia and lucent areas in the expanded diametaphyses allow differentiation.	Autosomal recessive disorder manifested in early childhood with small stature, dental anomalies, abnormal bone fragility, and occasionally neurologic symptoms.
Melorheostosis (Fig. 2.39)	Causes asymmetrical or uniform cortical thickening. Usually limited to one extremity, with a predilection for tubular bones where it presents as continuous or interrupted streaks of sclerotic areas.	When features of melorheostosis are present together with findings of osteopoikilosis and osteopathia striata, then the disorder is often referred to as *mixed sclerosing bone dystrophy* (Fig. 2.**40**).

(continues on page 32)

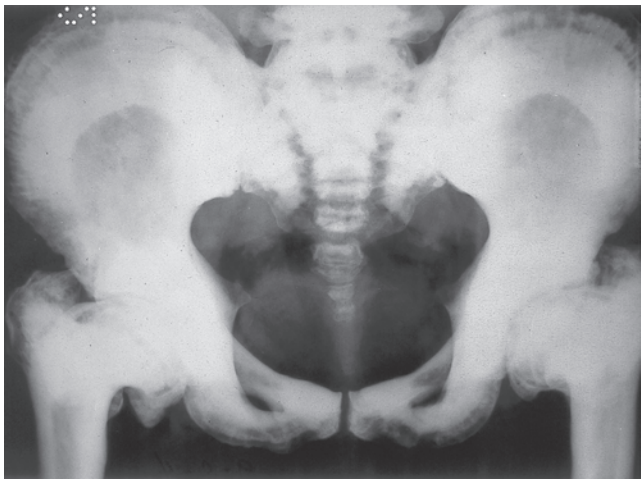

a

b

Fig. 2.**38** **Osteopetrosis**. Diffuse and symmetrical osteosclerotic involvement of the entire skeleton is characteristic. Note "bone-within-bone" appearance in the pelvis and tarsal bones (**a**) pelvis; (**b**) hand; (**c**) foot.

Fig. 2.**38 c**

Fig. 2.**40** **Mixed sclerosing bone dystrophy**. Features of osteopoikilosis, osteopathia striata and melorheostosis are seen.

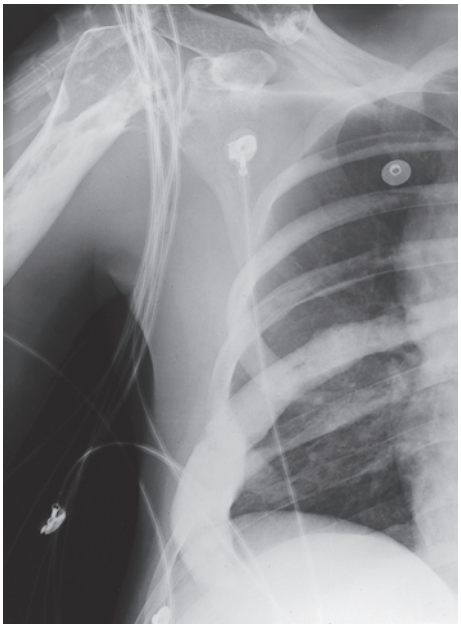

a

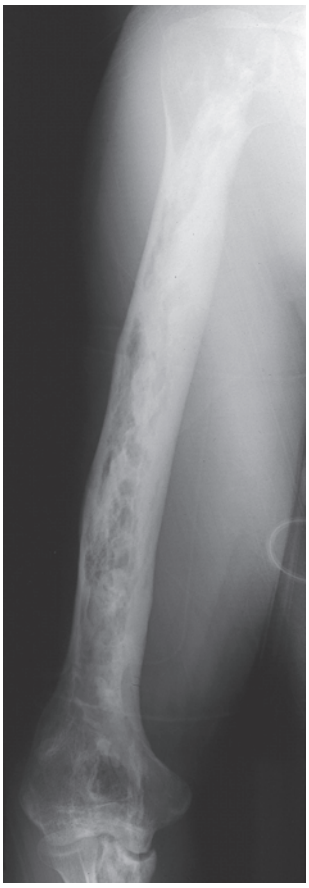

b

Fig. 2.**39 a**, **b** **Melorheostosis**. Extensive predominantly band-like ossificatins were seen in many bones of the right side of the patient shown here in the right hemithorax (**a**) and right humerus (**b**). The left side was normal.

Table 2.2 (Cont.) Generalized Diffuse Osteosclerosis

Disease	Radiographic Findings	Comments
Metastatic disease (extensive) (Fig. 2.41)	Generalized diffuse osteosclerosis.	Most commonly from carcinoma of prostate and breast.
Myelofibrosis (myelosclerosis, myeloid metaplasia) (Fig. 2.42)	Approximately half of the patients develop a diffuse (rarely patchy) osteosclerosis. Ribs, spine, pelvis, humeri, and femur are most often involved. Massive splenomegaly is usually apparent radiographically. Extramedullary hematopoiesis, evident as a paraspinal mass, may be present. Both findings may help to differentiate myelofibrosis from osteoblastic metastases, fluorosis, osteopetrosis, and renal osteodystrophy.	Clinically characterized by hepatosplenomegaly, anemia, thrombocytopenia.
Anemias and leukemias (Figs. 2.43 and 2.44)	Present radiographically more commonly with a loss of bone density and coarsening of the trabecular pattern. Generalized sclerosis may occur, particularly in *sickle cell anemia*.	Extramedullary hematopoiesis can be associated with all blood disorders. Splenomegaly is usually present except in the adult sickle cell patient (presumably because of multiple splenic infarctions).
Multiple myeloma	Uniform sclerosis is a very rare manifestation.	Characteristic bone marrow and laboratory findings.
Gaucher's disease (Fig. 2.45)	May present in the reparative stage with diffuse osteosclerosis. Characteristic for Gaucher's disease in the femur is the combination of avascular necrosis of the femoral head, Erlenmeyer's flask deformity of the distal end, and multiple osteolytic and/or sclerotic lesions in the shaft.	The radiographic findings described are seen in the chronic form of Gaucher's disease, whereas the acute infantile form is characterized by pathology in the respiratory and central nervous system and is usually fatal in the first year of life.

(continues on page 34)

Fig. 2.**41** **Osteoblastic metastases** from prostatic carcinoma. Generalized diffuse osteosclerosis is seen.

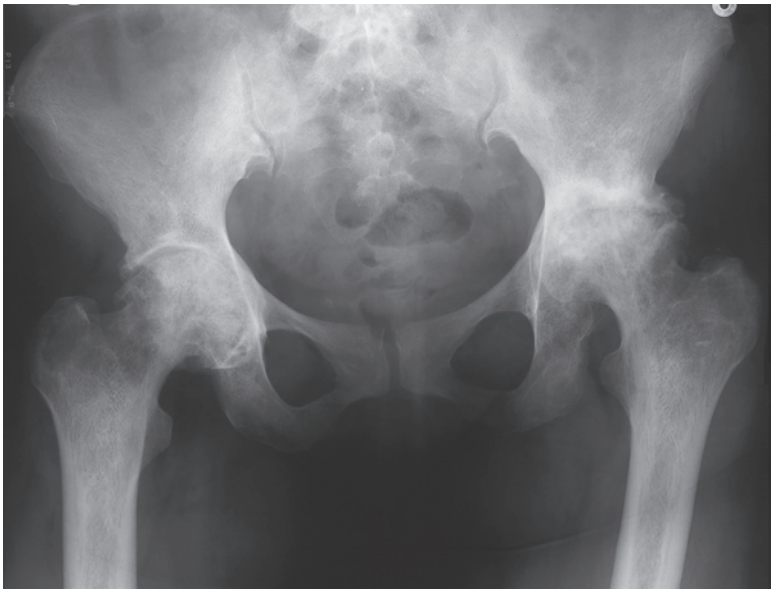

Fig. 2.**42** **Myelofibrosis**. Diffuse symmetric and somewhat patchy osteopenia is seen involving the lumbosacral area, pelvis and proximal femora.

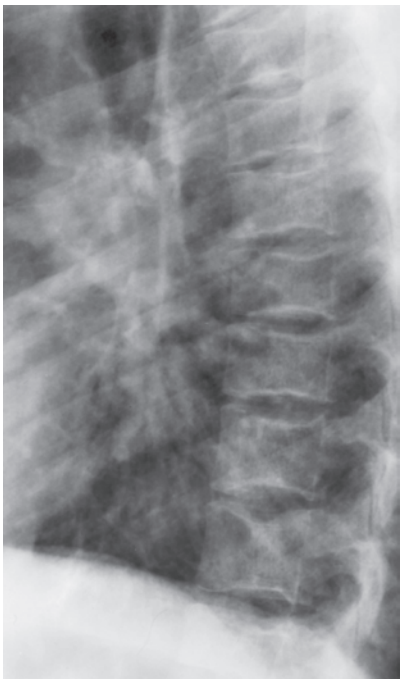

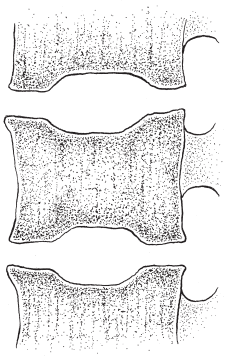

a

b

Fig. 2.**43** **Sickle cell anemia**. A nonuniform cuplike depression of only the central portions of the upper and lower endplates of several contiguous vertebral bodies is characteristic and assumed to be caused by local ischemia inhibiting central bone growth. The bone density may be decreased or increased and the trabecular pattern is often coarsened. **a**: thoracic spine; **b**: drawing.

Fig. 2.**44** **Leukemia**. A coarsened trabecular pattern and "cortical tunneling" (longitudinal striations in the cortex) with an overall increased bone density are seen in this child with acute leukemia.

Fig. 2.**45** **Gaucher's disease**. Avascular necrosis of the femoral ▷ head and sclerotic changes in the proximal femur are evident.

Table 2.2 (Cont.) Generalized Diffuse Osteosclerosis

Disease	Radiographic Findings	Comments
Erdheim-Chester disease (lipid granulomatosis) (Fig. 2.46)	Symmetric patchy or diffuse osteosclerosis and cortical thickening of the diaphyses and metaphyses of the major long bones, with relative sparing of the epiphyses and axial skeleton, are characteristic.	Affects men and women in the fifth through seventh decade. Xanthomatous patches in the eyelids and mild skeletal pain can be present, but patients may also be asymptomatic.
Paget's disease (Fig. 2.47)	The advanced stage of the polyostotic form may eventually result in a deformed and diffusely sclerotic skeleton. Enlargement of all involved bones by cortical thickening is a radiographic hallmark of the disease.	Common cause of osteosclerosis observed in an asymptomatic patient aged over 40. The radiographic diagnosis is supported by markedly elevated serum alkaline phosphatase and normal serum calcium and phosphorus levels.
Fibrous dysplasia (polyostotic form) (Fig. 2.48)	Similar to Paget's disease. Can present as diffuse sclerosis of the involved bone associated with widening and cortical thickening. The manifestations are predominantly unilateral, and bone deformities are common.	Clinically, "cafe-au-lait" pigmentations with irregular outline ("coast of Maine" appearance) are found in approximately one third of patients with the polyostotic form. Alkaline phosphatase is normal or only mildly elevated.
Mastocytosis	Can present throughout the skeleton as diffuse sclerosis that is not sharply demarcated from normal bone and often intermingled with osteolytic areas.	See also Table 2.**1**
Tuberous sclerosis	Can present as diffuse osteosclerosis similar to mastocytosis.	See also Table 2.**1**
Sarcoidosis	Diffuse osteosclerosis is a rare manifestation.	See also Table 2.**1**
Renal osteodystrophy (Fig. 2.49)	Features of osteomalacia, hyperparathyroidism, and sclerosis. The latter might be the dominant finding and is often combined with soft tissue calcifications. A "rugger jersey" spine (dense endplates with relatively lucent centers resulting in a striped appearance of the spine) is most characteristic.	Represents the skeletal response to chronic renal disease of any origin. In *primary hyperparathyroidism*, sclerosis is virtually limited to cases that are healing.
Oxalosis (Fig. 2.50)	Sclerotic, metaphyseal bands and "woolly" or "Paget-like" sclerosis are combined with features of renal osteodystrophy, including a more generalized form of osteosclerosis.	Deposition of calcium oxalate crystals as a primary hereditary (autosomal-recessive) disorder, or more commonly associated with chronic renal disease. Extensive nephrocalcinosis, nephrolithiasis, and extrarenal soft-tissue deposition of calcium oxalate occur.
Hypervitaminosis D, idiopathic hypercalcemia of infancy (Williams syndrome), intoxication with lead, bismuth, or phosphorus (Fig. 2.51)	Present with dense transverse metaphyseal bands and generalized sclerosis.	In children.
Fluorosis (Fig. 2.52)	Fluorosis progresses from coarsening of the trabecular structures to a dense uniform sclerosis. Characteristically, the findings are most pronounced in the axial skeleton, although all bones may be involved. Periosteal reaction may be present. Extensive ligamentous calcifications are characteristic, particularly in the sacrospinous and sacrotuberous ligaments.	Can be found at any age. Clinically, the most characteristic feature is mottling of the enamel of the teeth. Chronic fluorine intoxication occurs, when the drinking water contains excessive fluoride concentrations (endemic in certain regions of India) or with chronic fluoride therapy in too high dosages (e. g., for osteoporosis).

Fig. 2.**46** **Erdheim-Chester disease**. Inhomogeneous sclerosis with cortical thickening and relative sparing of the epiphysis is seen in the distal tibia.

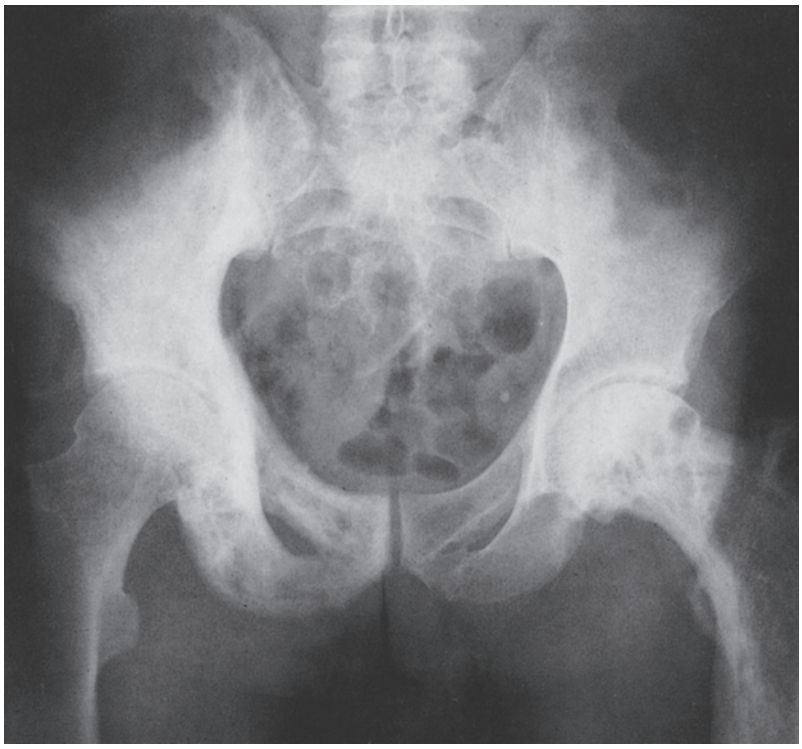

Fig. 2.**47** **Paget's disease**. Predominantly sclerotic involvement of the right hemipelvis, left ilium (inferior half) and left proximal femur is seen.

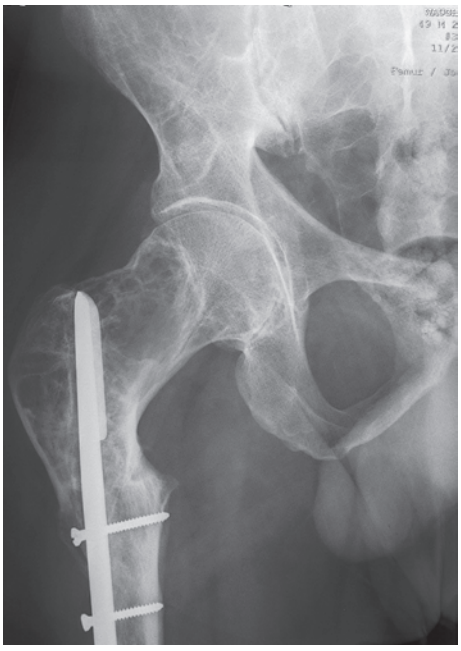

Fig. 2.**48** **Fibrous dysplasia (polyostotic form)**. Mixed osteolytic (some with ground glass appearance) and osteosclerotic involvement of the right hemipelvis and proximal femur is seen.

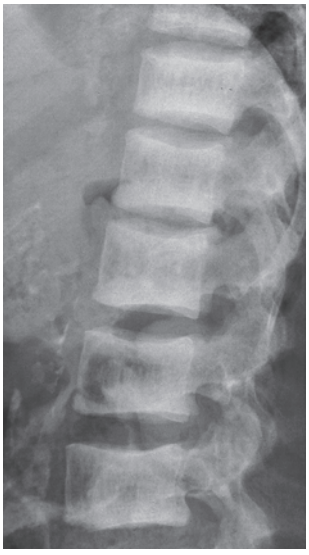

Fig. 2.**49** **Renal osteodystrophy**. Sclerosis is particularly dense at the endplates of the vertebral bodies, resulting in a characteristic "rugger jersey" spine appearance.

Fig. 2.**50** **Oxalosis**. Diffuse "woolly" sclerosis of the axial skeleton and proximal femora is associated with bilateral dense and small kidneys.

Fig. 2.**51** **Hypervitaminosis D**. Generalized sclerosis and transverse bands in slightly widened metaphyses are seen.

Fig. 2.**52** **Fluorosis**. Increased bone density varying from a markedly thickened and coarsened trabecular pattern to uniform sclerosis.

Table 2.3 Avascular Necrosis of the Bone

Location	Eponym or Name of Disease	Etiology	Time of Occurrence
Spine			
Vertebral body (vertebra plana)	Calvé-Kümmel-Verneuil	Idiopathic, posttraumatic, eosinophilic granuloma	Childhood
Vertebral epiphysis	Scheuermann	Idiopathic	Adolescence
Pelvis			
Iliac crest	Buchman	Idiopathic	Adolescence
Ischial apophysis	Milch	Idiopathic	Adolescence
Ischiopubic synchondrosis	Van Neck	Idiopathic	Childhood
Symphysis pubis	Pierson	Idiopathic	Adolescence
Upper extremity			
Clavicle (lower half of sternal end)	Friedrich	Idiopathic	Adulthood
Head of humerus	Hass	Idiopathic	Childhood
Head of humerus (Fig. 2.53)	Avascular necrosis	Post fracture and other causes similar to avascular necrosis of femoral head (see under this subject in this table)	Adulthood
Head of humerus	Osteochondritis dissecans	Idiopathic, posttraumatic	Adolescence, adulthood
Capitulum of humerus (Fig. 2.54)	Panner	Idiopathic, posttraumatic	Childhood, adolescence
Capitulum of humerus	Osteochondritis dissecans	Idiopathic, posttraumatic	Adolescence, adulthood
Head of radius	Brailsford	Idiopathic	Childhood
Distal ulna (epiphysis)	Burns	Idiopathic	Childhood
Hand			
Scaphoid	Preiser	Idiopathic	Childhood, adolescence
Scaphoid (proximal part)	Avascular necrosis	Posttraumatic	Adulthood
Lunate	Kienböck	Idiopathic, posttraumatic	Adulthood
Entire carpus	Caffey	Idiopathic (bilateral), posttraumatic	Childhood, adolescence
Heads of metacarpals	Dietrich	Idiopathic	Adolescence
Bases of phalanges	Thiemann	Idiopathic, posttraumatic	Adolescence

(continues on page 38)

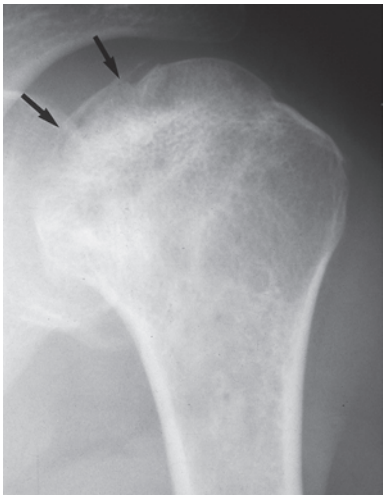

Fig. 2.**53** **Avascular necrosis of the humeral head**. Sclerotic and lytic changes in the humeral head with fragmentation of the joint surface (arrows) are seen.

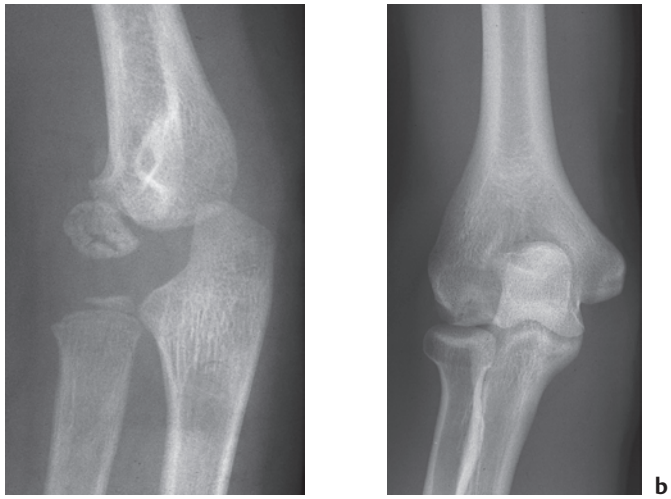

a **b**

Fig. 2.**54** **Avascular necrosis of the capitulum of the humerus** (**Panner**) (2 cases). **a:** Fragmentation of the slightly sclerotic capitulum humeri is seen (arrow). **b:** Sclerotic lesion in the capitulum humeri is seen with healing.

Table 2.3 (Cont.) Avascular Necrosis of the Bone

Location	Eponym or Name of Disease	Etiology	Time of Occurrence
Lower extremity			
Femoral head epiphysis (Fig. 2.55)	Legg-Calvé-Perthes	Idiopathic	Childhood
Femoral head epiphysis	Slipped capital femoral epiphysis	Idiopathic, posttraumatic	Adolescence
Femoral head	Osteochondritis dissecans	Idiopathic, posttraumatic	Adolescence, adulthood
Femoral head	Avascular necrosis	Idiopathic, degenerative and associated with a variety of diseases (e.g., congenital disorders, hematologic and reticuloendothelial diseases, posttraumatic (especially subcapital hip fracture), post-inflammatory diseases, endocrinologic and metabolic disorders, collagen diseases, pancreatic diseases, alcoholism, steroid therapy, post-irradiation, and caisson disease.	Adolescence, adulthood
Greater trochanter	Mandl	Idiopathic	Adolescence
Medial femur condyle (less commonly lateral femur condyle)	Osteochondritis dissecans	Idiopathic, posttraumatic	Adolescence, adulthood
Medial femur condyle (less commonly lateral femur condyle, rarely tibial condyles) (Fig. 2.55 a)	Ahlbäck (Spontenous osteonecrosis about the knee or SONC)	Idiopathic, stress (insufficiency) fractures	Adulthood (usually after age 60 with female predominance)
Medial or lateral femur condyle	Avascular necrosis	Posttraumatic and other causes similar to avascular necrosis of femoral head.	
Patella	Köhler	Idiopathic	Childhood
Patella (secondary ossification center at inferior aspect of patella)	Sinding-Larsen-Johansson	Idiopathic, posttraumatic	Adolescence
Patella	Osteochondritis dissecans	Idiopathic, posttraumatic	Adolescence, adulthood
Intercondylar spines of tibia	Caffey	Posttraumatic	Adolescence
Medial tibia condyle	Blount	Idiopathic, posttraumatic	Infancy, childhood, adolescence
Tibial tuberosity	Osgood-Schlatter	Idiopathic, posttraumatic	Childhood, Adolescence
Distal tibia (epiphysis)	Liffert-Arkin	Idiopathic, posttraumatic	Childhood
Foot			
Talus (Trochlea)	Diaz	Idiopathic	Childhood
Talus (Trochlea) (Fig. 2.56)	Osteochondritis dissecans	Idiopathic, posttraumatic	Adolescence, adulthood
Talus (Trochlea)	Avascular necrosis	Posttraumatic and other causes similar to avascular necrosis of femoral head (see under this subject in this table)	Adulthood
Epiphysis of calcaneus	Sever	Idiopathic	Adolescence
Navicular	Köhler	Idiopathic	Childhood
Navicular (Fig. 2.57)	Mueller-Weiss	Idiopathic, posttraumatic	Adulthood
Os tibiale externum	Haglund	Idiopathic, posttraumatic	Childhood, adolescence, adulthood
Base of fifth metatarsal	Iselin	Idiopathic	Adolescence
Head of metatarsals (most commonly first)	Osteochondritis dissecans	Idiopathic, posttraumatic	Adolescence, adulthood
Head of metatarsals (most commonly second) (Fig. 2.58)	Freiberg	Idiopathic, posttraumatic	Adolescence, adulthood
Base of phalanges	Thiemann	Idiopathic	Adolescence, adulthood

Fig. 2.**55** **Legg-Calvé-Perthes disease**. A flattened, fragmented and laterally displaced capital epiphysis is associated with a widened and shortened femoral neck.

Fig. 2.**55 a** **Ahlbäck's disease (spontaneous osteonecrosis about the knee or SONC)**. An osteochondral defect with mild surrounding sclerosis is seen in the weight-bearing portion of the medial femur condyle.

Fig. 2.**56** **Osteochondritis dissecans of the talus**. A small, oval-shaped bony fragment is seen in an articular defect located in the medial aspect of the talar dome (arrow).

Fig. 2.**57** **Avascular necrosis of the navicular bone (Mueller-Weiss).** A collapsed sclerotic navicular bone with secondary degenerative changes in the talonavicular joint is seen.

Fig. 2.**58** **Avascular necrosis of the head of the second metatarsal (Freiberg).** Sclerosis and flattening of the head of the second metatarsal is seen.

3 Periosteal Reactions

A periosteal reaction is a common response to a variety of insults to the bone. Important differential diagnostic clues may be obtained from both patterns and locations of periosteal reactions. After an acute incidence, it usually takes three weeks before a periosteal reaction can be diagnosed radiographically. Periosteal reactions should be classified as either *solid* or *interrupted*. Each of these two basic forms of periosteal reaction consist of several subtypes. Furthermore, it appears useful for the differential diagnosis to discriminate between conditions with localized or generalized periosteal reactions.

Solid periosteal reactions can be *thin* (1 mm or less in thickness) or *thick* (2 mm or more). A thin periosteal reaction might represent an early stage of a highly aggressive bone lesion or a chronic, benign process (Fig. 3.**1**). On the other hand, a thick periosteal reaction usually suggests a benign condition. Thick periosteal reactions may be further subdivided into *straight*, *elliptical*, and *undulating*, each subtype suggesting somewhat different diagnostic possibilities (Fig. 3.**2**).

An *interrupted periosteal reaction*, in general, signals an acute and rapidly progressing process requiring immediate attention. These periosteal reactions can be *laminated ("onion skin")*, *perpendicular ("sunburst")*, or *amorphous* (Fig. 3.**3**). A destructive bone lesion associated with any interrupted periosteal reaction suggests acute osteomyelitis or a malignancy.

A local elevation of the periosteum that is calcified at the site of its bone insertion is known as *"Codman's triangle"* (Fig. 3.**3b**). Originally considered as a sign of a malignant bone neoplasm, it has been recognized that it can also occur with benign processes such as osteomyelitis, subperiosteal hemorrhage, and fracture. When the periosteal reaction eventually blends with the adjacent cortex, cortical thickening occurs. However, cortical thickening may also develop by excessive endosteal or periosteal new bone formation without stripping the periosteum away from the cortex. The differential diagnoses of various bone lesions with periosteal reactions are discussed in Table 3.**1**.

Under a variety of degenerative, traumatic and inflammatory conditions, a periostitis is found at the insertions of many tendons and ligaments causing the appearance of *"whiskering"* (Fig. 3.**4**). The most common location is the pel-

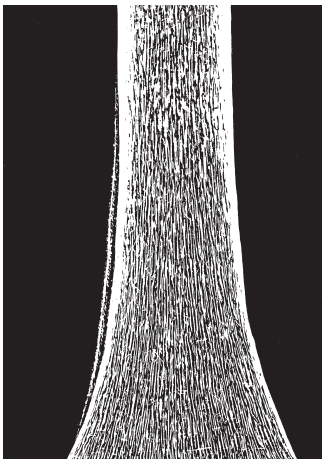

Fig. 3.**1** **Thin (1 mm or smaller) periosteal reaction**. This is an indeterminate finding, since it may indicate a chronic benign process that progresses slowly, if ever, to a solid thick periosteal reaction; or it may represent the earliest stage of an aggressive bone lesion that progresses rapidly to an interrupted periosteal reaction.

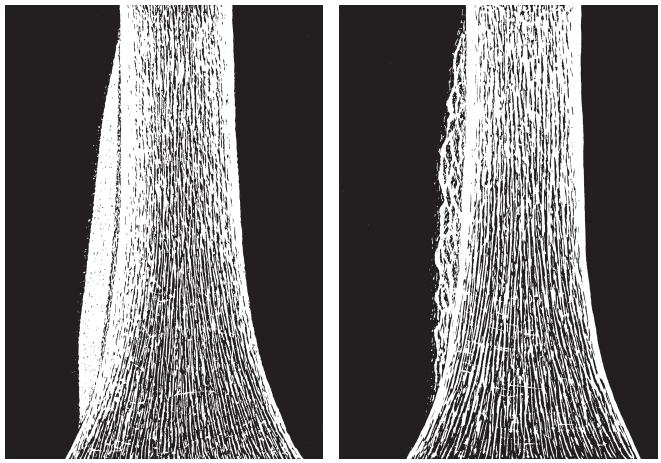

a **b**

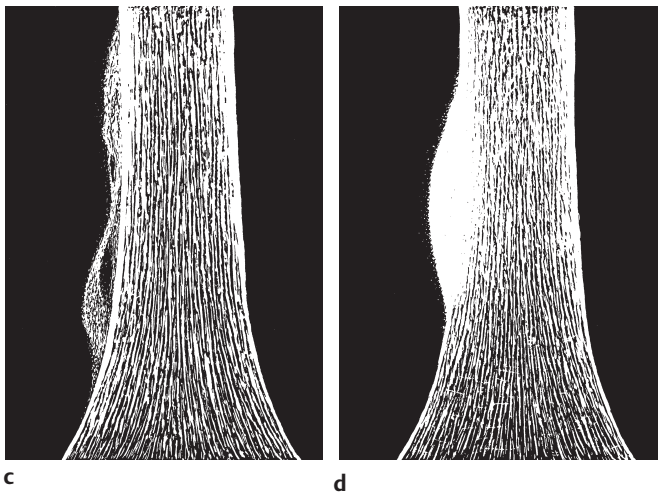

c **d**

Fig. 3.**2** **Solid periosteal reactions** indicating a benign bone lesion. **a** Thick (2 mm or larger) periostea! reaction. **b** Undulating periosteal reaction. **c** Periosteal cloaking. **d** Elliptical periosteal reaction.

vis, where the iliac crests, the ischial tuberosities and the ischiopubic rami are affected. Other sites of extrapelvic involvement include the femoral trochanters, the patella, the calcaneus, the dorsum of the foot, the inferior clavicular margin at the attachment of the coracoclavicular ligament, the humeral tuberosities, and the olecranon. As the periostitis progresses the "whiskers" become more prominent, and may transform into spurs or other bony excrescences referred to as *enthesophytes*. They tend to remain relatively ill-defined or fluffy in *ankylosing spondylitis* (Fig. 3.**5**), *Reiter's syndrome* and *psoriasis*. In these inflammatory conditions, erosions or sclerosis of the adjacent bone may be associated.

The enthesophytes in *diffuse idiopathic skeletal hyperostosis (DISH)* (Fig. 3.**6**) are bilateral and symmetrical, but without adjacent erosions or reactive bone sclerosis. These spurs are well demarcated and often irregular in outline, especially in the calcaneus. Degenerative disease of tendons and ligaments in the elderly may produce similar enthesophytes, but they tend to be less prominent and less symmetric.

Localized spurring at the insertions of tendons and ligaments occurs in conjunction with *chronic stress* or as *sequelae of an old injury*. Spur formations are commonly found in the calcaneus, patella and trochanters with *acromegaly*. Ligamentous and tendinous calcifications resembling DISH and predominantly involving the axial skeleton are encountered in *fluorosis*, *hypoparathyroidism*, and *vitamin D-resistant rickets* (adults), but may be associated in these conditions with osteosclerosis, which is particularly striking in fluorosis.

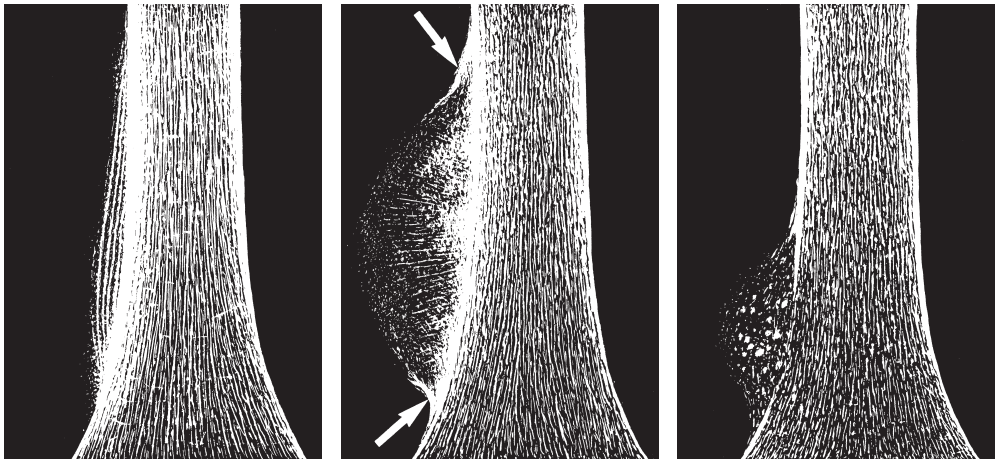

a b c

Fig. 3.**3** **Interrupted periosteal reactions** indicating an aggressive or malignant bone lesion. **a** Laminated ("onion skin") periosteal reaction. **b** Perpendicular ("sunburst") periosteal reaction and Codman's triangles at both ends (arrows). **c** Amorphous periosteal reaction.

Fig. 3.**4** **Whiskering**. Periostitis at the insertion of tendons and ligaments found with a variety of degenerative, traumatic and inflammatory conditions. Progression to formation of spurs or bony excrescences (enthesophytes) possible.

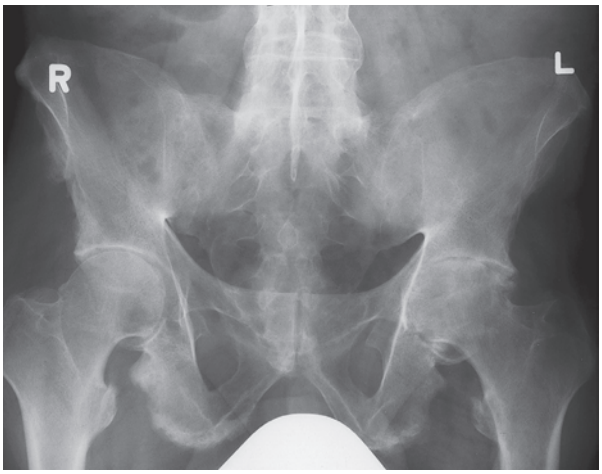

Fig. 3.**5** **Ankylosing spondylitis**. Fluffy enthesopathy along the iliac crests and ischia with sclerosis of the adjacent bones is associated with fusion of the sacroiliac joints and the visualized part of the lumbar spine. Note the delicate bridging syndesmophytes in the lumbar spine. Arthritic changes with circumferential (axial) joint space narrowing and early erosions are also seen in both hips.

Fig. 3.**6** **DISH**. Well defined enthesopathy with bony excrescences that can be differentiated in cortical and cancellous bone are associated with normal sacroiliac joints and fused lower lumbar spine by huge paravertebral ossifications.

Table 3.1 Diseases with Periosteal Reactions

Disease	Preferred Locations	Distribution	Periosteal Reactions	Comments
Physiologic periostitis in infants (Fig. 3.7)	Long bones	Generalized and symmetrical	Solid thin or thick	Develops in second or third month of life, especially in prematures.
Congenital syphilis (Fig. 3.8)	Long bones	Generalized and symmetrical	Solid thick or laminated	Associated with transverse striping of metaphyses and destructive lesions, initially involving the corners of the metaphyses adjacent to the cartilage plate.
Infantile cortical hyperostosis (Caffey's disease) (Fig. 3.9)	Mandible, clavicle, scapula, ribs, tubular bones (limited to diaphyses)	Solitary or multiple	Solid thick or laminated	Clinically tender soft-tissue swellings are associated with the affected bone. Onset occurs in the first five months of life.
Hypervitaminosis A	Tubular bones (especially ulna), metatarsals, clavicle, tibia, fibula (limited to diaphyses)	Generalized	Solid, undulating or occasionally laminated	Associated with tender soft masses in children usually between 1 and 3 years old. *Prostaglandin* infusions in neonates (to maintain patency of the ductus-dependent congenital heart disease) may result in similar bony changes. In older children and adolescents, periosteal reactions and hyperostosis in the axial and appendicular skeleton similar to DISH may bay be found with chronic administration of *retinoid drugs*.

(continues on page 44)

Fig. 3.7 **Physiologic periostitis in infants**. A solid, thin periosteal reaction is found along the medial aspect of the tibia and lateral aspect of the distal femur.

Fig. 3.8 **Congenital syphilis**. Solid, thick periosteal reactions are associated with destructive lesions in the radius and ulna and with irregular metaphyses.

Fig. 3.9 **Infantile cortical hyperostosis (Caffey's disease).** A laminated periosteal reaction is seen along the femur diaphysis.

Table 3.1 (Cont.) Diseases with Periosteal Reactions

Disease	Preferred Locations	Distribution	Periosteal Reactions	Comments
Scurvy (healing) (Fig. 3.10)	Long bones	Generalized	Solid thick	Caused by calcification of the subperiosteal hemorrhage.
Rickets (healing) (Fig. 3.11)	Long bones	Generalized	Solid thin, thicker laminated	Caused by calcification of the subperiosteal osteoid. Associated with mineralization of the zone of provisional calcification that appears as an irregular dense area in the epiphyseal cartilage, separated by a thin radiolucent line from the metaphysis.
Dysproteinemia	Tubular bones, mandible	Generalized and symmetrical	Solid thin or thick, or laminated	In children with bone pain and often with fever. Hyperphosphatemia may also be present.
Pachydermoperiostosis (primary hypertrophic osteoarthropathy) (Fig. 3.12)	Long tubular bones, especially radius, ulna, tibia and fibula. Less common in metacarpals, metatarsals, and phalanges, pelvis, ribs and clavicles.	Generalized and symmetrical. May extend from the diaphyses into the metaphyses and epiphyses (DD: Secondary hypertrophic osteoarthropathy, where it does not extend into the epiphyses).	Solid thick, often with shaggy, irregular excrescences	Familial condition with skin thickening and cortical thickening. Periosteal new bone formation tends to blend with thickened cortex. Almost exclusively found in males with predilection for blacks. Onset in adolescence.
Secondary hypertrophic osteoarthropathy (Fig. 3.13)	Diaphyses of tubular bones	Generalized and symmetrical	Solid thin or thick (often undulating and cloaking) or laminated	In patients with bronchogenic carcinoma, and occasionally with chronic diseases of lung, gastrointestinal tract, or cardiovascular system.
Osteosarcoma (Figs. 3.14 and 3.15)	Femur, tibia, humerus, and mandible	Localized	Solid thin, laminated, perpendicular (thin spicules) or amorphous. Codman's triangle occurs	*Periosteal sarcoma*: Limited to the cortex of long bone diaphyses (especially femur and tibia). Perpendicular periosteal reaction and Codman's triangle are characteristic. *Parosteal sarcoma*: a large radiodense lesion with smooth lobulated or irregular margins is attached to the external cortex (Fig. 3.**16**).

(continues on page 46)

Fig. 3.**10** **Scurvy** (healing). This characteristic periosteal reaction is caused by calcification of the subperiosteal hemorrhage.

Fig. 3.**11** **Rickets** (healing). This periosteal reaction is caused by calcification of the subperiosteal osteoid.

Fig. 3.**12** **Pachydermoperiostosis (primary hypertrophic osteoarthropathy.** A solid, thick, and shaggy periosteal reaction is seen

a

b

Fig. 3.**13a**, **b** **Secondary hypertrophic osteoarthropathy.** Solid thin and laminated, occasionally undulating periosteal reactions are seen in the radius and ulna (**a**) and tubular bones of the hand (**b**).

Fig. 3.**14** **Osteosarcoma (osteolytic)**. A poorly defined osteolytic lesion is seen in the distal femur associated with a large amorphous periosteal reaction posteriorly.

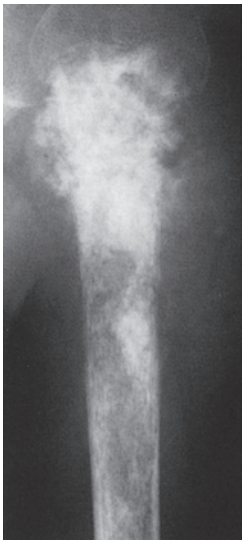

a

b

◁ Fig. 3.**15a**, **b** **Osteosarcoma (2 cases).** A permeative destructive lesion with osteoblastic areas and amorphous periosteal reaction, interspersed with thin perpendicular spicules, is seen in **a**. Cortical thickening with laminated periosteal reaction is seen in **b**.

Fig. 3.**16** **Parosteal osteosarcoma**. A large, radiodense lesion with irregular margins is attached posteriorly to the distal femur in characteristic location. ▷

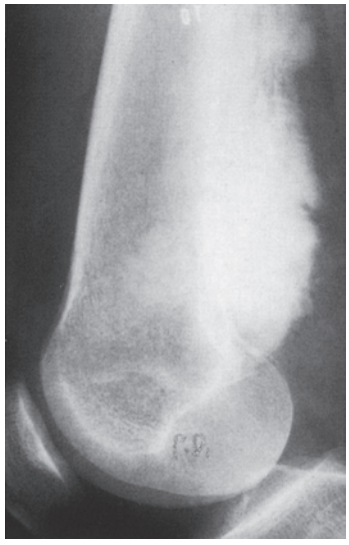

Table 3.1 (Cont.) Diseases with Periosteal Reactions

Disease	Preferred Locations	Distribution	Periosteal Reactions	Comments
Ewing's sarcoma (Figs. 3.17 and 3.18)	Under 20 yr: tubular bones Over 20 yr: flat bones	Localized	Solid thin, laminated or perpendicular (thin spicules). Codman's triangle occurs.	
Other sarcomas (e.g. chondrosarcoma, fibrosarcoma) and primary bone lymphoma (including reticulum cell sarcoma)	Long bones, flat bones	Localized	Solid thin, thick or amorphous. Rarely solid thick, laminated, perpendicular or amorphous. Codman's triangle is unusual.	Periosteal reactions are rare in these conditions. Cortical thickening in a chondroid matrix tumor suggests low-grade chondrosarcoma rather than enchondroma.
Leukemia and metastases (Figs. 3.19 and 3.20)	Long bones, ribs	Multiple	Solid thin or laminated. Perpendicular in skull. Rarely solid thick.	Interrupted periosteal reactions are common in children (e.g., leukemia and metastases from *neuroblastomas*). Solid periosteal reaction or localized cortical thickening is associated with metastases from *prostatic* and *breast carcinomas*.
Osteoid osteoma (Fig. 3.21)	Femur, tibia, fibula, humerus, vertebral arch	Localized	Elliptical and dense. Rarely solid thin.	Radiolucent intracortical nidus with or without central calcification is classical, but not always demonstrated.
Other benign tumors and cysts		Localized	Solid thin or thick.	Periosteal reactions usually associated with bone expansions and/or pathologic fractures.
Acute hematogenous osteomyelitis (Fig. 3.22)		Solitary, rarely multiple	Solid thin or thick, laminated or perpendicular (short and squat spicules). Codman's triangle occurs.	Earliest radiographic findings: bone destruction after 1 week, periosteal reactions after 2 weeks, and sequestrum formation after 3 weeks. Organisms: staphylococci, streptococci, salmonella (especially in sickle cell anemia), pseudomonas, klebsiella (often with intravenous drug abuse), less common: pneumococci, meningococci, brucella, fungi, viruses, and parasites.

(continues on page 48)

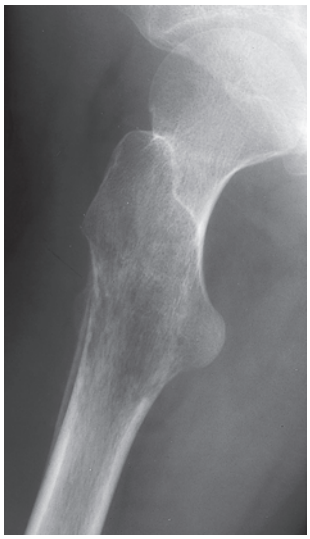

Fig. 3.**17** **Ewing's sarcoma**. A poorly defined permeative osteolytic lesion is seen in the proximal femur with beginning laminated periosteal reaction on its outer cortex.

Fig. 3.**18** **Ewing's sarcoma**. A barely perceptive permeative osteolytic lesion in the femur shaft is associated with laminated periosteal reactions including three Codman's triangles (arrows).

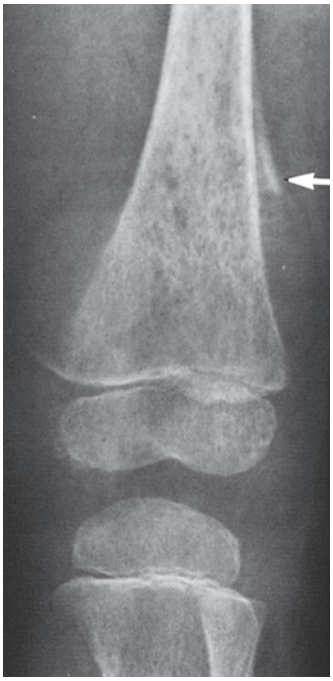

Fig. 3.**19** **Neuroblastoma metastasis**. A permeative lesion with a Codman's triangle (arrow) and a faint perpendicular periosteal reaction is seen. A solitary neuroblastoma metastasis is radiographically often indistinguishable from a Ewing's sarcoma.

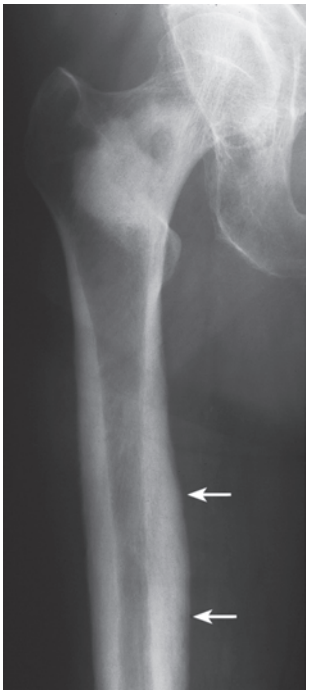

Fig. 3.**20** **Osteoblastic metastases (breast carcinoma)**. Besides a large osteoblastic metastases in the femoral neck and intertrochanteric area localized thickening of the cortex in the femur shaft is also evident (arrows).

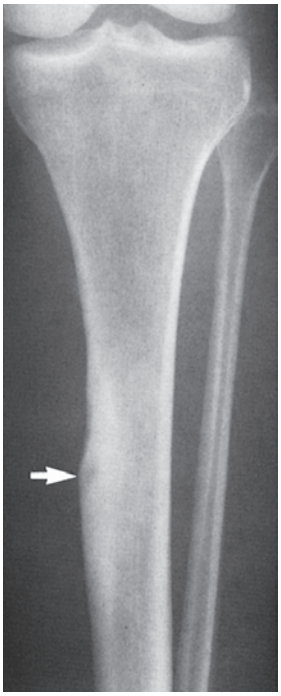

Fig. 3.**21** **Osteoid osteoma**. A dense, elliptical periosteal reaction with a nidus (arrow) is diagnostic.

Fig. 3.**22** **Acute osteomyelitis**. A destructive bone lesion surrounded by a laminated periosteal reaction is seen.

Table 3.1 (Cont.) Diseases with Periosteal Reactions

Disease	Preferred Locations	Distribution	Periosteal Reactions	Comments
Chronic osteomyelitis (Fig. 3.23)		Solitary, rarely multiple	Solid thick, often undulating and cloaking.	Thick periosteal reaction associated with sclerosis, and scattered radiolucent areas which may contain a dense bone sequestrum.
Osteomyelitis from contiguous infective source (Fig. 3.24)	Hands, feet or adjacent to decubitus ulcers	Localized	Solid thin or thick.	Periosteal reaction associated with bone destruction and sclerosis. Commonly found in diabetes mellitus, quadriplegia and vascular insufficiency.
Tuberculous osteomyelitis (Fig. 3.25)		Solitary, rarely multiple	Solid thin or thick.	Similar to hematogenous osteomyelitis, but osteopenia is more pronounced, whereas periosteal reactions and osteosclerosis are less. Similar findings as in tuberculosis are seen in *atypical tuberculosis bacilli* and *BCG osteomyelitis*.
Syphilis	Long bones, skull	Localized or generalized	Solid thin or thick, often undulating and with squat spicules, or laminated.	In early acquired syphilis, an extensive generalized periosteal reaction and cortical thickening is the most common osseous manifestation. The radiologic hallmark of the tertiary stage of the disease consists of dense bony sclerosis with areas of destruction (gumma formation).
Yaws	Long and short tubular bones, skull	Localized or generalized	Solid thin or thick, often undulating and with squat spicules, or laminated.	Occurs in tropical climates, and is usually acquired before puberty. Radiographic features similar to syphilis and *bejel* (prevalent in the Middle East). The causative organisms of these three spirochetal diseases are morphologically indistinguishable.
Tropical ulcer	Tibia (anterior aspect of middle and distal third)	Localized	Solid thick, elliptical or undulating.	Common in Central and East Africa.
Leprosy	Hands, feet	Solitary or multiple	Solid thin or thick, or laminated.	May be associated with bone destruction. Neuropathic bone manifestations are, however, much more common and characteristic.
Rheumatoid arthritis (juvenile)	Peripheral and axial skeleton: periarticular and at tendon and ligament insertions	Localized or generalized	Solid thin or thick or laminated.	Common in juvenile rheumatoid arthritis; very rare in adults, and never a dominant feature.
Psoriatic arthritis (Fig. 3.26)	As above, preferentially in hands	Localized or Generalized	Solid thin or thick or laminated.	Periosteal reactions not uncommon. Irregular bony excrescences characteristic.
Reiter's syndrome (Fig. 3.27)	Calcaneus, short tubular bones of foot, tibia, and fibula	Localized, seldom generalized	Solid thin or thick (often "fluffy") or laminated.	Periosteal reactions common.
Polyarteritis nodosa	Long tubular bones (preferentially lower limbs) and metatarsals	Generalized and symmetrical	Solid thin or thick, characteristically undulating.	Radiographically similar to hypertrophic osteoarthropathy. Pain and swelling of the lower extremity may be associated.

(continues on page 50)

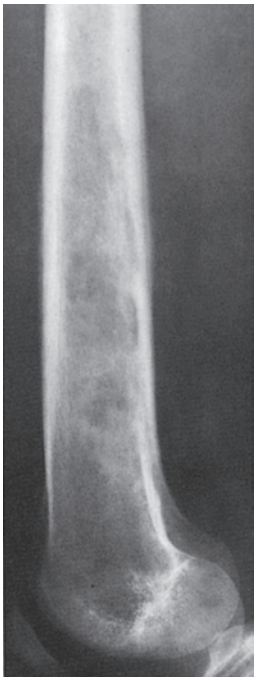

Fig. 3.**23** **Chronic osteomyelitis**. A poorly defined, mixed lytic and sclerotic lesion is associated with a solid periosteal reaction (serratia marcescens osteomyelitis in an intravenous drug abuser).

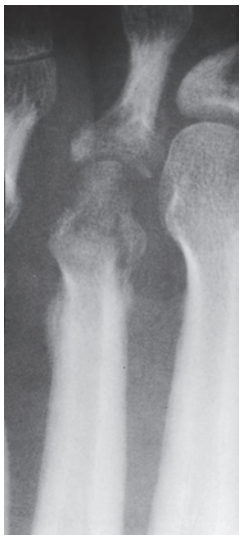

Fig. 3.**24** **Osteomyelitis in diabetes mellitus**. A destructive lesion around the third metatarsophalangeal joint with periosteal reaction is seen.

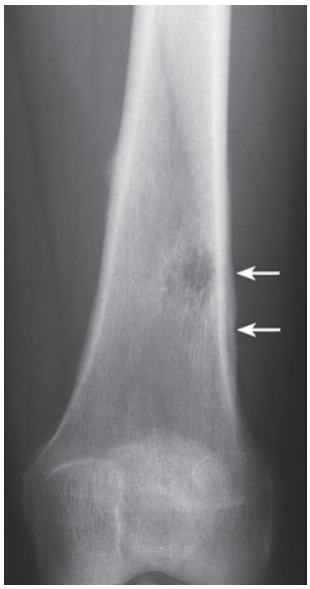

Fig. 3.**25** **Tuberculous osteomyelitis**. A poorly defined lytic lesion is associated with a thin solid periosteal reaction (arrows).

Fig. 3.**26** **Psoriatic arthritis**. Besides erosive arthritic changes extensive periostitis and sclerosis is seen producing an “ivory hand”.

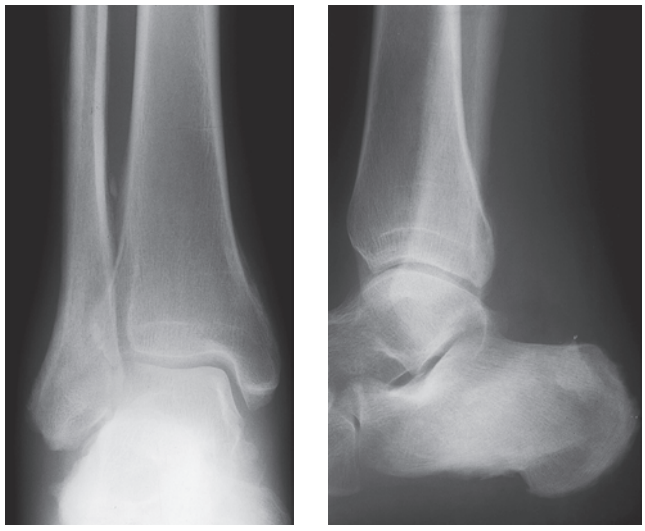

a **b**

Fig. 3.**27** **Reiter’s syndrome**. **a** Ill-defined periosteal reactions around the ankle and **b** fluffy “whiskering” in the posterior and inferior aspect of the calcaneus are quite characteristic.

Table 3.1 (Cont.) Diseases with Periosteal Reactions

Disease	Preferred Locations	Distribution	Periosteal Reactions	Comments
Fractures and stress fractures (Fig. 3.28)		Solitary or multiple	Solid thin or thick or laminated. Codman's triangle occurs.	Periosteal reactions are similar in traumatic and pathologic fractures.
Subperiosteal hemorrhages	Long tubular bones	Solitary or multiple	Solid thin or thick or laminated. Codman's triangle occurs.	Traumatic (including *battered child syndrome*) and *hemophilia*.
Electrical and thermal injuries	Upper extremity	Localized	Solid thin.	Osteolysis, osteosclerosis, periarticular calcifications and heterotopic bone formation are frequently associated.
Vascular and lymphatic disease (Fig. 3.29)	Lower extremity	Localized or generalized	Solid thin or thick, often undulating.	Any disease associated with venous and/or lymphatic stasis. Vascular calcifications and phleboliths may be associated.
Bone infarct	Long tubular bones	Solitary or multiple	Solid thin or thick.	Especially in sickle cell disease, where the periosteal reaction may also be caused by osteomyelitis. *Hand-foot syndrome:* infarctions of the short tubular bones causing periosteal reactions that are indistinguishable from osteomyelitis. Occurs in young children (average age 18 months) with sickle-cell disease.
Eosinophilic granuloma (Langerhans cell histiocytosis)		Solitary or multiple	Solid thin or thick. Rarely laminated.	Destructive bone lesions may contain bone sequestrum.
Gaucher's and other storage diseases	Long tubular bones, spine, and pelvis	Localized or generalized	Solid thin or thick, often undulating and cloaking.	Combination of avascular necrosis of the femoral head, Erlenmeyer flask deformity of the distal femur, circumscribed osteolytic lesions, and bone infarcts are characteristic for Gaucher's disease.
Thyroid acropachy (Fig. 3.30)	Tubular bones, particularly hands and feet	Bilateral and relatively symmetrical	Solid thin or thick, occasionally with short and squat spicules.	Usually one year and later after treatment with thyroidectomy or radioactive iodine.
Renal osteodystrophy (Fig. 3.31)	Long tubular bones, metatarsal, pubic rami	Generalized and symmetrical	Solid thin or thick, occasionally laminated.	Associated with findings of hyperpalathyroidism and osteosclerosis. Very rare in *primary hyperparathyroidism*.
Tuberous sclerosis	Tubular bones	Solitary or multiple	Solid thin or thick, often undulating.	
Neurofibromatosis	Long bones of lower extremity	Solitary or multiple	Solid thick, often undulating.	Pathogenesis of this manifestation is not clear.
Fluorosis	Tubular bones	Generalized and symmetrical	Solid thick, often undulating and cloaking.	Osteosclerosis and ossification of ligaments and tendons at their insertion.
Gardner's syndrome	Tubular bones	Multiple	Solid thin or thick, often undulating.	Osteomas and intestinal polyposis are associated.
DISH (diffuse idiopathic skeletal hyperostosis) (Fig. 3.32)	Spine, pelvis, lower extremity (commonly patella and calcaneus)	Multiple and often symmetrical	Solid thick.	Particularly at tendon and ligament insertions into bone ("whiskering").

Fig. 3.**28** **Stress fracture**. A healing stress fracture is seen in the fibula shaft with exuberant callus formation.

Fig. 3.**29** **Venous stasis**. A thick, undulating periosteal reaction in the proximal tibia, and particularly fibula is associated with extensive varicosis.

Fig. 3.**30** **Thyroid acropachy**. A thick, asymmetric, shaggy periostitis is seen in the fingers with predilection for the metacarpals and proximal phalanges.

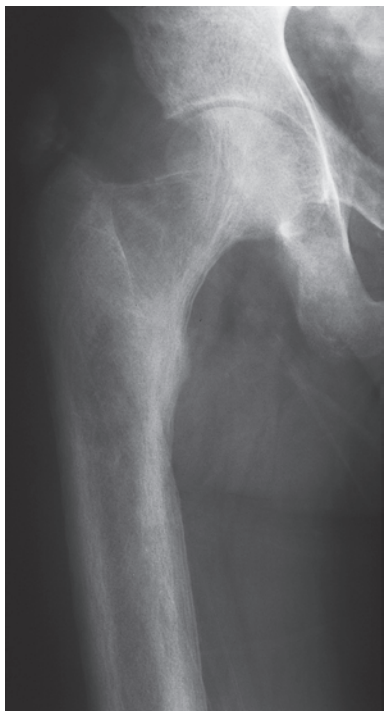

Fig. 3.**31** **Renal osteodystrophy**. Diffuse sclerosis is associated with a solid thick periosteal reaction in the lateral femur cortex and laminated in the medial femur cortex.

Fig. 3.**32** **DISH.** "Whiskering" along the iliac crest, ischiopubic ramus, and femoral trochanters associated with hypertrophic spurs at the superior and inferior margins of the acetabulum.

4 Trauma and Fractures

The radiologic diagnosis and differential diagnosis of an acute fracture is usually not associated with any problems. A sharply demarcated fracture line is the hallmark of an acute fracture. Depending on their radiographic appearances, fractures are classified into different types (Fig. 4.**1**). Occasionally, however, a frank fracture line cannot be demonstrated in undisplaced fractures immediately after injury even when films in several projections are taken. Demonstration of either a cortical break that has to be differentiated from a nutrient artery or disruption of the normal spongiosa pattern may be the only clue in these instances to diagnose a fracture. Magnetic resonance imaging or a nuclear medicine scan is otherwise required to arrive at the correct diagnosis.

In the presence of clinical evidence of a fracture, a zone of increased bone density or an abnormal angulation may suggest radiographically an acute fracture, although these findings can also be encountered in healing fractures and other bone diseases. At least some degree of soft-tissue swelling can be seen radiographically in virtually all acute fractures, but this finding is of little use to differentiate a fracture from a distortion or other soft-tissue injuries.

Fracture healing begins with an acute inflammatory response resulting in the organization of the fracture hematoma by invasion of fibrovascular tissue. At this stage, bone resorption along the fracture margins becomes evident and in undisplaced fractures may allow at this stage (several days after the injury incidence) an unequivocal radiographic diagnosis. Periosteal and endosteal callus formation usually becomes visible two to three weeks after injury and is first evident as a thin periosteal reaction and irregular mottled calcifications about the fracture, increasing with time in density, and finally developing bone texture. The healing process of a noncomplicated fracture from injury to consolidation takes one to several months. Fracture healing progresses more rapidly in oblique or spiral fractures, in a single fracture, and in younger patients. The healing process is slower in larger bones, in transverse fractures, in the presence of multiple fractures, and with increasing age of the patient.

A *delayed union* is found with poor reduction, incomplete immobilization, in the presence of infection, in vitamin C and/or D deficiencies, and in areas of preexisting bone disease (pathologic fractures). Infections are particularly common in *compound fractures*, where extensive soft-tissue damage is caused by either a fracture fragment piercing through the skin or by an object (e.g., a projectile) penetrating from the outside.

Malunion refers to a fracture that is healed with significant fracture fragment displacement and/or angulation. A *nonun-*

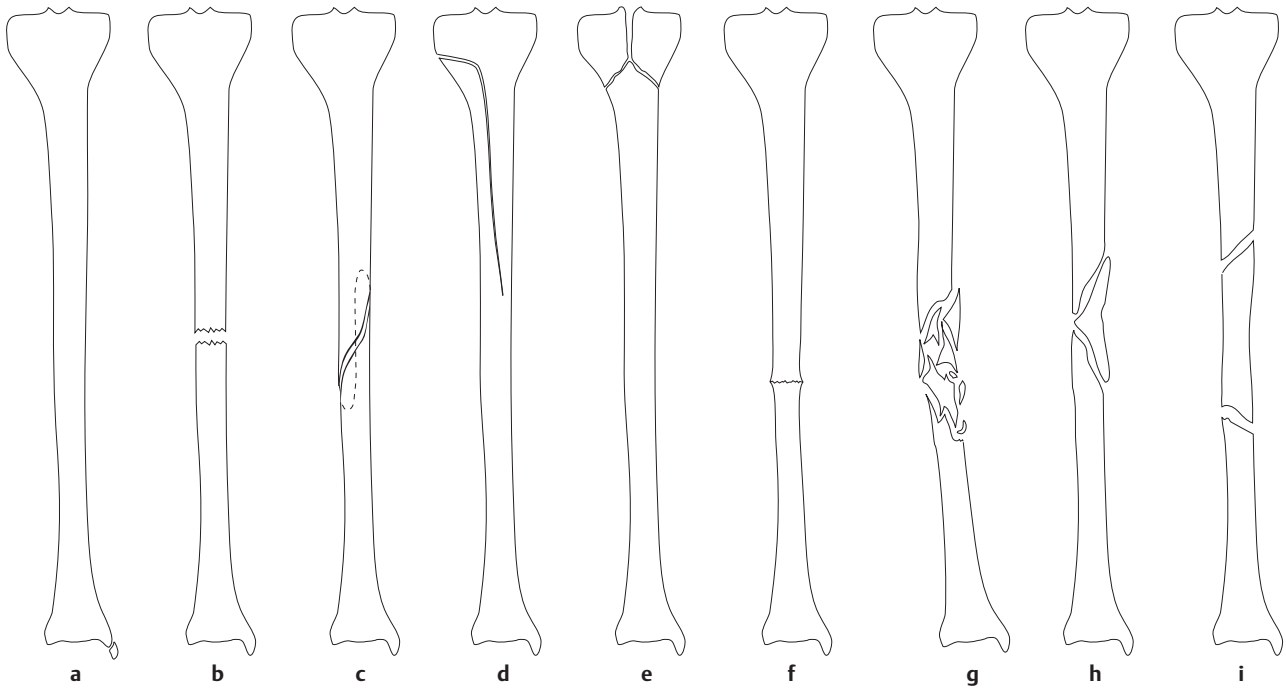

Fig. 4.**1** **Classification of fracture according to their radiographic appearance.** **a** Avulsion fracture (secondary to forcible tearing of ligament or tendon attachment). A chip fracture has the same radiographic appearance, but is caused by direct impact. **b** Transverse fracture (secondary to shearing force to opposite sides of a bone or to impact force along transverse axis). An oblique fracture (not shown) occurs secondary to impact along an oblique axis. **c** Spiral fracture (secondary to rotary-type injury). **d** Longitudinal fracture (secondary to impact force along longitudinal axis). **e** T-, V-, or Y-shaped fracture in proximity of joints (secondary to impact force along longitudinal axis). **f** Impacted fracture or compression fracture (secondary to impact force along longitudinal axis). **g** Comminuted fracture (secondary to severe external trauma or shattering effect of a projectile). **h** Fracture with butterfly fragment. **i** Segmental fracture.

ion is characterized by failure of fracture healing 6 to 9 months after injury. The fracture margins are well delineated and often sclerotic and a frank area of intervening translucency is present. Nonunion may result from the same complications associated with delayed union or by interposition of soft tissue between the fracture fragments. *Hypertrophic nonunion* is commonly caused by continued motion at the fracture site. In these cases the fracture line persists or excessive and prolonged bone resorption at the fracture margins occurs. Eventually the bone ends become sclerotic, and there is a varying degree of non-bridging external callus formation. *Atrophic nonunion* is thought to result from extensive bone death. The radiographic appearance is that of a persistent fracture line without demonstrable callus formation (Figs. 4.**2** and 4.**3**). Nonunion may eventually progress to *pseudarthrosis* formation (Fig. 4.**4**).

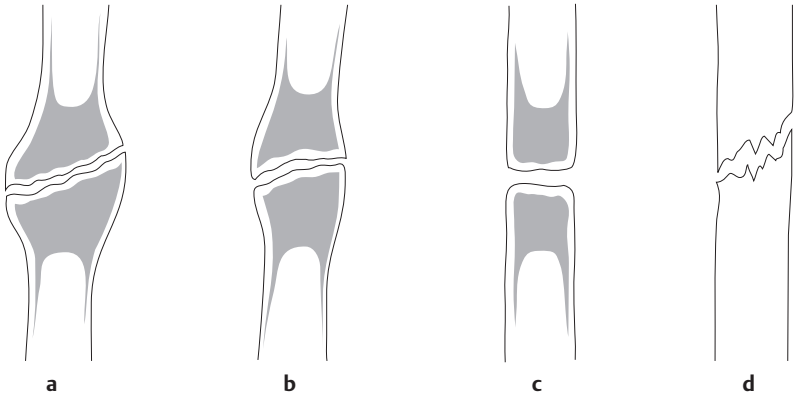

Fig. 4.**2** **Nonunion. a** Hypertrophic (elephant foot). **b** Hypertrophic (horse foot). **c** Oligotrophic. **d** Atrophic.

Fig. 4.**3** **Hypertrophic nonunion.** The distal tibia shaft fracture shows relatively smooth, sclerotic borders without endosteal or periosteal bony bridging of the fracture line, A healed fibula fracture is also evident.

Fig. 4.**4** **Pseudarthrosis** had developed 2 years after a fracture of ▷ the humerus that shows classical changes of Paget's disease.

Fracture healing in *osteogenesis imperfecta* is complicated by pseudarthrosis formation with a higher incidence than in normal bone. Pseudarthrosis is also a common feature in *neurofibromatosis*, where it is most often found in the lower two-thirds of the tibia (Fig. 4.**5**). Pseudarthrosis occurs also in *fibrous dysplasia*, which often demonstrates bone changes radiographically similar to neurofibromatosis. The two disorders can, however, often be differentiated by their skin manifestations. The cafe-au-lait spots in fibrous dysplasia are irregularly outlined ("coast of Maine" appearance), whereas they are smoothly outlined in neurofibromatosis ("coast of California" appearance). Furthermore, the presence of cutaneous fibromas is characteristic for the latter condition. *"Congenital pseudarthrosis"* is a rare condition that may or may not be related to neurofibromatosis or fibrous dysplasia (forme fruste?).

Fractures of the *proximal humerus* occur between one or all four major segments, which include the articular segment (anatomic neck fracture), the proximal humerus shaft (surgical neck fracture), the greater tuberosity and the lesser tuberosity. The modified *Neer four-segment classification* is based on the number of displaced segments. Any fracture that is not or only minimally (less than 1 cm) displaced and not or only minimally angulated (less than 45°) is disregarded. A one-part fracture may involve any or all four anatomic segments but there is no displacement or angulation between fracture fragments. A two-part fracture indicates that only one segment is displaced in relation to the three that remain undisplaced or are intact. A three-part fracture commonly consists of a displaced greater *or* lesser tuberosity fracture combined with a surgical neck fracture. A four-part fracture typically involves both greater and lesser tuberosity in addition to the surgical neck with displacement of all four segments. Two-part, three-part, and four-part fractures may be associated with either anterior or posterior dislocation. The involvement of the articular surface in an anterior fracture-dislocation is referred to as "head splitting" and in a posterior fracture-dislocation as "impression".

Fractures of the *elbow* may involve the distal humerus, and proximal radius and ulna. Extra-articular fractures of the distal humerus involve the epicondyles and supracondylar area. Intra-articular fractures of the distal humerus may involve either the trochlea or the capitellum alone (transcondylar fractures) or both (bicondylar or intercondylar fractures with or without supracondylar comminution). Fractures of the radial head are common in adults, but when nondisplaced or minimally displaced may be difficult to demonstrate with routine radiographic projections. An *Essex-Lopresti fracture* consists of a comminuted displaced fracture of the radial head associated with posterior subluxation of the distal ulna. Fractures of the proximal ulna may involve the coronoid process or the olecranon, but the former rarely occurs as an isolated injury.

A *Monteggia fracture* is the association of a proximal ulnar shaft fracture with dislocation of the radial head. Both the apex of angulation of the ulnar fracture and the dislocation of the radial head are anterior in type 1 (60%), posterior in type 2 (15%), lateral in type 3 (20%) and similar to type 1 but associated with a radius shaft fracture at the level of the ulnar fracture in type 4 (5%) (Fig. 4.**6**). A *Galeazzi fracture* consists of a fracture of the distal third of the radius with angulation apex dorsal and medial (ulnar) associated with dorsal and medial dislocation of the ulna in the distal radioulnar joint (Fig. 4.**7**).

Fractures of the *distal radius* include 1. *Colles fracture* (extra-articular, usually occurring about 2 to 3 cm from the articular surface with typically radial and dorsal displacement and angulation apex volar of the distal radius fracture fragment and frequent association of an ulnar styloid fracture). 2. *Smith fracture* (extra- or intra-articular fracture with volar displacement of the distal fragment). 3. *Barton fracture* (intra-articular oblique fracture of the dorsal distal radius) and 4. *Hutchinson or chauffeur's fracture* (fracture of the radial styloid process) (Fig. 4.**8**). The scaphoid is the most commonly fractured carpal bone. The fracture may be located in the distal pole (5%), tubercle (5%), waist (75%) or proximal pole (15%) (Fig. 4.**9**). Common complications of a

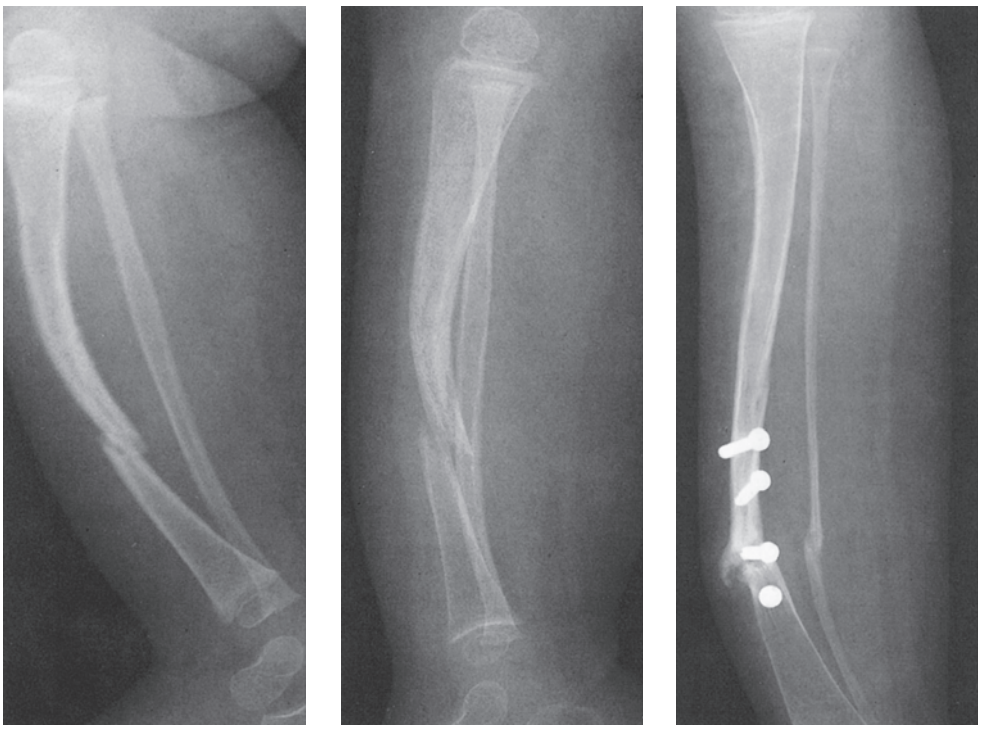

a b c

Fig. 4.**5** **Nonunion and pseudarthrosis formation in neurofibromatosis. a** A fracture is seen in the tibia that shows anterior bowing. **b** Six months after **a**. Periosteal callus formation and bone resorption occurred around the fracture fragments, but the fracture has not healed (nonunion). **c** Five years after **a**. Despite various conservative and surgical treatment attempts, the fracture has not healed, and a pseudarthrosis has formed. Note also the bowing and narrowing (overconstriction) of the fibula (characteristic of neurofibromatosis) in which a healed fracture is now seen.

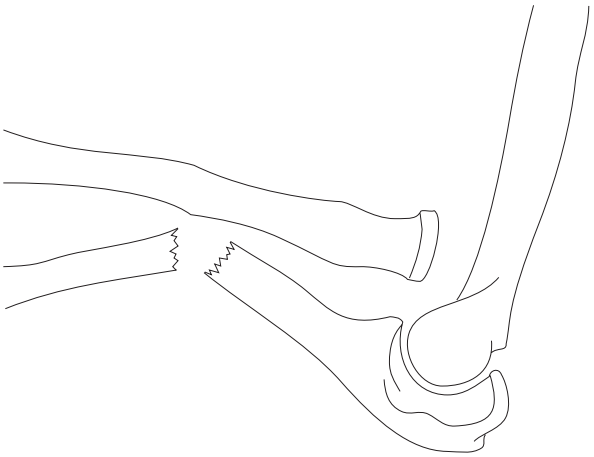

Fig. 4.6 **Monteggia fracture** (type 1). Fracture of the proximal ulnar shaft with anterior angulation at the apex and anterior dislocation of the radial head is seen.

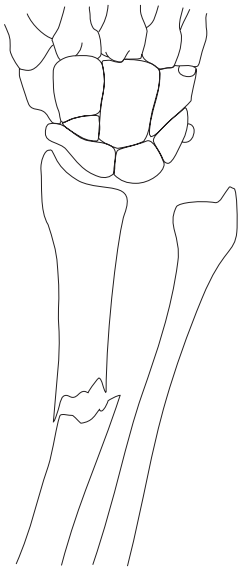

Fig. 4.7 **Galleazzi fracture**. Fracture of the distal radius with angulation apex medial and dorsal and posteromedial dislocation of the ulna in the distal radioulnar joint is diagnostic. The radius fracture fragments may also overlap.

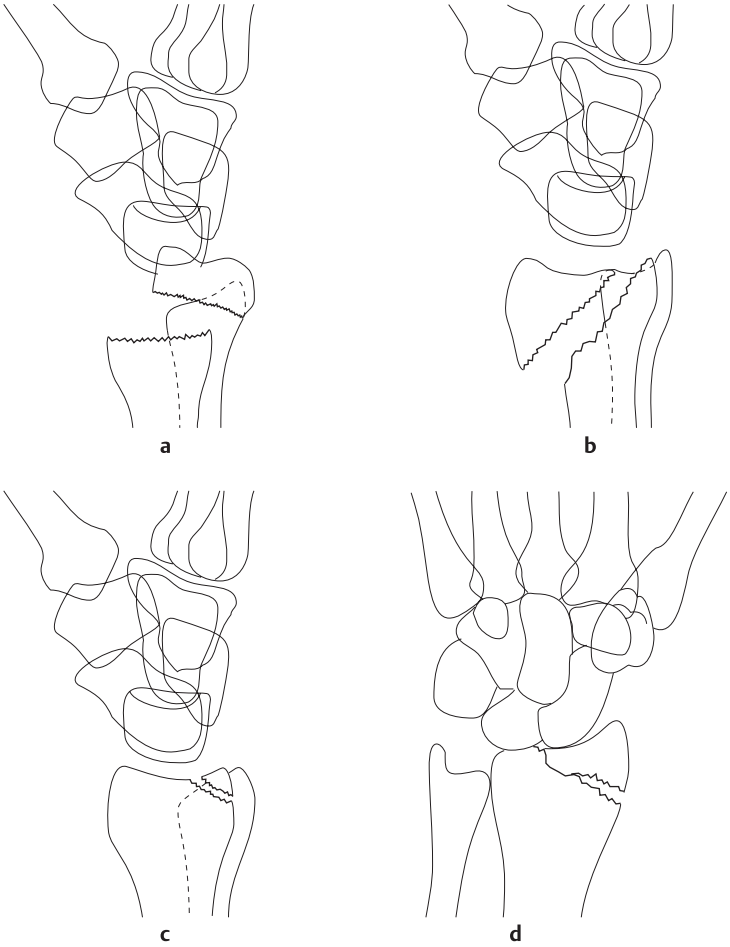

Fig. 4.8 **Distal radius fractures**. **a** *Colles fracture*: Dorsal displacement and angulation apex volar of distal fragment. **b** *Smith fracture*: Volar displacement of distal fragment. **c** *Barton fracture*: Intraarticular fracture of the dorsal distal radius. **d** *Hutchinson* or *chauffeur's fracture*: Fracture of the radial styloid process.

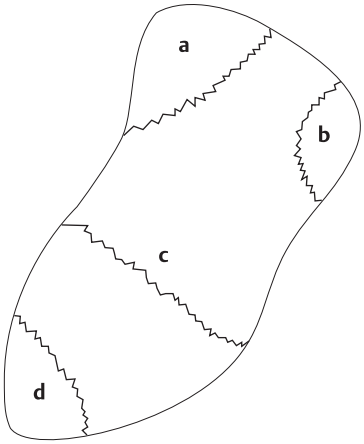

Fig. 4.9 **Scaphoid fractures** may involve distal pole (**a**), tubercle (**b**), waist (**c**) or proximal pole (**d**).

scaphoid waist fracture include nonunion and avascular necrosis of the proximal fracture fragment.

The most frequent ligamentous injuries of the carpal bones are centered around the lunate and include scapholunate dissociation, perilunate dislocation, midcarpal dislocation and lunate dislocation. *Scapholunate dissociation (rotary subluxation of the scaphoid)* (Fig. 4.**10**) is associated with an injury to the scapholunate ligament. The condition is diagnosed on the dorsovolar view of the wrist by either widening of the space between the scaphoid and lunate measuring more than 2 mm in the midline between these to carpal bones or more than 4 mm at their proximal border, respectively, (*Terry Thomas sign*) and/or a volar tilt of scaphoid producing a foreshortened scaphoid with characteristic ring shadow (*signet ring sign*). In *perilunate dislocation* the lunate is volarly rotated, but remains in articulation with the radius and the capitate is dorsally dislocated with regard to the lunate. In *lunate dislocation* the volarly rotated lunate is also completely volarly dislocated with regard to both the radius and capitate which remain aligned (Fig. 4.**11**). *Pericarpal dislocation* can be considered a stage between perilunate and lunate dislocation with anterior subluxation of the volarly tilted lunate with regard to the radius and complete dorsal dislocation in the lunocapitate joint. Perilunate dislocations may be associated with carpal bone fractures. The prefix "trans-" indicates which carpal bone(s) is/are fractured (e.g., trans-scaphoid perilunate dislocation).

Intra-articular fractures of the base of the first metacarpal may be simple (*Bennett fracture*) (Fig. 4.**12**) or comminuted (*Rolando fracture*). In these conditions the first metacarpal is frequently dorsally and radially dislocated or displaced, respectively, caused by the pull of the abductor pollicis longus. A *boxer's fracture* involves the neck of a metacarpal (most commonly the fifth) with characteristic dorsal angulation at the apex. A *gamekeeper's thumb* (*skier's thumb*) (Fig. 4.**13**) results from rupture of the ulnar collateral ligament of the first

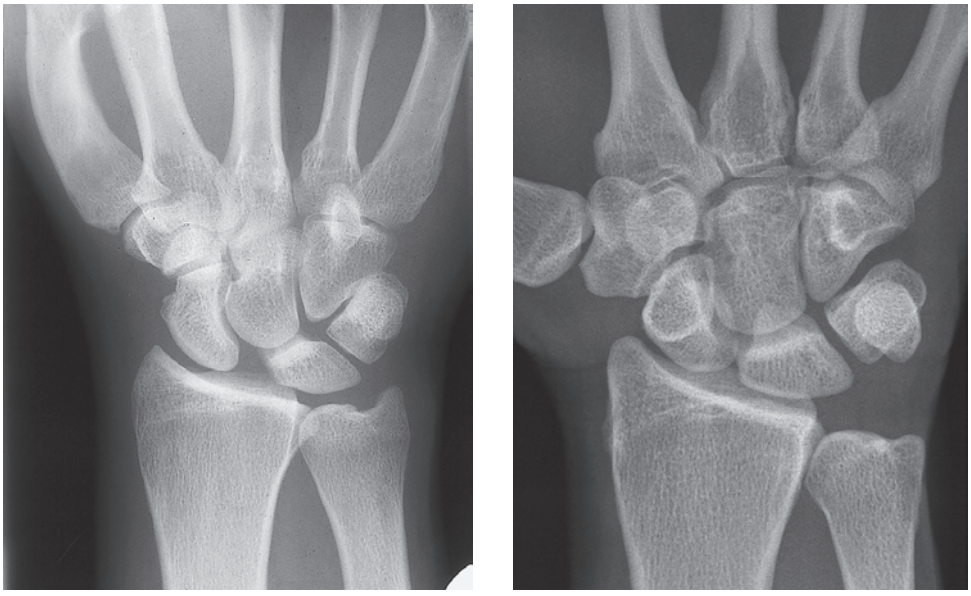

Fig. 4.**10 a, b** **Scapholunate dissociation** and rotary subluxation of the scaphoid. An injury to the scapholunate ligament is diagnosed by either widening of the distance between scaphoid and lunate (Terry Thomas sign) (**a**) or by rotary subluxation of the scaphoid producing the signet ring sign (**b**).

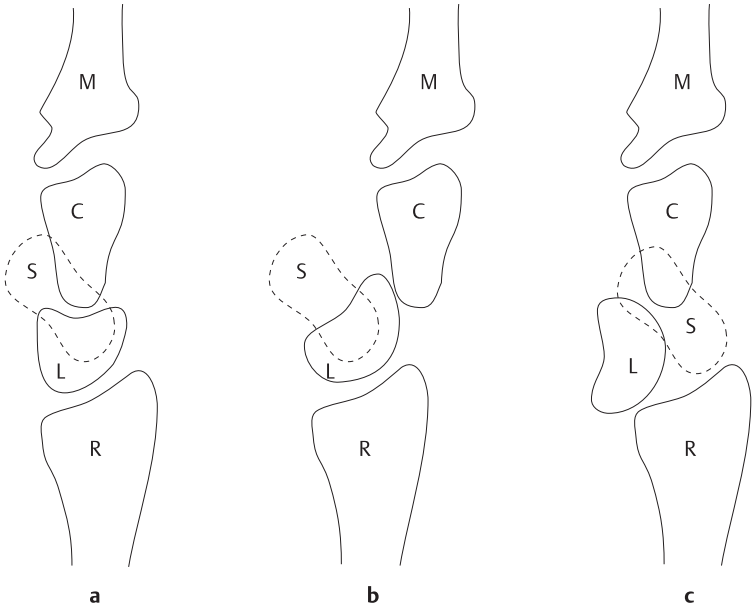

Fig. 4.**11** **Perilunate and lunate dislocation**. **a** Normal lateral wrist, **b** perilunate dislocation, **c** lunate dislocation. C: capitate. L: lunate. M: 3rd metacarpal. R: radius. S: scaphoid.

metacarpophalangeal joint that may be accompanied by the fracture of the base of the proximal phalanx.

In the *pelvis* stable and unstable fractures must be differentiated (Figs. 4.**14** and 4.**15**). In unstable fractures the pelvic ring formed by the sacrum and pelvis is totally disrupted in two or more places. Stable pelvic fractures include avulsion injuries (anterosuperior and anteroinferior iliac spines and ischial tuberosity) and/or complete disruption of the pelvic ring limited to a single location. Pelvic fractures may extend into the acetabulum where involvement of the dome (acetabular roof), anterior (iliopubic) wall or column and posterior (ilioischial) wall or column must be differentiated.

Fractures of the *proximal femur* may be classified as capital, subcapital, midcervical, basicervical, intertrochanteric and subtrochanteric (Fig. 4.**16**). Capital fractures are uncommon and usually associated with posterior hip dislocation. After healing they may be impossible to differentiate from avascular necrosis of the femoral head. Frequent complications of displaced femoral neck fractures are avascular necrosis of the femoral head and nonunion.

Fractures about the *knee* may involve the distal femur or the proximal tibia. Distal femur fractures may be extra-articular (supracondylar) or intra-articular (condylar or intercondylar). Fractures of the proximal tibia may involve, besides the intercondylar eminence, the lateral or, less frequently, the medial tibia plateau or both. The articular surface of the tibia plateau may be split, depressed or both. Cruciate ligament injuries are frequently associated with fractures extending into the intercondylar eminence of the tibia. A *Segond fracture* is an avulsion fracture of the lateral proximal tibia just distal to the joint line at the insertion of the reinforced capsule. This fracture has to be differentiated from an avulsion of *Gerdy's*

Fig. 4.**12** **Bennett fracture**. A simple intra-articular fracture (arrow) of the base of the first metacarpal with radial subluxation of the latter is seen.

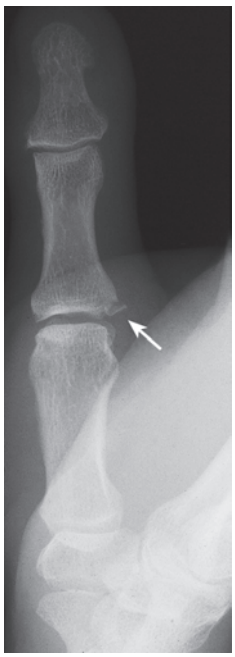

Fig. 4.**13** **Gamekeeper's (skier's) thumb**. A tiny avulsion fracture (arrow) of the ulnar aspect of the proximal phalanx of the thumb is seen.

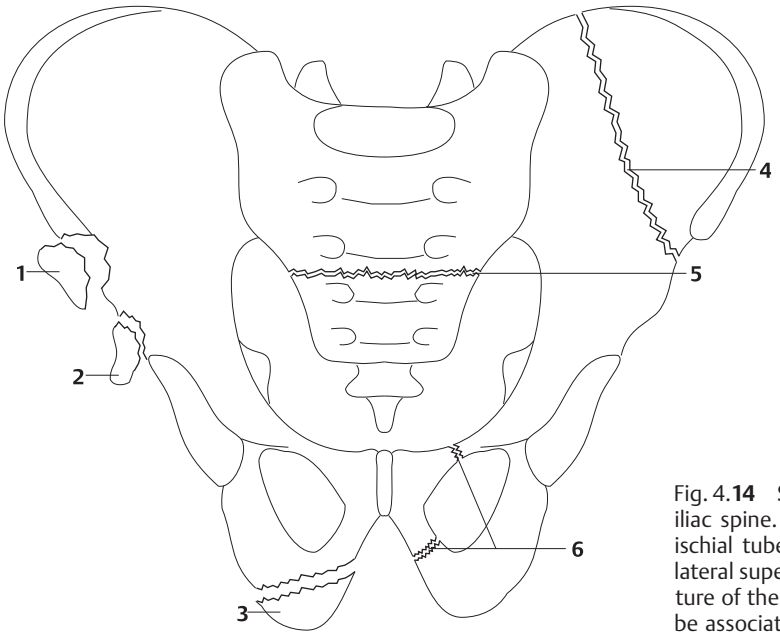

Fig. 4.**14** **Stable pelvic fractures**. **1** Avulsion of anterosuperior iliac spine. **2** Avulsion of anteroinferior iliac spine. **3** Avulsion of ischial tuberosity. **4** Iliac wing fracture. **5** Sacral fracture. **6** Unilateral superior and inferior pubic rami fractures (in addition a fracture of the contralateral superior *or* inferior pubic ramus may also be associated). DD: Straddle fracture in Fig. 4.**15**.

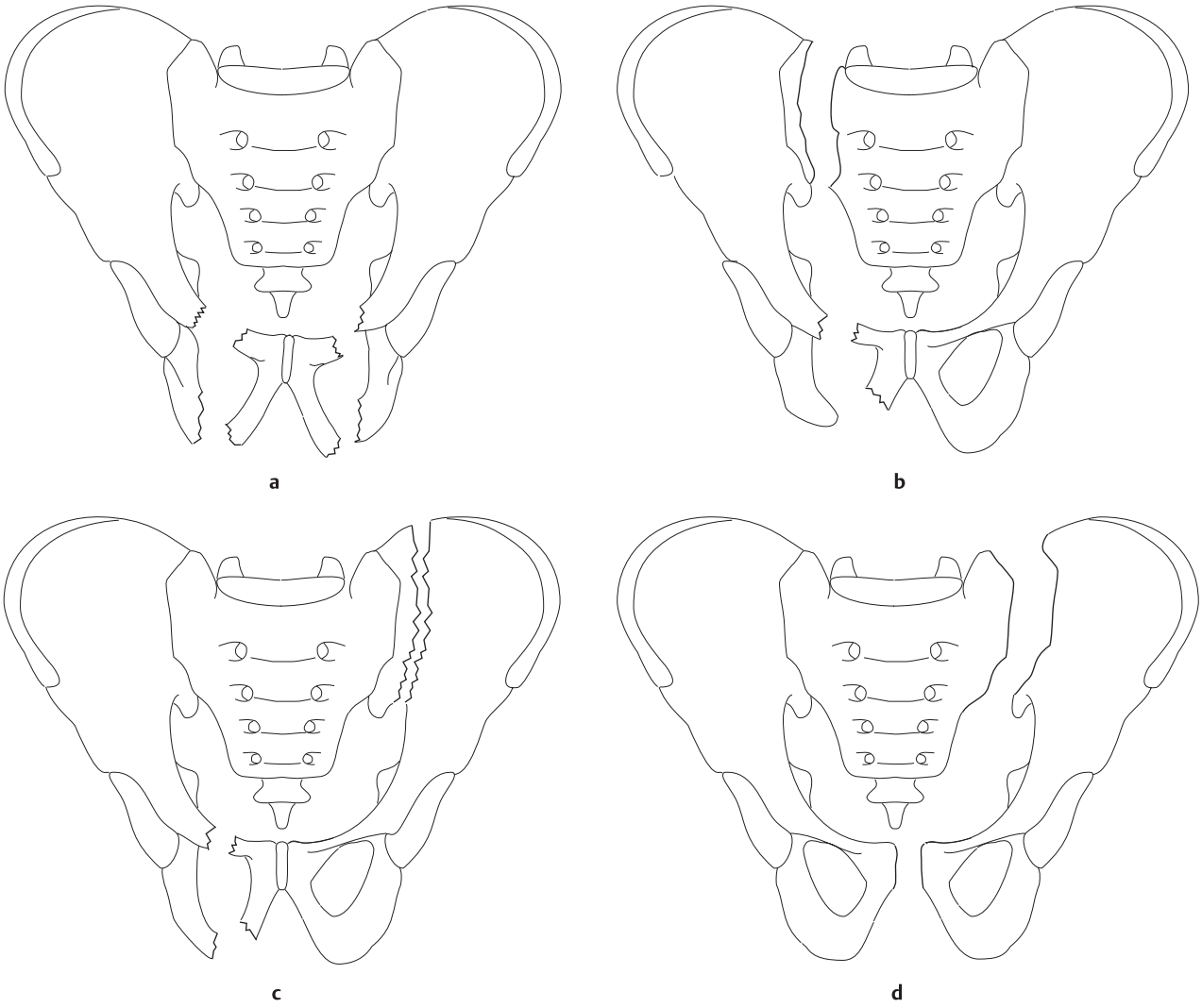

Fig. 4.**15** **Unstable pelvic fractures. a** Straddle fracture (both superior and inferior pubic rami (or ischial rami) are fractured. **b** Malgaigne fracture (instead of the sacral wing fracture the ipsilateral sacroiliac joint may be disrupted or the ilium along the ispilateral sacroiliac joint may be fractured). **c** Bucket handle fracture. **d** Pelvic "dislocation" (pubic diastasis associated with unilateral or bilateral sacroiliac joint disruption).

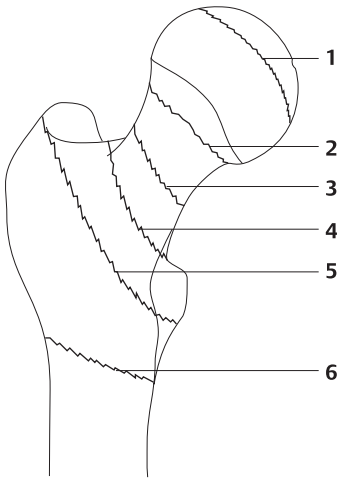

Fig. 4.**16** **Proximal femur fractures**: **1**: capital, **2**: subcapital, **3**: midcervical, **4**: basicervical, **5**: intertrochanteric, **6**: subtrochanteric. Fractures **1**–**4** are intracapsular, **5** and **6** extracapsular. Fractures **2**, **3**, and **4** are femur neck fractures.

tubercle (insertion of the iliotibial tract) that is located anterior to the Segond fracture and usually only visualized on an external oblique but not on a frontal radiograph.

Fractures of the *ankle* can be classified as unimalleolar, bimalleolar, trimalleolar or complex (comminuted fracture of the distal tibia and fibula). A fracture of the distal tibia caused by axial load is called *pilon fracture* when the fracture line extends into the articular surface of the distal tibia, the tibia plafond. Injuries of the ankle are commonly caused by inversion (supination, adduction) or eversion (pronation, abduction) of the foot and may be associated with external (lateral) rotation of the foot. These injuries may be ligamentous, osseous, or both. Depending on their radiographic presentation (Fig. 4.**17**) both mechanism and severity of the injury can be assessed. Osteochondral fractures of the lateral or less commonly the medial talar dome may be associated resulting from impingement of the talus on the fibula or tibia, respectively.

Fibular shaft fractures may be associated with ankle injuries. A *Dupuytren fracture* consists of a distal fibular fracture 2 to 7 cm above the ankle joint line associated with disruption of the distal tibiofibular syndesmosis and the medial collateral (deltoid) ligament. The same injury without disruption of the distal tibiofibular syndesmosis is termed *Pott fracture*. A *Maisonneuve fracture* (Fig. 4.**18**) is an eversion-lateral rotation type injury similar to the DuPuytren fracture and consists of a proximal fibula fracture, disruption of the tibiofibular syndesmosis and a medial malleolar fracture or torn medial collateral (deltoid) ligament.

Fractures of the talus tend to be vertical, typically involving the neck of the talus, or comminuted and occur most often from forced dorsiflexion of the foot. Osteochondral fractures

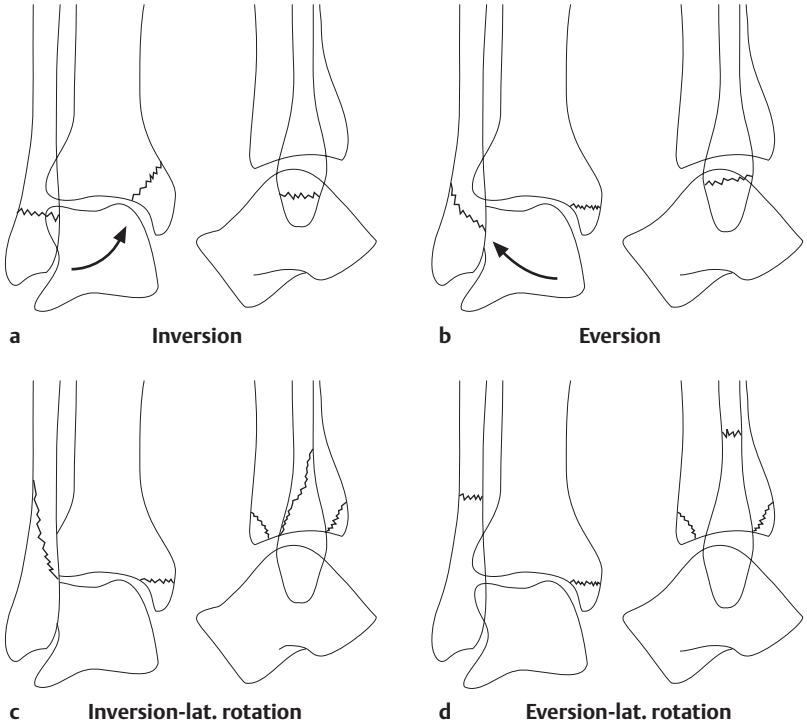

Fig. 4.**17** **Ankle fractures**. **a** Inversion injury (20 %). Horizontal (avulsion) fracture of the lateral malleolus and oblique (talar impaction) fracture of the medial malleolus, both originating at or below the joint line. **b** Eversion injury (10 %). Horizontal (avulsion) fracture of the medial malleolus and oblique (talar impaction) fracture of the lateral malleolus, both originating at or below the joint line. **c** Inversion-lateral rotation injury (60 %). Oblique (spiral) fracture of the distal fibula originating anteromedial at or up to 1.5 cm above the joint line and extending in dorsal and proximal direction. Fractures of the medial and posterior malleolus and anterior tibial tubercle may be associated. **D** Eversion-lateral rotation injury. Fracture of the medial malleolus associated with a horizontal supramalleolar (2 cm or higher above the joint line) fracture of the distal fibula. Fractures of the posterior malleolus and anterior tibial tubercle may be associated. Note that instead of a malleolar fracture the corresponding ligament may be torn. Widening of the mortise (injury to the tibiofibular syndesmosis consisting of the anterior and posterior tibiofibular ligaments, inferior transverse ligament [immediately distal the latter] and interosseous membrane) can be diagnosed when the distal tibia and fibula no longer overlap on the mortise view. Avulsion fractures of the anterior tibial tubercle and posterior malleolus indicate injuries of the anterior and posterior tibiofibular ligaments respectively, and are only found with rotational injuries (modified Lange-Hansen classification).

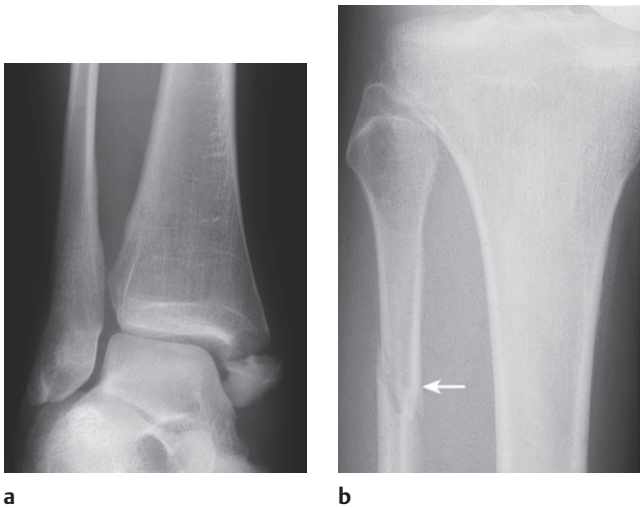

Fig. 4.**18 a, b** **Maisonneuve fracture**. A fracture of the medial malleolus with slightly widened mortise evident by the loss of the normal tibiofibular overlap is seen in (**a)**. Fracture of the proximal fibula (arrow) is associated indicating disruption fo the tibiofibular syndesmosis (**b**).

of the medial or lateral talar dome may be associated with inversion or eversion injuries of the ankle. Talar dislocations may be peritalar involving the talocalcaneal and talonavicular joints or total involving besides the aforementioned joints also the tibiotalar joint ("floating talus").

Seventy-five percent of *calcaneal fractures* extend into the subtalar (talocalcaneal) joint. Depression of the subtalar joint is diagnosed by the Böhler's angle (angle between lines drawn on lateral radiograph from the highest point of the subtalar joint to the anterior process of the calcaneus and posterosuperior aspect of the calcaneus respectively) measuring less than 28 degrees.

Chopart fracture-dislocation involves both the talonavicular and calcaneocuboidal joints and abutting bones. *Lisfranc fracture-dislocation* (Fig. 4.**19**) involves the tarsometatarsal joints. In the homolateral form all metatarsals are dislocated laterally, whereas in the divergent form the first metatarsal is dislocated dorso-medially and remaining metatarsal laterally. Associated fractures most often occur at the base of the second metatarsal, followed by the base of the third metatarsal and the first and second cuneiforms. A first ray separation is diagnosed when the joint space between the medial and intermediate cuneiform is widened.

An *intra-articular avulsion fracture of the base of the fifth metatarsal* has to be differentiated from a *Jones fracture* referring to an extra-articular transverse fracture of the proximal fifth metatarsal shaft. Jones fractures have a high incidence of non-union.

Cervical spine injuries are caused by hyperflexion (e.g. anterior wedge fracture, anterior subluxation, and bilateral locked facets with anterior subluxation of the superior vertebra), hyperextension (e.g. avulsion of anteroinferior corner of a vertebral body, typically at C2), hyperrotation (e.g. rotary atlanto-axial dislocation), hyperflexion and rotation (e.g. unilateral locked facet), lateral hyperflexion (e.g. unilateral uncinate process or pillar fracture) and vertical compression (e.g. burst fracture). A *Jefferson fracture* is a burst fracture of C1 presenting classically with bilateral disruption of both anterior and posterior arches and with lateral displacement of both lateral masses.

Dens (odontoid) fractures (Fig. 4.**20**) are classified based on their location: Type I fractures occur cephalad to the base of the dens, and are usually obliquely oriented. They are stable and must be differentiated from an ossiculum terminale (ossicle of Bergmann) at the tip of the dens. Type II fractures are unstable transverse fractures at the base of the dens and must be differentiated from an os odontoideum. Type III fractures extend from the base of the dens into the body of C2 and are usually stable injuries. They can be differentiated from type II fractures on the lateral radiograph by disruption of the normal "ring shadow" of the axis caused by the pedicles.

A *hangman's fracture* (Fig. 4.**21**) is a hyperextension injury of the axis presenting with bilateral pedicle fractures and varying degrees of anterior subluxation or frank dislocation of the body of C2. This fracture can be considered as trau-

Fig. 4.**19** **Lisfranc fracture-dislocation (homolateral form).** Lateral dislocation of all metatarsals is seen. Fractures of the bases of the second and third metatarsals are associated.

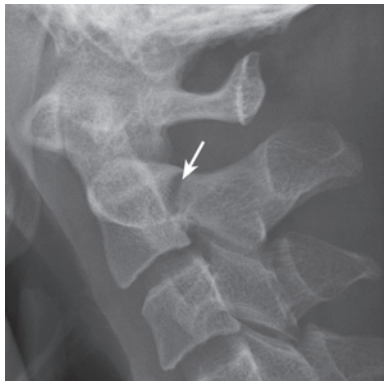

Fig. 4.**21** **Hangman's fracture.** Fracture of the pedicles of C2 (arrow) with only minimal anterior subluxation of the body of C2 is seen.

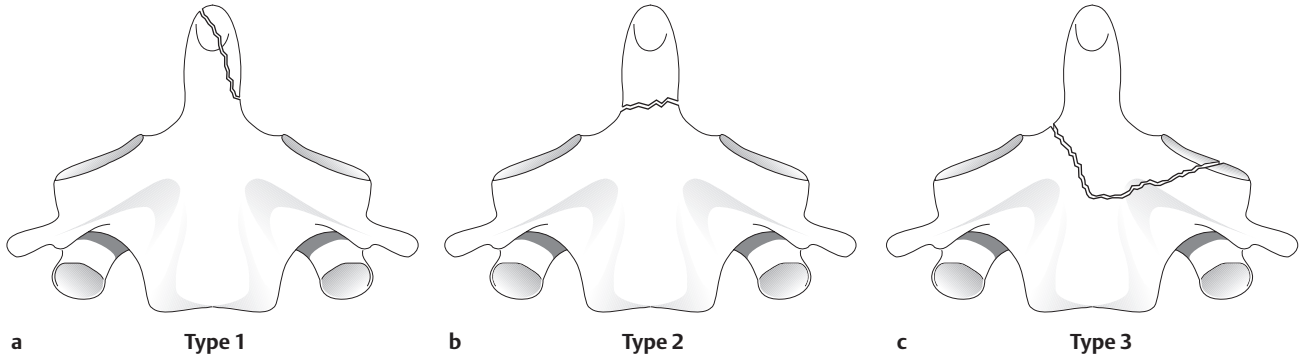

Fig. 4.**20** **Dens fractures.** **a** Type 1: Fracture (usually oblique) cephalad to the base of the dens. **b** Type 2: Transverse fracture at the base of the dens. **c** Type 3: Fracture extending from the base of the dens into the body of C2.

matic spondylolisthesis of C2 and is nowadays most commonly found in automobile accidents when the face strikes the windshield. A *clay-shoveler's fracture* (Fig. 4.**22**) is an oblique or vertical avulsion fracture of the spinous process of C6 or C7 (occasionally T1 to T3) caused by a sudden load on the flexed spine.

Teardrop fractures (Fig. 4.**23**) in the cervical spine may be associated with both hyperextension and hyperflexion injuries. In the extension teardrop fracture the avulsion arises from the anteroinferior corner of a vertebral body usually at the level of C2 or C3. This injury is in contrast to the flexion teardrop fracture stable and the triangular fracture fragment produced by hyperextension is small and does not exceed in size one quarter of the sagittal diameter of the vertebral body. However it has to be emphasized that many hyperextension injuries in the lower cervical region with few or no radiographic abnormalities may be unstable or result in severe neurologic damage. The flexion teardrop fracture is a highly unstable injury typically involving the lower cervical spine with C5 being most often affected. The vertebral body is divided into a smaller anteroinferior teardrop fragment and a larger posterior fragment. The teardrop fragment is frequently large but at most is only minimally anteriorly and inferiorly displaced whereas the remaining vertebral body is posteriorly displaced into the spinal canal.

Acute *thoracolumbar spine fractures* are best classified by mechanism of injury and location. For the latter the concept of the three-column spine is most useful. The anterior column comprises the anterior two-thirds of the vertebral body, the middle column the posterior third of the vertebral body and pedicles, and the posterior column the facet joints, lamina and spinous process. A column is also considered affected when the corresponding spinous ligaments are injured. Anterior and posterior one-column fractures are stable, whereas two- and three-column fractures and all fractures involving the middle column must be considered unstable.

Four types of major injuries can be discerned in the thoracolumbar spine (Fig. 4.**24**): 1. *Compression fractures* are flexion injuries resulting in compression of the anterior column. They present with anterior or less commonly lateral cortical buckling or wedging of a vertebral body. In severe compression fractures posterior ligamentous distraction injuries may be associated. 2. *Burst fractures* are the result of axial loading resulting in compression of both the anterior and middle columns with centropetal disruption. Characteristic radiographic findings include increased sagittal diameter of the vertebral body, increased interpediculate distance, retropulsion of the posterosuperior portion of the vertebral body and moderate to marked anterior wedging. 3. *Seat-belt injuries (Chance fractures)* are caused by hyperflexion of the spine resulting in distraction injuries of both the middle and posterior columns associated at times with anterior compression of the vertebral body. The radiographic findings depend on whether the injury is predominantly osseous or ligamentous. A horizontal splitting of the vertebra beginning in the spinous process or lamina and extending through the pedicles into the vertebral body without anteroposterior subluxation is characteristic. Ligamentous injuries can be diagnosed by widening of the interspinous distance, increased height of the intervertebral foramina, and perching or locking of the facet joints. 4. *Fracture-dislocation injuries* refer to the complete disruption of all three spinal columns. The hallmark of these severe, usually mixed osseous-ligamentous injuries is the presence of intervertebral subluxation or dislocation, while the loss of height of the involved vertebral bodies characteristically is commonly relatively small.

Traumatic fractures of the spine have to be differentiated from subacute or chronic compression fractures associated with osteopenia. These fractures are frequently located in the mid thoracic spine, whereas traumatic fractures are preferentially located in the thoracolumbar region. A narrow zone of increased density below the fractured endplate, produced by impacted trabeculae and/or attempted fracture healing, is commonly present in compression fractures associated with osteoporosis.

Fractures in children may present with special features. *Greenstick fractures* (Fig. 4.**25**) are incomplete fractures of the relatively soft growing bone perforating only one cortex and ramifying within the medullary cavity. *Bowing fractures* (Fig. 4.**26**) present as antero-posterior or lateral bending of the radius, ulnar or fibula without evidence of a bony break. Comparison radiographs of the opposite side are often required for correct diagnosis. *Torus (buckling) fractures* (Fig. 4.**27**) produce a buckling of the metaphyseal cortex in children and osteopenic adults.

Trauma to the bone in children and adolescents often involves the cartilage (growth) plate, as long as the epiphyses are not closed. These injuries can be classified into different types using the Salter-Harris method (Fig. 4.**28**). A Salter-Harris type III fracture in the lateral distal tibia epiphysis is referred to as *juvenile Tillaux fracture* (Fig. 4.**29**). A *triplane*

Fig. 4.**22** **Clay-shoveler's fracture**. Oblique fracture of the spinous process (arrow) of C7 is seen.

Fig. 4.**23** **Flexion teardrop fracture**. A fracture at C5 is seen consisting of the smaller anteroinferior teardrop fragment (arrow) and a larger posterior fragment that is posteriorly displaced into the spinal canal.

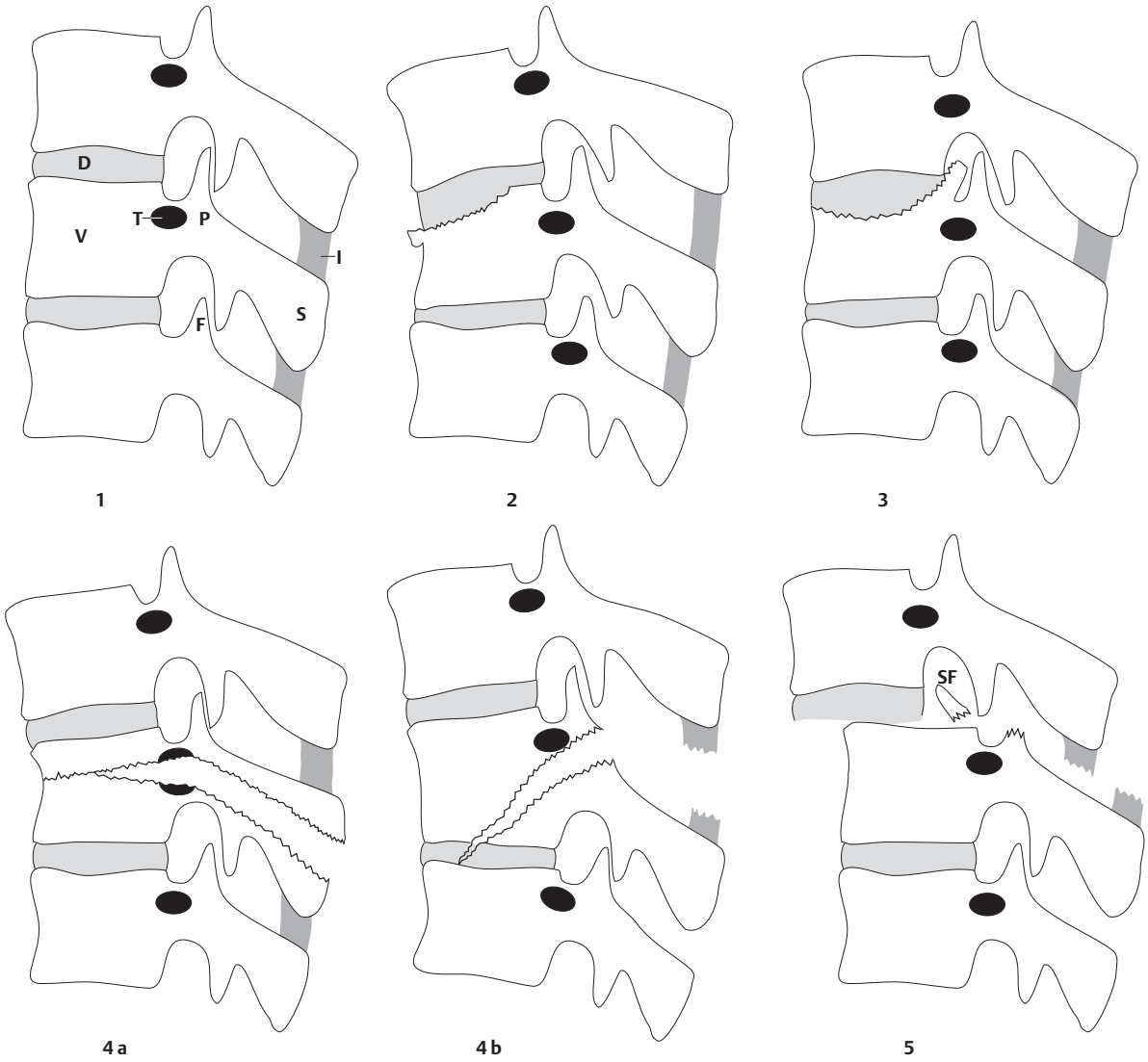

Fig. 4.**24** **Thoracolumbar spine fractures**. **1** Normal. **2** Compression fracture. **3** Burst fracture. **4** Chance fracture (4**a**: one-level, 4**b**: two-level). **5** Fracture-dislocation. D: Intervertebral disc. I: Interspinous ligament. F: Facet (apophyseal) joint. P: Pedicle. S: Spinous process. T: Transverse process. V: Vertebral body. SF in 5: Superior facet of the middle vertebra. Note that a torn interspinous ligament may also imply tears in the anterior and posterior longitudinal ligaments and ligamentum flavum.

Fig. 4.**25** **Greenstick fracture.** An incomplete ulnar fracture with bowing of its shaft and intact cortex on its radial side is seen in addition to the transverse overriding radius fracture.

Fig. 4.**26** **Bowing fracture.** A fracture of the radius shaft is associated with a marked bending deformity (bowing fracture) of the ulna without evidence of a cortical break.

fracture of the distal tibia in adolescents represents a variation of a Harris-Salter type IV injury (Fig. 4.**30**). Two, three or four fragments (parts) may result with two fragments being most common.

A *traumatic epiphysiolysis of the femur head* is particularly common in boys between 10 and 15 years of age, although a history of acute trauma is often not available. In these cases of *slipped capital femoral epiphyses (SCFE)*, repeated low-grade trauma is believed to be the triggering mechanism. The displacement of the femoral head in relation to the metaphysis is almost always in a posterior, inferior and medial direction (Fig. 4.**31**).

Multiple fractures and dislocations in an infant should raise the suspicion of an "*abused child syndrome*." More subtle find-

Fig. 4.**27** **Torus (buckling) fracture**. Buckling of the metaphyseal cortex of the distal radius (arrow) is seen.

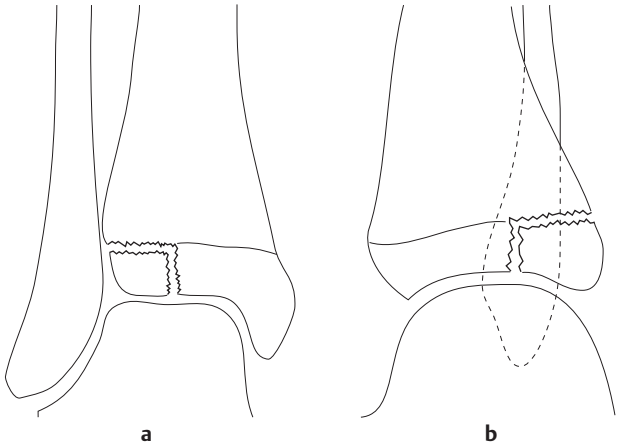

Fig. 4.**29** **Juvenile Tillaux fracture** is a Harris-Salter type III fracture involving the posteriolateral (shown here) or anterolateral aspect of the distal tibia epiphysis (**a**: anteroposterior, **b**: lateral).

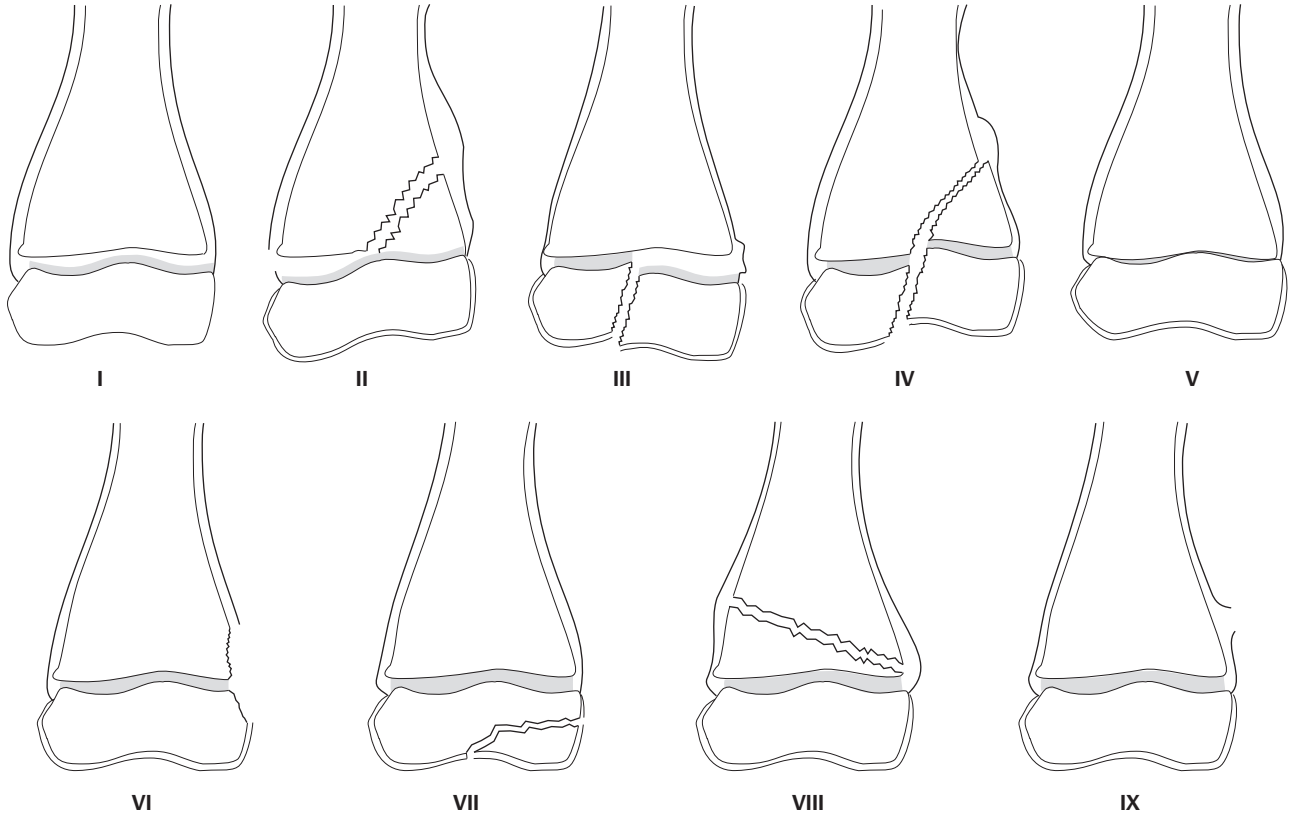

Fig. 4.**28** **Salter-Harris classification** of growth plate injuries (types I-V) with **Rang and Ogden's** additions (types VI-IX). Type **I**: Injury limited to the cartilage plate, which shows complete transverse laceration. The bone itself is intact. Prognosis is good. Type **II**: Incomplete transverse laceration of the cartilage plate associated with oblique fracture of the metaphysis. Triangular fracture fragment remains attached to the epiphysis. Prognosis is good. Type **III**: Incomplete transverse laceration of the cartilage plate associated with longitudinal fracture through the epiphysis. Prognosis is bad if the fracture is not reduced with smooth joint surface. Type **IV**: Oblique longitudinal fracture through epiphysis, cartilage plate, and metaphysis. Prognosis is bad if the fracture is not perfectly reduced. Type **V**: Crushing of the cartilage plate with intact bone. Premature closure of the plate and stoppage of growth is relatively common. Type **VI**: Trauma to the perichondrium with tethering of growth plate. Type **VII**: Fracture of the epiphysis. Type **VIII**: Fracture of the metaphysis. Type **IX**: Avulsion injury of the periosteum.

ings in this condition include injuries to the cartilage plate, metaphyseal fragmentation and avulsions, the latter producing a characteristic "bucket-handle" deformity, posttraumatic metaphyseal cupping and cortical thickening (Fig. 4.**32**).

The evaluation of *dislocations* requires radiologic examinations in at least two projections (Fig. 4.**33**). With a single projection, a dislocation as well as a potentially associated avulsion or compression fracture is easily missed. Traumatic, habitual, pathologic (secondary to joint disease), paralytic, and congenital dislocations are differentiated. There is no longer any contact between the two joint surfaces in a complete dislocation (luxation), whereas in subluxations (incomplete dislocations), a partial contact between the joint surfaces is still maintained.

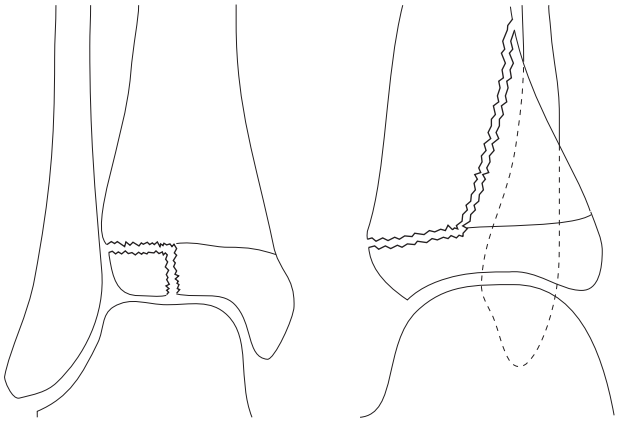

Fig. 4.**30** **Triplanar (triplane) fracture** (two-part) of the distal tibia in children consists of a vertical fracture of the epiphysis in the sagittal plane, a horizontal fracture in the axial plane through the lateral and anterior aspect of the growth plate and an oblique fracture of the metaphysis in the coronal plane extending from the growth plate to the posterior cortex of the tibia (**a**: anteroposterior, **b**: lateral).

Fig. 4.**31** **Traumatic epiphysiolysis (slipped capital femoral epiphysis).** The right femoral head is displaced medially, downward and backward. Note also the widening of the physis, the irregularities of the metaphysis, and the blurring of the junction between the metaphysis and the epiphyseal cartilage plate, all of which are early signs of an imminent slip. These findings are best appreciated when compared with the normal left hip.

a

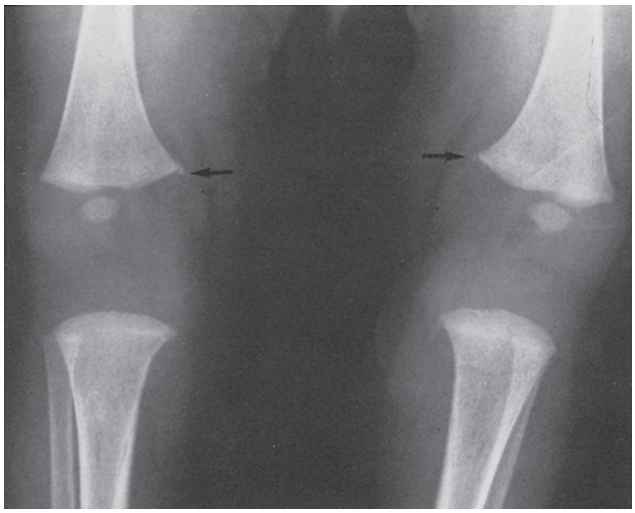

b

Fig. 4.**32 a, b** **Abused child syndrome. a** Healing fractures are seen in the humerus, radius, and ulna. **b** More recent avulsions of the metaphyseal corners (arrows) produce the characteristic "bucket-handle" deformity in infants.

Osteochondritis dissecans appears to be caused in a great majority, if not all cases, by stress, usually of chronic nature. The medial femur condyle is the most common site of involvement, but the disease has also been observed in the lateral femur condyle, the distal tibia, the talar dome, the capitulum of humerus (Fig. 4.**34**), the patella, and the heads of the femur, humerus, and metatarsals, especially the first. The bony fragment may still be located in the corresponding defect of the articular surface or may have become completely separated from the latter and form a loose intra-articular body. The differential diagnosis of loose intra-articular bodies is shown in Table 4.**1**.

Table 4.1 Differential Diagnosis of Loose Intra-Articular Bodies

Disease	Preferred Location	Number of Loose Bodies	Other Radiographic Findings	Comments
Osteochondritis dissecans	Knee	One	Defect (pit) in articular surface at the site of origin.	Preponderant in young males.
Osteochondromatosis (synovial) (Fig. 4.35)	Large joints, bursae	Multiple (often more than 10), relatively uniform in size, one-third not calcified	Joint effusion common.	Preponderant in young to middle-aged males. Hypertrophic cartilaginous synovial growths that may become detached, calcified and eventually ossified.
Trauma (chondral and osteochondral fractures)	None	One or more, not always calcified	Evidence of old trauma.	Secondary to avulsion of bone and/or cartilage (articular surface, meniscus).
Septic or tuberculous arthritis	None	One or more	Evidence of joint destruction and deformity.	Rare. Characteristic clinical history.
Degenerative joint disease	Weight-bearing joints	One or more detached spurs	Osteophytosis, sclerosis, subchondral cysts, and joint space narrowing.	Usually in elderly patients. *Synovial chondrometaplasia* may also occur simulating osteochondromatosis.
CPPD arthropathy (Fig. 4.36)	Large joints of upper and lower extremities	One or more	Similar to degenerative joint disease, but more destructive and progressive. Chondrocalcinosis and subchondral cyst formation are common and often prominent.	Elderly patients.
Avascular necrosis	Hip, knee, shoulder	One or more	Advanced stage with flattened or collapsed articular surface	Bone infarcts may also be present. May simulate osteochondritis dissecans in the knee, but is often bicondylar or bilateral.
Neuropathic arthropathy (hypertrophic form) (Fig. 4.37)	Weight-bearing joints	Multiple, varying size	Marked sclerosis, disintegration of articular surfaces and subluxation.	Loss of pain sensation (diabetes, syphilis [Charcot joint] and other neurologic disorders).

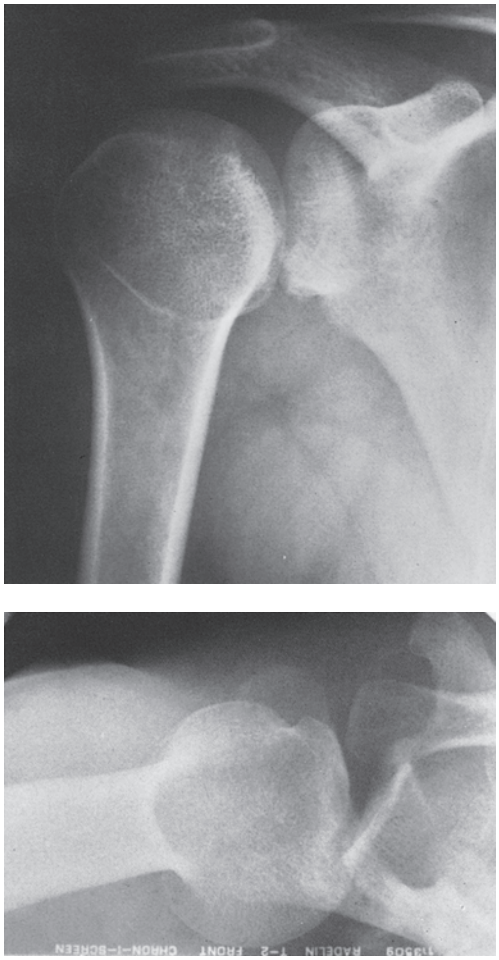

a

b

Fig. 4.**33 a, b** **Posterior dislocation of the shoulder with impaction fracture of the humeral head. a** In the oblique anteroposterior projection, the posterior dislocation is difficult to appreciate (normally there is a slight overlap between humeral head and glenoid fossa in this projection). **b** The axillary projection identifies clearly the posterior dislocation. Furthermore, an impaction fracture on the humeral head caused by the impingement of posterior ridge of the glenoid fossa is now evident.

Fig. 4.**34** **Osteochondritis dissecans.** A small bony fragment (arrow) is located in a subchondral defect of the capitulum of the humerus.

a b

Fig. 4.**35 a, b** **Osteochondromatosis** (2 patients). **a** Elbow, **b** knee. Multiple loose bodies are seen in both joints.

Stress fractures can be subdivided into fatigue fractures and insufficiency fractures. *Fatigue fractures* occur in normal bones with the application of an abnormal stress or torque caused by a new strenuous or repeated activity. *Insufficiency fractures* occur when normal stress is placed on an abnormal (osteopenic) bone. Stress fractures are usually symptomatic. They begin as small cortical cracks, and may progress to subcortical infraction and eventually a fracture running transversely across the bone (Fig. 4.**38**). If the fracture line cannot be demonstrated radiographically, magnetic resonance imaging (MRI) or a radionuclide examination are always positive and may provide an early diagnosis. MRI, however, has comparable sensitivity and superior specificity to bone scintigraphy in the assessment of stress fractures. Osteomyelitis and bone tumors such as osteosarcoma and osteoid osteoma can be differentiated from a stress fracture on the basis of both characteristic location and the typical history of stress fractures (Table 4.**2** and Fig. 4.**39**). At a later stage, periosteal reactions with subsequent localized callus formation and cortical thickening obscuring the fracture line, are found in the diaphyses of tubular bones (Fig. 4.**40**). In an epiphyseal and metaphyseal location (e.g., tibia plateau) and cancellous

Fig. 4.**36** **CPPD arthropathy.** Advanced arthritic changes with numerous calcific and osseous bodies in the joint space and suprapatellar bursa (arrow) are seen.

Fig. 4.**37** **Neuropathic arthropathy.** Fragmentation of the joint surfaces with several irregular loose bodies, sclerosis and subluxations are seen in the metatarsophalangeal joints.

a

b

Fig. 4.**38 a, b** **Stress fractures** (2 patients). (**a**) A transverse linear radiolucency (arrow) is associated with mild localized cortical thickening in the femur shaft. (**b**) The stress fracture presenting initially as poorly defined sclerotic band (arrow) in the medial aspect of the femoral neck progressed to a complete subcapital fracture.

Table 4.2 Stress Fractures (Fig. 4.39)

Location	Activity
1. Lower cervical or upper thoracic spinous process	Shoveling
2. Clavicle	Postoperative (radical neck dissection)
3. Coracoid process of scapula	Trap shooting
4. Ribs	Carrying heavy pack (first rib), golf, coughing
5. Humerus: distal shaft	Throwing a ball
6. Ulna: coronoid process shaft	Pitching a ball, throwing a javelin, pitchfork work, propelling wheelchair
7. Hook of hamate	Holding golf club, tennis racket, baseball bat
8. Lumbar vertebra: pars interarticularis (spondylolysis)	Ballet, lifting heavy objects, scrubbing floors
9. Femur: neck shaft	Ballet, running Ballet, marching, running, gymnastics
10. Pelvis: obturator ring	Stooping, bowling, gymnastics
11. Patella	Hurdling
12. Tibia	Running (proximal shaft in children, mid- and distal shaft in adults)
13. Fibula: proximal or distal shaft	Jumping, parachuting running
14. Calcaneus	Jumping, parachuting, prolonged standing, recent immobilization
15. Navicular	Stamping on ground, marching, running
16. Metatarsals	Marching, stamping on ground, prolonged standing, ballet, postoperative bunionectomy
17. Sesamoids of great toe	Prolonged standing

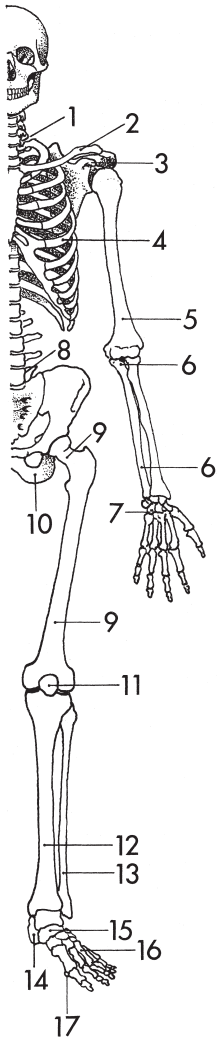

Fig. 4.**39** **Locations of stress fractures.** The numbers in the Fig. correspond to the numbers in Table 4.**2**.

a **b**

Fig. 4.**40 a, b** **Stress fractures**. (**a**) A healing stress fracture with extensive periosteal callus formation is seen in the second metatarsal. No other stress fracture was diagnosed at this time. Sequelae of arthroplasty including resection of the base of the proximal phalanx of the great toe are incidentally also evident. (**b**) Three months later the stress fracture in the second metatarsal has progressed in healing. A second healing stress fracture is now seen in the third metatarsal shaft and a new stress fracture with only minimal sclerosis in the neck of the fourth metatarsal (arrow).

bone, a band-like focal sclerosis usually without appreciable periosteal reaction is more characteristic (Fig. 4.**41**).

Osteoporosis and rheumatoid arthritis are the two most common conditions in which insufficiency fractures are encountered. *Reinforcement lines* (*bone bars)* presenting as well-defined, usually thin sclerotic lines extending partially or completely across the marrow cavity in patients with osteopenia have to be differentiated from poorly defined, band-like insufficiency fractures (Fig. 4.**42**). Reinforcement lines can be considered as unmasking of growth arrest lines occurring in childhood, although their pathogenesis is unclear. They are incidental findings without clinical relevance.

Pathologic fractures occur at sites of pre-existing abnormalities and are often caused by a minor trauma that would not fracture healthy bone (Figs. 4.**43** and 4.**44**). The radiographic differential diagnosis between pathologic and nonpathologic fracture can at times be difficult, particularly when the injury occurred days to weeks prior to the first radiologic examination. In these cases, bone resorption occurring at the site of a nonpathologic fracture may simulate an underlying pathologic lesion. On the other hand, a smaller underlying lytic or sclerotic bone lesion can be missed radiographically, particularly in the presence of displacement at the fracture site. In these cases, the demonstration of other lytic or sclerotic lesions as well as the absence of a history of trauma or the lack of fracture pain should suggest the possibility of a pathologic fracture. Pathologic fractures can also occur as early as five months after radiation therapy: that is, at a time when the bone does not reveal any radiation-induced changes.

Avulsion fractures (Fig. 4.**45**) at the site of ligament and tendon attachments can be differentiated from accessory ossicles by the lack of a clearly defined cortical margin characteristic of the latter condition (Figs. 4.**46** and 4.**47**). The diagnosis can be further supported by the demonstration of a cortical defect or irregularity in the adjacent bone. Avulsion injuries are caused by either a single violent traumatic event or repetitive injuries. They are particularly common in child-

Fig. 4.**41** **Stress fracture.** An irregular sclerotic band is seen paralleling the posterior border of the calcaneus (arrows).

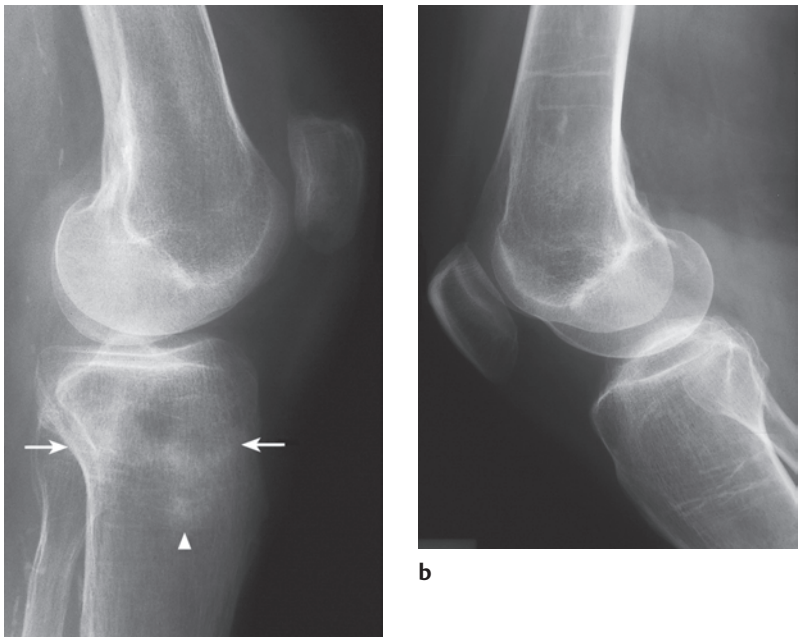

a b

Fig. 4.**42 a, b** **Insufficiency fractures versus einforcement lines (bone bars)**. (**a**) Osteopenia and a poorly defined sclerotic band (arrows) associated with a small sclerotic focus (arrowhead) are characteristic manifestations of insufficiency fractures. (**b**) Thin, well-defined sclerotic lines extending partially or completely across the distal femur and proximal tibia in osteopenia are virtually diagnostic for reinforcement lines (bone bars). In contrast to insufficiency fractures they have no clinical implications.

ren, since the physeal cartilage of an apophysis is considerably weaker than tendinous or ligamentous tissue. Several avulsion injuries about the pelvis and hips occur in young athletes including the anterior superior or inferior iliac spine, iliac crest, ischial tuberosity, pubic symphysis (adductor muscle insertion sites), and greater or lesser trochanter.

Calcifications and ossifications developing in a ligament after acute or repeated low-grade trauma can be impossible to differentiate from an ossicle, since both may be well corticated. A characteristic location (e. g., *Pellegrini-Stieda lesion* [Fig. 4.**48**] in the medial collateral ligament of knee) or the patient's history (e. g., *"rider's bone"* in the adductor muscles of the thigh) may, however, suggest the correct diagnosis.

Heterotopic bone formation in soft tissues following trauma is often termed myositis ossificans, since it occurs most commonly in muscle but is also found in tendons, ligaments, periosteum, and other connective tissues. It frequently develops after insertion of a joint prosthesis, particularly in the hip, and in paraplegic patients. Occasionally, myositis ossificans can mimic a parosteal sarcoma (Fig. 4.**49**). It can be distinguished from the latter by the fact that the periphery is both more dense and smoothly outlined ("eggshell calcification") and by the demonstration of a fine radiolucent line separating the lesion in its entire length from the adjacent bone (Fig. 4.**50**). A central amorphous calcification associated with a soft tissue mass is not found in myositis ossificans and suggests rather a synovial or extraosseous osteogenic sarcoma, where it is present in 30% and 50% of the cases, respectively.

Excessive callus formation following a fracture may occasionally have a tumor-like appearance. It is found in fractures that have not been properly immobilized. These fractures may not have been diagnosed because of a decreased sensitivity to pain secondary to a neurologic disorder. Since fractures are not immobilized in the battered child syndrome, excessive callus formation is common in that condition too. It is also associated with elevated steroid blood concentrations (e. g., Cushing's syndrome and steroid therapy).

Fig. 4.**45** **Avulsion fracture**. A fracture of the posterosuperior aspect of the calcaneus at the Achilles tendon insertion with superior displacement of the avulsed fracture fragment is seen.

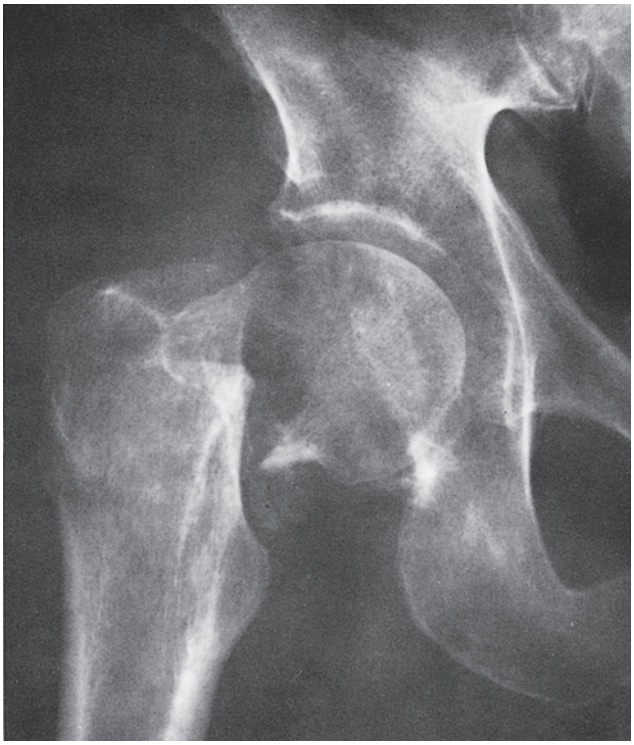

Fig. 4.**43** **Pathologic fracture.** A hip fracture through a large osteolytic metastasis from a renal cell carcinoma involving the femur neck is seen.

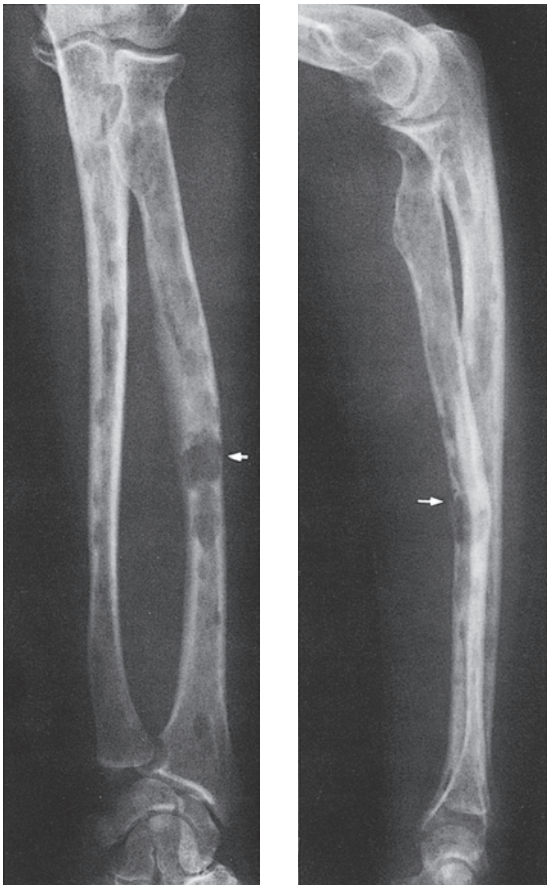

a **b**

Fig. 4.**44 a, b** **Pathologic fracture. a** The cortical break (arrow) is barely visible in the radius shaft of this patient with multiple myeloma in the anteroposterior projection. **b** In the lateral projection, the pathologic fracture (arrow) can be better appreciated because of some angulation of the radius at the fracture site.

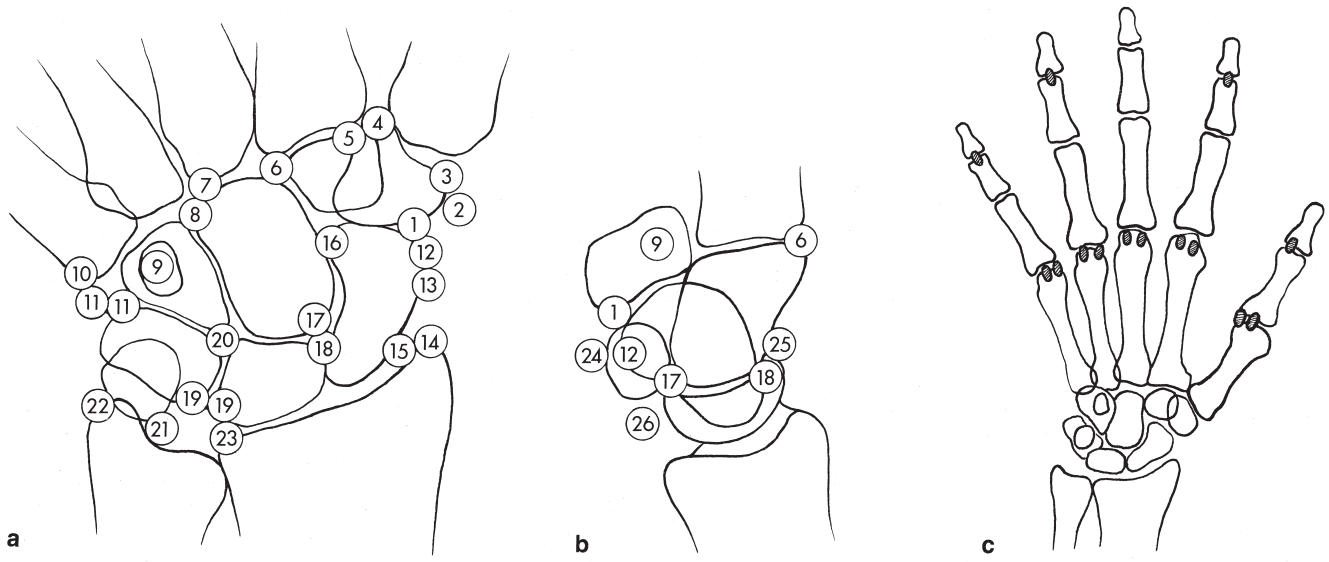

Fig. 4.**46** **Characteristic locations of accessory bones (numbered) and sesamoids (shaded) in the wrist and hand. a** Anteroposterior projection of the wrist. **b** Lateral projection of the wrist. **c** Anteroposterior projection of the hand:

1. epitrapezium
2. calcification (bursa, flexor carpi radialis)
3. paratrapezium
4. trapezium secundarium
5. trapezoides secundarium
6. os styloideum (carpal bone or carpe bossu)
7. ossiculum Gruberi
8. capitatum secundarium
9. os hamuli proprium
10. os vesalianum
11. os ulnare externum (calcifications in bursa or tendon)
12. os radiale externum
13. avulsion of the scaphoid, not an accessory bone
14. persisting center of ossification of the radial styloid process
15. accessory bone belween scaphoid and radius (paranaviculare)
16. os centrale carpi
17. hypolunatum
18. epilunatum
19. accessory bone belween lunatum and triquetrum
20. epipyramis
21. avulsion of the styloid process of the ulna (“triangulare”)
22. persistent nucleus of the styloid process of the ulna
23. small osseous element in the radioulnar joint
24. calcification on the pisiform
25. avulsion of the triquetrum, not an accessory bone
26. tendon or bursal calcification.

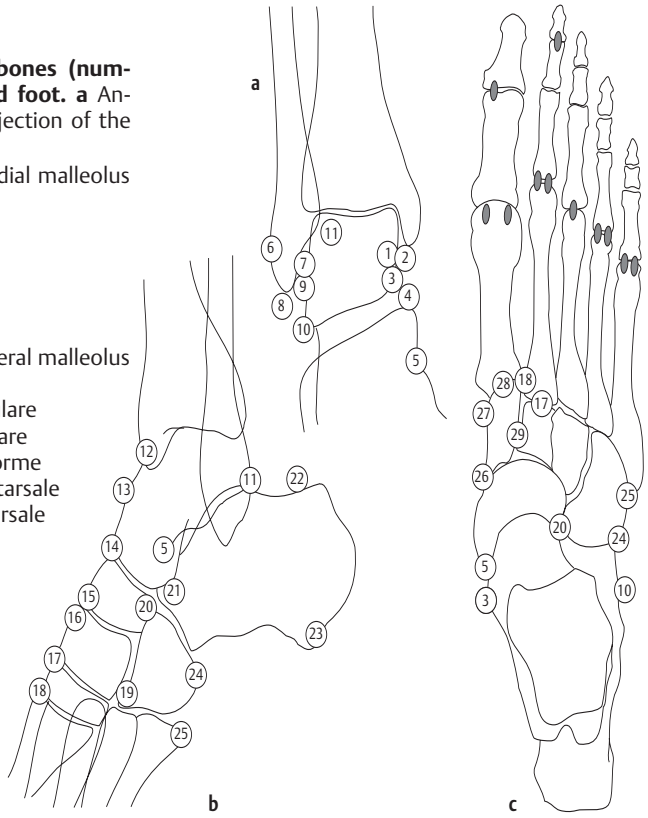

Fig. 4.**47** **Characteristic locations of accessory bones (numbered) and sesamoids (shaded) in the ankle and foot. a** Anteroposterior projection of the ankle. **b** Lateral projection of the ankle. **c** Anteroposterior projection of the foot.

1. accessory bone (or sesamoid) between the medial malleolus and the talus
2. os subtibiale
3. talus accessorius
4. os sustentaculi
5. os tibiale externum
6. os retinaculi
7. accessory ossicle (or sesamoid) between the lateral malleolus and the talus
8. os subfibulare
9. talus secundarius
10. os trochleare calcanei
11. os trigonum
12. os talotibiale
13. os supratalare
14. os supranaviculare
15. os infranaviculare
16. os intercuneiforme
17. os cuneometatarsale
18. os intermetatarsale
19. os unci
20. secondary cuboid
21. calcaneus secundarius
22. os accessorium supracalcaneum
23. os subcalcis
24. os peronaeum (peroneal ossicle)
25. os vesalianum
26. os cuneonaviculare mediale
27. sesamum tibiale anterius
28. os cuneometatarsale 1 plantare
29. os intercuneiforme.

Finally, fractures occurring in osteogenesis imperfecta may to heal with excessive callus formation.

Fractures extending to the articular surface result in a *joint effusion (hemarthrosis)*. In fractures of the radial head, a joint effusion displacing the anterior and/or posterior fat pad may be the only radiographic finding (Fig. 4.**51**). The demonstration of a *fat-fluid level* in the shoulder or knee is presumptive evidence of an intra-articular fracture but can only be demonstrated when the exposure is made with a horizontal beam (Fig. 4.**52**). *Pseudofractures (Looser's zones, Milkman's syndrome)* are assumed to be incomplete stress (insufficiency) fractures, presenting radiographically as narrow (2 to 3 mm) radiolucent bands lying perpendicularly to the cortex (Fig. 4.**53**). At a later stage, sclerosis develops around these lesions, making them more readily detectable. Pseudofractures are present in vitamin D deficiency (osteomalacia,

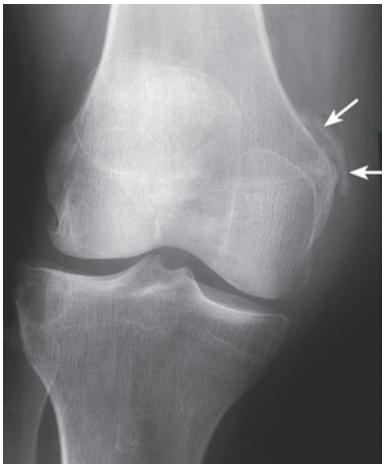

Fig. 4.**48** **Pellegrini-Stieda lesion**. A shell-like ossification (arrows) along the medial femur condyle developed within one month after an acute injury to the medial collateral ligament of the knee.

Fig. 4.**49** **Parosteal osteosarcoma.** The densely sclerotic lesion is solidly attached to the posterior cortex of the distal femur.

Fig. 4.**50** **Myositis ossificans (post-traumatic).** The ossification along the medial femur shaft is separated in its entire length from the adjacent bone.

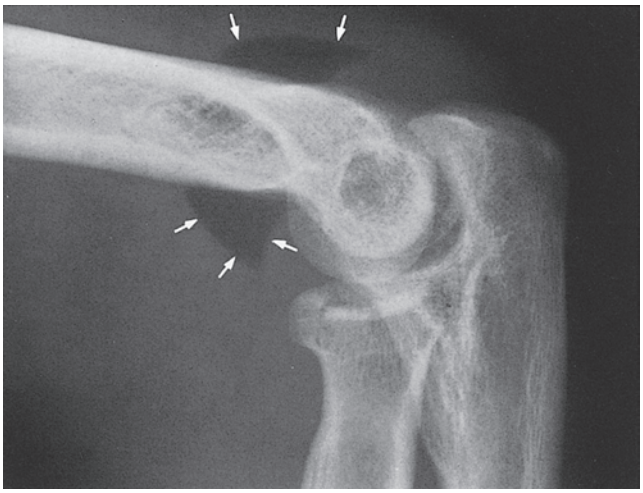

Fig. 4.**51** **Joint effusion (hemarthrosis) secondary to radial head fracture.** The joint effusion is evident from the positive posterior and anterior fat pad sign, evident as sail-like radiolucencies along the distal humerus (arrows). Demonstration of any radiolucent area posteriorly always indicates a joint effusion (positive posterior fat pad sign), whereas a small oblong radiolucent area along the anterior aspect of the distal humerus can be normal. The anterior fat pad sign is only indicative of a joint effusion when it assumes a triangular or sail-like shape, as in this case. Note also the fracture in the radial head, which not uncommonly escapes radiographic detection even when radiographs in multiple projection are taken.

rickets), renal osteodystrophy, Paget's disease, fibrous dysplasia, and hereditary hyperphosphatasia ("juvenile Paget's disease") or are rarely idiopathic. They are located in the femur (neck and shaft), pubic and ischial ramus, scapula, clavicle, ribs, ulna (proximal shaft), radius (distal shaft), metacarpals, metatarsals, and phalanges.

Nutrient arteries pierce the diaphyses of tubular bones obliquely. Their site of entry and angulation are fairly constant and, characteristically, the vessels point away from the dominant growing end of the bone (the end with the epiphyseal center in short tubular bones, or the end with the later fusing epiphysis in long bones). In the long tubular bones of the upper extremity they run towards the elbow, whereas in the lower extremity they run away from the knee ("to the elbow/go, from the knee/flee"). Nutrient arteries may be evident radiographically as oblique radiolucent cortical channels that should not be confused with fracture lines (Fig. 4.**54**).

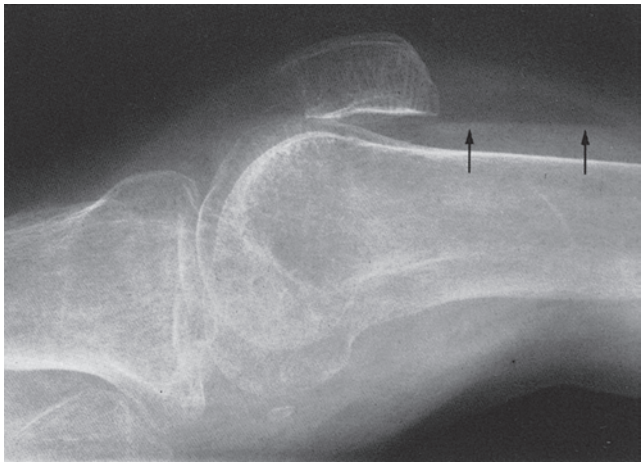

Fig. 4.**52** **Fat-fluid blood level secondary to tibia plateau fracture**. A fat-fluid level, pathognomonic of an intra-articular fracture, is seen in the suprapatellar bursa. It is caused by the lighter and more radiolucent fat (arrows) layering on top of the heavier blood in the joint (lipohemarthrosis). This finding can only be seen when the radiograph is taken with horizontal beam.

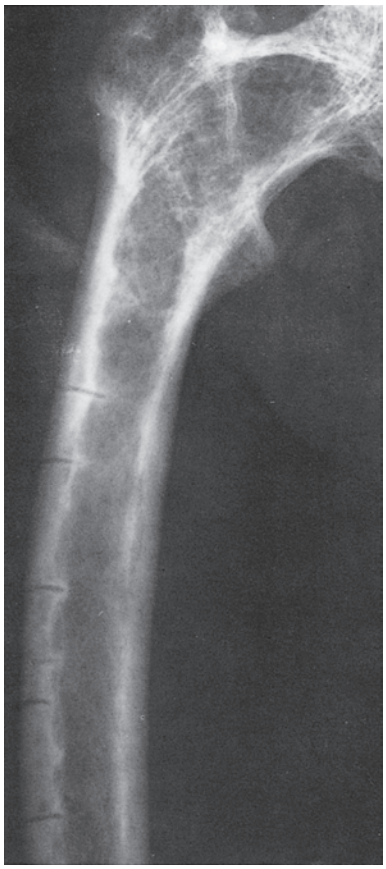

Fig. 4.**53** **Pseudofractures (Looser's zones) in Paget's disease.** Multiple pseudofractures are seen presenting as small radiolucent lines with adjacent sclerosis lying perpendicularly to the outer cortex of the femur shaft. Note also the bowing deformity, thickened cortices, and coarsened trabecular pattern of the femur characteristic of Paget's disease.

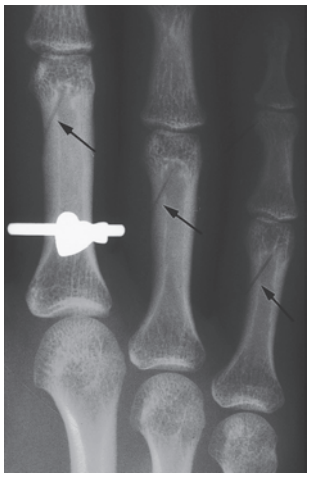

Fig. 4.**54** **Nutrient arteries.** Oblique radiolucent cortical channels are seen in characteristic location (arrows).

5 Localized Bone Lesions

Conventional radiography remains the primary imaging modality for the evaluation of skeletal lesions. The combination of conventional radiography, which has a high specificity but only an intermediate sensitivity, with radionuclide bone scanning, which has a high sensitivity but only a low specificity is still the most effective method for detecting and diagnosing bone lesions and differentiating between benign and malignant conditions. Conventional radiography, is, however, limited in delineating the intramedullary extent of a bone lesion and even more so in demonstrating soft-tissue involvement. Although magnetic resonance imaging frequently contributes to the characterization of a bone lesion, its greatest value lies in the ability to accurately assess the intramedullary and extraosseous extent of a skeletal lesion.

A solitary bone lesion is often a tumor or a tumor-like abnormality, but congenital, infectious, ischemic and traumatic disorders can present in similar fashion. Differentiation between a benign or malignant bone lesion is not always possible. Signs of an aggressive or malignant osseous lesion include rapid growth, large size, poor demarcation, cortical violation, interrupted periosteal reaction and soft tissue extension. Signs of a nonaggressive or benign osseous lesion include slow growth, small size, sharp margination, cortical expansion without cortical violation, solid periosteal reaction and no soft tissue extension. However these radiologic features are not infallible and many exceptions occur indicating the need for histologic confirmation in the appropriate setting.

In osteolytic lesions a **geographic, moth-eaten and permeative pattern of bone destruction** are commonly discerned. A *geographic lesion* (Figs. 5.**1** and 5.**2**) has a well-defined margin separating it clearly from the surrounding normal bone. The zone of transition of normal to abnormal bone is short and a sclerotic border of various thickness may surround the lesion. Geographic lesions are usually benign, especially when they are marginated by a sclerotic rim. Multiple myeloma and metastases, however, frequently present as geographic lesions without sclerotic borders (Table 5.**1**).

A *moth-eaten lesion* (Fig. 5.**3**) is a poorly demarcated focus of bone destruction with a long zone of transition from normal to abnormal bone indicating its aggressive nature and rapid growth potential. Malignant bone tumors, osteomyelitis and eosinophilic granulomas frequently present with this pattern of bone destruction (Table 5.**2**).

A *permeative lesion* (Fig. 5.**4**) represents the most aggressive bone destruction pattern with rapid growth. The lesion merges imperceptibly with the normal bone. Highly malignant tumors infiltrating the bone marrow such as round cell sarcomas (e.g. Ewing's sarcomas and lymphomas) typically are associated with this pattern of bone destruction. It is, however, also found in acute osteomyelitis and rapidly developing osteoporosis such as reflex sympathetic dystrophy. Infiltration of the cortex may also be associated with these conditions, presenting as cortical striation or tunneling.

Fig. 5.**1** **Geographic lesion**. A well-demarcated lesion with sclerotic border is seen in the distal femur (nonossifying fibroma).

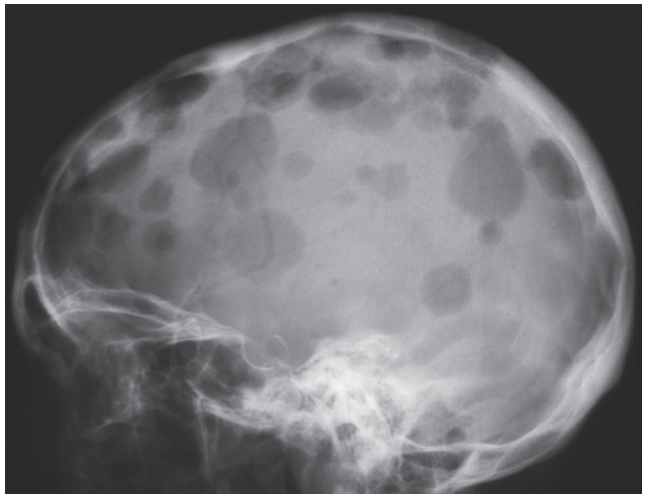

Fig. 5.**2** **Geographic lesions**. Multiple well-demarcated (punched-out) purely lytic lesions are seen in the vault of the cranium (multiple myeloma).

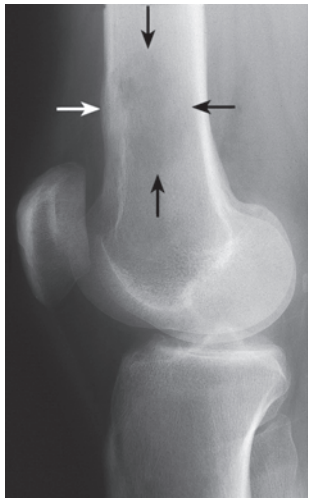

Fig. 5.**3** **Moth-eaten lesion**. A poorly demarcated osteolytic lesion (arrows) is seen in the distal femur (non-Hodgkin lymphoma).

Table 5.1 Solitary well defined osteolytic lesion

Subchondral cyst (associated with arthritis, osteonecrosis, or trauma)
Gout (intraosseous tophus)
Amyloidosis
Intraosseous ganglion
Simple (unicameral) bone cyst
Aneurysmal bone cyst
Epidermoid inclusion cyst
Glomus tumor
Intraosseous lipoma
Enchondroma
Chondroblastoma
Chondromyxoid fibroma
Nonossifying fibroma
Desmoplastic fibroma
Osteoblastoma
Giant cell tumor
Fibrosarcoma
Clear cell chondrosarcoma
Angiosarcoma
Plasmacytoma/multiple myeloma
Metastasis
Eosinophilic granuloma
Brown tumor (hyperparathyroidism)
Hemophilic pseudotumor
Osteonecrosis (bone infarct)
Brodie's abscess/cystic osteomyelitis
Fibrous dysplasia
Sarcoidosis

The cortex represents a barrier to nonaggressive lesions. Benign medullary processes may leave the endosteal surface intact or produce *endosteal scalloping* (Fig. 5.**5**). The latter finding is, however, also frequently seen with multiple myeloma and metastases. Progressive endosteal erosion associated with solid new periosteal bone deposition creates an expanded osseous contour indicative of a nonaggressive benign skeletal lesion. Aggressive skeletal lesions may penetrate the entire thickness of the cortex (Fig. 5.**6**) and sometimes induce a variety of interrupted periosteal reactions including onion-peel, sunburst and hair-on-end patterns or a

Table 5.2 Solitary poorly defined osteolytic lesion

Hemangioma
Chondroblastoma
Osteoblastoma
Giant cell tumor
Fibrosarcoma
Malignant fibrous histiocytoma
Chondrosarcoma
Osteosarcoma
Ewing's sarcoma
Angiosarcoma
Multiple myeloma
Metastasis
Lymphoma
Langerhans cell histiocytosis (eosinophilic granuloma)
Hemophilic pseudotumor
Osteonecrosis (bone infarct)
Osteomyelitis
Brodie's abscess
Sarcoidosis

Fig. 5.**4** **Permeative lesion.** A poorly defined osteolytic lesion merging imperceptibly with the normal bone is seen in the proximal femur. Note also the beginning laminated periosteal reaction in the subtrochanteric area (Ewing sarcoma).

Fig. 5.**5** **Endosteal scalloping.** Sharply demarcated erosions of the inner cortex of the radius and ulna caused by multiple osteolytic lesions is seen (multiple myeloma).

Codman's triangle. They are most commonly associated with osteosarcoma, Ewing's sarcoma, and osteomyelitis and are discussed in greater detail in chapter **3**.

The matrix of a skeletal lesion may be inhomogeneous because it contains areas of *calcification* or *ossification*. Calcifications appear as ring-like, flocculent or fleck-like radiodense areas (Figs. 5.**7** and 5.**8**). Intramedullary matrix calcification is primarily associated with cartilaginous tumors and bone infarcts (Table 5.**3**). Foci of intramedullary ossifications are more homogeneous and often ivory-like and are most often caused by bone islands, osteoblastic metastases and primary bone forming neoplasms (Fig. 5.**9**). They are discussed in detail in chapter **2**.

Table 5.3 Bone lesions with calcification

Intraosseous lipoma
Osteochondroma
Enchondroma
Periosteal (juxtacortical) chondroma
Bizarre parosteal osteochondromatous proliferation (BPOP)
Chondroblastoma
Dysplasia epiphysealis hemimelica (Trevor's disease)
Fibrocartilagenous mesenchymoma
Chondromyxoid fibroma
Osteoid osteoma (nidus)
Osteoblastoma (nidus)
Ossifying fibroma
Gnathic tumors (see chapter 11)
Chordoma
Chondrosarcoma (all variants)
Metastasis (especially thyroid carcinoma)
Gout (intraosseous tophus)
Osteonecrosis (bone infarct)
Intraosseous hematoma
Osteogenesis imperfecta (popcorn calcifications in enlarged epimetaphyses)

Fig. 5.**6** **Cortical penetration**. A poorly defined, mixed osteolytic and osteoblastic lesion is seen in the distal femur penetrating through the medial cortex. The lateral cortex is expanded and thinned but still intact (osteosarcoma).

Fig. 5.**7** **Matrix calcification**. A flocculent, ring-like cluster of calcification is seen in the distal femur (enchondroma).

Fig. 5.**8** **Matrix calcification**. An irregular, shell-like calcification is seen in the distal femur (bone infarct).

Fig. 5.**9** **Intramedullary ossification**. An irregular, ivory-like area of sclerosis is seen in the proximal humerus (enostosis or giant bone island).

Fig. 5.**10** **Septation.** A lytic lesion with extensive delicate trabeculation induced by the tumor is seen in the iliac wing. Note also the localized cortical violation (arrow) in the superolateral aspect of the lesion (aneurysmal bone cyst).

Fig. 5.**11** **Septation**. A large expansile lytic lesion with remaining remnants of the original bone matrix producing a septated appearance, is seen in the ilium (plasmacytoma).

Fig. 5.**12** **Ground glass appearance** . A slightly expansile osteolytic lesion with a hazy increase in density is seen in the proximal tibia (fibrous dysplasia).

Septation of the matrix represents another mechanism of new bone formation evoked by a neoplasm (Fig. 5.**10**). In other instances intratumoral septations represent the remnants of the original bone matrix largely destroyed by the neoplasm (Fig. 5.**11**). Septation is associated with both benign and malignant lesions. Delicate thin trabeculae typically are found in giant cell tumors and aneurysmal bone cysts, lobulated trabeculae in nonossifying fibromas, spiculated or radiating trabeculae in hemangiomas and irregular coarse trabecula in a variety of benign and malignant lesions, often of fibrous connective tissue origin (Table 5.**4**). A uniform hazy increase in radiodensity in an osteolytic lesion is termed *ground glass appearance*. It is most characteristic for fibrous dysplasia (Fig. 5.**12**), but is occasionally also found in simple (unicameral) bone cysts in the adult. The demonstration of a *sequestrum* (Fig. 5.**13**) representing a segment of

Table 5.4 Osteolytic lesions with trabeculation/septation

Simple (unicameral) bone cyst
Aneurysmal bone cyst
Intraosseous lipoma
Hemangioma
Chondromyxoid fibroma
Nonossifying fibroma
Ossifying fibroma
Giant cell tumor
Gnathic tumors (see chapter 11)
Adamantinoma
Ameloblastoma
Fibrosarcoma
Malignant fibrous histiocytoma
Osteosarcoma, teleangiectatic
Plasmacytoma/multiple myeloma
Metastasis (e.g. blowout-metastases from kidney, thyroid or lung)
Brown tumor (hyperparathyroidism)
Hemophilic pseudotumor
Fibrous dysplasia
Sarcoidosis

Fig. 5.**13** **Bone sequestrum**. A lytic lesion containing a small sclerotic sequestrum in its center is surrounded by dense sclerosis and cortical thickening in the tibia (chronic osteomyelitis). A healed fibula fracture is incidentally also seen.

dense necrotic bone is indicative of chronic osteomyelitis (Table 5.**5**).

Bone expansion can be associated with both benign and malignant lesions. In a slowly growing tumor the bone erosion on the inner cortex is compensated by bone apposition on the outer cortex (Fig. 5.**14**). In this instance the cortex remains intact at all times, but the thickness of this new cortical shell may be different when compared to the original cortex. The interface between normal and expanded cortex may be filled in with dense bone and often is referred to as *buttressing* (Fig. 5.**15**). It is found, among others, with eosinophilic granulomas, aneurysmal bone cysts and osteoblastomas. In rapidly growing tumors the new bone formation cannot keep up with the bone breakdown resulting in *cortical violation* or *frank destruction* (Fig. 5.**16**) (Tables 5.**6** and 5.**7**).

Table 5.5 Osteolytic lesions containing a sequestrum or bone fragment

Simple (unicameral) bone cyst with pathologic fracture (fallen fragment sign)
Fibrosarcoma (sequestered bone fragment)
Metastasis (sequestered bone fragment)
Bone lesion with pathologic fracture (fracture fragment)
Eosinophilic granuloma (sequestrum)
Comminuted fracture (intramedullary displaced cortical fragment)
Osteomyelitis (sequestrum)
Brodie's abscess (sequestrum)
Infected pin tract (ring sequestrum)
Button sequestrum in skull (eosinophilic granuloma, metastases, epidermoid, osteoblastoma, osteomyelitis, radiation necrosis, bone flap undergoing avascular necrosis, burr hole and normal variants)

Table 5.6 Expansile osteolytic lesion with intact cortex

Simple (unicameral) bone cyst
Aneurysmal bone cyst (eccentric)
Enchondroma
Chondromyxoid fibroma (eccentric)
Nonossifying fibroma (eccentric)
Desmoplastic fibroma
Osteoblastoma
Giant cell tumor (eccentric)
Fibrosarcoma
Chondrosarcoma
Eosinophilic granuloma
Brown tumor (hyperparathyroidism)
Hemophilic pseudotumor
Healing/healed fracture
Osteomyelitis (e.g. spina ventosa [phalanges or metacarpals] in tuberculosis)
Fibrous dysplasia

Fig. 5.**14** **Expansile lesion with intact cortex**. An expansile, multiloculated lesion with intact, thinned or thickened cortex is seen in the distal humerus (simple [unicameral] bone cyst).

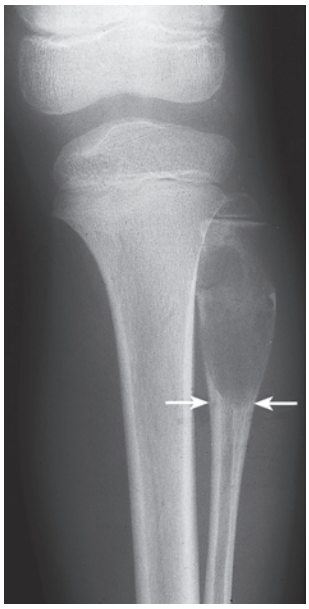

Fig. 5.**15** **Buttressing**. Localized cortical thickening (arrows) is seen in the proximal fibula at the interface between normal cortex and expanded cortex of the osteolytic lesion (aneurysmal bone cyst).

Fig. 5.**16** **Cortical destruction.** An eccentric, expansile, osteolytic lesion in the distal femur metaphysis and epiphyses broke through the cortex with only a few cortical remnants remaining (giant cell tumor).

The *location* of a solitary lesion within a bone provides an important clue to the correct diagnosis. In tubular bones the epiphysis is a common location for chondroblastomas, clear cell chondrosarcomas, metastases, lipomas, subchondral cysts, intraosseous ganglia and Brodie's abscesses. Giant cell tumors originate in the metaphysis, but quickly penetrate the closed growth plate and extend into the subchondral bone. Osteoid osteomas (intra-articular presentation), enchondromas and eosinophilic granulomas occasionally are also found in the epiphyses, but the diametaphysis is a more characteristic location for these tumors (Table 5.**8**). Lesions commonly located in the epiphyses are also found about the joints of flat bones, patella and carpal and tarsal bones.

Typical *metaphyseal lesions* include nonossifying fibroma which characteristically develops a short distance from the growth plate, chondromyxoid fibroma which abuts the growth plate, simple (unicameral) bone cyst, aneurysmal bone cyst, osteochondroma, Brodie's abscess, mesenchymal sarcomas such as osteosarcoma and chondrosarcoma and metastases. Common *diaphyseal lesions* include round cell tumors (e.g. Ewing's sarcoma and lymphoma), metastases, nonossifying fibromas, simple (unicameral) bone cysts in adults, enchondromas, osteoid osteomas, osteoblastomas, and fibrous dysplasia.

The diagnosis of a tubular bone lesion is also facilitated by the identification of its center with regard to the medullary canal and cortex. Typical *central lesions* include simple (unicameral) bone cysts, enchondromas, fibrous dysplasia and bone infarcts. *Eccentric lesions* include aneurysmal bone cysts, giant cell tumors and chondromyxoid fibromas. Typical *cortical lesions* are nonossifying fibromas and osteoid osteomas (Fig. 5.**17**). *Surface lesions* arise from the outer surface of the cortex (e.g. surface high-grade osteosarcoma). *Juxtacortical lesions* (Figs. 5.**18** and 5.**19**) can be divided into those originating from the deep layer of the periosteum (periosteal lesions) and those derived from the outer layer of the periosteum and growing in an exophytic pattern (parosteal lesions). Typical examples of juxtacortical lesions include the periosteal osteosarcoma and parosteal osteosarcoma (Table 5.**9**).

Table 5.7 Expansile osteolytic lesion with cortical violation

Aneurysmal bone cyst (eccentric)
Epidermoid inclusion cyst
Glomus tumor
Hemangioma (skull)
Chondromyxoid fibroma (eccentric)
Desmoplastic fibroma
Osteoblastoma
Giant cell tumor (eccentric)
Fibrosarcoma
Malignant fibrous histiocytoma
Chondrosarcoma
Osteosarcoma
Angiosarcoma
Plasmacytoma/multiple myeloma
Metastases (from kidney, thyroid, lung)
Hemophilic pseudotumor

Table 5.8 Common location of tubular bone lesions

Epiphyses
Subchondral cyst (associated with arthritis, osteonecrosis or trauma)
Gout (intraosseous tophus)
Amyloidosis
Intraosseous ganglion
Intraosseous lipoma
Chondroblastoma
Dysplasia epiphysealis hemimelica (Trevor's disease)
Giant cell tumor (originates in metaphysis)
Clear cell chondrosarcoma
Metastasis
Brodie's abscess

Metaphyses
Simple (unicameral) bone cyst
Aneurysmal bone cyst
Osteochondroma
Chondromyxoid fibroma
Periosteal desmoid
Nonossifying fibroma
Desmoplastic fibroma
Fibrosarcoma
Malignant fibrous histiocytoma
Chondrosarcoma
Osteosarcoma
Metastasis
Osteomyelitis
Brodie's abscess
Fibrous dysplasia

Diametaphysis
Simple (unicameral) bone cyst (in adults)
Intraosseous lipoma
Enchondroma
Periosteal chondroma
Nonossifying fibroma
Bone island
Osteoid osteoma
Osteoblastoma
Adamantinoma (especially anterior tibia)
Fibrosarcoma
Malignant fibrous histiocytoma
Ewing's sarcoma
Angiosarcoma
Multiple myeloma
Metastasis
Lymphoma
Langerhans cell histiocytosis (eosinophilic granuloma)
Brown tumor (hyperparathyroidism)
Hemophilic pseudotumor
Osteonecrosis (bone infarct)
Osteomyelitis
Fibrous dysplasia
Osteofibrous dysplasia (especially anterior tibia)

The knowledge of the *age of a patient* is fundamental to the correct interpretation of any bone lesion. Most benign symptomatic bone tumors are diagnosed in patients below the age of 30 years. Asymptomatic benign bone lesions are however a frequent incidental finding at any age. Primary malignant bone tumors in children and adolescents usually consist of osteosarcomas and Ewing's sarcomas. Neoplasms typically diagnosed between the age of 20 and 40 years include giant cell tumors, parosteal sarcomas and adamantimomas. Symptomatic bone tumors diagnosed at the age of 40 years and older must be considered malignant until proven otherwise with the vast majority being either metastases, lymphoma or multiple myeloma.

The differential diagnosis of localized bone lesions is discussed in Table 5.**10**.

Table 5.9 Cortical lesions

Localized elliptical cortical thickening
Osteoid osteoma
Osteomyelitis (chronic)
Stress fracture
Localized defect of external cortex
Periosteal desmoid (posteromedial aspect of distal femur)
Fibromatosis
Adamantinoma (especially anterior tibia)
Osteofibrous dysplasia (especially anterior tibia)
Ewing's sarcoma
Metastasis (especially from bronchogenic carcinoma)
Hyperparathyroidism including brown tumor
Gouty tophus
Adjacent soft tissue neoplasm or abscess
Subperiosteal osteomyelitis
Subperiosteal hematoma
Avulsion fracture/injury (chronic)
Juxtacortical tumors and tumor-like lesions
Parosteal lipoma (may induce cortical thickening or hyperostosis
Parosteal hemangioma (may induce cortical thickening or hyperostosis
Osteoma
Osteochondroma
Periosteal (juxtacortical) chondroma
Bizarre parosteal osteochondromatous proliferation (BPOP)
Periosteal (juxtacortical) desmoid
Peripheral chondrosarcoma
Periosteal chondrosarcoma
Periosteal osteosarcoma
Parosteal osteosarcoma
Parosteal myositis ossificans
Spurs (congenital, post-traumatic)
Enthesopathy
Osteophytosis

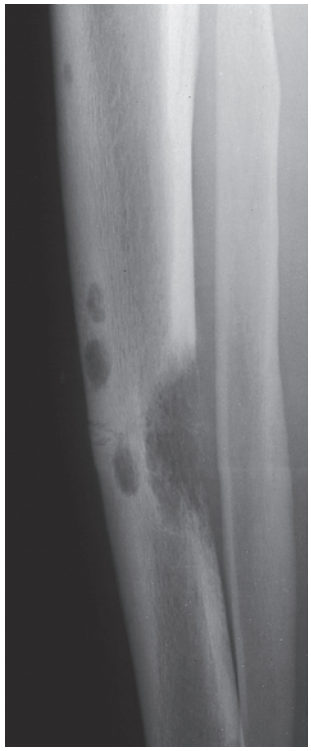

Fig. 5.**17** **Cortical lesions**. Multiple osteolytic lesions are seen within the cortex of the tibia. The largest lesion has extended from the cortex into the medullary space and adjacent soft tissue (metastases from bronchogenic carcinoma).

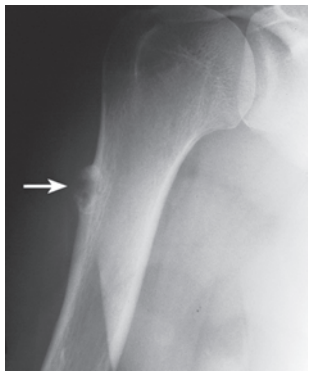

Fig. 5.**18** **Juxtacortical lesion**. A defect (arrow) with minimal punctate matrix calcifications is seen in the outer cortex of the proximal humerus surrounded by periosteal new bone formation (periosteal [juxtacortical] chondroma).

Fig. 5.**19** **Juxtacortical lesion**. An ossified mass with adjacent cortical thickening is seen in the posterior aspect of the distal femur (parosteal osteosarcoma).

Table 5.10 Localized bone lesions

Disease	Radiographic Findings	Comments
Subchondral cyst (Fig. 5.20)	Solitary or multiple defects measuring up to 3 cm in diameter with sclerotic border located in the subchondral bone (pressure segment) of a joint. Communication with joint may be present occasionally allowing gas to pass into the cyst (pneumatocyst).	Associated with osteoarthritis, calcium pyrophosphate dihydrate crystal deposition disease (CPPD), osteonecrosis (avascular necrosis) and rheumatoid arthritis). *Traumatic* cysts are the sequela of a bone injury, but may be larger and not necessarily associated with an arthritic process.
Intraosseous ganglion (Fig. 5.21)	Unilocular or multilocular, well-defined lytic epiphyseal lesion, often with sclerotic margin. The lesion does not communicate with the adjacent joint. Preferred locations are the medial malleolus of the tibia, femoral head, acetabulum and carpal bones.	A *herniation pit* (Fig. 5.**22**) is a well-circumscribed radiolucent defect usually measuring less than 1 cm in diameter with a thin sclerotic border in the superolateral aspect of the femoral neck caused by herniated synovium.
Simple (unicameral) bone cyst (Figs. 5.23, 5.24 and 5.25)	Centrally located, well-demarcated and often slightly expansile osteolytic lesion with cortical thinning is characteristic. The lesion may be septated or depict a scalloped inner margin. Most often located in long tubular bones (especially humerus and femur), initially in the metaphysis abutting the growth plate and with time migrating into the diaphysis. Pathologic fracture is relatively common with a fracture fragment occasionally located at the bottom of the cyst (fallen fragment sign).	Asymptomatic unless fractured. Usually diagnosed before the age of 20 years with a 3:1 male predominance. After that age bone cysts tend to appear more often in flat bones such as pelvis or calcaneus. *Echinococcal (hydatid) cysts* are found in 1 % of infected patients presenting with single or multiple expansile cystic lesions (“bunch of grapes”) preferentially located in the pelvis and sacrum.
Aneurysmal bone cyst (Figs. 5.26 and 5.27)	Presents most commonly as an eccentric, expansile osteolytic lesion with intact or disrupted cortex in the metaphysis of a long tubular bone. Extensive sclerosis at the interface between normal and expanded cortex (“buttressing”) may be present. Delicate thin trabeculation is characteristic and an expansile ballooning lesion may produce a “soap-bubble” appearance. Other common locations include the posterior elements of the spine and the pelvis, where a large soft tissue component may simulate a malignancy.	Primary lesions are usually diagnosed in the first, second or less frequently third decades of life with slight female predominance. Secondary aneurysmal bone cysts (20 %) are found in giant cell tumors and less frequently in osteoblastomas, simple bone cysts, nonossifying fibromas, teleangiectatic osteosarcomas, metastases, fibrous dysplasia, Paget’s disease, and others.

(continues on page 84)

Fig. 5.**20 Subchondral cyst**. Degenerative changes with a large subchondral cystic lesion with sclerotic margin is seen in the medial tibia plateau.

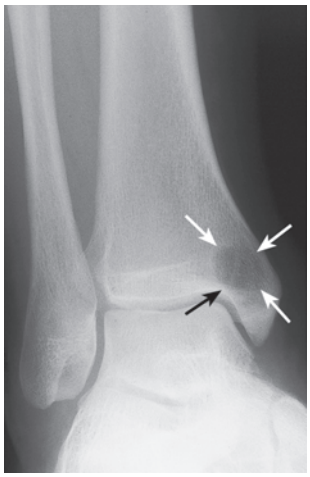

Fig. 5.**21 Intraosseous ganglion**. A small cystic lesion (arrows) with slightly sclerotic margin is seen in the medial malleolus in the absence of arthritis in the ankle.

Fig. 5.**22** **Herniation pit**. A cystic lesion (arrow) with sclerotic margin is seen in the anterolateral aspect of the femoral neck.

Fig. 5.**23** **Simple (unicameral) bone cyst**. A septated osteolytic lesion with cortical thinning is seen in the calcaneus.

Fig. 5.**24** **Simple (unicameral) bone cyst**. A multiloculated cystic lesion with expanded cortex is seen in the humerus.

Fig. 5.**25** **Simple (unicameral) bone cyst with fallen fragment sign**. A cystic lesion with pathologic fracture and a linear dense fragment at the bottom of the cyst is seen in the proximal humerus.

Fig. 5.**26** **Aneurysmal bone cyst**. An eccentric osteolytic lesion is seen in the proximal tibia abutting the open physis.

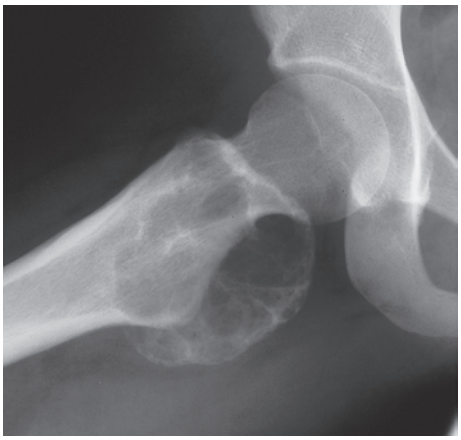

Fig. 5.**27** **Aneurysmal bone cyst**. An expansile trabeculated osteolytic lesion with "soap-bubble" appearance is seen originating from the greater trochanter.

Table 5.10 (Cont.) Localized bone lesions

Disease	Radiographic Findings	Comments
Epidermoid (inclusion cyst) Figs. 5.28 and 5.29)	Intraosseous lesion presents as well-defined osteolytic defect, often with sclerotic margin, occurring in the terminal phalanx of the hand or in the skull. The lesion may be expansile with thinning or destruction of the cortex. Skull lesions usually measure 1 to 5 cm in diameter and may be limited to the diploic space or extend through one or both tables. An irregularly shaped button sequestrum is usually present in larger skull lesions.	Usually diagnosed in the second to fourth decades of life with slight male predominance. A history of trauma is often present suggesting intraosseous implantation of ectodermal tissue with subsequent development of an epidermoid. The lesion is lined with a stratified squamous epithelium shedding keratin debris that breaks down and forms cholesterol.
Glomus tumor	Intraosseous glomus tumor presents as a well-defined osteolytic lesion in the terminal phalanges of the hand indistinguishable from an epidermoid on plain film radiography. Differentiation is however possible with MR imaging, where the glomus tumor depicts marked contrast enhancement, often with characteristic “salt and pepper” appearance.	Glomus tumors occur in patients of any age, typically are neither palpable nor visible and present in fingertips with aching pain and point tenderness. Secondary bone involvement from a soft tissue glomus tumor is much more common (e.g. temporal bone). In the hand such a lesion presents as shallow, well-marginated erosion in the adjacent bone, usually in the tuft of a terminal phalanx.
Lipoma (Fig. 5.30)	Well-circumscribed osteolytic lesion, often surrounded by a sclerotic border. Irregular thick bony ridges are frequently found in larger lesions. May contain a central calcified nidus (especially in the calcaneus). Demonstration of fatty tissue within the lesion by either CT or MR imaging is virtually diagnostic.	Besides the calcaneus intraosseous lipoma occur most commonly in the metaphyses of long tubular bones, especially the femur, tibia and fibula. A relatively typical location of larger lipomas is the femoral neck abutting the intertrochanteric line. In this location they resemble fibrous dysplasia. *Liposarcomas* rarely arise in bone.
Liposclerosing myxofibroma (Liposclerosing myxofibrous tumor, LSFMT) (Fig. 5.31)	Well defined lytic or “ground glass” lesion, often with markedly sclerotic-border occurring typically (80%) in the pretrochanteric and intertrochanteric region of the proximal femur. Fat is not always demonstrated with either CT or MRI.	Rare benign lesion commonly diagnosed as incidental finding or presenting with pain in patients between 20 and 70 years of age. Malignant transformation occurs in less than 10% of cases. May be a variant of fibrous dysplasia or represent a burned-out or infarcted intraosseous lipoma.

(continues on page 86)

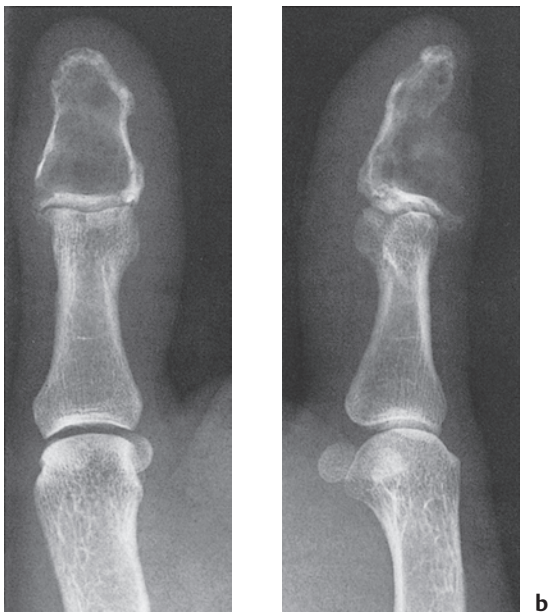

a b

Fig. 5.**28 a**, **b** **Epidermoid (inclusion cyst)**. An expansile osteolytic lesion is seen in the distal phalanx of the thumb.

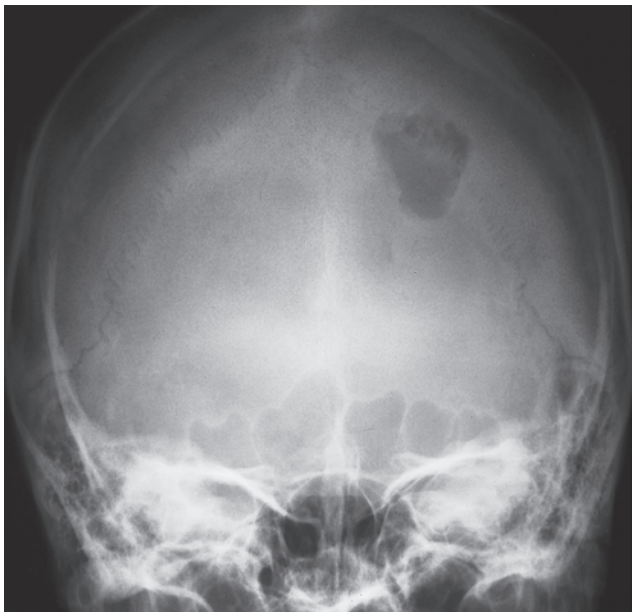

Fig. 5.**29** **Epidermoid (inclusion cyst)**. An irregular osteolytic lesion with slightly beveled margin is seen in the vault of the skull.

a

b

Fig. 5.**30 a**, **b** **Lipoma (2 cases)**. An osteolytic lesion in the calcaneus containing a small central calcified nidus (representing fat necrosis) is virtually diagnostic (**a**). A well-circumscribed osteolytic lesion with sclerotic border and irregular thick trabeculation in the femoral neck abutting the intertrochanteric line is quite characteristic (**b**). The demonstration of fatty content by either CT or MRI differentiates this lesion from fibrous dysplasia.

Fig. 5.**31** **Liposclerosing myxofibroma**. A round lesion with sclerotic margin is seen in the pretrochanteric region of the proximal femur (arrow).

Table 5.10 (Cont.) Localized bone lesions

Disease	Radiographic Findings	Comments
Hemangioma (Figs. 5.32, 5.33 and 5.34)	*Spine*: Coarse, vertical trabecular pattern ("corduroy" appearance) in the vertebral bodies is characteristic. Diameter of thickened vertical trabeculae is rather uniform (DD: Multiple myeloma, metastases and Paget's disease, which may present with irregular coarse trabecular thickening). Extension into the posterior elements, paraspinal tissues, and spinal canal is rare. *Skull*: Slightly expansile osteolytic lesion with radiating ("sunburst") pattern. *Tubular bones*: Poorly defined osteolytic lesion with lattice-like trabecular pattern.	Usually found in patients over 40 years of age with female predominance. Occasionally non-Hodgkin's lymphoma (especially the histiocytic type) and metastases (e.g. breast carcinoma) may simulate a hemangioma in the spine. *Cystic angiomatosis* (Fig. 5.**35**) is characterized by widespread cystic lesions often surrounded by a rim of sclerosis. They may progress to osteosclerotic lesions simulating metastases. The condition is frequently associated with widespread visceral involvement. *Cystic lymphangiomatosis* presents in a similar fashion. Accumulation of contrast material in lesions during lymphography is diagnostic.
Osteochondroma (Figs. 5.36 and 5.37)	Bony protuberance demonstrating cortical and medullary continuity with parent bone is diagnostic in the tubular bones. The lesion may be pedunculated (with narrow stalk and bulbous tip) or sessile (with a broad, flat base). Osteochondromas characteristically originate from the metaphyses and point away from the nearby articulation. The tip of the osteochondroma is covered by a hyaline cartilage cap that may contain regular stippled calcifications. A large cartilaginous cap containing irregular calcifications is suspicious of malignant transformation. Osteochondromas in the pelvis frequently are large and difficult to differentiate from lesions that have undergone malignant transformation. In the ribs osteochondromas frequently occur at the costochondral junction. Malignant transformation may be best assessed with MR imaging. A cartilage cap of 1 cm or less in thickness indicates a benign lesion, whereas a cap thicker then 2 cm is suspicious for malignant transformation.	Osteochondromas occur in children and adolescents as a slowly growing painless mass. They are intimately related to the physis and cease to enlarge with fusion of the adjacent growth plates. Rarely osteochondromas may develop in the adult after trauma. DD: 1. *Subungual exostosis* (Fig. 5.**38**) projects from the dorsomedial aspect of the tuft, usually of the great toe (80 %) or other distal phalanges of the foot or hand. 2. *Reactive bony excrescence* in medial portion of base of distal phalanx of great toe (normal variant). 3. *Turret exostosis* arises on dorsal surface of proximal or middle phalanx in a finger (post-traumatic). 4. *Supracondylar process of humerus* (Fig. 5.**39**): Spur originating from the anteromedial aspect of the distal humerus pointing towards the elbow (phylogenetic vestige). 5. *Pes anserinus spur* may mimic a small osteochondroma in the medial aspect of the proximal tibia (enthesophyte, occasionally associated with anserinus bursitis). 6. *Post-traumatic spurs* secondary to healed avulsion fractures. 7. *"Tug" lesions* at tendinous attachment sites in the lower extremity. *Hereditary multiple exostoses* (Fig. 5.**40**) present with multiple, usually bilateral and symmetric osteochondromas in the axial and appendicular skeleton associated with bone modeling deformities. In *metachondromatosis* (Fig. 5.**41**) multiple osteochondromas and enchondromas coexist, especially in the hands and feet.

(continues on page 88)

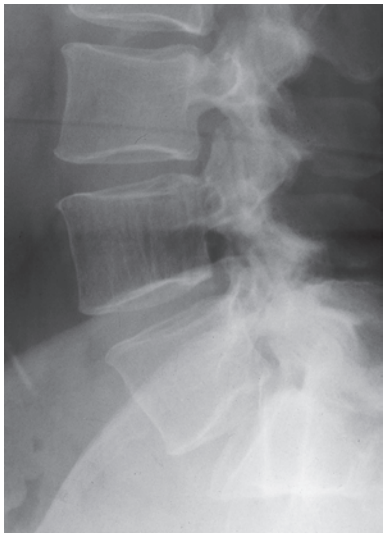

Fig. 5.**32** **Hemangioma**. A rather uniform coarse vertical striation pattern ("corduroy" appearance) seen in the vertebral body of L4 is virtually diagnostic.

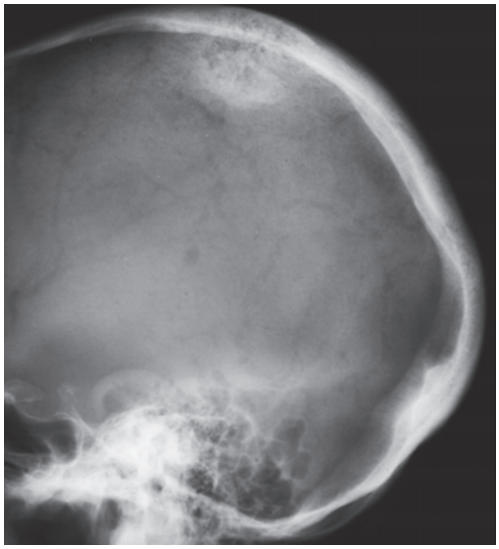

Fig. 5.**33** **Hemangioma**. A slightly expansile lesion with marginal sclerosis and characteristic radiating bony spicules within the lesion is seen in the vault of the skull.

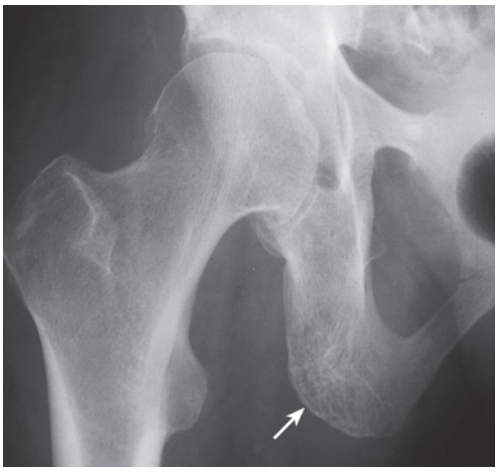

a

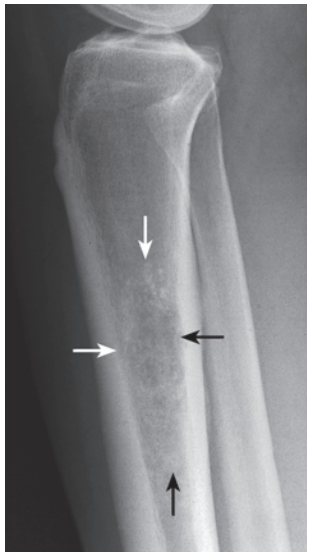

b

Fig. 5.**34 a**, **b** **Hemangioma** (2 cases). A poorly defined osteolytic lesion (arrows) with lattice-like trabecular pattern is seen in the ischiatic ramus (**a**) and proximal tibia (**b**).

Fig. 5.**35** **Cystic angiomatosis**. Multiple well-demarcated osteolytic lesions surrounded by sclerosis are seen in the pelvis and upper femur.

Fig. 5.**36** **Osteochondroma (pedunculated)**. A bony protuberance demonstrating cortical and medullary continuity with the tibia and pointing away from the knee is characteristic.

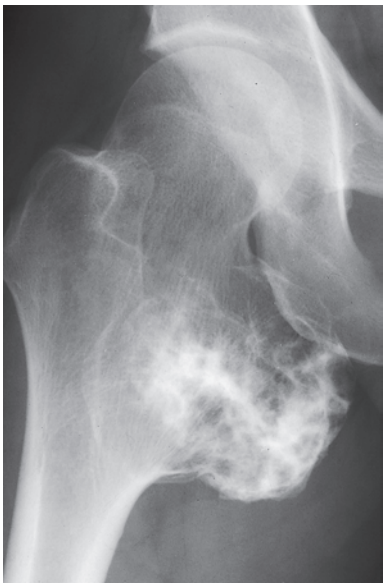

Fig. 5.**37** **Osteochondroma (sessile)**. A broad-based bony outgrowth from the lesser trochanter with calcified cartilage cap is seen. This lesion cannot be differentiated from a low-grade peripheral chondrosarcoma.

Fig. 5.**38** **Subungual exostosis**. An irregular bone protuberance originates from the dorsomedial aspect of the tuft of the great toe.

Table 5.10 (Cont.) Localized bone lesions

Disease	Radiographic Findings	Comments
Dysplasia epiphysealis hemimelica (Trevor's disease) (Fig. 5.42)	Lobulated osseous mass (articular chondroma) protruding from an epiphysis, carpal or tarsal bone. Presents initially in infants as irregular ossifications adjacent to the involved bone. Preferential involvement of the medial side of a lower extremity (e.g. distal femur, proximal and distal tibia and talus). Multiple bones in a single extremity are affected in two-thirds of cases.	Presents in children and young adults with swelling, pain and deformity localized to one side of the body.
Enchondroma (Figs. 5.43 and 5.44)	Well-circumscribed, often lobulated, osteolytic lesion with endosteal scalloping composed of hyaline-type cartilage with varying degrees of calcifications. Preferred locations are the metaphyses of the long tubular bones and the diaphyses in the short tubular bones of the hands and feet. Cortical expansion and pathologic fractures are frequent findings in the hands and feet, but malignant transformation is very rare in these locations. Transformation to chondrosarcoma in the long tubular and flat bones should be suspected with an enlarging radiolucent area, the disappearance of pre-existing calcifications or pathologic fracture.	Enchondromas are usually discovered in the third and fourth decades of life as incidental findings. The presence of pain should arouse suspicion of malignant transformation. Low-grade chondrosarcomas in the long tubular bones and axial skeleton are difficult if not impossible to differentiate from benign enchondromas. *Enchondromatosis (Ollier's disease*) (Figs. 5.**45** and 5.**46**) is characterized by multiple, asymmetrically distributed enchondromas, either exclusively or predominantly involving one side of the body. The affected bones often are shortened and deformed. After cessation of growth the lesion no longer increases in size unless malignant transformation has taken place, estimated to occur in 5 to 30 % of patients. *Maffucci's syndrome* (Fig. 5.**47**) consists of multiple enchondromas and soft tissue hemangiomas containing multiple phleboliths.

(continues on page 90)

Fig. 5.**39** **Supracondylar process**. A spur is seen originating from the anteromedial aspect of the distal humerus and pointing towards the elbow.

Fig. 5.**40** **Hereditary multiple exostoses**. Besides multiple osteochondromas modeling deformities in both the proximal and distal radius and ulna are also evident.

Fig. 5.**41** **Metachondromatosis**. Multiple osteochondromas and enchondromas are seen in the hand.

Fig. 5.**42** **Dysplasia epiphysealis hemimelica (Trevor's disease)**. An enlarged medial malleolus with an irregular, lobulated and partially calcified mass in its tip is seen. Calcified lesions are also present in the medial aspect of the talus and navicular bone.

Fig. 5.**43** **Enchondroma**. A lesion containing flocculent, punctate and circular calcifications is seen in the proximal humerus. An old avulsion fracture of the greater tuberosity is incidentally also present.

Fig. 5.**44** **Enchondroma**. An expansile osteolytic lesion with slightly sclerotic margin and faint matrix calcification is seen in the middle phalanx of the third finger.

Table 5.10 (Cont.) Localized bone lesions

Disease	Radiographic Findings	Comments
Periosteal (juxtacortical) chondroma (Figs. 5.48 and 5.49)	Calcified (50%) soft tissue mass with erosion of the adjacent cortex and varying degree of periostitis. Metaphyses of long bones and hands are most commonly affected.	All ages are affected but the tumor is usually diagnosed under age 30. Slight male predominance.
Bizarre parosteal osteochondromatous proliferation (BPOP) (Fig. 5.50)	Well-marginated sessile or pedunculated mass of heterotopic ossification arising from the cortical surface without medullary continuity between the lesion and the adjacent bone is characteristic.	Occurs usually in the hands and feet (occasionally in long tubular bones) without age and sex predilection. A history of trauma is evident in some patients.
Chondroblastoma (Figs. 5.51 and 5.52)	Well-defined, often lobulated lytic lesion involving the epiphysis or apophysis of a long tubular bone with or without thin sclerotic border and matrix calcification (> 50%) is characteristic. A solid periosteal reaction in the adjacent metaphyseal shaft can be induced by bone marrow edema surrounding the lesion. Approximately 10% of chondroblastomas occur in the hands and feet with predilection for the talus and calcaneus.	Benign cartilaginous lesion occurring between the ages of 5 and 25 years with slight male predominance.

(continues on page 92)

Fig. 5.**45** **Enchondromatosis (Ollier's disease)**. Multiple enchondromas are seen in the hand sparing the thumb and distal phalanges.

Fig. 5.**46** **Enchondromatosis (Ollier's disease)**. Multiple enchondromas are associated with severe modeling deformities in the distal femur, tibia and fibula.

Fig. 5.**47** **Maffucci's syndrome**. Multiple enchondromas are associated with multiple soft tissue hemangiomas containing numerous phleboliths.

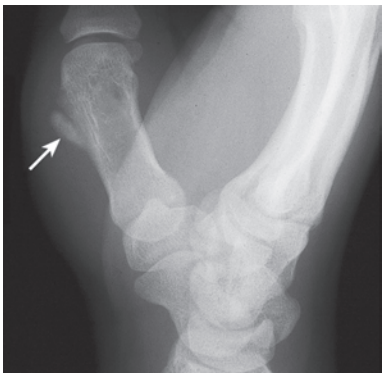

Fig. 5.**48** **Periosteal (juxtacortical) chondroma**. A cortical defect with surrounding sclerosis and adjacent soft tissue calcifications (arrow) is seen in the first metacarpal bone.

Fig. 5.**49** **Periosteal (juxtacortical) chondroma**. An eccentric osteolytic lesion with sclerotic margin, buttressing (arrow), and faint matrix calcifications is seen in the proximal fibula.

Fig. 5.**50** **Bizarre parosteal osteochondromatous proliferation (BPOP)**. A "mushroom cap"-like ossified mass (arrow) arising from the distal aspect of the first metatarsal bone is seen.

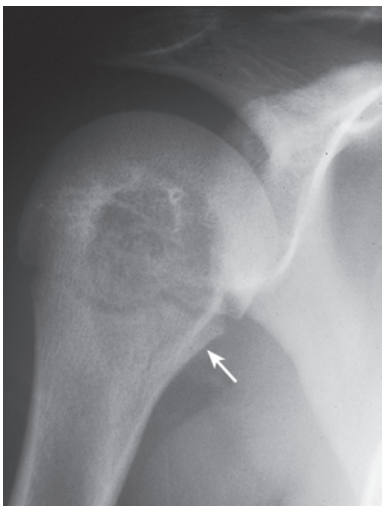

Fig. 5.**51** **Chondroblastoma**. A slightly lobulated osteolytic lesion with faint matrix calcification is seen in the humeral head. A solid periosteal reaction (arrow) and slight diffuse sclerosis of the metaphysis adjacent to the lesion is also evident.

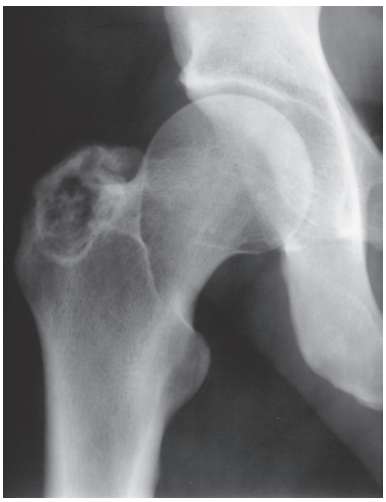

Fig. 5.**52** **Chondroblastoma**. A lytic lesion with sclerotic margin and matrix calcification is seen in the tip of the greater tuberosity.

Table 5.10 (Cont.) Localized bone lesions

Disease	Radiographic Findings	Comments
Chondromyxoid fibroma (Fig. 5.53)	Eccentric metaphyseal osteolytic lesion with cortical expansion, coarse trabeculation, endosteal scalloping and scalloped sclerotic medullary border is commonly seen. Destruction of the cortex resulting in a hemispherical osseous defect or "bite" without periosteal reaction is characteristic of larger lesions. Predilection for the long tubular bones of the lower extremity, but occasionally also found in pelvis and foot.	Uncommon benign cartilaginous lesion occurring between the ages of 5 and 25 years with slight male predominance and presenting with slowly progressive pain, tenderness, swelling and restriction of motion is typical. *Fibrocartilagenous mesenchymoma* is a very rare solitary expansile osteolytic lesion with spotty or ring-like calcifications, cortical destruction and soft tissue invasion originating most often in the metaphysis of long tubular bones. Age distribution is similar to chondromyxoid fibroma.
Periosteal (juxtacortical) desmoid (Fig. 5.54)	Saucer-like defect in the posteromedial cortex of the distal femur often associated with adjacent sclerosis, periostitis and soft-tissue swelling.	Occurs between the age of 10 and 20 as sequelae of acute or chronic trauma at the adductor magnus tendon insertion in the linea aspera.
Nonossifying fibroma (Figs. 5.55, 5.56 and 5.57)	Small lesions present as round or oblong, well delineated, radiolucent areas in the cortex with normal or sclerotic adjacent bone. They typically arise in the metaphysis at a short distance from the physis. Larger lesions present as a well delineated, eccentric, ovoid osteolytic area in the diametaphyses. They frequently have a multiloculated appearance and both cortical expansion and thinning may be evident. The long tubular bones, especially the tibia and femur, are most frequently affected. With time the lesions may spontaneously disappear or become sclerotic.	Usually diagnosed in patients under the age of 20. Smaller lesions are referred to as *benign fibrous cortical defects*. They are asymptomatic and diagnosed as incidental finding on routine radiography and occasionally are multifocal. They usually regress spontaneously or less commonly enlarge and migrate with growth into the diaphyses eventually being referred to as nonossifying fibromas. Pathologic fractures in larger lesions are not uncommon. *Jaffe-Campanacci syndrome* consists of multiple nonossifying fibromas associated with café-au-lait spots, mental retardation and hypogonadism. *Benign fibrous histiocytomas* (Fig. 5.**58**) are histologically identical to nonossifying fibromas, but present as slightly more aggressive lesions in patients over age 20 without site predilection.
Desmoplastic fibroma (Fig. 5.59)	Central osteolytic lesion with trabeculated, soap bubble or honeycomb pattern in the metaphyses of long tubular bones, mandible or pelvis. Slight bony expansion with endosteal erosion and limited periosteal bone formation may be associated.	Rare benign neoplasm occurring in the second or third decades of life. Pain and swelling are the leading clinical symptoms or a pathologic fracture may be the presenting feature.

(continues on page 94)

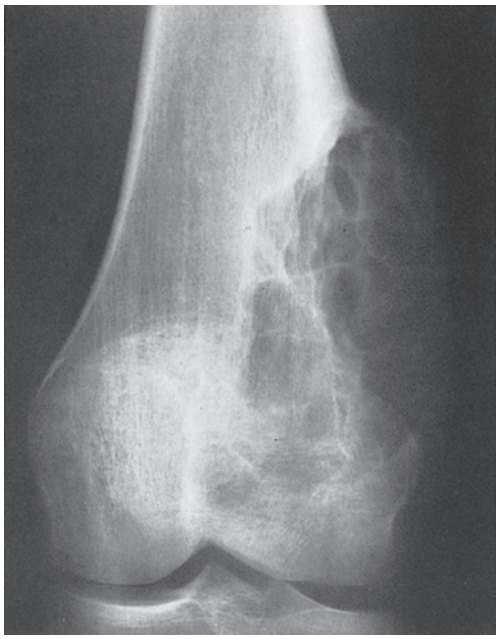

Fig. 5.**53** **Chondromyxoid fibroma**. An expansile eccentric osteolytic lesion with irregular trabeculation, dissolved cortex, and scalloped sclerotic medullary border is seen in the distal femur metaphysis.

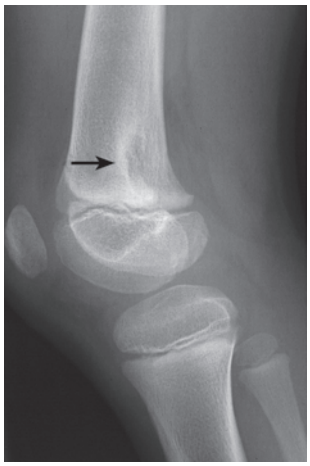

Fig. 5.**54** **Periosteal (juxtacortical) desmoid**. A saucer-like defect in the posteromedial cortex of the distal femur with adjacent sclerosis in a child with unfused physis is virtually diagnostic.

Fig. 5.**55** **Nonossifying fibroma**. A slightly oblong eccentric lesion with multiloculated appearance and sclerotic margin is seen in the distal femur metaphysis.

Fig. 5.**56** **Nonossifying fibroma**. A large oblong eccentric osteolytic lesion with sclerotic margin and pathologic fracture is seen in the distal tibia.

Fig. 5.**57** **Nonossifying fibroma (healed)**. An oblong eccentric sclerotic focus is seen in the distal tibia.

Fig. 5.**58** **Benign fibrous histiocytoma**. A central intramedullary lesion with sclerotic margin and trabeculation is seen in the proximal humerus shaft.

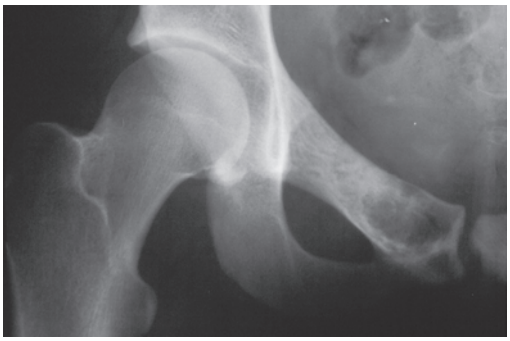

a

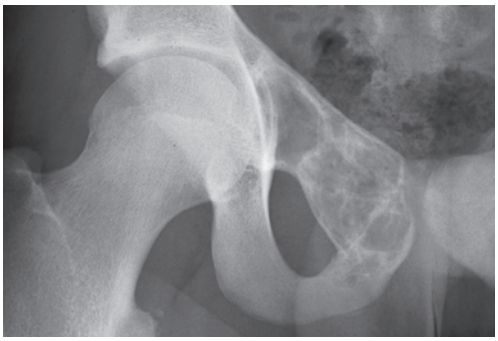

b

Fig. 5.**59 a**, **b** **Desmoplastic fibroma (2 cases)**. A central, relatively poorly defined, slightly expansile osteolytic lesion with honeycombing and surrounding new bone formation is seen in the superior pubic ramus and body of both patients.

Table 5.10 (Cont.) Localized bone lesions

Disease	Radiographic Findings	Comments
Bone island (enostosis) (Figs. 5.60 and 5.61)	Single or multiple intraosseous foci of homogeneously dense bone most often found in the pelvis, proximal femurs and spine. They may be round, ovoid or oblong and are aligned with the long axis of the trabecular architecture. Tiny bone spicules radiating from the periphery of the lesion are quite characteristic. A somewhat radiolucent center may occasionally be encountered. Range in size from a few millimeters to a few centimeters.	Incidental finding in all age groups. Lesions may slowly increase or decrease in size over years. Bone scintography is usually negative. (DD: osteoblastic metastases). A *curettaged* and *methylmethacrylate cemented bone lesion* may resemble a large enostosis. *Osteopoikilosis:* Numerous small sclerotic foci with symmetric distribution in periarticular locations.
Osteoma (Fig. 5.62)	Mass of either uniformly dense compact bone or less dense cancellous bone protruding from the skull and facial bones (especially the paranasal sinuses). Rarely osteomas arise from the cortical surface of the clavicle, pelvis and tubular bones.	*Gardner's syndrome:* Autosomal dominant disease consisting of multiple osteomas, colonic polyposis and soft tissue tumors (especially desmoids). *Tuberous sclerosis:* Multiple osteoma-like lesions may be associated, especially in the metacarpals and metatarsals.
Osteoid osteoma (Figs. 5.63, 5.64, 5.65, 5.66 and 5.67)	*Diaphysis of long tubular bones*: Cortical radiolucent lesion (nidus) measuring less than 1 cm in diameter surrounded by a zone of uniform bone sclerosis (elliptical thickening of the cortex) is virtually diagnostic. The nidus is not always identified with plain film radiography and occasionally has a calcified center. *Intra-articular location*: A nonconspicuous small radiolucent focus often without significant reactive sclerosis may be present inducing a synovial inflammatory response that may result in secondary arthritic changes. *Carpal and tarsal bones*: A partially or completely calcified lesion without or only mild reactive sclerosis is characteristic. *Spine*: An osteosclerotic focus in the posterior elements is the most common presentation. A scoliotic deformity is usually associated with the lesion and is located near its apex on the concave side of the curve.	Occurs in patients between 7 and 25 years of age with a male predominance of 3 to 1. Pain is the hallmark of the disease, usually more dramatic at night and ameliorated by aspirin. Bone scintigraphy shows an unusual intense uptake in the center of the lesion (nidus) differentiating it from chronic cortical osteomyelitis with small abscess formation. Localized cortical thickening caused by a stress fracture typically is associated with a transverse linear radiolucency. In the lumbar spine a unilateral osteosclerotic focus about a pedicle is frequently caused by a hypertrophied intra-articular pars caused by *unilateral spondylysis* of the contralateral side.

(continues on page 96)

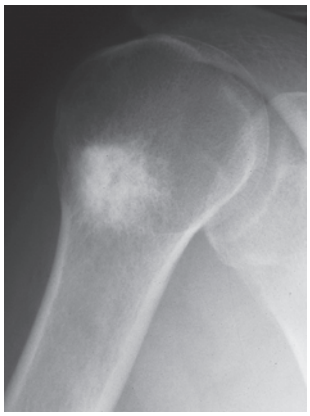

Fig. 5.**60 Enostosis (large bone island)**. An osteoblastic lesion with tiny bone spicules radiating from its periphery is seen in the proximal humerus metaphysis.

Fig. 5.**61 Enostosis (large bone island)**. An irregular shaped large osteoblastic lesion with minimally spiculated border is seen in the ilium.

Fig. 5.**62** **Osteoma**. A slightly lobulated dense bone mass is seen protruding into the frontal sinus.

Fig. 5.**63** **Osteoid osteoma**. Elliptical cortical thickening is seen in the femur shaft. The nidus is not identified in this case with conventional film radiography.

Fig. 5.**64** **Osteoid osteoma**. An expansile cortical lesion (arrow) with only minimal surrounding sclerosis is seen in the proximal phalanx of the index finger.

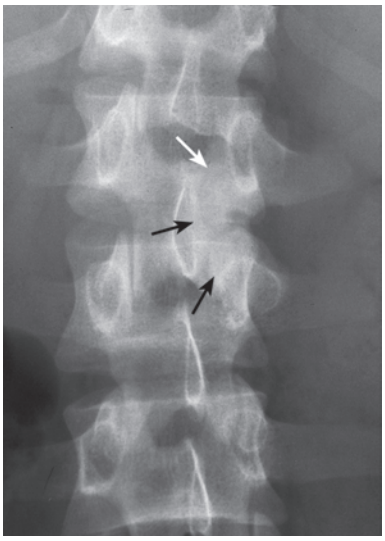

Fig. 5.**66** **Osteoid osteoma**. An osteosclerotic focus (arrows) is seen in the left posterior elements of L1 located at the apex on the concave side of the associated mild scoliosis.

Fig. 5.**65** **Osteoid osteoma**. An osteolytic lesion (arrows) with calcified center (target lesion) is seen in the lateral cuneiform that depicts an overall slight increase in density with the exception of its lateral and distal aspect.

Table 5.10 (Cont.) Localized bone lesions

Disease	Radiographic Findings	Comments
Osteoblastoma Figs. 5.68 and 5.69)	*Long tubular bones*: Osteoblastomas typically originate in either the medullary or cortical bone of the diaphysis and present as expansile osteolytic lesions, often with areas of calcification or ossification, surrounding bone sclerosis and frequently exuberant solid periosteal reaction. *Spine*: A well-defined expansile osteolytic lesion that is partially or extensively calcified and surrounded by mild sclerosis at best, is commonly found in the posterior elements. *Hands, feet and pelvis*: Slightly expansile lytic lesions with varying degrees of matrix calcification/ossification and surrounding reactive sclerosis are the most common presentation	Usually diagnosed in the second and third decades of life with a male predominance of 2 to 1 and similar clinical presentation as in osteoid osteomas. The size of the nidus (actual size of the osteolytic lesion) may be used to differentiate between osteoblastomas (>2 cm) and osteoid osteomas (<2 cm). *Aggressive (malignant) osteoblastomas* are differentiated from the typical (conventional) osteoblastomas by a more aggressive pattern of tumor behavior including a much greater likelihood to recur. The radiologic features of both types are similar, but cortical violation with tumor extension into the neighboring soft tissues is suggestive of aggressive osteoblastomas.
Giant cell tumor (Figs. 5.70 and 5.71)	In the long tubular bones (85%) a giant cell tumor presents as an eccentric expansile osteolytic lesion, often with a delicate trabecular pattern ("soap bubble" appearance) extending from the metaphysis into the subchondral bone. The margins of the lesion may be well or poorly defined, but sclerosis and periosteal reactions are typically absent. Cortical breakthrough with spread into the adjacent soft tissues occurs. Occasionally the tumor is found in pelvis, sacrum, ribs, vertebral bodies, hands and feet.	Occurs usually in the third and fourth decades of life with equal sex distribution. Tumor recurrence is about 50% in excised and grafted lesions, but markedly reduced when cemented with methylmethacrylate instead of bone grafts. *Malignant giant cell tumors* (including malignant transformation of a benign giant cell tumor) account for about 5%. The *giant cell (reparative) granuloma* (Fig. 5.**72**) has a more benign course and similar histologic and radiologic features as the giant cell tumor, although cortical violation with spread into neighboring soft tissues does not occur and a predilection for facial bones and short tubular bones of the hands and feet exists.

(continues on page 98)

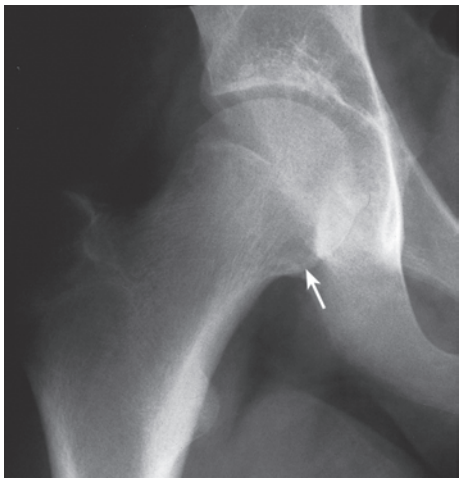

Fig. 5.**67** **Osteoid osteoma (intra-articular)**. A nonconspicuous radiolucent focus (arrow) without periosteal reaction is seen medially at the junction between femoral head and neck.

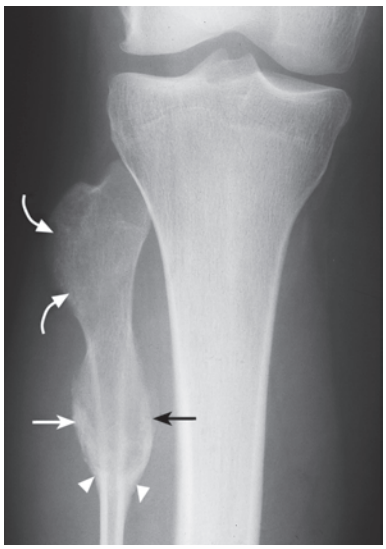

Fig. 5.**68** **Osteoblastoma**. An osteolytic lesion with exuberant solid periosteal reactions (arrows) and buttressing (arrowheads) is seen in the proximal fibular diaphysis. A second cortical lesion (curved arrows) with faint matrix calcification near the fibular head was caused by a **periosteal (juxtacortical) chondroma**.

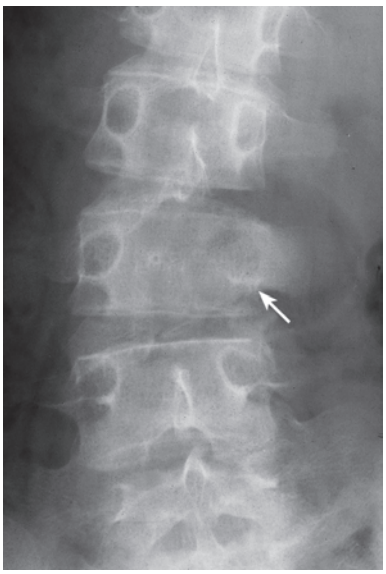

Fig. 5.**69** **Osteoblastoma**. An expansile osteolytic lesion with enlargement of the pedicle (arrow) and faint surrounding sclerosis is seen in the left posterior elements of L3 at the apex on the concave side of the associated scoliosis.

Fig. 5.**70** **Giant cell tumor**. A poorly demarcated osteolytic lesion with faint trabeculation and cortical violation is seen in the distal femur.

Fig. 5.**71** **Giant cell tumor**. An expansile, well-demarcated osteolytic lesion with "soap bubble" appearance is seen in the distal radius.

Fig. 5.**72** **Giant cell reparative granuloma**. A slightly expansile osteolytic lesion is seen in the base of the fifth metatarsal.

Table 5.10 (Cont.) Localized bone lesions

Disease	Radiographic Findings	Comments
Chordoma (Figs. 5.73 and 5.74)	Destructive expansile osteolytic lesion with large soft tissue mass and intratumoral calcifications in about half the cases is characteristic. Originates from the sacrum and coccyx (60%), clivus (30%) and spine, especially C2 (10%). Sacral lesions characteristically grow anteriorly. In the spine vertebral collapse, sclerosis (ivory vertebra) and enlarged neural foramina are additional manifestations.	Saccrococcygeal chordomas occur in 40- to 60-year-old patients with male predominance. Spheno-occipital chordomas are usually diagnosed in 20- to 40-year-old patients without sex predilection. The *chondroid chordoma* is a variant comprising one-third of all clivus chordomas with better prognosis and particularly prominent calcifications. Hematogeneous metastases may eventually develop in about one-third of all chordomas.
Adamantinoma (angioblastoma) (Fig. 5.75)	Single or multiple, central or eccentric, multilocular, slightly expansile, sharply or poorly delineated osteolytic lesions with or without reactive sclerosis in the diaphysis of the tibia (85%) with preferential involvement of its anterior cortex or other long tubular bones. Occasionally cortical destruction, exuberant periostitis and a soft tissue mass are associated.	Usually diagnosed in the third and fourth decades of life with slight male predominance. History of trauma is frequent. Local swelling is the major clinical finding. DD: *Osteofibrous dysplasia*. See under fibrous dysplasia at the end of this table.
Ameloblastoma (Fig. 5.76)	Presentation ranges from unilocular cyst to multilocular, often trabeculated lesion with cortical expansion or destruction and occasionally large soft tissue mass in the mandible or, much less commonly, the maxilla.	Usually diagnosed in the fourth and fifth decades of life without gender predilection. See chapter **11** for differentiation from other gnathic lesions.
Fibrosarcoma (Figs. 5.77, 5.78 and 5.79)	Well or poorly marginated osteolytic lesion with general lack of both periosteal reaction and osteosclerosis is typical. Irregular thin or thick intra-tumoral septation, cortical violation and soft tissue mass are frequently associated. Dystrophic calcifications and sequestered bone fragments are occasionally seen within the tumor. Preferential involvement of the metaphyses of the long tubular bones (70%) with frequent extension into the diaphyses and epiphyses.	Rare malignant bone tumor occurring in the third to sixth decades of life without gender predilection. The histologic spectrum of fibrosarcomas ranging from well differentiated to poorly differentiated lesions is reflected in the greatly variable radiologic presentation. May complicate Paget's disease, bone infarcts, radiation necrosis and chronic osteomyelitis.

(continues on page 100)

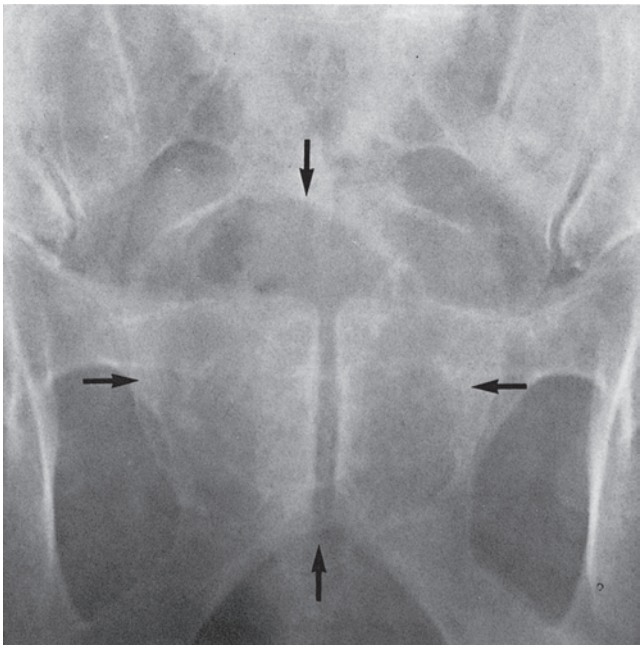

Fig. 5.**73** **Chordoma**. An osteolytic lesion (arrows) with slightly sclerotic margin and faint matrix calcification is seen in the sacrum.

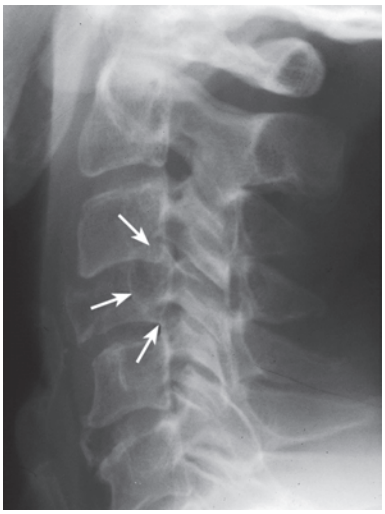

Fig. 5.**74** **Chordoma**. A hemispherical expansile osteolytic lesion (arrows) with slightly sclerotic margin originating in the posterior aspect of the vertebral body of C4 led to the infiltration of the remaining vertebral body with subsequent pathologic compression fracture.

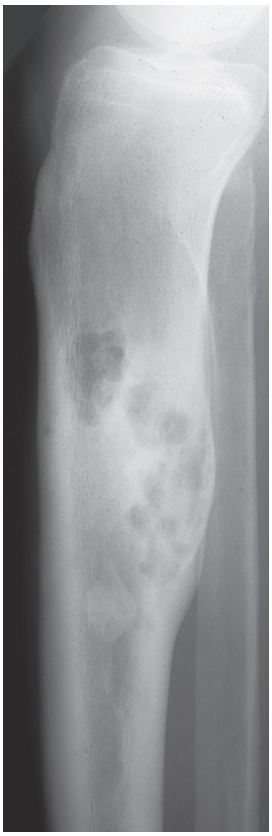

Fig. 5.**75** **Adamantinoma**. A slightly expansile, well to poorly demarcated, multilocular lesion with reactive surrounding sclerosis is seen in the tibia.

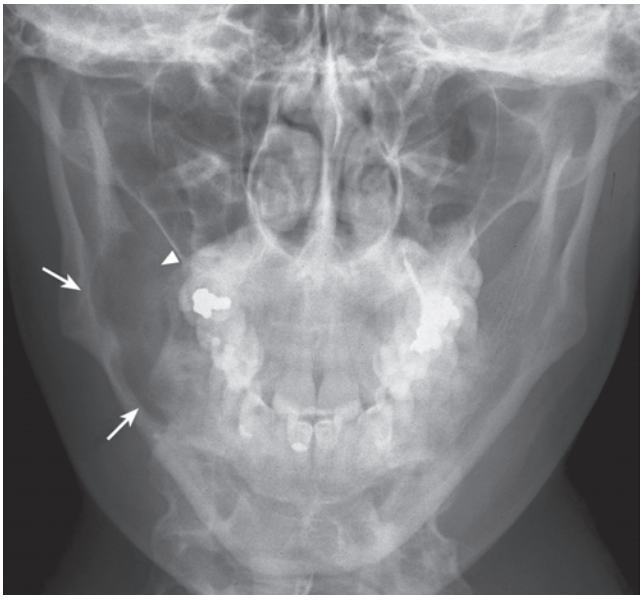

Fig. 5.**76** **Ameloblastoma**. An expansile, multiloculated, osteolytic lesion with both endosteal scalloping (arrows) and cortical violation (arrowhead) is seen in the right mandible.

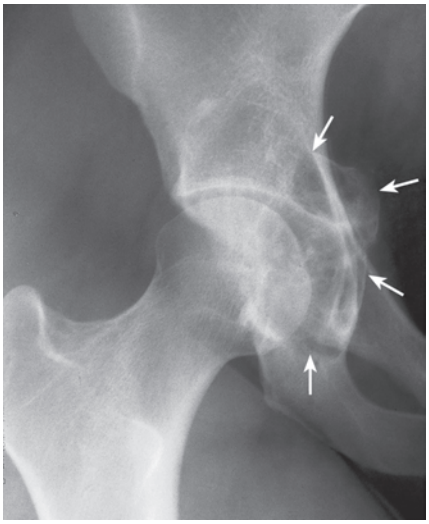

Fig. 5.**78** **Fibrosarcoma**. An expansile trabeculated lesion is seen in the innominate bone of the acetabulum (arrows).

Fig. 5.**77** **Fibrosarcoma**. A poorly demarcated lytic lesion with endosteal scalloping is seen in the femur diaphysis.

Fig. 5.**79** **Fibrosarcoma**. A poorly defined osteolytic lesion is seen in the iliac bone above the acetabulum.

Table 5.10 (Cont.) Localized bone lesions

Disease	Radiographic Findings	Comments
Malignant fibrous histiocytoma (Figs. 5.80 and 5.81)	A poorly defined osteolytic lesion with cortical destruction, large soft tissue mass and absence of both periosteal reaction and new bone formation is the most common presentation. The ends of long tubular bones from diaphysis to epiphysis are affected in 75 percent of cases with strong predilection for the lower extremity. Osseous expansion is unusual but may be observed in flat bones such as pelvis, ribs, scapula, and sternum.	Occurs at any age, but the majority of cases are diagnosed in the fifth, sixth and seventh decades of life with slight male predominance. The lesion cannot be radiographically differentiated from a highly malignant fibrosarcoma. May develop in abnormal bone such as Paget's disease and bone infarcts or secondary to radiation therapy.
Chondrosarcoma, central (Figs. 5.82, 5.83 and 5.84)	A slightly expansile, multilobulated osteolytic lesion with cortical thickening, endosteal erosion and scattered stippled or irregular calcifications is characteristic. Matrix calcification representing the most specific finding is only present in about two-thirds of the cases. Lesions without matrix calcifications are virtually impossible to differentiate from fibrosarcomas. Demonstration of a poorly defined osteolysis, cortical violation and large soft tissue mass indicate a highly aggressive lesion, but an interrupted periosteal reaction typically is absent. However more often a geographic destruction pattern is present suggesting a less malignant process. The tumor has a predilection for the metaphyses of the long tubular bones (especially femur and humerus) and flat bones (especially pelvis) and the vertebrae.	Occurs usually between 30 and 60 years of age with male predominance. The tumor arises either de novo in the medullary cavity or is caused by malignant transformation of an enchondroma. Low-grade chondrosarcomas are extremely difficult to differentiate from enchondromas. Irregular matrix calcifications (as opposed to punctate, ring and arc-like calcifications), large areas of noncalcified tumor matrix, poorly defined osteolysis and cortical thickening (even solid) suggest all malignancy.
Chondrosarcoma, peripheral (Figs. 5.85 and 5.86)	Malignant transformation of a benign osteochondroma is suggested by demonstration of scattered and irregular calcifications in the cartilaginous cap of the tumor, associated soft tissue mass (non-calcified cartilage cap) and destruction or pressure erosion of the adjacent bone. Differentiation of an osteochondroma from a peripheral chondrosarcoma is not reliably possible on the basis of conventional radiography and supplementation with other imaging techniques such as bone scintigraphy and MRI is required.	Local pain and growth of an osteochondroma in adulthood suggests clinically malignant transformation. The risk of malignant transformation is much higher in patients with hereditary multiple exostoses (estimated to be up to 25 %) than in a solitary osteochondroma (about 1 %) Rarely a peripheral chondrosarcoma develops de novo from the periost (*periosteal* or *juxtacortical chondrosarcoma*).

(continues on page 102)

Fig. 5.**80** **Malignant fibrous histiocytoma**. A highly aggressive permeative lesion involving the femoral head, neck, and intertrochanteric region without periosteal reaction is seen.

Fig. 5.**81** **Malignant fibrous histiocytoma**. A highly destructive lesion originating in the distal radius and extending into the distal ulna and carpal bones is seen.

Fig. 5.**82** **Central chondrosarcoma (low grade)**. A slightly expansile lesion with extensive stippled calcifications, and endosteal scalloping is seen in the proximal tibia diaphysis. This lesion cannot be differentiated radiographically from an enchondroma.

Fig. 5.**83** **Central chondrosarcoma**. A well to poorly demarcated osteolytic lesion with irregular matrix calcification and new cortical bone formation is seen in the proximal femur.

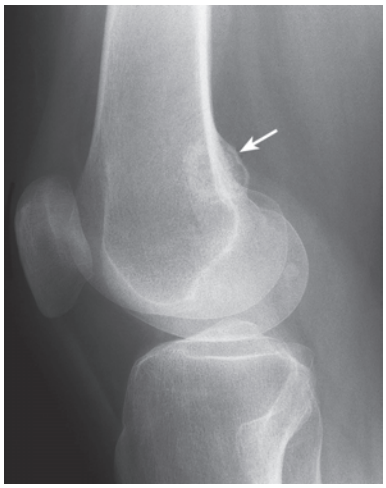

Fig. 5.**84** **Cortical chondrosarcoma (low grade)**. A small expansile cortical lesion (arrow) with faint matrix calcification and sclerotic margin originates from the posterior aspect of the distal femur metaphysis.

Fig. 5.**85** **Peripheral chondrosarcoma**. A broad-based bony protuberance with extensive irregular calcifications of the cartilaginous cap is seen originating from the posterior tibia metaphysis.

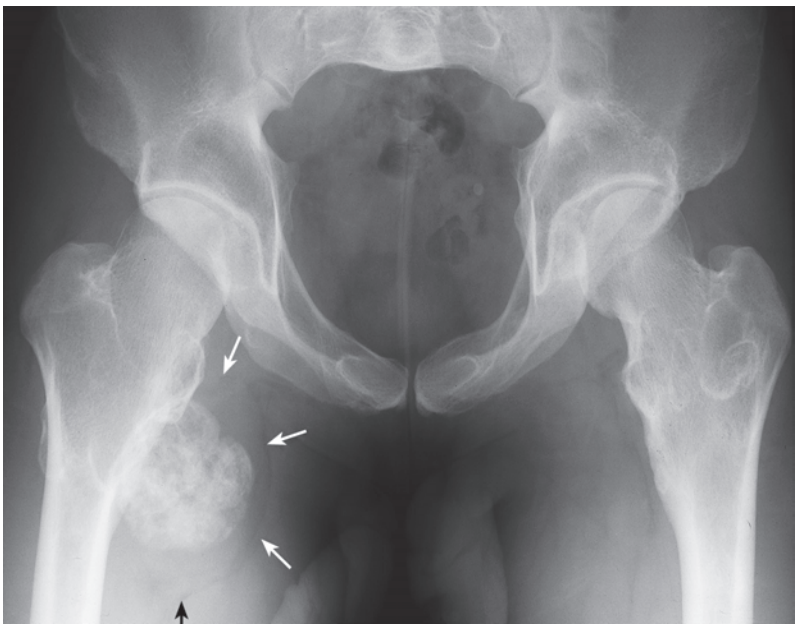

Fig. 5.**86** **Malignant transformation of osteochondroma in hereditary multiple exostoses.** Multiple exostoses with modeling deformities of the pelvis and both proximal femora is seen. The large exostosis originating beneath the right lesser trochanter with cartilage cap calcifications is associated with a soft mass (arrows) indicating malignant transformation.

Table 5.10 (Cont.) Localized bone lesions

Disease	Radiographic Findings	Comments
Clear cell chondrosarcoma (Fig. 5.87)	Poorly or well defined (sclerotic borders), slightly expansile epiphyseal lesion with central calcifications in about one-third of the cases is characteristic. Most frequent locations are the proximal ends of the femur, humerus and tibia.	Rare cartilaginous bone tumor occurring between 25 and 50 years of age with slight male predominance. Radiographic features are virtually identical to a chondroblastoma.
Dedifferentiated chondrosarcoma (Fig. 5.88 and 5.89)	Features of low-grade chondrosarcoma (nonexpansile osteolytic lesion with intact cortex and matrix calcifications) and of highly anaplastic sarcoma (expansile, poorly defined osteolytic lesion with cortical destruction and large soft tissue mass, but usually without calcification) are characteristic. The transition between these two tumor components is usually abrupt. Distribution of the tumor is similar to conventional chondrosarcoma with femur, humerus and pelvis being the most frequent sites of involvement.	Occurs in patients over 50 years of age without gender predilection. Presents with pain, soft tissue swelling or pathologic fracture (one-third of patients). The prognosis is very poor.
Mesenchymal chondrosarcoma (Fig. 5.90)	Features are indistinguishable from a high-grade conventional chondrosarcoma and include poorly defined osteolysis, matrix calcifications, cortical expansion and violation and soft tissue mass. Most frequent sites of involvement are femur, ribs and spine.	Occurs usually between 20 and 40 years of age and has a poor prognosis. Metastases to lymph nodes and other bones is not unusual. Approximately 50 percent of mesenchymal chondrosarcomas arise in the soft tissues.
Osteosarcoma (Figs. 5.91, 5.92, 5.93, and 5.94)	*Conventional osteosarcoma* presenting as a poorly defined intramedullary lesion most often originating in the metaphyses of long tubular bones with varying degrees of osteolysis and osteosclerosis is most characteristic. The tumor may however be purely osteolytic or osteoblastic. Cortical destruction associated with an interrupted periosteal reaction in the form of a Codman's triangle or with perpendicular ("hair-on-end" or "sunburst"), laminated ("onion skin") or amorphous appearance is most characteristic. Large soft tissue masses are commonly found in tumors with cortical violation. Most common sites of involvement are the long tubular bones (80 %), especially the femur, tibia and humerus. Osteosarcomas are relatively infrequent in the pelvis, spine and facial bones, and rare in the remaining skeleton. *Teleangiectatic osteosarcomas* commonly present as large, often expansile and predominantly lytic lesions, often with cortical violation and tumor extension into the soft tissues, but without significant periosteal reaction and sclerosis. *Small cell osteosarcomas* commonly present as large predominantly osteolytic lesions, extending from the metaphysis to the diaphysis of a long tubular bone associated with interrupted periosteal reaction and large soft tissue masses. They resemble Ewing's sarcomas. *Intraosseous low grade osteosarcomas* present as purely osteosclerotic and mixed osteolytic/osteoblastic lesions often limited to the medullary portion of the diametaphyses of long tubular bones, especially of the tibia and femur. Irregular cortical thickening may however be associated. The tumor is frequently mistaken for a benign osteosclerotic process.	Osteosarcomas most commonly present in the second and third decades of life with pain, swelling, restriction of motion and pyrexia. Men are more frequently affected than women. In the elderly they may be a complication of Paget's disease or radiation therapy. *Gnathic osteosarcomas* present as purely osteoblastic, osteolytic or mixed lesions in the mandible or less frequently maxilla, occur in the middle-aged and elderly, and have a relatively benign course. *Intracortical osteosarcomas* are rare and originate in the cortices of the tibia and femur, presenting as slightly expansile osteolytic lesions with surrounding sclerosis. *Osteosarcomatosis* refers to simultaneous involvement of more than one skeletal site. It has to be differentiated from a unicentric lesion with distal skeletal metastases.

(continues on page 104)

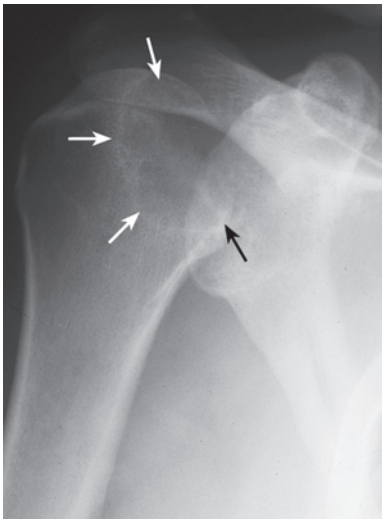

Fig. 5.**87** **Clear cell chondrosarcoma**. An ovoid osteolytic lesion (arrows) with slightly sclerotic border is seen in the humeral head.

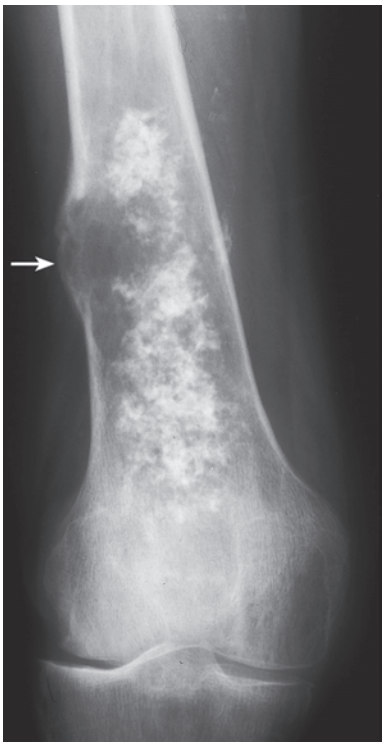

Fig. 5.**88** **Dedifferentiated chondrosarcoma**. A well-differentiated chondrosarcoma with extensive matrix calcification is seen in the distal femur associated with a poorly demarcated expansile osteolytic focus with cortical violation (arrow).

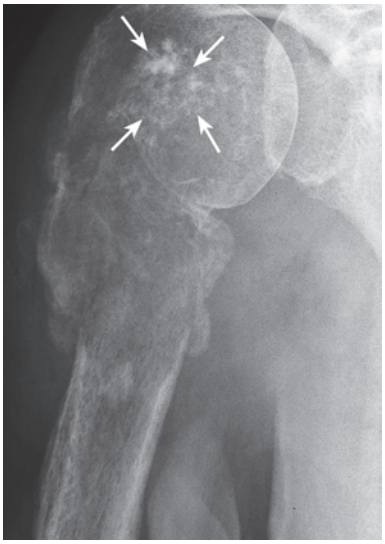

Fig. 5.**89** **Dedifferentiated chondrosarcoma**. A focus of punctate calcifications (arrows) in the humeral head is associated with a highly destructive permeative lesion with multiple pathologic fractures involving the proximal humerus shaft.

Fig. 5.**90** **Mesenchymal chondrosarcoma**. A highly destructive lesion with extensive irregular matrix calcification, cortical violation and large soft tissue mass is seen originating from the lateral aspect of the femoral neck and greater trochanter.

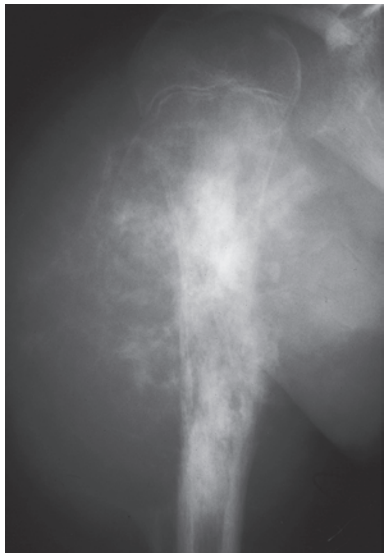

a

b

Fig. 5.**91 a**, **b** **Osteosarcoma (2 cases)**. A destructive osteoblastic lesion with extensive amorphous periosteal reaction and large soft tissue mass is seen in the proximal humerus shaft. A mixed, but predominantly osteolytic, relative poorly defined osteolytic lesion with cortical violation is seen in the distal femur.

Table 5.10 (Cont.) Localized bone lesions

Disease	Radiographic Findings	Comments
Periosteal osteosarcoma (Fig. 5.95)	Oblong dense lesion arising from the diaphyseal surface of a long tubular bone with irregular thickening and occasionally saucerization of the adjacent cortex is typical. A Codman's triangle and radiating or cloud-like osseous proliferation are frequently associated. Femur, tibia and humerus are the most common sites of involvement.	Usually diagnosed in the second and third decades of life with better prognosis than conventional osteosarcomas, but worse than parosteal osteosarcomas. Radiologic and histologic features of periosteal osteosarcomas and periosteal (juxtacortical) chondrosarcomas are similar if not identical. A *surface high-grade osteosarcoma* arises from the external surface of the cortex with clinical, histologic and radiologic features comparable to a conventional osteosarcoma.
Parosteal osteosarcoma (Fig. 5.96)	A large radiodense oval or round mass with smooth, lobulated, or irregular margins attached in sessile fashion to the external metaphyseal cortex of a long tubular bone is characteristic. A thin radiolucent line may separate the lesion outside its attachment (pedicle) from the cortex which itself may be thickened. With progressive enlargement the tumor tends to wrap around the bone. Ossification within the tumor proceeds from its base to the periphery and may be homogeneous or contain radiolucent areas. Tumor extension into the medullary bone is unusual. The most characteristic location is the posterior surface of the distal femur.	Most common type of osteosarcoma arising on the surface of a bone. Affected patients are adults most often in the third and fourth decades of life. Symptoms are typically insidious and include pain, swelling and a palpable mass. The prognosis is better than in both conventional and periosteal osteosarcomas. DD: *Post-traumatic myositis ossificans* (Figs. 5.**97** and 5.**98**) can be differentiated from a parosteal osteosarcoma by the demonstration of a fine radiolucent line separating the lesion in its entire length from the adjacent bone. Furthermore the ossification in myositis ossificans is evenly radiodense throughout the lesion and its periphery is sharply delineated.

(continues on page 106)

Fig. 5.**92 Osteosarcoma**. A poorly demarcated, mixed osteolytic and osteoblastic lesion is seen in the iliac wing.

Fig. 5.**93 Osteosarcoma**. A purely osteosclerotic lesion is seen in the distal femur consistent with a low-grade intraosseous osteosarcoma.

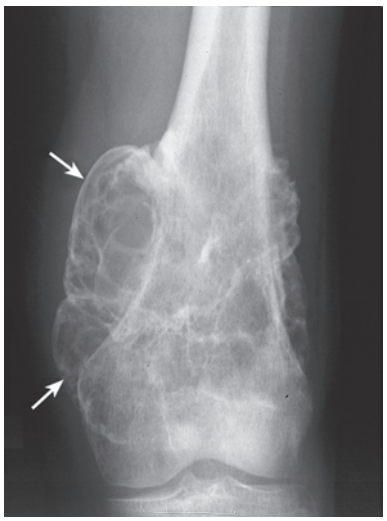

Fig. 5.**94 Telangiectatic osteosarcoma with aneurysmal bone cyst.** A poorly defined, slightly expansile, trabeculated, osteolytic lesion with cortical violation is associated with an aneurysmal bone cyst (arrows) presenting as better defined eccentric lesion with "soap-bubble" appearance.

Fig. 5.**95 Periosteal osteosarcoma.** An oblong dense soft tissue lesion arising from the posterior femur diaphysis with cloud-like and radiating osseous proliferation is seen.

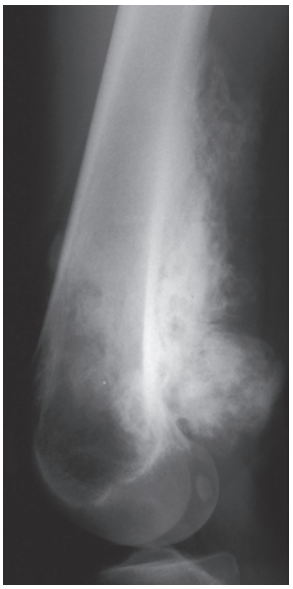

a

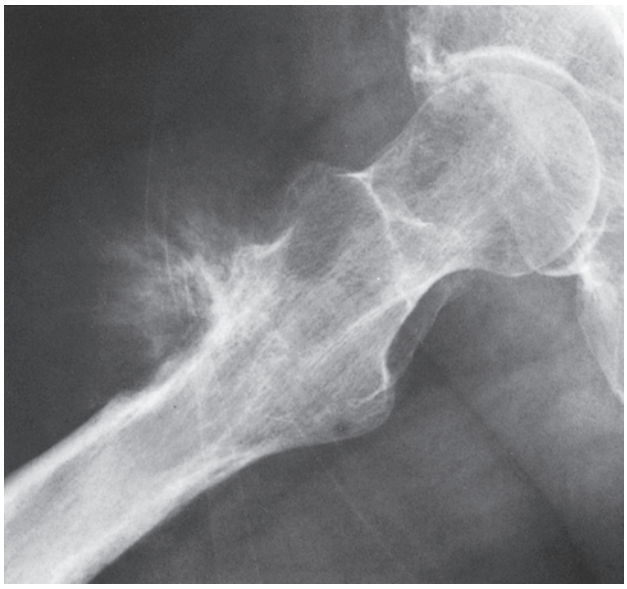

b

Fig. 5.**96 a**, **b** **Parosteal osteosarcoma (2 cases)**. **a**: A large heterogeneous ossified mass containing radiolucent areas originates from the posterior surface of the distal femur and wraps around the shaft causing the inhomogeneous appearance of the latter. The tumor periphery is irregular and poorly defined. **b**: A partly ossified mass is attached by a sclerotic stalk to the irregular anterior cortex of the femur in the subtrochanteric area. The tumor ossification is concentrated around its stalk and gradually fades out towards the tumor periphery.

Fig. 5.**97** **Posttraumatic myositis ossificans**. Following a complicated distal radius shaft fracture extensive heterotopic bone formation developed around the fracture site simulating a malignant osseous tumor.

Fig. 5.**98** **Posttraumatic myositis ossificans**. An ossified lesion with a complete rim of thin peripheral calcification ("eggshell calcification") is wrapping around the distal ulna. The lesion is separated in its entire length by a fine radiolucent line from the adjacent bone.

Table 5.10 (Cont.) Localized bone lesions

Disease	Radiographic Findings	Comments
Ewing sarcoma (Figs. 5.99, 5.100, 5.101, and 5.102)	A poorly defined osteolytic lesion with cortical violation and large soft tissue mass is characteristic. In tubular bones an interrupted periosteal reaction of the laminated ("onionskin") or less commonly perpendicular ("sunburst" or "hair-on-end") pattern is characteristically associated. Saucerization of the cortex is a rare but relatively characteristic manifestation of the disease. In flat and irregular bones osteosclerosis can be the dominant radiographic feature. The tumor can affect any bone, but has a predilection for the diametaphyses of long tubular bones and overall the lower half of the skeleton. The most common locations include femur, tibia, humerus, pelvis and sacrum.	Usually diagnosed between the ages of 5 and 30 years (peak 10 to 15 years) with slight male predominance. Involvement of the tubular bones occurs more often in children, whereas involvement of the flat bones is more commonly found in young adults. Patients present with localized pain and swelling occasionally combined with fever and leukocytosis. The tumor is rare in blacks. *Primitive neuroectodermal tumors (PNET)* (Fig. 5.**103**) have similar histologic and imaging features, but epiphyseal involvement, pathologic fractures, and distant metastases occur more frequently when compared to Ewing's sarcoma.
Angiosarcoma (Fig. 5.104)	Solitary or multiple, poorly or well demarcated lesions most commonly located in the medulla or cortex of long tubular bones, pelvis, spine and skull. Cortical thinning or violation and/or mild expansion without periostitis is occasionally associated.	Occurs in the fourth and fifth decades with male predominance. If multicentric it may simulate multiple myeloma, metastases, cystic angiomatosis, and cystic osteomyelitis (e.g. tuberculous or fungal). *Hemangioendothelioma* refers to a low-grade malignant angiosarcoma. *Hemangiopericytoma* is a borderline malignant tumor, with similar imaging features.
Plasmacytoma (Figs. 5.105 and 5.106)	Presents as an expansile trabeculated osteolytic lesion with cortical thinning and violation measuring up to several centimeters in diameter or as a well marginated purely osteolytic focus with endosteal scalloping. Rarely it may present as a sclerotic lesion (e.g. ivory vertebra). Most common locations are spine and pelvis. Complications in the spine include transdiscal tumor spread and pathologic fractures resulting sometimes in complete dissolution of a vertebral body.	Plasmacytoma may be considered a solitary manifestation of multiple myeloma with conversion to the latter occurring as late as 20 years after initial diagnosis. Plasmacytoma affects younger patients than multiple myeloma with about half the patients being 50 or younger at the time of diagnosis. It frequently presents with neurologic symptoms and radiographically may be mistaken for a giant cell tumor.

(continues on page 108)

Fig. 5.**99** **Ewing sarcoma**. A permeative osteolytic lesion with cortical violation and beginning laminated ("onionskin") periosteal reaction is seen in the proximal humerus shaft.

Fig. 5.**100** **Ewing sarcoma**. Extensive laminated ("onionskin") periosteal reaction and cortical tunneling is seen in the proximal femur shaft, while the permeative osteolytic lesion is barely perceptible.

Fig. 5.**101** **Ewing sarcoma**. A poorly demarcated mixed osteolytic and osteoblastic lesion involving the entire iliac wing is seen.

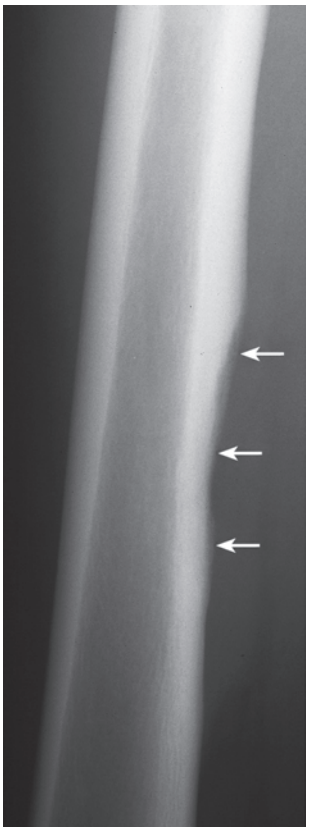

Fig. 5.**102** **Ewing sarcoma**. Saucerization of the femoral cortex (arrows) is the only manifestation of the disease in this case.

Fig. 5.**103** **Primitive neuroectodermal tumor (PNET)**. A poorly defined, mixed osteolytic and osteoblastic lesion in the distal tibia with cortical violation and beginning amorphous periosteal reaction on its lateral side and early laminated periosteal reaction on its medial side is seen.

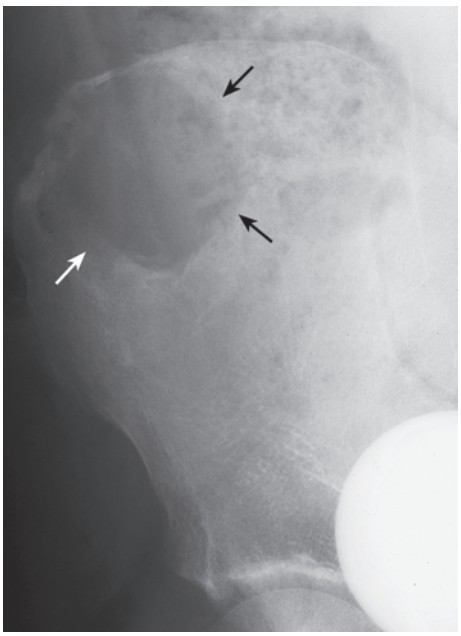

Fig. 5.**104** **Angiosarcoma**. A poorly demarcated osteolytic lesion (arrows) with cortical violation is seen in the ilium.

Fig. 5.**105** **Plasmacytoma**. An expansile osteolytic lesion with trabeculation is seen in the ilium.

Table 5.10 (Cont.) Localized bone lesions

Disease	Radiographic Findings	Comments
Multiple myeloma (Figs. 5.107, 5.108, 5.109, 5.110 and 5.111)	Multiple well marginated ("punched out") or poorly delineated osteolytic lesions of relatively uniform size are characteristic. Endosteal scalloping is typically present with larger lesions in the long tubular bones. Diffuse osteopenia without well-defined areas of osteolysis is another common presentation. Periosteal new bone formation is exceedingly rare. Focal or multiple sclerotic lesions are an unusual initial presentation, but may develop after chemotherapy, irradiation or pathologic fracture. Preferred locations in order of decreasing frequency are spine, ribs, skull, pelvis, long tubular bones, and clavicles (distal end). Spine: Preferential osteolytic destruction of the vertebral bodies, sometimes associated with irregular thickening of the remaining vertebral trabeculae, relative sparing of the posterior elements, scalloping of the anterior margins of the vertebral bodies (pressure erosions from adjacent soft tissue lesions), and paraspinal or extradural tumor extension are common. Pathologic compression fractures are a frequent complication.	Occurs in patients over 40 years of age with male predominance, presenting with bone pain, anemia, hypercalcemia, proteinuria (including Bence-Jones proteins), and monoclonal gammopathy (high erythrocyte sedimentation rate, abnormal electrophoresis). *Waldenström's macroglobulinemia* presents with similar clinical and radiographic findings but the radiographic features are usually less conspicuous.

(continues on page 110)

Fig. 5.**106** **Plasmacytoma**. An expansile trabeculated osteolytic lesion ("soap bubble appearance") originating from the scapular spine is seen.

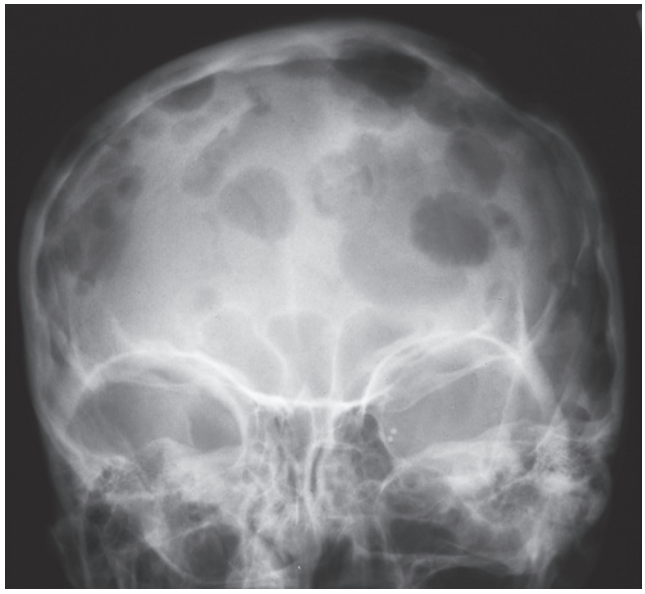

Fig. 5.**107** **Multiple myeloma**. Multiple well-demarcated ("punched-out") osteolytic lesions are seen in the vault of the skull.

◁ Fig. 5.**108** **Multiple myeloma**. Innumerable well-defined osteolytic lesions of relatively uniform size are seen scattered throughout the humerus and the visualized part of the scapula.

Fig. 5.**109** **Multiple myeloma**. Numerous well to poorly defined osteolytic lesions are scattered throughout the pelvis and proximal femora.

Fig. 5.**110** **Multiple myeloma**. Patchy osteopenia and tiny foci of increased bone density are evident throughout the thoraco-lumbar spine besides several compression fractures.

Fig. 5.**111** **Multiple myeloma**. Osteopenia with a prominent vertical trabecular pattern ("corduroy" appearance) is seen in all vertebral bodies of the lumbar spine.

Table 5.10 (Cont.) Localized bone lesions

Disease	Radiographic Findings	Comments
Metastases (Figs. 5.112, 5.113, 5.114, 5.115, and 5.116)	Solitary, or more commonly, multiple osteolytic, osteoblastic or mixed osteolytic-osteoblastic lesions with preferential involvement of the red marrow containing skeleton (spine, pelvis, ribs, skull, femora and humeri) is characteristic. Osteolytic metastases may be well or poorly marginated. Osteoblastic metastases may be focal or diffuse. In the spine, besides the vertebral bodies, the posterior elements including the pedicles are frequently also involved (DD multiple myeloma). Purely osteolytic metastases commonly arise from carcinomas of lung, kidney, thyroid and lymphoma. Purely osteoblastic metastases are most often associated with prostatic and breast carcinomas, but also with Hodgkin's lymphoma, carcinoids and medulloblastomas. Periosteal reactions are highly unusual in metastatic disease except in prostatic and breast carcinomas, gastrointestinal malignancies and neuroblastomas. Neither osseous expansion nor soft tissue masses are typically associated with bone metastases except in rib lesions, osteolytic metastases from carcinomas originating in the kidney, thyroid, lung and liver and osteoblastic metastases from prostatic and breast carcinomas. One or more sclerotic vertebral body (ivory vertebra) is most often caused by prostatic or breast carcinoma metastases, but also found with Hodgkin's lymphoma and Paget's disease. Pathologic fractures are a frequent complication, especially in the spine. Response of an osteolytic metastasis to treatment (e.g. chemotherapy or radiation therapy) is evident by progressive sclerosis proceeding from the periphery towards the center of the lesion with eventual reduction in size or disappearance of the osteolytic focus. The appearance of osteosclerotic foci during therapy is usually caused by progression of the disease, but may also indicate a healing response of pre-existing osteolytic metastases that could initially not be identified on radiographs. A positive treatment response of osteoblastic lesion is evident by decrease and eventual disappearance of the sclerotic focus.	Bone metastases are by far the most common skeletal malignancy occurring either by hematogenous spread or direct tumor extension. They most frequently originate from carcinomas of breast, prostate, lung, kidney, thyroid and gastrointestinal tract. Breast carcinoma metastases tend to be mixed, or, less commonly purely osteolytic or osteoblastic, often extensive and frequently associated with pathologic fractures. Prostate carcinoma metastases are characteristically osteoblastic, may be expansile (simulating Paget's disease) or associated with periostitis. Bronchogenic carcinoma metastases are typically osteolytic or mixed and occasionally expansile. An eccentric erosion of the external cortex of a long tubular bone ("cookie-bite" sign) is rare, but quite characteristic for a bronchogenic carcinoma metastasis manifestation. Kidney and thyroid carcinoma metastases are often solitary, purely osteolytic lesions that may be expansile and depict a septated (bubbly) appearance. Gastrointestinal tract metastases cover the whole spectrum from purely osteolytic to purely osteoblastic. Metastases from colon or rectum carcinoma may occasionally resemble an osteosarcoma and depict a sunburst periosteal reaction. Metastatic bone disease with unknown primary most often originates from prostate, lymphoma, breast, lung, kidney, thyroid or colon.

(continues on page 112)

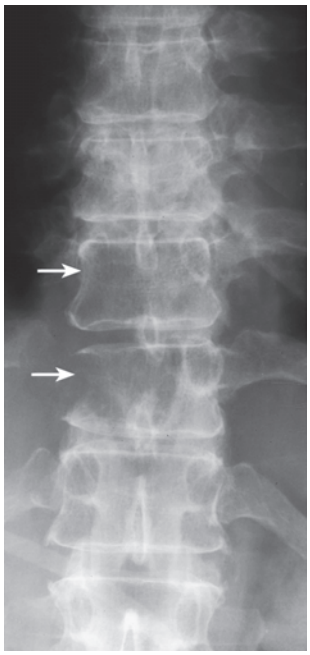

Fig. 5.**112 Metastases from bronchogenic carcinoma**. Scattered predominantly osteolytic metastases are seen in the thoracic spine with main involvement of the right pedicles and posterior elements of T10 and T11 (arrows) producing an "empty vertebral box" sign on that side.

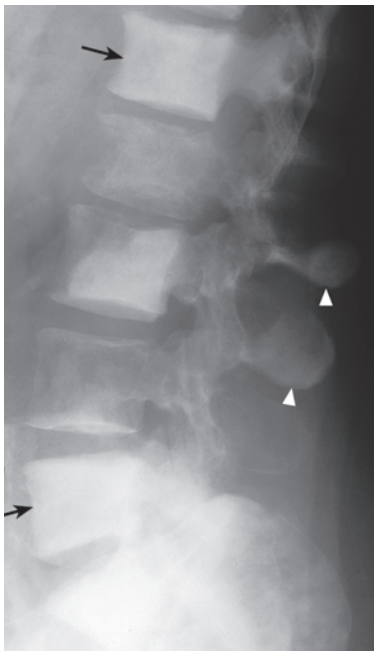

Fig. 5.**113 Metastases from breast carcinoma**. Predominantly osteoblastic metastases involving all vertebral bodies including the posterior elements of the lumbar spine. Ivory vertebrae are seen at L1 and L5 (arrows). Osteoblastic foci (arrowheads) are evident in the spinous processes of L2 and L3.

Fig. 5.**114** **Metastases from prostatic carcinoma**. Multiple bilateral expansile and purely osteoblastic metastases originating from the ribs are seen.

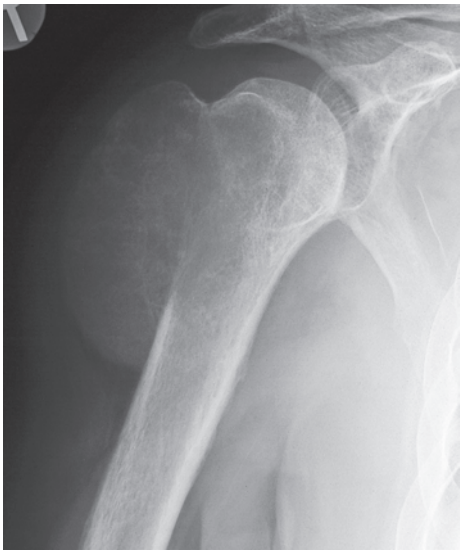

a

b

Fig. 5.**115 a**, **b** **Metastasis from renal cell carcinoma before (a) and after (b) radiation therapy**. A purely lytic, markedly expansile ("blow-out") lesion is seen originating from the dorsal aspect of the proximal humerus shaft (**a**). After radiation therapy the lesion became partially ossified depicting a trabeculated pattern and a well-demarcated sclerotic margin (**b**).

Fig. 5.**116** **Cortical metastases from bronchogenic carcinoma**. Multiple purely osteolytic lesions are seen in the cortex of the tibia. The largest lesion located posteriorly has broken through the cortex on both its inner and outer surface.

Table 5.10 (Cont.) Localized bone lesions

Disease	Radiographic Findings	Comments
Lymphoma (Figs. 5.117, 5.118, 5.119, 5.110 and 5.121)	Preferential sites of involvement include spine, pelvis, scapula and ribs. In long tubular bones involvement of the diametaphyses of the femur and tibia about the knee is most common. *Non-Hodgkin lymphoma* typically presents as solitary or, more often, multiple poorly defined osteolytic lesions. *Histiocytic lymphoma* (primary or secondary) frequently has a mixed osteolytic-osteoblastic appearance and may resemble Paget's disease without bony expansion. Purely osteoblastic lesions are uncommon in non-Hodgkin's lymphoma. *Hodgkin's disease* of the bone is always caused by secondary involvement. Its presentation ranges from purely osteolytic to purely osteoblastic lesions. Diffuse sclerosis of a vertebral body (ivory vertebra) is not an unusual manifestation. Osteolytic lesions tend to be poorly defined and are associated with periostitis in one-third of the cases.	Secondary involvement of bone caused by hematogenous spread or, less frequently, by direct invasion occurs in one-third of patients with non-Hodgkin's lymphoma and in 10 % with Hodgkin's disease. Primary bone lymphoma is much less common, accounts for approximately 5 % of all primary malignant bone tumors, is usually of the histiocytic-type (previously called reticulum cell sarcoma), and typically occurs in older patients with a 2:1 male predominance. *Burkitt's lymphoma* presents as expansile osteolytic lesions associated with a soft tissue mass. Involvement of the facial bones (especially the maxilla) is most characteristic in children of tropical Africa. Nonendemic Burkitt's lymphoma may be associated with immune dysfunction (e.g., organ transplantation and AIDS). *Mycosis fungoides* is a T-cell lymphoma with primary involvement of the skin. Discrete or poorly defined osteolytic lesions may be associated in the appendicular skeleton.
Leukemia (Figs. 5.122, 5.123 and 5.124)	Diffuse osteopenia with medullary widening and cortical thinning in tubular bones and vertebral compressions are the most common presentation. Moth-eaten or permeative osteolysis may be found in both tubular and flat bones. Radiolucent and/or radiodense metaphyseal bands, as well as periosteal new bone formation are particularly common in children. Complications may include intra-articular and subperiosteal hemorrhages, septic arthritis, osteomyelitis, osteonecrosis and secondary gout. *Granulocytic sarcomas (chloromas)* present as single or multiple, often expansile lytic lesions in the skull, spine, ribs, sternum and long tubular bones, usually in acute myelogenic leukemia.	Leukemias are classified based on cell maturity (acute with immature or blastic cells versus chronic with mature cells), cell morphology (myeloid versus lymphoid) or cell origin (thymus-derived T-cells versus blood marrow derived B-cells). Skeletal abnormalities are similar for all forms of leukemias, but are most common in acute childhood leukemias, where they occur in over 50 % of cases, and least common in chronic leukemias.

(continues on page 114)

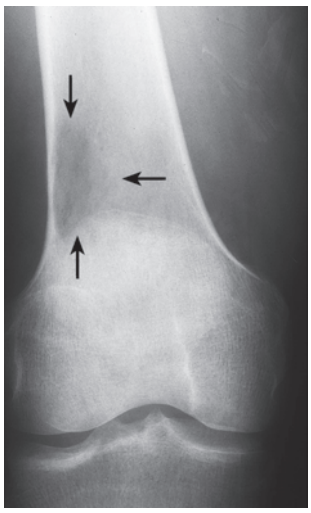

Fig. 5.**117** **Non-Hodgkin lymphoma**. A poorly defined (moth-eaten) osteolytic lesion (arrows) is seen in the distal femur.

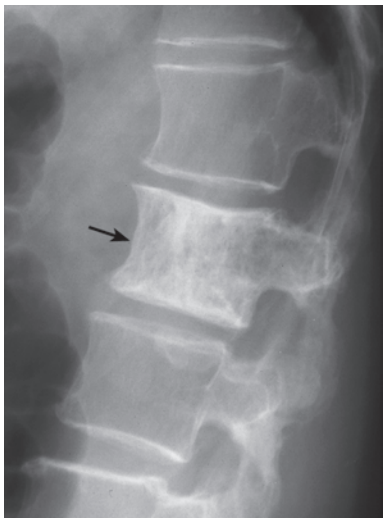

Fig. 5.**118** **Non-Hodgkin lymphoma (histiocytic type)**. A mixed osteolytic and osteoblastic lesion with coarse irregular predominantly vertical trabeculation involving both the vertebral body and pedicles of L2 (arrow) is seen.

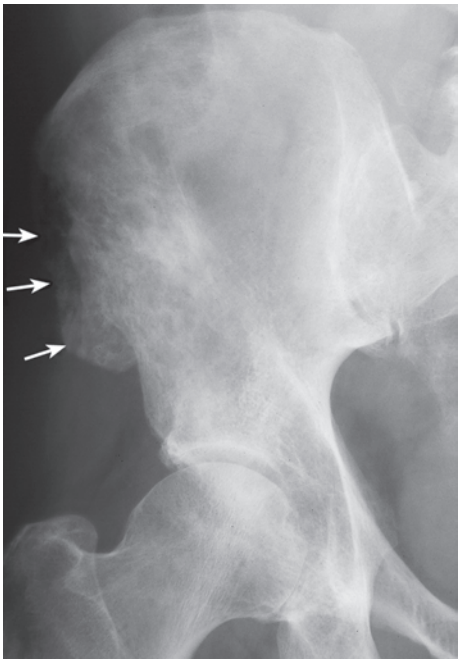

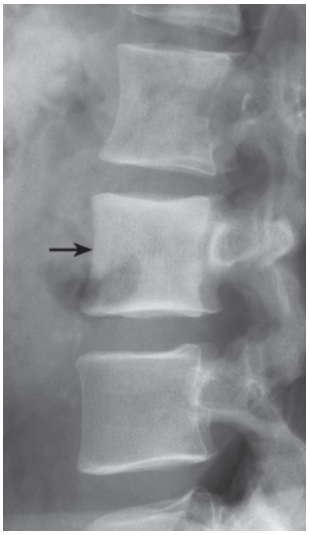

Fig. 5.**120** **Hodgkin's disease**. An ivory vertebral body is seen at L3 (arrow).

◁ Fig. 5.**119** **Non-Hodgkin lymphoma (histiocytic type)**. A mixed osteolytic and osteoblastic lesion is seen in the ilium. The lesion differs from Paget's disease by the absence of enlargement of the involved bone. Furthermore cortical violation (arrows) is also evident in this particular case.

Fig. 5.**121** **Hodgkin's disease**. Several relatively poorly defined osteoblastic lesions are seen in the distal femur and the proximal tibia and fibula.

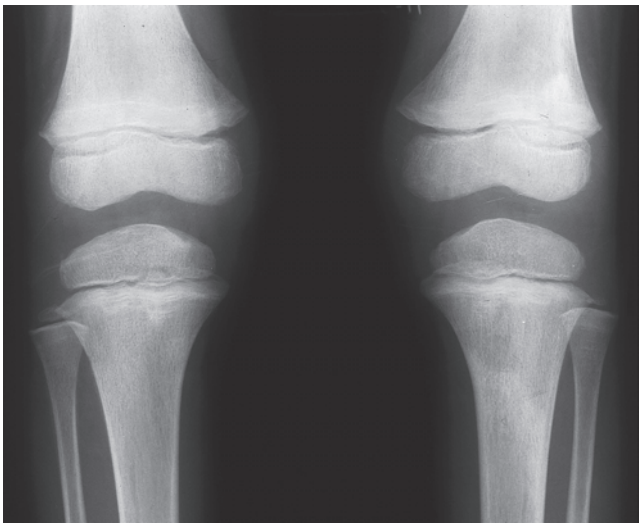

Fig. 5.**122** **Leukemia**. Sclerotic bands traversing all metaphyses about both knees are seen in this child.

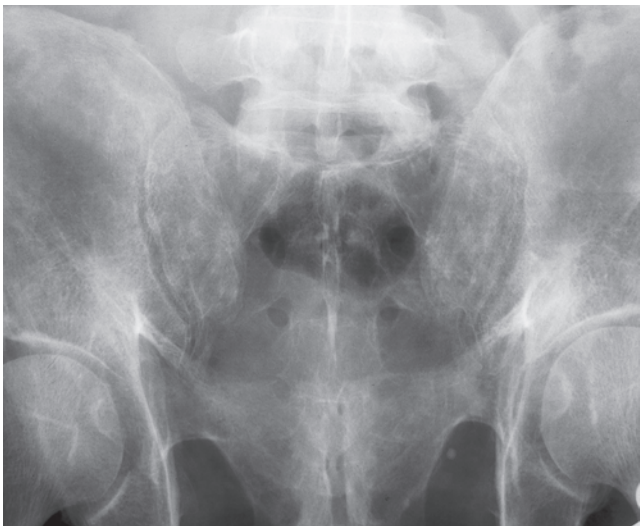

Fig. 5.**123** **Leukemia**. Innumerable tiny and poorly defined osteolytic and osteoblastic foci are scattered throughout the pelvis.

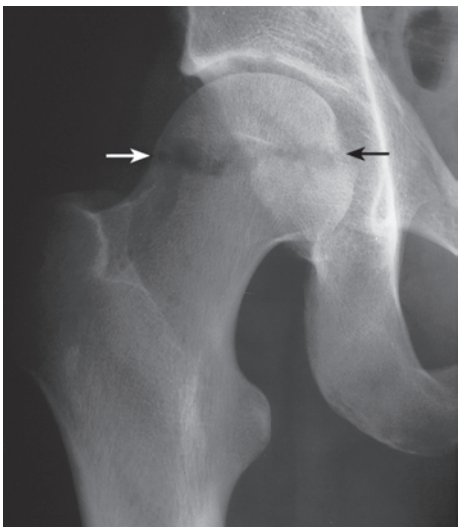

Fig. 5.**124** **Granulocytic sarcoma (chloroma)**. A barely perceptive permeative osteolytic lesion with pathologic fracture (arrows) is seen involving the femoral head and neck.

Table 5.10 (Cont.) Localized bone lesions

Disease	Radiographic Findings	Comments
Langerhans cell histiocytosis (Figs. 5.125, 5.126 and 5.127)	*Eosinophilic granuloma* presents as solitary or, less commonly, multiple lesions with preferential involvement of skull, mandible, spine, ribs and the diametaphyses (rarely epiphyses) of long tubular bones. Relatively well defined radiolucent areas with endosteal scalloping with or without slight bone expansion and periosteal new bone formation are typical in the long bones and may mimic osteomyelitis or even Ewing's sarcoma. Well-defined lytic lesions with or without sclerotic borders may be found in the skull and pelvis. A radiodense focus (button sequestrum) is frequently observed in skull lesions. Larger osteolytic areas in the skull typically depict beveled edges caused by the uneven destruction of the inner and outer tables. In the mandible radiolucent lesions about the teeth may lead to the "floating teeth" appearance. In the spine a collapsed vertebral body (vertebra plana) with intact intervertebral spaces or, less frequently, a lytic and occasionally slightly expansile lesion involving the vertebral body and/or the posterior elements may be found.	Langerhans cell histiocytosis comprises three major conditions. 1. *Eosinophilic granuloma* is both the most common and most benign variant representing approximately 70 % of cases. It is usually diagnosed between the age of 5 and 20. 2. *Hand-Schüller-Christian disease* is characterized by the triad of exophthalmos, diabetes insipidus and large lytic skull lesions ("geographic skull"). 3. *Letterer-Siwe disease* is the acute disseminated variant in children under age 2. Bone lesions are less common, but may include multiple widespread lytic lesions in the skull ("raindrop" pattern). Spontaneous healing of a solitary lesion occurs, typically progressing from the periphery towards its center and eventually resulting in its disappearance or transformation into a sclerotic focus.
Amyloidosis (Fig. 5.128)	Osteolytic lesions of variable size with endosteal scalloping simulating multiple myeloma preferentially located in the proximal humerus or proximal femur is the most common presentation. Subchondral amyloid deposition may result in avascular necrosis. Pathologic fractures are a relatively common complication. Subchondral cyst formation and erosions in the hand and wrist associated with periarticular or diffuse osteoporosis may simulate rheumatoid arthritis, although extensive nodular soft tissue masses, well-defined cystic lesions with or without surrounding sclerosis and preservation of the joint space are more characteristic for amyloidosis.	Musculoskeletal abnormalities are the result of amyloid deposition in bone, synovium and soft tissue. *Primary amyloidosis* occurs in patients above the age of 40 with male predominance. It may be associated with multiple myeloma. *Secondary amyloidosis* is associated with chronic renal disease, rheumatoid arthritis, lupus erythematosus, ulcerative colitis, chronic suppurative disease, and lymphoproliferative disorders.
Brown tumor in hyperparathyroidism (Fig. 5.129)	Single or multiple, occasionally expansile, well to poorly defined osteolytic lesions of the axial and appendicular skeleton. Eccentric or cortical location is not unusual. Common sites of involvement are facial bones, pelvis, ribs and femora. They may undergo necrosis and liquefaction producing cysts, or with proper treatment (removal of the parathyroid adenoma) become increasingly sclerotic.	Brown tumors are more commonly associated with primary than secondary hyperparathyroidism. Other manifestations of hyperparathyroidism are usually also apparent and include osteopenia, subperiosteal, endosteal and subchondral bone resorption, intracortical tunneling, chondrocalcinosis, and para-articular and vascular calcifications. Bone sclerosis is common in secondary hyperparathyroidism.

(continues on page 116)

Fig. 5.**125 Eosinophilic granuloma**. An irregular, relatively well-defined osteolytic lesion with minimal endosteal scalloping, slight bone expansion and beginning periosteal reaction on its anterior margin is seen in the proximal radius shaft.

Fig. 5.**126 Eosinophilic granuloma**. A well defined, trabeculated osteolytic lesion with sclerotic margin and cortical violation is seen in the ilium.

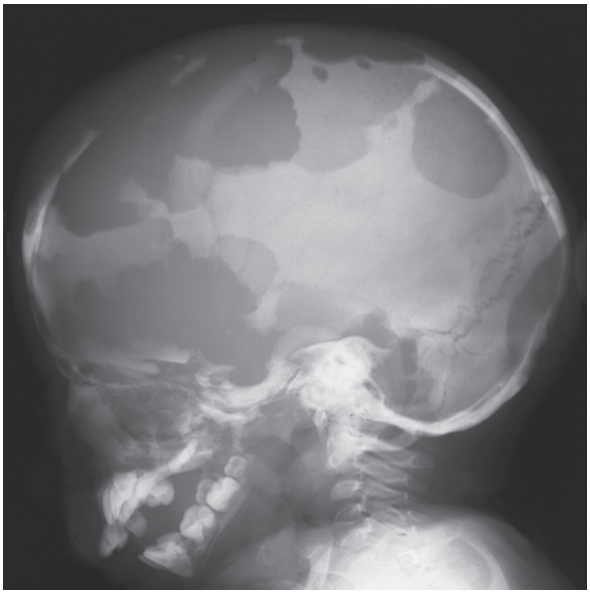

Fig. 5.**127** **Hand-Schüller-Christian disease**. Large, well-demarcated osteolytic lesions are seen in the vault of the cranium giving the appearance of a continental map ("geographic skull").

a

b

Fig. 5.**128 a**, **b** **Amyloidosis (2 cases)**. A large well-demarcated osteolytic lesion with endosteal scalloping is seen in the proximal femur shaft in this patient with multiple myeloma (**a**). A similar lesion is present in the second patient with chrome renal failure (**b**).

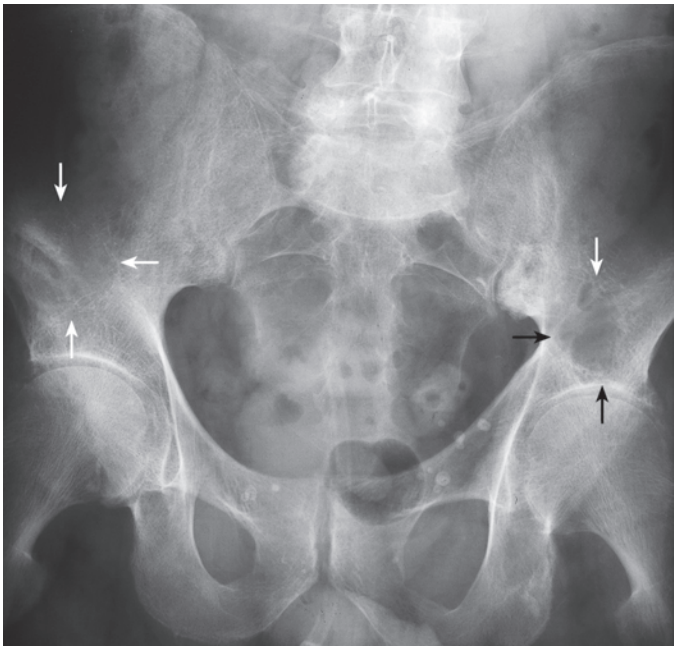

a

b

Fig. 5.**129 a**, **b** **Brown tumors in primary hyperparathyroidism**. Multiple poorly to well defined osteolytic lesions, some with trabeculation, are seen in the pelvis (arrows) and tibia. Most tibial lesions are cortical based (**a**: pelvis, **b**: tibia).

Table 5.10 (Cont.) Localized bone lesions

Disease	Radiographic Findings	Comments
Hemophilic pseudotumor (Figs. 5.130 and 5.131)	Central (intraosseous) or eccentric (subperiosteal), well-demarcated osteolytic lesion, are often associated with either solid or interrupted periosteal reaction and a large soft tissue mass. Minimal to massive calcification within the lesion is occasionally also encountered. Rarely, more than one bone contains a pseudotumor. Preferred locations are pelvis, femur, tibia and hand.	Lesions are late sequelae of intramedullary or periosteal hemorrhage occurring in fewer than 2 % of hemophiliacs. Hemophilic arthropathy including dense joint effusions and joint contractures, avascular necrosis, especially of the femoral head and talus, spontaneous fractures and soft tissue hematomas may also be evident.
Intraosseous tophus in gout (Fig. 5.132)	One or more cystic lesions often with partial calcification may be found in the subchondral and deeper osseous areas simulating enchondromas. Larger intraosseous calcifications may mimic bone infarcts. These findings are most frequently seen is the hands and feet. Association with characteristic findings of gouty arthropathy is diagnostic.	Occurs in approximately 5 % of patients with chronic gouty arthritis. Intraosseous urate deposition with subsequent calcifications usually originate from the adjacent joint, penetrate the cartilaginous surface and extend into the adjacent spongiosa.
Osteonecrosis (bone infarct and avascular necrosis) (Figs. 5.133, 5.134, 5.135 and 5.136)	Early signs are nonspecific and include mottled osteopenia, poorly defined osteolytic lesion(s), or patchy osteopenic and sclerotic areas. Findings are however more characteristic in an advanced late stage. In the diametaphyses they include a serpiginous peripheral rim of sclerosis surrounding an oblong area of bone rarefaction. Periostitis and matrix calcifications are frequently associated. Intramedullary calcifications are often the only finding and are typically shell-like whereas the calcifications in chondroid matrix tumors tend to be irregular and central and are surrounded by a rim of noncalcified, often slightly radiolucent tumor matrix. Solid periosteal reactions and cortical thickening may be associated with both conditions, but in the case of chondroid matrix tumor suggest a low-grade chondrosarcoma rather than enchondroma. Typical findings of osteonecrosis in the epiphyses include subchondral cyst(s) with sclerotic rim, arc-like subchondral radiolucency (crescent sign), subchondral fragmentation and eventually collapse of the articular surface, with considerable sclerosis and secondary degenerative changes in the affected joint.	Osteonecrosis can be divided in bone infarction, occurring more frequently in the metadiaphyseal regions of long bones (e.g. femur, humerus, and tibia) than in the axial skeleton and in avascular necrosis involving the subarticular bone. Solitary bone infarcts are frequently diagnosed as an incidental finding. Osteonecrosis may be idiopathic (25 %) or associated with hematological and reticuloendothelial diseases (e.g. *sickle cell* and *Gaucher's disease*), collagen vascular diseases (e.g. *lupus erythematosus*), trauma (e.g. *subcapital hip fracture*), *renal transplantation*, *alcoholism*, *steroid use*, *pancreatitis*, *gout*, *irradiation* and *caisson disease*. *Radiation osteitis (osteonecrosis)* presents with a mixture of osteopenia, osteosclerosis and coarse trabeculation. Round to ovoid radiolucent lesions within the cortex of long tubular bones are quite characteristic as opposed to endosteal scalloping caused by tumor recurrence. Bony changes are dose-dependent with a minimal dose of 3000 cGy required and occur at the earliest one year after irradiation, at a time, when a nuclear medicine scan does longer depict an increased uptake. *Calcified intraosseous hematomas* may present radiographically similar to a calcified bone infarct.

(continues on page 118)

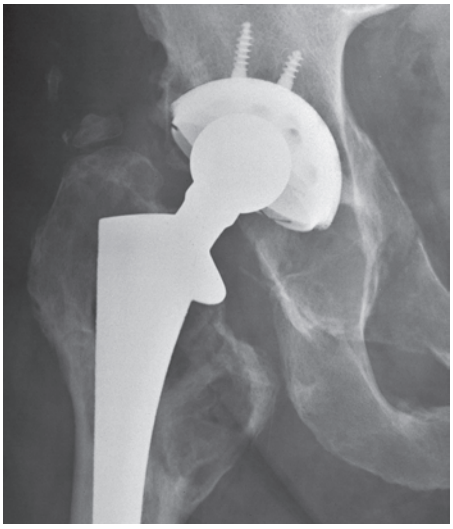

Fig. 5.**130** **Hemophilic pseudotumor**. Expansile osteolytic lesion with trabeculation developed in the greater and lesser trochanter as well as in the ischium and pubic bone adjacent to the components of the total hip prosthesis inserted 12 years earlier.

Fig. 5.**131** **Hemophilic pseudotumor**. A large expansile osteolytic lesion surrounded by a thin rim of solid new bone formation (arrows) and containing extensive central calcifications is seen in the ilium.

Fig. 5.**132** **Intraosseous tophi in gout**. Well-demarcated osteolytic lesions with faint calcifications are seen in the fourth and fifth finger resembling enchondromas.

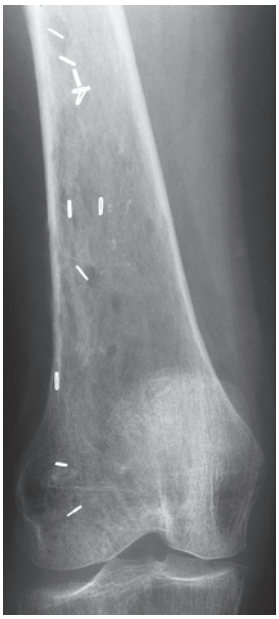

Fig. 5.**133** **Osteonecrosis (bone infarct)**. Patchy demineralization and poorly defined osteolytic lesions seen in the distal femur are the earliest radiographic findings in osteonecrosis.

Fig. 5.**134** **Osteonecrosis (bone infarct)**. An oblong shell-like calcification is seen in the distal tibia. A healing distal fibula fracture and a posttraumatic osteochondral defect in the medial talar dome are also present.

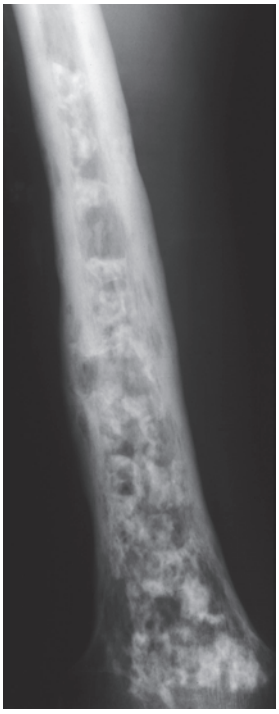

Fig. 5.**135** **Radiation osteonecrosis**. Extensive bone infarction limited to the field of irradiation is diagnostic. Findings include widespread calcifications in the medulla and irregular cortical thickening with numerous round to oblong intracortical lucencies.

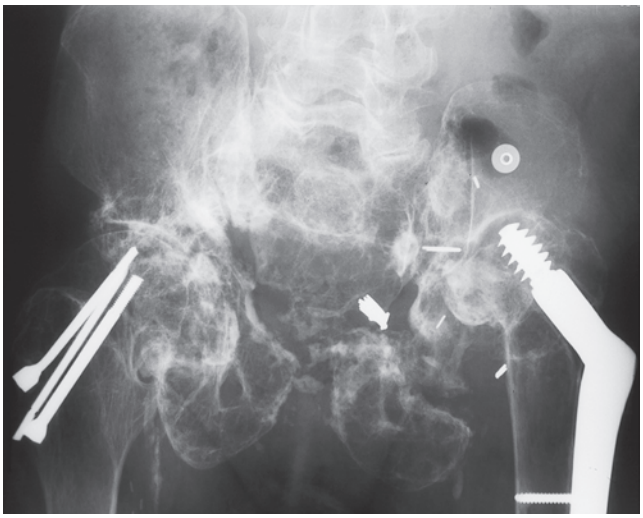

Fig. 5.**136** **Radiation osteonecrosis**. A dysplastic osteopenic pelvis with extensive calcifications and numerous pathologic fractures and bilateral avascular necrosis of the femoral heads are the consequences of pelvic irradiation during childhood.

Table 5.10 (Cont.) Localized bone lesions

Disease	Radiographic Findings	Comments
Healing or healed fracture and stress fracture (Figs. 5.137 and 5.138)	Osteosclerosis and callus formation may simulate chronic osteomyelitis or an osteoid osteoma, respectively. Demonstration of a fracture line in an area of localized elliptical cortical thickening of a long tubular bone (as opposed to a round or ovoid intracortical abscess or nidus) is diagnostic.	In the absence of proper clinical information a healed fracture resulting in localized bony expansion and deformities can at times be difficult to differentiate from fibrous dysplasia.
Pigmented villonodular synovitis (PVNS) (Fig. 5.139)	Subchondral pressure erosions may be found at margins of "tight" joints such as hip, ankle, and wrist. They are caused by an often slightly dense appearing soft tissue mass due to hemosiderin deposition in both the effusion and synovial proliferation. Calcifications, osteoporosis and joint space narrowing are typically absent. Pressure erosions in the knee (most commonly involved joint) are uncommon.	Monoarticular proliferative synovial disorder presenting with insidious onset of swelling, pain of long duration and decreased range of motion occurring typically in young adults. A hemorrhagic (chocolate-brown) joint effusion in the absence of trauma is characteristic.
Osteomyelitis (acute) (Figs. 5.140, 5.141 and 5.142)	*Hematogenous osteomyelitis* presents initially in the medullary space with focal osteoporosis, endosteal scalloping, and osteolysis due to hyperemia, edema, abscess formation and trabecular destruction. Progression of the disease to the Haversian and Volkmann's canals results in cortical fissuring with subsequent destruction and subperiosteal abscess formation. A periosteal reaction (laminated or, less commonly, spiculated) is a characteristic finding at this stage. After one month, a sequestration (detached necrotic cortical bone presenting as radiodense bony spicule surrounded by granulation tissue and newly formed cortical bone (involucrum) may be evident. An opening in the involucrum is termed a cloaca. Sinus tracts leading to the skin surface are often evident. Occasionally intraosseous gas may be seen. In both infants and adults extension of the disease process into the adjacent joint is common whereas in childhood (1–16 years of age) the open growth plate represents an effective barrier to the spread of the infection from the metaphysis to the epiphysis and joint, respectively. *Osteomyelitis from a contiguous soft tissue infection* typically presents as focal osteoporosis due to edema with subsequent cortical erosion. Periostitis is another less frequent initial finding. Cortical destruction and bone marrow infection with abscess formation may ensue.	Affects all ages but is commonly found in children, diabetics, and intravenous drug abusers. Occurs by hematogenous route, spread from contiguous infection or direct implantation (punctures, penetrating injury and postoperative infection). Pyogenic osteomyelitis in children is most often caused by staphylococcus aureus, streptococci, escherichia coli, and hemophilus influenzae. Gram-negative organisms are not uncommon in adults and intravenous drug abusers. *Tuberculous osteomyelitis* (Figs. 5.**143** and 5.**144**) arises most commonly secondary to septic arthritis. Spinal involvement accounts for approximately 50 % of skeletal tuberculosis. Compared to pyogenic osteomyelitis osteoporosis is more pronounced, whereas new bone formation is less extensive. *Tuberculous dactylitis* ("spina ventosa") (Fig. 5.**145**) refers to cystic expansion of the short tubular bones of the hands and feet with varying degrees of periostitis. *Cystic tuberculosis* presents as one or multiple well-defined osteolytic foci without sclerosis preferentially in the peripheral skeleton. *Fungal osteomyelitis* (Fig. 5.**146**) resembles a tuberculous infection. Solitary or multiple osteolytic lesions with discrete margins, mild surrounding sclerosis and little or no periosteal reaction are a common presentation.

(continues on page 120)

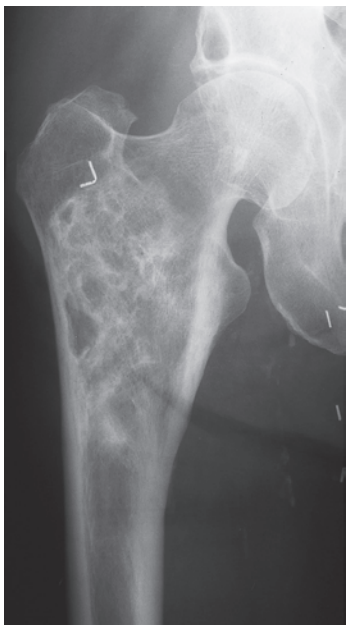

Fig. 5.**137 Healed fracture**. A widened proximal femur shaft with mixed osteolytic and osteoblastic texture is seen mimicking fibrous dysplasia. An ovoid subchondral cyst is incidentally seen in the lateral aspect of the acetabular roof.

Fig. 5.**138 Healed stress fracture**. A localized elliptical cortical thickening is seen in the medial aspect of the proximal femur shaft.

Fig. 5.**139** **Pigmented villonodular synovitis**. Several well-demarcated defects (pressure erosions) are seen in the lateral aspect of the femoral neck and head as well as in the acetabulum where they induced a reactive sclerosis.

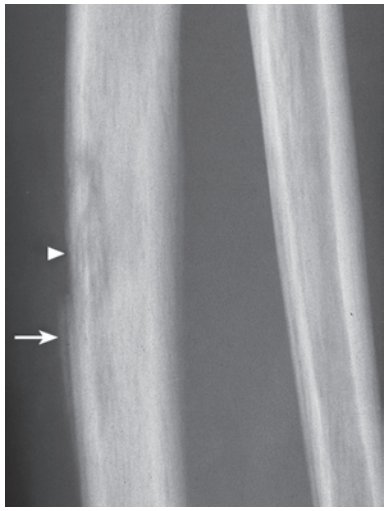

Fig. 5.**140** **Acute osteomyelitis**. Patchy demineralization, and beginning endosteal scalloping, cortical fissuring (arrowhead) and laminated periosteal reaction (arrow) are seen in the radius shaft representing the earliest radiographic manifestations of acute hematogenous osteomyelitis.

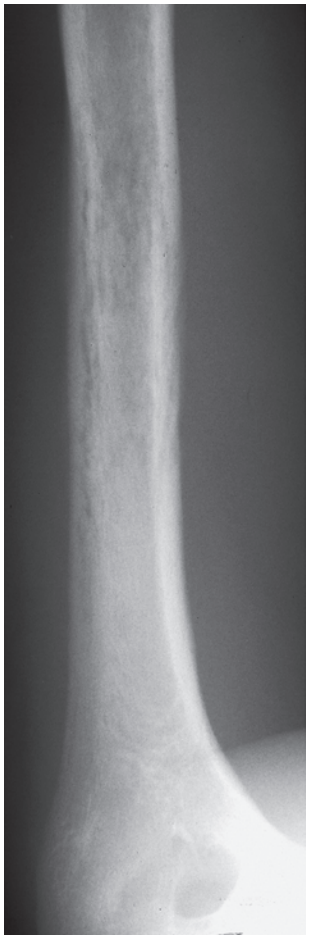

a

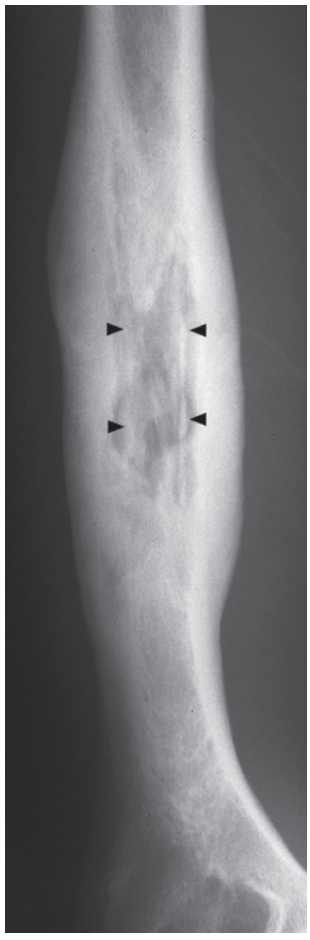

b

Fig. 5.**141** **a**, **b** **Osteomyelitis**. A permeative osteolytic lesion with cortical fissuring and beginning sequestration of a large bone fragment in its center is seen in the humerus shaft (**a**). One year later an expansile lesion with extensive new cortical bone formation is found (**b**). The lesion depicts endosteal scalloping and contains the sequestered bone fragment (arrowheads).

Fig. 5.**142** **Osteomyelitis in diabetic foot**. Besides neuropathic arthropathy manifestations in the first and fifth toe, osteolytic destruction of the second toe including the head of the second metatarsal is seen caused by osteomyelitis originating from an infected neuropathic skin ulcer in the second toe indicated by a metallic marker.

Table 5.10 (Cont.) Localized bone lesions

Disease	Radiographic Findings	Comments
Brodie's abscess (Figs. 5.147 and 5.148)	Usually solitary, lytic and often elongated lesion with sclerotic border typically in the metaphyses of long bones. Epiphyses, diaphyses, flat and irregular bones (e.g. carpus and tarsus) are less common locations. In the epiphysis a circular well-defined osteolytic lesion is typical. In the diaphysis the abscesses may be found in central, subcortical or cortical locations. In the cortex the abscess is surrounded by periosteal new bone formation simulating an osteoid osteoma or a stress fracture.	Subacute pyogenic osteomyelitis (smoldering indolent infection), usually of staphylococcal origin is common in children, in whom the lesion is typically located in the proximal or distal tibia metaphysis and sometimes connected to the growth plate by a tortuous channel. Histologically a central purulent or mucoid fluid collection is surrounded by inflammatory granulation tissue and spongy bone eburnation. The lesion may occasionally contain a central sequestrum.
Osteomyelitis (chronic) (Fig. 5.149)	Thick irregular sclerotic bone with radiolucencies and extensive periosteal new bone formation is characteristic. Signs of remaining activity or reactivation include a change from the previous exam, poorly defined areas of osteolysis, thin laminated periosteal reaction, poorly defined bony excrescences, and demonstration of a sequestrum, sinus tract or soft tissue abscess. *Sclerosing osteomyelitis of Garré* (Fig. 5.**151**) is a low-grade infection without purulent exudate presenting as focal or circumferential cortical thickening and sclerosis in the mandible (most commonly) or diaphyses of long tubular bones. In the latter location osteoid osteoma, stress fracture and *Ribbing's disease* (hereditary multiple diaphyseal sclerosis with typically asymmetric distribution) must be considered in the differential diagnosis.	*Late acquired syphilis* resembles chronic osteomyelitis. Thickened sclerotic long bones caused by endosteal and periosteal new bone formation and ill-defined lytic lesions (gumma formation) are characteristic. *Chronic recurrent multifocal osteomyelitis (CRMO, chronic symmetric plasma cell osteomyelitis)* (Fig. 5.**150**) presents most commonly in children with a protracted clinical course and often symmetric involvement of the medial ends of the clavicles and metaphyses of long bones with a combination of osteolysis and osteosclerosis and extensive periosteal reaction and new bone formation. *SAPHO syndrome* (*s*ynovitis. *a*cne, *p*ustulosis, *h*yperostosis, *o*steitis) may be a related condition. *Epidermoid carcinoma* occurs in 1 % of osteomyelitis at the site of a chronically draining sinus and is evident as an enlarging soft tissue mass eroding the osteomyelitic bone.

(continues on page 122)

Fig. 5.**143** **Tuberculous osteomyelitis**. A large multiloculated osteolytic lesion without significant reactive sclerosis is seen in the acetabular roof and adjacent ilium. The infection most likely originated from the hip where signs of tuberculous arthritis including joint space narrowing and early erosive changes in the femoral head are evident.

Fig. 5.**144** **Tuberculous spondylitis**. An erosive lesion on the antero-inferior aspect of L5 is associated with marked disc space narrowing between L5 and S1.

Fig. 5.**145** **Tuberculous dactylitis ("spina ventosa")**. Expansile fusiform enlargement of the first metacarpal depicting a permeative osteolytic pattern is seen.

Fig. 5.**146** **Fungal osteomyelitis (coccidioidomycosis)**. A solitary osteolytic lesion with discrete margin and mild surrounding sclerosis is seen in the olecranon.

Fig. 5.**147** **Brodie's abscess**. An osteolytic lesion with sclerotic margin and multiloculated appearance is seen in the proximal tibia metaphysis. The lesion is connected on its superomedial border by an osteolytic defect (channel) to the growth plate.

Fig. 5.**148** **Brodie's abscess**. An oblong osteolytic lesion with surrounding sclerosis and minimal periostitis is seen in the distal tibia.

Fig. 5.**149** **Chronic osteomyelitis.** A thick sclerotic distal humerus shaft containing several radiolucencies is seen.

Fig. 5.**150** **Chronic recurrent multifocal osteomyelitis**. A thickened sclerotic distal tibia with several medullary and cortical osteolytic foci is seen.

Fig. 5.**151** **Sclerosing osteomyelitis of Garré**. Circumferential cortical thickening and sclerosis is seen in the tibia diaphysis.

Table 5.10 (Cont.) Localized bone lesions

Disease	Radiographic Findings	Comments
Gorham's disease (vanishing bone disease) (Fig. 5.152)	Progressive, often massive osteolysis without attempt of repair (no periosteal or osteosclerotic reaction) spreading across joints or intervertebral spaces is characteristic. Preferential locations are the hip and shoulder regions, although any bone can be affected. Tapering or "pointing" of the long bones at the sites of osteolysis is typical. In the pelvis a rapidly destructive arthropathy of the hip presenting with destruction of primarily the femur head must be differentiated. This condition may be idiopathic, may represent unusual aggressive forms of osteoarthritis, osteonecrosis, CPPD or HADD, or may occur after intra-articular corticosteroid injections. *Proximal femoral focal deficiency (PFFD)* (Fig. 5.**153**) characterized by partial absence of the proximal femur is diagnosed in infancy.	Occurs sporadic at any age without sex predilection, but is usually diagnosed before the age of 40 years. Histologically a nonmalignant proliferation of angiomatous and fibrous tissue is evident. Other osteolysis syndromes diagnosed in infancy or childhood include acro-osteolysis of *Hajdu and Cheney*, *Joseph*, or *Shinz*, *carpal-tarsal osteolysis* (hereditary or associated with nephropathy), *Farber's disease* (elbows, wrists, knees and ankles) and *Winchester's syndrome* (carpal and tarsal areas and elbows).
Fibromatosis (Fig. 5.154)	Solitary or multiple soft tissue masses with erosions of the adjacent bone or osteolytic lesions. Cortical hyperostosis may be associated with bone involvement.	Variety of benign, but often aggressive fibrous proliferations presenting in both children and adults as tumor-like soft tissue lesions. Involvement of the adjacent bone is not uncommon in infantile forms of the disease.
Membranous lipodystrophy (polycystic lipomembranous osteodysplasia) (Fig. 5.155)	Symmetric and slowly progressive lytic lesions are found in the carpal and tarsal bones and the ends of long and short tubular bones. Bone deformities may eventually occur from pathologic fractures.	Rare hereditary disorder of adipose tissue affecting primarily the bones and brain. Presents commonly in the second or third decade of life with painful bones and joints and subsequently with presenile dementia.
Paget's disease (osteitis deformans) (Fig. 5.156, 5.157, 5.158, 5.159, 5.160, 5.161, and 5.162)	Monostotic or more commonly polyostotic asymmetric lesions with preferential involvement of the pelvis, femur, tibia, spine, skull, scapula, and humerus. The pattern of involvement ranges from purely osteolytic (e.g., osteoporosis circumscripta in the calvarium, and V- or flame-shaped defect in the diaphyses of long bones) to purely osteosclerotic (e.g., ivory vertebra). The mixed pattern (e.g., "picture frame vertebra" and "cotton wool" appearance of the skull) that is usually associated with bony enlargement, cortical thickening, and coarse trabeculation represents the most common manifestation. In long bones the disease characteristically progresses from an epiphysis to the diaphysis. Bone softening may result in bowing deformities of the long bones, acetabular protrusion, biconcave compression of vertebral end plates, and basilar invagination. Complications include cortical stress fractures (single or multiple horizontal radiolucent lines in the convex aspect of the deformed bone (lateral aspect of the femoral neck and shaft, anterior aspect of tibia), transverse pathologic fractures, and sarcomatous degeneration.	Common disorder of middle-aged and elderly patients that is often diagnosed as an incidental finding on radiographs obtained for unrelated purposes. The disease is present in 10 % of patients over the age of 80 years and rare in patients under 40. Laboratory findings include elevated alkaline phosphatase and hydroxyproline levels in the serum and abnormally high hydroxyproline urine levels. Serum acid phosphatase values are normal. Neoplastic involvement in Paget's disease includes sarcomatous degeneration, giant cell tumor, aneurysmal bone cyst, and superimposition of metastases, multiple myeloma and lymphoma. Sarcomatous degeneration occurs in approximately 1 % of patients usually over 55 years of age. Predominantly osteolytic osteosarcomas (60 %), malignant fibrous histiocytoma/fibrosarcomas (25 %) and chondrosarcomas (10 %) are the most frequent tumors found in sarcomatous degeneration.

(continues on page 125)

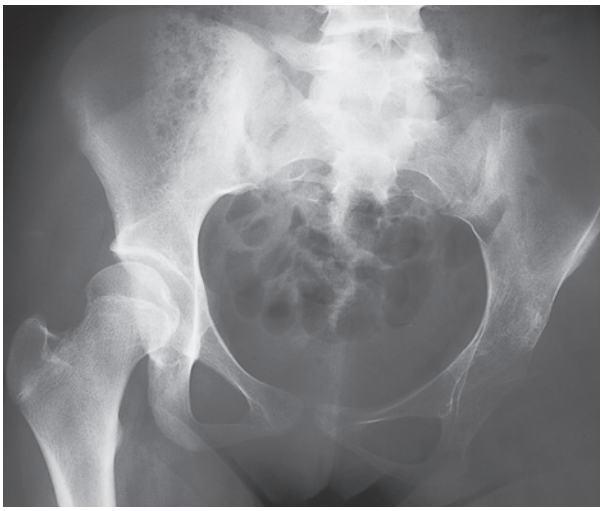

Fig. 5.**152** **Gorham's disease (vanishing bone disease)**. Complete osteolysis of the left proximal femur and beginning osteolysis of the left acetabulum and adjacent innominate bone without either periosteal reaction or reactive sclerosis is seen.

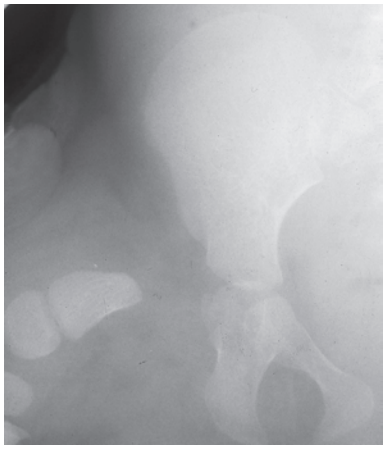

Fig. 5.**153** **Proximal femoral focal deficiency (PFFD)**. Dysplastic acetabulum and absent proximal femur are seen.

Fig. 5.**154** **Fibromatosis**. Osteolytic lesions with pathologic fractures are seen in the distal tibia and fibula in this aggressive infantile form.

Fig. 5.**155** **Membranous lipodystrophy**. Well-demarcated cystic lesions are seen in the carpal bones.

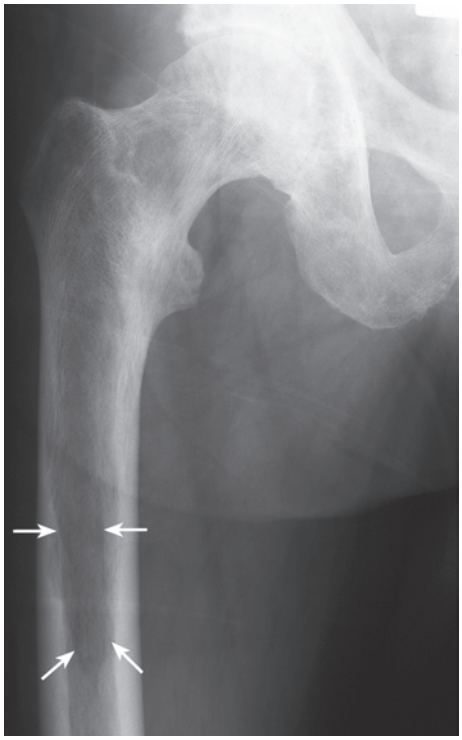

Fig. 5.**156** **Paget's disease**. Mixed osteolytic and osteosclerotic form is seen in the proximal femur and pelvis and a predominantly osteolytic form with V- or flame-shaped osteolytic defect (arrows) in the femur shaft.

Fig. 5.**157** **Paget's disease**. Mixed osteolytic and osteosclerotic form is seen in the distal femur and proximal tibia. Findings include bony expansion, coarse trabeculation, thickened cortices, bowing deformities and a pseudoarthrosis in the distal femur.

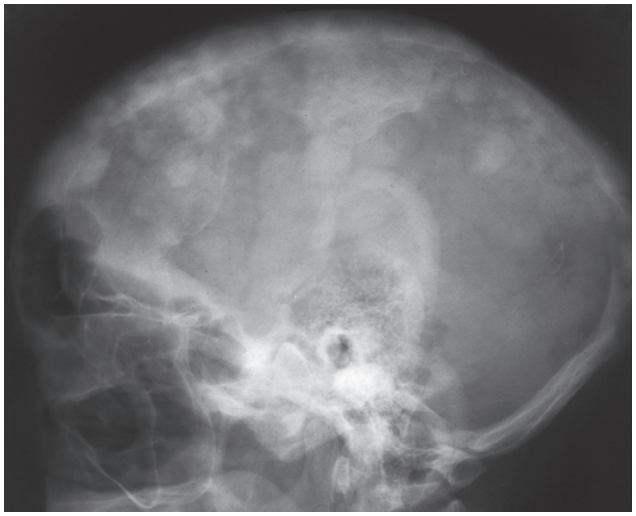

Fig. 5.**158** **Paget's disease**. Sclerotic skull base, thickened vault (especially the inner table of the frontoparietal bone) and multiple sclerotic foci ("cotton wool" appearance) are diagnostic.

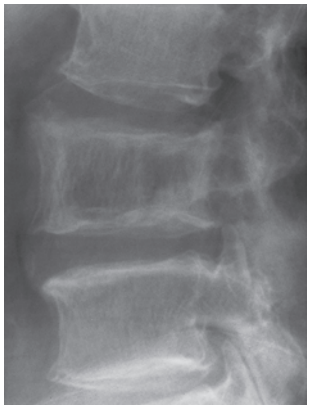

Fig. 5.**159** **Paget's disease**. An enlarged vertebral body with coarse vertical striations and sclerotic margins ("picture frame vertebra") is seen in L3.

Fig. 5.**160** **Paget's disease**. A slightly enlarged "ivory vertebra" is seen at L4.

Fig. 5.**161** **Aneurysmal bone cyst in Paget's disease**. A well-demarcated cortical lesion (arrow) with sclerotic border originates from the anterior cortex of the distal femur with characteristic findings of Paget's disease.

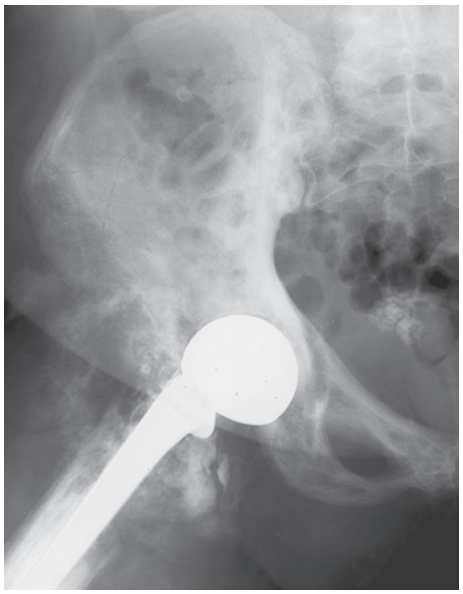

Fig. 5.**162** **Osteosarcoma in Paget's disease**. A huge, partly ossified soft tissue mass is seen originating from the destructed proximal femur shaft around the hemiarthroplasty. Characteristic features of Paget's disease are present in the right hemipelvis and femur.

Table 5.10 (Cont.) Localized bone lesions

Disease	Radiographic Findings	Comments
Fibrous dysplasia (Figs. 5.163, 5.164, 5.165 and 5.166)	Solitary or multiple, often slightly expansile radiolucent lesions that may have a hazy quality ("ground glass" appearance). The matrix may also be uniformly dense, partially calcified or ossified, or thick dense bands may be present. A curvilinear sclerotic rim may outline lytic lesions. The monostotic form (75 %) commonly involves a rib, femur, tibia, humerus, and mandible, whereas the polyostotic form (25 %) frequently involves the skull and facial bones, pelvis, spine and shoulder girdle besides the long tubular bones. Polyostotic fibrous dysplasia may be unilateral or bilateral and may affect several bones of a single limb or both limbs. Solitary lesions in the long bones are located in the diaphyses or, less commonly, metaphyses. Bowing deformities are frequent in the polyostotic form.	Usually diagnosed before the age of 30. In the *McCune-Albright syndrome* precocious female sexual development and café-au-lait spots are associated with the polyostotic form. DD: *Neurofibromatosis*, where more irregularly contoured and darker café-au-lait spots are frequently associated with similar bone lesions. *Ossifying fibromas* are closely related to fibrous dysplasia and occur in the facial bones (especially mandible) and tubular bones (especially anterior aspect of tibia). In the latter location they are also referred to as *osteofibrous dysplasia* (Fig. 5.**167**).

(continues on page 127)

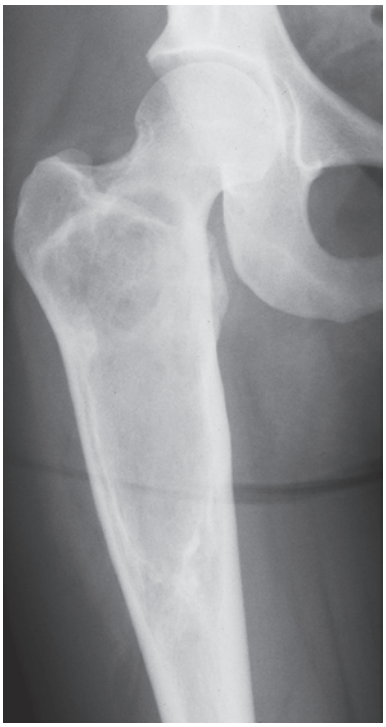

Fig. 5.**163** **Fibrous dysplasia**. Slightly expansile, inhomogeneous lesion with "ground glass" appearance that is partially surrounded by a sclerotic margin is seen in the proximal femur.

Fig. 5.**164** **Fibrous dysplasia**. A slightly expansile, septated osteolytic lesion is seen in the distal humerus. Sclerotic expansion is evident in the proximal ulna. Osteolytic lesions with endosteal scalloping are present in the mid ulnar shaft.

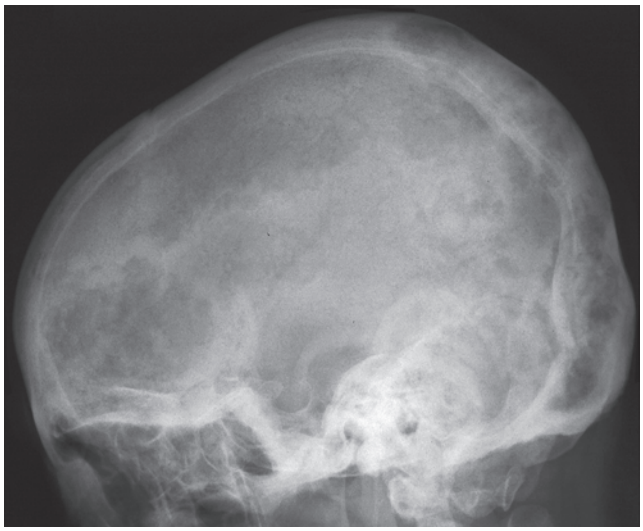

a

b

Fig. 5.**165 a**, **b** **Polyostotic fibrous dysplasia**. Extensive mixed osteolytic and osteoblastic lesions are seen. In the skull (**a**) the paranasal sinuses, base and vault are involved. Marked widening of the diploic space and expansion of primarily the outer table is best appreciated in the parieto-occipital area. Trabeculated osteolytic lesions with a hazy quality ("ground glass" appearance) are seen in the ilium and proximal femur (**b**). Slight bony expansion and beginning bowing deformity is also evident in the femoral neck and intertrochanteric area.

Fig. 5.**166** **Fibrous dysplasia**. Extensive mixed osteolytic and osteoblastic lesions with trabeculation and calcifications are seen in the ilium and hip. Coxa vara deformity ("shepherd's crook") is also evident.

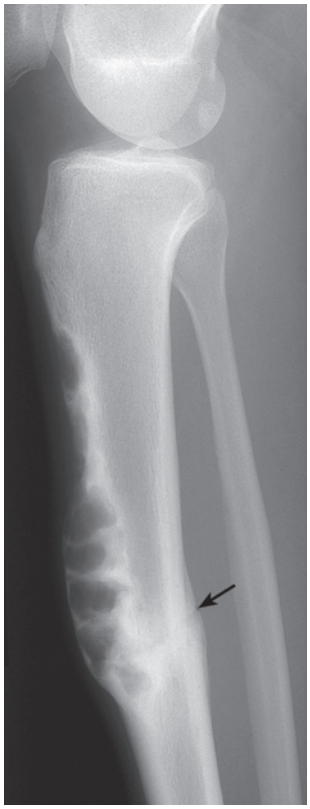

Fig. 5.**167** **Osteofibrous dysplasia**. An expansile multiloculated osteolytic lesion is seen originating from the anterior cortex of the tibia shaft that appears somewhat irregularly thickened. A healing pseudofracture (arrow) is also evident.

Table 5.10 (Cont.) Localized bone lesions

Disease	Radiographic Findings	Comments
Sarcoidosis (Fig. 5.168)	A solitary or multiple osteolytic lesions with a coarsened or lace-work trabecular pattern that may be associated with endosteal scalloping or cortical violation without periosteal reaction is the most common presentation. Purely osteolytic ("punched-out") cystic lesions or purely osteosclerotic foci are less common presentations. The hand is the predominant site of involvement, where acrosclerosis or acro-osteolysis may also be present.	Osseous sarcoidosis is usually associated with either skin lesions or pulmonary disease.
Foreign body granuloma (Figs. 5.169, 5.170 and 5.171)	Presents typically as scalloped osteolytic lesion with or without sclerotic margins about a prosthetic component. Larger expansile lesions may become trabeculated and eventually break through cortex without inciting a periosteal reaction.	Foreign body reaction to prosthetic components such as polymethylmethacrylate cement, polyethylene and silicone. Rarely an intraosseous foreign body granuloma is found that is not associated with joint replacement surgery or any other known cause of accidental foreign body implantation.

Fig. 5.**168 a, b Sarcoidosis**. Multiple osteolytic lesions with a honeycomb or lace-work trabecular pattern, some of which depict endosteal scalloping or cortical violation without periosteal reaction are seen in the hand (**a**) and foot (**b**).

Fig. 5.**169 Foreign body granulomas**. An expansile trabeculated lesion with sclerotic margin is seen in the proximal femur shaft wrapping around the femoral component of the total hip prosthesis. A similar smaller second lesion is evident just below the acetabular component.

Fig. 5.**170 Foreign body granulomas**. An aggressive osteolytic lesion with delicate trabeculation and cortical violation is surrounding the loose femoral component of the dislocated total hip prosthesis. A similar second lesion with bony expansion but without cortical violation is found around the loose acetabular component.

Fig. 5.**171 Foreign body granuloma**. An oblong eccentric lesion with sclerotic margin resembling a nonossifying fibroma is seen in the posterior aspect of the distal femur metaphysis (arrows). No history of accidental foreign body implantation was available in this case.

6 Joint Diseases

A multitude of radiologic changes occur in articular disorders. No single radiographic finding is however diagnostic for a specific arthropathy, since individual lesions in many conditions appear similar. The combinations of various radiologic parameters may lead to an accurate diagnosis, especially when pertinent clinical and laboratory findings are taken into consideration. The time and sequence of arthritic abnormalities observed with respect to the evolution of the disease may also offer important clues to the correct diagnosis. For example a rapidly progressing, destructive arthritic process involving a single joint is virtually diagnostic for septic (pyogenic) arthritis. Certain diseases such as rheumatoid arthritis show radiologic manifestations in a relatively early phase. Other arthritides such as gout depict radiographic abnormalities only late in their clinical course.

Proper radiographic analysis of any arthropathy must include the following criteria: 1. Number of joints involved (monoarticular versus polyarticular). 2. Distribution pattern of involved joints. 3. Joint space width. 4. Erosion. 5. Subchondral cysts. 6. Fragmentation of subchondral bone and loose intra-articular bodies. 7. Reactive (productive) bony changes (subchondral sclerosis, osteophytosis, enthesopathy, periostitis). 8. Osteoporosis (periarticular or generalized). 9. Joint deformities. 10. Chondrocalcinosis and periarticular soft tissue calcifications. 11. Joint effusions and para-articular soft tissue abnormalities.

Monoarticular arthritis (Table 6.1)

An arthritic process involving a single joint is commonly found in infectious arthritis, gout, secondary osteoarthritis and avascular necrosis. In pyogenic and tuberculous arthritis joint space narrowing, joint effusion and periarticular osteoporosis are characteristically present in the early stage followed by poorly defined bone destruction. Since periarticular osteoporosis and joint space narrowing are not present in gout, osteoarthritis and avascular necrosis, every monoarticular disease depicting these two radiographic abnormalities must be considered infectious in origin until proven otherwise. Osseous erosions and cysts in gout are sharply marginated as opposed to the poorly defined bone destruction in infectious arthritis. Osteoarthritis secondary to trauma may at times be difficult to differentiate from gout in small joints without proper clinical history and laboratory findings, since osseous erosions may simulate post-traumatic defects. Avascular necrosis in the early stage presents with normal radiographic findings. Subsequently patchy lucent and sclerotic areas may be seen in the subchondral bone on one side of a joint, followed by a diagnostic arc-like subchondral lucency (crescent sign) and eventually fragmentation and collapse of the involved bone.

Polyarticular arthritis (Table 6.2)

Rheumatoid arthritis, seronegative spondylarthropathy (psoriatic arthritis, Reiter's syndrome, ankylosing spondylitis and enteropathic arthropathy), gout, calcium pyrophosphate dihydrate crystal deposition disease (CPPD), osteoarthritis and neuropathic arthropathy are the most common polyarticular joint disorders. A symmetrically distributed articular disorder presenting with concentric joint space loss, erosions, osteoporosis, and fusiform soft tissue swelling is characteristic for rheumatoid arthritis. An erosive arthritis process involving both synovial and fibrocartilagenous joints (e.g. pubic symphysis and manubriosternal

Table 6.1 Monoarticular disease

Infectious arthritis:
pyogenic
tuberculous
fungal
Gout
Hydroxyapatite deposition disease (HADD)
Traumatic arthritis
Secondary osteoarthritis
Avascular necrosis (osteonecrosis)
Pigmented villonodular synovitis
Synovial osteochondromatosis
Osteochondritis dissecans

Table 6.2 Polyarticular disease

Osteoarthritis
Erosive osteoarthritis
Rheumatoid arthritis
Psoriatic arthritis
Reiter's syndrome
Ankylosing spondylitis
Gout
Calcium pyrophosphate dihydrate crystal deposition disease (CPPD)
Hemochromatosis
Ochronosis
Multicentric reticulohistiocytosis
Hemophilia
Acromegaly
Jaccoud's arthritis
Systemic lupus erythematosus
Scleroderma
Multiple epiphyseal dysplasia

Table 6.3 Distribution patterns of polyarticular diseases

Involvement	Disease
Bilateral symmetric	Primary osteoarthritis Erosive osteoarthritis Rheumatoid arthritis Ankylosing spondylitis CPPD Hemochromatosis Ochronosis Multicentric reticulohistiocytosis Neuropathic osteoarthropathy Hemophilia Acromegaly Jaccoud's arthritis Systemic lupus erythematosus Scleroderma Multiple epiphyseal dysplasia
Asymmetric	Secondary osteoarthritis Psoriatic arthritis Reiter's syndrome Gout
Distal interphalangeal joints (hand)	Osteoarthritis Erosive osteoarthritis Psoriatic arthritis Gout Multicentric reticulohistiocytosis Scleroderma
Proximal interphalangeal joints (hand)	Osteoarthritis Erosive osteoarthritis Rheumatoid arthritis Psoriatic arthritis Gout Multicentric reticulohistiocytosis Scleroderma
Metacarpophalangeal joints	Secondary osteoarthritis Rheumatoid arthritis Gout CPPD Hemochromatosis Jaccoud's arthritis Systemic lupus erythematosus
First carpometacarpal joint	Osteoarthritis Rheumatoid arthritis Gout Systemic lupus erythematosus
Common carpometacarpal joint Midcarpal joint	Rheumatoid arthritis Gout Osteoarthritis (scaphotrapeziotrapezoidal joint) Rheumatoid arthritis (including triquetropisiform joint) Gout CPPD (scaphotrapeziotrapezoidal joint)
Radiocarpal joint	Secondary osteoarthritis Rheumatoid arthritis Gout CPPD Hemochromatosis
Distal radioulnar joint	Rheumatoid arthritis Gout Scleroderma

joints) and the ligamentous attachments in the pelvis, femur and calcaneus in an often asymmetric fashion is characteristic for a seronegative spondylarthropathy. This diagnosis is further supported by the absence of osteoporosis, the presence of bony proliferation and intra-articular osseous fusion, and involvement of the spine and sacroiliac joints. Gouty arthropathy is characterized by asymmetric involvement of the appendicular skeleton, eccentric osseous erosions, bony proliferation, preservation of the joint space and absence of osteoporosis. In CPPD articular and periarticular calcifications are combined with joint space narrowing, eburnation, cyst formation, fragmentation and collapse. The presence of significant osteophytosis and the general absence of both intra-articular and extra-articular calcifications differentiates osteoarthritis from CPPD. Otherwise the radiographic findings in these two disorders are very similar, though fragmentation and bone collapse are less common in osteoarthritis. Neuropathic osteoarthropathy in an early stage may resemble osteoarthritis and CPPD, but extensive sclerosis associated with joint fragmentation, fractures and subluxations/dislocations is virtually diagnostic in a more advanced case.

Distribution patterns of articular diseases

(Table 6.3)

Symmetric joint involvement is typical of rheumatoid arthritis, primary osteoarthritis, CPPD and neuropathic arthropathy, whereas an asymmetric distribution of the affected joints favors the diagnosis of a seronegative spondylarthropathy, secondary osteoarthritis and gout.

In the hand nonerosive arthritic changes involving the distal interphalangeal joints suggests osteoarthritis, whereas erosive arthritic changes in the distal interphalangeal joints are common in psoriatic arthritis, erosive osteoarthritis and gout. Involvement of the proximal interphalangeal joints is common in rheumatoid arthritis and all aforementioned conditions affecting the distal interphalangeal joints. CPPD does not affect the interphalangeal joints, but has a predilection for the second and third metacarpophalangeal joints and the radiocarpal joint. Involvement of the metacarpophalangeal joints is common in both rheumatoid and psoriatic arthritis, but these joints are usually spared by both primary and erosive osteoarthritis.

In the wrist erosive arthritic changes without site predilection are very common in rheumatoid arthritis and gout and less frequent in psoriatic arthropathy. Both primary osteoarthritis and CPPD have a predilection for the first carpometacarpal joint and the joint between the scaphoid and trapezium-trapezoid.

In the foot primary osteoarthritis is typically located in both the first metatarsophalangeal joint (hallux rigidus), where it may be associated with hallux valgus deformity, and in the first tarsometatarsal joint. Rheumatoid arthritis commonly affects the interphalangeal joint of the great toe, both the metatarsal-phalangeal and tarsometatarsal joints, the talonavicular and the posterior subtalar joints. Seronegative arthropathies potentially affect any joint of the forefoot, but the most severe changes commonly occur in the metatarsophalangeal joints and the interphalangeal joint of the great toe. Gout shows a predilection for the first metatarsophalangeal joint and to a lesser degree the interphalangeal joint of the great toe, the metatarsophalangeal joints 2 to 5 and the tarsometatarsal joints, although any joint in the

forefoot and midfoot can be affected. Neuropathic arthropathy in diabetes may involve the metatarsophalangeal joints and all joints of the midfoot and hindfoot.

Arthritic involvement of the calcaneus most commonly affects the sites of insertion of the Achilles tendon posteriorly and the plantar aponeurosis (fascia) inferiorly, as well as the posterosuperior aspect of the calcaneus that abuts the retrocalcaneal bursa. Retrocalcaneal bursitis leads to unilateral or bilateral erosions at this site in rheumatoid arthritis. Localized retrocalcaneal bursitis not related to a systemic arthritic process is termed *Haglund's syndrome* (Fig. 6.**1**). The condition is aggravaled by a prominent bony protuberance at the postero-superior aspect of the calcaneus (Haglund's deformity). The hallmark of the seronegative spondyloarthropathies are fluffy periostitis about the posterior and inferior aspect of the calcaneus and broadbased spurs (entesophytes) at the attachment of the Achilles tendon and plantar aponeurosis (Fig. 6.**2**). Erosions at these sites as well as near the retrocalcaneal bursa are not a dominant radiographic feature in these conditions. In osteoarthritis well-defined and typically narrow-based calcaneal spurs are found at the osseous tendon attachments. Similar bony excrescenses are associated with acromegaly, diffuse idiopathic skeletal hyperostosis (DISH) and CPPD (Fig. 6.**3**). In the latter condition linear calcific deposition in the Achilles tendon and plantar fascia may also be present. In gout tophaceous nodule in and about the Achilles tendon can lead to erosion near its calcaneal insertion.

In the knee bilateral and symmetric involvement of all three compartments (medial and lateral femorotibial space and patellofemoral joint) with marked joint space narrowing, osteoporosis and erosions is virtually diagnostic of rheumatoid arthritis. A tricompartmental distribution may also be found in seronegative spondylarthropathies, but the involvement is frequently asymmetric and less severe than in rheumatoid arthritis and periosteal new bone formation may be pronounced. In osteoarthritis the medial compartment is typically more severely affected than the lateral compartment resulting frequently in varus deformity. Significant degenerative changes in the patellofemoral joint may be associated. The compartmental distribution of CPPD in the knee is similar to osteoarthritis, but there is no preferential involvement of the medial compartment and both extensive chondrocalcinosis and rapid progression of the arthritic process including osseous destruction and fragmentation favor the former diagnosis. Isolated degenerative-like arthropathy of the patellofemoral joint should also raise the possibility of CPPD. Neuropathic arthropathy is characterized by disorganization of one or both knees including subluxation, fragmentation and extensive sclerosis.

In the hip the pattern of joint space loss may be useful to differentiate various articular diseases. Circumferential (axial or concentric) loss of joint space leads to migration of the femoral head in axial direction along the axis of the femoral neck (Fig. 6.**4**). Circumferential loss of joint space is associated with rheumatoid arthritis where both hips are affected in symmetric fashion. A unilateral (monoarticular) concentric loss of joint space suggests an infectious process but is also found with idiopathic chondrolysis of the hip. In ankylosing spondylitis a similar bilateral concentric joint space loss is found as in rheumatoid arthritis, but the presence of osteophytosis, commencing on the superolateral aspect of the femoral head and progressing to a collar about the femoral head-neck junction, is distinctive of the former disorder. Hip involvement in both psoriatic arthritis and Reiter's syndrome is similar to ankylosing spondylitis but un-

Fig. 6.**1** **Haglund's syndrome**. Extensive erosive changes in the posterosuperior aspect of the calcaneus are associated with new bone formation and localized soft tissue mass secondary to retrocalcaneal bursitis.

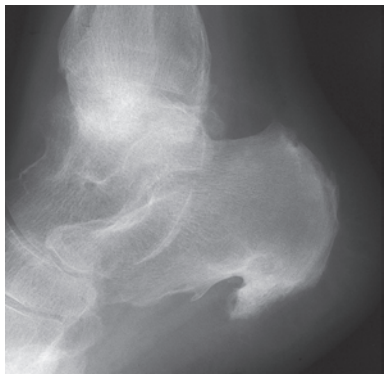

Fig. 6.**2** **Inflammatory calcaneal spur (enthesophyte).** A broad-based plantar calcaneal spur is associated with fluffy periostitis about the posterior and inferior aspect of the calcaneus (Reiter's syndrome).

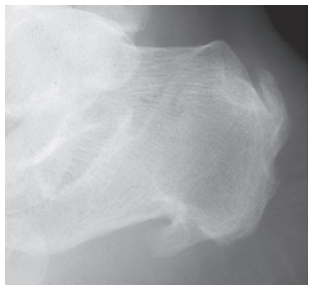

Fig. 6.**3** **Degenerative calcaneal spurs (enthesophytes)**). Two well-defined calcaneal spurs depicting cancellous bone outlined by cortical margins are seen at the insertions of the Achilles tendon posteriorly and plantar aponeurosis inferiorly (acromegaly).

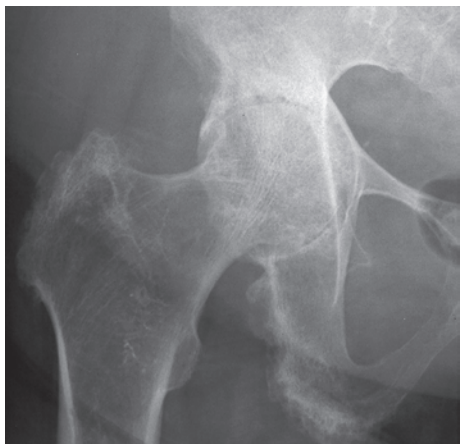

Fig. 6.**4** **Circumferential loss of joint space**. Concentric (axial) narrowing of the joint space is associated with tiny articular erosions, extensive fluffy enthesopathy along the ischium and greater trochanter and fused sacroiliac joints. Mild protrusio acetabuli is also present (ankylosing spondylitis).

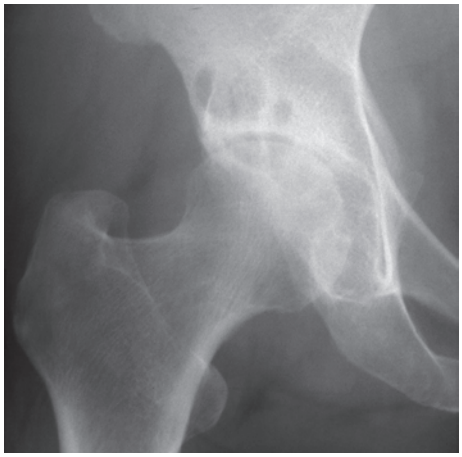

Fig. 6.**5** **Asymmetric loss of joint space**. Narrowing of the joint space is limited to the superior (weight-bearing area of the hip and is associated with reactive sclerosis and subchondral cyst formation (osteoarthritis).

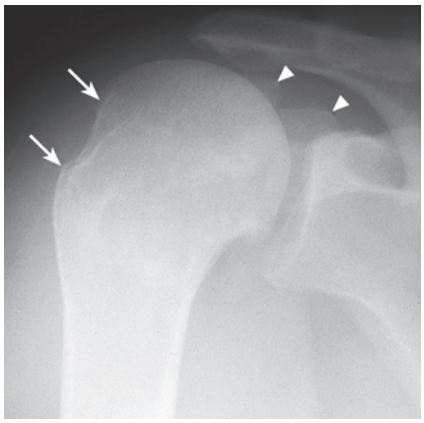

Fig. 6.**6** **Hatchet sign**. An erosion limited to the lateral aspect of the humeral head (arrows) produces a deformity reminiscent of a hatchet. This finding is typically associated with ankylosing spondylitis or fungal arthritis as in this case. It should not be confused with a Hill-Sachs defect secondary to an anterior shoulder dislocation. Loose intra-articular bony fragments (arrowheads) and a decreased distance between humeral head and inferior aspect of the acromion indicating a chronic rotator cuff tear are also seen.

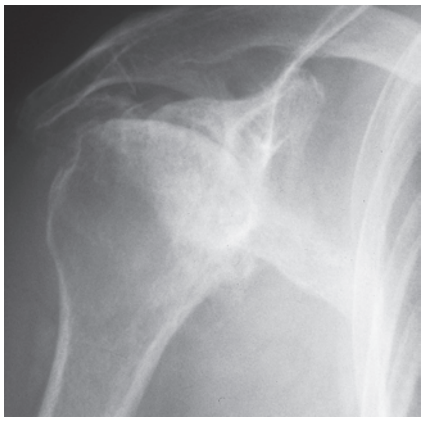

Fig. 6.**7** **Milwaukee shoulder**. Cloud-like calcification in the rotator cuff and subacromial bursa projecting between the distal acromion and humeral head are associated with destructive shoulder arthritis and chronic rotator cuff tear evident by the decreased distance between humeral head and inferior aspect of the acromion.

common. In CPPD unilateral or bilateral concentric loss of joint space is associated with sclerosis, osteophytosis, cyst formation and eventually fragmentation of the femoral head. The demonstration of chondrocalcinosis in the acetabular labrum and pubic symphysis further supports the diagnosis of CPPD. Even in advanced cases of osteonecrosis (avascular necrosis) of the femoral head with bony collapse and fragmentation the joint space remains largely preserved. In osteoarthritis the loss of joint space narrowing is limited to the weight-bearing superior aspect of the joint or less frequently, to its medial aspect (Fig. 6.**5**). Besides the subchondral sclerosis, osteophytosis and cyst formation, cortical thickening or buttressing of the medial femoral neck cortex may also be apparent in this condition. *Protrusio acetabuli* (see Fig. 6.**4**) is associated with rheumatoid arthritis, ankylosing spondylitis, osteoarthritis (medial migration pattern), infection, acetabular trauma, Paget's disease and osteomalacia.

In the shoulder region bilateral symmetric loss of joint space in the glenohumeral joints combined with widened eroded acromioclavicular joints is characteristic for rheumatoid arthritis. Ankylosing spondylitis presents in similar fashion, but a large bony defect (erosion) on the superolateral aspect of the humeral head, the "hatchet" deformity (Fig. 6.**6**), the absence of osteoporosis and the presence of bony proliferation about the osseous erosions are clues to differentiate it from rheumatoid arthritis. Severe osteoarthritis in the glenohumeral joint is usually associated with previous trauma or overuse and is therefore most often unilateral. Acromioclavicular joint degeneration is frequent in middle-aged and elderly persons and may lead to shoulder impingement syndrome with the development of spurs protruding inferiorly from this joint and the adjacent undersurface of the acromion. In CPPD an advanced degenerative-like process in the glenohumeral joint may be associated with chondrocalcinosis. Calcium hydroxyapatite crystal deposition disease (HADD) presenting initially with cloud-like calcifications in the rotator cuff or subacromial bursa may progress to a destructive arthropathy of the glenohumeral joint with chronic rotator cuff tear, the so-called *Milwaukee shoulder syndrome* (Fig. 6.**7**).

Joint space width (Tables 6.**4** and 6.**5**)

Analysis of the width of the joint space may provide important clues in the differential diagnosis of arthritic disorders. In these conditions the joint space may be narrowed, normal or widened. Furthermore joint space narrowing may be symmetric or asymmetric and occur early or late in the disease process. Symmetric joint space loss involving an entire joint early in the disease process is suggestive of an infectious or inflammatory arthritic disorder. An asymmetric joint space narrowing in the large joints of the lower extremity is indicative of osteoarthritis. In this condition subchondral sclerosis usually precedes a radiographically appreciable joint space loss. Advanced erosive or destructive joint disease with relatively well-maintained joint space and asymmetric joint involvement suggests gout and osteonecrosis, respectively. A widened joint space is typically associated with large joint effusions, especially in children, and hemathrosis secondary to trauma, hemophilia or other bleeding disorders. Joint laxity in neuromuscular disorders frequently presents with a widened joint space too. A *drooping shoulder* (Fig. 6.**8**) is an inferior "subluxation" of the humeral head caused by either a large hemarthrosis

(e.g. in intra-articular proximal humerus fractures), any neurologic or muscular disorder affecting the supporting musculature or any direct injury of the capsule or rotator cuff itself. True subluxations and dislocations typically present also as joint space widening, but in certain projections these conditions may occasionally mimic a joint space narrowing. A considerable widening of the joint space in the fingers and toes can be found in psoriatic arthropathy when severe destruction of the subchondral bone is present. This condition has to be differentiated from sequelae of resection arthroplasties consisting of removal of one or both articular surfaces in an interphalangeal joint. A *widened acromioclavicular joint* (Fig. 6.**9**) is a frequent finding in rheumatoid arthritis and psoriatic arthropathy, but also encountered in infectious arthritis, traumatic separation, post-traumatic osteolysis (e.g. weight lifters), acromioplasty with resection of the distal clavicle, and hyperparathyroidism.

Erosions (Table 6.6)

Marginal articular erosions at osseous surfaces that do not possess protective cartilage are typical for early rheumatoid arthritis (Fig. 6.**10**). The erosions typically are poorly defined and without sclerotic margin. In the hand and wrist symmetric involvement with predilection for the proximal interphalangeal and metacarpophalangeal joints, trapezium, capitate, scaphoid, triquetrum and pisiform, and both the

Table 6.4 Narrowed joint space

Osteoarthritis (often asymmetric in weight-bearing joints)
Rheumatoid arthritis
Psoriatic arthritis
Reiter's syndrome
Ankylosing spondylitis
CPPD
Hemochromatosis
HADD
Ochronosis
Infectious arthritis
Hemophilia
Multiple epiphyseal dysplasia
Endstage of any arthritic process

Table 6.5 Widened joint space

Subluxation or dislocation (congenital, traumatic)
Hemarthrosis or large joint effusion
Joint laxity (neuromuscular, traumatic)
Psoriasis
Neuropathic osteoarthropathy
Acromegaly
Pigmented villonodular synovitis
Synovial osteochondromatosis
Synovial neoplasm
Resection arthroplasty

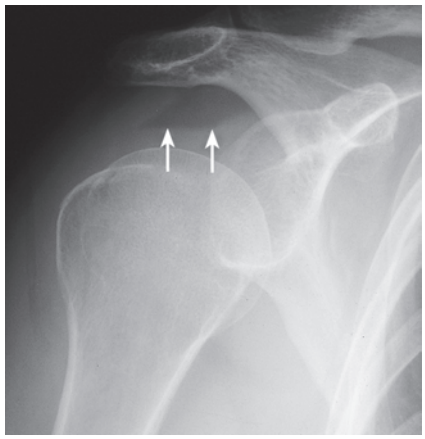

Fig. 6.**8** **Drooping shoulder**. A large lipohemarthrosis with fat-blood level (arrows) secondary to a nondisplaced greater tuberosity fracture produces inferior subluxation of the humeral head evident by the increased distance between the latter and the inferior aspect of the acromion.

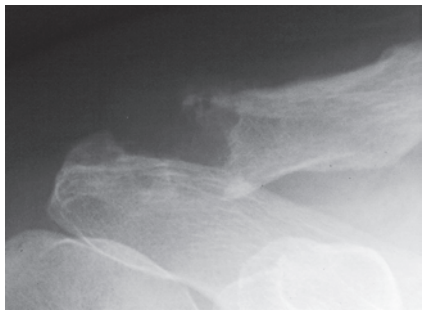

Fig. 6.**9** **Widening of the acromioclavicular joint** is caused by erosion of the distal clavicle and to a lesser degree the distal acromion (secondary hyperparathyroidism).

Fig. 6.**10** **Erosions in rheumatoid arthritis**. Multiple preferentially marginal erosions with symmetric distribution and characteristic localization (sparring of the distal interphalangeal joints) are seen.

Fig. 6.**11** **Erosions in psoriatic arthritis**. Multiple marginal erosions are associated with extensive bony proliferation evident as irregular excrescences with spiculated appearance. Note also the involvement of the distal interphalangeal joints and the partial resorption of the tufts on the third and fourth finger.

Table 6.6 Erosions

Erosive osteoarthritis
Rheumatoid arthritis
Psoriatic arthritis
Reiter's syndrome
Ankylosing spondylitis
Gout
HADD
Amyloidosis
Multicentric reticulohistiocytosis
Infectious arthritis
Scleroderma
PVNS (pressure erosions)
Synovial osteochondromatosis (pressure erosions)
Articular defects simulating erosions in CPPD, osteonecrosis, osteochondritis dissecans and osteochondral fractures

Fig. 6.**12** **Erosions in gout**. Eccentric erosions with overhanging edge (arrow) and associated soft tissue mass is seen about the distal interphalangeal joint.

Fig. 6.**13** **Fragmentation of the articular surface in frostbite**. Fragmentation of the distal articular surfaces of the proximal phalanx of the fifth finger and middle phalanx of the fourth finger secondary to osteonecrosis is seen. The remaining less exposed fingers were intact.

radial and ulnar styloid is characteristic. A poorly defined monoarticular erosive arthritic process suggests an infectious etiology. In psoriatic arthropathy (Fig. 6.**11**) marginal erosions characteristically are associated with adjacent bony proliferation evident as irregular excrescences with spiculated appearance. In gout (Fig. 6.**12**) one or more eccentric erosions with sclerotic margin and over-hanging edge may be evident. In erosive osteoarthritis the combination of osteophytosis and sharply marginated erosions in central location of the joint are characteristic. Fragmentation of an articular surface (e.g. in CPPD, osteonecrosis or secondary to trauma) may result in a defect that can mimic a true erosion (fig. 6.**13**).

Subchondral cysts (Table 6.7)

Single or multiple radiolucent lesions with sclerotic margins are commonly found with osteoarthritis, CPPD, and osteonecrosis (Fig. 6.**14**). In both osteoarthritis and osteonecrosis these cysts are typically located within the pressure segment of the joint, whereas in CPPD they are more widespread and frequently unusually large. A subchondral cyst occasionally is the sequela of a bone injury that becomes evident over a period of months after the traumatic episode (traumatic cyst). In rheumatoid arthritis the subchondral cysts frequently originate in the chondro-osseous junction and do not depict a surrounding sclerotic margin. An intraosseous ganglion presents as a solitary subchondral cystic lesion with sclerotic margin anywhere in the subchondral bone of a joint not affected by an arthritic process. Furthermore subchondral cysts can be mimicked by intraosseous gouty tophus, a Brodie's abscess and variety of neoplasms (e.g. chondroblastoma, giant cell tumor, intraosseous lipoma, clear cell chondrosarcoma, and skeletal metastases).

Fragmentation of subchondral bones and loose intra-articular bodies (Tables 6.8 and 6.9)

Fragmentation of the articular surface (Fig. 6.15) is commonly associated with CPPD, osteonecrosis, neuropathic arthropathy, far advanced osteoarthritis, and trauma (osteochondral fractures) resulting frequently in one or more loose intra-articular bodies. Detached osteophytes in osteoarthritis may also lead to loose intra-articular bodies. Joint destruction secondary to pyogenic or tuberculous arthritis may also be associated with loose intra-articular bony fragments. In osteochondritis dissecans the solitary osteochondral fracture fragment may be still located in the original articular defect (pit) or freely mobile in the joint. In synovial osteochondromatosis a large number of calcified/ossified loose bodies located within and around the involved joint and ranging in size from a few millimeters to several centimeters is characteristic.

Reactive (productive) bony changes

In osteoarthritis of weight-bearing joints sclerosis of the subchondral bone is frequently the first radiographic sign of the disease, since the causative joint cartilage degeneration

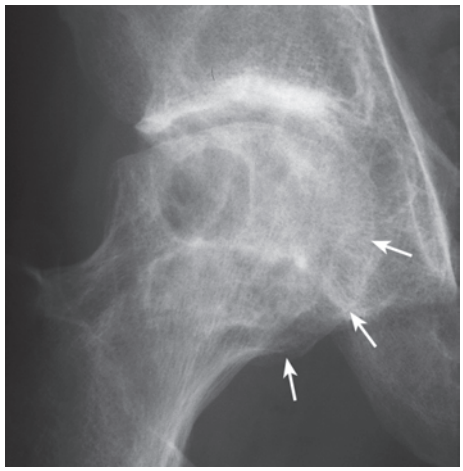

Fig. 6.14 **Subchondral cyst in avascular necrosis (osteonecrosis)**. A cystic lesion with sclerotic margin is seen in the weight-bearing portion of the deformed and flattened femoral head. Secondary degenerative changes including remodeling and new bone formation (buttressing) along the medial aspect of the femoral head and neck (arrows) are also evident in this patient with sickle cell disease.

Table 6.7 Subchondral cystic lesions

Osteoarthritis
Rheumatoid arthritis
Gout
CPPD
Amyloidosis
Avascular necrosis (osteonecrosis)
Post-traumatic cyst without secondary osteoarthritis
Hemophilia
Infectious (Brodie's abscess)
Intraosseous ganglion
Intraosseous lipoma
Chondroblastoma
Giant cell tumor
Clear cell chondrosarcoma
Metastasis

Fig. 6.15 **Fragmentation of subchondral bone in osteoarthritis**. Degenerative changes in the weight-bearing portion of the hip are seen including subchondral cyst formation and beginning fragmentation of both acetabular dome and femoral head.

Table 6.8 Fragmentation of articular surface

Intra-articular fracture
Osteoarthritis (advanced stage)
CPPD
HADD
Ochronosis
Infectious arthritis
Avascular necrosis (osteonecrosis)
Neuropathic osteoarthropathy
Osteochondritis dissecans

Table 6.9 Loose intra-articular bodies

Intra-articular fracture
Osteoarthritis (advanced stage)
CPPD
HADD
Ochronosis
Infectious arthritis
Avascular necrosis (osteonecrosis)
Neuropathic osteoarthropathy
Osteochondritis dissecans
Synovial osteochondromatosis

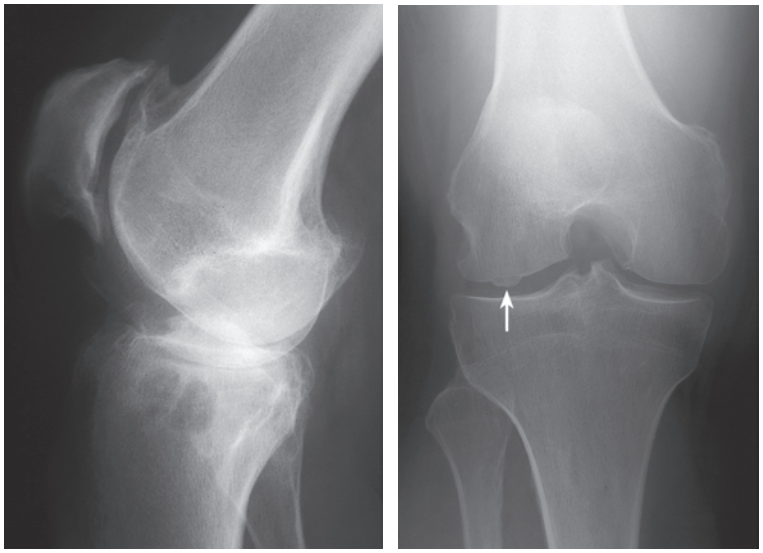

Fig. 6.**16 a, b** **Osteophytosis in osteoarthritis**. **a**: Marginal osteophytes are seen in the patellofemoral joint. **b**: A central (interior joint) osteophyte (arrow) presents as button-like excrescence originating from the subchondral bone largely denuded from its cartilage.

Fig. 6.**17** **Enthesopathy in DISH**. Extensive well-defined bony proliferation is seen bilaterally along the iliac wings, ischiatic bones and greater and lesser trochanters. Note also the paravertebral ossifications in the lower lumbar spine and the normal sacroiliac joints.

can only be appreciated when a substantial loss of cartilage has occurred resulting in joint space narrowing. *Osteophytosis* (Fig. 6.**16**) is the hallmark of primary and secondary degenerative joint disease. *Marginal osteophytes* develop in the periphery of the articular surface of a joint and appear as lips of new bone. Less common are *central (interior joint) osteophytes* appearing as button-like or flat bony excrescences that may be demarcated at their bases by remnants of the original cartilage simulating occasionally loose intra-articular bodies.

Enthesopathy refers to bony proliferation at the site of osseous attachment of ligaments and tendons. Enthesophytes (Fig. 6.**17**) are commonly found with seronegative spondyloarthropathies and diffuse idiopathic skeletal hyperostosis (DISH). In the spine these conditions are characteristically associated with syndesmophytes (ossifications of the outer portion of the annulus fibrosus) or paravertebral ossification, respectively. The thin and vertically oriented, symmetric syndesmophytes in ankylosing spondylitis and enteropathic spondylarthropathy differ from the broader asymmetric syndesmophytes of psoriasis and Reiter's syndrome. Degenerative enthesophytes in osteoarthritis tend to be sharply marginated as opposed to the inflammatory enthesophytes associated with the seronegative spondylarthropathies that depict a more fluffy and often spiculated appearance.

Arthropathies commonly associated with periostitis (periosteal new bone formation) include psoriatic arthropathy, Reiter's syndrome, septic arthritis and juvenile rheumatoid arthritis. Intra-articular bone apposition on the medial aspect of the femoral neck is termed *buttressing*. It is most commonly observed with osteoarthritis and osteonecrosis, but occasionally is caused by a stress fracture or an adjacent osteoid osteoma.

Osteoporosis

In both the elderly patient and in advanced arthropathies of any etiology the presence of osteopenia is of little differential diagnostic value, since the finding may be either coincidental (e.g. senile osteoporosis) or caused by disuse. Periarticular or generalized osteoporosis are important radiographic features of rheumatoid, pyogenic, and tuberculous

arthritis. These arthropathies have to be differentiated from reflex sympathetic dystrophy (Sudeck's osteodystrophy) and transient regional osteoporosis in which severe periarticular osteoporosis and articular pain are present in the absence of any radiographic joint abnormalities. Osteoporosis typically is not a feature of osteoarthritis, CPPD, gout and seronegative spondylarthropathies.

Joint deformities

Subluxations and dislocations are commonly caused by trauma, but are also associated with congenital and developmental diseases, neuromuscular disorders and most arthropathies. An erosive arthritic process associated with multiple joint deformities suggests the diagnosis of either rheumatoid arthritis or a seronegative spondylarthropathy such as psoriatic arthritis. The hand deformities associated with these diseases are depicted in Fig. 6.**18**. Similar hand and wrist deformities in the absence of erosions may be found with systemic lupus erythematosus or Jaccoud's arthritis secondary to rheumatic fever.

Common toe deformities include hallux valgus (valgus deformity in first metatarsophalangeal joint), hammer toe (hyperextended metatarsophalangeal, flexed proximal interphalangeal, hyperextended distal interphalangeal joints), claw toe (hyperextended metatarsophalangeal, flexed proximal interphalangeal and distal interphalangeal joints), curly toe (flexed proximal interphalangeal and distal interphalangeal joints), mallet toe (flexed distal interphalangeal joint), and cross-over toe (dorsal superimposition of a deviated toe over a neighboring toe). In rheumatoid arthritis spreading of the metatarsals, lateral deviation of the first to fourth toes in the metatarsophalangeal joints, and cock-up toe (hyperextended metatarsophalangeal joint with subluxation of the phalanx above the metatarsal head) are also frequently associated. Subluxation associated with articular fragmentations, osteophytosis and eburnation is most frequently found in neuropathic arthropathy.

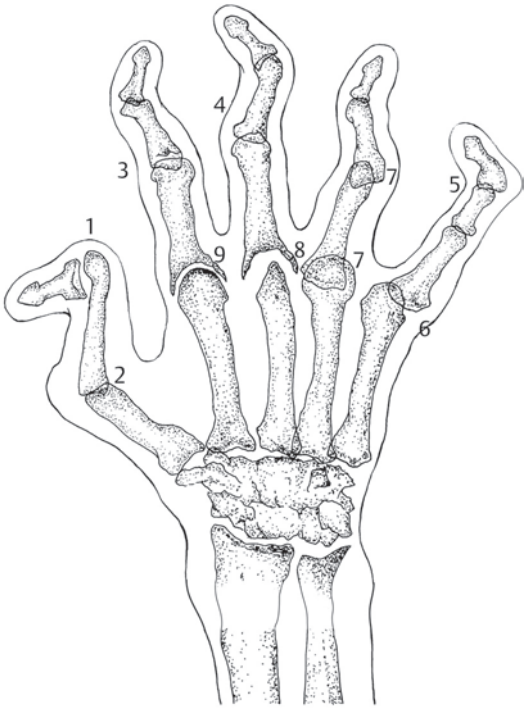

Fig. 6.**18** **Hand deformities in inflammatory arthritis**. 1. Hyperextension and subluxation of the distal phalanx of the thumb. 2. Hyperextension at interphalangeal joint and flexion at the first metacarpophalangeal joint (Z-shaped deformity or hitchhiker's thumb). 3. Hyperextension distal interphalangeal and flexion proximal interphalangeal joint (boutonnière deformity). 4. Flexion distal interphalangeal and hyperextension proximal interphalangeal joint (swan-neck deformity). 5. Flexion distal interphalangeal joint (mallet finger). 6. Ulnar deviation at metacarpophalangeal joint. 7. Overriding dislocations at metacarpophalangeal and/or proximal interphalangeal joints ("telescoping" "opera-glass" deformity or "main en lorgnette"). 8. Whittled metacarpal head projecting in expanded base of proximal phalanx ("pencil-in-cup" deformity). 9. Erosion and compression of metacarpophalangeal joint ("ball-in-cup" or "cup-in-saucer" deformity). Boutonnière, and swan-neck deformities and ulnar deviation are more common in rheumatoid arthritis than psoriatic arthropathy, whereas "telescoping", "pencil-in-cup" and "ball-in-cup" deformities are more common in psoriatic arthropathy than rheumatoid arthritis.

Chondrocalcinosis and periarticular soft tissue calcifications (Tables 6.**10**, 6.**11** and 6.**12**)

Calcification of articular cartilage is termed chondrocalcinosis (Fig. 6.**19**). It is the hallmark of calcium pyrophosphate dihydrate crystal deposition disease (CPPD). However chondrocalcinosis due to pyrophosphate and less frequently other crystals is also associated with many other conditions, most commonly with primary and post traumatic osteoarthritis and hyperparathyroidism. Periarticular soft tissue calcifications (Fig. 6.**20**) are frequently caused by calcium hydroxyapatite crystals, although other crystals such as calcium pyrophosphate dihydrate may be associated too. Extensive periarticular soft tissue calcifications are most commonly found with scleroderma (Fig. 6.**21**) and secondary hyperparathyroidism (renal osteodystrophy) whereas smaller and less conspicuous periarticular calcifications are typical for calcific tendinitis and bursitis, respectively.

Table 6.10 Chondrocalcinosis

Osteoarthritis (primary, secondary, post-traumatic)
Gout
CPPD
Hemochromatosis
Wilson's disease
HADD
Ochronosis
Acromegaly
Oxalosis

Joint effusions

Joint effusions are commonly associated with synovial inflammation and trauma. In the absence of an injury a large monoarticular joint effusion suggests an infectious arthritic process. Joint effusions can only be differentiated from paraarticular soft tissue swelling when the capsule of the affected joint is separated by a layer of fat from the surrounding tissues. This is the case in the elbow, knee and ankle where joint effusions can be reliably diagnosed by conven-

Fig. 6.**19** **Chondrocalcinosis in CPPD**. Extensive calcification is seen in the lateral and to a lesser degree medial meniscus.

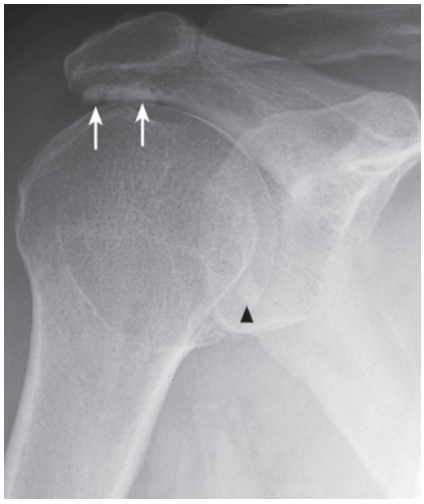

Fig. 6.**20** **Calcific tendinitis**. A localized calcification is seen in the supraspinatus tendon (arrows) of the rotator cuff. A smaller calcification is also present in the long biceps head tendon (arrowhead).

Fig. 6.**21** **Soft tissue calcification in scleroderma** is seen about the olecranon and dorsal aspect of the proximal ulna.

tional radiography (Fig. 6.**22**). Massive joint effusions may cause widening or pseudosubluxation of the involved joint such as inferior subluxation of the humeral head ("drooping shoulder") or widening of the distance between triquetrum and pisiform in a large radiocarpal joint effusion (Fig. 6.**22d**). After an intra-articular fracture a lipohemarthrosis can be diagnosed by the presence of a fat-blood level when the radiograph is obtained with horizontal beam technique. Occasionally intra-articular gas is also found in the absence of penetrating injury. Following a fracture or dislocation gas (mostly nitrogen) may accumulate in the joint, besides blood and bone marrow, in the form of one or more air bubbles as a result of negative intra-articular pressure. Such a pneumohemarthrosis or pneumolipohemarthrosis, respectively, is particularly common in the hip. A pyogenic arthritis caused by a gas-producing organism may also present with a large joint effusion containing gas. This condition has to be differ-

Table 6.11 Intervertebral disc calcification

Degenerative spine disease
Post-traumatic
CPPD
Hemochromatosis
Ochronosis
Acromegaly
Amyloidosis
Hyperparathyroidism
Paraplegia (e.g. poliomyelitis)
Spinal fusion of any etiology (e.g. congenital, surgical, traumatic, inflammatory, infectious, degenerative, DISH)

Table 6.12 Periarticular soft tissue calcification

Post-traumatic dystrophic calcification/myositis ossificans
Post-surgical dystrophic calcification/heterotopic bone formation
Paralysis
Thermal injury
Calcific tendinitis and bursitis
Gout
CPPD
HADD
Infectious arthritis (especially tuberculous)
Scleroderma and other connective tissue diseases
Hyperparathyroidism and renal osteodystrophy
Hypoparathyroidism
Hypervitaminosis D
Milk-alkali syndrome
Calcinosis circumscripta and tumoralis
Sarcoidosis

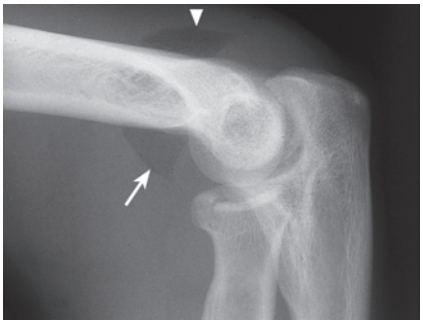

a

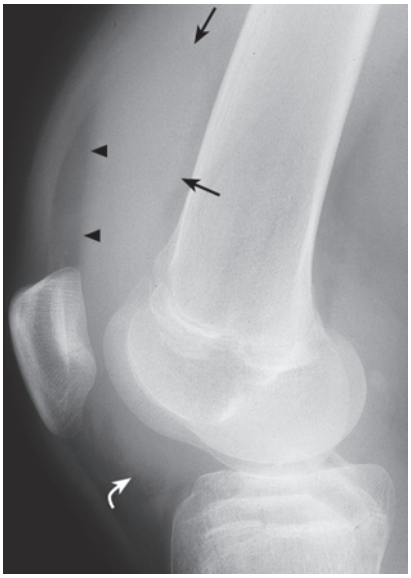

b

c

d

Fig. 6.**22 a, b, c, d** **Joint effusions**. **a: Elbow**: Visualization of the posterior fat pad (arrowhead) is diagnostic. The anterior fat pad can normally be seen, but its elevation by the intra-articular fluid may produce a "sail" configuration (arrow) indicative of an effusion. A radial head fracture is also evident. **b: Knee**: Fluid accumulation in the suprapatellar bursa (arrows) that connects with the knee is diagnostic. The joint effusion (curved arrow) may also displace the inferior patellar fat pad anteriorly. A fat-fluid (blood) level (arrowheads) can be seen in the suprapatellar bursa in a post-traumatic lipohemarthrosis, when the examination is performed with horizontal beam technique. **c: Ankle**: A larger anterior (arrows) and smaller posterior (arrowhead) soft tissue bulge is characteristic. **d: Wrist**: Anterior subluxation of the pisiform is caused by the large hemarthrosis in the radiocarpal joint secondary to intra-articular fractures of the distal radius and ulna.

entiated from a transient, linear or crescent-shaped intra-articular vacuum phenomenon (gas in the intra-articular cavity) that is an occasional incidental finding (Fig. 6.**23**) indicating the absence of a significant joint effusion. Gas within a meniscus or disc is usually associated with degenerative disease.

Para-articular soft tissue abnormalities

(Table 6.**13**)

Fusiform para-articular soft tissue swelling commonly occurs with rheumatoid arthritis and psoriatic arthropathy, whereas sausage-like swelling of an entire digit is quite characteristic for the latter condition. Subcutaneous nodules are frequently associated with rheumatoid arthritis (Fig. 6.**24**) and are characteristically located in dorsal and lateral aspects of the fingers, about the olecranon, ischial tuberosities, femoral trochanters and the Achilles tendon region. Gouty tophi presenting as nodular soft tissue masses are commonly found in the knees, hands, ankles, elbows and may rarely calcify. In osteoarthritis of the hand Heberden's nodes about the distal interphalangeal joints and Bouchard's nodes about the proximal interphalangeal joints are posterolateral soft tissue nodules which in a more advanced stage may be associated with a bony outgrowth (osteophyte).

The differential diagnosis of articular disorders is discussed in Table 6.**14**.

Fig. 6.**23** **Vacuum phenomenon.** A crescent-shaped radiolucent line is seen in the glenohumeral joint indicating the absence of a joint effusion.

Fig. 6.**24** **Subcutaneous soft tissue nodules in rheumatoid arthritis** are seen in the dorsal and lateral aspects of the fingers.

Table 6.13 Para-articular soft tissue nodules and swelling

Osteoarthritis (Heberden's nodes, Bouchard's nodes, bunion)
Rheumatoid arthritis (fusiform soft tissue swelling and rheumatoid nodules)
Rheumatic fever (similar to rheumatoid arthritis)
Psoriatic arthritis (fusiform soft tissue swelling and sausage finger)
Gout (tophi)
Multicentric reticulohistiocytosis (skin nodules and xanthomas)
Neuropathic osteoarthropathy
Infectious arthritis (fusiform soft tissue swelling and abscess formation)
Trauma (fusiform soft tissue swelling)
Foreign body granuloma (volar)
Hemophilia (hematomas)
Amyloidosis
Pigmented villonodular synovitis
Sarcoidosis (subcutaneous nodules)
Synovial cyst
Ganglion
Myositis ossificans (ossified)
Calcinosis circumscripta and tumoralis (calcified)
Xanthomatosis (subcutaneous nodules)
Weber-Christian disease (subcutaneous nodules)
Tumors (benign and malignant)
Aneurysm

Table 6.14 Differential Diagnosis of Articular Disorders

Disease	Characteristic Location	Radiographic Findings	Comments
Rheumatoid arthritis (RA) (Figs. 6.25, 6.26, 6.27, 6.28, 6.29, 6.30, and 6.31)	Symmetric polyarticular involvement of the synovial joints of the appendicular skeleton. Hands: Metacarpophalangeal and proximal interphalangeal joints including interphalangeal joints of the thumbs, with relative sparing of the distal interphalangeal joints. Wrists: Distal radioulnar joint including ulnar styloid, radiocarpal joint including radial styloid process and pisiform-triquetral joint. Feet: Medial aspects of the metatarsal heads, except in the fifth digit, where erosions on the lateral aspect may be the earliest manifestation. Interphalangeal joint of great toe (medial aspect) and calcaneus (erosions at insertions of Achilles tendon and plantar aponeurosis). Acromioclavicular joint (resorption of distal clavicles). Glenohumeral joints Elbows Hips (circumferential loss of joint space and protrusio acetabuli). Knees (symmetric involvement of the medial and lateral compartments). Ankles Cervical spine: Subluxations (anterior, lateral or vertical at C1-C2, less frequently at one or more subaxial levels). Vertical subluxation (telescoping) at the C1-C2 level may result in basilar invagination. Multilevel subluxations produce a “doorstep” or “stepladder” appearance.	Fusiform periarticular soft tissue swelling, regional osteoporosis and joint space narrowing associated with marginal and central erosions are the hallmark of the disease. The first erosions are frequently found in the metacarpophalangeal and proximal interphalangeal joints of the hands and the ulnar styloids. Besides marginal erosions originating typically in the bare bone areas of a joint without protective cartilage coverage, compressive erosions due to collapse of osteoporotic bone and surface erosions due to resorption of bone beneath inflamed tendons are also encountered. Synovitis resulting in fluid accumulation in joints, bursae and tendon sheaths is more difficult to appreciate with conventional radiographic technique. Progression of the disease leads to complete destruction of the involved joints and eventually to bony fusion, though the latter is rather uncommon. Subluxations and dislocation are frequent. In the hands flexion and extension contractures result in boutonnière or swan neck deformities of the fingers, hitchhiker deformity in the thumb and ulnar deviation in the metacarpophalangeal joints. In the wrist both volar (palmar) flexion instability (VISI) and dorsiflexion instability (DISI) occur besides dorsal subluxation of the distal ulna. Erosions may progress to extensive osteolysis in the distal clavicle, elbow and distal ulna. A chronic rotator cuff tear evident by progressive elevation of the humeral head (narrowing of the space between humerus and inferior surface of the acromion that typically becomes concave) is common in the advanced stage. In the spine diffuse narrowing of the disc spaces and facet joints without osteophytosis is characteristic.	Type III hypersensitivity connective soft tissue disorder with female predominance presenting clinically with morning stiffness, para-articular soft tissue swelling, especially of the wrist, hand and feet, and subcutaneous nodules at dorsal pressure points (e.g. olecranon). High sedimentation rate and positive rheumatoid factor in 90 % are characteristic laboratory findings. Extra-articular manifestations (75 %) are found in the lung (pulmonary fibrosis and rheumatoid nodules), pleura (unilateral or, less frequently, bilateral pleural effusions, usually not associated with parenchymal lung disease), cardiovascular system (pericarditis, myocarditis, aortitis and vasculitis), and lymphatic system (mild adenopathy and rarely splenomegaly). In *cystic rheumatoid arthritis* (Fig. 6.**32**) well-defined subcortical lesions often with sclerotic margins are the dominant radiographic feature, often in the absence of significant osteoporosis, joint space narrowing and erosions. In this condition 50 % of patients are seronegative and there is no sex predilection. *Felty syndrome:* Rheumatoid arthritis associated with splenomegaly and neutropenia. *Sjögren’s syndrome:* Connective tissue disorder with keratoconjunctivitis sicca, xerostomia and articular findings similar to rheumatoid arthritis.

(continues on page 144)

Fig. 6.**25** **Rheumatoid arthritis**. Osteopenia and erosive arthritic changes involving the hand and wrist with sparing of the distal interphalangeal joints are seen.

Fig. 6.**26** **Rheumatoid arthritis**. Osteopenia and erosive arthritic changes are associated with finger deformities including hitchhiker's thumb, swan neck deformities in digits 2 and 3, and boutonnière deformity in digit 5.

Fig. 6.**27** **Rheumatoid arthritis**. Severe osteopenia and erosive arthritic changes are associated with subluxations/dislocations and ulnar deviation in the metacarpophalangeal joints 2 to 5, ulnar subluxation in the radiocarpal joint and scapholunate dissociation.

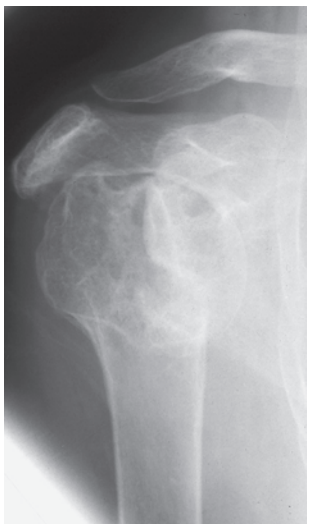

a

b

Fig. 6.**28 a, b** **Rheumatoid arthritis** (2 cases). **a** Shoulder: Extensive erosive changes in the glenohumeral joint and resorption of the distal clavicle are seen. **b** Elbow: Joint space narrowing and early erosions are evident.

Fig. 6.**29** **Rheumatoid arthritis**. Concentric (axial) joint space narrowing is associated with osteopenia, erosions and small subchondral cysts. Beginning osteophytosis is indicative of early secondary degenerative changes.

Fig. 6.**30** **Rheumatoid arthritis**. Small erosions (arrow) with minimal surrounding sclerosis are seen in the posterosuperior aspect of the calcaneus. Generalized osteopenia and a large ankle joint effusion (arrowheads) are also evident.

Fig. 6.**31** **Rheumatoid arthritis**. Early erosions about the dens associated with anterior atlanto-axial subluxation are seen.

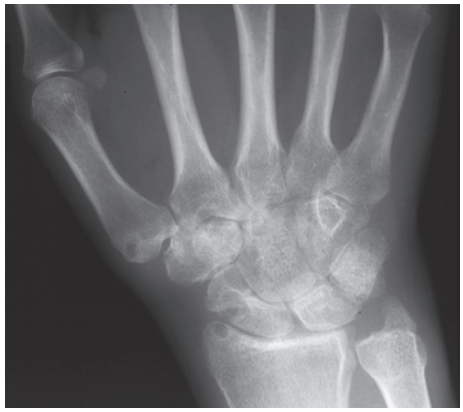

Fig. 6.**32** **Cystic rheumatoid arthritis**. Small well-defined subchondral cysts, some with sclerotic margins, are the dominant radiographic feature.

Table 6.14 (Cont.) Differential Diagnosis of Articular Disorders

Disease	Characteristic Location	Radiographic Findings	Comments
Juvenile rheumatoid arthritis (JRA, chronic juvenile arthritis) (Figs. 6.33, 6.34, 6.35 and 6.36)	Symmetric, polyarticular. Hands (metacarpophalangeal and interphalangeal joints). Wrists, Feed (metatarsophalangeal, interphalangeal and intertarsal joints). Knees Hips Elbows Cervical spine Temporomandibular joint	Periarticular fusiform soft tissue swelling, osteoporosis and joint subluxations are common, similar to rheumatoid arthritis of the adult (RA). In contrast to the latter joint space narrowing and erosions are late manifestations in JRA, intra-articular bony ankylosis, periostitis and epiphyseal compression fractures are common and synovial cysts are rare. Growth disturbances including epiphyseal enlargement and either overgrowth or undergrowth of long bones with reduced diameters (overconstriction) are characteristic.	Rheumatoid arthritis in patients under 16 years of age with female predominance. Three types are differentiated: 1. Juvenile-onset adult type rheumatoid arthritis (15%) 2. Juvenile-onset ankylosing spondylitis (5%) 3. Still's disease (75%). Systemic and/or articular symptoms with negative rheumatoid factor. Three subtypes: a) Systemic disease. Acute febrile onset with skin rash, generalized lymphadenopathy, hepatosplenomegaly, pericarditis and myocarditis are usually associated with mild articular manifestations. b) Polyarticular disease. c) Para-articular or mono-articular disease: Usually confined to large joints. Associated iridocyclitis may lead to blindness.

(continues on page 145)

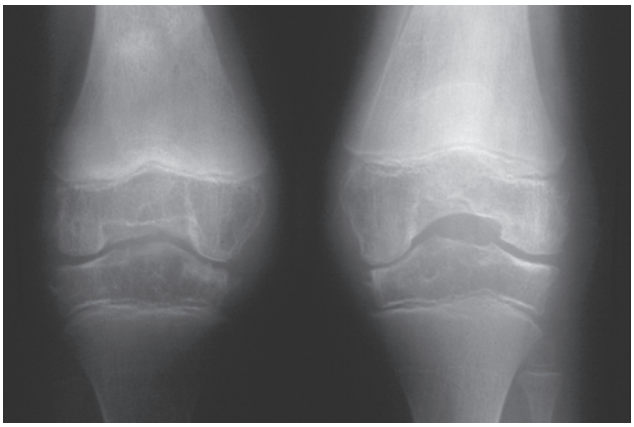

Fig. 6.**33** **Juvenile rheumatoid arthritis**. Osteopenia, joint space narrowing and overgrowth of the epiphyses including widening of the intercondylar notch in the distal femora are seen.

◁ Fig. 6.**34** **Juvenile rheumatoid arthritis**. Severe generalized osteopenia and advanced erosive arthritis in both hips with right coxa valga and left coxa vara deformity are seen. Early erosive changes are evident in both sacroiliac joints.

Fig. 6.**35** **Juvenile rheumatoid arthritis**. Extensive erosive/destructive changes are seen in the elbow associated with overconstricted distal humerus and proximal radial and ulnar shafts.

Fig. 6.**36** **Juvenile rheumatoid arthritis**. A completely fused C-spine with uniformly marked disc space narrowing and severe osteopenia is seen.

Table 6.14 (Cont.) Differential Diagnosis of Articular Disorders

Disease	Characteristic Location	Radiographic Findings	Comments
Ankylosing spondylitis (Fig. 6.37, 6.38 and 6.39)	Symmetric involvement of synovial and fibrocartilagenous joints and sites of ligamentous and tendinous attachments (entheses). Sacroiliac joints Lumbar spine Thoracic spine Cervical spine (late) Tendinous insertion in pelvis ("whiskering") Pubic symphysis Hips Shoulders Sternoclavicular joints	Bilateral and symmetric involvement of the sacroiliac joints is the hallmark of the disease. Both synovial and ligamentous portions are affected, but involvement of the ilium is typically more severe. Erosive changes progress from loss of articular definition to superficial erosions, fraying of the subchondral bone and widening of the joint. Proliferative bony changes progress from focal sclerosis of the subchondral bone to irregular bony bridges and eventually complete ankylosis. In the spine syndesmophytes (thin vertical ossifications of the outer fibers of the annulus fibrosus) connecting the anterior and lateral corners resulting eventually in a bamboo spine formation and straightening (squaring) of the anterior vertebral margins are diagnostic. Other findings include increased sclerosis of the corners of the vertebral bodies ("shiny corner" sign), discal ballooning (biconvex shape of the disc secondary to osteoporosis), "dagger" sign (ossification of the interspinous ligament producing a central radiodense line on frontal radiographs) and "trolley-track" sign (three vertical lines on frontal radiographs related to the ossifications of the interspinous ligaments and apophyseal joints). The hip involvement is typically bilateral and symmetric with concentric joint space narrowing and osteophytosis. In the shoulder diffuse joint space narrowing and erosive changes predominantly in the superolateral aspect of the humeral head that may progress to complete destruction of that part ("hatchet" sign) are characteristic.	Chronic inflammatory disease primarily affecting the spine with male predominance of 4:1 to 10:1 and clinical onset with low back pain and stiffness at the age of 15–35 years. Histocompatibility antigen HLA-B27 is positive in 96 %. Three times less common in blacks than Caucasians. Symmetric bilateral involvement of joints and sites of ligamentous attachment with subtle erosions and new bone formation (osteitis) with preferential involvement of the axial skeleton and large joints is characteristic. Erosive lesions in the spine at the discovertebral junction are termed Andersson lesions or, when located in the anterior margin, Romanus lesions. Complications of the ankylosed spine include fractures typically through a fused disc. Due to their instability these fractures are associated with significant morbidity and mortality, especially in the cervical region. Hand and wrist involvement occurs in 30 % of patients, but is rarely a dominant feature of the disease. Radiographic findings in these locations are similar to psoriatic arthropathy.

(continues on page 147)

Fig. 6.**37** **Ankylosing spondylitis**. Symmetric bilateral sacroiliitis with erosions and joint space narrowing, mild concentric (axial) narrowing of both hips and extensive fluffy enthesopathy along the ischiatic bones are characteristic.

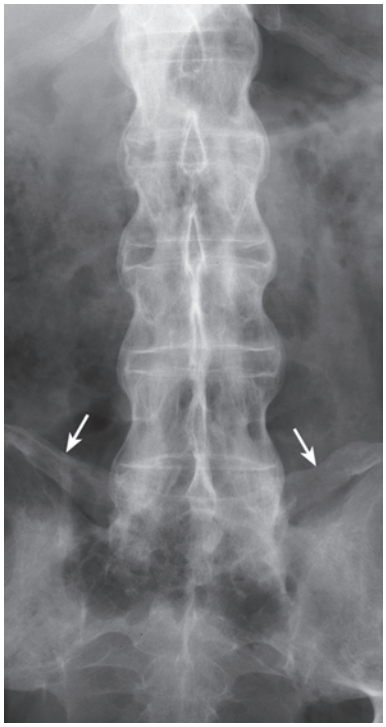

a

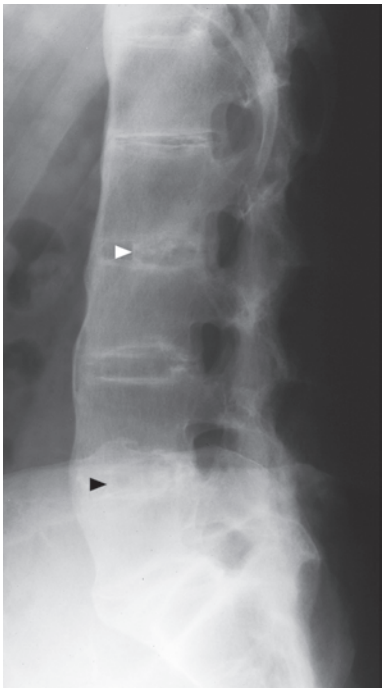

b

Fig. 6.**38 a, b** **Ankylosing spondylitis**. Fusion of the lumbar spine by delicate vertical syndesmophytes produces a "bamboo spine". Bilateral fused sacroiliac joints and ossification of both the interspinous ligament producing the "dagger" sign and the iliolumbar ligaments (arrows) are also evident in the anteroposterior projection (**a**). On the lateral film (**b**) straightening of the anterior vertebral margins, central disc calcifications (arrowheads) and either discal ballooning or discal narrowing are seen.

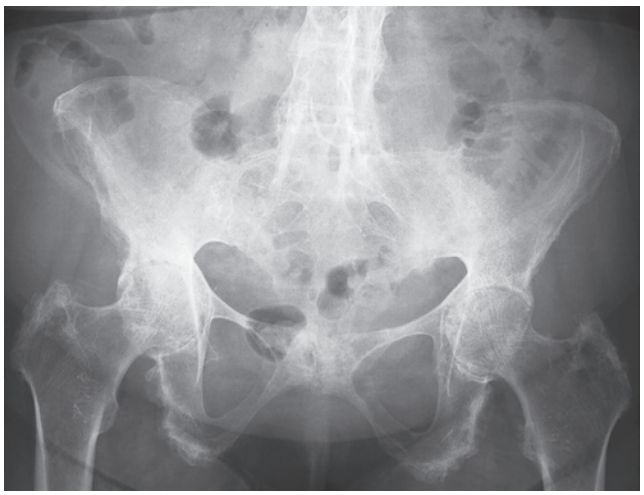

Fig. 6.**39** **Ankylosing spondylitis**. Generalized osteopenia, fusion of the lower lumbar spine and bilateral sacroiliac joints, marked concentric (axial) narrowing of the joint space in both hips with mild protrusio acetabuli on the right side, erosion and blurring of the subchondral bone with adjacent eburnation in the pubic symphysis, and extensive fluffy enthesopathy along the ischiatic bones and greater trochanters are seen.

Table 6.14 (Cont.) Differential Diagnosis of Articular Disorders

Disease	Characteristic Location	Radiographic Findings	Comments
Psoriatic arthritis (Figs. 6.40, 6.41, 6.42, 6.43, 6.44, 6.45 and 6.46)	Asymmetric polyarticular involvement of synovial and fibrocartilagenous joints and sites of tendinous and ligamentous attachments (entheses). Hands: Distal interphalangeal joints, proximal interphalangeal joints, metacarpophalangeal joints and tufts (tuftal resorption is almost always associated with nail involvement). Feet: Interphalangeal joints, metatarsophalangeal joints and tufts. Sacroiliac joints Sternoclavicular joints Acromioclavicular joints Spine Calcaneus Pubic symphysis	Fusiform soft tissue swelling about the involved joint or, less commonly, sausage-like swelling of entire digit is typical. Osteoporosis is not prominent or absent. Diffuse loss of joint space (similar to rheumatoid arthritis) is characteristic, but in the small joints of the fingers and toes considerable widening of articular space is not uncommon. Erosive/destructive changes tend to progress from the joint margins to the center. "Pencil-in-cup", or "ball-in-cup", "cup-and-saucer" appearance are quite characteristic in the digits. Bone proliferation is typically associated with erosive changes and may produce irregular excrescences with spiculated appearance. Exuberant periostitis and new bone formation in an entire phalanx may result in an ivory phalanx. Bony ankylosis is quite common in an advanced stage, especially in the hands and feet. Enthesopathy (bony proliferation at ligament and tendon attachment sites) occurs at the posterior and inferior surfaces of the calcaneus, femoral trochanters, the ischial tuberosities, medial and lateral malleoli, olecranon, radial tuberosity, and about the knees including the patella. Deformities in the hand and feet are less frequent than in rheumatoid arthritis. Sacroiliac joint involvement tends to be bilateral, but often somewhat asymmetric. Findings include erosions, sclerosis and widening or narrowing of the joint space, whereas complete ankylosis is relatively rare. In the spine thin and curvilinear to thick and fluffy paravertebral ossifications may be found with preferential involvement of the lower thoracic and upper lumbar spine. They may involve only one side of the spine, or when bilateral, may be asymmetric (DD: ankylosing spondylitis). In the cervical spine extensive proliferation along the anterior surface and both narrowing and sclerosis of the apophyseal joints are characteristic manifestations.	Arthritic changes are present in less than 5% of patients with psoriasis. Skin disease is present in 85% of patients with arthritic onset, but occasionally arthritis may antedate dermatological changes. HLA-B27 is positive in 80% of patients whereas the rheumatoid factor is negative. Types: 1) True psoriatic arthritis (polyarthritis with distal interphalangeal joint involvement). 2) Seronegative polyarthritis simulating rheumatoid arthritis (DD: Psoriasis with coincidental rheumatoid arthritis). 3) Sacroiliitis and spondylitis. 4) Peripheral arthritis and sacroiliitis (combination of types 1 and 3) Radiographic features that differentiate psoriatic arthritis from rheumatoid arthritis in the hand include: 1) Lack of osteoporosis. 2) Tuftal resorption. 3) Asymmetric distribution of joint involvement 4) Involvement of the distal interphalangeal joints and relative sparing of the wrists. 5) Occasional widening of the articular space secondary to destruction of marginal and subchondral bone. 6) Bone proliferation including exuberant periosteal reaction, ankylosis and ivory phalanx formation 7) Sausage-finger.

(continues on page 150)

Fig. 6.**40** **Ankylosing spondylitis**. Erosive arthritic changes are seen in the hand and wrist that are indistinguishable from psoriatic arthritis.

Fig. 6.**42** **Psoriatic arthritis**. Erosive arthritic changes involving primarily the proximal and distal interphalangeal joints and the wrist are seen. The margins of the erosions are frequently indistinct because of the associated new bone formation. Bony ankylosis of the distal interphalangeal joint of the index finger is also evident.

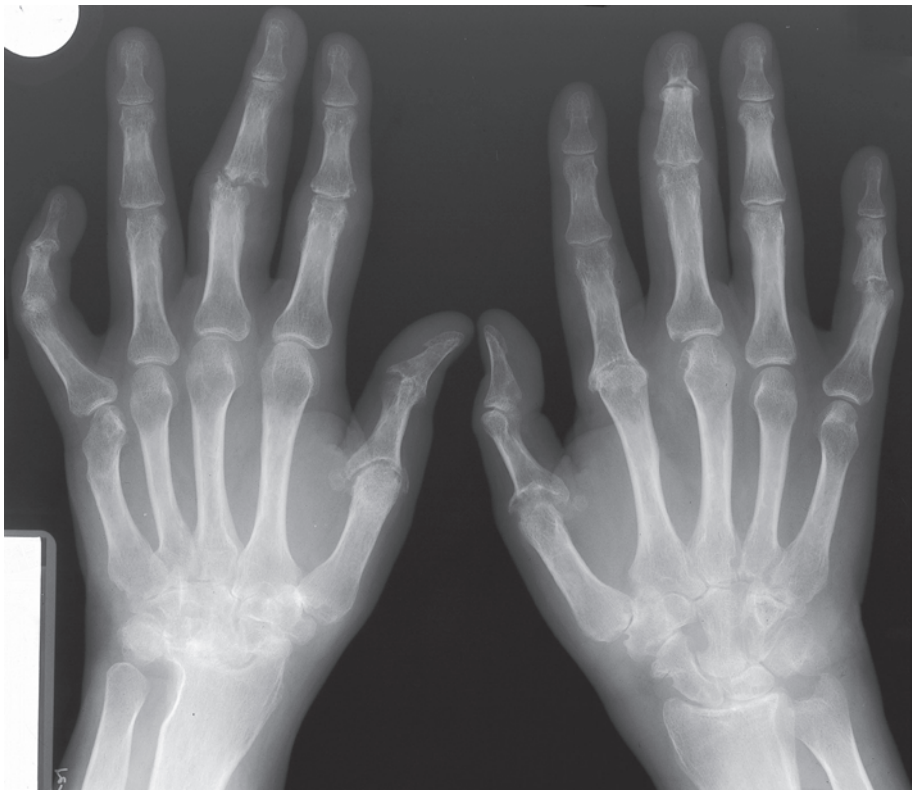

Fig. 6.**41** **Psoriatic arthritis**. Erosive arthritic changes with both asymmetric distribution and severity of joint involvement in both hands and wrists are seen.

Fig. 6.**43** **Psoriatic arthritis**. Severe destruction of the subchondral bone is seen in the hand and wrist leading to considerable widening of the articular space in several fingers.

Fig. 6.**44** **Psoriatic arthritis**. Erosions associated with bone proliferation are seen in the interphalangeal joint of the great toe, the first tarsometatarsal joint and the dislocated metatarsophalangeal joints 2 to 5. Tuftal erosions are also evident in several toes.

Fig. 6.**45** **Psoriatic arthritis**. Erosions of the bone adjacent to the intervertebral spaces of C4/5 and C5/6 with fluffy anterior syndesmophyte formation and beginning bony bridging.

Fig. 6.**46** **Psoriatic arthritis**. Fusion of the lumbar spine by large asymmetric syndesmophytes is seen. Narrowed bilateral sacroiliac joints with early erosions and mild reactive sclerosis on the right side are also present.

Table 6.14 (Cont.) Differential Diagnosis of Articular Disorders

Disease	Characteristic Location	Radiographic Findings	Comments
Reiter's syndrome (triad of arthritis, urethritis, and conjunctivitis) (Figs. 6.47, 6.48 and 6.49)	Usually asymmetric polyarticular involvement of synovial and fibrocartilagenous joints and entheses with preferential involvement of the lower extremity. Foot: Metatarsal phalangeal and interphalangeal joints including sesmoids. Calcaneus Ankle Knee Pubic symphysis Sacroiliac joints Spine Hand (especially proximal interphalangeal joints)	Periarticular osteoporosis may accompany acute episodes, but is not a prominent feature of the chronic stage. Loss of joint space and erosions are more frequently found in smaller than larger joints. Superficial bone resorption also occurs beneath inflamed bursae and tendon sheaths. Fluffy periosteal bone proliferation is characteristic, especially in the posterior and plantar aspect of the calcanei, ischial tuberosities and trochanters, but also in the metatarsal, metacarpal and phalangeal shafts, the malleoli and the knees. Sacroiliac joint involvement is common (in excess of 50% in advanced disease) and is usually bilateral symmetric or asymmetric. Osseous erosions associated with adjacent sclerosis varying from mild to severe predominate characteristically on the iliac site of the joint. In the lower thoracic and upper lumbar spine thin or thick vertical osseous bridges may extend across the intervertebral disc and initially are separated by a clear space from the lateral margin of the adjacent vertebral bodies. Spinal involvement is typically asymmetric.	Peak onset occurs between 15 and 35 years of age with male predominance. HLA-B27 is positive in 75% of patients. Transmission occurs in association with either epidemic dysentery or sexual intercourse. Urethritis is frequently the initial manifestation. Associated mucocutaneous lesions include balanitis circinata and keratosis blennorhagica in soles and palms. Conjunctivitis may progress to uveitis and keratitis. Seventy percent of patients develop radiographic bony alterations. Acute attacks may be associated with soft tissue swelling and osteoporosis. Radiographic features of Reiter's syndrome are virtually indistinguishable from psoriatic arthritis. Compared to the latter condition preferential involvement of the lower extremities, less frequent involvement of the spine and relatively rare bony ankylosis of the small joints of the hands and feet are favoring the diagnosis of Reiter's syndrome.
Enteropathic arthritis (Figs. 6.50, 6.51 and 6.52)	Monoarticular to bilateral symmetric Sacroiliac joints Spine Knees Ankles Feet Shoulder Elbows Wrists Hands	Central type: Symmetric involvement of the sacroiliac joints and spine indistinguishable from ankylosing spondylitis. Peripheral type: Monoarticular or pauciarticular acute synovitis presenting with soft tissue swelling and periarticular osteoporosis. A close temporal association between exacerbation of intestinal and arthritic findings is characteristic. Chronic changes are rare and include joint space narrowing, erosions and cyst formation mimicking rheumatoid arthritis. Clubbing of fingers and rarely periostitis of tubular bones simulating hypertrophic osteoarthropathy may also be found.	The incidence of arthritic changes: Ulcerative colitis 12% Crohn's disease 10% Whipple's disease 75% (predominantly peripheral type) Salmonella 2% Shigella 2% Yersinia 30% Intestinal bypass surgery 3% Hepatic disease (cirrhosis, hepatitis) 2% (exclusively peripheral type) Pancreatic disease 1% (exclusively peripheral type; associated osteonecrosis common). Intestinal infections caused by salmonella and yersinia may also cause septic arthritis and osteomyelitis by hematogenous spread.

(continues on page 152)

Fig. 6.**47** **Reiter's syndrome**. Erosions with partial destruction of the metatarsal head and beginning fluffy bone proliferation are seen in the 5th metatarsal phalangeal joint. Joint space narrowing and beginning bony proliferation without erosions are evident in the interphalangeal joint and metatarsophalangeal of the great toe.

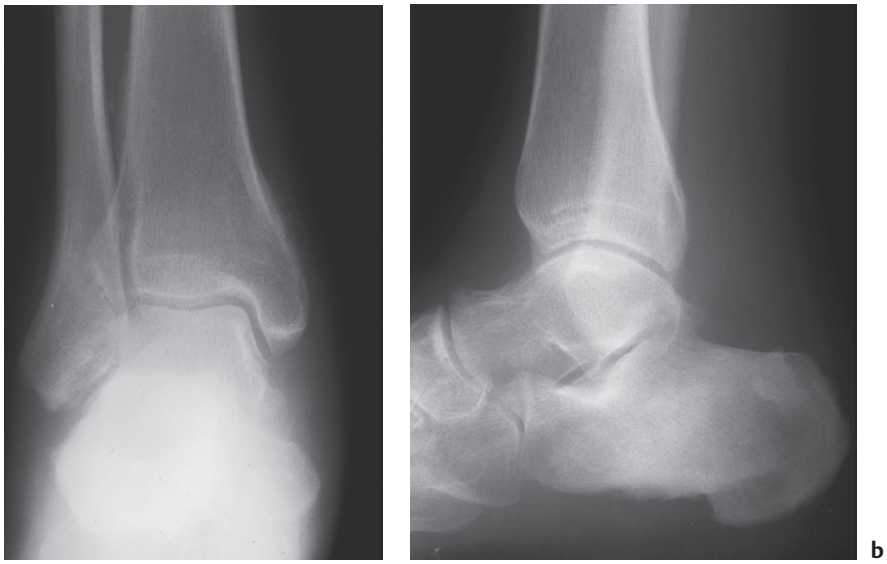

a **b**

Fig. 6.**48 a, b** **Reiter's syndrome**. Extensive fluffy periostitis is seen in the medial aspect of the distal tibia metaphysis and about the lateral malleolus in **a**, and about the posterior and inferior aspect of the calcaneus in **b**.

Fig. 6.**49** **Reiter's syndrome**. Erosive arthritic changes with bone proliferation are seen in the several joints of the hand and the wrist. Note also the diffuse soft tissue thickening of digits 2 and 3 (sausage fingers).

Fig. 6.**50** **Enteropathic arthritis (Crohn's disease)**. Bilateral fused sacroiliac joints and delicate syndesmophyte formation in the lumbar spine are evident.

Table 6.14 (Cont.) Differential Diagnosis of Articular Disorders

Disease	Characteristic Location	Radiographic Findings	Comments
Jaccoud's arthritis (Fig. 6.*53*)	Bilateral symmetric Hands	Bilateral symmetric deforming nonerosive arthropathy. Ulnar deviation and flexion deformities of the metacarpophalangeal joints, especially in the fourth and fifth finger are characteristic. Hyperextension of the interphalangeal joints may be associated. Joint space narrowing and erosions are typically absent. Foot involvement with lateral deviation and subluxation of the metatarsophalangeal joints is less common.	Post-rheumatic fever arthropathy. Rheumatic fever is characterized by fever, carditis and polyarthritis following an episode of beta-hemolytic streptococcal infection. Reversible nature of the articular deformities is characteristic, but occasionally deformities may become fixed.
Systemic lupus erythematosus (Fig. 6.54)	Bilateral symmetric Hands Feet Hips Knees Ankles Shoulders	Bilateral symmetric deforming nonerosive arthropathy of the hands occurs in 25 % of patients. Subluxation of the metacarpophalangeal joints with ulnar deviation, swan-neck and boutonnière deformities of the fingers and hyperextension of the interphalangeal joint of the thumb are characteristic. Joint space narrowing and erosions are rare. Occasionally hook erosions on the radial and volar aspects of the metacarpal heads are found, presumably produced by capsular pressure. Associated foot abnormalities may include hallux valgus deformity, metatarsophalangeal joint subluxations and splaying of the forefoot. Instability in knees, shoulders and atlanto-axial joint may also be present. Osteonecrosis is, besides deforming nonerosive arthropathy, the other classic feature of the disease occurring in up to 40 % of patients. The femoral heads are most commonly affected site, but humeral heads, femoral condyles, tibial plateaus, talar domes, and the small bones of hands, wrists and feet are also frequently involved. Signs of avascular necrosis in these joints and cystic changes in the carpal bones are the corresponding radiographic features. Acrosclerosis and tuftal resorption complete the radiographic picture.	Relatively common connective tissue disorder with 10:1 female predominance and typical onset during childbearing age. Three times more common in blacks. Laboratory findings include antinuclear DNA antibodies (87 %), LE cell formation (78 %), hypergammaglobulinemia (77 %), anemia (78 %) and leukopenia (77 %). Nonspecific bilateral polyarthralgia involving hands, wrists, shoulders and knees is present in 90 % of patients. Myositis and spontaneous tendon rupture are common and usually associated with systemic or local steroid therapy. Soft tissue calcifications occur, but are much less common than in either scleroderma or dermatomyositis. Osteomyelitis and septic arthritis (bacterial and mycotic) are relatively frequent complications. Both steroid administration and renal disease are major contributing factors to the susceptibility for infection. The deforming nonerosive lupus arthropathy differs from Jaccoud's arthropathy in the hand only by the site of involvement. In the former all metacarpophalangeal joints including the thumb are typically involved, whereas the latter has a preference for the fourth and fifth finger.

(continues on page 154)

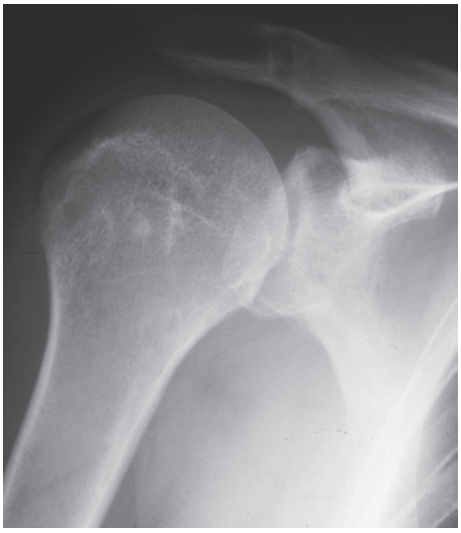

Fig. 6.**51** **Enteropathic arthritis (Crohn's disease)**. Erosions with fluffy spiculated bone proliferation are limited to the greater tuberosity.

Fig. 6.**52** **Enteropathic arthritis (Crohn's disease)**. Juxta-articular osteoporosis and scattered early erosions are evident in the hand and wrist best appreciated in the volar aspect of the interphalangeal joint of the thumb and the ulnar aspect of the fifth carpometacarpal joint. Nonspecific arthritis with para-articular soft tissue swelling is seen in the distal interphalangeal joints of the third and fourth fingers.

Fig. 6.**53** **Jaccoud's arthritis**. Ulnar deviation without erosions is seen in the metacarpophalangeal joints. It is most severe in the fifth digit where it progressed to complete dislocation.

Fig. 6.**54** **Systemic lupus erythematosus**. Ulnar deviation in the metacarpophalangeal joints and hitchhiker's deformity of the thumb are seen.

Table 6.14 (Cont.) Differential Diagnosis of Articular Disorders

Disease	Characteristic Location	Radiographic Findings	Comments
Scleroderma (Fig. 6.55)	Monoarticular to bilateral symmetric. Hands (distal and proximal interphalangeal joints and metacarpophalangeal joints). Wrists (first carpometacarpal joint and distal radioulnar joint) Sternoclavicular joints Acromioclavicular joints Mandible (thickening of the periodontal membrane resulting in a widened periodontal gap between the tooth and the mandible is a characteristic finding).	Acro-osteolysis and soft tissue calcifications are the hallmark of the disease. Resorption of the tufts leads to "penciling" of the phalanx. Calcifications present as small punctate deposits at the phalangeal tip to more wide spread conglomerate deposits with periarticular distribution. Acrosclerosis (hyperostosis of the tuft) associated with soft tissue atrophy is another presentation. Nonspecific articular involvement of the hands and wrist may eventually progress to erosive destructive changes with or without intra-articular calcifications. Involvement ranges from monoarticular (e.g. first carpometacarpal joint) to bilateral symmetrical. Foot abnormalities are less frequent and usually limited to the metatarsophalangeal joints. Thinning of the 3rd to 6th ribs posteriorly, and resorption of both the proximal and distal ends of the clavicle and the distal acromion can also be found.	Autoimmune disease with 3:1 female predominance and peak age of 30 to 50 years. May be associated with CREST syndrome (*C*alcinosis of skin and subcutaneous tissue, *R*aynaud's phenomenon, *E*sophageal dysmotility, *S*clerodactyly and *T*elangiectasia). Musculoskeletal abnormalities of scleroderma associated with other collagen vascular disease (e.g. rheumatoid arthritis or systemic lupus erythematosus) is referred to as mixed connective tissue disease or overlap syndrome, respectively. Soft tissue calcifications frequently occur also about large joints. (DD: Milk-alkali syndrome, hypervitaminosis D, renal osteodystrophy and tumoral calcinosis). *Dermatomyositis* (Fig. 5.**56**) presents with similar radiographic features as scleroderma, but both extensive linear subcutaneous and intermuscular fascial plane calcifications are typical for the former disorder.
Vasculitides	Hands Wrists Hips Knees Ankles	Nonspecific (periarticular soft tissue swelling, osteoporosis and joint effusions) or absent.	*Polyarteritis nodosa* (occasionally with periosteal new bone formation) *Giant cell (temporal) arteritis* *Polymyalgia rheumatica* *Henoch-Schönlein (anaphylactoid) purpura* *Cryoglobulinemia* (occasionally with small subchondral cysts) *Erythema nodosum*
Familial Mediterranean fever (Fig. 6.57)	Bilateral asymmetric Sacroiliac joints (unilateral or bilateral) Hips Knees	Osteoporosis Epiphyseal overgrowth in children. Articular erosions, sclerosis and fusion may eventually develop.	Rare genetic disorder predominantly in Sephardic Jews, Armenians and Arabs presenting with multiple episodes of fever associated with peritonitis, pleuritis and synovitis.
Relapsing polychondritis (Fig. 6.58)	Bilateral asymmetric Sacroiliac joints (unilateral or bilateral)	Bilateral sacroiliitis with joint space loss, erosion and eburnation without spinal alterations. Nonspecific findings in peripheral joints, sternoclavicular joints, manubriosternal and costochondral junctions ranging from usually mild nonerosive to occasionally multilating arthritis. Extra-articular findings include tracheal stenosis and calcifications of the auricular cartilage.	Episodic inflammation of cartilaginous tissue (e.g. external ear, nose, larynx, trachea, ribs and joints) and ocular structures (e.g. conjunctiva, sclera and urea) occurring in all age groups with peak in fourth decade.
Behçet's syndrome (Figs. 6.59 and 6.60)	Monoarticular or oligoarticular Knees Small peripheral joints Sacroiliac joints	Monoarticular or oligoarticular involvement with periarticular soft tissue swelling and osteoporosis and rarely joint space narrowing and small erosions	Triad of recurrent oral and genital ulcerations and ocular inflammation characteristic. Occurs at all ages (peak age 30 years) with male predominance.

(continues on page 156)

Fig. 6.**55** **Scleroderma**. Osteopenia, soft tissue calcifications and resorption of the tufts in the thumb, index and middle finger are seen. The small cystic lesion in the distal aspect of the first metacarpal is an incidental finding most likely representing a small enchondroma.

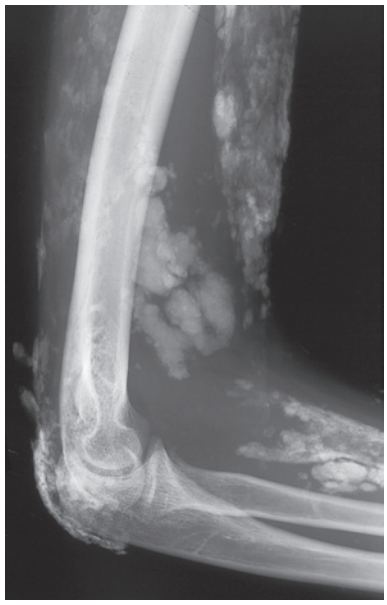

Fig. 6.**56** **Dermatomyositis**. Extensive subcutaneous and intermuscular fascial plane calcifications are evident.

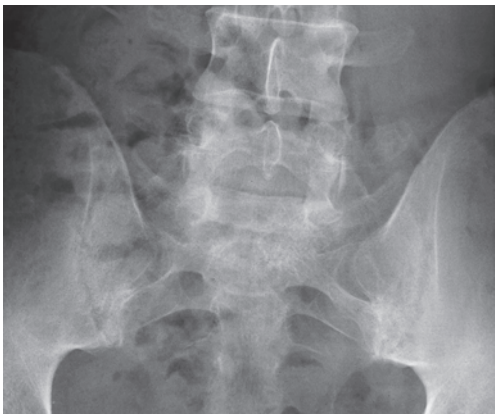

Fig. 6.**57** **Familial Mediterranean fever**. Osteopenia, joint space narrowing and early erosions are seen in both sacroiliac joints.

Fig. 6.**58** **Relapsing polychondritis**. Early erosions with reactive sclerosis are seen in both sacroiliac joints.

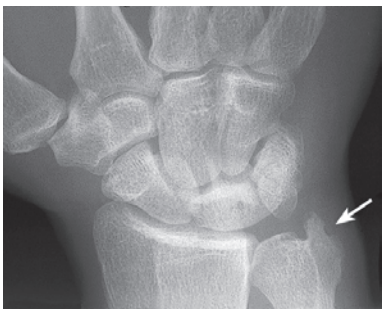

Fig. 6.**59** **Behçet's syndrome**. Minimal scattered erosive changes are seen in the wrist with the largest erosion being located in the ulnar styloid (arrow).

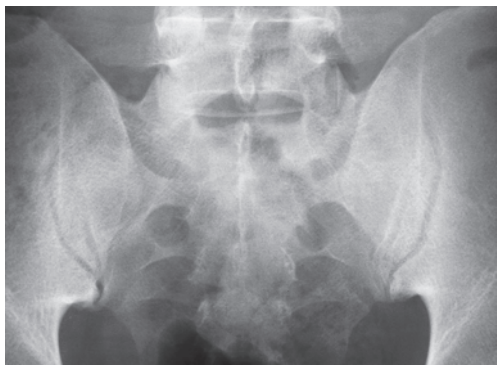

Fig. 6.**60** **Behçet's syndrome**. Early erosions are seen in both sacroiliac joints (same patients as in Fig. 6.**59**).

Table 6.14 (Cont.) Differential Diagnosis of Articular Disorders

Disease	Characteristic Location	Radiographic Findings	Comments
Hemophilia (Figs. 6.61 and 6.62)	Bilateral, not always symmetric Knees Ankles Elbows	Dense appearing (hemosiderin deposition) joint effusions and periarticular soft tissue swelling, osteoporosis, joint space narrowing, cartilaginous and osseous joint destruction with secondary sclerosis, osteophytosis and subchondral cyst formation and epiphyseal overgrowth (secondary to chronic hyperemia) are characteristic. Widening of the intercondylar femoral notch and squaring of the inferior pole of the patella, tibiotalar slanting in the ankle and widening of the trochlear and radial notches of the ulna in the elbow may be associated. Intraosseous hemorrhage may lead to osteonecrosis (especially in the femoral head and talar dome) and hemophilic pseudotumor formation simulating a variety of benign or malignant lesions and infections.	Occurs in approximately 1 in every 10,000 males due to X-linked deficiency of coagulation factor VIII (hemophilia A, 90% of patients) or factor IX (hemophilia B or Christmas disease, 10% of patients). Von Willebrand's disease (autosomal dominant with factor VIII and platelet deficiency) may occasionally present with similar features in both genders. Radiographic features of hemophilia and juvenile rheumatoid arthritis in large joints are virtually indistinguishable. Involvement of the spine and hands, bony ankylosis and growth inhibition are however findings only associated with juvenile rheumatoid arthritis.
Gout (Figs. 6.63, 6.64, 6.65, 6.66, 6.67, 6.68 and 6.69)	Monoarticular or asymmetric polyarticular involvement typical. Feet: Involvement of first metatarsophalangeal joint most characteristic with erosion frequently located on medial or dorsal aspect of first metatarsal head. Other metatarsophalangeal joints, interphalangeal joints, tarsometatarsal joints and intertarsal joints may also be affected. Hands: Distal and proximal interphalangeal joints are most commonly involved, but metacarpophalangeal joints and wrists may also be affected. Elbows: Bilateral olecranon bursitis with erosive and proliferative changes in the adjacent olecranon virtually pathognomonic. Knees Sacroiliac joints	Erosions caused by tophi may be intra-articular, para-articular or at a considerable distance from the joint and are typically surrounded by a sclerotic border producing a "punched out" appearance. An elevated bony spicule may form over the eroding tophus producing the "overhanging edge" sign that is found in almost half of the cases and quite characteristic. Bone proliferation may occasionally produce club-shaped metacarpal, metatarsal and phalangeal heads ("mushrooming"), enlarged ulnar styloids and thickened diaphyses. Tophi typically present as eccentric juxta-articular, lobulated soft tissue masses occasionally containing calcific deposits. Intra-osseous calcified tophi may mimic enchondromas in the hand. Calcium pyrophosphate deposition disease (CPPD) is occasionally associated presenting with chondrocalcinosis of the menisci of knee, pubic symphysis and triangular fibrocartilage of the wrist. Osteonecrosis is another associated complication.	Hyperuricemia is the hallmark of the disease. Deposition of urate crystals occurs in para-articular soft tissues, joints and bone causing inflammation and destruction. The disease is caused by either overproduction of uric acid or decrease in renal urate excretion. There is a 20:1 male predominance with the first attack occurring typically in the 5th decade of life, although any age is possible, in women the disease commences in the postmenopausal period. Stages: 1) Asymptomatic hyperuricemia 2) Acute gouty arthritis: Monoarticular or polyarticular attacks presenting with pain, tenderness and swelling, but usually without radiographic bony abnormality. 3) Chronic tophaceous gout: Develops eventually in fewer than half of the patients with recurrent acute attacks. *Secondary gout* rarely causes radiographically apparent arthropathy and is associated with myeloproliferative disorders and sequelae of their treatment and with chronic renal failure. *Lesch-Nyhan syndrome*: X-linked enzyme deficiency of uric acid metabolism presenting with mental retardation is associated with self-mutilation (amputation of fingertips), gouty erosions and retarded skeletal maturation. *Saturnine gout* is a complication of chronic lead poisoning caused by contamination of alcoholic beverages. *Type 1 glycogen storage disease* may also be associated with gouty arthritis

(continues on page 159)

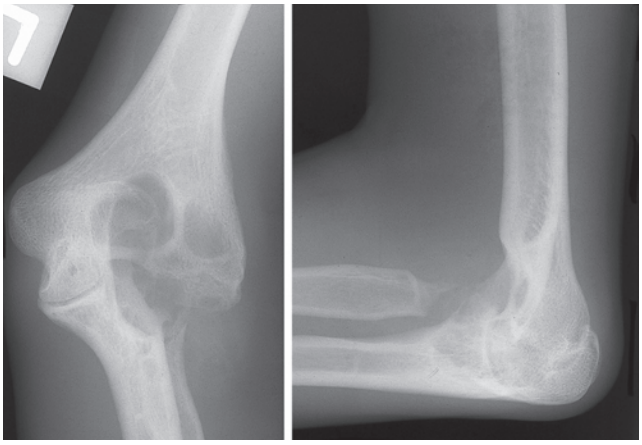

a b

Fig. 6.**61 a, b** **Hemophilia**. Erosive/destructive changes with subchondral cyst formations are seen in the elbow in anteroposterior (**a**) and lateral (**b**) projections.

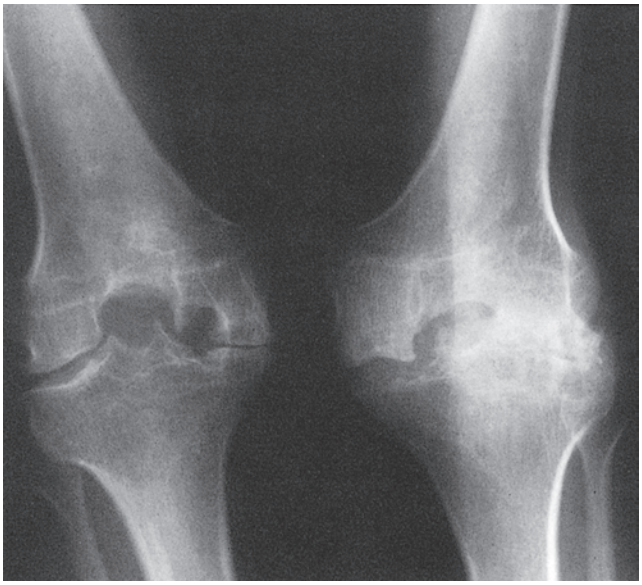

Fig. 6.**62** **Hemophilia**. Osteoporosis, widened intercondylic notch and joint space narrowing and destruction of the adjacent bone are seen bilaterally. Furthermore extensive reactive sclerosis with subchondral cyst formations is present in the lateral compartment of the left knee.

Fig. 6.**63** **Gout**. Well defined erosions with small bony spicules associated with a soft tissue mass are seen in the distal interphalangeal joint. Osteoporosis and joint space narrowing typically are absent.

Fig. 6.**64** **Gout**. A large dense soft tissue mass surrounding the distal interphalangeal joint of the fifth finger where small subchondral and marginal erosions are seen, the latter with tiny overhanging bone spicules. Erosive and cystic changes with beginning bone proliferation are also seen in the wrist and distal radioulnar joint, most notably in the proximal aspect of the triquetrum.

Fig. 6.**65** **Gout**. A large erosion with considerable amount of new bone formation is seen on the medial aspect of the first metatarsal head and neck without involvement of the articular surface of the adjacent joint. Only minimal erosive/cystic changes are seen in the other metatarsal heads and about the interphalangeal joint of the great toe.

Fig. 6.**66** **Gout**. A large soft tissue mass with scattered calcifications is seen eroding the adjacent olecranon.

Fig. 6.**67** **Gout**. A large tophus (arrows) with sclerotic margin is seen in the patella. Joint space narrowing with small erosions and subchondral cysts and reactive sclerosis is seen in the medial compartment of the knee.

Fig. 6.**68** **Gout**. Well defined erosions of varying sizes and large cysts with or without sclerotic margins are seen in the distal tibia, lateral malleolus and talus.

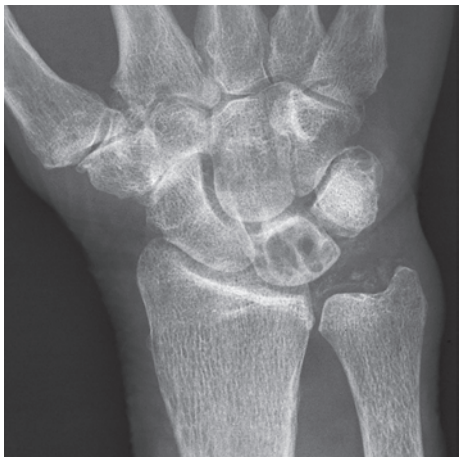

Fig. 6.**69** **Gout and CPPD**. A multiloculated cystic lesion in a slightly expanded lunate is associated with chondrocalcinosis in the triangular fibrocartilage. A smaller cyst with sclerotic margin is evident in the distal aspect of the triquetrum.

Table 6.14 (Cont.) Differential Diagnosis of Articular Disorders

Disease	Characteristic Location	Radiographic Findings	Comments
Calcium pyrophosphate dihydrate crystal deposition disease (CPPD) (Figs. 6.70, 6.71, 6.72 and 6.73)	Bilateral and symmetric distribution. Knees Wrists Metacarpophalangeal joints (especially 2nd and 3rd) Pubic symphysis Hips Intervertebral discs	Chondrocalcinosis is the hallmark of the disease and refers to linear or punctate calcifications of both the fibrocartilagenous cartilage (e.g. menisci of the knee, triangular fibrocartilage of the wrist, pubic symphysis, annulus fibrosus of the intervertebral disc, and acetabular and glenoid labra) and the hyaline cartilage (e.g. wrist, knee, elbow, hip and shoulder). The calcifications in the fibrous cartilage tend to be irregular, thick and shaggy and in the hyaline cartilage thin and linear. Synovial, capsular, tendinous, bursal and ligamentous calcifications are frequently associated. Arthritic changes of CPPD and osteoarthritis are very similar and include joint space narrowing and subchondral sclerosis. In CPPD, however, subchondral cysts tend to be larger and more numerous, and subchondral bone collapse and fragmentation with formation of intra-articular loose bodies are much more common, whereas osteophytosis is often less prevalent. CPPD also tends to affect joints that are not commonly involved in osteoarthritis, such as the metacarpophalangeal joints, midcarpal and radiocarpal compartments of the wrist, elbows and shoulders. In the knee the medial compartment is most frequently involved, similar to primary osteoarthritis, but isolated involvement of either the patellofemoral or lateral compartment is somewhat suggestive of either CPPD or post-traumatic osteoarthritis. In the wrist a predilection for the radiocarpal compartment results in "degenerative" changes between the distal radius and the proximal carpal row. The scaphoid moves proximally and appears compressed and deformed by the adjacent radius, whereas the lunate moves distally and hereby producing a "stepladder" appearance. This pattern is also referred to as scapholunate advanced collapse (SLAC) and, besides CPPD is also found a sequela of occupational or accidental trauma. Isolated "degenerative" changes in the second and third metacarpophalangeal joints including collapse of the metacarpal heads are another quite characteristic CPPD manifestation. Irregular, beaklike osteophytes on the radial aspects of the metacarpal heads may be associated. In the hip CPPD may be suggested when advanced degenerative changes are associated with concentric loss of joint space.	Most common crystalline deposition arthropathy affecting primarily the middle-aged and elderly population without sex predilection. Clinically CPPD may be asymptomatic or mimic osteoarthritis, rheumatoid arthritis, neuropathic arthropathy or gout, the latter beginning frequently referred to as *pseudogout*. CPPD is usually idiopathic, but a hereditary form is also recognized. A variety of diseases have been associated with CPPD including osteoarthritis, diabetes mellitus, gout, hyperparathyroidism, hemochromatosis, and Wilson's disease. Chondrocalcinosis may be found in both primary and post-traumatic osteoarthritis and thus the demonstration of cartilage calcification should not automatically lead to the diagnosis of CPPD arthropathy, particularly since the accumulation of other crystals than calcium pyrophosphate dihydrate (CPP) might be responsible for this finding. *Wilson's disease* (hepatolenticular degeneration) is a rare autosomal recessive disease with excessive copper retention caused by the inability of the liver to excrete it into the bile. It presents with degenerative changes in the brain, especially the basal ganglia, hepatic cirrhosis and diagnostic greenish-brown Kayser-Fleischer corneal rings. Articular changes in the metacarpophalangeal joints, wrist, hand, foot, hip, shoulder, elbow resemble CPPD or osteochondritis dissecans. Additional radiographic findings include osteoporosis and fluffy new bone formation at sites of capsular, ligamentous or tendinous attachments. In the spine wedged vertebral bodies with irregular plates and Schmorl's nodes simulate Scheuermann's disease.

(continues on page 161)

Fig. 6.**70** **CPPD**. Chondrocalcinosis of the triangular fibrocartilage associated with severe arthritic changes in the second and third metacarpophalangeal joint is a characteristic presentation. Other typical findings seen in this case include calcifications of the lunotriquetral ligament, joint space narrowing in the radiocarpal and scaphotrapeziotrapezoidal joints, tiny, beak-like osteophytes on the radial side of the second and third metacarpal heads and capsular calcifications about the third metacarpophalangeal joint.

a

b

Fig. 6.**71 a, b** **CPPD**. Faint calcifications in the triangular fibrocartilage are associated with advanced arthritic changes in the radiocarpal joint including sclerosis and compression of the proximal scaphoid that appears embedded in the distal radius and increased scapholunate distance. This pattern is also referred to as scapholunate advanced collapse (SLAC). Multiple small cysts in other carpal bones and "degenerative" changes in the scaphotrapeziotrapezoidal joint without involvement of the first carpometacarpal joint are also seen in (**a**). One year later significant progression of the arthritic process including a new large subchondral cyst formation in the distal radius is seen in **b**.

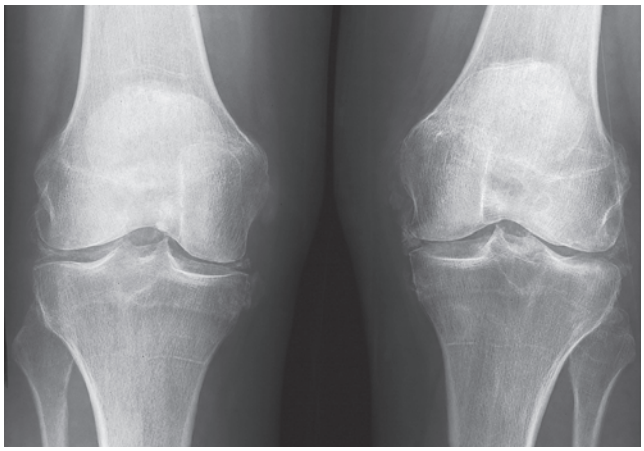

Fig. 6.**72** **CPPD**. Chondrocalcinosis in the menisci and calcifications of the joint capsule and collateral ligaments, respectively, are seen in both knees.

Fig. 6.**73** **CPPD**. Disc space narrowing with faint calcifications of the intervertebral discs, sclerosis of the adjacent plates and mild osteophytosis is seen.

Table 6.14 (Cont.) Differential Diagnosis of Articular Disorders

Disease	Characteristic Location	Radiographic Findings	Comments
Calcium hydroxyapatite crystal deposition disease (HADD) (Figs. 6.74, 6.75 and 6.76)	Tendons Bursae Joint capsule Shoulder	Periarticular hydroxyapatite (HA) crystal deposition is found in calcific tendonitis and bursitis. It is much more common than intra-articular HA deposition and almost always precedes the latter. Intra-articular HA crystal accumulation leads to joint space narrowing, destruction of subchrondral bone, subchondral sclerosis, intra-articular debris and joint disorganization. In the shoulder a chronic rotator cuff tear is invariably associated resulting in superior migration of the humeral head with possible erosion of the adjacent inferior aspect of the acromion and distal clavicle. The condition is *termed cuff tear arthropathy* or *Milwaukee shoulder syndrome.* HADD may also involve the knee (often limited to the lateral compartment), hip, elbow and the small joints of the hands and feet.	Periarticular HADD affects both men and women and is particularly common between 40 and 70 years of age. Symptoms include pain, tenderness, local edema and restricted motion. HA deposits are however also frequently found in asymptomatic patients. HADD arthropathy simulates CPPD, but does not produce the characteristic calcifications found in chondrocalcinosis. Cloud-like intra-articular opacities may however be evident in HADD. In *mixed calcium phosphate deposition disease* both HA and CPP crystals are found in the aspirated synovial fluid. This condition is not uncommon and should be expected when radiographically chondrocalcinosis and periarticular calcifications are present to a similar extend.

(continues on page 162)

Fig. 6.**74** **HADD (Milwaukee shoulder)**. Rotator cuff calcifications are associated with a chronic rotator cuff tear evident by the superior migration of the humeral head with markedly decreased distance between the humeral head and distal acromion with eroded inferior margin and concave demarcation. Arthritic changes in the glenohumeral joint including a minimally deformed humeral head are also present.

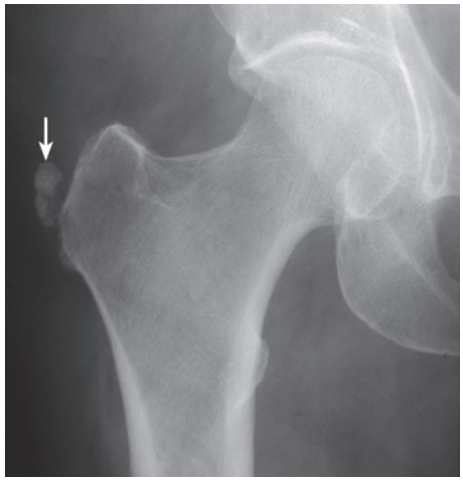

Fig. 6.**75** **HADD (trochanteric bursitis)**. A calcification (arrow) adjacent to the greater trochanter is seen.

Fig. 6.**76** **HADD (housemaid's knee)**. Multiple calcifications are noted in an enlarged subcutaneous infrapatellar bursa. ▷

Table 6.14 (Cont.) Differential Diagnosis of Articular Disorders

Disease	Characteristic Location	Radiographic Findings	Comments
Hemochromatosis (Fig. 6.77)	Metacarpophalangeal joints Wrists	Findings are almost identical to CPPD including chondrocalcinosis, but are commonly associated with a more uniform loss of joint space and osteoporosis. Characteristic involvement of the metacarpophalangeal joints (primarily 2nd and 3rd, less commonly 1st, 4th and 5th) include symmetric joint space loss, sclerosis, subchondral cysts, and fragmentation or flattening of the metacarpal heads. Compared to CPPD, the 4th and 5th metacarpophalangeal joints are more frequently involved, irregular beak-like osteophytes on the radial aspects of the metacarpal heads are more prevalent, the wrist involvement tends to be more widespread with diffuse affection of all midcarpal and common carpometacarpal joints, but with relative sparing of radiocarpal compartment.	*Primary hemochromatosis* is an inherited disorder with abnormal iron deposition resulting in cirrhosis, diabetes, skin pigmentation and heart failure. It has a 10:1 male predominance with symptoms occurring after the age of 40 years. *Secondary hemochromatosis* is associated with an increased intake of iron such as multiple blood transfusions in myeloproliferatory disorders and refractory anemias. An arthropathy is found in approximately one-third of patients commencing typically in the small joints of the hands and eventually progressing to the large joints.
Ochronosis (alkaptonuria) (Fig. 6.78)	Bilateral, not always symmetric Spine Hips Knees Shoulders Sacroiliac joints Pubic symphysis	In the spine widespread, often laminated disc space calcifications involving both nucleus pulposus and annulus fibrosis with predilection of the lumbar spine is most characteristic. Associated findings include marked uniform disc space narrowing at all levels, multiple vacuum phenomena and osteoporosis. Progressive discal ossification and bony bridging eventually results in a bamboo spine. Extraspinal manifestations in large joints resemble CPPD. Findings include asymmetric or symmetric joint space loss, severe subchondral sclerosis, and eventually collapse and fragmentation of the articular surface with intra-articular loose bodies. In contrast to CPPD subchondral cysts are absent or inconspicuous, whereas severe involvement of both the sacroiliac joints and pubic symphysis with eburnation and fragmentation is suggestive of ochronosis.	Rare hereditary metabolic disease with inability to metabolize homogentisic acid that is excreted by the kidneys. The urine is colorless when passed but darkens when exposed to light. Ochronotic pigmentation of the ears and sclera is usually first observed at the age of 20 to 30 years. Symptoms and signs of ochronotic arthropathy usually appear in the fourth decade of life.

(continues on page 164)

Fig. 6.**77** **Hemochromatosis**. Symmetric joint space loss with mild subchondral sclerosis and large beak-like osteophytes (arrows) on the radial aspects of the metacarpal heads are seen in the second and third metacarpophalangeal joints.

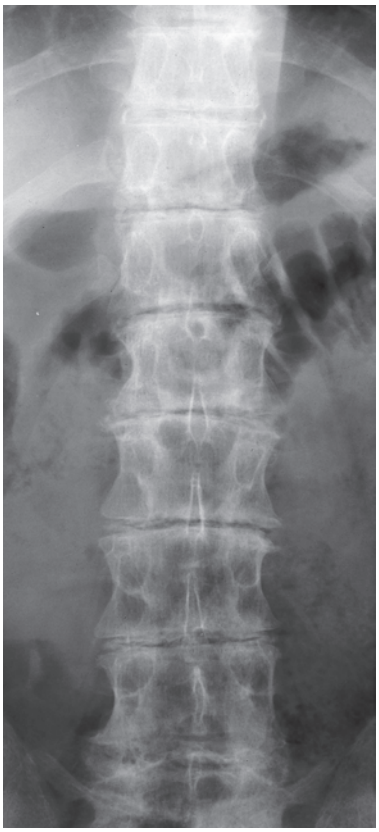

a

b

Fig. 6.**78 a, b** **Ochronosis**. Marked uniform disc space narrowing with irregular and slightly sclerotic endplates, discal calcification and multiple vacuum phenomena is seen in anteroposterior (**a**) and lateral (**b**) projection throughout the lumbar and visualized lower thoracic spine. The syndesmophytosis in this case is rather minimal. Grade 1 anterolisthesis of L5 against S1 is also present secondary to spondylolysis at L5.

Table 6.14 (Cont.) Differential Diagnosis of Articular Disorders

Disease	Characteristic Location	Radiographic Findings	Comments
Acromegaly (Fig. 6.79)	Bilateral symmetric Hands Feet Mandible Spine Soft tissue thickening (heel, phalanges)	Hands and feet: Soft tissue thickening of the phalanges, joint space widening (especially metacarpophalangeal and metatarsophalangeal joints), thickening and squaring or overconstriction of phalanges, metacarpals and metatarsals, enlargement of the tufts and bases of the terminal phalanges, enlarged sesmoids and large enthesophyles at ligament and tendon attachment sites. Spine: Enlarged intervertebral disc, increased anteroposterior and lateral diameters of the vertebral bodies with exaggerated concavity of their posterior aspects. Premature osteoarthritis with prominent osteophytosis is seen at a later stage, especially in the weight-bearing joints and spine.	Hypersecretion of growth hormone due to eosinophilic adenoma or hyperplasia of the pituitary gland leads to gigantism in the immature skeleton and acromegaly in the mature skeleton. Stimulation of endochondral ossification results in enlargement of the costochondral junctions (acromegalic rosary). Stimulation of periosteal bone formation leads to enlargement of the mandible, phalanges, metacarpals, metatarsals and various tuberosities. Cartilage proliferation results in widened articular and intervertebral spaces.
Amyloidosis (Figs. 6.80 and 6.81)	Monoarticular to bilateral asymmetric Hand Wrists Shoulders Hips	Articular involvement includes asymmetric soft tissue masses, periarticular osteoporosis, erosions and cystic lesions with or without surrounding sclerosis and preservation of the joint space. Joint contractures and subluxations may also be present. Avascular necrosis may complicate amyloidosis in larger joints. Periarticular amyloid nodules or masses are frequently observed about the olecranon, shoulder, hand and wrist, where they can cause the carpal tunnel syndrome. Osteolytic lesions producing endosteal scalloping and, occasionally pathologic fractures and generalized osteoporosis are additional manifestations.	Primary amyloidosis occurs without coexistent disease or is associated with multiple myeloma. Secondary amyloidosis is associated with various chronic diseases including rheumatoid arthritis, sepsis, inflammatory disorders such as Crohn's disease, neoplasm and chronic hemodialysis. Primary amyloidosis is more frequent in men with an onset between 40 and 80 years. Amyloid joint disease shares many radiographic features with gout, xanthomatosis and pigmented villonodular synovitis.
Multicentric reticulohistiocytosis (lipoid dermatoarthritis) (Fig. 6.82)	Bilateral symmetric Hands Feet Wrists Shoulders Elbows Hips Knees Ankles Spine Sacroiliac joints	Predilection of the interphalangeal joints of the hands and feet with erosions originating at the joint margins and spreading centrally associated with soft tissue nodules is characteristic. The erosions are well circumscribed resembling defects seen in gout. The joint space is frequently preserved. Osteoporosis and new bone formation are absent. Progression to arthritis mutilans is seen in about one-third of cases. Severe erosive destructive changes in the cervical spine, especially the atlantoaxial joint is also a common manifestation. Erosions and bony ankylosis may be observed in the sacroiliac joints.	Uncommon systemic disease of unknown cause with female predominance and typical onset in middle age. In approximately two-thirds of patients polyarthritis is the first manifestation of the disease, followed after months to years by eruption of red to purple skin nodules measuring up to 1 cm in diameter. Patients may also reveal xanthomas preferentially involving the eyelids. Abnormal laboratory findings include anemia, hypercholesterolemia and elevated erythrocyte sedimentation rate.

(continues on page 166)

Fig. 6.**79 a, b** **Acromegaly**. Soft tissue thickening of the phalanges, joint space widening (especially metacarpophalangeal and metatarsophalangeal joints) enlarged tufts and bases of the terminal phalanges and prominent metacarpal and metatarsal heads are seen in the hand (**a**) and foot (**b**).

Fig. 6.**80** **Amyloidosis**. Osteopenia and multiple carpal cysts with relatively well preserved joint spaces are seen in the wrist.

Fig. 6.**81** **Amyloidosis in chronic renal failure**. Poorly defined osteolytic lesions are seen in acetabular dome, femoral head and proximal femur shaft. In the former two locations the lesions are surrounded by an irregular and poorly demarcated sclerosis.

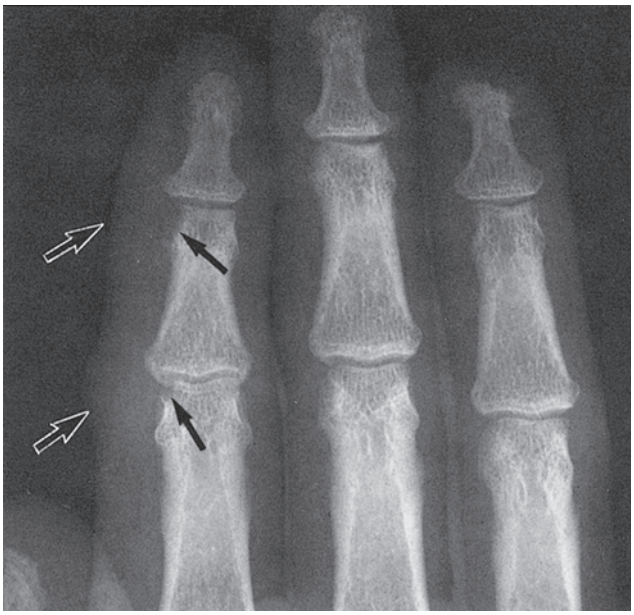

Fig. 6.**82** **Multicentric reticulohistiocytosis**. Soft tissue nodules (white arrows) are associated with marginal erosions (black arrows) in the proximal and distal interphalangeal joints of the index finger.

Table 6.14 (Cont.) Differential Diagnosis of Articular Disorders

Disease	Characteristic Location	Radiographic Findings	Comments
Osteoarthritis (degenerative joint disease (Figs. 6.83, 6.84, 6.85, 6.86, 6.87, 6.88, 6.89 and 6.90)	*Primary osteoarthritis:* Oligo-articular to polyarticular, often bilateral and relatively symmetric Hand (interphalangeal joints, rarely metacarpophalangeal joints). Wrist (first carpometacarpal joint, scaphotrapezio-trapezoidal joint) Hip Knee Foot (first metatarsophalangeal joint, tarsometatarsal joints and talonavicular joint) Acromioclavicular joint	Joint space loss, subchondral sclerosis, cyst formation and osteophytosis are the hallmark of osteoarthritis. The joint space loss in weight-bearning articulations typically is asymmetric and localized predominantly in the area that is subjective to excessive pressure (e.g. superior or weight-bearing portion of the hip, medial compartment of the knee). Subchondral sclerosis typically is confined to the area of joint space narrowing with progressive obliteration of this space. The sclerosis may extend both vertically and horizontally into the adjacent bone. Subchondral cysts (geodes) form within the pressure segment of the subchondral bone. The cysts commonly are multiple, and of variable size and depict sclerotic margins. They may or may not communicate with the joint. Osteophytosis: Marginal (peripheral) osteophytes are most common, developing as lips of new bone around the edges of the articular cartilage. Central osteophytes are button-like or flat excrescences within the articular surface denuded of cartilage. Thickening of the intra-articular cortex on the medial aspect of the femoral neck is termed buttressing and represents a periosteal osteophyte. Capsular osteophytes originating from the capsular attachment sites may be found in the interphalangeal joints producing the “seegull sign” as dorsal talar beak in the talonavicular joint. Degenerative enthesopathy may produce bony excrescences in the trochanters and ischial tuberosities and spurs in the calcaneus, patella and olecranon. Bony proliferation may be seen at syndesmotic insertion sites. Flattening and collapse of the articular surface may become apparent in a more advanced stage which is not always caused by the development of secondary avascular necrosis. Both joint effusions and synovial proliferation are not prominent features in osteoarthritis. Large effusions should suggest an inflammatory, infectious or traumatic arthritic process. Complications of osteoarthritis include malalignment (e.g. varus or, less commonly, valgus deformity and lateral subluxation in the knee, lateral displacement of the femoral head, radial subluxation in the first carpometacarpal joint, and radial or ulnar deviation in the interphalangeal joints) and the formation of loose intra-articular cartilagenous or osseous bodies.	Osteoarthritis is by far the most common joint disorder, one of the most common chronic diseases in the elderly and a leading cause of disability. There is a poor correlation between clinical symptoms and radiographic findings. The correlation between joint degeneration and advancing age is not linear. Rather, an age related predisposition to osteoarthritis appears to increase exponentially after the age of 50. Osteoarthritis refers to degenerative disease of synovial joints. Abnormalities, however, predominate in the cartilaginous and osseous tissues, whereas alterations in the synovium are generally mild. Primary (idiopathic) osteoarthritis occurs in the absence of any underlying abnormality. Secondary osteoarthritis refers to joint degeneration produced by a pre-existing condition. *Secondary osteoarthritis* (Figs. 6.**91**, 6.**92** and 6.**93**) is associated with pre-existing articular disease or deformity, trauma and chronic overuse and thus frequently involves articular sites that are not commonly affected in primary osteoarthritis. Secondary osteoarthritis may follow inflammatory or infectious arthritis, episodes of minor or major trauma, and congenital disorders. Chronic athletic and occupational overuse is associated with joint degeneration at specific locations: Workers using vibrating or pneumatic tools (e.g. miners or jackhammer operators) develop arthritic changes in the elbows, wrists and hands (especially carpal cysts), ballet dancers in the ankles and feet, football and soccer players in the ankles, feet, hips and knees, cyclists in the patellofemoral joints, boxers and wrestlers in the hands, wrists, elbows, and baseball players in the shoulder and elbows. *Sacroiliac joints* (Fig. 6.**94**): Besides focal or diffuse, well-defined subchondral sclerosis with or without loss of joint space, erosions are occasionally also seen in degenerative sacroiliac joint disease. An anterior bridging osteophyte is not uncommon and may mimic an osteoblastic metastasis centered over the sacroiliac joint. Subchondral cysts are relatively uncommon, but may contain gas (pneumatocyst) even in the absence of a vacuum phenomenon in the sacroiliac joint. *Rapidly destructive osteoarthritis of the hip* refers to an osteolytic destruction of the hip without osteophytosis within weeks. Besides osteoarthritis, CPPD, HADD and osteonecrosis have also been implicated (Fig. 6.**95**).

(continues on page 169)

Fig. 6.**83** **Osteoarthritis**. Arthritic changes including joint space narrowing and osteophytosis are seen in all interphalangeal joints,he first carpometacarpal joint and the scaphotrapeziotrapezoidal joint whereas the metacarpophalangeal joints are spared. Osteopenia and a fracture of the base of the proximal phalanx of the fifth finger are incidentally also present. Calcification of the triangular fibrocartilage is also evident.

Fig. 6.**84** **Osteoarthritis**. Advanced degenerative changes including joint space narrowing, sclerosis, subchondral cyst formation and mild lateral subluxation are present in the first carpometacarpal joint.

Fig. 6.**85** **Osteoarthritis**. Joint space narrowing in the superolateral aspect of the hip is associated with adjacent subchondral cyst formation in the acetabulum and femoral head. Considerable osteophytosis is also seen in the acetabulum.

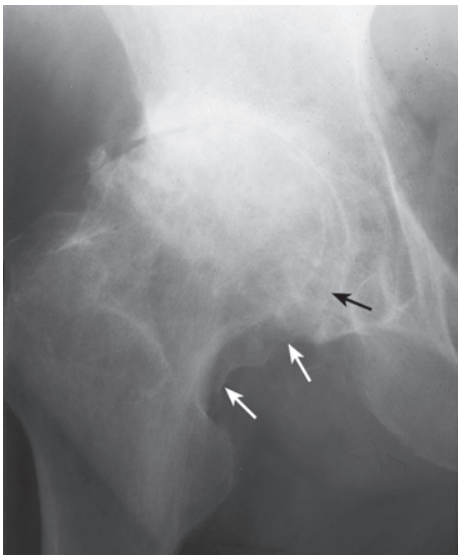

Fig. 6.**86** **Osteoarthritis**. Joint space narrowing limited to the weight-bearing portion of the hip associated with subchondral sclerosis is seen. New bone formation (buttressing) along the medial aspect of the femoral head and neck is also evident (arrows).

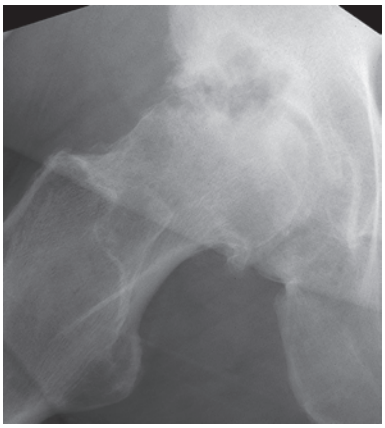

Fig. 6.**87** **Osteoarthritis**. Advanced degenerative changes with fragmentation of the subchondral bone of both the femoral head and acetabulum in the weight-bearing portion of the hip is evident.

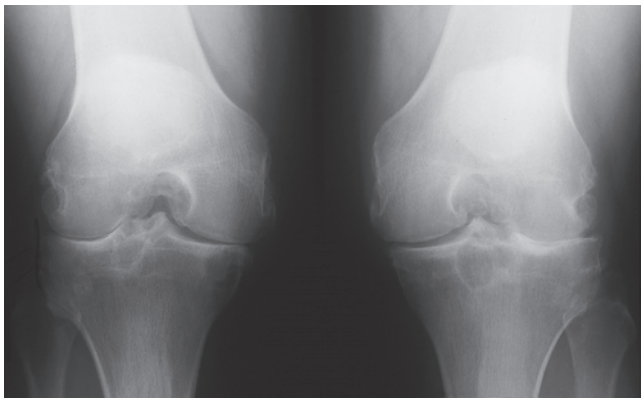

Fig. 6.**88** **Osteoarthritis**. Advanced degenerative changes with joint space narrowing, sclerosis, osteophytosis, subchondral cysts and loose bodies in the intercondylar notch are seen in both knees.

Fig. 6.**89** **Osteoarthritis (hallux rigidus)**. Advanced degenerative changes with joint space narrowing, extensive subchondral sclerosis and osteophytosis are seen in the first metatarsophalangeal joint.

Fig. 6.**90** **Osteoarthritis**. Hypertrophic degenerative changes with inferior spurring are seen in the acromioclavicular joint causing impingement on the supraspinatus muscle and tendon (impingement syndrome).

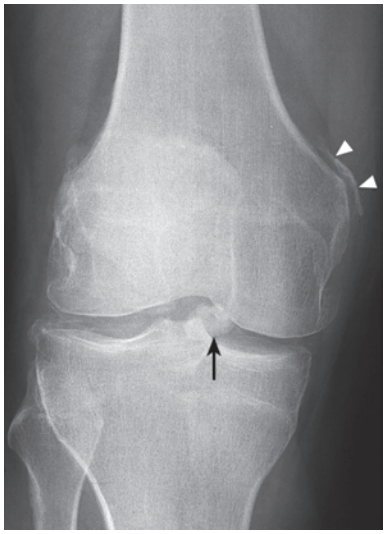

Fig. 6.**91** **Post-traumatic osteoarthritis**. Chondrocalcinosis in the lateral meniscus, a large intra-articular loose body (arrow) and a shell-like ossification (arrowheads) along the medial femoral condyle (Pellegrini-Stieda ossification) indicative of a chronic medial collateral ligament injury are seen.

a

b

Fig. 6.**92 a**, **b** **Chronic overuse osteoarthritis. a Javelin thrower:** Degenerative changes including subchondral sclerosis, mild osteophytosis and healed fracture of the tip of the olecranon are seen in a javelin thrower. **b Jackhammer operator:** Multiple carpal cysts and early degenerative changes in the radiocarpal and distal radioulnar joints are seen in a patient with normal bone mineralization.

Table 6.14 (Cont.) Differential Diagnosis of Articular Disorders

Disease	Characteristic Location	Radiographic Findings	Comments
Erosive osteoarthritis (Fig. 6.96)	Bilateral symmetric Interphalangeal joints of the hand	Findings of advanced osteoarthritis (joint space narrowing, subchondral sclerosis and prominent marginal osteophytes) are associated with erosions. They commonly originate in the central portion of the joint as sharply marginated defects. Their central location differs from the marginal erosions seen in rheumatoid and psoriatic arthritis. Progression to bony ankylosis is not infrequent. In contrast to psoriatic arthritis the distribution pattern tends to be bilateral symmetric.	Presents clinically with acute inflammatory episodes including painful Heberden's and Bouchard's nodes (marginal osteophytes and soft tissue thickening about the distal and proximal interphalangeal joints, respectively) in women (male/female ratio is 1:10). May be associated with primary (noninflammatory) osteoarthritis in other joints of the hand and wrist.

(continues on page 170)

Fig. 6.**93** **Post-traumatic scapholunate advanced collapse (SLAC)**. Sclerosis and compression of the proximal scaphoid secondary to a healed fracture, scapholunate dissociation, and proximal migration of the scaphoid with obliteration of the radioscaphoid space are seen. Mild compression, rotation and sclerosis of the lunate with degenerative changes in the lunocapitate joint are also associated.

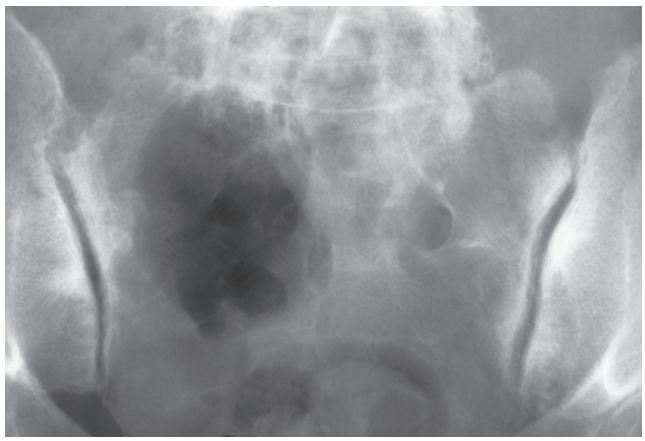

Fig. 6.**94** **Osteoarthritis in the sacroiliac joints**. Bilateral well-defined subchondral sclerosis without erosions or joint space narrowing is seen.

Fig. 6.**95** **Rapidly destructive osteoarthritis of the hip.** Bilateral osteolytic destruction of both acetabula and femoral heads is seen. On the right side the process is further advanced and involves also the femoral neck.

Fig. 6.**96** **Erosive osteoarthritis**. Joint space narrowing, subchondral sclerosis and osteophytosis are associated in several interphalangeal joints with central erosions. Degenerative changes with small subchondral cyst formation are also seen in both first carpometacarpal joints. ▷

Table 6.14 (Cont.) Differential Diagnosis of Articular Disorders

Disease	Characteristic Location	Radiographic Findings	Comments
Degenerative disease of the spine (Figs. 6.97, 6.98, 6.99, 6.100, and 6.101)	Middle and lower cervical spine Lower lumbar spine	Degeneration of the intervertebral disc (*osteochondrosis*) may present with disc space narrowing, reactive sclerosis of the adjacent endplates, osteophytosis and vacuum phenomena (gas) within the disc. (DD: vacuum phenomenon within a vertebral body suggests ischemic necrosis). Degenerative disc calcification is uncommon. In children nucleus pulposus calcification occurs in the cervical spine as an isolated finding and may rupture into the adjacent vertebral body, intervertebral foramen or spinal canal. Large anterolateral osteophyte formations caused by disc displacement in that direction is referred to as *spondylosis deformans*. Superior and inferior disc displacement produces a cartilagenous (Schmorl's) node evident as a radiolucent lesion surrounded by a sclerotic rim. Posterior and posterolateral disc displacement is of greatest clinical significance because of its relationship with neurological structures, but cannot be assessed with plain film radiography. Degenerative changes in the apophyseal (facet) joints (*spondylarthrosis*)are also common and present with joint space narrowing, bony eburnation and osteophytosis. Ligamentous laxity may result in mild anterolisthesis (not associated with pars defect) or retrolisthesis. The neural foramina in the cervical spine below C2 may be encroached by osteophytes, frequently originating from the uncovertebral (Luschka's) joints.	Conditions associated with degenerative disease of the spine include costovertebral osteoarthritis, Baastrup's disease and Bertolotti's syndrome. *Costovertebral osteoarthritis*: The costovertebral joints are located between the head of the ribs and the vertebral bodies and between the necks and tubercles of the ribs and the transverse processes. Degenerative changes, predominant in the articulations of the 11th and 12th ribs, include joint space narrowing, bony eburnation and osteophytosis and may progress to complete bony ankylosis with pagetoid appearance of the posterior portion of the affected rib. *Baastrup's disease*: Extensive disc space loss or excessive lordosis of the lumbar spine leads to approximation and contact of the often unusually large spinous processes. Degenerative changes including reactive sclerosis and osteophytosis may develop between the "kissing spines" and may be associated with considerable pain. *Bertolotti's syndrome*: Degenerative changes may be found in the articulations between the transverse processes of a transitional vertebra in the lumbosacral junction and the adjacent sacral wing. The relationship of back pain to this finding is however debated.

(continues on page 172)

a

b

Fig. 6.**97 a, b Degenerative disease of the spine (spondylosis deformans)**. Anterolateral osteophytosis throughout the lumbar spine is the dominant radiographic manifestation seen in anterolateral (**a**) and lateral (**b**) projection.

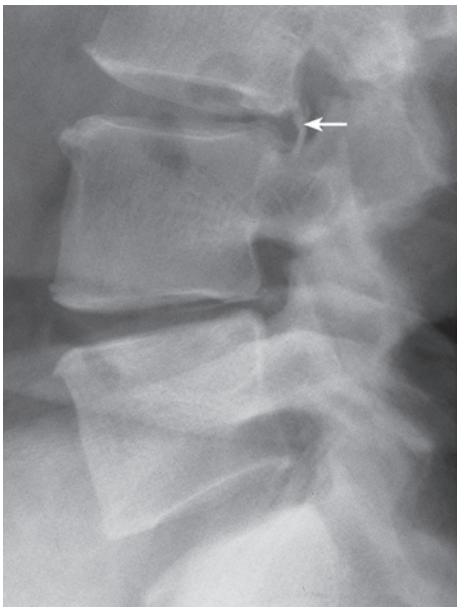

Fig. 6.**98** **Degenerative disease of the spine (osteochondrosis)**. Narrowing of the intervertebral space with relatively little osteophytosis is the dominant radiographic manifestation best seen at L4/5. Less severe disc space narrowing with calcification of the posterior longitudinal ligament (arrow) that is posteriorly displaced by the bulging disc and small anterior osteophyte formation is seen at L3/4.

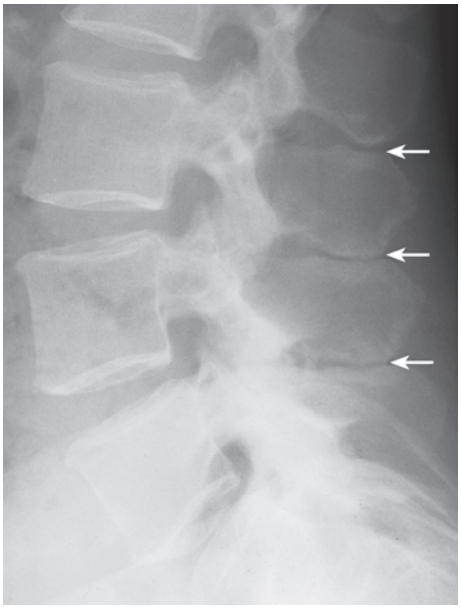

Fig. 6.**99** **Degenerative disease of the spine (spondylarthrosis and Baastrup's disease)**. Spondylarthrosis: Degenerative changes in the apophyseal (facet) joints presenting with joint space narrowing, bony eburnation and osteophytosis are seen in all segments of the lumbar spine. Baastrup's disease: Degenerative changes including reactive sclerosis are also seen between the unusually large spinous processes (arrows) which appear in contact with each other ("kissing spines").

Fig. 6.**100** **Bertolotti's syndrome**. Partial sacralization of L5 is seen. Degenerative changes between the enlarged left transverse process of this transitional vertebra and the adjacent sacral wing are evident by the extensive sclerosis at the contact site of these two parts.

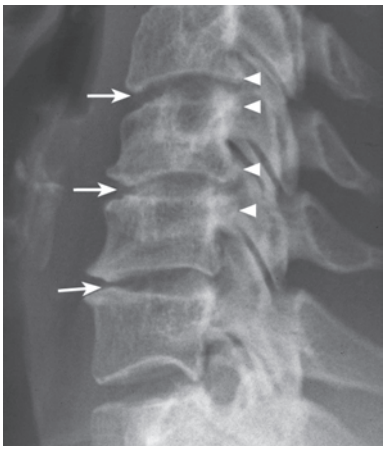

a

b

Fig. 6.**101 a, b** **Degenerative cervical spine disease**. Disc space narrowing with mild osteophytosis is seen between C4/5, C5/6, and C6/7 (arrows). Small osteophytes (arrowheads) protruding posteriorly into the spinal canal are seen in **a**. Encroachment of the right neural foramina by small osteophytes (arrows) originating from the uncovertebral (Luschka's) joints are evident in **b**.

Table 6.14 (Cont.) Differential Diagnosis of Articular Disorders

Disease	Characteristic Location	Radiographic Findings	Comments
Diffuse idiopathic skeletal hyperostosis (DISH, Forestier's disease) (Figs. 6.102 and 6.103)	Spine (especially lower thoracic and upper lumbar area) Pelvis Calcaneus Patella Olecranon	Diagnostic criteria in the spine include: 1. Flowing ossifications along the anterolateral aspect of at least 4 contiguous vertebral bodies. 2. Relative preservation of the disc space and absence of significant degenerative signs such as reactive sclerosis and vacuum phenomena in the involved segment. 3. Absence of bony ankylosis in the apophyseal joints and no evidence of sacroiliitis. Pelvis: Bony proliferation ("whiskering") in the iliac crests, ischial tuberosities and trochanters. Broad osteophytes at the lateral acetabular edges, inferior portions of the sacroiliac joints and superior aspect of pubic symphysis. Ossifications of iliolumbar, sacrotuberous and sacroiliac ligaments. Enthesophytes without adjacent reactive bone sclerosis or erosions at numerous sites, most commonly in the calcaneus, patella and olecranon.	Common ossifying diathesis characterized by bone proliferation at sites of tendinous and ligamentous attachment (entheses). Presents usually with mild symptoms of restricted spinal motion and tendinitis in patients over 50 years of age with 3:1 male predominance. The cause of DISH is unknown. It might be considered a hypertrophic variant of spondylosis deformans. Bony hyperostosis of the spine somewhat similar to DISH is associated with endocrine disorders such as acromegaly, hypoparathyroidism and diabetes mellitus. Hyperostosis of the spine and ligamentous calcifications are also found with fluorosis, but the latter condition is associated with diffuse osteosclerosis of the axial skeleton. Prolonged therapy for skin disorders with retinoid drugs (e.g. Acutane®), which are chemically similar to vitamin A, may also induce hyperostosis in both the axial and appendicular skeleton. Excessive heterotopic bone formation after prosthetic hip or knee replacement is frequently observed with DISH. *Ossification of the posterior longitudinal ligament (OPLL)* (Fig. 6.**104**) affects the cervical spine and is often associated with DISH.

(continues on page 174)

a

b

Fig. 6.**102 a, b** **DISH**. Huge paravertebral flowing ossifications with preservation of the disc spaces are noted throughout the lumbar spine in anteroposterior (**a**) and lateral (**b**) projection. Note also the absence of bony ankylosis in the apophyseal (facet) joints and the normal sacroiliac joints.

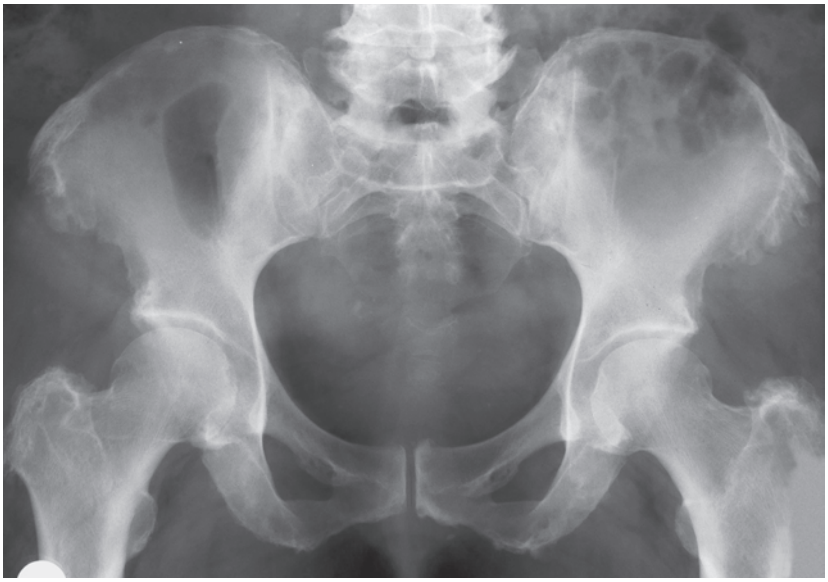

Fig. 6.**103** **DISH**. Symmetrical bony proliferation ("whiskering") is seen in the iliac crests, greater trochanters and to a lesser degree in the ischial tuberosities.

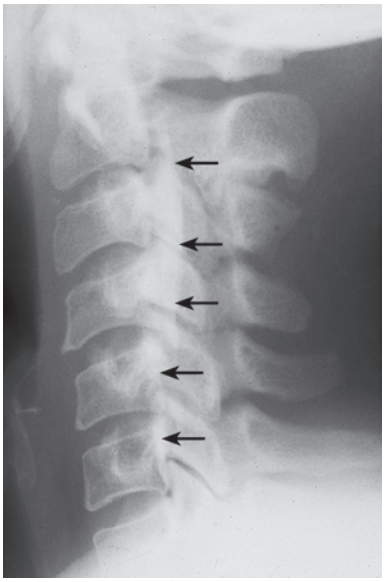

Fig. 6.**104** **Ossification of the posterior longitudinal ligament (OPLL)** is seen in the cervical spine (arrows).

Table 6.14 (Cont.) Differential Diagnosis of Articular Disorders

Disease	Characteristic Location	Radiographic Findings	Comments
Neuropathic osteoarthropathy (Charcot joint) (Figs. 6.105, 6.106, 6.107, 6.108, 6.109 and 6.110)	Congenital indifference to pain and meningomyeloceles: Knees Ankles Intertarsal joints Syringomyelia: Shoulders Elbows Tabes dorsalis: Hips Knees Ankles Spine Diabetes mellitus: Midfoot Forefoot Leprosy: Hands Feet	Persistent joint effusion, often with cartilaginous and osseous debri (detritic synovitis) resulting from fragmentation of the articular surface are early findings. More advanced abnormalities include progressive rapid bone resorption or extensive joint destruction with marked sclerosis and osteophytosis, intra-articular osseous fragments, subluxations, massive effusions and fractures of neighboring bones. The end result is a completely disorganized joint with predominant features of bone resorption, new bone formation, or both. *Diabetic foot*: Fragmentation, sclerosis, subluxations or dislocations are characteristically found in the tarsometatarsal joints resembling a Lisfranc fracture/dislocation. Collapse of the plantar arch with talar malalignment and fragmentation of various tarsal bones is also a common manifestation. Flattening and fragmentation of the metatarsal heads resembling Freiberg's infarction or partial to complete resorption of the metatarsal heads and adjacent proximal phalanges with tapering of the remaining shafts are other presentations. Furthermore ischemic and infectious processes are frequently superimposed on the neuropathic changes in the diabetic foot.	Hypertrophic bone changes are caused by repetitive trauma/microtrauma with attempted repair. Atrophic resorptive changes are caused by sympathetic dysfunction resulting in hyperemia and bone resorption. Congenital causes include myelomeningoceles and congenital indifference to pain. Acquired causes include brain and cord injuries or tumors, syringomyelia, tabes dorsalis, diabetes mellitus and leprosy. *Axial neuropathic osteoarthropathy* is usually productive and best described as greatly exaggerated degenerative changes in the spine with malalignment, profound reactive sclerosis and osteophytes reaching mammoth proportions. Osteolytic or destructive changes are less common and may result in rapid disintegration of vertebral bodies and/or apophyseal joints that can mimic infection or metastases. It is relatively common in *tabes dorsalis* with preferential involvement of the lumbar spine, but also seen in *syringomyelia* where it primarily affects the cervical spine. *Congenital indifference to pain* becomes manifest in infancy or childhood. Findings include amputation of fingers and toes caused by self-mutilation and fractures of the long bones with frequent epiphyseal separation. *Leprosy:* Skeletal abnormalities occurring on a neurological basis are much more frequent and severe than those produced by direct leprous infiltration. Acro-osteolysis and tapered resorption of the end of phalanges, metacarpals and metatarsals resulting in "licked candy stick" appearance are characteristic.

(continues on page 176)

Fig. 6.**105 Neuropathic osteoarthropathy (syringomyelia).** Advanced arthritis with destruction of the glenoid, intra-articular fragments, sclerosis and osteophytosis is seen. Superior migration of the humeral head indicating a chronic rotator cuff tear is also evident.

Fig. 6.**106** **Neuropathic osteoarthropathy (syringomyelia)**. A completely disorganized elbow with multiple fracture fragments and extensive sclerosis is seen.

Fig. 6.**108** **Neuropathic osteoarthropathy (congenital indifference to pain)**. Extensive soft tissue swelling is associated with multiple fractures in the distal tibia and talus, angular deformity of the ankle, numerous loose fracture fragments, sclerosis and periostitis.

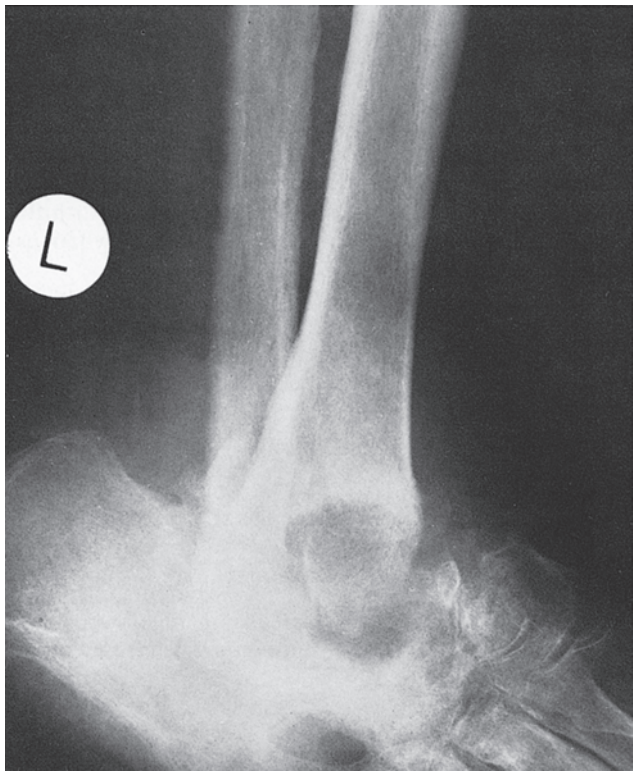

Fig. 6.**107** **Neuropathic osteoarthropathy (tabes dorsalis)**. Destruction of the ankle, subtalar and talonavicular joints with collapsed plantar arch and extensive sclerosis is seen.

Fig. 6.**109** **Diabetic foot**. Multiple healing fractures with extensive callus formation in the mid and forefoot are associated with a collapsed and disrupted Lisfranc joint. Arteriosclerotic calcifications characteristically are also present.

Fig. 6.**110** **Leprosy**. Multiple subluxations/dislocations and extensive osteolysis are seen in the forefoot resulting in a tapered appearance of many metatarsals and phalanges (“licked candy stick” appearance).

Table 6.14 (Cont.) Differential Diagnosis of Articular Disorders

Disease	Characteristic Location	Radiographic Findings	Comments
Pyogenic (septic) arthritis (Figs. 6.111, 6.112, 6.113 and 6.114)	Monoarticular Hip Knee Spine	Every monoarticular inflammatory arthritic process should be considered infectious until proven otherwise. Acute stage: Para-articular soft tissue swelling, joint effusion (frequently producing widening of the joint space in children) and juxta-articular osteoporosis followed by diffuse joint space narrowing due to rapid destruction of the articular cartilage and marginal and central bony erosions. Subacute/chronic stage: Subchondral bone destruction with reactive bone sclerosis, secondary degenerative changes and eventually bony ankylosis may be found. In the spine disc space narrowing and loss of normal definition of the adjacent endplates progressing rapidly to frank destruction of the subchondral bone plate or enlarging destructive foci is characteristic. After 2 to 3 months reparative changes become evident in the form of reactive sclerosis. In children a hematogenous infection of the intervertebral disc alone ("diskitis") without involvement of the neighboring vertebral bodies may occur as long as the blood supply to the discs remains intact. Diskitis may occur in adults by direct inoculation of the offending agent during diagnostic or surgical procedures. Sacroiliac joint infection typically is unilateral differentiating it from many other arthritic processes that are frequently bilateral.	A hematogenous infection-induced arthritis is either caused by direct infiltration and subsequent multiplication of the viable organism or without direct contamination of the joint. The latter is referred to as *reactive arthritis* and found with rheumatic fever and Lyme disease where it is caused by an antigen-mediated immune response to the offending organism. A sympathetic joint effusion adjacent to a site of inflammation may also mimic an acute infectious arthritic process. *Routes of infectious joint contamination* include *hematogenous spread, contiguous spread* (intra-articular extension of osteomyelitis or neighboring soft tissue abscess) and *direct implantation* (penetrating trauma or iatrogenic procedure). In infants and children monoarticular involvement of the knee or hip is the most common presentation. In the adult the lumbar spine and knee are the most common sites of involvement. Common organisms include staphylococcus aureus and streptococcus pyogenes at all ages, hemophilus influenza in children, and neisseria gonorrhoeae (often more than one joint involved) and brucella in adults. A prompt and definite diagnosis requires an arthrocentesis, blood cultures and possibly bone biopsy (spine).

(continues on page 178)

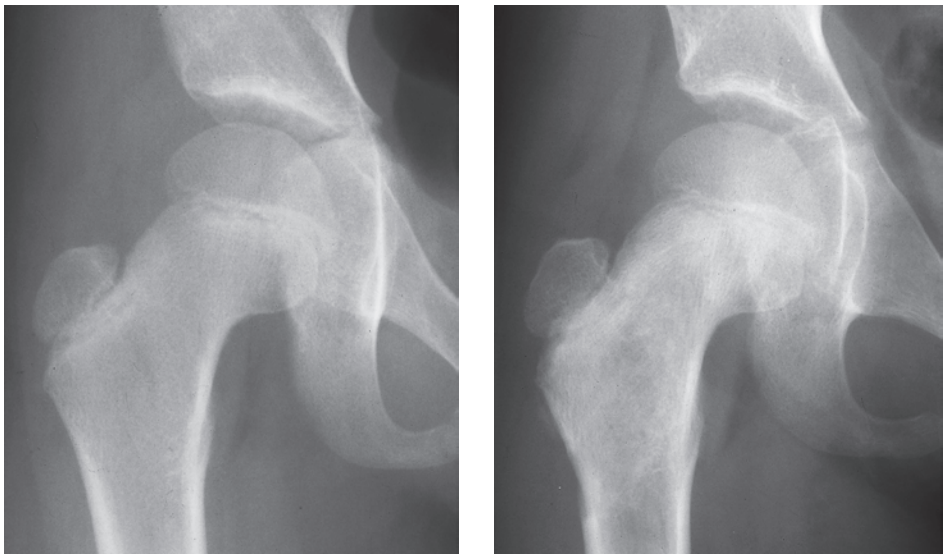

Fig. 6.**111 a, b Pyogenic (septic) arthritis**. A joint effusion evident by the slight lateral subluxation of the femoral head is the only abnormality seen in **a**. Six weeks later narrowing of the joint space, especially medially, due to destruction of the articular cartilage and poorly defined mixed osteolytic and osteosclerotic areas in the femoral neck and adjacent shaft are seen in **b**.

Fig. 6.**112** **Pyogenic (septic) arthritis**. Joint space narrowing with destruction and fragmentation of the subchondral bone in the medial talar dome and adjacent tibia plafond is seen. Beginning periostitis in the distal tibia and fibula is also evident.

a

b

Fig. 6.**113 a, b** **Pyogenic (septic) arthritis**. Joint space narrowing and poorly defined osteolytic and osteosclerotic lesions are seen in the femoral head and proximal neck in **a**. One year later marked disease progression with destruction and fragmentation of both the femoral head and acetabulum, osseous debris accumulation in the hip with lateral subluxation of the femoral head, extension of the osteomyelitic process into the intertrochanteric area and beginning repair (sclerosis of the acetabular roof with adjacent osteophyte formation) is seen in **b**.

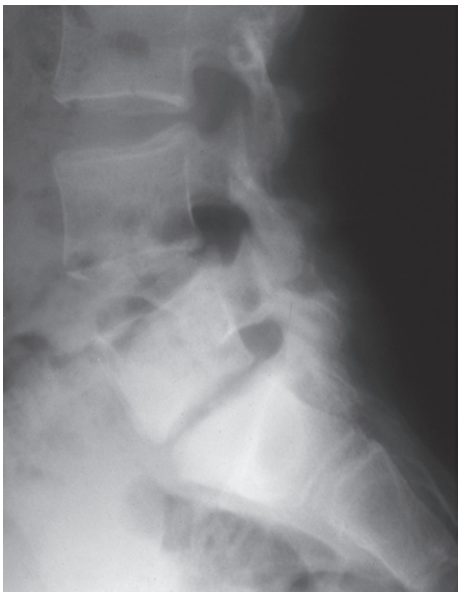

Fig. 6.**114** **Diskitis**. Narrowing of the intervertebral space between L5 and S1 with slightly irregular adjacent endplates and marked sclerosis of the adjacent bone is seen.

Table 6.14 (Cont.) Differential Diagnosis of Articular Disorders

Disease	Characteristic Location	Radiographic Findings	Comments
Tuberculous arthritis (Figs. 6.115, 6.116 and 6.117)	Monoarticular Spine Hip Knee	Tuberculous spondylitis most commonly affects the thoracolumbar area. It may involve more than one intervertebral disc and has a predilection for the anterior aspect of the vertebral body. Extension into the adjacent ligaments and soft tissue is frequent allowing osseous or disc invasion at distant sites or leading to the formation of a psoas abscess that tends to calcify. A gibbus deformity in the thoracolumbar area may be the end result. In the appendicular joints Phemister's triad is characteristic consisting of juxta-articular osteoporosis, marginal erosions and gradual narrowing of the joint space. Compared to a pyogenic arthritis a delay in destruction of the articular cartilage or intervertebral disc, absence of reparative sclerosis, and calcification of the associated soft tissue abscesses are all suggestive of tuberculosis.	Skeletal tuberculosis can affect persons of all ages, but less than 1% of patients infected with tuberculosis have bone or joint manifestations. Tuberculous spondylitis is the most frequent skeletal manifestation presenting with an insidious onset of back pain, stiffness, local tenderness and possibly fever. Appendicular tuberculous arthritis may present with pain, swelling, weakness, muscle wasting and a draining sinus. Globally tuberculosis is the leading infectious cause of morbity and mortality. In industrialized nations the disease has retreated from the general population, affecting selected groups. In the United States an upsurge in tuberculosis has been noted since 1985 that is linked to the HIV epidemic.
Fungal arthritis (Fig. 6.118)	Monoarticular Large appendicular joints Spine	Joint involvement is usually caused by direct extension from an adjacent osseous focus and rarely by direct hematogenous implantation. Soft tissue swelling, effusion, joint space narrowing, erosions or bony destruction, with or without osteoporosis are observed in these cases.	Usually in patients with compromised immune system. Cryptococcosis, North American blastomycosis, coccidioidomycosis, histoplasmosis, sporotrichosis (especially hand and foot), and candidiasis are common organisms. *Madura foot*: Single or multiple osseous defects to extensive destruction with periostitis and sclerosis leading to extensive intra-articular osseous fusion ("melting snow" appearance).
Viral arthritis	Monoarticular to polyarticular Peripheral joints Often polyarticular	Nonspecific joint effusion without bony involvement. Chronic arthropathy following rubella vaccination/infection is occasionally seen resembling juvenile rheumatoid arthritis	Transient arthritis associated with rubella, mumps, mycoplasma infections, and hepatitis. Osteomyelitis and arthritis (suppurative and nonsuppurative) were in the past well-known complications of smallpox (variola).
HIV infection (AIDS) (Fig. 6.119)	Oligoarticular to polyarticular Knee Ankle Foot Hand	Reiter's-like asymmetric oligoarticular or polyarticular involvement of preferentially the lower extremity with considerable enthesopathy, especially in the foot (AIDS-foot). Peripheral arthropathy similar to psoriatic arthritis is also found. Involvement of the axial skeleton with the exception of the sacroiliac joint is uncommon.	HIV shares certain aspects of cellular immune deficiency elements with seronegative spondylarthropathies such as Reiter's syndrome and psoriasis. Septic, tuberculous and fungal arthritis are not uncommon in AIDS patients either (Figs. 6.**120** and 6.**121**). This infective arthritic process is monoarticular and, besides the knee and the sacroiliac joint, the larger joints of the upper extremity, and the acromioclavicular and sternoclavicular joints are frequently affected.

(continues on page 180)

Fig. 6.**115** **Tuberculous spondylitis**. Marked disc space narrowing and a destructive lesion with fragmentation affecting the anterior aspect of the adjacent two vertebral bodies resulting in focal kyphosis (gibbus deformity) is seen at L1/2.

Fig. 6.**116** **Tuberculous arthritis**. Severe localized osteopenia associated with joint space narrowing and multiple small erosions is seen in the wrist involving the radiocarpal, intercarpal and carpometacarpal joints. The normal contralateral wrist in this patient differentiates this condition radiographically from rheumatoid arthritis.

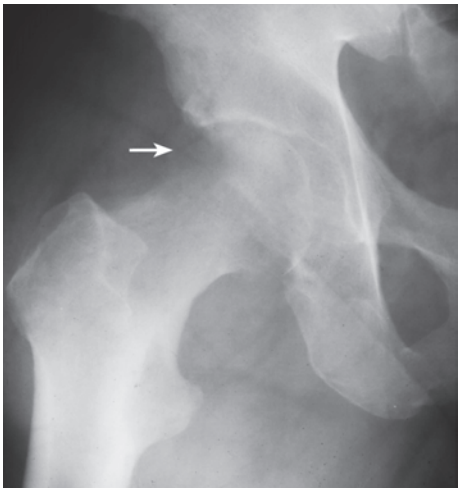

Fig. 6.**117** **Tuberculous arthritis**. Juxta-articular osteopenia, joint space narrowing and a poorly defined erosion (arrow) in the lateral aspect of the femoral head are seen.

Fig. 6.**118** **Fungal arthritis**. A well defined triangular osseous defect with sclerotic margin is seen in the greater tuberosity. Several poorly defined osteolytic lesions with surrounding sclerosis in the humeral head and glenoid are also seen in this patient with AIDS.

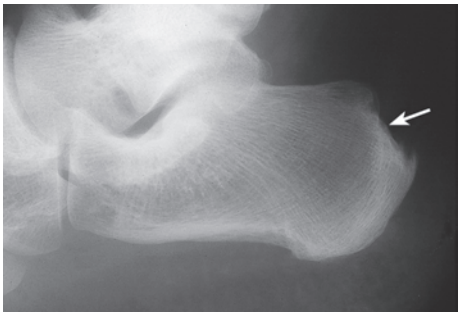

Fig. 6.**119** **HIV infection**. An erosive lesion (arrow) with minimal spiculated new bone formation is seen in the superolateral aspect of the calcaneus.

Table 6.14 (Cont.) Differential Diagnosis of Articular Disorders

Disease	Characteristic Location	Radiographic Findings	Comments
Pigmented villonodular synovitis (PVNS) (Figs. 6.122, 6.123 and 6.124)	Monoarticular Knee Hip Ankle Elbow Wrist	Dense appearing soft tissue swelling around the involved joint due to hemosiderin deposition in synovial proliferation and joint effusion. Pressure erosions and cysts are common in joints with tight capsule (e.g. hip, ankle, wrist). Osteoporosis and intra-articular calcifications/loose bodies are absent. Joint space is preserved until very late in the disease.	Highly vascularized, tumor-like synovial proliferation with multinucleated giant cells ingesting hemosiderin. Occurs typically in adults in the 3rd and 4th decade of life. Hemorrhagic (chocolate-brown) effusions in the absence of trauma are characteristic.
Synovial osteochondromatosis (Figs. 6.125, 6.126 and 6.127)	Usually monoarticular Occasionally bilateral Knee Hip Elbow Shoulder	Multiple calcified/ossified synovial nodules or loose bodies ranging in size from a few millimeters to several centimeters are characteristic. One-third of chondromas are not calcified. Lesions may cause pressure erosions in the adjacent bone (e.g. hip) and widening of the joint space. No osteoporosis is evident. Secondary osteoarthritis occurs in advanced disease from chronic mechanical irritation by the loose bodies. Malignant transformation to chondrosarcoma is extremely rare.	Presents in the 3rd to 5th decades of life with chronic joint pain, limitation of motion and locking with 3:1 male predominance. *Synovial chondrometaplasia* occasionally occurs in the elderly patient with advanced primary osteoarthritis causing chronic synovial inflammation and subsequently secondary osteochondromatosis. Differential diagnosis includes *synovial hemangioma*, *lipoma arborescens* and pigmented villonodular synovitis.

(continues on page 182)

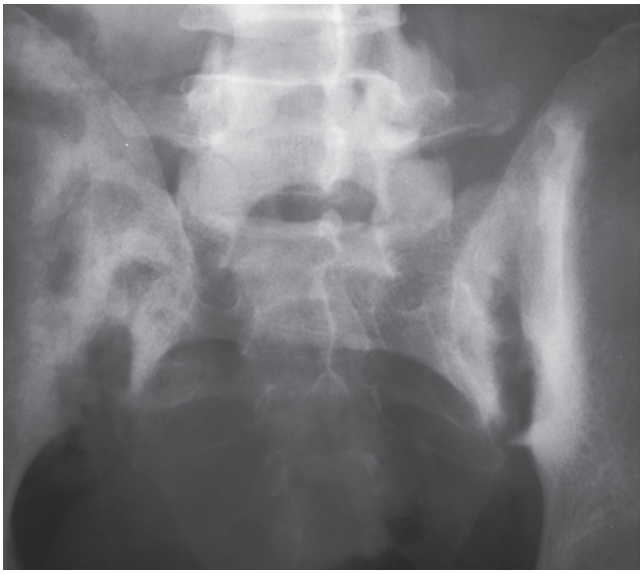

a

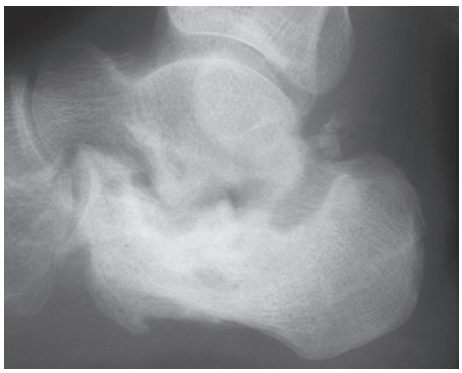

b

Fig. 6.**120 a, b** **Septic arthritis in AIDS** (2 cases). **a** Widening of both sacroiliac joints caused by erosion and destruction of the adjacent bone with extensive sclerosis is seen. The bilateral involvement is unusual for septic arthritis. **b** Destruction of the subtalar joint is associated with extensive sclerosis primarily of the calcaneus.

Fig. 6.**121** **Tuberculous arthritis in AIDS**. Osteolysis of the proximal phalanx of the fifth finger with a coarsened, reticulated pattern reminiscent of sarcoidosis is seen extending into the proximal interphalangeal joint.

Fig. 6.**122** **Pigmented villonodular synovitis**. Extrinsic pressure erosions present as scalloped extrinsic osteolytic lesions in the lateral aspect of the femoral neck and acetabulum.

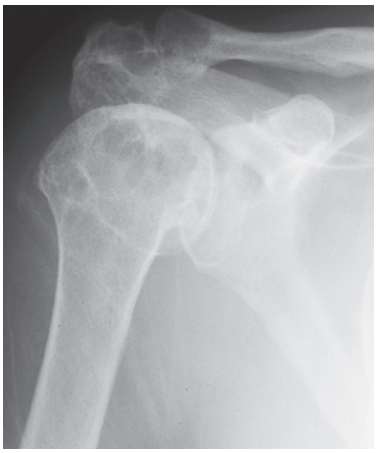

Fig. 6.**123** **Pigmented villonodular synovitis**. Multiple lobulated cystic lesions often with minimally sclerotic margins are seen in the humeral head, acromion and distal clavicle.

Fig. 6.**124** **Pigmented villonodular synovitis**. A large soft mass along the distal ulna outlined by two metallic skin markers is associated with multiple erosions/cystic lesions in many carpal bones and the bases of metacarpals 3 to 5.

Fig. 6.**125** **Synovial osteochondromatosis**. Multiple ossified loose bodies are seen in the knee joint, suprapatellar bursa and popliteal (Baker) cyst (arrow).

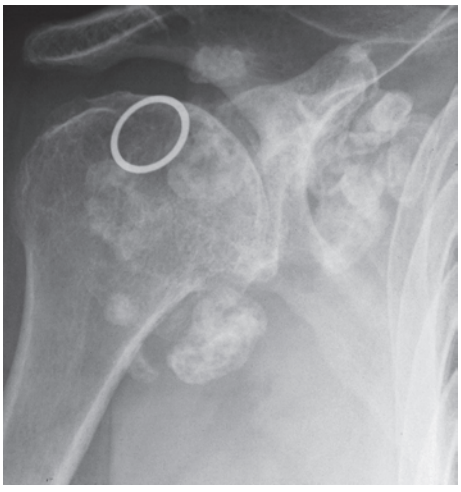

Fig. 6.**126** **Synovial osteochondromatosis**. Multiple calcified or ossified loose bodies are seen in the glenohumeral joint including the axillary and subscapular recesses.

Fig. 6.**127** **Synovial osteochondromatosis**. Innumerable small calcified loose bodies are seen in a hugely enlarged hip joint.

Table 6.14 (Cont.) Differential Diagnosis of Articular Disorders

Disease	Characteristic Location	Radiographic Findings	Comments
Osteochondritis dissecans (osteochondral fracture) (Figs. 6.*128*, 6.129, 6.130 and 6.131)	Knee: Medial femoral condyle. Less commonly lateral femoral condyle, tibia, and patella. Talus: Lateral and medial dome Elbow: Capitellum Shoulder: Humeral head and glenoid	Osteochondral fracture with characteristic location. The spectrum ranges from an in situ lesion with intact articular cartilage over a detached osteochondral body still located in the original pit (mouse bed) to a completely detached osteochondral fragment (mouse) away from the pit evident as a subchondral defect with sclerotic margin. Soft tissue swelling and joint effusions are frequently associated. Knee: The most common location is the nonweight-bearing portion of the medial femoral condyle at the intercondylar notch (70%). Other locations in the knee include the weight-bearing portions of either the medial or lateral femoral condyle and rarely the anterior aspect of the lateral femoral condyle and the medial facet of the patella	Presents most commonly in male adolescents and young adults with pain aggravated by motion, clicking and locking or maybe asymptomatic. It represents a subchondral fatigue fracture, but a single traumatic event is occasionally identified (especially in the talus). A purely cartilaginous lesion cannot be appreciated by plain film radiography and requires MR imaging or CT arthrography for accurate diagnosis. Avascular necrosis of the knee may also present with findings resembling osteochondritis dissecans, but in this condition frequently both knees or both condyles in the same knee are affected.

(continues on page 183)

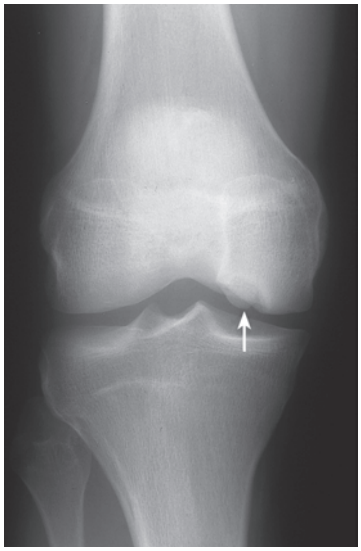

Fig. 6.**128 Osteochondritis dissecans**. A 1 cm oval shaped bony fragment (arrow) is seen in an osteochondral defect (pit), located classically along the lateral non-weight-bearing segment of the medial femur condyle. At a later stage, the bony fragment may become dislodged from the pit and found as a loose body anywhere in the knee joint.

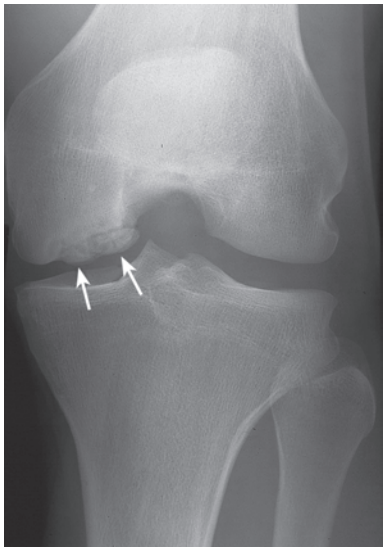

Fig. 6.**129 Osteochondritis dissecans**. An osteochondral defect extending from the intercondylar notch to the weight-bearing segment of the medial femur containing two osteochondral fracture fragments (arrows) is seen (extended classic variant).

Fig. 6.**130 Osteochondritis dissecans**. A radiolucent line separates an oval shaped osseous body (arrow) from the medial talar dome. The lesion is referred to as in-situ when the articular cartilage covering the osseous fragment remains intact.

Fig. 6.**131 Osteochondral fracture**. An acute osteochondral fracture (arrow) is seen in the lateral talar dome. In the subacute/chronic stage this lesion may be impossible to differentiate from osteochondritis dissecans.

Table 6.14 (Cont.) Differential Diagnosis of Articular Disorders

Disease	Characteristic Location	Radiographic Findings	Comments
Avascular necrosis (osteonecrosis) (Figs. 6.132, 6.133, 6.134, 6.135, 6.136, 6.137 and 6.138)	Monoarticular, occasionallly bilateral Hip Knee Talus Scaphoid Shoulder	Articular involvement affecting only one site of the joint is characteristic. In an early stage plain film findings are absent or nonspecific and include mixed lytic and sclerotic changes producing a mottled appearance of the subchondral bone with preservation of the joint space. An arc-like subchondral lucent line (crescent sign in femoral head) is more specific. Progression of the disease results in subchondral cyst formation, fragmentation and eventually collapse of the affected epiphysis. At this stage loose intra-articular bony fragments are frequently present. The endstage is severe secondary osteoarthritis involving the entire joint. Post-traumatic avascular necrosis is most frequent in the femoral head (subcapital fracture, dislocation, or slipped capital femoral epiphysis), talar dome (talar neck fracture), humeral head (anatomic neck fracture, or severe fracture-dislocation), and proximal pole of scaphoid (scaphoid waist fracture).	For early diagnosis of avascular necrosis either radionuclide bone scintigraphy or magnetic resonance imaging is required. Primary avascular necrosis is uncommon in the adult except in the lunate (*Kienböck's disease*) and the knee (*Alhbäck's disease*). It is, however, common in children and adolescents (see Chapter 2). Secondary avascular necrosis is associated with trauma (fracture or dislocation), hemoglobinopathies (e.g. sickle cell anemia), exogeneous or endogeneous hypercortisolism, transplantation, alcoholism, pancreatitis, caisson disease, small vessel disease (e.g. systemic lupus erythematosus), Gaucher's disease, gout and radiation therapy. In many of these conditions more than one joint is involved and bone infarcts in the diametaphyses of the long bones may also be evident. *Ahlbäck's disease* or *spontaneous osteonecrosis of the knee (SONC)* usually occurs in patients over 60 years of age with female predominance. It presents with flattening of the weight-bearing portion of the medial femoral condyle. Involvement of the lateral condyle, tibial plateau or both knees are all uncommon. Progression of the disease results in further depression of the affected condyle with increased sclerosis and possible loose body formation. More recently a stress (insufficiency) fracture rather than osteonecrosis has been implicated as cansative factor for this condition.

(continues on page 185)

Fig. 6.**132** **Avascular necrosis**. Early avascular necrosis presents with mixed lytic and sclerotic changes in both femoral heads without alteration of their shape. An arc-like subchondral lucent line (crescent sign) seen in the right femoral head (arrow) is a more specific finding and indicates progression of the disease. Sequelae from bilateral core decompression are evident by the oblique tracks extending from the greater trochanters to the femoral heads. Post-traumatic diastasis of the pubic symphysis is incidentally also present.

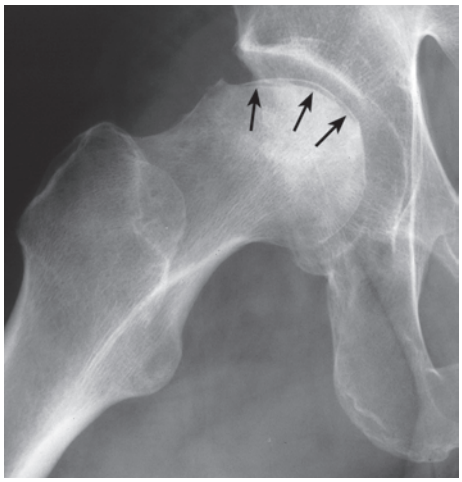

Fig. 6.**133** **Avascular necrosis**. An arc-like subchondral lucent line (crescent sign) is seen (arrows).

Fig. 6.**134** **Avascular necrosis**. Fragmentation of the femoral head in the weight-bearing segment results in flattening and collapse of the femoral head.

Fig. 6.**135** **Avascular necrosis**. Localized fragmentation of the humeral head in its superomedial aspect is seen. The osteochondral fracture fragment with crescent sign resides in an irregular pit with sclerotic margin. A large subchondral cyst infero-lateral to the pit is also evident.

Fig. 6.**136** **Avascular necrosis**. A large detached osteochondral fragment is seen in the weight-bearing portion of the sclerotic medial femur condyle in this patient with systemic lupus erythematosus.

Fig. 6.**137** **Idiopathic avascular necrosis of the lunate (Kienböck's disease)**. A compressed, sclerotic lunate with several small cysts is seen.

Fig. 6.**138** **Spontaneous osteonecrosis of the knee (Ahlbäck's disease)**. An irregular osteochondral defect with sclerotic border is seen in the weight-bearing portion of the medial femur condyle

Table 6.14 (Cont.) Differential Diagnosis of Articular Disorders

Disease	Characteristic Location	Radiographic Findings	Comments
Multiple epiphyseal or spondyloepiphyseal dysplasia (Figs. 6.139)	Polyarticular, bilateral, symmetric Hips Knees Ankles Shoulders Wrists	Epiphyseal centers of long bones are late in appearance and fragmented. After ossification they have a mulberry-like appearance and are commonly displaced. After puberty the affected articular surfaces of the long bones remain irregular and abnormal in shape and the joints may appear dysplastic. Femoral heads and condyles are flattened and often fragmented and deformities include coxa vara, genu valgum or varum, tibiotalar slant and V-shaped deformities of the wrist. Secondary osteoarthritis is present before the 3rd or 4th decade of life.	Heterogeneous group of dysplasias with minimal to advanced spinal changes (spinal beaking to platyspondyly). Radiographic differential diagnosis includes *cretinism*, *avascular necrosis*, *mucopolysaccharidosis*, *juvenile rheumatoid arthritis* and in the hip *Legg-Calvé-Perthes disease* and *Meyer's dysplasia* (delayed and fragmented epiphyseal ossification resulting eventually in normal hip, bilateral in 50 % of cases).

(continues on page 186)

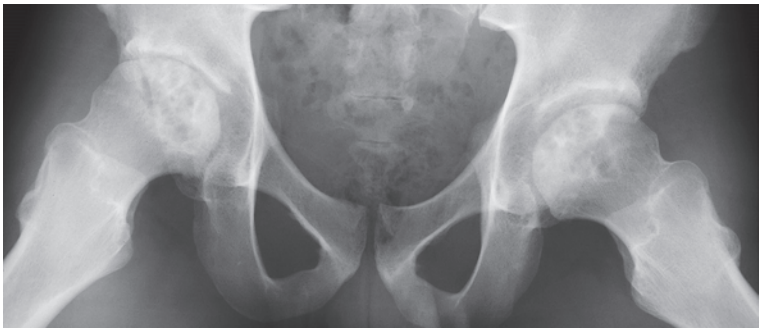

a

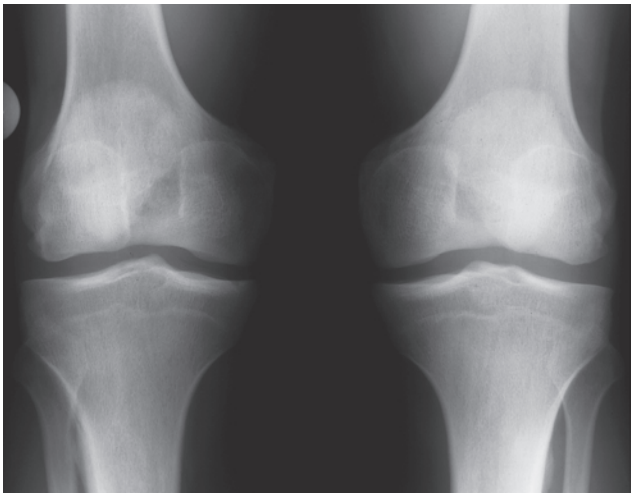

b

c

Fig. 6.**139 a, b, c Spondyloepiphyseal dysplasia tarda (X-linked)**. **a**: Slightly deformed femoral heads with extensive sclerosis and numerous small cystic lesions are associated with mildly dysplastic shallow acetabuli. **b**: Bilateral dysplastic knees with shallow intercondylar notches and hypoplastic tibial spines are seen. **c**: Dysplastic vertebral bodies with characteristic osseous humps in their central and posterior portions causing narrowing of the disc spaces posteriorly and widening anteriorly are seen.

Table 6.14 (Cont.) Differential Diagnosis of Articular Disorders

Disease	Characteristic Location	Radiographic Findings	Comments
Hyperparathyroidism (Figs. 6.140 and 6.141)	Bilateral, symmetric sacroiliac joints Sternoclavicular joints Acromioclavicular joints Pubic symphysis	Subchondral bone resorption in the axial or less commonly appendicular skeleton may mimic an erosive arthritic disease.	Other radiographic findings include osteopenia, acro-osteolysis, subperiosteal bone resorption, chondrocalcinosis, soft tissue calcifications and brown tumors. Osteosclerosis is a feature of secondary hyperparathyroidism (renal osteodystrophy).
Sarcoidosis (Fig. 6.142)	Monoarticular to polyarticular Hands Feet	Articular involvement in the chronic form is usually an extension of the osseous disease causing destruction and collapse of the joint	In the acute form radiographic findings are nonspecific and include soft tissue swelling, effusions and occasionally osteopenia affecting small and medium-sized joints.
Foreign body synovitis (Figs. 6.143 and 6.144)	Associated with prosthetic joint implants	A joint effusion is the initial presentation. Tiny radiopaque particles may be evident in the joint fluid and synovial lining when the synovitis is induced by radiopaque bone cement. Subsequently subchondral cysts and erosions, often with thin sclerotic margins may be found. Osteoporosis is not a prominent finding differentiating this condition from infection.	Caused by shed particles from a joint prosthesis secondary to normal wear or damaged prosthesis. May induce a foreign body synovitis and subsequent osseous involvement of the affected joint. Particles of polymethylmethacrylate, silicone and polyethylene are the most common offending agents.

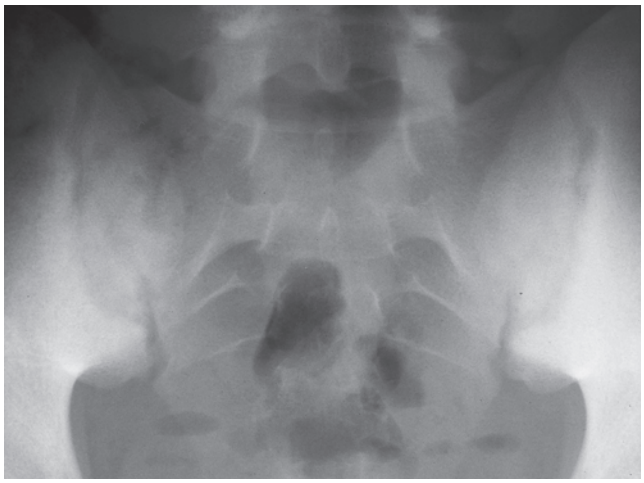

Fig. 6.**140** **Hyperparathyroidism (secondary)**. Bilateral widening of the sacroiliac joint with diffuse sclerosis, especially of the iliac bones is seen.

Fig. 6.**141** **Hyperparathyroidism**. Subchondral erosions imitating articular disease are seen in the distal interphalangeal joints of the second and fifth finger, the interphalangeal joint of the thumb and the first carpometacarpal joint. Other findings include heavy calcification of the triangular fibrocartilage, subperiosteal resorption along the radial margin of several phalanges, acro-osteolysis and a small brown tumor in the distal aspect of the proximal phalanx of the third finger.

Fig. 6.**142** **Sarcoidosis**. Soft tissue lesions are associated with a coarsened lacework trabecular pattern or small cysts in many phalanges and distal metacarpals. Articular involvement of the interphalangeal joint of the thumb is an extension of the osseous involvement of the distal phalanx. Note also the acro-osteolysis in several fingers.

Fig. 6.**143** **Cement synovitis**. A unicompartmental (Repicci) prosthesis is seen in the medial compartment of the knee with signs of loosening of the femoral component and wear of the tibial component. Osteoarthritis is evident in the lateral knee compartment and patello-femoral joint. A small joint effusion with slightly distended suprapatellar bursa outlined by tiny radiopaque cement particles is seen (arrows).

a

b

Fig. 6.**144 a, b** **Silicone-induced arthritis**. An intact silicone implant is seen in the first carpometacarpal joint following arthroplasty including trapezectomy for degenerative joint disease in **a**. Six years later partial collapse of the implant and osteolysis about its stem in the proximal first metacarpal is evident in **b**. In addition extensive erosive and cystic changes occurred in many carpal bones.

7 Joint and Soft-Tissue Calcification

Deposition of calcium in abnormal locations may take two forms: *calcification or ossification*. They can be roentgenologically differentiated from each other. Calcification is seen as structureless density; ossification shows organization into trabeculae and cortex (Figs. 7.**1** and 7.**2**).

Calcification of soft tissues is classified as *metastatic* (disturbance of calcium or phosphorus metabolism leading to ectopic calcification in primarily normal tissue), *calcinosis* (deposition of calcium in soft tissues in the presence of normal calcium metabolism), or *dystrophic* (calcium deposition in damaged tissues without generalized metabolic derangement). Ossification of soft tissues is usually due to *myositis ossificans* or *tumoral ossification* of soft tissues.

Tables 7.**1–6** present the differential diagnosis of calcification or ossification of joints and soft tissues of the extremities.

Fig. 7.**2 a** **Myositis ossificans.** Bone formation in the soft tissues of the upper arm after trauma.

Fig. 7.**1** **Structureless calcifications (arrows) in the soft tissues of the hand.** Chronic renal failure.

Fig 7.**2 b** Total hip prosthesis is the most common reason of myositis ossificans (different patient than 7.**2 a**).

Table 7.1 Intra-articular calcified or ossified body (single or multiple)

Associated Disorders	Common Locations and Remark
***Degenerative joint disease* with detached spur.**	Knee and other large joints. May resemble synovial osteochondromatosis, but usually contains one or few calcifications.
***Fracture* with avulsed fragment in joint (bone, articular cartilage meniscus).**	Occurs especially in avulsed medial epicondyle of pediatric elbow. Cartilaginous fragments may or may not calcify.
***Osteochondrosis dissecans* (Fig. 7.5)**	Knee, elbow, hip, shoulder, ankle; similar to synovial osteochondromatosis, but only one or few calcifications. A residual pit in the articular surface.
***Synovial osteochondromatosis* (Fig. 7.3)**	Knee, hip, elbow, shoulder. Multiple small calcified or ossified densities within the joint capsule. Some of the synovial chondromas remain uncalcified and are not detected on plain films.
***Neuropathic joint* (Fig. 7.4, 14.53)**	Knee, hip, ankle, shoulder. Disintegration of joint surfaces, sclerosis and malalignment. May occur in diabetes, syringomyelia, syphilis and leprosy
Intra-articular tumor calcification *(synovial sarcoma, intra-capsular chondroma).*	Knee. Associated with a soft-tissue mass. A tumor may simulate a loose body.
Sequestrum from *tuberculous* or *pyogenic arthritis*.	Rare. Associated with arthritis or postarthritic deformity

a

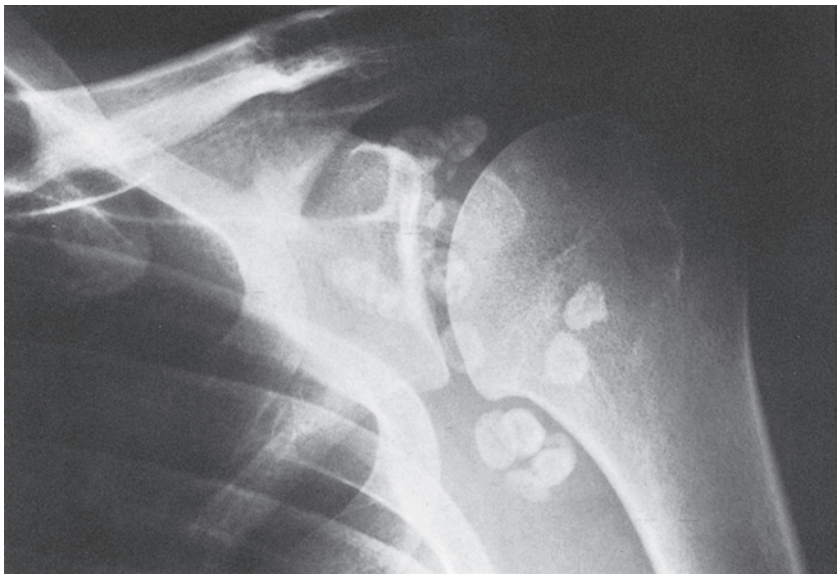

Fig. 7.3 **Synovial osteochondromatosis.** **a** Shoulder joint. **b, c** Knee joint. There is severe secondary osteoarthritis in the knee joint.

Fig. 7.3 b, c ▷

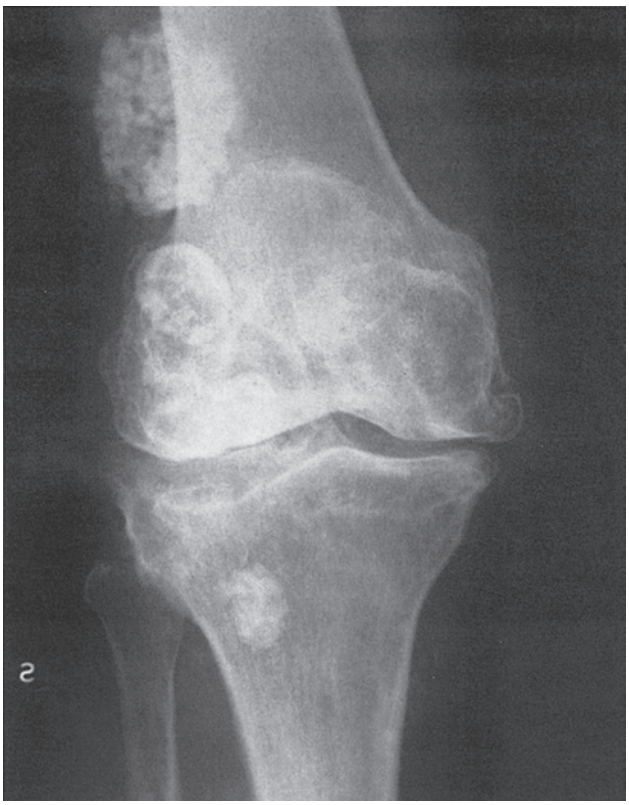

b

c

Fig. 7.**3 b, c**

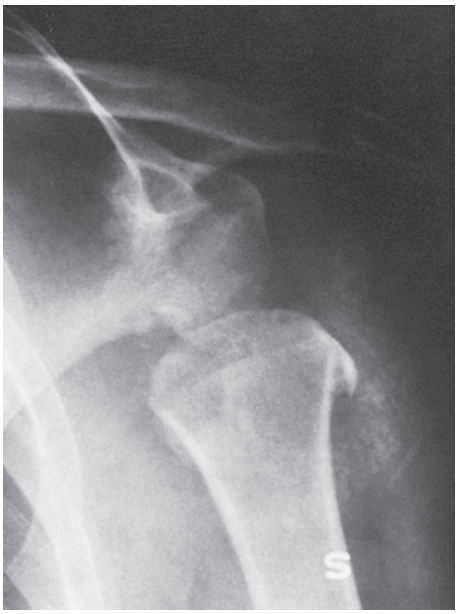

Fig. 7.**4** **Syringomyelia.** Destruction of the glenoid fossa and humeral head, which is displaced inferiorly. The joint cavity contains calcific fragments.

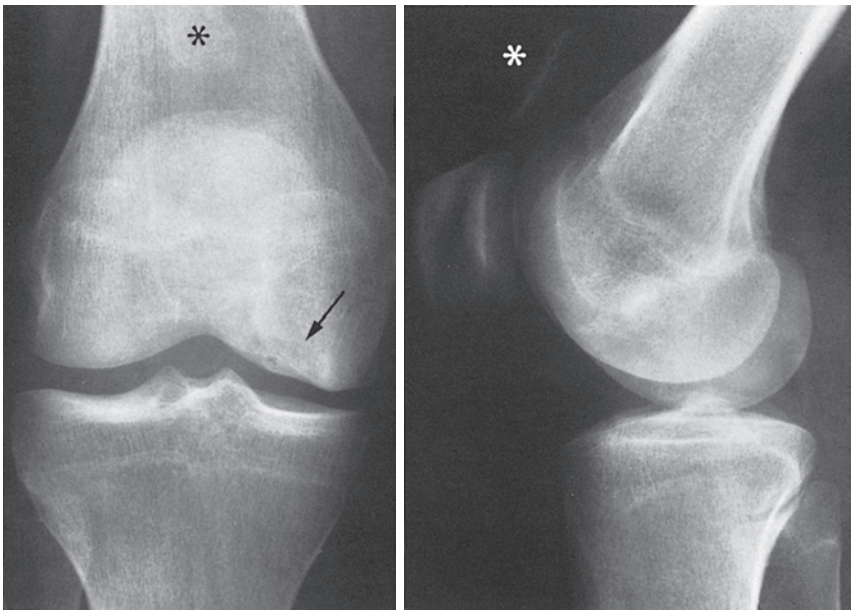

Fig. 7.**5 a** Anteroposterior and **b** lateral views of the knee with osteochondrosis dissecans. A residual pit in the articular surface of the medial femoral condyle is demonstrated (arrow) and the calcified loose body is seen above the patella (asterisk).

Table 7.2 Calcification of articular cartilage or meniscus

Associated Disorders	Common Locations and Remark
Calcium pyrophosphate dihydrate (CPPD deposition disease) *"Pseudogout"* (Figs. 7.6 and 7.7).	Knees, wrists, hips. May be associated with various degrees of secondary osteoarthritis.
Idiopathic, *primary osteoarthritis, trauma*	Calcification of cartilage without crystal arthropathy.
Secondary *osteoarthritis.*	Premature osteoarthritis with chondrocalcinosis.
Hyperparathyroidism, renal osteodystrophy	Wrists, knees, hips, shoulders, elbows. Seen also in oxalosis with secondary renal failure.
Gout	Knee. Chondrocalcinosis is a secondary manifestation.
Ochronosis (alkaptonuria)	Menisci, intervertebral disks. Intervertebral disk calcification is also seen in *hypervitaminosis D, hypophosphatasia, ankylosing spondylitis, spondylosis* and *disk degeneration*
***Acromegaly* (Fig. 7.8)**	Knee. Cartilage proliferation widens joint spaces. Calcification may happen.
Hemochromatosis	Autosomal recessive hereditary disorder in which iron accumulation causes the diseace. 20–60 % of patients may have chondrocalcinosis. Calcification may be similar to CPPD.
Wilson's disease	Rare autosomal recessive disorder characterized by copper accumulation. Affects particularly basal ganglia and liver. In skeletal system it causes osteopenia, subchondral bone fragmentation and chondrocalcinosis.

Fig. 7.**6** Chondrocalcinosis in CPPD with calcification of menisci and articular cartilage of the knee.

Fig. 7.**7** **CPPD (pyrophosphate arthropathy).** Calcification in the region of the triangular cartilage of the wrist (arrow). Osteoarthritic changes in the joint surfaces of the larger multangular bone.

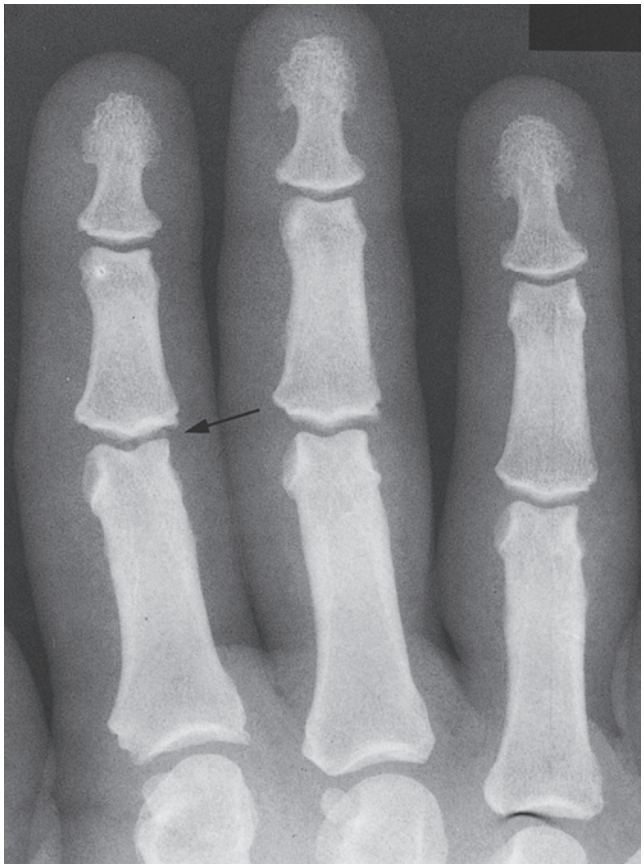

Fig. 7.**8** **Acromegaly.** Widening of the joint spaces and calcification of the proximal interphalangeal joint cartilage of the index finger (arrow).

Table 7.3 Periarticular soft tissue calcification or ossification

Associated Disorders	Common Locations and Remark
Hyperparathyroidism* (Fig. 7.9)** ***Renal osteodystrophy	Associated with other radiographic signs of hyperparathyroidism.
Other disorders of calcium and phosphate metabolism *(hypoparathyroidism, chronic hemo dialysis, widespread bone destruction, vitamin D intoxication, milk-alkali syndrome, etc.)*	Ligamentous subcutaneous and intracranial calcifications sometimes occur. Not seen in postsurgical hypoparathyroidism.
***Scleroderma* (Fig. 7.10)**	Most common in hands. Association of generalized calcinosis of the skin with scleroderma is called *Thibierge-Weissenbach syndrome*. The tetrad of skin calcification, Raynaud's phenomenon, sclerodactyly, and telangiectasia (*CRST syndrome*) is a variant of scleroderma.
***Dermatomyositis* (Fig. 7.11)** ***Polymyositis* (Fig. 7.12)**	Associated with generalized or localized calcinosis of subcutaneous tissues.
Polyarteritis nodosa ***Raynaud's syndrome*** ***Rheumatoid arthritis*** ***Systemic lupus erythematosus***	Periarticular calcifications in these connective tissue diseases are rare. May be reversible in systemic lupus erythematosus.
Sarcoidosis	Large periarticular soft-tissue masses with or without calcifications are a rare manifestation.

(continues on page 194)

Fig. 7.**9** Periarticular (arrows) and vascular calcifications in hyperparathyroidism.

Fig. 7.**10** **Scleroderma.** Periarticular soft-tissue calcification in one finger and a soft-tissue defect in another.

Table 7.3 (Cont.) Periarticular soft tissue calcification or ossification

Associated Disorders	Common Locations and Remark
Gout	Periarticular calcified lump associated with chondrocalcinosis is diagnostic of gout. Most commonly occurs at the first metatarsophalangeal joint, the insertion of the Achilles tendon and the olecranon bursa.
***Ochronosis* (alkaptonuria)**	Periarticular calcification occurs in spine and large joints.
Ehlers-Danlos syndrome	See subcutaneous calcifications, table 7.**5**.
Werner's syndrome (adult progeria)	Periarticular ligamentous calcifications, especially about the knees, may occur in this rare condition. Other radiographic findings include osteoporosis, premature atherosclerosis with calcification, and osteoarthritis.
HADD *(hydroxyapatite deposition disease)* (Fig. 7.14)	Examples: shoulder (calcific tendinitis, periarthrosis). Hip (calcified trochanteric bursa).

(continues on page 195)

Fig. 7.**11** **Dermatomyositis in a child.** Periarticular soft-tissue calcifications around the knee have some resemblance to synovial osteochondromatosis.

Fig. 7.**12** **Polymyositis and Raynaud's syndrome.** Extensive soft tissue calcifications around thumb, fewer calcification at distal ends of other fingers.

Fig. 7.**13** **Calcinosis Interstitialis universalis.** Calcific deposits in the toes are as in scleroderma, but there are no other abnormalities.

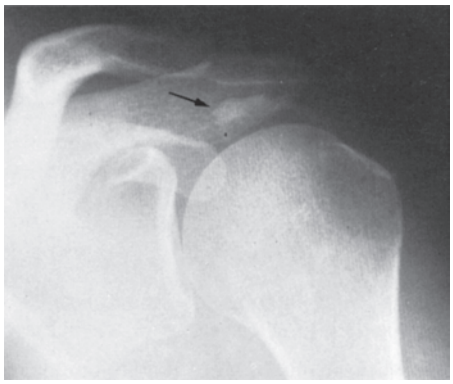

Fig. 7.**14** **Hydroxyapatite deposition disease.** Calcification of the subacromial bursa of the shoulder.

Table 7.3 (Cont.) Periarticular soft tissue calcification or ossification

Associated Disorders	Common Locations and Remark
***Myositis ossificans (localisata)* (Fig. 7.15)**	Calcification occurs about one month after trauma (hematoma, capsular or ligamentous damage), later it ossifies. Also common around joint replacement and in association with chronic neurological diseases (paraplegia). Ossification is always separated from bone by a radiolucent zone, unlike a malignant bone tumor.
***Posttraumatic calcification* (Fig. 7.16)**	Pellegrini-Stieda calcification in the proximal attachment of the medial collateral ligament of the knee is a common presentation.
***Synovial sarcoma* (Fig. 7.17)**	Most common in knee. Only small percentage of these tumors are intra-articular. The periarticular mass often contains calcific flecks, but not extensive calcification.
Pigmented villonodular synovitis	Most common in knee. A high-density lobulated mass may sometimes appear calcified due to hemosiderin deposits, although the tumor calcifies extremely rare.
Healed tuberculous arthritis* (Fig. 7.18)** ***(Caries sicca)	Large joints, spine. Fibrous ankylosis and extensive soft-tissue calcification often occurs.
Pseudotumoral calcinosis (lipocalcinogranulomatosis)	Usually painless calcifications, most often of the bursae in the vicinity of joints (hip, elbow, shoulder) or near bony protuberances. If cystic, may show layering of calcific fluid. Small calcific nodules may progress to a large solid lobulated tumor. The joint is not involved.

Fig. 7.**15** **Calcified hematoma near the ankle joint.**

Fig. 7.**16** **Pellegrini-Stieda calcification.** Curvilinear soft tissue calcification at medial aspect of the femoral condyle.

Fig. 7.**17** **Synovial sarcoma of the knee joint.** A large soft- tissue mass and small calcifications near the joint space (arrows).

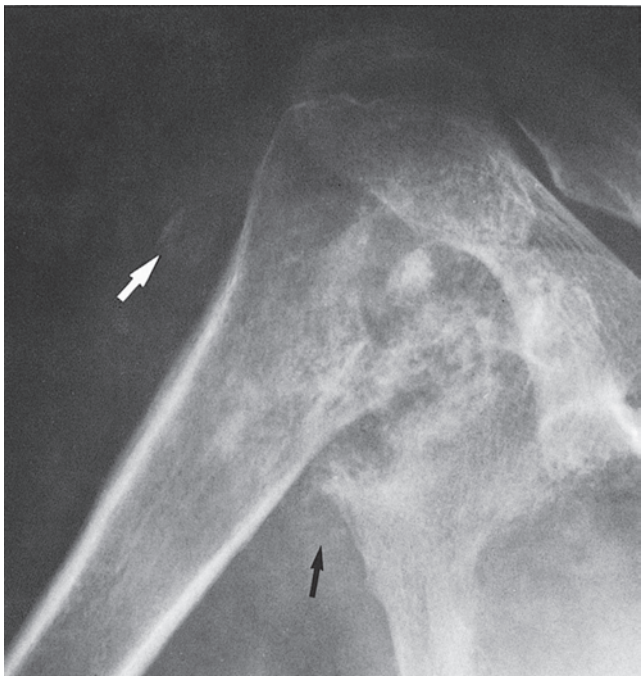

Fig. 7.**18** **Healed tuberculous arthritis of the right shoulder.** Severe deformity and soft-tissue calcifications (arrows).

Table 7.4 Connective tissue and muscular calcification or ossification (Figs. 7.19–7.26)

Associated Disorders	Common Locations and Remark
Idiopathic universal calcinosis **(Fig. 7.13)** **Scleroderma** **Dermatomyositis (Figs. 7.19–20)** ***systemic lupus erythematosus*** **(rarely)** ***Carbon monoxide poisoning*** **(rare).**	Variable: neck, thorax, limbs. Usually no ossification takes place.
Myositis ossificans progressiva **(rare) (Fig. 7.2)**	A rare hereditary connective tissue disorder. Ectopic ossification in early childhood. Neck, shoulders, proximal arms, pelvis. Associated with short first metacarpals and metatarsals and finger or toe anomalies.
Parasitic calcifications:	
– **Cysticercosis** ***(Taenia solium)*** **(Fig. 7.22)**	Multiple, ovoid (about 1 cm long and 3 mm thick) calcifications have their long axis along muscle planes.
– **Hydatid disease** ***(Echinococcus)***	If calcifications occur in muscle, they tend to parallel the long axis of the limb.
– **Guinea worm disease** ***(Dracunculus medinensis)***	Small irregular or linear serpinginous calcifications measuring up to several cm (calcified female worm) in legs, abdominal, or thoracic muscles.
– **Loiasis** ***(Filaria loa loa)***	U- or V-shaped calcific dots in web spaces.
– **Schistosomiasis** ***(Schistosoma haematobium)***	Fibrosis and granulomatous calcification, more commonly in the lower urinary tract.
– **Trichinosis** ***(Trichinella spiralis)***	1 mm or less, rarely visible radiographically.
– ***Armillifer armillatus.***	Multiple, comma-shaped peritoneal or pleural calcifications.

(continues on page 198)

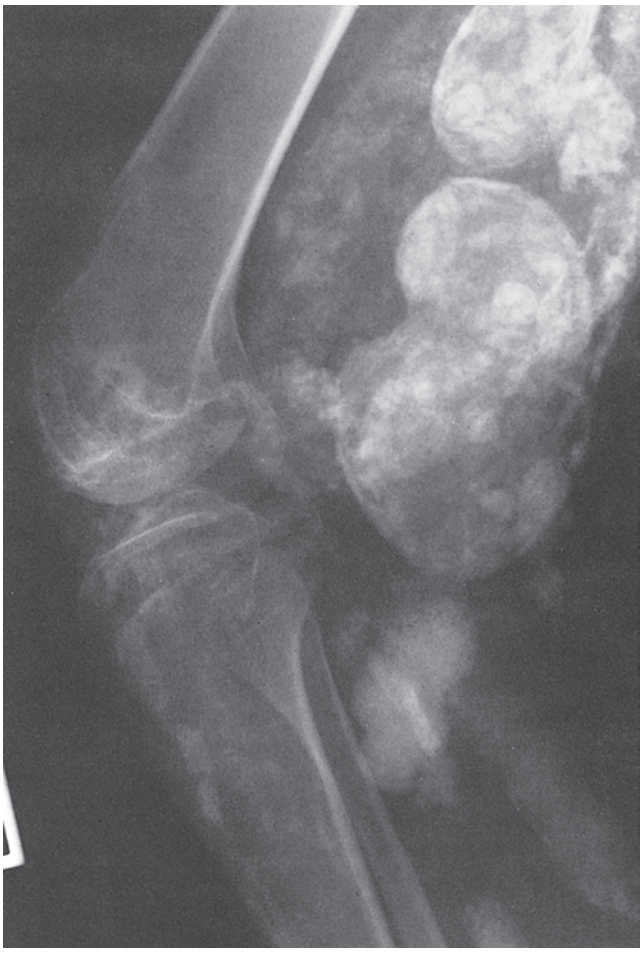

Fig. 7.**19** **Dermatomyositis.** Extensive connective tissue calcification in the leg.

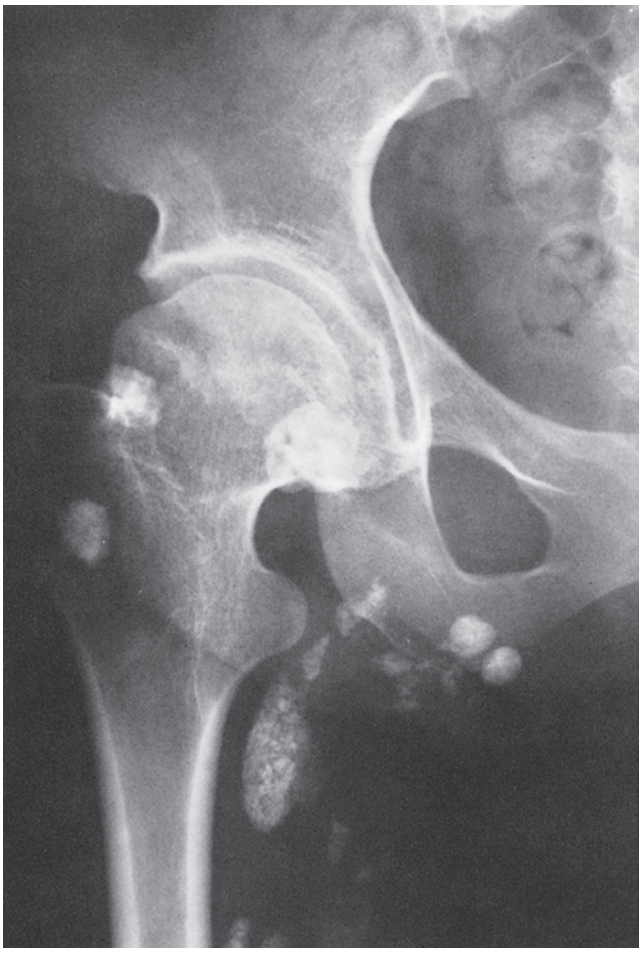

Fig. 7.**20** **Dermatomyositis.** Calcification of connective tissues.

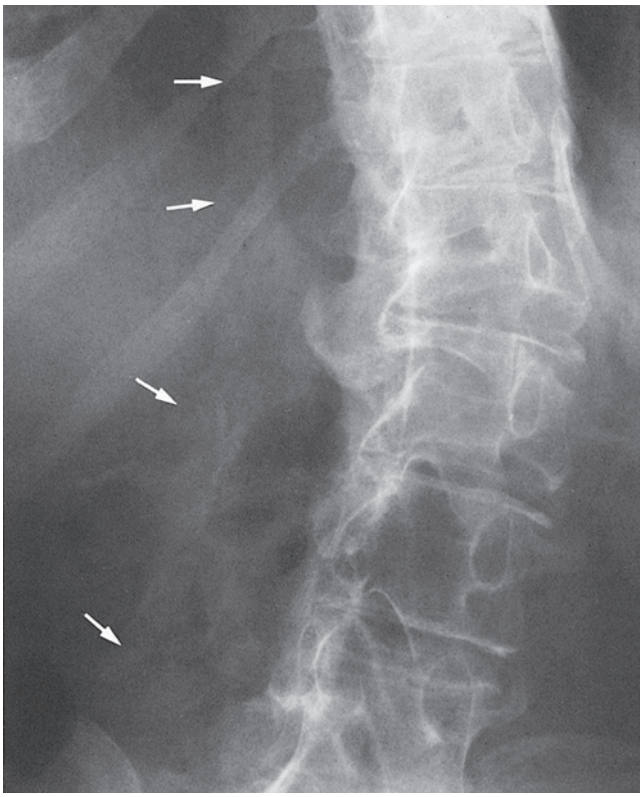

Fig. 7.**21** **Myositis ossificans progressiva.** Paraspinal soft-tissue ossification (arrows) associated with myositis in this region.

Fig. 7.**22** **Cysticercosis.** Multiple ovoid calcifications in the soft tissues of the leg.

Table 7.4 (Cont.) Connective tissue and muscular calcification or ossification (Figs. 7.19–7.26)

Associated Disorders	Common Locations and Remark
Idiopathic or degenerative **(Fig. 7.23)**	Ligaments of the shoulder girdle and pelvis often calcify in normal individuals.
Fluorosis	Paraspinal sacrotuberal and iliolumbal ligaments can calcify extensively in fluorosis. Sclerosis of the axial skeleton is more diagnostic.
Traumatic or postoperative **(Fig. 7.2 B)**	Common around total hip replacement.
Periosteal due to *hematoma* (Fig. 7.24)	In early phase may mimic periosteal sarcoma, but is denser at the periphery, whereas sarcoma is denser at the center.
Neurological causes, especially *paraplegia*	Myositis ossificans around hip joints is a common presentation.
Tumors:	
– **Osteosarcoma**	Rarely develops in the soft tissues, and may show fuzzy or spicular calcification.
– **Chondrosarcoma**	
– **Fibroma**	Small calcific flecks may be present in both benign and malignant tumors.
– **Fibrosarcoma**	
– **Synovial sarcoma**	Most tumors are extra-articular and commonly show calcific flecks.
– **Lipoma (Fig. 7.25)**	Both benign and malignant tumor may contain extensive ossification. Predilection in medial thigh and popliteal areas.
– **Liposarcoma (Fig. 7.26)**	
– **Metastases**	Bone-forming metastases occur in the carcinomas of the colon, breast, and urinary tract.
Leprosy	Nerve abscesses of tuberculous leprosy are seen as soft-tissue masses which may calcify.

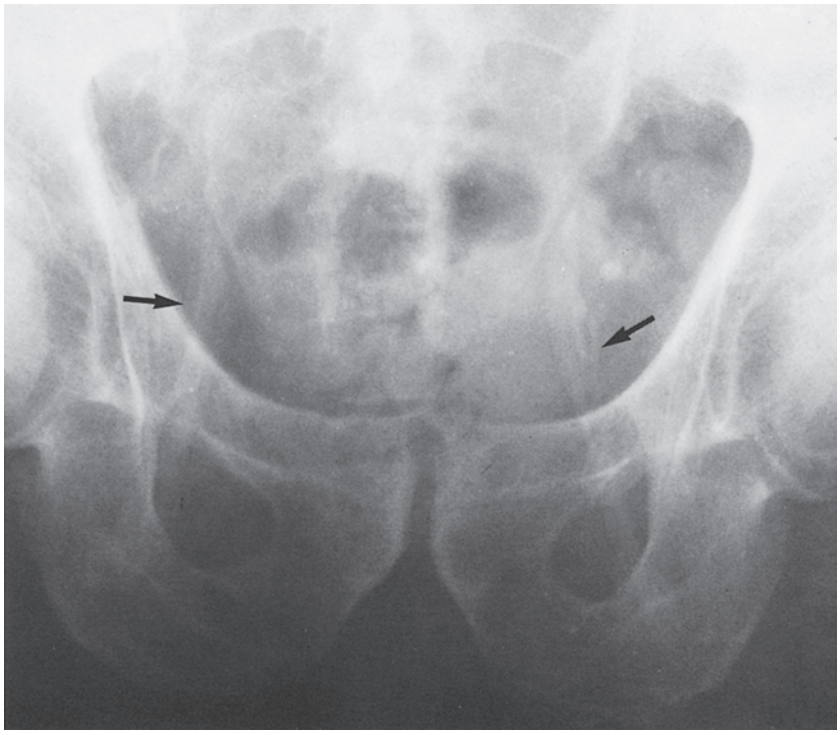

Fig. 7.**23** Calcified sacrotuberous ligaments (arrows), an incidental finding.

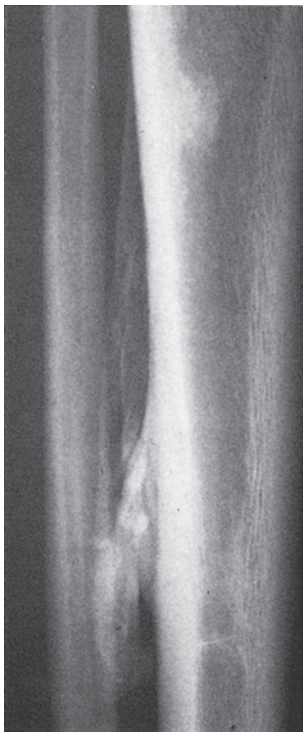

Fig. 7.**24** **Calcification of periosteum and the interosseus ligament following hematoma.**

Fig. 7.**25** **Lipoma.** A low-density mass in the arm has a well-defined outline. It contains a calcified spot characteristic of fat necrosis (arrow).

Fig. 7.**26** **Liposarcoma of the thigh with calcification.**

Table 7.5 Subcutaneous calcification or ossification

Associated Disorders	Common Locations and Remark
***Dermatomyositis* and other causes of generalized or circumscribed interstitial calcinosis. (Fig. 7.27)**	Thighs, abdomen, thorax, shoulders, neck, hands, feet.
Ehlers-Danlos syndrome	Generalized inherited disorder of connective tissue and loose joints. Fatty nodules in the subcutaneous tissue of the extremities may calcify. They may mimic phleboliths, having central lucencies.
Pseudoxanthoma elasticum	Hereditary systemic disorder with widespread premature degeneration of elastic fibers. Middle and deep layers of the dermis may calcify, as well as tendons, ligaments, and large vessels.
Basal cell nevus syndrome	Soft-tissue calcification can be a feature of this inherited disorder characterized by multiple basal cell carcinomas, palmar pits, dentigerous cysts of the mandible, anomalies of the spine and ribs, and brachydactyly, as well as neurologic abnormalities.
Postinjection or traumatic fat necrosis (or heavy metals)	Irregular dense deposits in buttocks may contain heavy metals, but calcification of fat necrosis may follow injections of antibiotics etc.
Venous thrombosis ***Varicose veins***	Lower extremities, subcutaneous ossification secondary to chronic venous stasis.

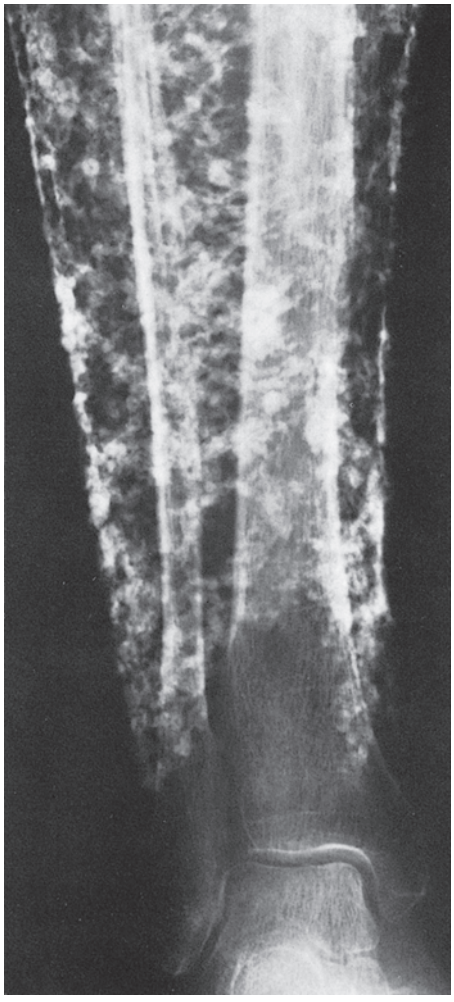

Fig. 7.**27** **Dermatomyositis** with extensive subcutaneous calcification.

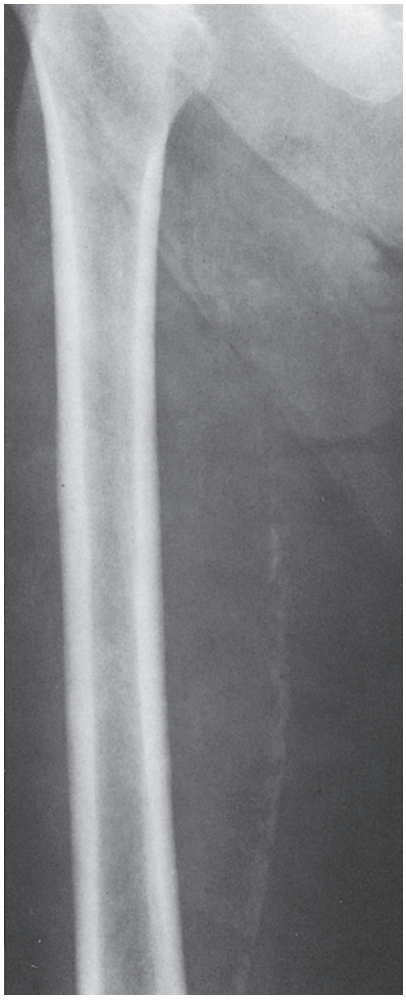

Fig. 7.**28** **Atheromatous calcifications** in the arteries of the thigh.

Table 7.6 Differential Diagnosis of Vascular calcifications

Findings	Associated Disorders	Common Locations and Remarks
Atheromatous calcifications (patchy) (Fig. 7.28)	*Arteriosclerosis* *Aneurysm* *Takayasu's arteritis*	Causes of premature atherosclerosis: familial hyperlipemia; secondary hyperlipemia (e.g., diabetes)
Mainly medial sclerosis of arteries evident as parallel lines (Monckeberg's medial sclerosis) (Fig. 7.29)	*Idiopathic hypercalcemia syndromes* *Nephropathies*	Hypercalcemia syndromes: hyperparathyroidism, hypervitaminosis D, immobilization, milk-alkali syndrome, sarcoidosis, idiopathic, paraneoplastic, or secondary to massive bone destruction.
Calcified thrombus (rare)	*Venous thrombosis, varicose veins*	Seen as an irregular calcification along the course at an artery or, more commonly, a vein.
Phlebolith (small rounded opacities, characteristically with central lucencies) (Fig. 7.30)	*Normal* *Angiomatous malformation Hemangioma* *Varicose veins*	Common in pelvis, more rarely spleen, ankle, orbits. Usually a localized collection of phleboliths. Cavernous hemangioma associated with enchondromatosis is called *Mafucci's syndrome*. Lower extremities.

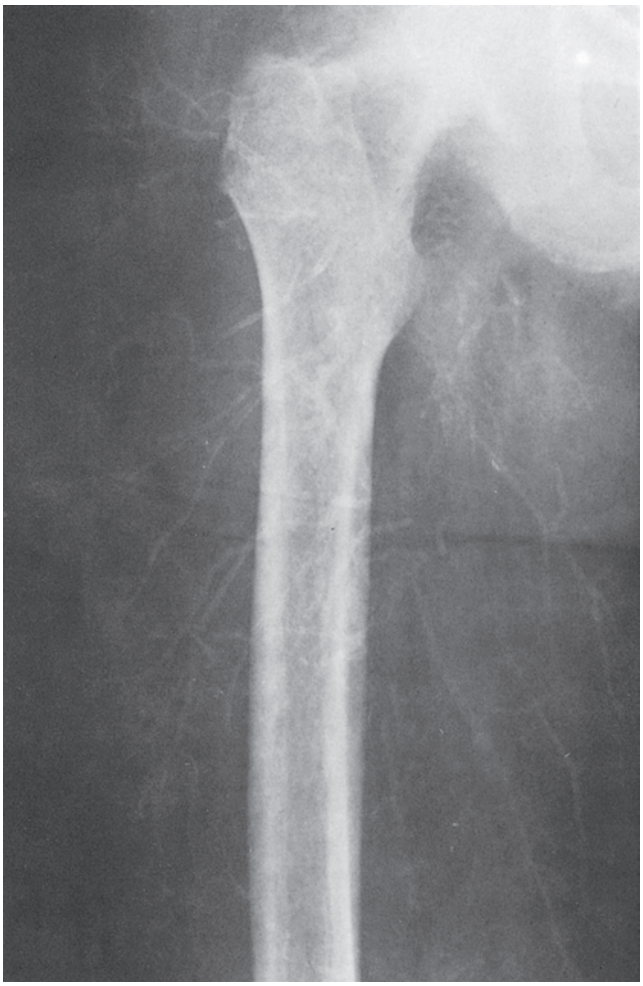

Fig. 7.**29** **Medial sclerosis** of the branches of the femoral artery. **A case of renal failure.**

Fig. 7.**30** **Soft-tissue calcification associated with varicose veins.** Both ossifications (myositis ossificans) and calcified phleboliths (arrow) are seen.

8 Skull

Calcifications

Calcifications are a common finding on skull radiographs. With computed tomography, many more calcifications within the skull can be appreciated that escape detection with plain film radiography. Numerous artifacts on the scalp (e.g., dirt, fragments, ointments, and braids) may simulate intracranial calcifications and therefore must be taken into consideration (Fig. 8.**1**).

Physiologic Intracranial Calcifications

Physiologic and pathologic intracerebral calcifications occur, although the boundaries between the two can be blurred. Locations of characteristically physiologic calcifications are summarized in Table 8.**1** and Fig. 8.**2**.

Table 8.1 Physiologic Intracranial Calcifications

Pineal
Habenula
Choroid plexus
Dura (falx, tentorium)
Ligaments (petroclinoid and interclinoid)
Pituitary
Internal carotid artery (cavernous portion)
Basal ganglia and dentate nucleus

A *calcified pineal* is found in 5 % of children under the age of 10 and in almost two-thirds of the adult population (Fig. 8.**3**). With CT scanning, a considerably higher rate of pineal calcification is found. It appears amorphous or ring-like, and varies considerably in size but measures usually less than 1 cm. A pineal calcification exceeding 1 cm in diameter suggests neoplasm, either a pinealoma or even more commonly a teratoma. A calcified aneurysm of the vein of Galen may occasionally also simulate an abnormal pineal calcification.

The pineal lies midline in the anteroposterior projection. A displacement of a pineal more than 3 mm to one side of the midline suggests an intracranial mass lesion displacing the pineal away from the midline. On the lateral radiograph, the pineal projects approximately 3 cm above the highest posterior elevation of the pyramids. Numerous methods have been described to assess pineal displacement in this projection, but since their usefulness is rather limited, they will not be discussed in this context.

The *habenula* is located a few millimeters anterior to the pineal and calcifies in almost one-third of patients (Fig. 8.**3**). Habenular calcification characteristically assumes the shape of a "C" open posteriorly. Habenular displacement by intracranial lesions occurs in the same way as pineal displacement.

Although the *choroid plexus* can calcify in all ventricles, it most commonly occurs in the atrial portions of the lateral ventricles (junction of the body of the lateral ventricles with the posterior and temporal horns), projecting on the lateral view approximately 2 to 3 cm behind and slightly below the pineal (Fig. 8.**3**). In the anteroposterior projection, plexus

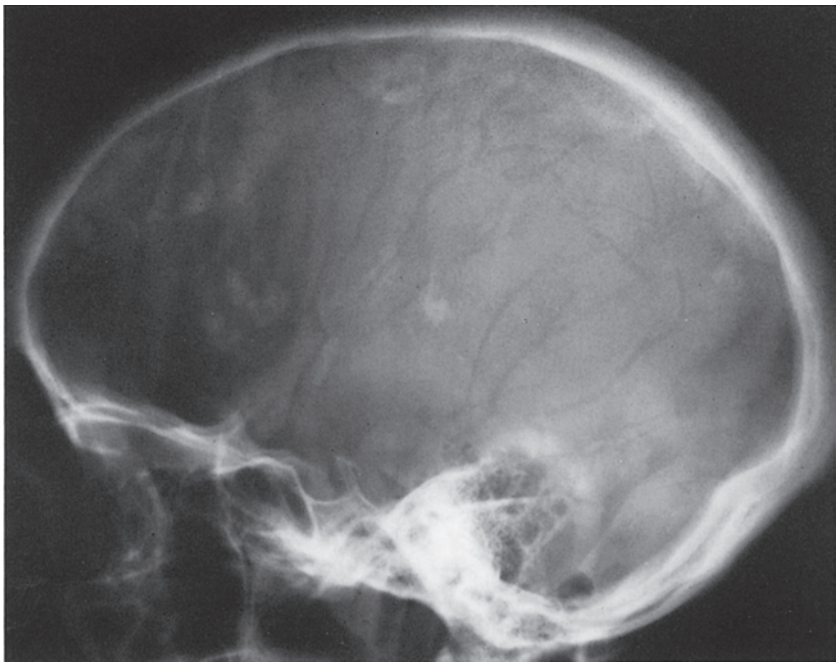

Fig. 8.**1** **Artifacts.** Corn rows (tight African-style braiding of the hair) simulate scattered intracranial calcifications

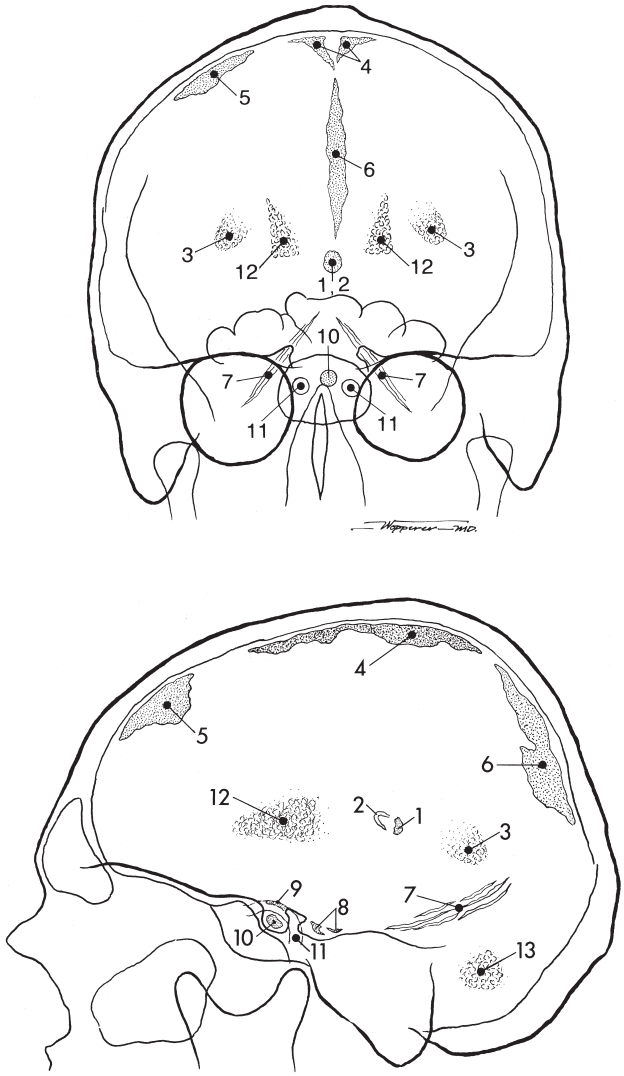

Fig. 8.**2 a, b** **Physiologic intracranial calcifications** in **a** anteroposterior and **b** lateral projection. 1 pineal; 2 habenula; 3 choroid plexus; 4 falx around sagittal sinus; 5 dura; 6 falx (free edge); 7 tentorium; 8 petroclinoid ligament; 9 interclinoid ligament; 10 pituitary; 11 internal carotid artery (cavernous portion); 12 basal ganglia; 13 dentate nuclei.

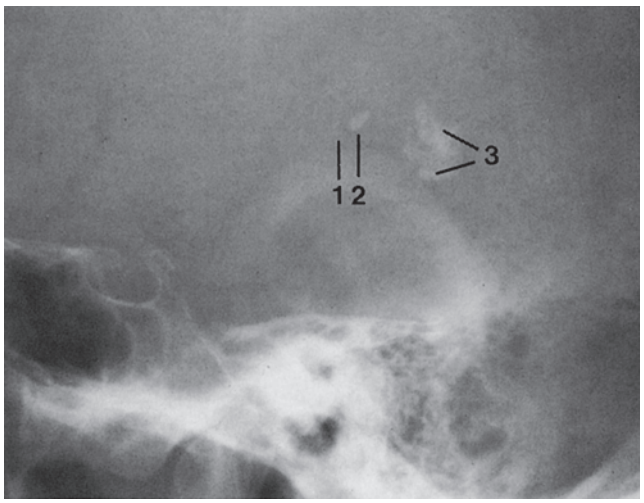

Fig. 8.**3** **Physiologic intracranial calcifications.** From anterior to posterior: 1 C-shaped habenula, 2 pineal gland, and 3 the two superimposed choroid plexuses are seen projecting just above the ear.

calcifications project approximately 3 cm from the midline and are usually symmetrical, although some disparity in size between the two sides occurs occasionally. The amount of calcification can vary greatly and is of no clinical significance. The calcifications have a characteristically fine to coarse granular appearance, occupying a circular area of 1 cm or more in diameter. Extensive plexus calcifications can be found in neurofibromatosis.

Calcification of dura, falx, and/or *tentorium* occurs in approximately 10% of cases, and each has quite a characteristic appearance (Fig. 8.**4**). Dural calcification around the sagittal sinus has a V-shaped appearance at the vertex in the anteroposterior projection. Calcifications in this area may occasionally be caused by calcified *Pacchionian (arachnoid) granulations* (diverticula-like outpouchings of the arachnoid space penetrating the dura mater and projecting into the lumen of the main sinuses and adjacent venous lakes). Falx calcifications are normally situated anteriorly, and are evident as linear streaks or lamellae in one or both leaves of the falx. Calcifications in the free edge of the tentorium have an inverted V-shape on the anteroposterior projection. The amount of calcification in the dura, falx, and tentorium usually has no clinical significance, particularly when the calcification is more or less diffuse. Falx and dura calcifications have been found in two thirds of patients with *basal cell nevus syndrome (Gorlin),* and extensive dura calcifications have been reported in *pseudoxanthoma elasticum.*

Calcifications of the petroclinoid and interclinoid (diaphragma sella) *ligaments* are common in the elderly. The former lies between the tip of the dorsum sella and the apex of the petrous bone, whereas the latter may result in interclinoid (sellar) bridging.

Pituitary calcifications are rarely recognizable on skull films, as opposed to histologic examinations. On skull films, they may represent calculi.

Arteriosclerotic calcifications of the internal carotid artery are commonly seen as it passes through the cavernous sinus. These calcifications can range from a small flake to complete visualization of the carotid syphon (8.**5**). On the lateral view, these calcifications are superimposed on the sella turcica, whereas ring-like calcifications may be seen on either side of the sella in anteroposterior projection.

Basal ganglia calcifications are found in a number of diseases (see "pathologic calcifications"), but are most often found incidentally in a healthy adult and have no clinical implications. The calcifications range from punctate to conglomerate densities in characteristic locations: on the anteroposterior examinations, the calcifications are symmetrical and parasagittal, whereas on the lateral view, they may assume a gentle curve, roughly paralleling the squamosal suture. However, sclerosis along the squamosal suture, presenting on the lateral view occasionally as a dense band (see Fig. 8.**26b**), should not be confused with basal ganglia calcifications.

Calcifications in the dentate nucleus of the cerebellum are less common than in the basal ganglia, but are found in the same conditions. On the lateral skull film, these calcifications are often obscured by the mastoid air cells, but are best seen in the occipital (Towne's) view as symmetrical crescent-shaped densities.

Pathologic Calcifications

Pathologic intracranial calcifications can be subdivided into localized or scattered. Localized calcifications are often suggestive of a specific disease process when both location and

Fig. 8.**4** **Physiologic Intracranial calcifications.** Extensive calcifications of the falx (midline and V-shaped around the sagittal sinus) and tentorium (tent-like above the foramen magnum) are seen. Incidentally, small parasagittal radiolucencies are also noted, representing Pacchionian (arachnoid) granulations.

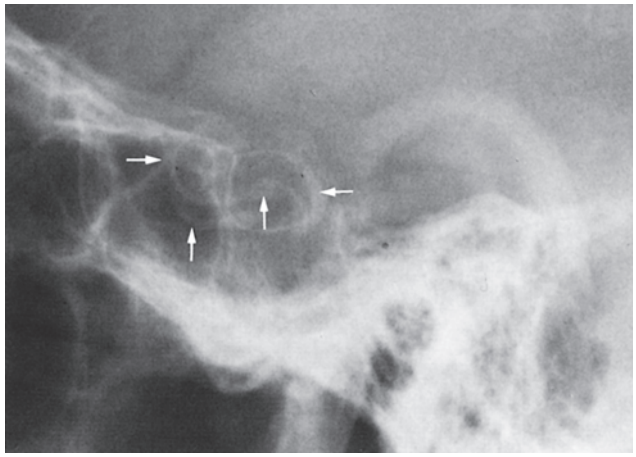

Fig. 8.**5** **Internal carotid artery calcifications.** Both completely calcified carotid syphons (arrows) are superimposed on the sella turcica.

shape of the calcification are taken into account. Scattered intracerebral calcifications are virtually limited to a variety of infectious processes, tuberous sclerosis and metastatic carcinomatosis (e.g., from breast carcinoma). Pathologic intracranial calcifications are summarized in Fig. 8.**6**.

Intracranial tumors represent the largest fraction of localized intracerebral calcifications. Their differential diagnosis is shown in Table 8.**2**.

Vascular lesions that calcify include (1) aneurysm, (2) arteriovenous malformations, and (3) old hemorrhages (intracerebral, subdural).

Arterial aneurysms occur most commonly in the region of the circle of Willis and calcify in less than 1%. Ring-like or arc-like calcifications are characteristic. Erosion of the adjacent bone may occur. A *calcified aneurysm of the vein of Galen* is rare, and is usually associated with obstructed hydrocephalus.

Calcifications in *arteriovenous malformations* are present on skull films in slightly less than 20%. Multiple small peripheral ring shadows combined with scattered flecks or streaks of calcification are almost always pathognomonic. Increased vascular markings in the skull are often an associated radiologic finding. A double-track ("tramline") calcification in the posterior parietal and/or occipital area is virtually diagnostic of the *Sturge-Weber syndrome* (meningofacial angiomatosis) (Fig. 8.**13**). In these cases, an ipsilateral port wine-colored nevus flammeus of the face in the distribution of the trigeminal nerve is almost invariably present. Mental retardation, seizure disorders, and contralateral hemiplegia may also be associated. The ipsilateral hemispheric brain atrophy may be evident radiographically

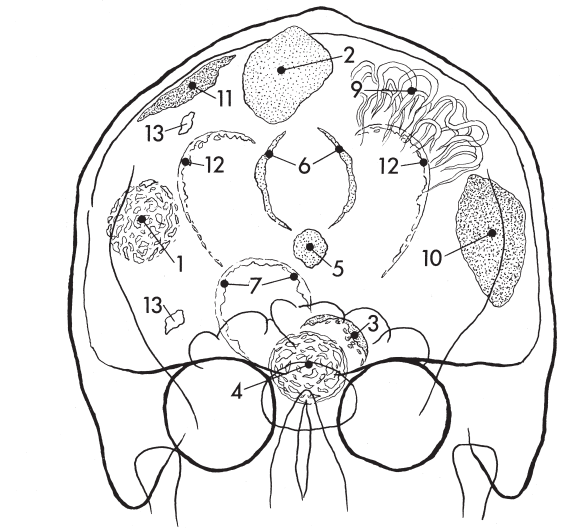

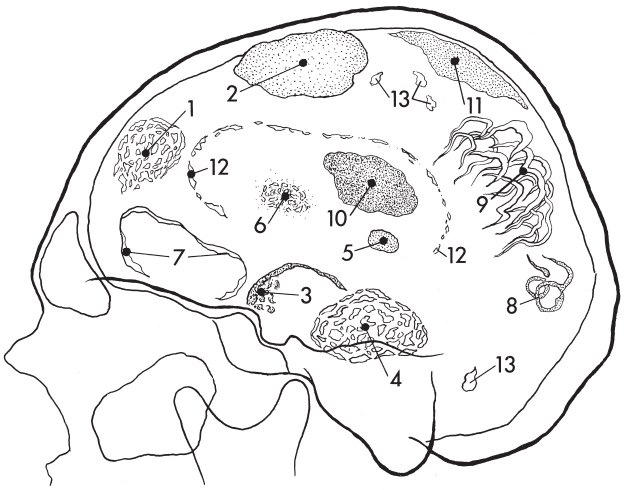

Fig. 8.**6a, b** **Pathologic intracranial calcifications** in anteroposterior and lateral projection. 1 Glioma; 2 meningioma; 3 craniopharyngioma; 4 chordoma; 5 pinealoma or teratoma; 6 corpus callosum lipoma; 7 aneurysm; 8 arteriovenous malformation; 9 Sturge-Weber syndrome; 10 old intracerebral hemorrhage ("brain stone") or granuloma; 11 old subdural or epidural hematoma; 12 cytornegalic inclusion disease or congenital toxoplasmosis; 13 tuberous sclerosis.

Table 8.2 Brain Tumors

Tumor	Preferred Location	Calcifications	Comments
Glioma:			
Astrocytoma	Adults: Central white matter of cerebrum Children: Cerebellum (40%), brainstem (20%), supratentorial (30%)	8% Grade 1 (well-differentiated): 25% Grade 2 (anaplastic): 6% Grade 3 (glioblastoma multiforme): 2%	50% of all brain tumors are gliomas of which four-fifths are astrocytomas and oligodendrogliomas. Gliomas are found in patients of all ages. Glioma calcification ranges from a few ill-defined dots and/or irregular linear streaks to a dense calcified nodule.
Oligodendroglioma (Fig. 8.7)	Frontal lobe	50%	
Ependymoma (Fig. 8.8)	Ventricles	15%	
Medulloblastoma	Infratentorial	Rare (<10%)	Highly malignant posterior fossa tumor usually diagnosed in infancy and childhood. It is a primitive neuroectodermal tumor (PNET).
Choroid plexus papilloma	Ventricles	25%	
Meningioma (Fig. 8.9)	Parasagittal, base of skull, falx, tentorium	5% to 15% (granular, curvilinear, or dense nodular ["ball of calcium"])	15% of all intracranial tumors. Predominantly in the middle-aged and elderly, rarely in children. M:F = 1:3. Associated and often diagnostic radiographic findings in 50%: 1 local hyperostosis; 2 increased meningeal vascular markings; and 3 enlarged foramen spinosum.
Craniopharyngioma (Fig. 8.10a)	Suprasellar	75% (nodular and/or curvilinear)	Usually but not always associated with sellar abnormalities. Bimodal age distribution with peaks in 1st and 2nd decades (75%) and 5th decade.
Teratoma (Fig. 8.10b)	Midline (half in pineal region)	75% (may contain teeth, etc.)	
Dermoid (cerebral)	Midline, most often posterior fossa	Almost always	Majority in children and adolescents. DD: epidermoid ("cholesteatoma") which is not necessarily midline, occurs at all ages and may be either extradural (rarely calcified) or intradural (commonly calcified).
Pinealoma	Pineal region	50% (pineal calcification exceeding 1 cm in diameter)	Majority in the first 2 decades of life, strong male predominance.
Pituitary adenoma	Pituitary fossa	Rare (4%)	Calcifications occur only in large, usually chromophobe or rarely eosinophil adenomas, which are always associated with an abnormal sella.

(continues on page 208)

Fig. 8.**7** **Oligodendroglioma.** A tumor calcification is seen in the frontal lobe projecting just above the sphenoid wing (arrows).

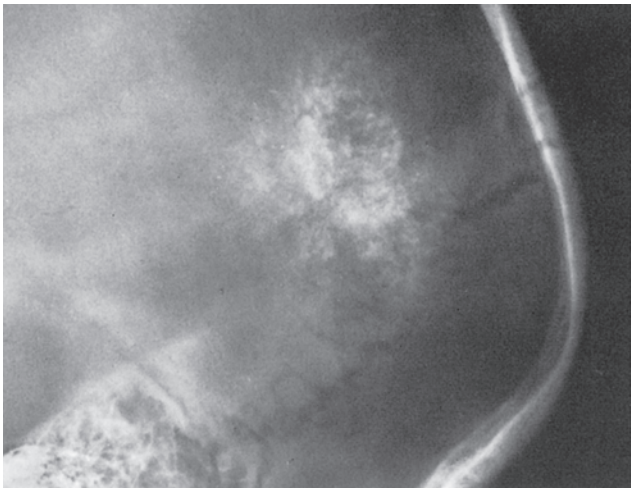

Fig. 8.**8** **Ependymoma.** A tumor calcification is seen projecting above the lambdoid suture.

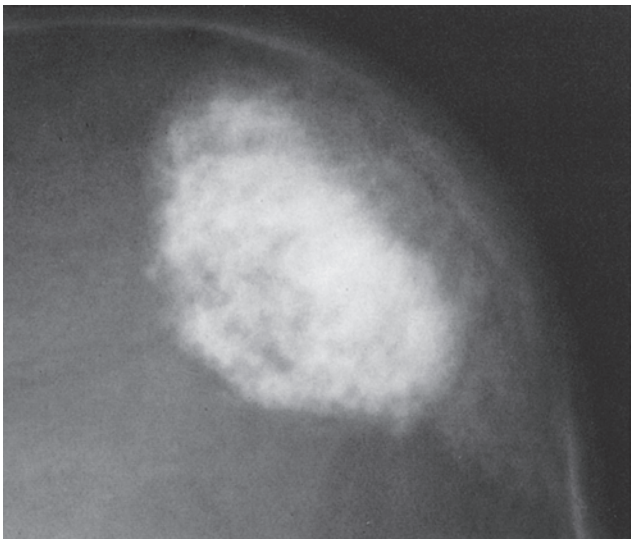

Fig. 8.**9** **Meningioma.** A dense tumor calcification is seen with thickening of the adjacent inner table of the skull.

Fig. 8.**10 a** **Craniopharyngioma.** Nodular tumor calcifications in semicircular configuration are seen above a normal-sized sella. Although sellar abnormalities are commonly associated with this tumor, a normal-sized sella, as in this case, is not unusual in young children. Note the poor definition of the dorsum sellae secondary to increased intracranial pressure.

Fig. 8.**10 b** **Pineal teratoma.** A large calcified mass is seen midline.

Table 8.2 (Cont.) Brain Tumors

Tumor	Preferred Location	Calcifications	Comments
Chordoma (Fig. 8.11)	Skull base (clivus)	70 % (retrosellar, parasellar or suprasellar)	Predominantly in 3th and 4th decade. Usually associated with destruction of clivus. Extension to sella (destruction) and nasopharynx (soft-tissue mass) possible. Calcifications are particularly prominent in chondroid chordomas, a more benign variant.
Enchondroma, osteochondroma, chondrosarcoma	Dura, skull base	50 %	Mimic meningiomas and chordomas.
Osteoma	Cranial vault, sinuses	Very dense, homogeneous ossification.	Protrudes from the outer or inner table of the cranial vault; in the latter case, it may mimic a meningioma.
Lipoma (Fig. 8.12)	Corpus callosum	2 curvilinear calcifications with concavity facing the midline around the area of the corpus callosum. Lipoma can sometimes be recognized as a radiolucent mass.	Corpus callosum lipoma usually diagnosed as incidental finding when calcified.
Von Hippel-Lindau disease	Orbits (retina) and cerebellum	Rare	Autosomal inherited disorder producing hemangioblastomas in both the cerebellar hemispheres and retina, associated with renal cysts and carcinomas. Pheochromocytomas and polycythemia may also be present.
Metastases	None	Rare	(e.g., from osteogenic sarcoma, mucinous adenocarcinoma of colon)
Other tumors	None	Extremely rare	(e.g., angioma, neurofibroma, hamartoma, etc.)

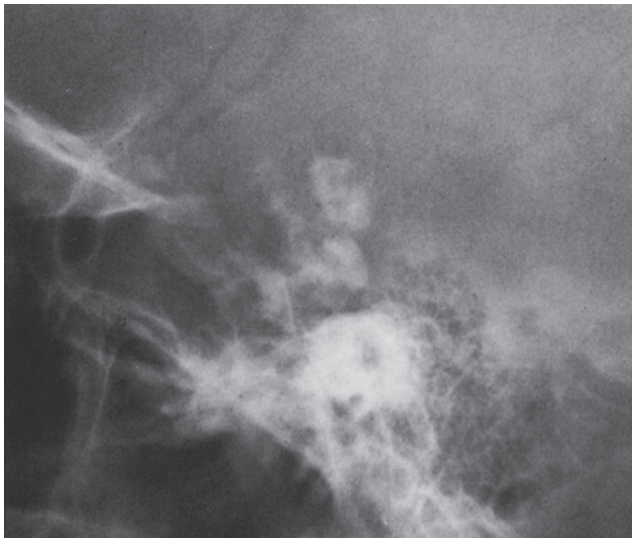

Fig. 8.**11** **Chordoma.** Predominantly retrosellar tumor calcifications and destruction of clivus with sellar extension are seen.

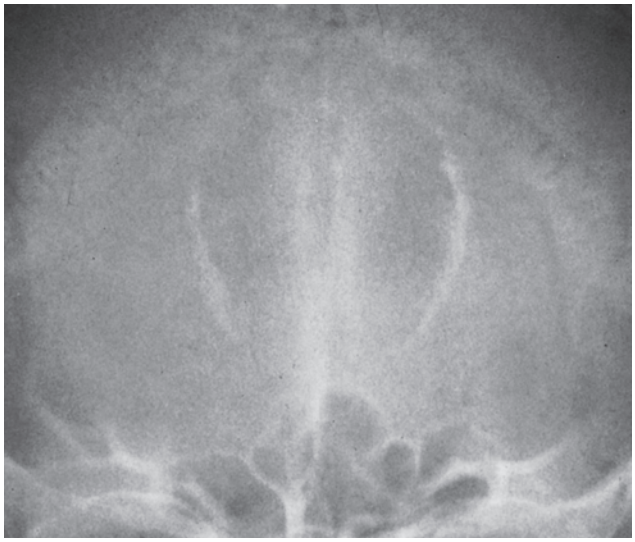

Fig. 8.**12** **Corpus callosum lipoma.** Two curvilinear calcifications with the concavity, facing the midline, are diagnostic.

Fig. 8.**13** **Sturge-Weber syndrome.** Extensive double-track ("tramline") calcifications in the posterior parietal and occipital area extending into the temporal lobes are seen. Ipsilateral large mastoid air cells are also present.

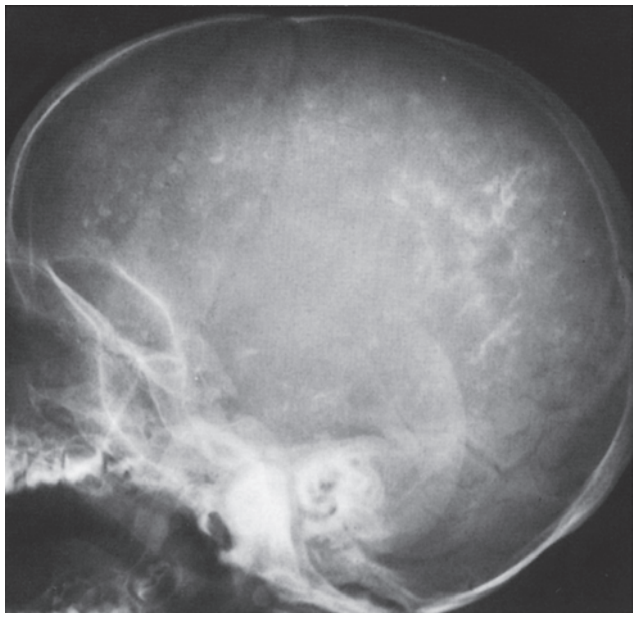

Fig. 8.**14** **Congenital toxoplasmosis.** Scattered calcifications around the enlarged lateral ventricles, characteristically sparing the subtentorial area, are seen.

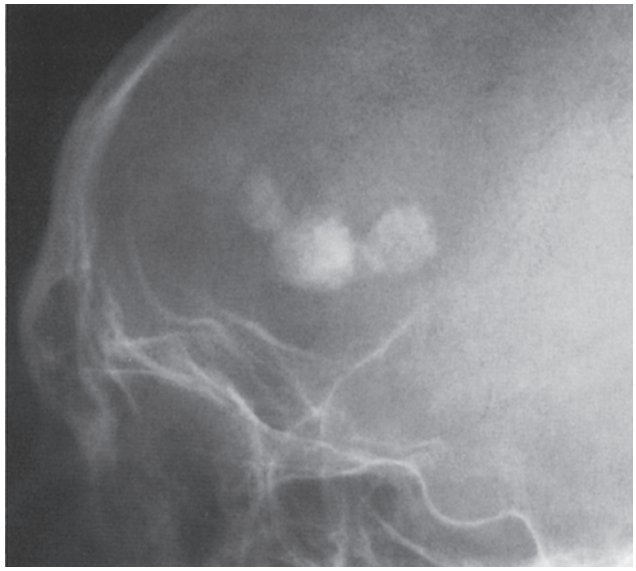

Fig. 8.**15** **Cryptococcosis.** Round calcifications are seen in the frontal lobe area.

as elevated skull base and compensatory enlargement of the ipsilateral mastoid air cells with increased aeration.

Calcifications in *intracranial hemorrhages* occur. An *intracerebral hematoma* of either traumatic or spontaneous origin may ultimately result in a dense nodular and amorphous calcification ("brain stone"). *Cerebral infarcts* may rarely calcify also. *Subdural* and less frequently *epidural hematomas* can result on occasion in a thin calcified layer over the hemispheres. The extent of calcification may vary from a small focus to a huge deposit that envelops large portions of one or both hemispheres.

Numerous *inflammatory conditions* (infections and infestations) may result in intracranial calcifications. When they are located in the brain they are commonly scattered. *Congenital cytomegalic inclusion disease* is by far the most important diseases in this group, although other viral encephalitides (e.g., *polio, herpes*, and *rubella*) have been implicated as a cause of intracerebral calcifications. The incidence of calcification in cytomegalic disease is estimated at approximately 25 %. The calcifications are found in the periphery of the often enlarged first and second ventricles.

Calcifications secondary to *congenital toxoplasmosis* occur in approximately half of the patients, and are virtually indistinguishable from cytomegalic inclusion disease (Fig. 8.**14**). Other parasitic infestations that can cause scattered intracerebral calcifications are *cysticercosis* (scattered nodular calcifications 1–3 mm in diameter) , *trichinosis* (punctate calcifications of 1 mm or less) and *paragonimiasis* (punctate to cystic, often in clusters and measuring up to 3–4 cm in diameter). Rarely, *echinococcal disease* may cause one or several larger intracranial calcifications.

Tuberculosis is for all practical purposes the only bacterial infection that has to be included in the differential diagnosis of intracranial calcifications. It may present as a single nodule, or less commonly as multiple calcified intracerebral nodules. A healed *brain abscess*, a *syphilitic gumma*, or a granuloma caused by a fungal infection (e.g., *cryptococcosis*, Fig. 8.**15**) are rare causes of similar localized intracerebral calcifications. Irregular calcifications resulting from tuberculous meningitis are found in the subarachnoid cisterns and project radiographically around and above the sella. Basal arachnoiditis produced by fungal diseases (e.g., *coccidioidomycosis*) can result in a similar radiographic picture.

Scattered intracerebral calcifications are found in 50% of patients with *tuberous sclerosis*. In contrast to toxoplasmosis and cytomegalic inclusion disease, the intracerebral calcifications in tuberous sclerosis are much more variable in size (lesions may exceed 1 cm in diameter), do not have a paraventricular distribution, and can also be found subtentorially (e.g., dentate nuclei). Calcifications occur also in the basal ganglia. Small areas of localized hyperostosis of the skull are often associated with tuberous sclerosis, and may actually be confused with intracerebral calcifications. In *neurofibromatosis* granular unilateral or bilateral temporal lobe calcifications may be found that appear to extend along the choroid plexus of the temporal horn. Scattered cerebral calcifications occur also with *metastatic carcinomatosis* (e.g., from breast neoplasms) or rarely develop after irradiation or a variety of other insults to the brain resulting in scarring and proliferation of neuroglial cells *(gliosis)*.

When the *basal ganglia* and *dentate nucleus calcifications* are not idiopathic, *primary hypoparathyroidism* appears to be the most frequent cause (Fig. 8.**16**), whereas these calcifications are rarely seen following surgical removal of the parathyroids. The calcifications in *pseudohypoparathyroidism* are radiographically indistinguishable. Calcifications of the basal ganglia and dentate nuclei may also be found in diseases associated with scattered intracerebral calcifications (e.g., tuberous sclerosis, or less commonly toxoplasmosis) and rarely in a few other conditions such as *Fahr's disease* (idiopathic familial cerebrovascular ferrocalcinosis), *lead* and *carbon monoxide intoxications, birth anoxia*, and certain congenital or acquired neurological disorders.

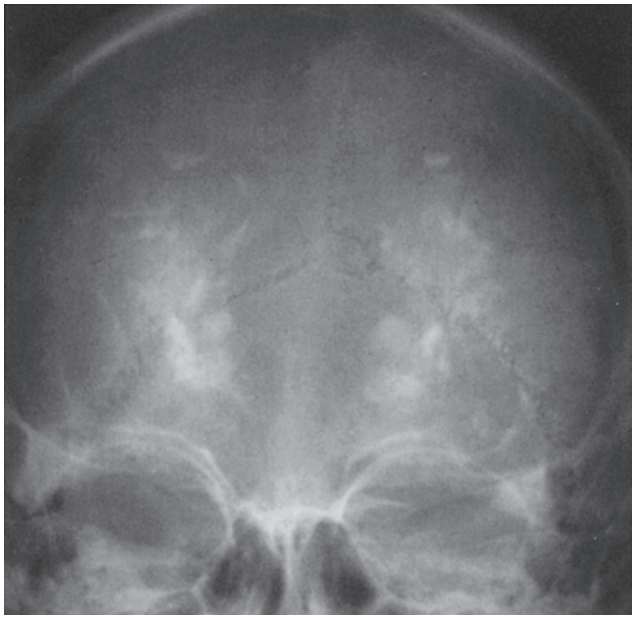

Fig. 8.**16** **Primary hypoparathyroidism.** Extensive calcifications of the basal ganglia are seen. Calcifications of the dentate nuclei were also present, but cannot be recognized in this projection.

Vascular Markings, Sutures, and Fracture Lines

Vascular structures are responsible for a wide range of radiolucent markings in the normal skull (Fig. 8.**17**). With the exception of *emissary veins* that connect the venous systems inside and outside the skull and may produce bony channels, which are not wider than 2 mm, vascular structures cause indentations only on one table of the skull. Meningeal arteries and veins and dural sinuses produce indentations on the inner table that are fairly constant in position and thus relatively easily recognizable. *Pacchionian (arachnoid) granulations*, which are arachnoid extensions projecting into the lumen of the main sinuses and adjacent venous lakes, may erode through the inner table into the diploe. They most frequently produce irregular defects in the parasagittal area and the region around the torcula (see Fig. 8.**4**).

Diploic veins, on the other hand, are extremely variable in size, shape, and number. Besides diploic veins, there are *diploic lakes* that appear as irregular oval or round radiolucencies, rarely exceeding 2 cm in diameter. Occasionally larger and slightly expansile defects originating from the diploe can be found when a diploic vein forms a larger outpouching (Fig. 8.**18**). Diploic veins may resemble osteolytic lesions. The demonstration of an irregular and well-demarcated contour,

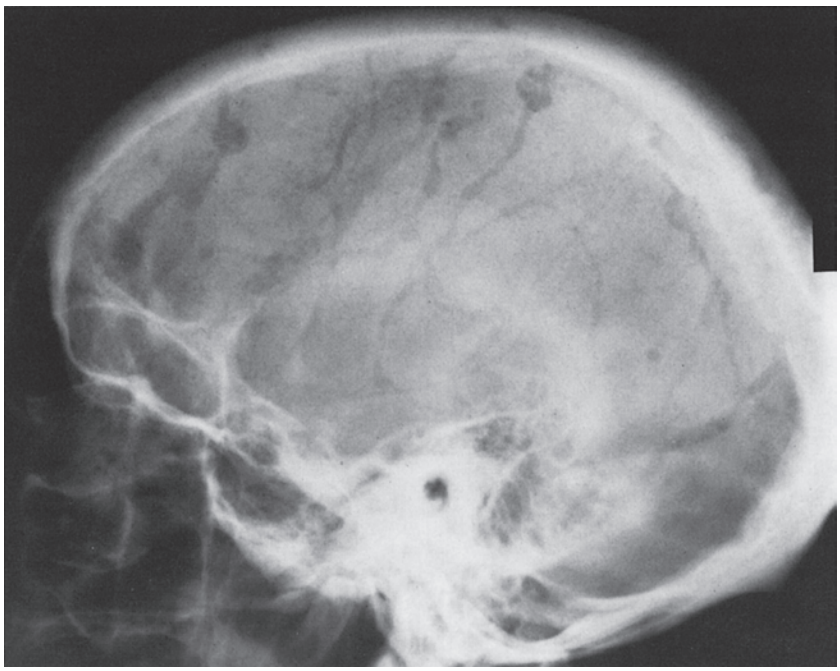

Fig. 8.**17** **Normal vascular structures.** A wide range of radiolucent markings are seen in the skull.

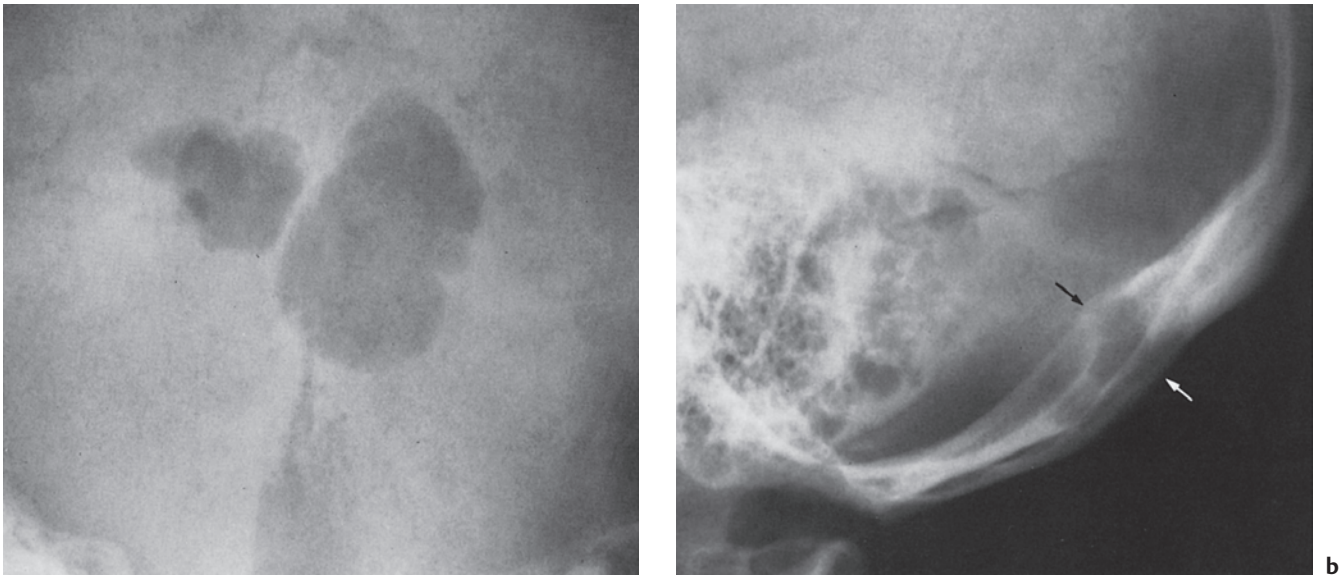

a b

Fig. 8.**18 a, b** **Venous lakes.** Two unusually large well-defined, irregular radiolucencies are seen in the occiput. These large outpouchings of the diploic vein are slightly expansile as seen on the lateral projection (arrows). A single defect would be indistinguishable from an epidermoid originating from the diploe.

which is characteristic for venous lakes, may be helpful to differentiate them from osteolytic lesions.

The outer table may be indented by the *supraorbital artery* and the *middle branch of the superficial temporal artery*. The former is located in the frontal bone above the orbits, whereas the latter runs vertically across the temporal squama and fades out in the inferior part of the parietal bone (Fig. 8.**19**).

Vascular grooves have to be differentiated from *acute fractures*, which are usually more radiolucent, since they extend through both the inner and the outer table. Fracture lines also have very sharp and distinct margins (Fig. 8.**20**). Occasionally a fracture presents as an apparent dense line when the margins overlap in relation to the roentgen beam. This occurs most often with depressed fractures. *Sutures* may also be confused with acute fractures, when the suture in the outer table with the characteristic serrated appearance is obliterated and only the suture in the inner table remains visible as a relatively straight line. Sutures can, however, be differentiated from fractures by their constant anatomic location, their decreased radiolucency, and their less well-defined margins. Traumatic separation of a suture (diastasis) occurs occasionally in the adult. In children, traumatic suture diastasis has to be differentiated from raised intracranial pressure. In the latter condition, erosion of the dorsum sella, increased convolutional markings, and pineal displacement may also be found. A suture which is normally obliterated can occasionally persist (e.g., the metopic suture in the frontal bone or the mendosal and midsagittal sutures in the occipital bone) and should not be confused with a fracture line (Fig. 8.**21**).

Wormian bones are small bones occurring within a suture, most commonly within the lambdoidal suture (Fig. 8.**22**). They have no clinical significance and are found in healthy persons. However, a higher than normal incidence of multiple wormian bones has been found in a variety of congenital disorders such as *osteogenesis imperfecta, cretinism (hypothyroidism), cleidocranial dysostosis, progeria, hypophosphatasia, rickets*, and many others.

Compared with tubular bones, the osseous healing of skull fractures is slow and often incomplete, with only fibrous tissue formation. Such old fractures may persist as radiolucent lines, which are often difficult to differentiate from vascular markings and sutures.

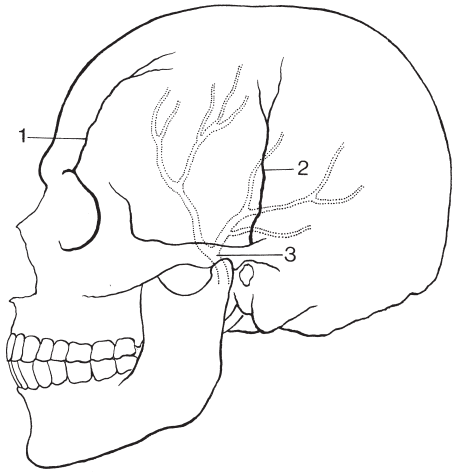

Fig. 8.**19** **Arterial grooves** on the outer and inner table. They have a constant anatomic location and should not be mistaken for fracture lines. 1 Supraorbital artery (outer table), 2 middle branch of the superficial temporal artery (outer table), and 3 middle meningeal artery (inner table). (Modified from Schunk H, Marayama Y Acta Radiol. 1960; 54: 186).

A *localized increase in vascular markings* can be a very important finding in the diagnosis of a *meningioma* when the increased vascular markings are associated with a calcified lesion or a local hyperostosis. It can be found relatively frequently in *arteriovenous malformations* which are calcified in almost 20% of cases.

Hypervascular primary or secondary tumors of the skull may also be associated with increased vascular markings. They may be observed in Paget's disease or fibrous dysplasia too, although the radiographic changes in these conditions are usually diagnostic by themselves. Because of a great variation in healthy persons, a generalized increase in the vascular markings is difficult to diagnose, but could indicate collateral circulation in cases with occlusion of major arteries or veins.

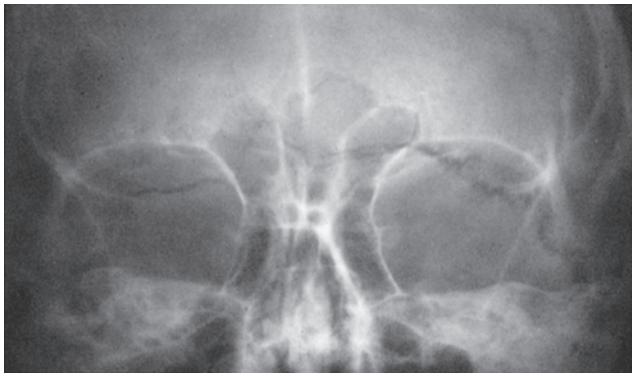

Fig. 8.**20** **Fracture and suture diastasis.** Note the sharp and distinct margins of the fracture line projecting into the right orbit and the traumatic separation of the left lambdoid suture, whereas the normal lambdoid suture projecting into the frontal sinus has an indistinct margin and is barely visible.

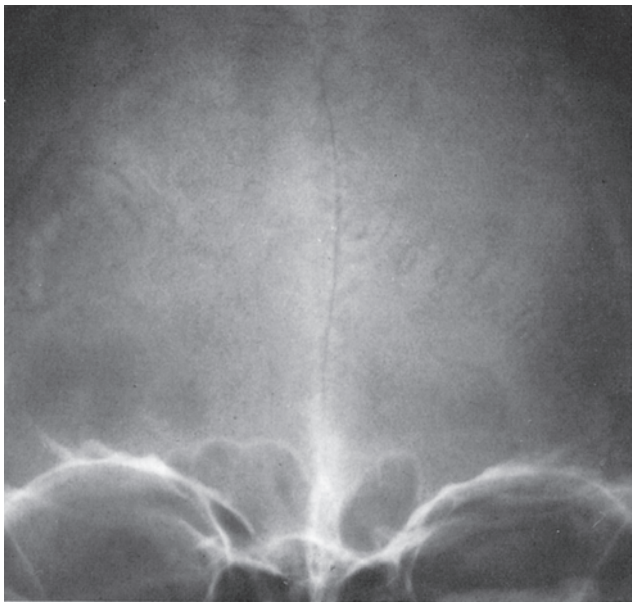

Fig. 8.**21** **Metopic suture.** This suture is normally obliterated, but may occasionally persist and present as a poorly defined radiolucent line in the middle of the frontal bone, and should not be confused with a fracture.

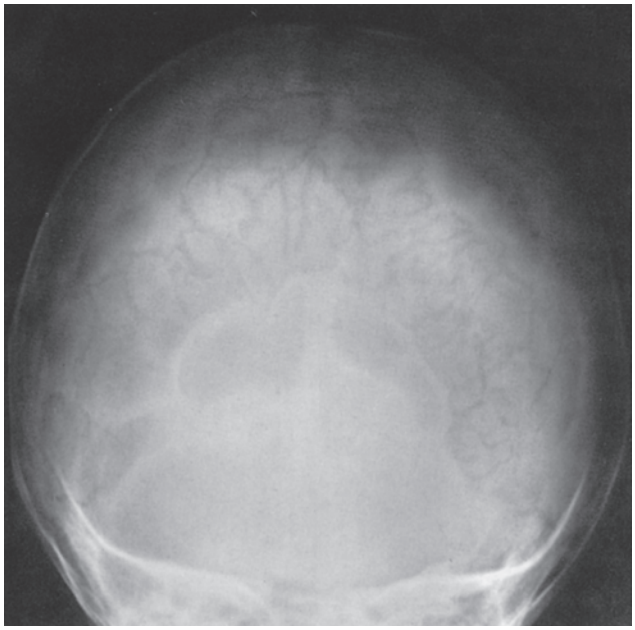

Fig. 8.**22** **Wormian bones.** Numerous small bones are seen in the lambdoidal suture.

Osteosclerotic Lesions of the Vault of the Skull

For the differential diagnosis, sclerotic changes of the skull vault are best divided into localized and diffuse lesions.

Localized Sclerosis (Single or Multiple Osteoblastic Lesions) of the Skull Vault

As described in more detail in Chapter 2, the differential diagnosis of solitary or multiple localized sclerotic lesions includes benign tumors (e.g., *osteoma, osteochondroma*), malignant tumors (e.g., *osteosarcoma, metastases*) (Fig. 8.**23**), *chronic osteomyelitis* (Fig. 8.**24**), *ischemic necrosis* (especially in bone flaps), *radiation osteonecrosis* (Fig. 8.**25**), *fibrous dysplasia, neurofibromatosis, Paget's disease* ("cotton wool" appearance), *mastocytosis*, and *tuberous sclerosis* (often associated with scattered intracerebral calcifications). Formation of a band-like sclerosis along sutures is relatively common and without any clinical significance. Such a sclerosis along the squamosal suture should not be confused on the lateral view with calcifications in the basal ganglia (Fig. 8.**26**). *Hyperostosis frontalis interna* is an idiopathic irregular thickening of the inner table, mainly of the frontal bone (Fig. 8.**26**). The lesions are characteristically bilateral and symmetrical and spare the midline. They are most commonly found in women over 40 years of age, and progress at a very slow pace over the years. Thickening of the inner tables of other cranial bones or a more generalized thickening of the inner tables occur rarely. The latter condition is called *hyperostosis interna generalisata.*

An *ossified cephalhematoma* or *subdural hematoma* may also present as a localized area of increased density contiguous with either the outer or inner table, respectively (Fig. 8.**27**). *Meningiomas* invading the skull vault may present as localized thickening of the inner table (commonly in the parasagittal region or sphenoidal ridge) and may progress until they involve the whole thickness of the skull (Fig. 8.**28**) .When the lesion is protruding outside the skull vault, sunburst spiculations may be present (Fig. 8.**29**).

Besides meningiomas, a localized *osteoblastic lesion with sunburst spiculations* can also be seen with *osteosarcomas, osteoblastic metastases* (e.g., from neuroblastomas), and hemangiomas (Fig. 8.**30**); *diffuse sunburst spiculations* of the vault with the exception of the occipital bone inferior to the internal occipital protuberance are encountered in severe anemias, particularly in *thalassemia* and to a lesser degree in *sickle cell anemia.*

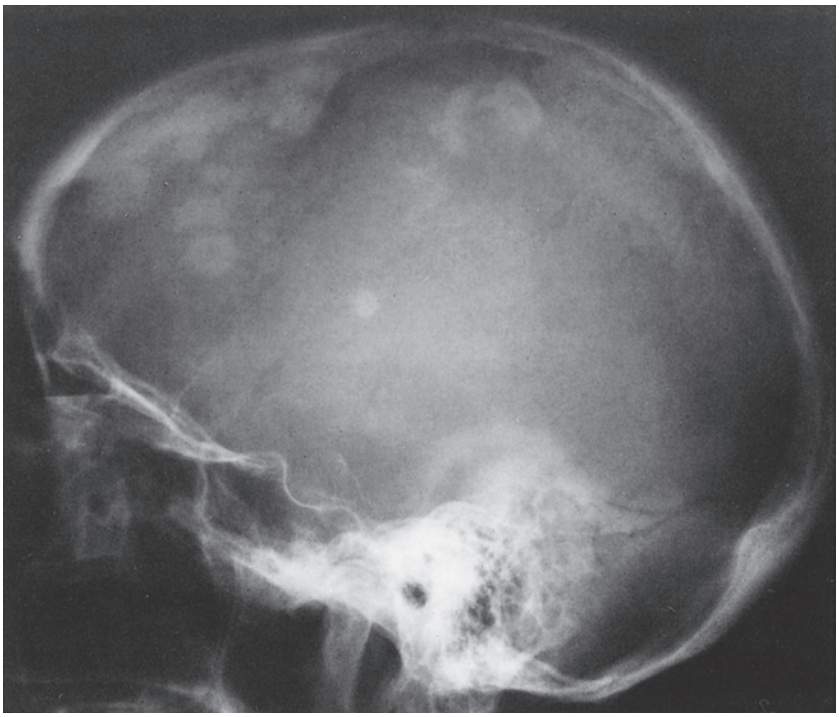

Fig. 8.**23** **Osteoblastic metastases** from breast carcinoma. Round lesions of increased density are particularly well seen in the frontal area. Note also the normal thickness of the skull that helps to differentiate this condition from Paget's disease. Incidentally physiologic occipital thinning presenting as increased radiolucency of the squama occipitalis is also noted.

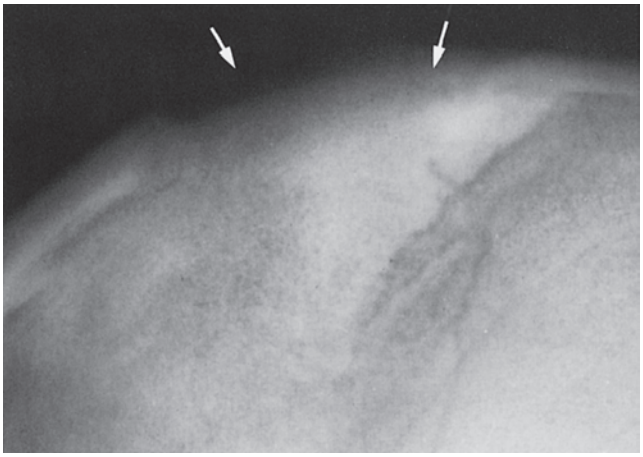

Fig. 8.**24** **Chronic osteomyelitis.** A defect (arrows) seen in the frontal bone with adjacent sclerosis.

Fig. 8.**25** **Radiation osteonecrosis.** Extensive mixed lytic and sclerotic bone involvement is found around a large surgical defect in the occiput.

Diffuse Sclerosis of the Skull Vault

A diffuse increase in bone density of the cranium may be caused by an abnormal osteoblastic response in the diploe triggered, for example, by osteoblastic metastases or myelofibrosis. Both sclerotic obliteration of the diploic space and thickening of the calvarium are the hallmark of *osteopetrosis* (Fig. 8.**31**) and many other constitutional diseases, such as *pyknodysostosis, van Buchem's disease* (generalized cortical hyperostosis) (Fig. 8.**32**), *Engelmann–Camurati disease* (progressive diaphyseal dysplasia), *osteopathia striata* (Fig. 8.**33**), *melorheostosis* and *hyperphosphatasia*, which have already been discussed in Chapter 2. In these conditions, diffuse sclerosis of the calvarium is commonly associated with osteosclerosis in other bones too. Similar radiographic findings are found in children with *hypervitaminosis D, idiopathic hypercalcemia of infancy* (Williams syndrome), *hypoparathyroidism* and *pseudohypoparathyroidism.*

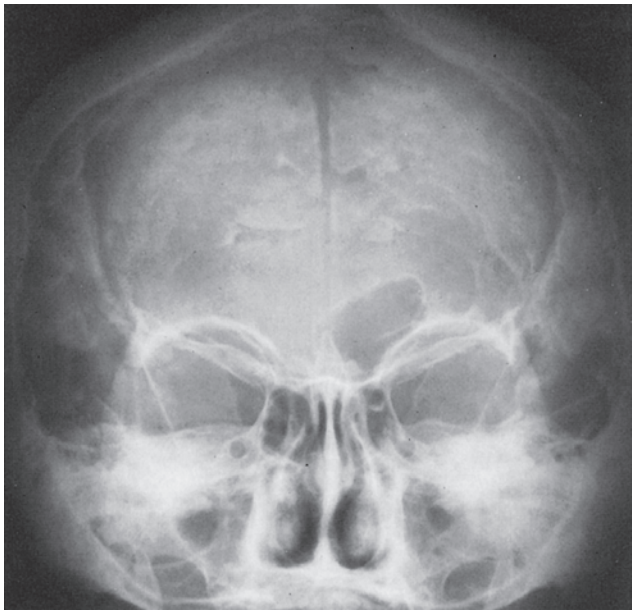

a

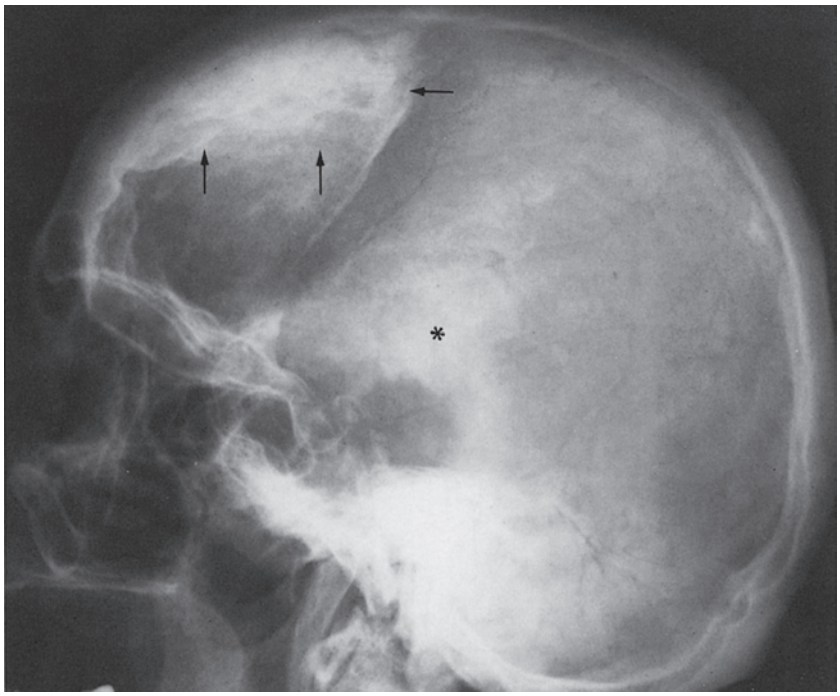

b

Fig. 8.**26 a, b** **Hyperostosis frontalis interna.** Symmetrical thickening of the inner tables, mainly of the frontal bone, is seen (arrows). Incidentally, a wide sclerotic band in the area of the squamosal suture is also evident in the lateral projection (asterisk).

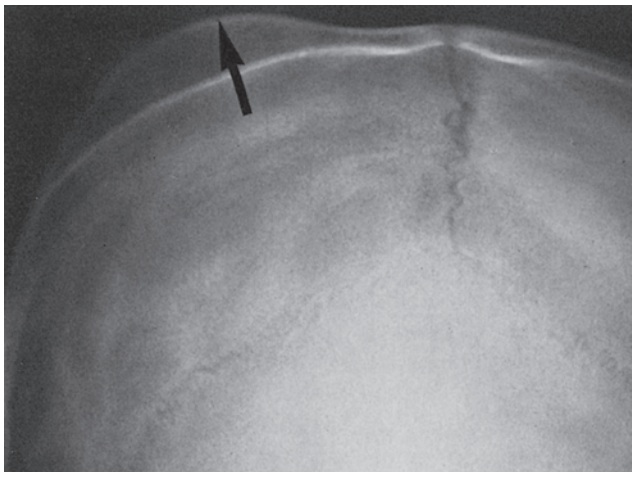

a

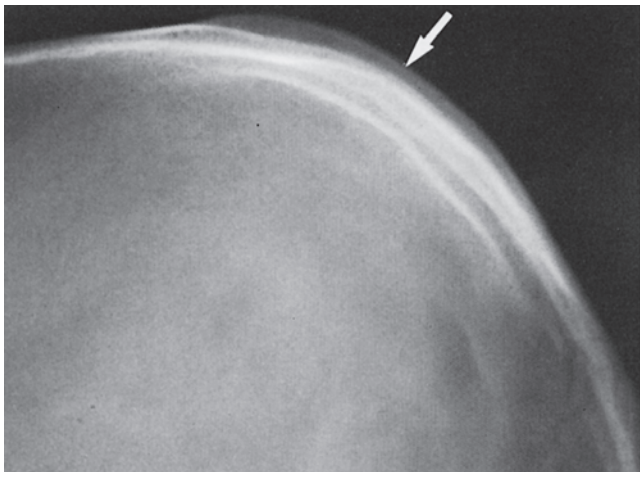

b

Fig. 8.**27 a, b** **Cephalhematoma.** Ossification of the elevated periosteum over the parietal bone produces a localized thickening of the skull.

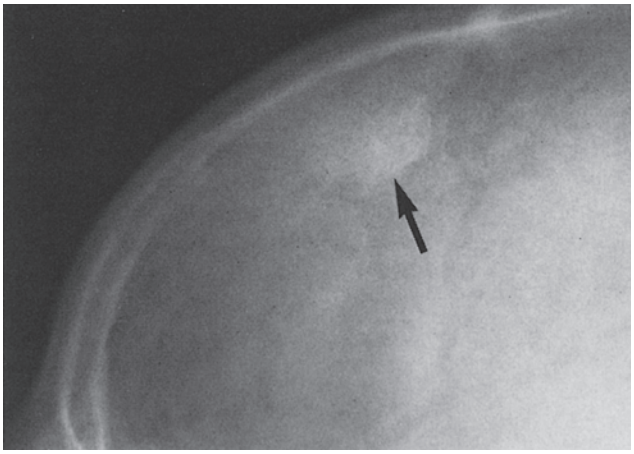

Fig. 8.**28** **Meningioma.** A localized thickening of the inner table is seen (arrows).

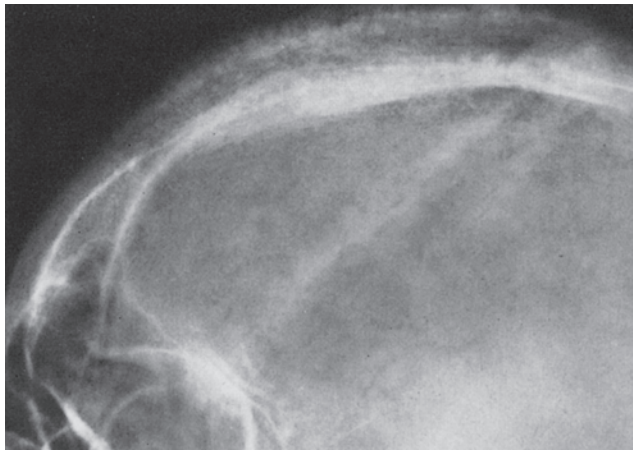

Fig. 8.**29** **Meningioma.** Localized thickening of both tables and the diploe as well as sunburst spiculations are seen.

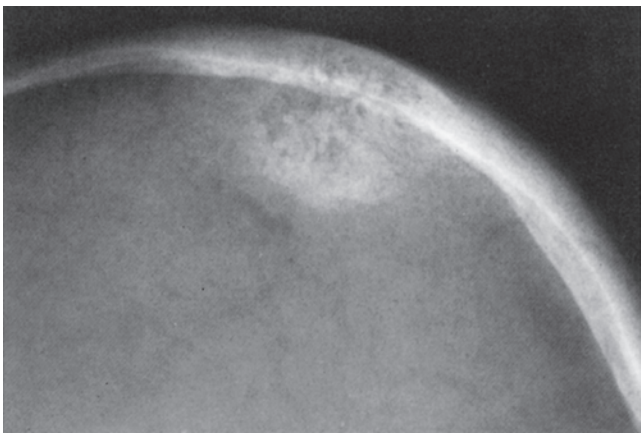

◁ Fig. 8.**30** **Hemangioma.** A slightly expansile lesion with marginal sclerosis and characteristic radiating bony spicules within the lesion is seen.

Fig. 8.**31** **Osteopetrosis.** Extensive sclerosis of the skull with complete obliteration of the diploic space and marked thickening of the calvarium is present. Note also the sclerosis and thickening of the facial bones and particularly of the mandible.

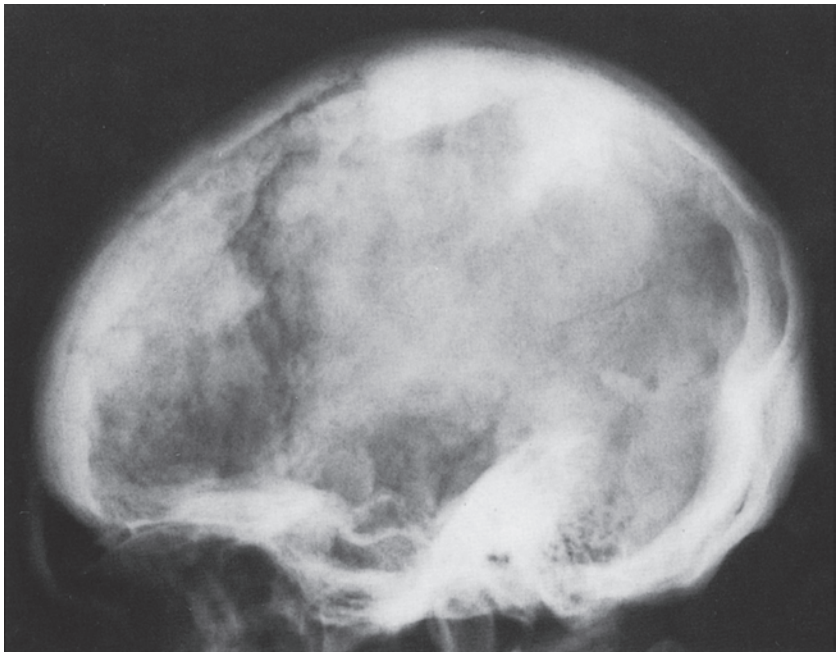

Fig. 8.**32** **Van Buchem's disease (generalized cortical hyperostosis).** Extensive hyperostosis of the entire skull is evident.

Fig. 8.**33** **Osteopathia striata.** Macrocephaly and sclerosis of the skull are occasionally associated with the more characteristic bony changes of this disease in the tubular and flat bones, representing a distinct autosomal dominant syndrome.

An increase in density of the skull vault may, however, also be the result of an abnormally thick calvarium. A great variation in the normal range of the thickness of the calvarium exists. A dense skull caused by an increased width of both outer and inner tables and the diploe, and observed as an isolated finding, has no clinical significance and may be called *idiopathic.*

Thickening of the skull has been observed with *chronically increased intracranial pressure*. In childhood, both *cerebral atrophy* and *successful relief of increased intracranial pressure* (e.g. following surgery for hydrocephalus) may result in generalized calvarial thickening.

In *acromegaly*, thickening of the calvarium, particularly of the inner table, is associated with a large frontal sinus, exces-

Fig. 8.**34** **Acromegaly.** Thickening of the skull, particularly of the inner table, prominent external occipital protuberance, excessive pneumatization of the mastoids, enlarged sella with straightening of the dorsum, and a large mandible (not shown) are characteristic. The frontal sinuses appear normal in this case, but are usually enlarged in this condition.

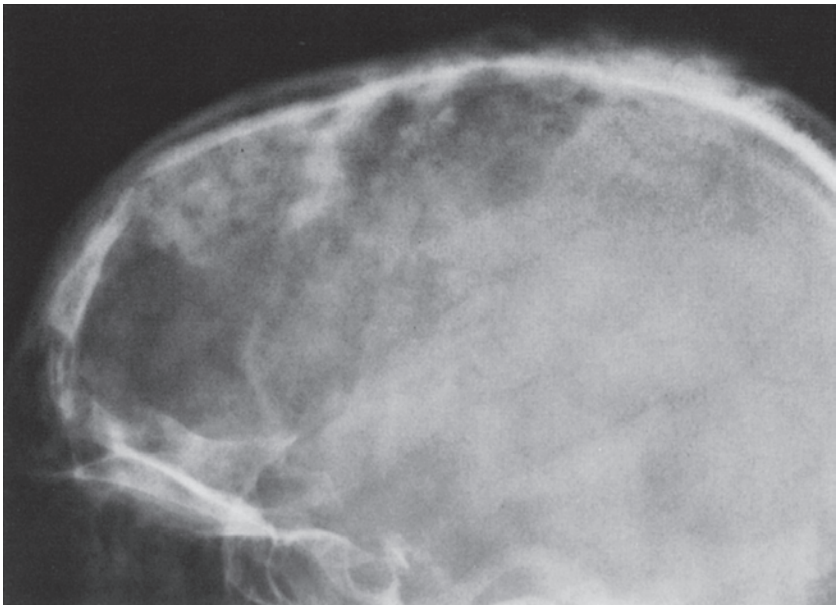

Fig. 8.**35** **Fibrous dysplasia.** Mixed lytic and sclerotic lesions are seen in the frontoparietal area. The disorder involves the outer table, that appears interrupted and expanded on the top of the vault, whereas the inner table remains intact in the entire skull.

sive pneumatization of the mastoids, prominent external occipital protuberance, and enlarged sella turcica (Fig. 8.**34**).

Sclerosis of the calvarium in *fibrous dysplasia* can be extensive but is usually not uniform. It is generally caused by expansion of the outer table while the inner table is usually not involved. Irregular radiolucencies can also be present (Fig. 8.**35**). Sclerosis of the skull base and/or paranasal sinuses by fibrous dysplasia is commonly associated with involvement of the vault of the skull.

In the combined destructive and sclerotic phase of *Paget's disease*, both inner and outer tables are thickened and the diploe is markedly widened and contains irregular areas of sclerosis ("cotton wool" appearance, Fig. 8.**36**). In the sclerotic phase, a uniform thickening of the calvarium can be found with loss of differentiation between the tables and the diploe. Petrous pyramids and paranasal sinuses are often involved also.

The skull changes in *congenital hemolytic anemias* (e.g., thalassemia, sickle cell anemia) and less commonly in *acquired anemias* (e.g., iron deficiency) and *cyanotic congenital heart disease* result from erythroid hyperplasia of the marrow causing widening of the diploic space with external displacement and thinning of the outer table, which can assume a sunburst appearance (Fig. 8.**37**). The thickened diploe and outer table can often no longer be differentiated, whereas the inner table usually remains clearly defined.

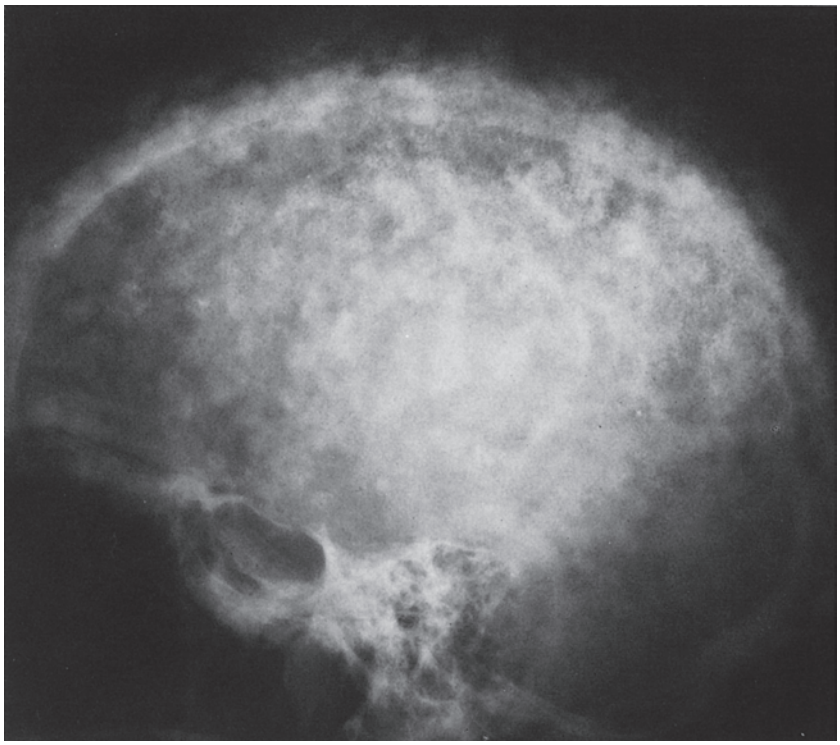

Fig. 8.**36** **Paget's disease.** Thickening of both the outer and inner table, widening of the diploë, loss of differentiation between tables and diploë, and irregular areas of sclerosis ("cotton wool" appearance) are diagnostic.

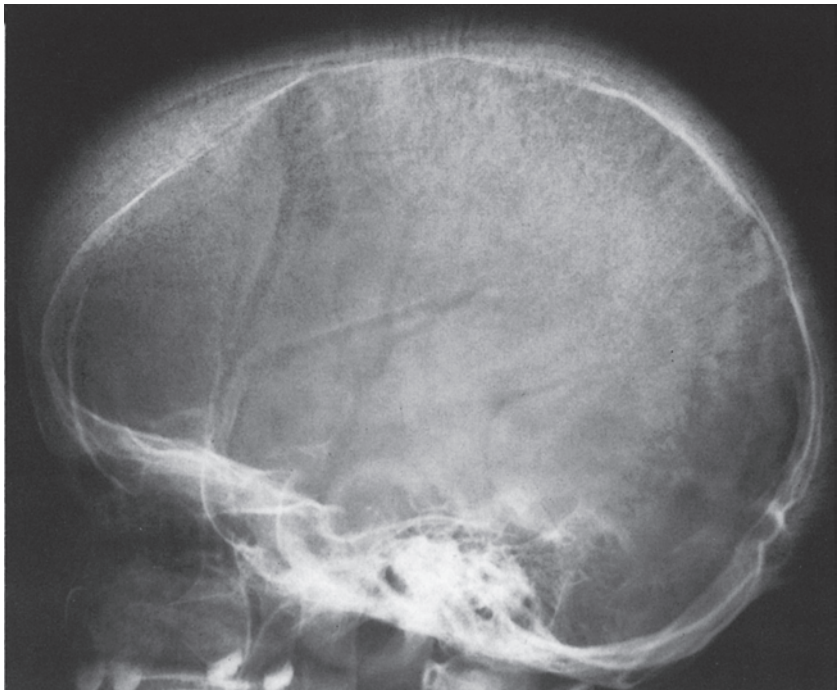

Fig. 8.**37** **Thalassemia.** Widening of the diploe and thinning of the outer table with sunburst appearance and sparing of the occipital bone below the internal occipital protuberance are characteristic. Poor pneumatization of the sinuses is also associated.

Characteristically, the occipital bone inferior to the internal occipital protuberance is not involved, because of the lack of bone marrow in this area. With the exception of thalassemia, where poor pneumatization of the sinuses can be found, there is no involvement of the paranasal sinuses. In *hyperparathyroidism*, granular deossification *("salt and pepper" skull)* with loss of the sharp definition of both the outer and inner table is typical. Small cyst-like lesions are also occasionally seen (Fig. 8.**38**). A "salt and pepper"-like skull can occasionally be found as a normal variant; more commonly, it is associated with osteopenia of any etiology. However, in these conditions the outer and inner table remain sharply defined (Fig. 8.**39**).

Long-term *phenytoin therapy* may also be associated with diffuse calvarial thickening, besides radiographic evidence of rickets and osteomalacia, respectively. In *fluorosis* (secondary to chronic fluorine poisoning of the drinking water or in response to fluorine treatment of osteoporosis) calvarial

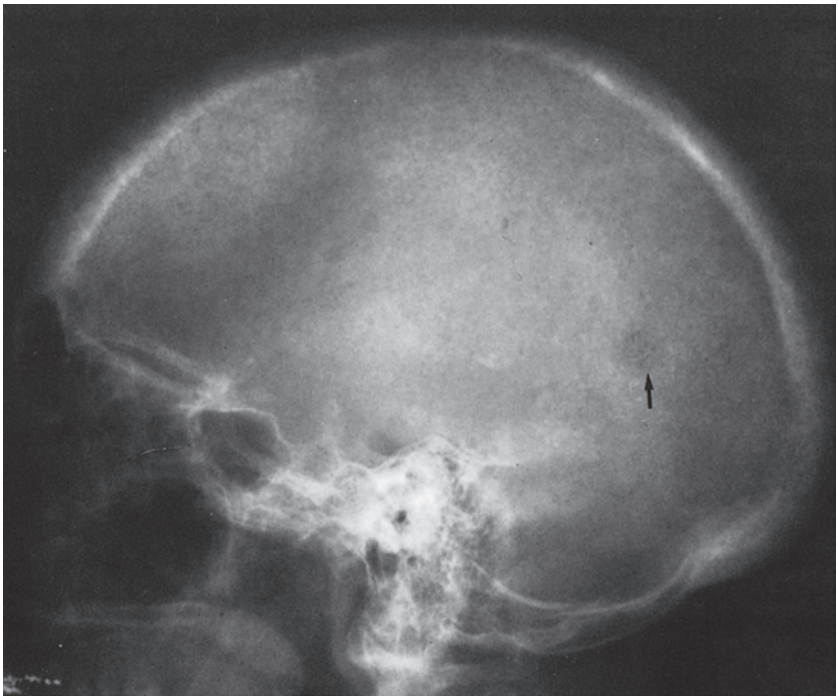

Fig. 8.**38** **Primary hyperparathyroidism.** Thickening of the calvarium with granular deossification ("salt and pepper" skull) and loss of definition of the tables are seen. A small cyst-like brown tumor is evident in the posterior parietal area (arrow),

Fig. 8.**39** **Senile osteoporosis.** Granular deossification of the skull similar to the hyperparathyroidism in Fig. 8.**38** is seen. However, in contrast to the latter condition, both tables are still well defined and evident as distinct thin lines.

sclerosis occurs, but is less prominent than in the axial skeleton. Finally, *proper treatment of hyperparathyroidism* and *rickets* may also induce a generalized sclerosis of the skull. Similarly, *hypervitaminosis D* and *idiopathic hypercalcemia of infancy* (Williams syndrome) are further rare causes of diffuse osteosclerosis in children that may also affect the skull.

Solitary or Multiple Bone Defects in the Skull

When a bone defect is diagnosed in the skull, tangential views of the lesions are useful in determining whether the erosion is caused by an extracranial or intracranial mass, or originates within the bone. If the thinning of the skull is caused by pressure from an adjacent benign mass, then the bone defect has a curved and usually smooth appearance, and the thinning increases progressively from the periphery

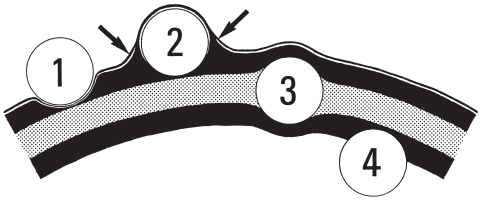

Fig. 8.**40** **Nondestructive expansile lesions** originating from the vault of the skull or adjacent to it. (Solid black bands: outer and inner table, respectively; crosshatched area: diploë; black line: periosteum.) 1 Lesion originates from the scalp outside the periosteum. An extrinsic defect is produced in the outer table. 2 Lesion originates beneath the periosteum. An extrinsic defect in the outer table similar to 1 is produced, but in addition there is new bone formation by the elevated periosteum. This is usually most pronounced at both edges, where the new bone assumes a triangular shape (arrows). 3 Lesion originates form the diploë. Symmetrical erosion and expansion of both tables result. 4 Lesion originates from the meninges or brain. An extrinsic defect is produced on the inner table.

Fig. 8.**41** **Button sequestrum.** A radiodense focus is seen within a lytic cranial lesion (eosinophilic granuloma).

Fig. 8.**42** **"Doughnut lesion".** A small round lytic defect surrounded by a sclerotic margin is evident.

to the center of the lesion. An erosion along the outer table indicates a scalp lesion, whereas an erosion on the inner table reflects an intracranial abnormality. Expansile lesions originating in the diploë erode and/or displace both inner and outer tables (Fig. 8.**40**).

Extracranial lesions eroding the vault or base of the skull are relatively rare and either of neoplastic or inflammatory origin. They are almost invariably associated with a soft-tissue mass or abnormality that can be diagnosed clinically. Carcinoma of the nasopharynx and sphenoid sinus, and glomus jugulare tumors, may invade the base of the skull, whereas skin carcinomas (rodent ulcers) may invade the skull vault. Pressure defects on the outer table of the skull may be produced by epidermoid cysts.

Lesions originating from the meninges and brain destroy the inner table first. Besides primary and secondary intracranial neoplasms, common causes for these are chronic subdural hematomas and abscesses, vascular structures and abnormalities (arteriovenous malformations and aneurysms), and cystic lesions (porencephalic cysts and meningoceles). Differential diagnosis of intracranial lesions causing bone destruction is rarely possible with conventional radiography unless other characteristic features (e.g., calcifications or location) are present.

Occasionally, a radiodense focus is found within a lytic cranial lesion and termed button sequestrum (Fig. 8.**41**). *Button sequestra* are found with eosinophilic granulomas, metastases (especially from breast carcinoma), epidermoids, osteomyelitis (including tuberculosis and syphilis), radiation necrosis, bone flaps undergoing avascular necrosis, and burr holes. A button sequestrum can also be mimicked by a radiolucent vascular channel forming a loop around a center of normal bone.

"Doughnut lesions" are small radiolucent areas in the skull surrounded by a sclerotic margin of variable thickness (Fig. 8.**42**). They often contain a central area of sclerosis simulating a button sequestrum. They are usually discovered incidentally on routine skull radiographs, and have no clinical significance.

A great variety of lesions originate from the skull itself, causing solitary or multiple bone defects. The differential diagnosis of lytic skull lesions is summarized in Table 8.**3**.

Abnormal Sella Turcica

There is a great variation in size and configuration of a normal sella turcica. On a lateral skull film, the greatest anteroposterior dimension of the normal sella ranges from 4 to 16 mm (average 10.5 mm), and its greatest depth (diaphragma sellae to floor) ranges from 4 to 12 mm (average 8.1 mm).

A *small sella* diagnosed as an incidental finding on a skull radiograph has no clinical significance and can be considered as a normal variant. A small sella has been described with hypopituitarism and several congenital syndromes and abnormalities,

The sella may demonstrate an abnormal shape without necessarily being enlarged. A *double-floor sella* on the lateral view suggests an intrasellar tumor with asymmetrical ex-

(continues on page 227)

Table 8.3 Solitary or Multiple Bone Defects in the Vault of the Skull

Disease	Radiographic Findings	Comments
Pacchionian (arachnoid) granulations (see Fig. 8.4)	Irregular smooth erosions in the inner table, located usually in the parasagittal area within 3 cm of the midline.	Pacchionian granulations are diverticula-like outpouchings of the subarachnoid space penetrating the dura mater and projecting into the lumen of the main sinuses and adjacent venous lakes. They may erode through the inner table into the diploic space.
Vascular markings (see Figs. 8.17 and 8.18)	Diploic veins and lakes may produce irregular, well demarcated oval or round radiolucencies, rarely exceeding 2 cm.	Other vascular structures may cause channel-like lucencies in the skull.
Parietal foramina (Fig. 8.43)	Smoothly marginated symmetric, parasagittal defects measuring up to 3 cm in diameter in the posterior parasagittal region.	Normal variant (nonossification of embryonal rests in parietal fissure) through which emissary veins pass.
Parietal thinning (Fig. 8.44)	Symmetric, crescent-shaped thinning of the superior portion of the parietal bones.	Normal variant in elderly males involving the outer tables.
Lacunar skull (craniolacunia, Lückenschädel) (Fig. 8.45)	Multiple radiolucent areas of calvarial thinning in newborns and infants, producing a pattern of exaggerated convolutional impressions.	Mesenchymal dysplasia of calvarial ossification. Usually associated with another malformation such as meningoceles of the skull or spine, hydrocephalus (e.g., in aqueductal stenosis) or Arnold-Chiari malformation. Spontaneous regression within first 6 months of life. DD: *Convolutional impressions* (normal variant visible between 2 and 8 years of age) and *"hammered silver" appearance* caused by increased intracranial pressure.
Meningocele, meningoencephalocele (Fig. 8.46)	Round to oval midline defect with smooth and often slightly sclerotic margins. Defect varies greatly in size and involves both inner and outer table. Frontal and occipital bone are the most common locations.	Congenital defect with herniation of meninges with or without brain. *Cranium bifidum* refers to a congenital midline defect without herniation.
Epidermoid (Fig. 8.47)	Solitary lytic and often expansile lesion measuring up to several cm in diameter. Its borders are always well-marginated and may be scalloped and sclerotic. Occasionally, a button sequestrum can be found.	Benign tumor caused by either posttraumatic implantation or congenital inclusion of epidermal elements. Appearance varies considerably with site of origin (e.g., scalp, diploë, or dura; see Fig. 8.**40**).
Dermoid	Small radiolucent defect without sclerotic margin, usually occurring in the midline.	Benign cystic lesion caused by congenital inclusion of elements from all dermal layers.
Arachnoid cyst	Smooth defect, often with a thin sclerotic rim.	Usually congenital, rarely traumatic or inflammatory in origin. Localized pressure causes thinning and outward bowing of the skull (see also posttraumatic [leptomeningeal] cyst in this table).
Primary bone tumors (benign and malignant)	Solitary, rare	Usually mixed lytic-sclerotic or predominantly sclerotic appearance.
Metastases (Fig. 8.48)	Usually multiple; irregular, ill-defined radiolucencies ("moth-eaten"); clear-cut defects occasionally with larger lesions. Button sequestrum (central nidus of intact bone in lytic defect) occurs, especially in breast carcinoma metastases.	Most frequent pathologic cause. All primaries that can produce lytic bone metastases, but breast carcinoma metastases are most common DD: vascular markings, Pacchionian (arachnoid) granulations.

(continues on page 224)

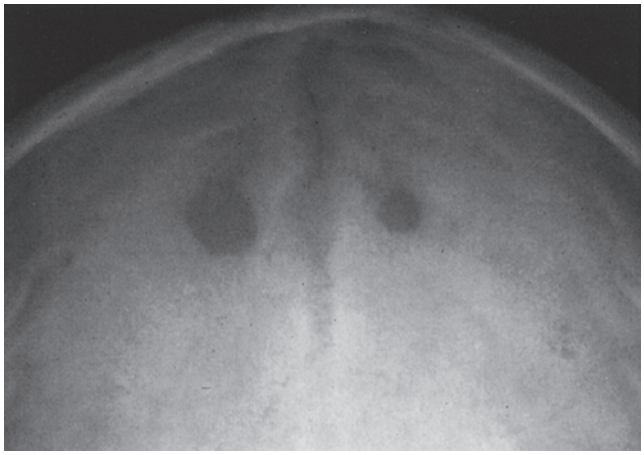

Fig. 8.**43** **Parietal foramina.** Two symmetrical parasagittal defects are seen in characteristic location.

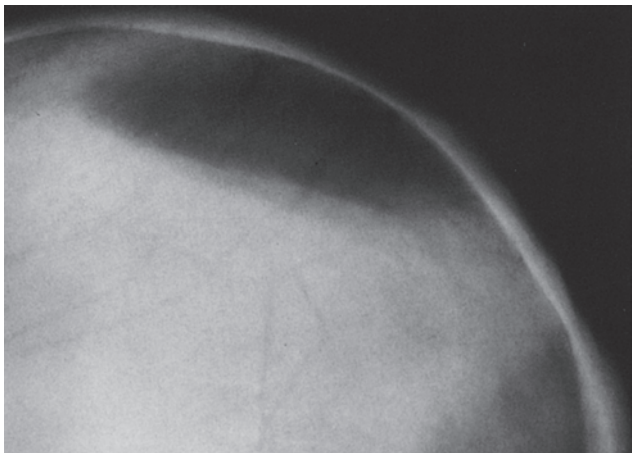

Fig. 8.**44** **Parietal thinning.** An oblong radiolucent area is seen in the parietal bone, which is symmetrical and caused primarily by thinning of the outer tables.

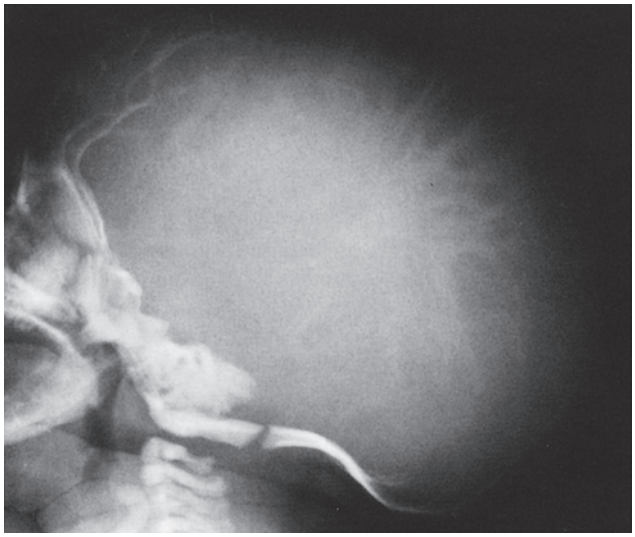

Fig. 8.**45** **Lacunar skull.** A pattern of exaggerated convolutional impressions is caused by multiple areas of calvarial thinning

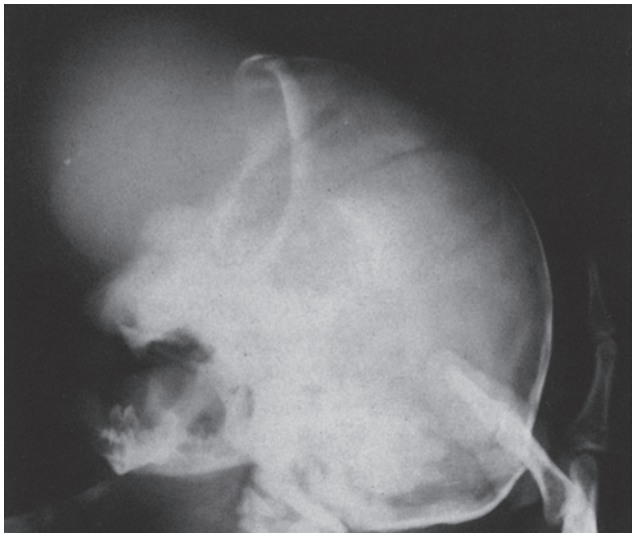

Fig. 8.**46** **Meningoencephalocele.** Round, midline defect in the frontal bone with the meningoencephalocele evident as a soft-tissue mass.

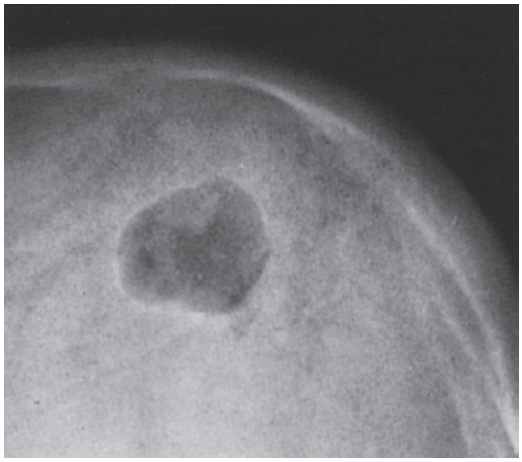

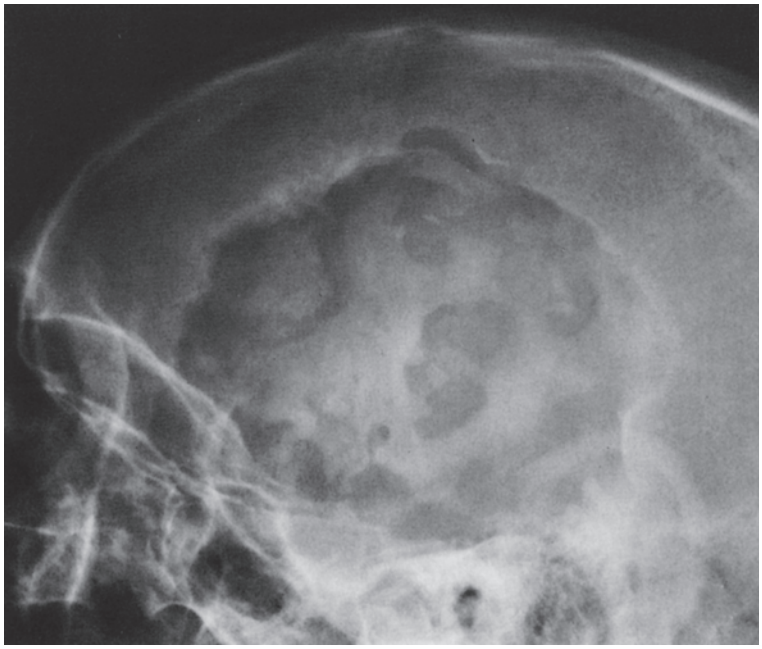

Fig. 8.**47** **Epidermoids** (2 cases), **a** A relatively small lytic lesion with slightly sclerotic margins is seen. **b** A large defect with scalloped margins containing irregular bony fragments is evident.

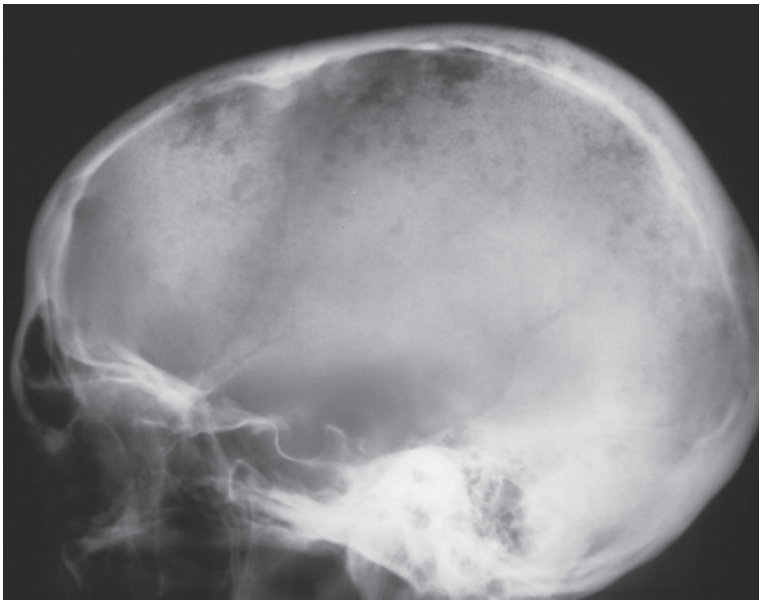

a

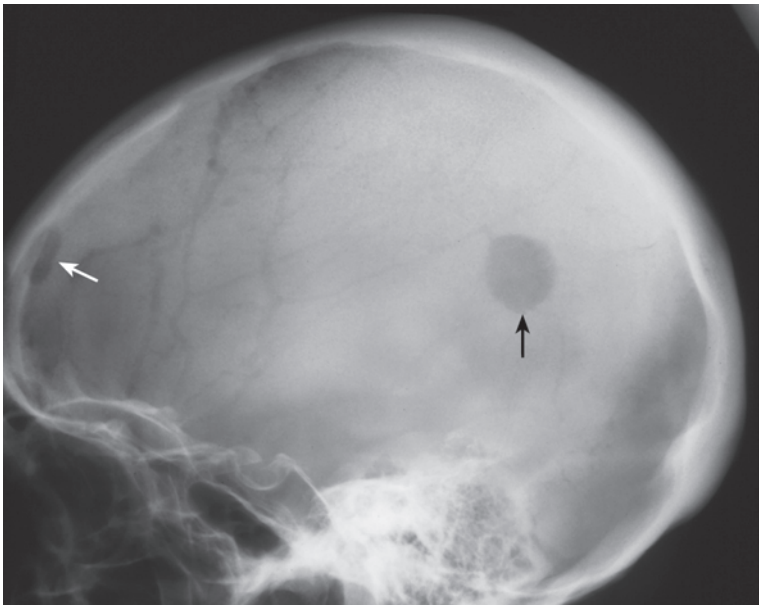

b

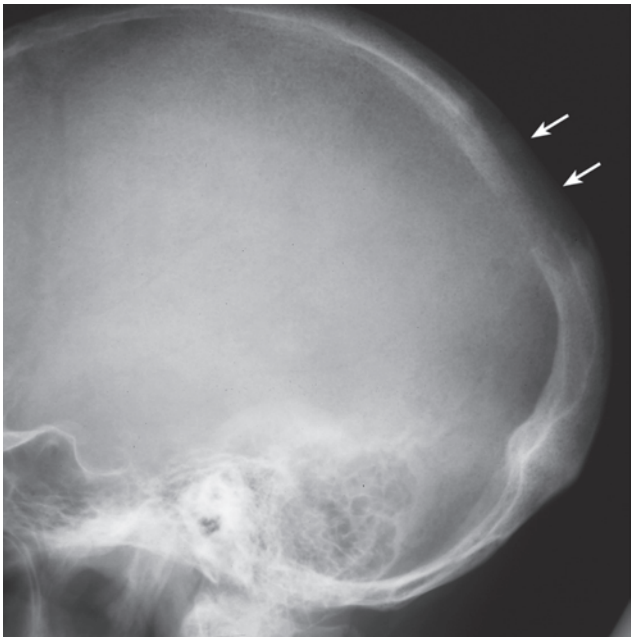

c

Fig. 8.**48** **Osteolytic metastases** (3 cases). **a** Multiple irregular, ill-defined and partially confluent radiolucencies ("moth-eaten" appearance) are seen (breast carcinoma). **b** Two well-defined ("punched-out" osteolytic lesions (arrows) are seen (thyroid carcinoma). **c** A large osteolytic lesion (arrows) extending along the diploic space with destruction of the outer table is seen in the parieto-occipital region (bronchogenic carcinoma).

Table 8.3 (Cont.) Solitary or Multiple Bone Defects in the Vault of the Skull

Disease	Radiographic Findings	Comments
Lymphoma, leukemia, malignant reticulosis	Multiple small erosions that can become confluent.	
Multiple myeloma (plasmacytoma) (Fig. 8.49)	Multiple (rarely solitary) sharply circumscribed ("punched-out") lesions are characteristic. May, however, also present similar to metastases.	Almost always in patients over 40 years of age.
Langerhans cell histiocytosis (eosinophilic granuloma, Hand-Schüller-Christian disease) (Figs. 8.50 and 8.51)	Solitary or multiple. Margins are usually well defined and often beveled and may become sclerotic. Button sequestra occur. Undulating margin when several lesions become confluent ("geographic skull").	Usually in patients under 40 years of age.
Hemangioma (Fig. 8.30)	Solitary, Slightly expansile lesion with or without some marginal sclerosis. Virtually diagnostic when radiating bone spicules are present within the lesion.	
Neurofibromatosis (Fig. 8.52)	Lytic defects in occipital and temporal bone occur, but are rare. A round to oval calvarial defect involving the left lambdoid suture and extending toward the midline is considered to be most typical.	Neurofibromatosis more commonly involves the base of the skull (defects in sphenoid wing and posterior superior wall of the orbit are virtually diagnostic).
Fibrous dysplasia (Fig. 8.53)	Single or multiple but rarely purely lytic.	Usually mixed lytic and sclerotic pattern in the vault.
Paget's disease (Fig. 8.54)	Osteoporosis circumscripta: Destructive phase of Paget's disease in the vault . Area of destruction well demarcated, bilateral, and involving primarily the outer table of more than one bone in the calvarium.	In patients over 40 years of age. DD: Physiologic symmetrical *thinning of the squama occipitalis* is a common finding, best seen on lateral views.
Osteomyelitis (acute) (Fig. 8.55)	Irregular, poorly defined lytic areas, which may coalesce. Button sequestrum may be present.	Usually spread by continuity from infection adjacent to calvarium (e.g., paranasal sinus, middle ear, scalp) or secondary to fracture. Hematogenous spread to the skull is rare.
Tuberculosis	Solitary, round, sharply defined, purely lytic lesion, rarely containing a sequestrum.	
Syphilis	Multiple, poorly defined lytic lesions that may coalesce and contain one or more scattered sequestra.	
Fungal infections	Solitary or multiple, simulating either tuberculosis or metastases.	
Sarcoidosis	Solitary or multiple small purely lytic lesions.	
Burr holes, craniotomies	Edges of lesions initially beveled and smooth, but may become irregular with new bone formation.	Enlarged parietal foramina (symmetrical parasagittal defects in posterior parietal region) must be differentiated from burr holes (see Fig. 8.**40**).

(continues on page 226)

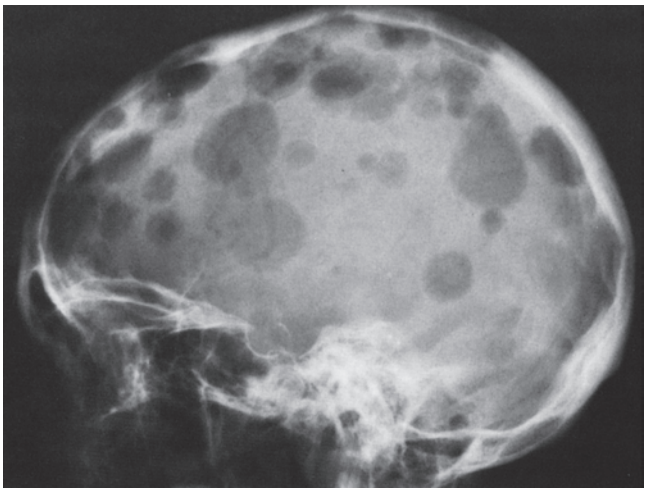

Fig. 8.**49** **Multiple myeloma.** Multiple, sharply circumscribed ("punched-out") lytic lesions are characteristic.

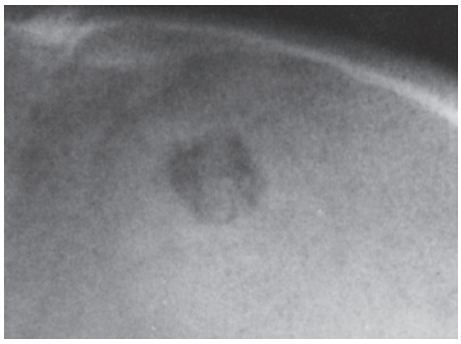

Fig. 8.**50** **Langerhans cell histiocytosis** (eosinophilic granuloma). A solitary relatively well-defined lytic lesion with button sequestrum (central nidus of intact bone) is seen.

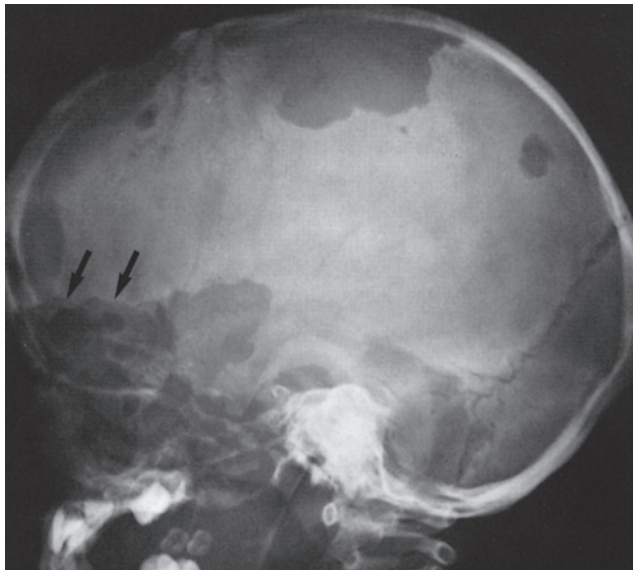

Fig. 8.**51** **Langerhans cell histiocytosis** (Hand-Schüller-Christian disease). Destructive lesions with undulating and beveled margins are seen, resulting in the "geographic skull" appearance. The beveled margin (arrows) indicates that the outer and inner table are unevenly destroyed. ▷

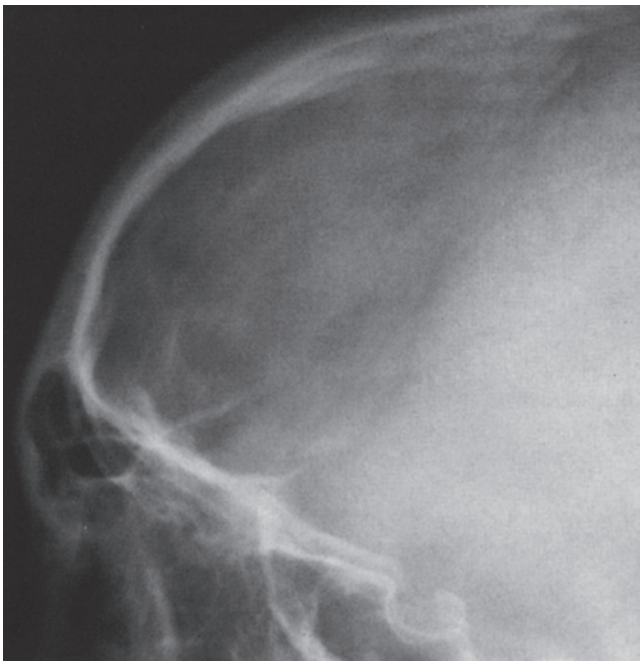

Fig. 8.**52** **Neurofibromatosis.** A predominantly lytic area in the frontoparietal area is an unusual location in this disorder.

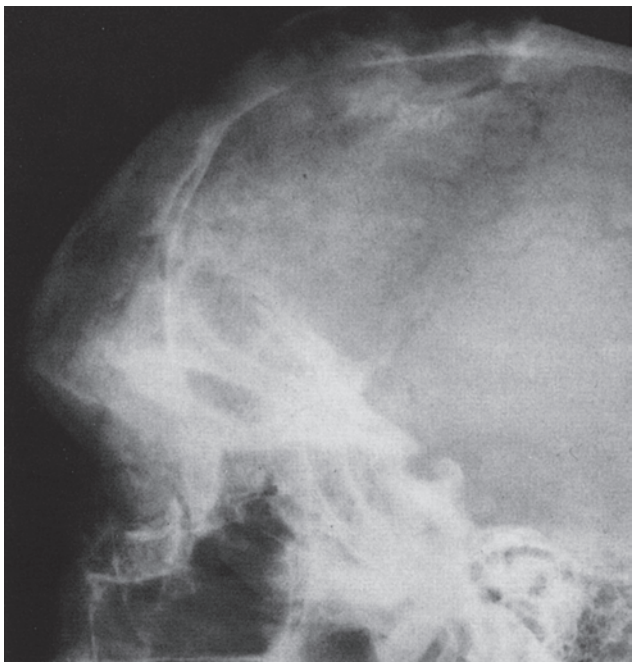

Fig. 8.**53** **Fibrous dysplasia.** Extensive sclerosis of the skull base and paranasal sinuses is associated with expansile and predominantly lytic lesions originating from the outer table of the frontal bone, whereas the inner table appears intact.

Table 8.3 (Cont.) Solitary or Multiple Bone Defects in the Vault of the Skull

Disease	Radiographic Findings	Comments
Posttraumatic (leptomeningeal) cyst (Fig. 8.56)	Solitary, often large defect with scalloped and beveled margin (inner table more eroded than outer table).	
Fibrosing osteitis	Solitary, poorly defined, lytic defect often with slightly sclerotic margin in outer table secondary to a fracture. Button sequestrum may be found.	Caused by transformation of fragmented bone into fibrous tissue.
Radiation osteonecrosis	Scattered small and irregular lytic defects occurring a year or more after irradiation. Button sequestrum occurs.	A mixed pattern of lytic and sclerotic lesions is more characteristic.
Brown tumors and hemorrhagic cysts in primary hyperparathyroidism (Fig. 8.38)	Solitary or multiple poorly defined lesion(s) surrounded by granular demineralization ("salt and pepper" skull). After treatment (removal of parathyroid adenoma), cysts are often better demarcated because of the remineralization of the surrounding bone.	After treatment, brown tumors heal by filling in with bone and may eventually disappear or persist as sclerotic foci for many years.

a

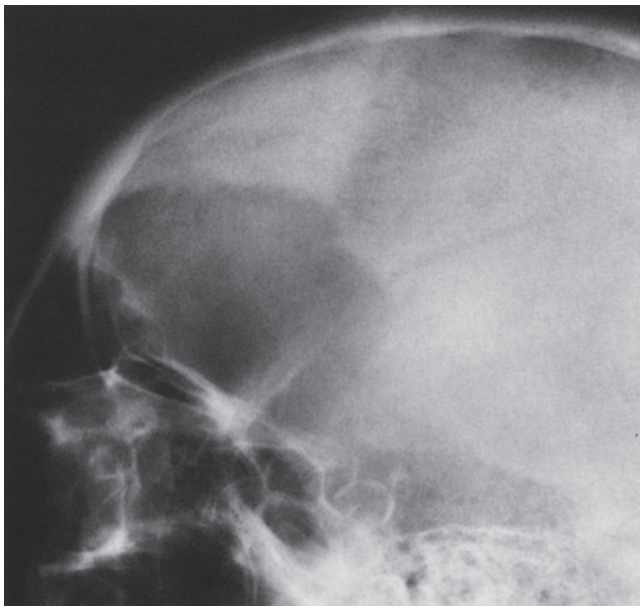

b

Fig. 8.**54 a, b Paget's disease.** A large, well-demarcated and somewhat asymmetric area of destruction in the frontal bone with extension into the temporal squama is seen (osteoporosis circumscripta). Incidentally calcification of the carotid syphon that projects on the lateral view into the sella is also present.

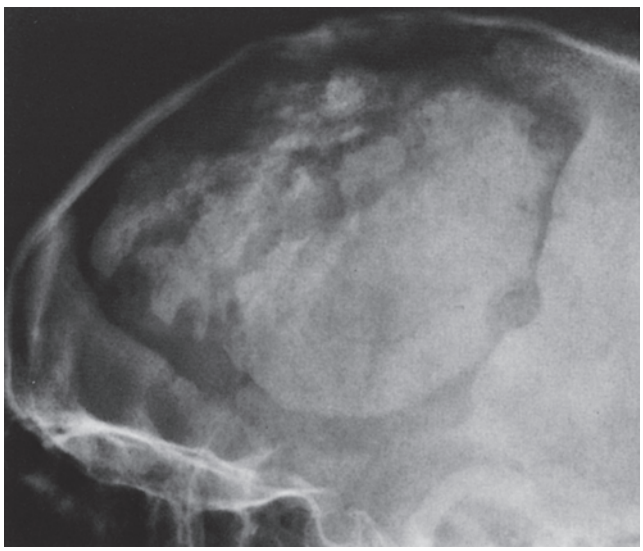

Fig. 8.**55 Osteomyelitis in bone flap.** Destruction of the anterosuperior part of the bone flap is evident, while its posteroinferior portion is not affected.

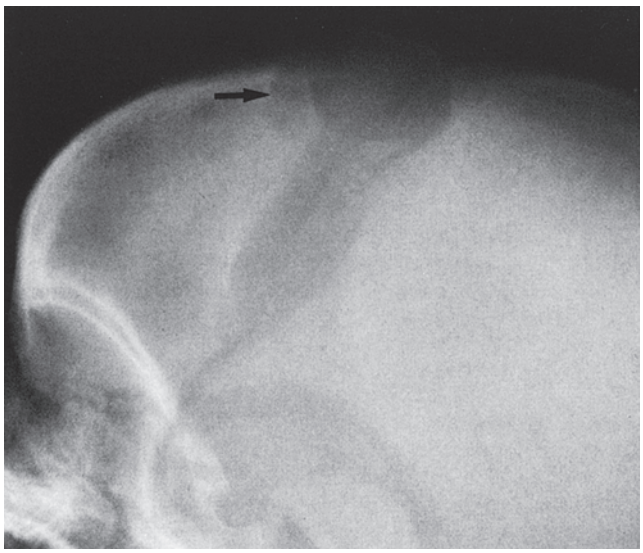

Fig. 8.**56 Posttraumatic (leptomeningeal) cyst.** A large defect with beveled margin (arrow) is seen six weeks after skull fracture during birth.

pansion (Fig. 8.**57**). Both a normally tilted sella and a superimposed bony structure (e.g., from the sphenoid sinus or carotid sulcus) may simulate a pathologic double floor and must be differentiated from the latter.

The *J-shaped sella* refers to an elongated sella with a shallow anterior convexity caused by the sulcus chiasmaticus. It is more commonly seen in healthy children than adults. An enlarged sulcus chiasmaticus is a common finding in a *glioma of the optic chiasm* (Fig. 8.**58**). It is a rare finding in pituitary tumors extending anteriorly and in suprasellar tumors. In children, it can also be associated with *Hurler's syndrome* (mucopolysaccharidosis type 1) and with *chronic low-grade hydrocephalus*.

The *dorsum sella* shows a range of normal variations. On the lateral view, both the anterior and posterior margins consist of a well-defined cortex outlining a medulla of varying thickness and spongy texture. Pneumatization of the dorsum sella results occasionally from the extension of a large sphenoid sinus into the dorsum. In chronically elevated intracranial pressure or prolonged arterial hypertension, loss of definition of the entire dorsum sella occurs (see Fig. 8.**10a**),whereas the anterior cortex of the dorsum remains characteristically intact in osteopenia.

Enlargement of the sella turcica is caused by many intrasellar and parasellar mass lesions, which are summarized in Table 8.**4**

Table 8.4 Enlarged Sella Turcica

Disease	Radiographic Findings	Comments
Empty sella syndrome (Fig. 8.59)	Sella slightly enlarged and globular. No erosions, destructions, or posterior displacement of the dorsum.	Probably caused by a developmental defect in the diaphragma sellae allowing the prolapse of a small fluid-containing pocket of arachnoid into pituitary fossa. Enlargement of sella caused by fluid-transmitted pulsations. CT and MRI are diagnostic.
Increased intracranial pressure	Enlargement begins with erosion of the anterior cortex of the dorsum, proceeds to the floor of the sella, and may result in complete dissolution of the dorsum. Anterior and posterior clinoids can be thinned or eroded.	In chronically raised intracranial pressure caused by intracranial masses, cerebral edema, over-production of cerebrospinal fluid, obstruction of cerebrospinal fluid pathways or intracranial venous thrombosis.
Pituitary tumor (Fig. 8.60)	Ballooned sella with undercutting of the anterior clinoid processes, unequal downward displacement of the floor (double-floor appearance), and backward bowing to complete destruction of the dorsum.	Chromophobe adenomas virtually always produce considerable sellar enlargement. Eosinophil adenomas produce usually some enlargement of the sella and give rise to acromegaly. Basophil adenomas (causing Cushing's syndrome) and prolactin secreting microadenomas (causing amenorrhea and galactorrhea) do not generally cause any sellar abnormality. Adenocarcinomas are rare and cause an extremely rapid enlargement of the sella.
Craniopharyngioma (Fig. 8.61)	Elongated sella with short curved dorsum characteristic, but more often sellar changes indistinguishable from pituitary tumor.	Suprasellar tumor found predominantly in children and young adults. Calcified in 75 % but incidence of calcification decreases with age. DD: Similar sellar changes in other juxtasellar or suprasellar tumors (meningiomas and, less commonly, other benign or malignant tumors originating in the adjacent structures, and metastases).

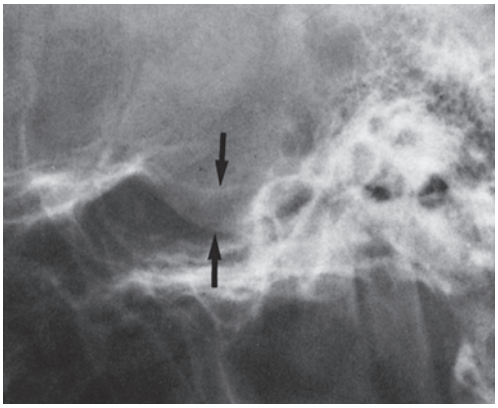

Fig. 8.**57** **Double-floor sella.** Asymmetric growth of an eosinophil adenoma of the pituitary gland caused a double-floor sella (arrows).

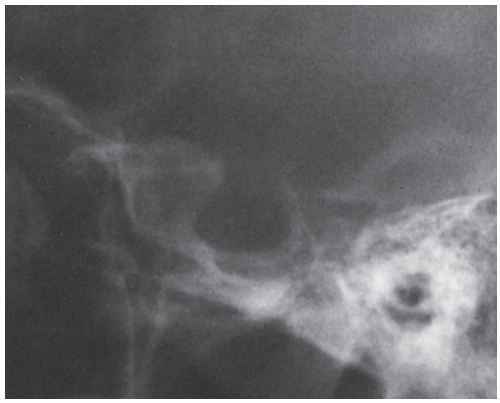

Fig. 8.**58** **J-shaped sella.** A glioma of the optic chiasm undercutting the anterior clinoid processes caused this sellar configuration and enlargement. Note also the straightening and partial destruction of the dorsum.

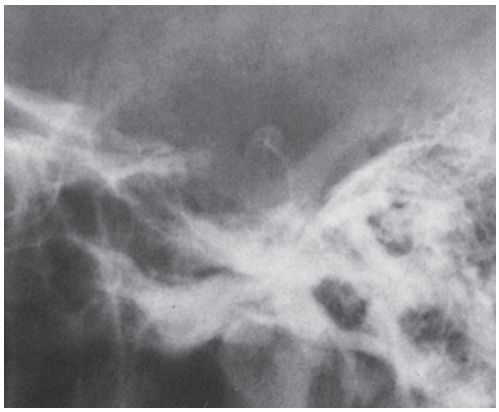

Fig. 8.**59** **Empty sella syndrome.** A slightly enlarged and globular-appearing sella with an intact and normally configurated dorsum is characteristic. However, a relatively small pituitary adenoma can occasionally produce identical radiographic changes.

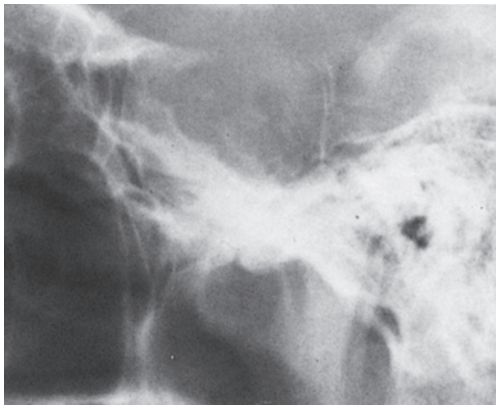

Fig. 8.**60** **Chromophobe pituitary adenoma.** An enlarged sella with undercutting of the anterior clinoid processes and straightening and destruction of the dorsum is seen.

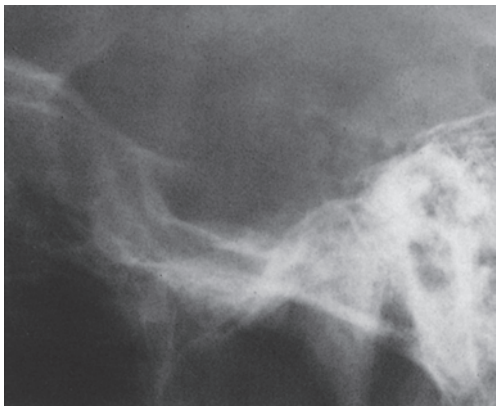

Fig. 8.**61** **Craniopharyngioma.** An enlarged and elongated sella with completely destroyed dorsum is seen (see also Fig. 8.**10 a**).

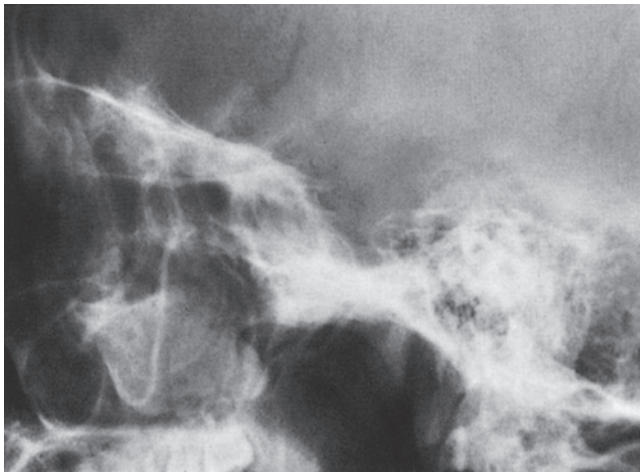

Fig. 8.**62** **Langerhans cell histiocytosis.** Sellar destruction is associated with sclerotic lesions in the base of the skull and facial bones.

Fig. 8.**63** **Carcinoma of the sphenoid sinus.** The sellar destruction is caused by direct invasion of the sphenoid sinus carcinoma that is often evident as a soft-tissue density in the sinus.

Basilar Invagination and Platybasia

Basilar invagination (impression) means elevation of the floor of the posterior fossa with invagination of the margins of the foramen magnum upward into the skull. This condition is readily diagnosed on radiographs taken either in anteroposterior or lateral projection (Fig. 8.**64**). Basilar invagination is often associated with platybasia (flattening of the base of the skull), in which an increased basal angle is found (Fig. 8.**65**). Basilar invagination and platybasia are found in a variety of congenital anomalies (e.g., *osteogenesis imperfecta, Klippel-Feil deformity, Arnold-Chiari malformation*, and *cleidocranial dysostosis*) and in acquired diseases producing bone softening. *Paget's disease* (Fig. 8.**65b**), *osteomalacia*, *hyperparathyroidism* and *rheumatoid arthritis* are the most common causes in the adult which produce these findings.

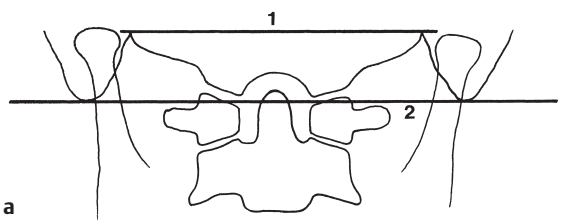

a

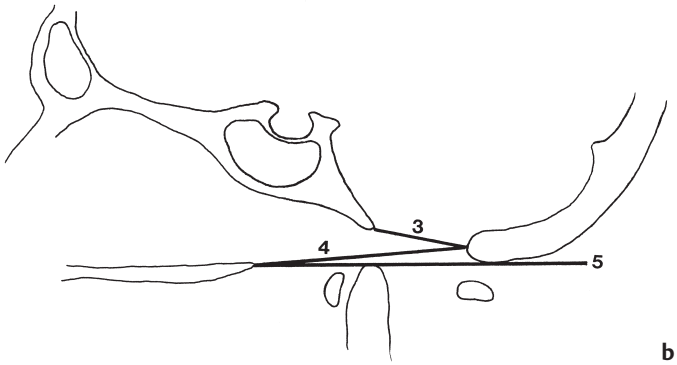

b

Fig. 8.**64 a, b Radiologic assessment of basilar invagination** **a** in anteroposterior and **b** lateral projection. 1 Digastric line. Tip of odontoid process is normally located below this line. 2 Bimastoid line. Tip of odontoid process projects normally not more than 10 mm above this line. 3 Foramen magnum or McRae line. Tip of odontoid process projects normally below this line. 4 Chamberlain line (hard palate to posterior margin of foramen magnum). Tip of odontoid process projects normally not more than 3 mm above this line. 5 McGregor line (hard palate to outer contour of occiput). Tip of odontoid process projects normally not more than 5 mm above this line

Sclerosis of the Base of the Skull

The following differential diagnosis is limited to those diseases that either frequently involve the base of the skull or are exclusively found in this area. Virtually all disorders presenting elsewhere in the skeleton with osteoblastic lesions or diffuse osteosclerosis may involve the base of the skull also. This is a particularly common finding in all constitutional diseases associated with osteosclerosis (Fig. 8.**66**). For a complete differential diagnosis, the reader is referred to Chapter 2.

Meningiomas may arise from various locations at the base of the skull such as cribriform plate, planum sphenoidale, tuberculum sellae, clinoid processes, and petrous bone. They cause a localized thickening and sclerosis of the involved bone (Fig. 8.**67**). Erosions of neighboring bony structures may also be associated. Differentiation from localized fibrous dysplasia can be difficult, but the presence of tumor calcification and the demonstration of trabeculae in the thickened sclerotic bone are only found with meningiomas and may help to distinguish these two entities.

Carcinomas originating in the ear, sphenoid sinus, and nasopharynx and invading the base of the skull are usually destructive, but may become sclerotic after radiotherapy. *Lymphoepitheliomas* (nonkeratinizing squamous cell carcinomas) of the nasopharynx or paranasal sinuses occasionally produce a localized sclerotic reaction in the adjacent bone before any treatment has been instituted.

Low-grade and chronic infections in the sphenoid sinus and mastoids produce localized sclerosis combined with poor pneumatization of the area. A localized sclerosis in the middle ear may be caused by chronic inflammation. Sclerotic changes in *otosclerosis* can only be appreciated with computed tomography, but not with conventional radiography.

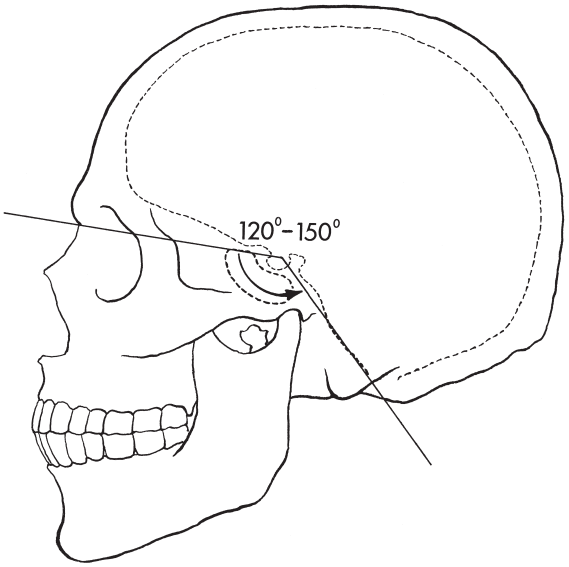

a

Fig. 8.**65 a Radiologic assessment of the basal angle** (angle between a line drawn through the nasion and the roof of the sphenoid sinus and a line paralleling the slope of the clivus or drawn through the tuberculum sella and the anterior margin of the foramen magnum). The normal basal angle ranges form 120 to 150 degrees (mean 135 degrees). An angle larger than 150 degrees indicates platybasia, whereas an angle smaller than 120 degrees indicates basal kyphosis. Platybasia is usually associated with basilar invagination, and basal kyphosis with prognathism.

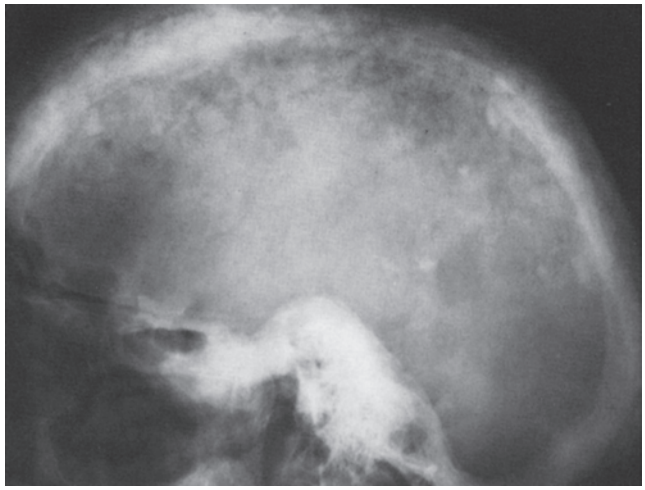

b

Fig. 8.**65 b Basilar invagination and platybasia in Paget's disease** evident as marked sclerosis of the base of skull. Note also the characteristic changes of Paget's disease in the vault of the skull.

Fig. 8.**66** **Craniometaphyseal dysplasia.** Sclerosis of the base of the skull and facial bones with obliteration of all paranasal sinuses is seen. With the exception of a localized area of dense sclerosis in the frontal bone the vault of the skull is not affected, which is usually the case in this condition.

Fig. 8.**68** **Fibrous dysplasia.** Extensive sclerosis and thickening of the base of the skull with extension into the frontal bone is seen. The trabecular pattern in both the sclerotic and "ground glass" appearing areas is characteristically effaced.

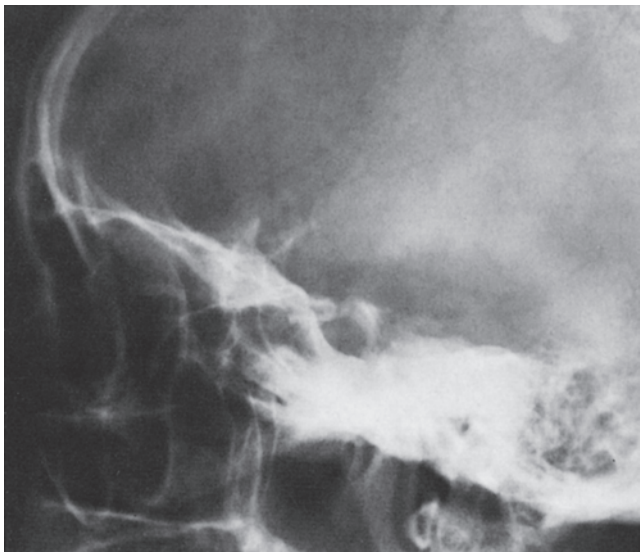

Fig. 8.**67** **Meningioma.** Sclerosis and thickening of the base of the skull was caused by a sphenoidal meningioma.

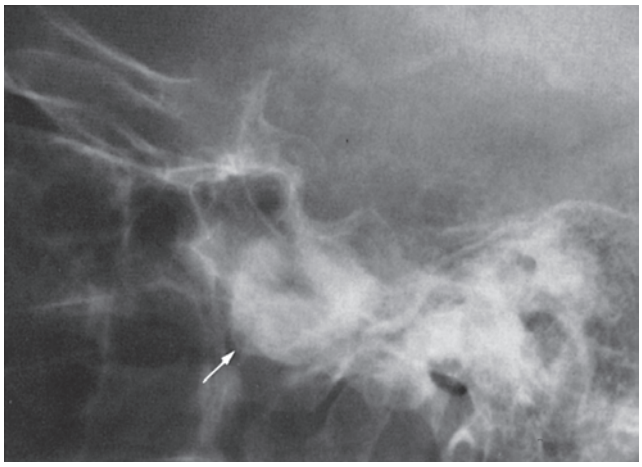

Fig. 8.**69** **Paget's disease.** Involvement of the base of the skull is seen, including a localized area of dense sclerosis (arrow).

Sclerotic changes caused by *fibrous dysplasia* in the base of the skull can be localized, but are often more widespread than in a meningioma, and manifestations of fibrous dysplasia may be found elsewhere in the skull. The bone changes may be purely sclerotic or a mixture of sclerosis and radiolucencies. The bone of fibrous dysplasia does not contain trabeculae and, for its thickness, does not appear very dense (Fig. 8.**68**).

Paget's disease can present as widespread sclerosis of the skull base usually associated with involvement of the vault and/or facial bones (Fig. 8.**69**). Encroachment of foramina and fissures occurs causing nerve compression symptoms.

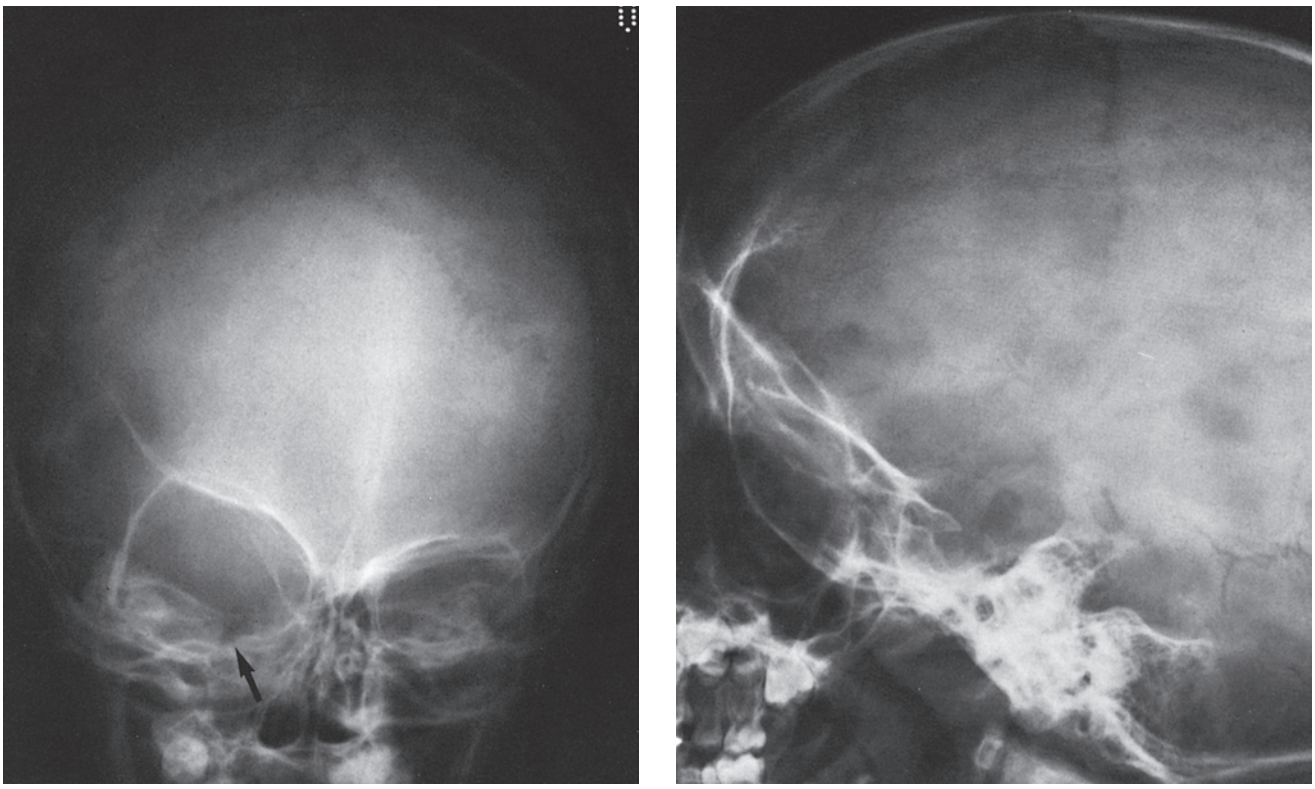

Fig. 8.**70 a, b** **Neurofibromatosis.** Asymmetry of the skull with enlarged right orbit, absent right superior orbital fissure, and erosion of the tip of the right petrous apex (arrow) are characteristic.

Basilar impression is a common finding with Paget's disease involving the base of the skull (see Fig. 8.**65b**).

In *Langerhans cell histiocytosis*, sclerotic involvement of the base of the skull is usually associated with destructive lesions, particularly in the sellar and parasellar region (see Fig. 8.**62**).

Erosion, Destruction or Lytic Defects in the Base of the Skull

Lytic lesions in the base of the skull may be caused by a variety of conditions that often can be differentiated from each other on the basis of location and radiographic appearance.

In *neurofibromatosis*, a unilateral defect in the sphenoid wings with absent superior orbital fissure and orbital enlargement can be found (Fig. 8.**70**). The disease may also be bilateral and erode the clinoid processes and the tip of the petrous apex.

Acoustic neuroma is the most common tumor of the inner ear, found usually in the middle-aged or elderly patient. The tumor presents radiographically as erosion and expansion of the internal auditory canal or erosion of the petrous apex (Fig. 8.**71**). Comparison with the normal contralateral side facilitates the diagnosis, but one has to keep in mind the fact that complete symmetry between the two sides is only seen in approximately 50% of healthy subjects. The length of the internal auditory canal varies greatly from individual to individual (3–16 mm; average 7–9 mm). Its diameter is more constant and should not exceed 5 mm. A diameter larger than 5 mm or a side difference in excess of 1 mm should raise the suspicion of a tumor.

A osteolytic defect projecting into the middle ear or the antrum mastoideum is most commonly caused by a *cholesteatoma* (Fig. 8.**72**). Primary cholesteatomas that are developmental in origin are rare. Secondary cholesteatomas

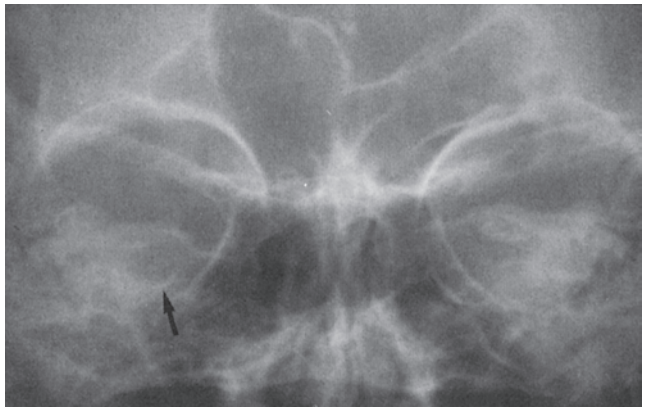

Fig. 8.**71** **Acoustic neuroma.** A localized erosion and expansion of the right internal auditory canal near the petrous apex is seen (arrow).

Fig. 8.**72** **Cholesteatoma.** A large round defect in the antrum mastoideum (arrow) is seen besides significant sclerosis of the mastoid indicating chronic mastoiditis (Schüller's view).

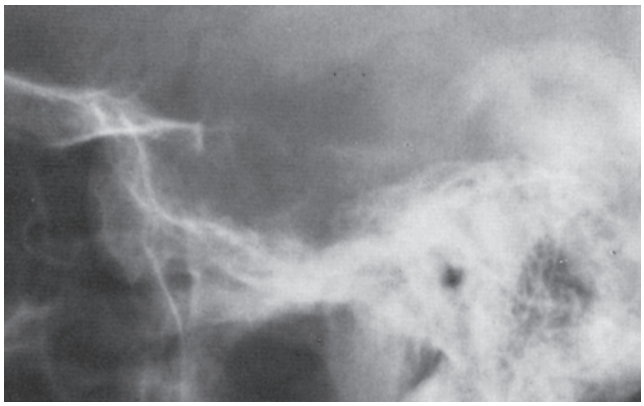

Fig. 8.**73** **Chordoma.** Destruction of the clivus, petrous pyramids and sella is seen (see also Fig. 8.**11**).

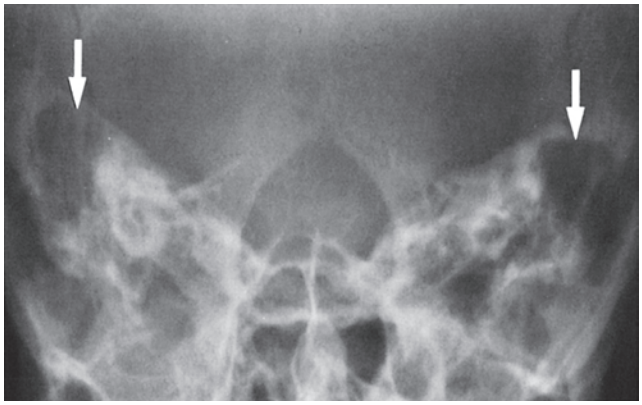

Fig. 8.**74** **Langerhans cell histiocytosis.** Two large areas of destruction simulating bilateral cholesteatomas are seen in the petrous bones (arrows). On the left side, the tumor had been removed one month earlier, with a surgical defect remaining that is impossible to differentiate from the original lesion.

Table 8.5 Destructive Lesions Affecting the Petrous Pyramid, Middle Ear and Antrum

A. Petrous pyramid

Neoplasm
- Acoustic neurinoma
- Meningioma
- Glioma
- Neuroma of the trigeminal and facial nerve
- Chordoma
- Glomus jugulare tumor
- Epidermoid (cerebellopontine angle cistern)
- Carcinoma of the nasopharynx
- Parotid tumors

Petrositis (Gradenigo's syndrome: diplopia, periorbital pain, and otorrhea)

Aneurysm (e.g., intrapetrous carotid artery)

Langerhans cell histiocytosis

B. Middle ear, antrum, and mastoids

Choleastoma (primary and secondary)

Neoplasm
- Carcinoma, primary or metastatic
- Sarcoma
- Glomus tumor

Abscess

Granuloma

Surgical defect

Langerhans cell histiocytosis

are the result of ear infections and are quite common. A surgical defect following the excision of a cholesteatoma is usually impossible to differentiate from a cholesteatoma by conventional radiography. A large mastoid air cell can at times mimic a lytic defect in this area and must be differentiated. A summary of all destructive lesions involving the petrous pyramid, middle ear, and antrum is given in Table 8.**5**.

Glomus tumors are locally invasive chemodectomas arising in the chemoreceptor organs located in the jugular fossa or rarely in the hypotympanum of the middle ear. The glomus jugulare tumor erodes the jugular foramen and the interior aspect of the midpetrous pyramid in the early stage, whereas in a later stage, it may extend into the middle ear and the posterior fossa. Women are three times more frequently affected than men.

Chordomas originate from notochordal remnants found in the clivus and entire dorsal spine. The clivus is the second most common origin of this tumor, after the sacrococcygeal region. A destructive lesion of the clivus, dorsum sella, and petrous pyramid is virtually diagnostic when associated with a dense retrosellar calcification that is found in 70% of patients (Fig. 8.**73**).

Meningiomas and *gliomas* may erode into the base of the skull causing a localized bone destruction, although an area of increased bone density is a more common manifestation in the former tumors.

Carcinomas of the nasopharynx, paranasal sinuses, and mastoids as well as a variety of *primary or metastatic bone tumors* have to be considered in the differential diagnosis when a destructive lesion is found in the base of the skull.

Surgical defects can simulate a neoplastic lesion and may be impossible to differentiate from a local tumor recurrence on a single examination. Proper patient history and/or follow-up examinations are usually required for a correct diagnosis (Fig. 8.**74**).

Langerhans cell histiocytosis (histiocytosis X) can mimic different diseases in the skull base and produce one or more lytic lesions. Sella turcica, sphenoid wings, petrous pyramids, and mastoid air cells are most often involved. Sellar destruction is not necessarily associated with diabetes insipidus, and vice versa. In the middle ear, the disease simulates unilateral or bilateral otitis media with or without cholesteatomas both clinically and radiographically (Fig. 8.**74**).

An *aneurysm of the internal carotid artery* may, depending on its location, cause erosion of the dorsum sella, petrous pyramid, carotid canal, and superior orbital fissure. The latter may also be eroded by a *carotid cavernous fistula* that is usually the consequence of a fracture involving the base of the skull.

9 Orbits

Calcifications

Calcifications within the soft tissues of the orbits are uncommon, but their radiologic demonstration often has clinical significance and may be pathognomonic of a specific disease. Calcifications of the lens presenting as a circular density of approximately 7 mm on the posteroanterior projection and as an oval density on the lateral view occur in *cataracts*.

In *retrolental fibroplasia* (retinopathy developing in premature infants with oxygen being the primary offending agent), flecks of intravitreal calcifications are found that may be combined in a more advanced stage with lenticular calcifications (Fig. 9.**1**).

Finely stippled to conglomerate calcifications in children are seen with *retinoblastomas*, which are bilateral in approximately 20 %. Calcifications can also be found in intraorbital *meningiomas, gliomas, dermoids, angiomas, aneurysms, hematomas*, and *arteriovenous malformations*. These calcifications are similar in appearance to the previously described intracranial calcifications of the same lesions (Chapter 8). Multiple phleboliths have been reported in *venous malformations* and *cavernous hemangiomas* of the orbit. In *von Hippel–Lindau disease* (retinal, intracranial, and sometimes visceral angiomatosis) calcifications, though rare, may occur.

Bacterial and *parasitic infections* may rarely cause intraorbital calcifications. *Mucoceles* from the frontal or ethmoidal sinus may erode into the orbital cavity. Gross calcification of the cyst-like wall of a mucocele occurs in 5 % of these cases. *Phthysis bulbi* refers to shrinkage and wasting of the eye, usually the sequelae of severe, longstanding ophthalmic disease (e.g., trauma with intraocular foreign body, rupture of the globe, and chronic inflammatory disease). Calcification of the choroid, vitreous body and lens is common in this condition. In systemic conditions such as *hypercalcemia (e.g., hyperparathyroidism)* and *connective tissue disease*, intraorbital calcifications may occasionally be found. An intraorbital *foreign body* has to be differentiated from a pathologic calcification when the density of both is similar. The radiographic demonstration of even the smallest amount of intraorbital air *(orbital emphysema)* after a traumatic incident is virtually diagnostic of a fracture into an adjacent paranasal sinus, most commonly secondary to a fracture of the lamina papyracea of the ethmoid sinus (Fig. 9.**2**).

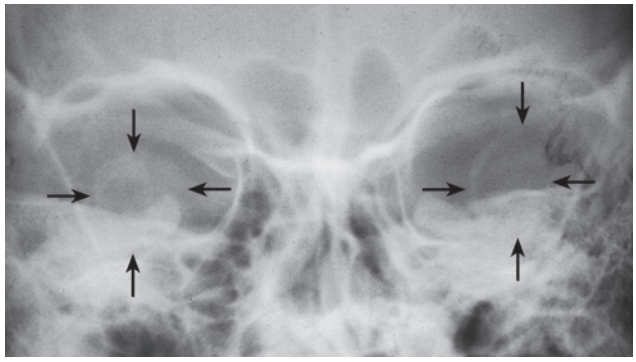

Fig. 9.**1** **Retrolental fibroplasia.** Lenticular calcifications (arrows) are seen in both orbits in this far advanced stage of the disease.

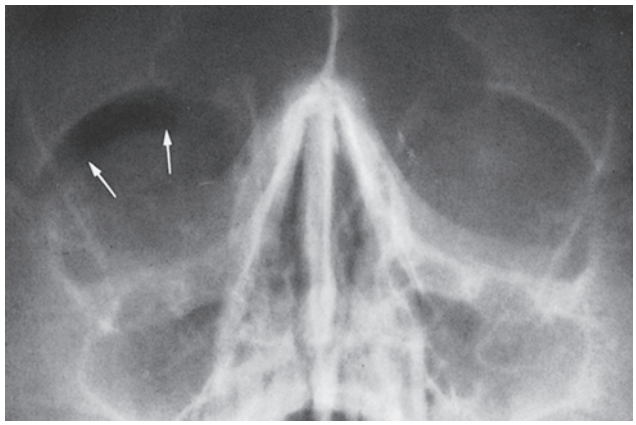

Fig. 9.**2** **Orbital emphysema.** A crescent-shaped radiolucency (arrows) is seen under the right orbital roof post fracture of the lamina papyracea of the ethmoid sinus, which cannot be appreciated on this examination,

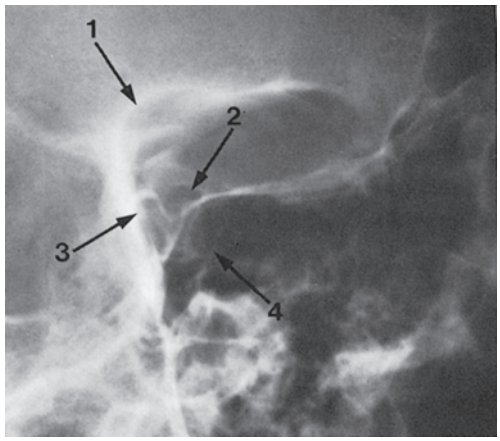

Fig. 9.**3** **Lacrimal gland tumor.** An ovoid radiolucent defect with a relatively poorly defined inferior margin is seen in the superolateral aspect of the orbit caused by deepening of the normally shallow fossa of the lacrimal gland in this location (arrow 1). Note also the oval-shaped optic canal (arrow 2), the pneumatized anterior clinoid projecting laterally to the optic canal (arrow 3), and the caroticoclinoid canal projecting inferiorly to it (arrow 4) on this standard optic canal projection.

Erosions and Bony Defects in the Orbit

Dermoids and *epidermoids* occur most often in the superolateral portion of the orbit near its anterior margin. They grow slowly and produce a smoothly marginated defect often with slightly sclerotic margins.

Lacrimal gland tumors are benign mixed neoplasms that deepen the normal shallow fossa of the lacrimal gland in the superolateral quadrant of the orbit (Fig. 9.**3**). They do not produce a sharply marginated bony defect as observed with dermoid tumors in the same location. Rarely, lacrimal gland tumors undergo malignant transformation and cause irregu-

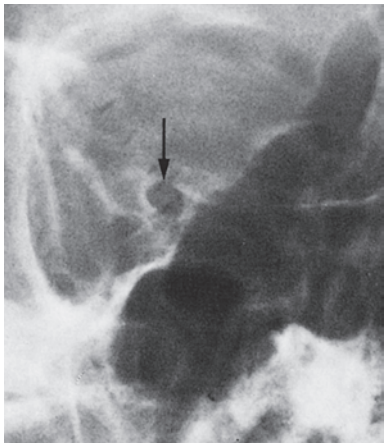

a

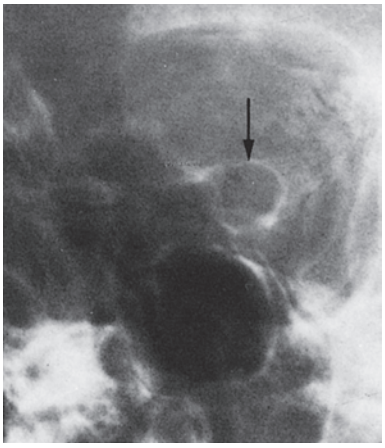

b

Fig. 9.4 **a, b Optic nerve glioma.** A concentric enlargement of the left optic canal measuring 10 mm in diameter is seen in **b** (arrow). The normal right optic canal is shown for comparison in **a** (arrow).

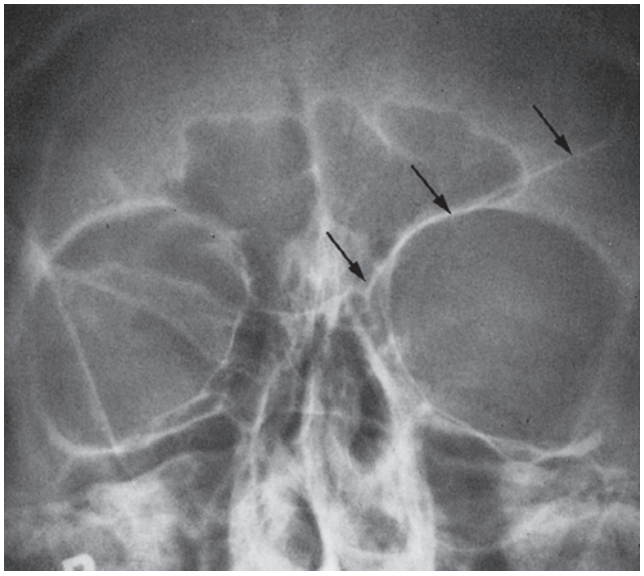

Fig. 9.5 **Neurofibromatosis.** Agenesis of the greater and lesser wings of the left sphenoid with absence of the superior orbital fissure and marked elevation of the sphenoid ridge (arrows) is seen in the enlarged left orbit ("empty orbit" sign). Hypoplasia of the left ethmoidal cells is also evident.

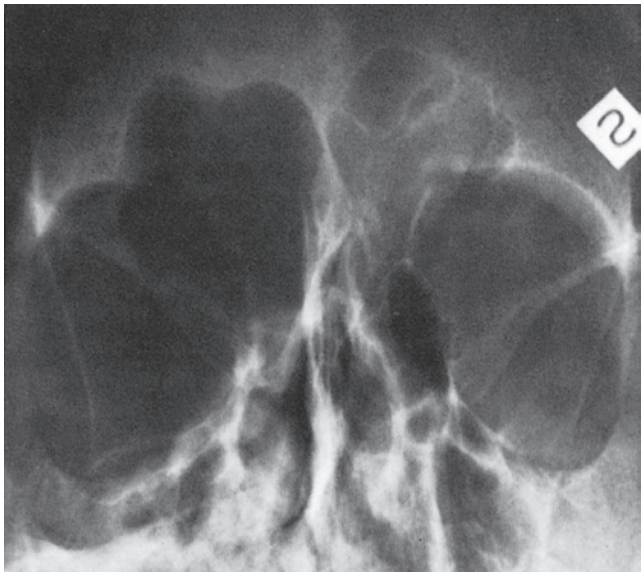

◁ Fig. 9.6 **Mucocele of the frontal sinus** invading the right orbit and ethmoidal cells. A mucocele of the frontal sinus, which appears relatively radiolucent because of the considerable thinning of its walls that overcompensates the loss of aeration caused by the mucocele itself, has destroyed the right orbital roof and ethmoidal cells.

larly marginated lytic defects with or without a diffuse increase in density of the surrounding bone.

Hemangiomas and *retinoblastomas* in children, and *melanomas* in adults, are relatively common primary orbital tumors, but destruction of the orbital wall is unusual.

Carcinomas invading the orbit from the *nasopharynx* and *paranasal sinuses* can cause irregular bone destruction. *Gliomas* and *meningiomas* may also produce local areas of destruction, although a purely lytic involvement of the orbital wall by a meningioma is unusual. A *glioma* of the optic nerve produces localized enlargement of the optic canal (Fig. 9.**4**). This is the most common cause of a concentrically enlarged optic canal. *Orbital pseudotumors* consist of a variety of chronic inflammatory conditions that rarely produce changes on conventional radiographic examinations. Enlargement of the superior orbital fissure or optic canal occurs exceptionally with lesions located posteriorly in the orbits.

Neurofibromatosis can be associated with unilateral orbital enlargement, large lytic defects in the orbital roof, walls, and floor, enlargement of the optic canal or superior orbital fissure and hypoplasia of the ipsilateral maxillary and ethmoid sinuses. Agenesis of the sphenoid wings produces the characteristic "empty orbit" sign (Fig. 9.**5**). Besides neurinomas and neurofibromas, gliomas and meningiomas are also found in this condition.

Metastases, lymphomas, multiple myeloma, and *primary bone* and *soft-tissue tumors* may involve the orbit, occasionally causing a destructive lesion. They must be considered in the differential diagnosis of an osteolytic or osteoblastic orbital bone lesion, but their presentation is not different from other locations.

Sinusitis may spread from the frontal sinus and less commonly from the ethmoid and maxillary sinuses into the soft tissue of the orbit. In such cases destruction of the intervening bone is common, but some increase in bone density along the margins is often present, suggesting the inflammatory etiology of the lesion. Similarly, a *mucocele* from an adjacent paranasal sinus may slowly erode into the orbit, causing a bony defect with smooth margins (Fig. 9.**6**).

Table 9.1 Erosion and Enlargement of Optic Canal and Superior Orbital Fissure

Disease	Optic Canal	Superior Orbital Fissure
Increased intracranial pressure	Rare; concentric, bilateral	Rare; bilateral erosions of the margins of superior orbital fissures.
Glioma	Glioma of the optic nerve is the most common cause of concentric enlargement.	
Meningioma	Meningioma involving the optic nerve sheet. Rare. Enlargement concentric.	Rare. In meningiomas that originate from the middle fossa.
Pituitary tumor, craniopharyngioma or chordoma extending anteriorly	Unilateral or bilateral erosions beginning at the lateral wall.	Chromophobe adenomas are the second most common cause of superior orbital fissure widening.
Carcinoma of sphenoid sinus	Destruction of optic canal (particularly medial wall).	Rare
Intraorbital mass extending posteriorly	Rare (e.g., retinoblastoma)	Rare
Metastases	Rare	Rare
Inflammatory lesions	Rare. Concentric enlargement by granulomas (e.g., sarcoid, tuberculosis). Erosion of medial wall by mucocele of sphenoid sinus.	Rare (e.g., mucocele of sphenoid sinus).
Orbital pseudotumor	Rare	Rare
Aneurysm	Ophthalmic artery: concentric enlargement. Internal carotid artery (cavernous portion): lateral wall erosion.	Aneurysm of internal carotid artery (cavernous portion) most common cause of superior orbital fissure enlargement.
Arteriovenous malformation	Concentric enlargement with ophthalmic artery involvement.	Superior orbital fissure enlarged with ophthalmic vein involvement (e.g. , carotid-cavernous sinus fistula).
Orbital varix		Congenital dilatation of orbital veins that can occasionally cause an enlargement of the superior orbital fissure.
Langerhans cell histiocytosis (histiocytosis X)	Localized destruction of the optic canal is rare.	Limitation of destructive lesions to superior orbital fissure is uncommon.
Neurofibromatosis	Concentric enlargement of optic canal usually caused by associated optic nerve glioma.	Congenital enlargement of superior orbital fissure that is not associated with any mass lesion (orbital dysplasia) occurs. Neurofibromas and posterior orbital encephalocele can occasionally enlarge the superior orbital fissure but are not always associated with neurofibromatosis.

Langerhans cell histiocytosis produces irregularly marginated defects in the orbit. With healing, either spontaneously or after therapy, the margin of the lesion may become sclerotic. The lesions can vary considerably in size and seem to have a predilection for the roof and lateral wall of the orbit.

Conditions causing a more localized enlargement of the optic canal and superior orbital fissure are summarized in Table 9.**1**. The diameter of the *optic canal* ranges from 4 to 6 mm and its radiographic appearance varies considerably. In healthy subjects it is usually oval and rarely truly circular. Normal variants include “figure-of-eight” and “keyhole” appearances, the latter being essentially an incomplete “figure-of-eight.” Pneumatization of the anterior clinoid may create the appearance of a second canal projecting laterally to the true optic canal. The caroticoclinoid canal is a developmental anomaly found in approximately 35 % of skulls and projects inferiorly to the true optic canal (see Fig. 9.**3**).

The *superior orbital fissure* is the largest communication between middle fossa and orbit and has the shape of an inverted comma. Variations in size and shape are common, however, and an asymmetry between the two orbital fissures is found in 9 % of cases.

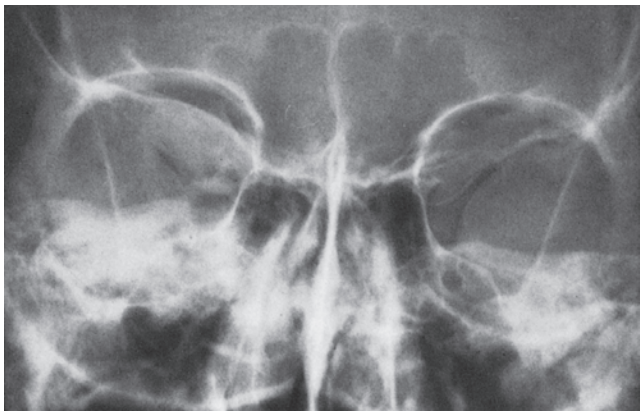

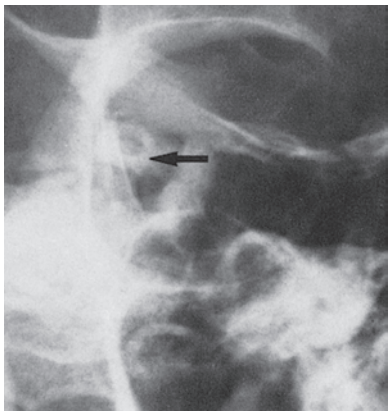

Fig. 9.**7 a, b Meningioma.** Significant sclerosis of the lesser and greater right sphenoid wings with marked narrowing of the right superior orbital fissure and right optic canal (arrow in **b**) is seen.

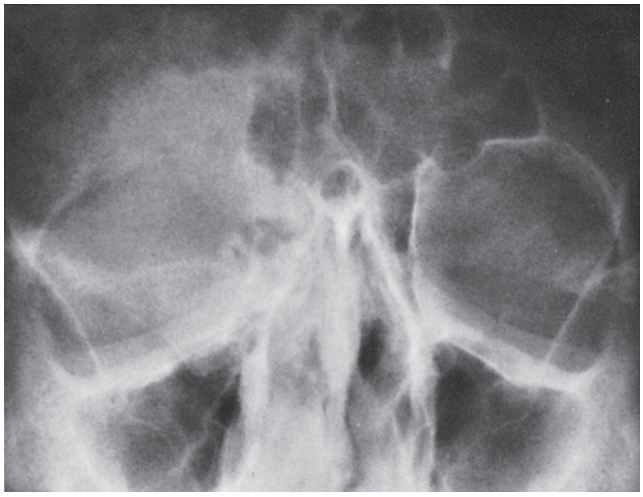

Fig. 9.**8** **Fibrous dysplasia.** Sclerosis and thickening of the right facial bones including roof and posterior wall of the orbit is seen.

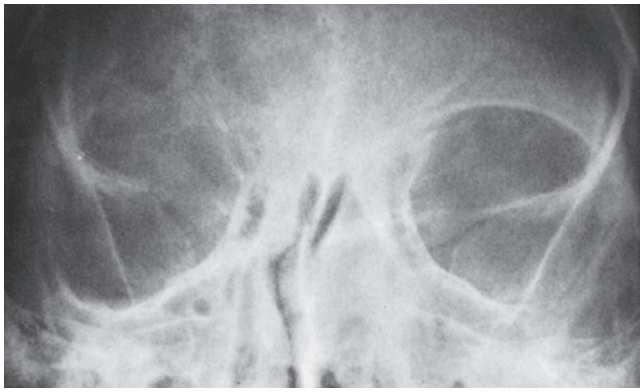

Fig. 9.**9** **Langerhans cell histiocytosis.** Sclerosis and destruction of the superomedial wall of the right orbit with involvement of the adjacent frontal sinus and ethmoidal cells is evident.

Fig. 9.**10** **Craniometaphyseal dysplasia.** Symmetrical sclerosis of both orbits is associated with sclerotic changes in the base of the skull and facial bones.

10 Nasal Fossa and Paranasal Sinuses

The paranasal sinuses consist of the frontal sinus, sphenoid sinus, maxillary antra, and ethmoidal air cells. They communicate with the nasal fossa and are lined with a mucous membrane contiguous with that of the nasal cavity. These are two important factors for the understanding of the development and spread of any pathologic process. Pneumatization and expansion of the sinuses occurs during the first and second decade of life, reaching its full extent only in early adulthood. The size of the sinuses varies greatly from individual to individual and even between the right and left side of the same individual. *Unilateral* or *bilateral hypoplasia* is not uncommon and has no clinical significance, except in some congenital syndromes where it might be a finding in a much wider spectrum of radiographic abnormalities (e.g., hypoplastic maxillary antra in *dysostosis cleidocranialis*). Enlarged paranasal sinuses are a constant feature of *acromegaly*, but as an isolated finding are best disregarded.

Since the paranasal sinuses are air-containing cavities, soft-tissue changes occurring in them can already be well demonstrated by conventional radiographic technique. Complete opacification of a sinus may at times be more difficult to appreciate than less severe mucosal thickening that is still contrasted by air. As a rule of thumb, the maxillary antra should normally have a similar transparency as the orbits in the Water's view. Fluid accumulation in a paranasal sinus can easily be demonstrated using a horizontal roentgen beam. In this case the fluid will accumulate in the deepest part of the sinus and form a sharp interface with the air topping it. It must, however, be remembered that when using a vertical beam, any fluid accumulation in a sinus produces a diffuse loss of translucency that is indistinguishable from mucosal thickening.

An *air–fluid level in a sinus* is caused by the accumulation of blood, pus, or exudate produced by the mucosa. An air–fluid level produced by blood is most commonly the result of a *fracture* (Fig. 10.**1**). Occasionally the only radiographic clue to a paranasal sinus fracture consists of a localized soft-tissue swelling caused by mucosal or submucosal bleeding. This is particularly common in *blow-out fractures of the orbit*, presenting as a small, soft-tissue bulge on the antral roof (Fig. 10.**2**). A more extensive hemorrhage can cause a complete loss of translucency of the involved paranasal sinus. In the maxillary antrum, a soft-tissue hematoma of the overlying cheek must be differentiated from a hemorrhage within the sinus, since both can cause a generalized loss of translucency. Clinical examination of the patient and radiographs in different projections allow differentiation between these two conditions.

Fractures of the paranasal sinus can sometimes only be diagnosed radiographically by demonstrating the leak of air from a sinus into a neighboring structure. *Orbital emphysema* is encountered with maxillary and ethmoidal sinus fractures (see Fig. 9.**2**). Air within the cranial cavity *(pneumocephalus)* may result from a fracture involving the frontal or ethmoid sinus.

Acute sinusitis is the most common cause of an air–fluid level in a paranasal sinus. Although air–fluid levels occur with allergic sinusitis, they are more common with infectious sinusitis. The latter condition is often limited to one sinus, and mucosal thickening paralleling the bony walls is characteristically found. In allergic sinusitis a diffuse involvement of the nose (swelling of the turbinates) and all sinuses is usually present. In this condition, the mucosal thickening often produces a scalloped lining, and polyp formations are frequently encountered.

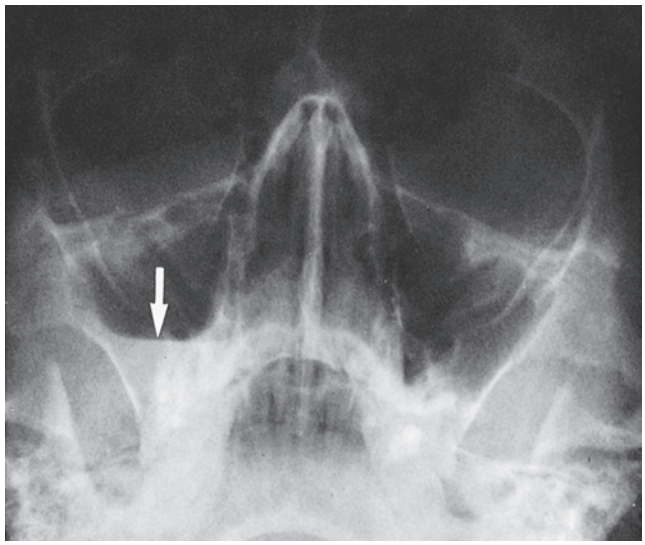

Fig. 10.**1** **Air-fluid (blood) level secondary to trauma.** A fracture in the right antral roof with bleeding into the right maxillary antrum evident by the air-fluid level (arrow) is seen.

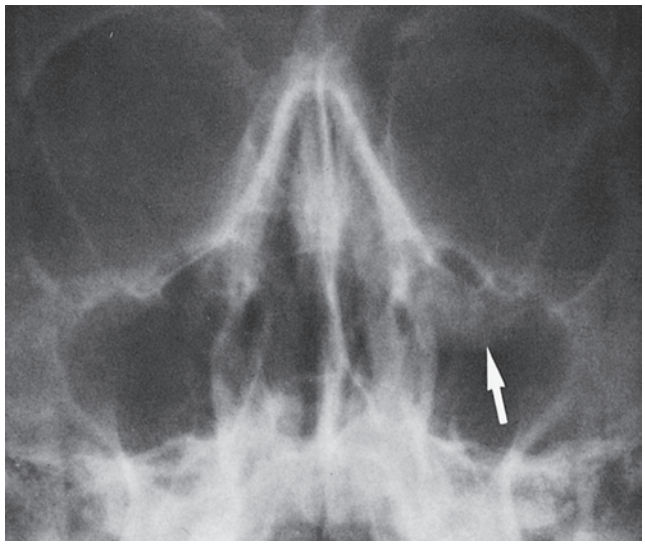

Fig. 10.**2** **Blow-out fracture of the left orbit.** A polypoid soft-tissue mass (arrow) hanging from the left antral roof is the only radiographic evidence of this fracture.

A soft-tissue thickening or mass with or without destruction of the adjacent bone can, however, be found in many other conditions, which will be discussed in Table 10.**1**. Asymmetry of the sinuses between the right and left side or localized osteosclerosis in a sinus wall can also produce a unilateral decrease in translucency that should not be confused with soft-tissue thickening within a sinus (Fig. 10.**3**).

Benign and malignant tumors of cartilagenous or osseous origin may occasionally develop in the facial bones. Their presentation, however, does not differ from any other location and their differential diagnosis has been covered in Chapter **5**. A *rhinolith* in the nasal cavity should not be mistaken for such a lesion (Fig. 10.**4**).

Table 10.1 Soft-tissue Thickening or Mass in Paranasal Sinuses

Lesion	Radiographic Appearance	Comments
Benign tumors (see Fig. 10.18)	Variable, ranging from a localized soft-tissue mass to a dense bony lesion (osteoma).	Except for osteomas, these tumors are very rare and include *lipomas*, *hemangiomas* , *dermoids* and *chondromas*.
Carcinoma (Figs. 10.5 and 10.6)	Soft-tissue mass associated almost invariably with bone destruction. Sclerotic reaction of infiltrated bone occurs on rare occasions.	Usually found in patients over 50. Squamous cell carcinoma is by far the most common histologic type.
Sarcoma	Findings indistinguishable from carcinoma except when new bone is formed (e.g. , osteosarcoma).	Rare. All ages. *Benign mesenchymal neoplasms* are even less common.
Extrinsic neoplasm invading sinus (Fig. 10.7)	Usually malignant but also benign (e.g., chordoma, enchondroma, pituitary adenoma in sphenoid sinus, and juvenile angiofibroma.	*Juvenile angiofibroma*: Highly vascular tumor originating in nasopharynx of adolescent males. May bow the posterior wall of the maxillary antra anteriorly or invade the adjacent sinuses, orbits and even the cranium.
Odontogenic lesions (cysts, tumors)	Limited to the base of maxillary antra.	For differential diagnosis see Chapter 11.
Lymphoma (usually nonHodgkin) (Fig. 10.8)	Involvement often bilateral with soft-tissue thickening (occasionally polypoid) and frequently bone erosions.	Lymphadenopathy is usually the dominant clinical feature.
Wegener's granulomatosis (Fig. 10.9)	Unilateral or more commonly bilateral soft tissue thickening, often associated with erosion and/or sclerosis of the adjacent bone.	Usually associated with pulmonary, vascular, and renal disease. *Limited form of Wegener's granulomatosis*: Confined to respiratory tract including nasal cavity and paranasal sinuses and of relatively good prognosis.
Midline granuloma	Ulcerating granulomatous masses with progressive destruction of paranasal sinuses, nose, and hard and soft palate.	Destructive process may erode through the skin, resulting in mutilation of the face. Without proper treatment, the disease is fatal. Good response to high-dose local radiotherapy. The sinus involvement is radiographically indistinguishable from Wegener's granulomatosis, but there is neither pulmonary nor renal involvement.
Fibrous dysplasia (Fig 10.10)	Expansion and nonhomogeneous opacification of the involved sinuses. Associated with predominantly sclerotic involvement of the adjacent facial bones.	Similar findings in *ossifying fibromas* that can be regarded as localized form of fibrous dysplasia in facial bones. *"Leontiasis ossea"* (deformity and bilateral enlargement of the face) is caused by widespread involvement of the frontal and facial bones by fibrous dysplasia.

(continues on page 240)

Fig. 10.**3** **Osteoblastic metastases** from breast carcinoma. The poorly defined increased density in the right frontal sinus is caused by osteoblastic bone metastases and should not be mistaken for soft-tissue thickening in this sinus.

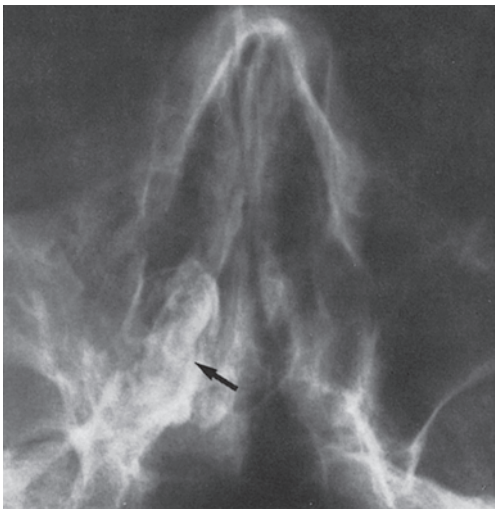

Fig. 10.**4** **Rhinolith.** An irregular sclerotic lesion is seen in the right nasal cavity (arrow).

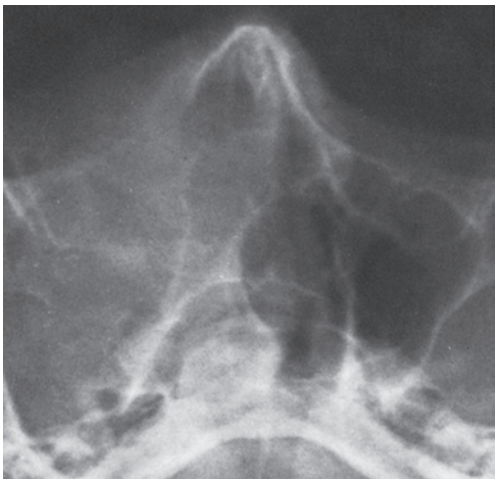

Fig. 10.**5** **Carcinoma of the right maxillary antrum.** A large soft-tissue mass originating from the right maxillary antrum with extensive destruction of the facial bones including the nose is seen.

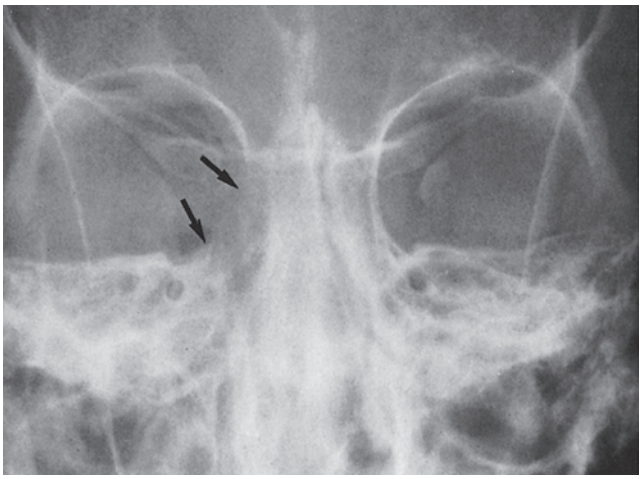

Fig. 10.**6** **Carcinoma of the right ethmoid sinus.** Opacification of the ethmoidal air cells with destruction of the adjacent medial wall (arrows) of the right orbit is seen.

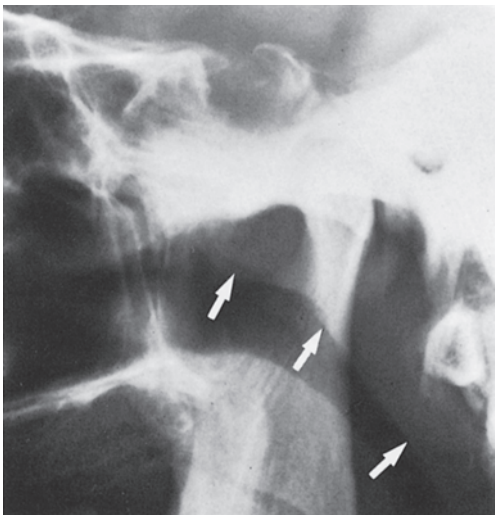

Fig. 10.**7** **Carcinoma of the nasopharynx** with invasion into the sphenoid sinus and pituitary fossa. The carcinoma, evident in the nasopharynx as increased soft-tissue density (arrows), has invaded into the sphenoid sinus, which is opacified, and destroyed the floor of the pituitary fossa.

Fig. 10.**8** **Non-Hodgkin's lymphoma.** Complete obliteration of both maxillary antra by soft-tissue masses is seen. There is also a suggestion of bony erosions in both the left maxillary roof, where the infraorbital foramen can no longer be outlined, and the inferolateral wall of the left antrum, which can barely be recognized

Fig. 10.**9** **Wegener's granulomatosis.** Complete opacification of the right maxillary antrum with destruction of its superomedial wall and a soft-tissue mass protruding into the adjacent orbit is evident. Soft-tissue thickening including a round granulomatous mass is also present in the roof of the left maxillary antrum, but its wall appears to be intact.

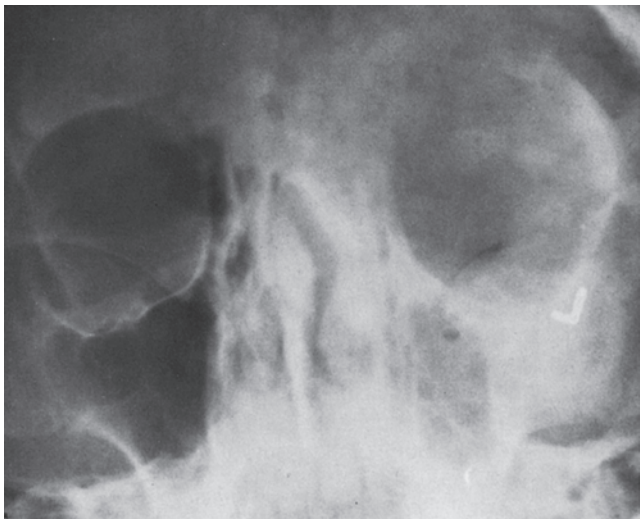

Fig. 10.**10** **Fibrous dysplasia.** Enlargement of the left half of the face and left orbit by predominantly sclerotic lesions and nonhomogeneous opacification of the left maxillary antrum are seen. Involvement of the frontal bone is also evident.

Table 10.1 (Cont.) Soft-tissue Thickening or Mass in Paranasal Sinuses

Lesion	Radiographic Appearance	Comments
Neurofibromatosis (Fig. 10.11)	Deformed and enlarged facial bones and sinuses associated with large soft-tissue masses (neurofibromas) which may erode into the adjacent bones.	Changes in skull and orbit are more common and characteristic.
Paget's disease (Fig. 10.12)	Obliteration of sinuses occurs occasionally, but is solely caused by thickening and sclerosis of the bone without soft-tissue involvement.	Involvement of skull is much more common and characteristic.
Sinusitis – acute (Figs. 10.13 and 10.14)	Air-fluid levels, soft-tissue swelling, and polyps. Secondary osteomyelitis of adjacent bone is very rare.	Allergic or infectious. Infectious sinusitis is usually secondary to upper respiratory tract infections (e.g. , streptococci, staphylococci, or viral infections). Maxillary sinusitis can also be of dental origin.
Sinusitis, chronic granulomatous (Fig. 10.15)	Nasal and/or upper respiratory tract diseases are associated and usually prominent. Soft-tissue swelling, polypoid lesions, bone destruction, and sclerosis occur in sinuses.	*Bacterial*: tuberculosis, syphilis, leprosy, glanders (*Pseudomonas mallei*), listeriosis, yaws, actinomycosis, and *rhinoscleroma* (probably caused by *Klebsiella rhinoscleromatis*). *Fungal*: aspergillosis, blastomycosis, histoplasmosis, coccidioidomycosis, cryptococcosis, mucormycosis, sporotrichosis, rhinosporidiosis. *Idiopathic*: sarcoidosis, erythema nodosum.
Polyp and cyst (Fig. 10.16)	Smooth spherical or domeshaped opacities which may alter slightly their convex borders in different projections when the lesions are cystic and not under tension. Broadbased cystic lesions originating from the floor of the maxillary sinus may mimic occasionally an airfluid level. Sinus is uniformly opaque when completely occupied by lesion. The walls of the sinus are not affected.	"Polyp": Inflammatory hypertrophic swelling of mucosa. "Cyst": 1. Encapsulated exudate, pus, or blood. 2. Retention cyst containing mucus or serous material. 3. Surgical: Ciliated cyst developing in maxillary sinus post Caldwell-Luc operation (surgical production of window connecting the antrum with the inferior meatus of the nose).

(continues on page 242)

Fig. 10.**11** **Neurofibromatosis.** Enlarged right half of the face associated with huge soft-tissue masses (neurofibromas), that have eroded the adjacent bone is evident.

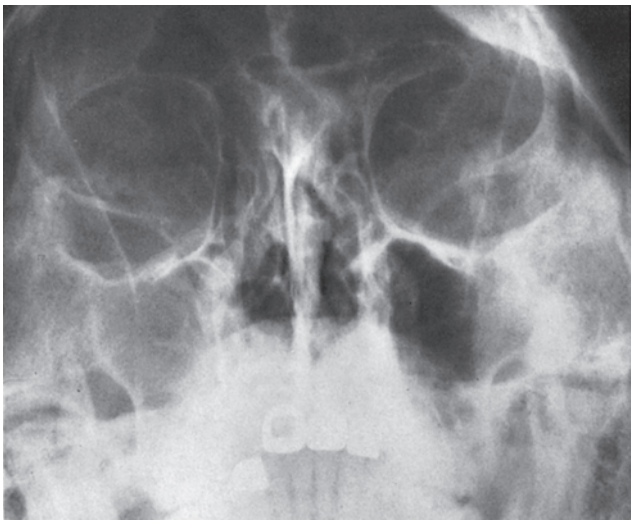

Fig. 10.**12** **Paget's disease.** Thickening and sclerosis of the facial bones bilaterally with complete obliteration of the right maxillary antrum is seen. Note also the sclerotic changes in the left skull vault.

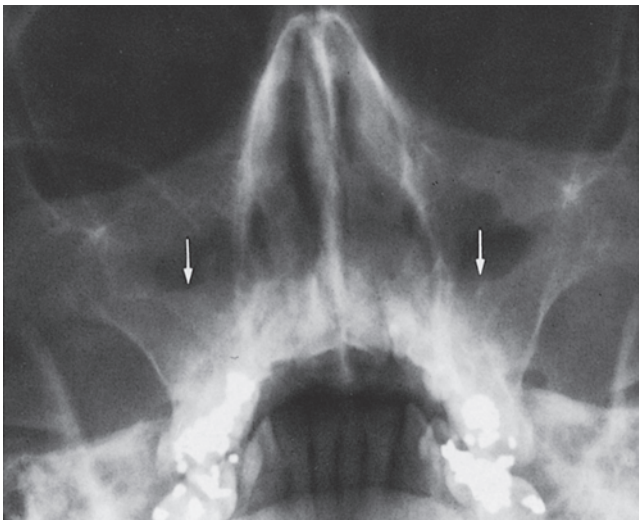

Fig. 10.**13** **Acute sinusitis.** Bilateral soft-tissue thickening and air-fluid levels (arrows) are seen in both maxillary antra. A viral upper respiratory tract infection preceded this examination.

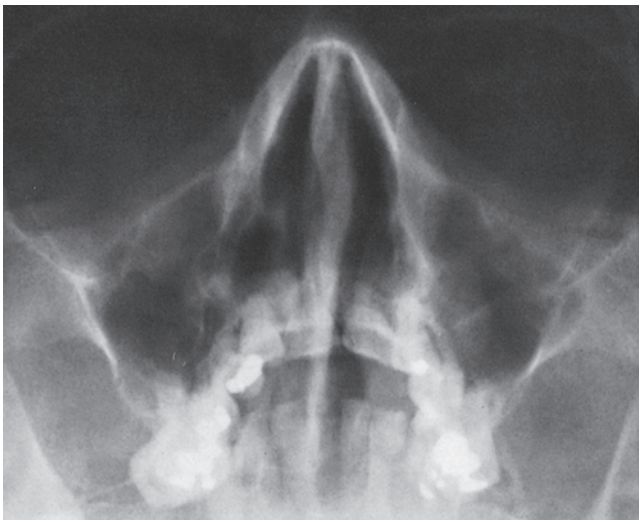

Fig. 10.**14** **Acute sinusitis.** Polypoid soft-tissue thickening in both maxillary antra is found in this patient with allergic history.

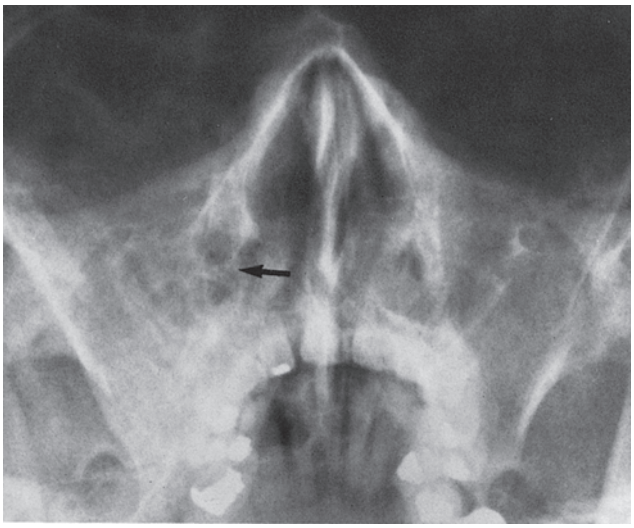

Fig. 10.**15** **Chronic granulomatous sinusitis.** Complete opacification of both maxillary antra with localized destruction of the medial wall on the right side (arrow) is caused by aspergillosis.

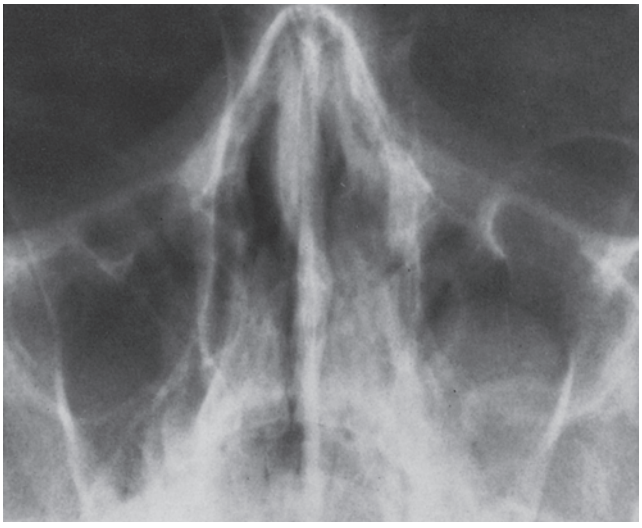

Fig. 10.**16** **Retention cyst.** A large polypoid soft-tissue density is seen in the base of the left maxillary antrum.

Table 10.1 (Cont.) Soft-tissue Thickening or Mass in Paranasal Sinuses

Lesion	Radiographic Appearance	Comments
Mucocele (Fig. 10.17)	Most common in frontal sinus, May occasionally produce an increased translucency of involved sinus when thinning of the adjacent bone outweighs the increased density from the fluid content. Erodes into neighboring structures (see also Fig. 9.**6).**	Develops when ostium of sinus remains closed after an infection has subsided. Retained aseptic fluid produces changes by pressure erosion. *Osteomas*, which are also most commonly found in the frontal sinus, have a much greater density than mucoceles and should not be confused with the latter (Fig. 10.18).
Fracture (see Fig. 10.1)	Localized submucosal hematoma may simulate polyp (e.g., blowout fracture: polypoid mass on antral roof). Air-fluid (blood) level may be present. Partial to complete sinus opacification may be found in an acute fracture or as sequela of an old fracture. Complex facial fractures include *blowout fractures of the orbit* (see Fig. 10.**2**), *tripod fracture* (Fig. 10.**19**), and *Lefort fractures* (Fig. 10.**20**).	In *barotrauma* (e.g., among divers and pilots of unpressurized aircraft) similar changes can be found. In this condition, polypoid mucosal swelling to complete opacification of a sinus is caused by submucosal hemorrhage, mucosal thickening, and/or outpouring of secretion.

Fig. 10.**17** **Mucocele.** A slightly lobulated soft-tissue mass is seen in the base of the left frontal sinus that is unusually large.

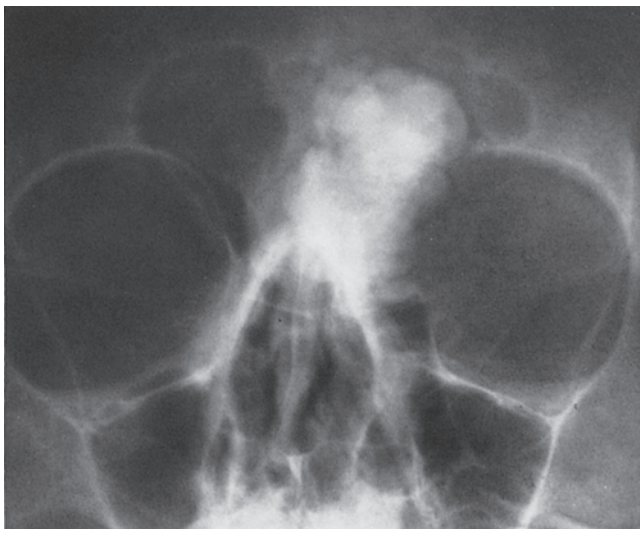

Fig. 10.**18** **Osteoma.** A very dense, structureless, and lobulated lesion involving the left frontal and ethmoidal sinuses is seen.

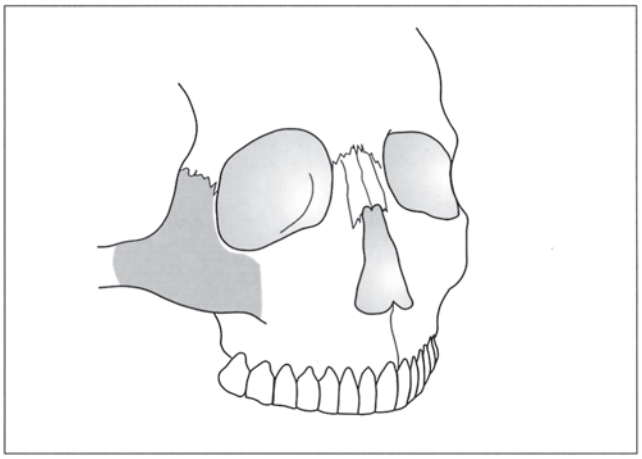

Fig. 10.**19** **Tripod fracture.** Fracture sites include the frontozygomatic suture, zygomatic arch, and lateral wall of maxillary sinus with the anterior orbital rim.

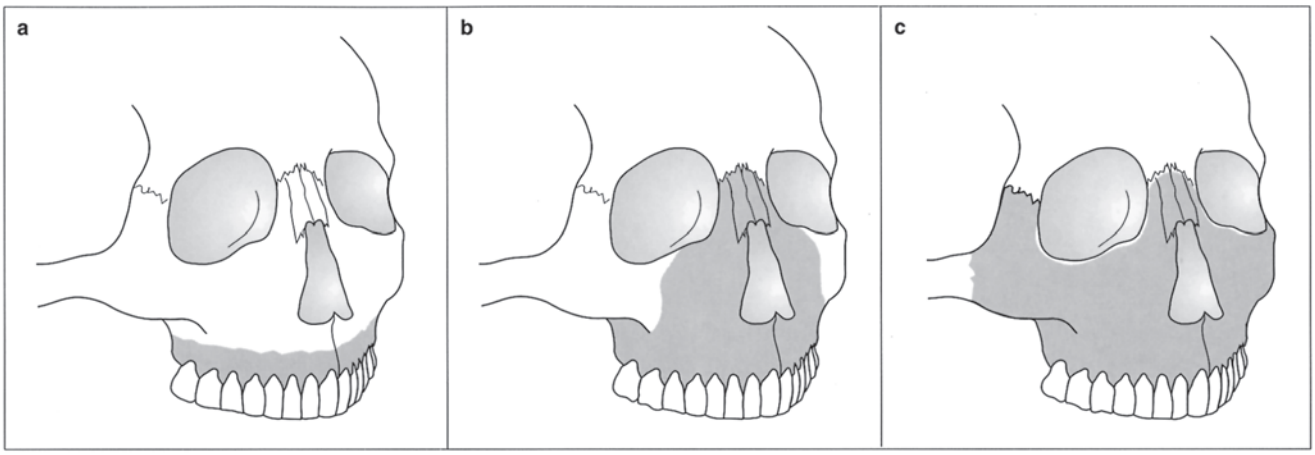

Fig. 10.**20** **Lefort fractures. a** Lefort I: horizontal fracture line extending across the floor of the maxillary sinus above the dentition line ("floating palate"). **b** Lefort II: fracture runs vertically through the maxilla and across the nasal bridge and back to the pterygoid plates ("floating maxilla"). **c** Lefort III: fracture line passes across the bridge of the nose, orbits, and frontozygomatic sutures into the zygomatic arches and pterygoid plates ("floating face").

11 Jaws and Teeth

Calcifications in the soft tissues around the jaws may be caused by the same conditions as anywhere else in the body. They are commonly arteriosclerotic in origin or due to calcified lymph nodes secondary to granulomatous disease. These conditions must, however, be differentiated from *salivary gland calcifications*, which are usually caused by salivary calculi. They are radiopaque in approximately 80% because of their high calcium carbonate content and occur most often in the submandibular glands, less commonly in the parotid glands, and virtually never in the sublingual glands. A salivary stone tends to be oval in shape and usually has a relatively homogeneous density (Fig. 11.**1**).

Dysfunction of the temporomandibular joint may affect as many as 25% of the adult population and causes a variety of clinical symptoms ranging from headache to myofascial pain. This entity has gained increasing attention in recent years and is now referred to as temporomandibular joint syndrome. Unfortunately, plain film radiography is generally of little use in evaluating this condition, since in the vast majority of cases the disorder is related to an abnormality of the meniscus that divides this joint, and hence arthrography, computed tomography, or magnetic resonance imaging is required for proper diagnosis. In far-advanced cases, flattening or atrophy of the mandibular head, flattening of the articular tubercle, sclerosis, cysts, and spur formations around the joint may be seen with conventional radiographic technique (Fig. 11.**2**).

In the jaws, many pathologic conditions are related to the teeth. The emphasis in the remaining part of this chapter is on the differential diagnosis of these odontogenic lesions. The radiographic presentations of nonodontogenic lesions that may be confused with odontogenic lesions will be briefly discussed. For a more complete differential diagnosis of nonodontogenic lesions, the reader should refer to Chapters 1, 2, and 5.

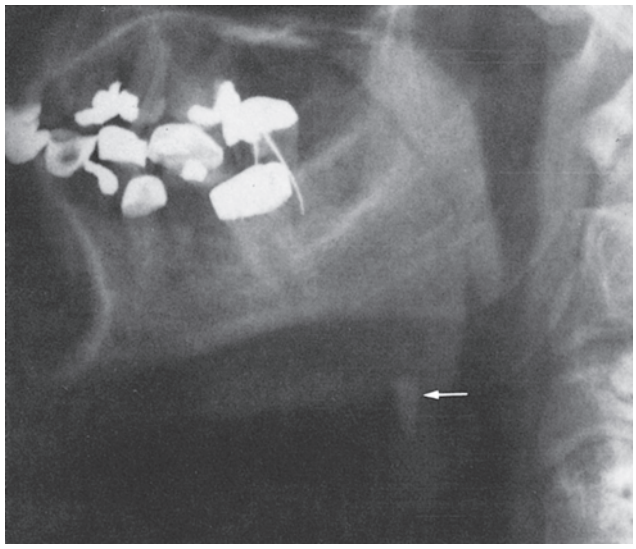

Fig. 11.**1** **Submandibular gland calculus.** An ovoid soft-tissue calcification (arrow) is seen below the right mandibular angle.

Fig. 11.**2** **Advanced degenerative changes in the temporomandibular joint** (tomography). Anterior spur and degenerative cyst are seen in the deformed and sclerotic head of the condylar process. There is also considerable flattening of the articular tubercle located anteriorly to the glenoid fossa, with significant sclerosis of both these structures.

Periodontal Abnormalities

The periodontium represents the supporting structure of the teeth comprising gingiva, periodontal ligament (membrane), alveolar bone, and cementum (Fig. 11.**3**). Radiographically, the cementum outlining the roots of the teeth cannot be differentiated from dentin. The periodontal membrane, evident radiographically as a radiolucent line of less than 1 mm in width, separates the root of a tooth in its socket from the alveolar bone of the jaw. A thin cortical line, the lamina dura, demarcates the latter from the periodontal membrane. From this observation, it becomes obvious that periodontal pathology can manifest itself radiographically as loss of lamina dura, widening of the periodontal membrane, or both. These subtle changes cannot, however, be appreciated with conventional x-ray technique, and require special dental films with high resolution for proper evaluation. Excessive bone resorption around the root of a tooth is commonly referred to as *"floating tooth."*

Resorption of the lamina dura is common in primary and secondary *hyperparathyroidism*. In this condition, it is usually not associated with an appreciable widening of the periodontal membrane space. Reappearance of the lamina dura occurs after proper treatment. A generalized loss of the

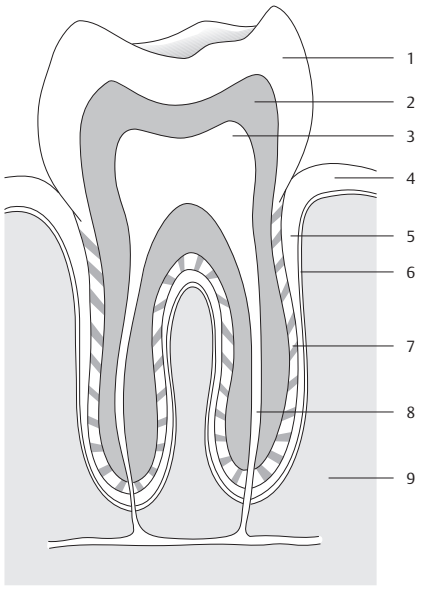

Fig. 11.**3** **Anatomy of a normal molar tooth.** 1 Enamel; 2 dentin; 3 pulp; 4 gum; 5 periodontal membrane; 6 lamina dura; 7 cement; 8 apical canal; 9 alveolar bone.

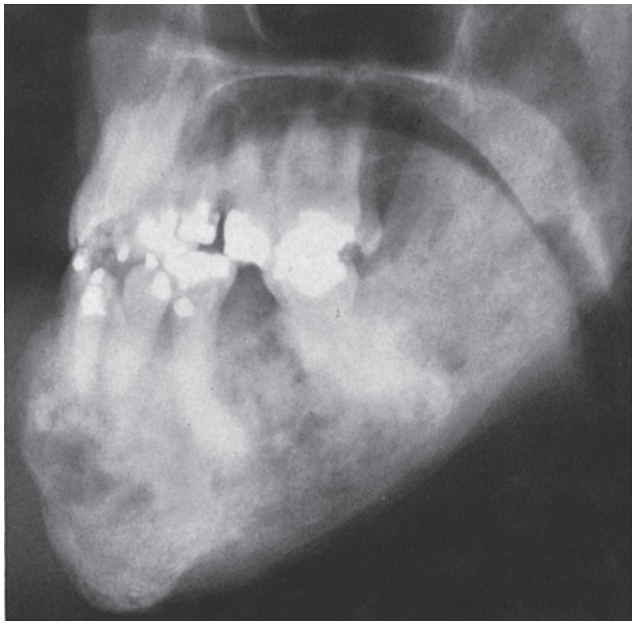

Fig. 11.**4** **Paget's disease.** Thickening and sclerosis of the mandible resulted in an apparent loss of the lamina dura around the teeth.

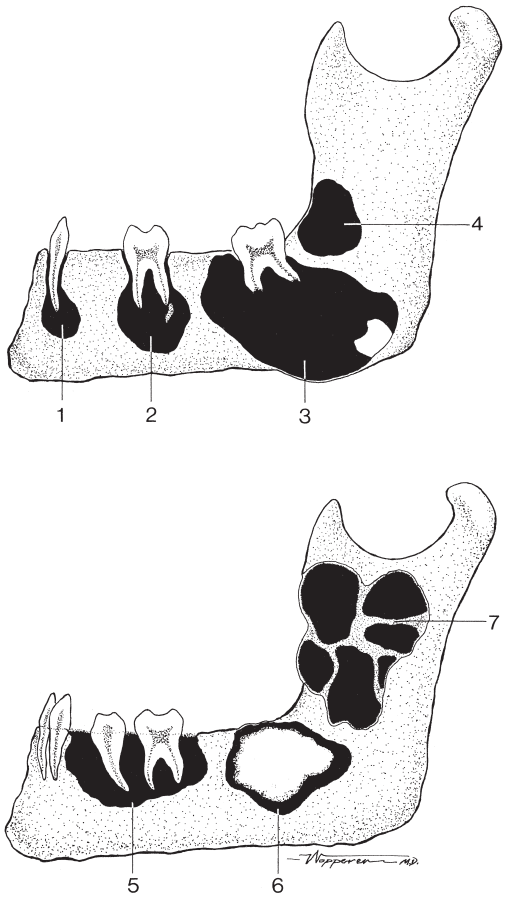

Fig. 11.**5 a, b** **Lytic mandibular lesions.** 1 Dental granuloma; 2 periodontal cyst (occasionally containing small root remnant); 3 dentigerous cyst; 4 primordial cyst; 5 "floating teeth" (e.g., eosinophilic granuloma; 6 odontoma); 7 ameloblastoma.

lamina dura can also be found with *osteoporosis* of any etiology (e.g., senile, steroid therapy, Cushing's syndrome), but in these cases remnants of the lamina can often still be recognized unless the osteoporosis has progressed so far that the correct diagnosis can easily be established by other radiographic findings. In both *periodontosis* (non-inflammatory, degenerative) and *periodontitis* (inflammatory), resorption of bone including the lamina dura occurs characteristically around the neck and proximal part of the root of a tooth while the lamina dura around the apex remains intact. If the process proceeds to a *periodontal abscess*, resorption of the entire lamina dura combined with widening of the periodontal membrane space may be found.

The radiographic absence of lamina dura is not only the result of its resorption but may also be caused by an increase in bone density of the adjacent cancellous bone as seen, for example, in *sclerosing osteomyelitis*. The radiographic loss of lamina dura observed in *Paget's disease* (Fig. 11.**4**), *fibrous dysplasia*, and *osteomalacia* is commonly the result of both bone resorption and sclerosis.

The width of a normal periodontal membrane space measures radiographically less than 1 mm. Generalized *widening of the periodontal membrane space* with intact lamina dura is characteristic for *scleroderma*, but may also be found in patients with the *habit of forcibly clenching the teeth*. The most common cause for a localized widening of the periodontal gap associated with resorption of the lamina dura is a severe inflammation such as *periodontal abscess*. More extensive bone resorption around one or several teeth produces radiographically the impression of *"floating teeth."* In addition to a periodontal abscess, this finding is common in *eosinophilic granuloma (Langerhans cell histiocytosis)*, but may also be encountered in any other condition producing a large lytic lesion such as *ameloblastoma, lymphoma, leukemia, multiple myeloma, metastases,* and *odontogenic lesions*.

Localized lytic lesions of odontogenic origin can represent an inflammatory, cystic, or neoplastic process or may be a developmental anomaly. The most common lytic lesions in

the mandible are shown schematically in Fig. 11.**5**, while their more complete differential diagnosis is discussed in Table 11.**1**.

Only a few localized sclerotic lesions are unique for the jaw. *Odontomas* consist of an irregular opaque mass of different dental tissues such as enamel, dentin and cementum surrounded by a radiolucent line or band representing the fibrous capsule. Symmetric and bilateral sclerotic bony protuberances are occasionally found in the midline of the palate or along the lingual surface of the mandible (primarily in the canine-premolar region) and are termed *torus palatinus* and *mandibularis*, respectively. These are benign static growths without clinical significance. They must be differentiated from *osteomas*, which are protruding mass lesions composed of abnormally dense bone that is formed in the periosteum. They are most common in the skull and facial bones.

Table 11.1 Differential Diagnosis of Lytic Lesions in the Jaw

Lesion	Radiographic Appearance	Comments
Periodontal abscess	Localized poorly to well-defined defect in the periphery of a tooth.	*Periodontitis* is an extension of gingivitis to the underlying periodontal tissues. An abscess develops usually in a periodontal pocket that is partially or completely occluded, or is occasionally caused by a foreign body lodged in the periodontium.
Periapical abscess	Localized poorly to well-defined defect around the apex of a tooth.	Results from progression of pulpitis. In the acute stage, the tooth is extremely painful and tender to percussion. In the chronic stage, draining sinuses to the oral cavity, maxillary antra and even the surface of the skin may occasionally develop.
Periapical granuloma	Round or oval, fairly well-circumscribed radiolucency rarely exceeding 1 cm in diameter. May ultimately be transformed into periodontal cyst.	Forms as the reparative process following the resolution of a periapical abscess.
Periodontal cyst (dental, radicular or apical cyst) (Fig. 11.6)	Sharply defined radiolucent lesion with thin sclerotic margin, measuring from a few millimeters to several centimeters. Rarely remnants of the root of a primary tooth are found within the lesion. Bone expansion can be found with an enlarging cyst.	Most common cyst of jaw. Epithelium-lined sac, usually situated at the apex of the root. Acquired and probably of inflammatory origin (see periapical granuloma). A *residual cyst* (Fig. 11.**7**) is a cystic lesion remaining after tooth removal. Occasionally infected, particularly when root of tooth is retained (residual infection). *Multiple cysts* are rare and either developmental or associated with extensive caries.
Dentigerous cyst (follicular cyst) (Fig. 11.8)	Sharply defined, oval or round radiolucent lesion varying in size from 1 cm to a large expansile defect involving both the body and ramus of the mandible. The lesion characteristically contains the *crown of an unerupted tooth.*	Arises from the follicle of an unerupted tooth and is usually found in young persons. Cysts eventually destroyed by late tooth eruption have been referred to as "*eruptive cysts*."

(continues on page 248)

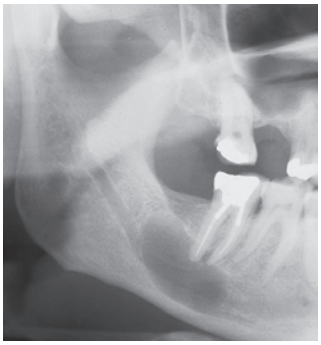

Fig. 11.**6** **Periodontal cyst**. A well defined radiolucent lesion with very thin sclerotic margins involving the apex of the roots of the last molar is seen.

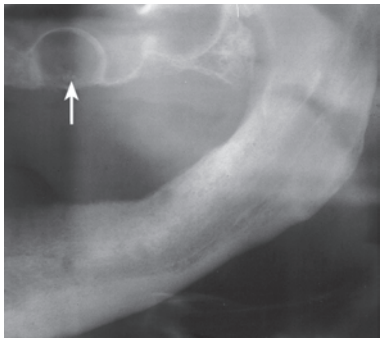

Fig. 11.**7** **Resdiual cyst.** A cystic lesion with sclerotic border is seen in the maxilla (arrow). Irregular thickening and sclerosis of the left body and ramus of the mandible is also evident due to *sclerosing osteomyelitis of Garré.*

Fig. 11.**8** **Dentigerous cyst.** A sharply defined, lytic lesion containing a molar crown is seen involving the left body of the mandible.

Table 11.1 (Cont.) Differential Diagnosis of Lytic Lesions in the Jaw

Lesion	Radiographic Appearance	Comments
Primordial cyst (Fig. 11.9)	Purely lytic, well-marginated, unilocular, round or oval lesion most commonly located posterior of the third molar in the angle or ramus of mandible.	Develops from embryonal tooth sac before any calcified structures have been formed.
Keratocyst (Fig. 11.10)	Radiolucent, often multiloculated lesion with smooth or scalloped border located in the body or ramus of the mandible. Occurs frequently in conjunction with impacted tooth. Differentiation from an ameloblastoma is often not possible.	Account for 5 to 10 % of all jaw cysts and have a high recurrence rate. Multiple keratocysts can be found in *Gorlin's syndrome*, where they are associated with nevoid basal cell carcinomas and soft tissue calcifications. Other bony abnormalities include small flame-shaped cystic lesions and sclerotic foci, bifid ribs and anomalies of the spine and hands.
Fissural cyst	Most commonly located in midline of mandible or maxilla (e.g., incisive canal cyst or nasopalatine cyst), rarely lateral (e.g., globulomaxillary cyst between lateral incisor and canine tooth).	Arises from the epithelial remnant of an existing fissure or suture (sites of embryonic fusions).
Solitary bone cyst of the mandible (traumatic cyst) (Fig. 11.11)	In general relatively poorly defined and irregular radiolucency of varying size usually located in the body of the mandible. Larger lesions characteristically have a scalloped superior border that appears to undulate around the roots of teeth into the interdental bone. The teeth are neither splayed nor loosened.	Occurs most often in younger persons. History of trauma often present ("traumatic" or "hemorrhagic" cyst). May regress spontaneously.
Ameloblasioma (adamantinoma) (Fig. 11.12)	Unilocular or more commonly multilocular cystic (bubble-like) appearance often with coarse trabecular structures filling in part of the cystic cavities. Size varies from 1 cm to huge tumors causing cortical expansion or destruction with deformity of the face. Rarely, a small tumor mimics a simple cyst.	Most common tumor of the mandible that can occur at any age but is usually diagnosed after 30 years of age. Local invasion into surrounding structures and even distant metastases occur. *Adenoameloblastoma* (Fig. 11.**13**) and *ameloblastic fibroma* are rare tumors occurring both in the first two decades of life. They are clinically less aggressive than ameloblastomas. Clusters of calcifications and retained teeth may be found in these lesions.
Calcifying epithelial odontogenic tumor (Pindborg tumor) (Fig. 11.14)	Similar to ameloblastoma, but more dense when the characteristic honeycomb appearance is present within the lesion.	Clinical behavior similar to ameloblastoma: Locally invasive and tendency to recur.

(continues on page 250)

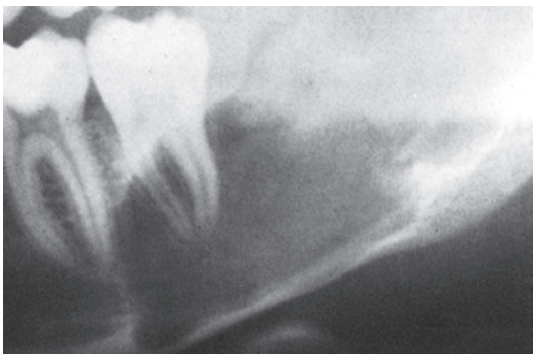

Fig. 11.**9** **Primordial cyst.** A well-defined cystic lesion is seen in the angle of the left mandible.

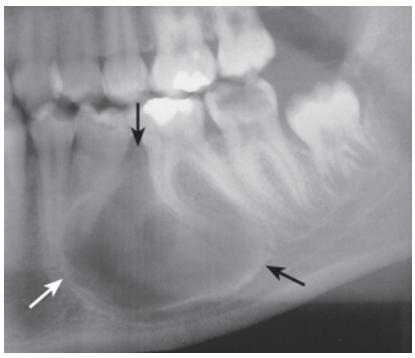

Fig. 11.**10** **Keratocyst**. A lytic lesion with partially sclerotic border (arrows) is seen in the body of the left mandible.

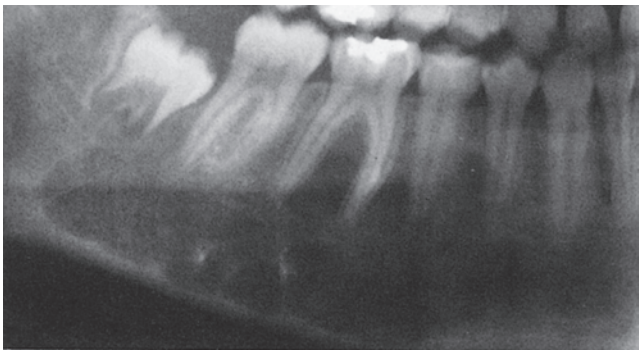

Fig. 11.**11** **Solitary (traumatic) cyst of the mandible.** A poorly-defined radiolucency with scalloped margins involving large portions of the right mandibular body extends superiorly between the roots of the teeth.

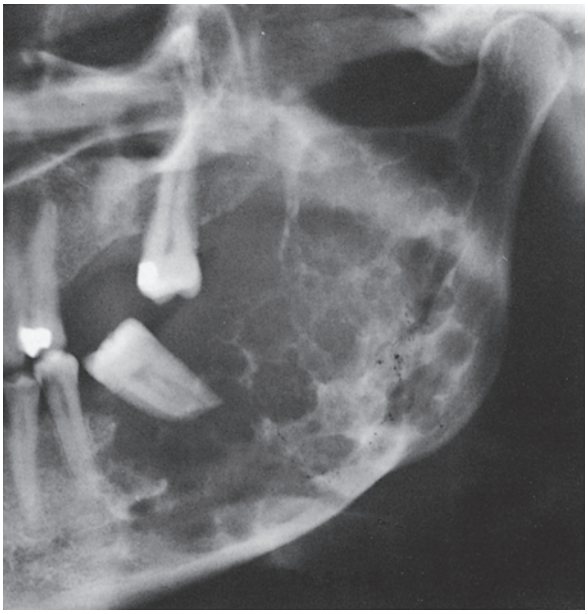

Fig. 11.**12 a, b** **Ameloblastoma** (2 cases). **a** A multilocular cystic and slightly expansile lesion with cortical thinning involves the left ramus and part of the adjacent body of the mandible. **b** A more aggressive lesion with soap-bubble appearance in similar location caused destruction of the cortex and resorption of the roots of an encroached molar.

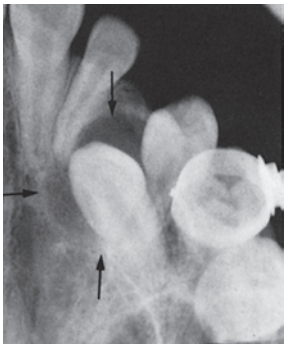

Fig. 11.**13** **Adenoameloblastoma.** A cystic lesion (arrows) associated with an unerupted tooth is characteristic.

Fig. 11.**14** **Calcifying epithelial odontogenic tumor** (Pindborg). A lytic lesion with honeycomb appearance and small calcifications is seen.

Table 11.1 (Cont.) Differential Diagnosis of Lytic Lesions in the Jaw

Lesion	Radiographic Appearance	Comments
Odontoma (Figs. 11.15–21)	Well-circumscribed lesion containing varying amounts of different dental tissues evident usually as radiopaque material.	Odontomas represent abnormal developments of dental tissue and should be regarded rather as hamartomatous lesions than true neoplasms. Histologically ameloblastic (Fig. 11.**15**), complex (Fig. 11.**16**), and compound odontomas (Fig. 11.**17**), dentinoma (Fig. 11.**18**), odontogenic fibromyxoma (Fig. 11.**19**), and cementoma (Fig. 11.**20**) are distinguished. Hypercemtosis (Fig. 11.**21**) is excessive formation of cementum on the surface of the root of a tooth.

(continues on page 251)

Fig. 11.**15** **Ameloblastic odontoma.** A well-circumscribed cystic lesion containing a crown of a molar and amorphous opaque material is seen.

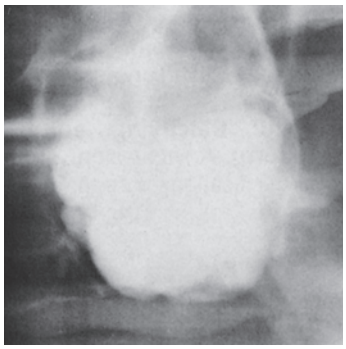

Fig. 11.**16** **Complex odontoma.** A cystic lesion containing a very dense and homogeneous mass with a somewhat irregular outline is evident

Fig. 11.**17** **Compound odontoma.** A lesion containing several dwarfed and misshapen teeth is seen.

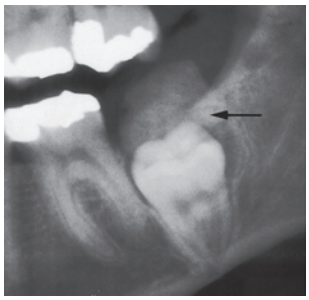

Fig. 11.**18** **Dentinoma.** A radiopaque lesion (arrow) projects characteristically on top of the crown of an unerupted molar.

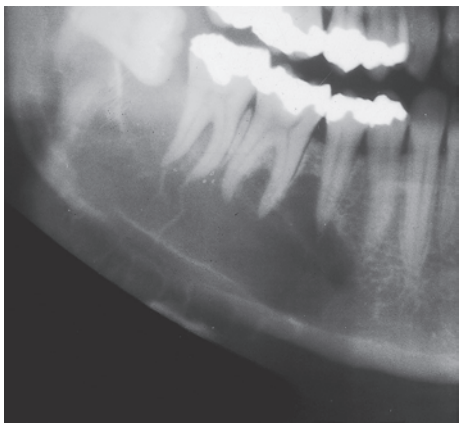

Fig. 11.**19** **Fibromyxoma.** A poorly-defined radiolucent lesion extending superiorly between the roots of the teeth and eroding the inferior cortex is seen in the body of the mandible. The lesion is traversed by a few very delicate septa, some of which appear to extend beyond the eroded inferior cortex, giving it the appearance of a perpendicular periosteal reaction.

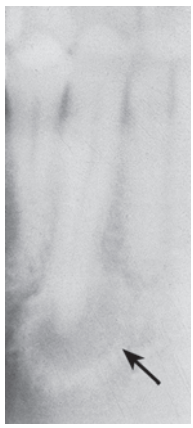

Fig. 11.**20** **Cementoma**. A slightly radiopaque lesion with sclerotic border (arrow) is around the right lower canine.

Fig. 11.**21** **Hypercementosis**. Poorly defined radiopaque material (cement) is formed around the apex of the root of the left second mandibular molar.

Table 11.1 (Cont.) Differential Diagnosis of Lytic Lesions in the Jaw

Lesion	Radiographic Appearance	Comments
Stafne's mandibular defect (Fig. 11.22)	Round cyst-like lesion with dense sclerotic border located anterior to the mandibular angle. The continuity of the inferior border may be interrupted.	Developmental defect in the mandible caused by an accessory salivary gland. Sialography is diagnostic. Incidental finding in routine dental or mandibular radiography.
Nonodontogenic benign tumor	Similar to counterparts occurring elsewhere (see Chapter 5).	Rare. Aneurysmal bone cyst, giant cell tumor, hemangioma, neurofibroma, etc.
Gnathic osteosarcomas (Figs. 11.23 and 11.24)	Purely lytic, mixed or purely osteoblastic lesion originating in the mandible or less frequently in the maxilla.	Account for 8 % of all osteosarcomas. Differ from conventional osteosarcomas by the older age of onset (average age about 30 years) and decreased tendency for metastases.
Nonodontogenic primary malignant tumor (Fig. 11.25)	Similar to counterparts occurring elsewhere (see Chapter 5).	Rare. Fibrosarcoma, Ewing's sarcoma, chondrosarcoma, lymphoma and plasmacytoma occur.
Metastases (Fig. 11.26)	Similar to counterparts elsewhere (see Chapters 1, 2, and 5).	Hematogenous or per continuitatem from malignancy of oral or nasal cavity, salivary gland or skin.

(continues on page 252)

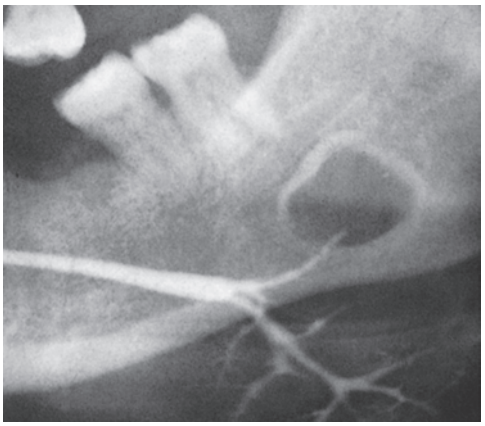

Fig. 11.**22** **Stafne's mandibular defect.** A round, cyst-like defect with a dense sclerotic border located anterior to the mandibular angle is caused by an accessory salivary gland . Sialography demonstrates the accessory duct draining this area.

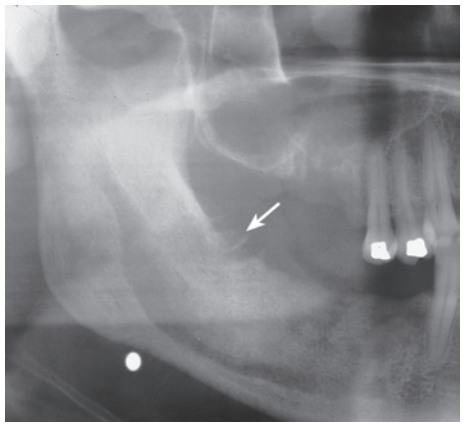

Fig. 11.**23** **Gnathic osteosarcoma**. A poorly defined, mixed osteolytic and osteoblastic lesion with violation of the superior cortex and small radiating spicule formation (arrow) is seen in the right body and angle of the mandible.

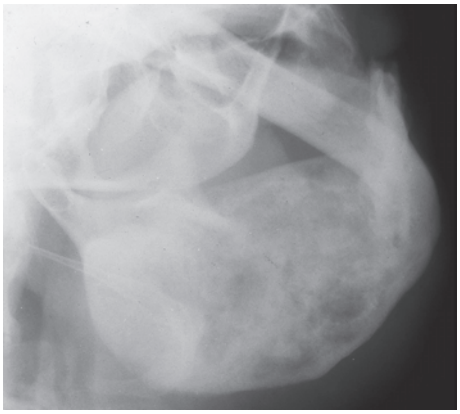

Fig. 11.**24** **Gnathic osteosarcoma**. A relatively well marginated and predominantly osteoblastic lesion with marked expansion but no definite cortical violation is seen in the body and ramus of the mandible.

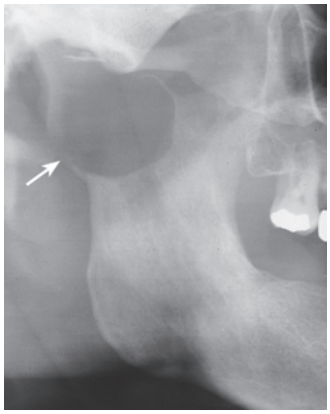

Fig. 11.**25** **Burkitt's lymphoma**. An expansile, well-defined, purely osteolytic lesion with minimal cortical violation (arrow) is seen in the ramus and condylar process of the right mandible.

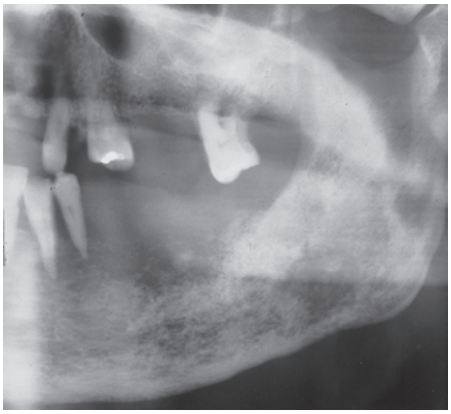

Fig. 11.**26** **Bronchogenic carcinoma metastasis.** A poorly defined, destructive osteolytic lesion is seen in the left mandible.

Table 11.1 (Cont.) Differential Diagnosis of Lytic Lesions in the Jaw

Lesion	Radiographic Appearance	Comments
Fibrous dysplasia (Fig. 11.27 and 11.28)	Expansile, lytic-to-sclerotic, fairly well circumscribed, unilateral lesion. Polyostotic form less common. The *ossifying fibroma* (/Fig. 11.**29)** of the jaw is a well-circumscribed slowly growing, expansile lesion measuring up to 5 cm in diameter with radiographic features similar to fibrous dysplasia.	"*Leontiasis ossea*" (deformity and bilateral enlargement of the face) is usually caused by widespread involvement with fibrous dysplasia. Similar changes, but usually without the sclerotic component, can be found in *neurofibromatosis* (Fig. 11.**30**).
Cherubism (hereditary fibrous dysplasia of the jaw)	Symmetrical enlargement of the mandible (especially in the region of the angles) by fibrous and cystic changes. Tooth anomalies (agenesis, noneruption, and displacement) are associated. Maxillary tuberosities are occasionally also involved.	Histologically indistinguishable from fibrous dysplasia, but autosomal dominant inherited and without manifestations outside the jaws. Develops as early as one year of age, and regresses after puberty.
Paget's disease (see Fig. 11.4)	Lytic, mixed, and sclerotic phase of the disease occurs. Loss of lamina dura in the involved bone. Gross enlargement of the mandible in the mixed and sclerotic phase is common.	Rarely in patients under 40 years of age.
Langerhans cell histiocytosis (eosinophilic granuloma) (Fig. 11.31)	Lytic lesion with "teeth floating in space" characteristic.	
Hyperparathyroidism	Generalized loss of lamina dura without widening of the periodontal membrane, Brown tumors (often multiple) may be evident as cystic lesions.	

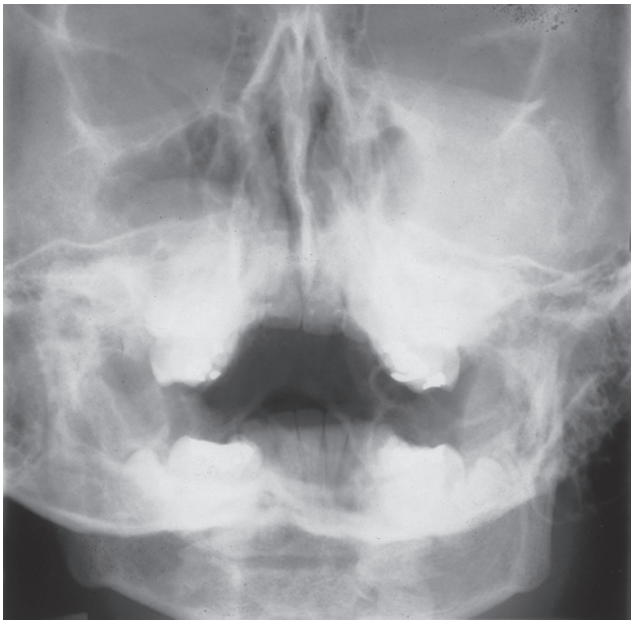

Fig. 11.**27** **Fibrous dysplasia.** Deforming sclerotic lesions are seen in the facial bones with main involvement of the left maxilla.

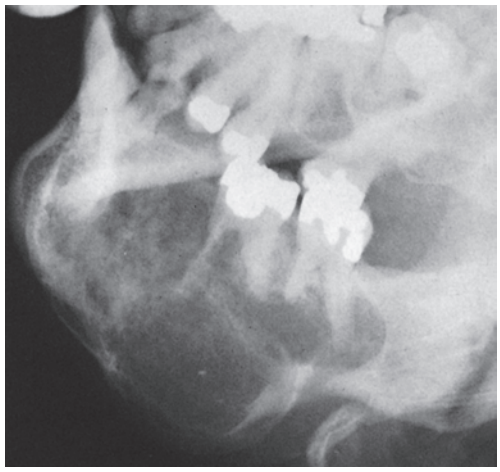

Fig. 11.**28** **Fibrous dysplasia.** An expansile, mixed lytic and sclerotic lesion is seen in the right mandibular body.

Fig. 11.**29** **Ossifying fibroma.** A lobulated, mixed osteolytic and osteoblastic lesion with slight bone expansion is seen in the body of the mandible.

Fig. 11.**30** **Neurofibromatosis.** Multiple, poorly defined, lytic areas are seen in the grotesquely, but somewhat asymmetrically enlarged mandible.

Fig. 11.**31** **Langerhans cell histiocytosis** (eosinophilic granuloma). A lytic lesion is seen in the left mandible around the last molar, that appears to float in space.

12 Spine and Pelvis

Spine

The development, structure, and function of the spine is complex. Consequently a great number of either primary or secondary abnormalities are encountered in various portions of the spinal column. Intraspinal lesions may not cause an abnormality on plain films despite serious clinical symptoms. In such cases MRI is advisable. In order to detect all available information from plain films, one should inspect them in a systematic fashion, paying attention to a number of different features.

The *alignment* of vertebrae in the normal spine includes a forward curvature (kyphosis) in the thoracic portion and a backward curvature (lordosis) in the cervical and lumbar portions. *Loss of normal curve* or straightening of the spine, often secondary to muscular spasm of variable etiology, may be difficult to evaluate in films taken on a Bucky table. The true extent of anteroposterior curves, as well as eventual lateral curvatures (*scoliosis*), is better evaluated in a weight-bearing (standing) position, if such positioning is not contraindicated by acute spinal trauma. Likewise, slippage of one vertebral body on the next either *forward* (*spondylolisthesis*) or *backward* may be better appreciated by taking flexion and extension views in a weight-bearing position.

A number of congenital or acquired diseases cause either general or local changes in the *size, shape, structure,* and/or *density* of the vertebral bodies and neighboring disk spaces. Such changes may or may not involve the neural arch. Plain films do not show intervertebral disks. For the evaluation of disk degeneration, protrusion or prolapse, MRI should be used. Facet joints are seen in plain films but for accurate evaluation of facet joint abnormalities and associated effects on root channels or spinal canal, a multislice CT examination or MRI is required.

Tables 12.**1** and 12.**2** are lists of some cardinal roentgen features of the spine and pelvis, respectively. They may serve as a reference point for differential diagnosis.

The *occipitovertebral junction* is developmentally a specialized area presenting a number of congenital anomalies. The latter as well as some acquired abnormalities of the upper cervical spine have radiographic features not seen elsewhere in the spinal column, and are presented in Table 12.**3**. Table 12.**5** presents a list of localized abnormalities involving the spine and their radiographic characteristics. Tumors involving the pelvis are presented together with tumors of the spine in Table 12.**6**. A more detailed discussion of bone tumors, including spine and pelvic bones, is found in Chapter 5.

Cervical spine fractures are caused by hyperflexion, hyperextension, hyperrotation, hyperflexion and rotation, lateral hyperflexion, and vertical compression. Fractures of spinal column are summarized in Table 12.**4**.

Pelvis

Sacrum and coccyx are an integral part of the pelvis, although they essentially belong to the spine. Localized abnormalities of the sacrum, coccyx, and the rest of the pelvic girdle are therefore presented here together. Localized processes in the pelvic bones are not different radiographically from similar lesions in any flat bone. Abnormal *size and shape of the pelvis* may be typical of some congenital syndromes.

Involvement of *sacroiliac joints* may have great differential diagnostic significance. Early changes in the sacroiliac joints may be difficult to recognize, especially in young patients, whose sacroiliac joints are not completely ossified. *CT* and *MRI* cross-sectional images are helpful in demonstrating subtle changes. The involvement of sacroiliac joints in arthritides has been discussed already in Chapter 6, and is only briefly summarized in Table 12.**2**. Table 12.**7** presents localized lesions usually involving the pelvis only.

Conditions Involving Both Spine and Pelvis

Abnormal size and shape of the pelvis may be typical of some congenital syndromes. Often they also present with spinal abnormalities. Many of the rare congenital syndromes are not included. The reader should consult texts of pediatric bone radiology in cases of rare congenital osteochondrodysplasias. Table 12.**8** presents some congenital and acquired conditions with both pelvic and spinal radiographic findings.

Fractures of Spine

Fractures of the spine are summarized in Table 12.**4**. All seven cervical vertebral bodies must be visible on radiographs. In a case when good quality radiographs can not be obtained one has to consider CT imaging. Multiple fractures occur frequently. Multislice CT with reformats is nowadays highly recommended when serious spinal fracture is suspected. Multislice CT often reveals fractures not seen on radiographs.

Table 12.1 Some Radiographic Changes Characteristic of the Spine and Their Differential Diagnosis

Radiographic Finding	An Alphabetical List of Causes
Kyphosis, scoliosis or kyphoscoliosis 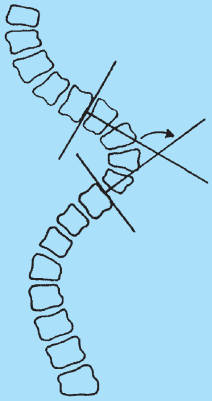	Chest wall abnormality (congenital or postoperative rib abnormality) Chronic unilateral lung disease Congenital spinal anomaly (e.g., fused vertebrae, vertebral hypoplasia or hemivertebra, dysraphism, rachischisis) Congenital syndromes (achondroplasia, cretinism, mucopolysaccharidosis, neurofibromatosis, osteogenesis imperfecta, etc.) Fracture, traumatic or pathologic, dislocation Idiopathic or postural Infection (spondylitis, tbc) Neoplastic (metastatic, multiple myeloma, primary tumor) Neuromuscular disorders Osteoid osteoma of the spine Osteoporosis (most often senile or postmenopausal) Paget's disease Rheumatoid or ankylosing spondylitis Scheuermann's disease (adolescent kyphosis) Neurotrophic spine (Charcot spine) Spasm due to an abdominal or retroperitoneal disease
Atlantoaxial subluxation (> 3 mm, children > 5 mm) 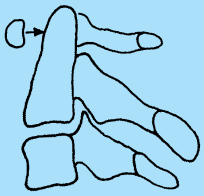	Ankylosing and psoriatic spondylitis Congenital cervicobasilar anomaly Down's syndrome Juvenile rheumatoid arthritis Morquio's syndrome Pseudogout Retropharyngeal abscess in a child Rheumatoid arthritis (common, see Chapter 6) Trauma (fracture or torn ligaments)
Increased diameter of one or more vertebrae 	Acromegaly Benign bone tumor (hemangioma, giant cell tumor, aneurysmal bone cyst, osteoblastoma) Butterfly vertebra Compression fracture Fibrous dysplasia Paget's disease (sclerosis, framed) Hydatid disease (echinococcus) (uncommon) Scheuermann's disease (increased sagittal diameter) (common) (Degenerative ligamentous ossification)
Increased height of one or more vertebrae 	Arachnodactyly Compensatory growth (from non-weight bearing) Congenital or block vertebra
Biconcave vertebral bodies 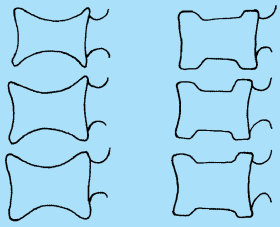 **"Fish vertebra"** **Steplike endplate depression**	Gaucher's disease (fish vertebra) Hereditary spherocytosis (fish vertebra) Homocystinuria (fish vertebra) Osteopenia (fish vertebra) (common) Renal osteodystrophy (fish vertebra) Sickle cell anemia (central steplike endplate depression or fish vertebra) Thalassemia major (rarely) (fish vertebra)

(continues on page 257)

Table 12.1 (Cont.) Some Radiographic Changes Characteristic of the Spine and Their Differential Diagnosis

Radiographic Finding	An Alphabetical List of Causes
Squared vertebral bodies 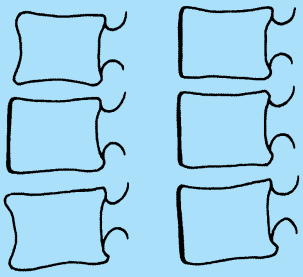	Ankylosing spondylitis (common) Paget's disease Psoriatic arthritis Reiter's syndrome Rheumatoid arthritis
Dense vertebra, solitary or multiple 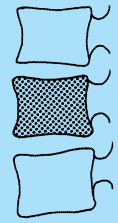 	Homogeneously dense or "ivory" Fluorosis Lymphoma (especially Hodgkin) Myelosclerosis Osteoblastic metastases Osteopetrosis Paget's disease Sclerotic or patchy, nonhomogeneous All the above, plus: Bone island Fracture (compression or healing) Hemangioma Idiopathic hypercalcemia Intervertebral disk disease Mastocytosis Nondiscogenic sclerosis (idiopathic) Osteoblastoma Osteomyelitis Renal osteodystrophy Radiation therapy Sarcoidosis Sarcoma (osteosarcoma, chondrosarcoma, Ewing's) Sickle-cell anemia Tuberous sclerosis
Collapse or flattening of one or more vertebrae 	Aseptic necrosis (Kummel-Verneuil's syndrome) Congenital platyspondyly syndromes (e.g., achondroplasia, mucopolysaccharidosis, osteogenesis imperfecta) Eosinophilic granuloma Fracture (traumatic or pathologic) (common) Hemangioma Hyperparathyroidism Lymphoma Metastasis (pedicle involvement common) Myeloma, plasmocytoma (pedicle involvement rare) Osteomalacia Osteomyelitis Osteoporosis Paget's disease Scheuermann's disease
Anterior scalloping of one or more vertebral bodies 	Aneurysm of aorta Inflammatory lymphadenopathy Lymphoma Metastatic lymph nodes Tuberculosis (spondylitis anterior)

(continues on page 258)

Table 12.1 (Cont.) Some Radiographic Changes Characteristic of the Spine and Their Differential Diagnosis

Radiographic Finding	An Alphabetical List of Causes
Posterior scalloping of one or more vertebral bodies	Achondroplasia Acromegaly Congenital syndromes (arachnodactyly, mucopolysaccharidosis, etc.) Increased intraspinal pressure Neurofibromatosis I (von Recklinghausen's disease) Syringomyelia Tumor of spinal canal
Enlarged intervertebral foramen 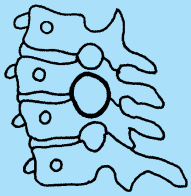	Congenital absence of pedicle Lateral meningocele Neurofibroma, neurinoma (common) Tumor (chordoma, dermoid, lipoma, lymphoma, meningioma, neuroblastoma) Vertebral artery aneurysm or tortuosity
Vertebral pedicle erosion or destruction 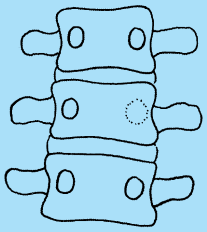	Benign bone tumor (aneurysmal bone cyst, giant cell tumor, hemangiopericytoma) Congenital absence Eosinophilic granuloma Granulomatous disease (tuberculosis, fungus) Intraspinal neoplasm or cyst (neurofibroma, meningioma) Metastasis (common) Multiple myeloma (rare) Syringomyelia
Localized widening of interpedicular distance 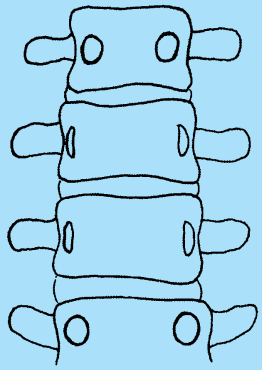	Diasthematomyelia Intrathecal tumors (e.g., ependymoma) Myelocele or meningomyelocele Rotation of vertebra in scoliosis (apparent widening) Hurler's syndrome Morquio's syndrome
Calcification of one or more intervertebral discs (either annulus fibrosus, nucleus pulposus, or both) 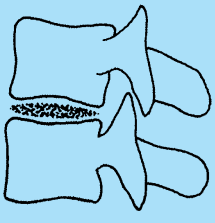	Acromegaly Ankylosing spondylitis Degenerative disk disease Hemochromatosis Hyperparathyroidism Hypervitaminosis D Idiopathic Ochronosis Poliomyelitis Pseudogout Spinal ankylosis for any reason (congenital, DISH, surgical) Transient calcification (in children)

(continues on page 259)

Table 12.1 (Cont.) Some Radiographic Changes Characteristic of the Spine and Their Differential Diagnosis

Radiographic Finding	An Alphabetical List of Causes
Syndesmophytes Ossification of the annulus fibrosus. Thin, vertical, and symmetrical. 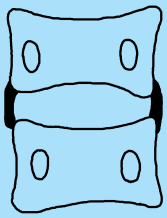	Ankylosing spondylitis Fluorosis Ochronosis (Alkaptonuria)
Paravertebral ossification Ossification of paravertebral connective tissue. Separated from the edge of the vertebral body and disc. 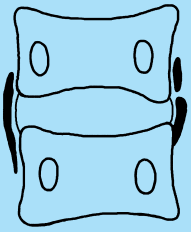	Fluorosis Hypoparatyroidism Psoriatic arthropathy Reiter's syndrome
Osteophytes Arising from the vertebral margin with no gap and having a claw appearance 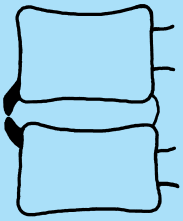	Acromegaly Stress response (spondylosis)
Traction spurs The tip not protruding beyond the horizontal plane of the vertebral endplate 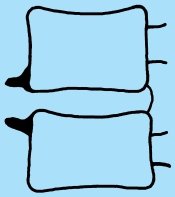	Shear stresses across the disc
Anterior Ossification Undulating ossification of the anterior longitudinal ligament, intervertebral disc, and paravertebral connective tissue 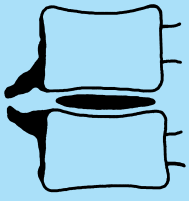	Diffuse Idiopathic Skeletal Hyperostosis (DISH)

Table 12.2 Some Radiographic Changes Characteristic of the Pelvis and Their Differential Diagnosis

Radiographic Finding	An Alphabetical List of Causes
Abnormal size or shape of pelvis 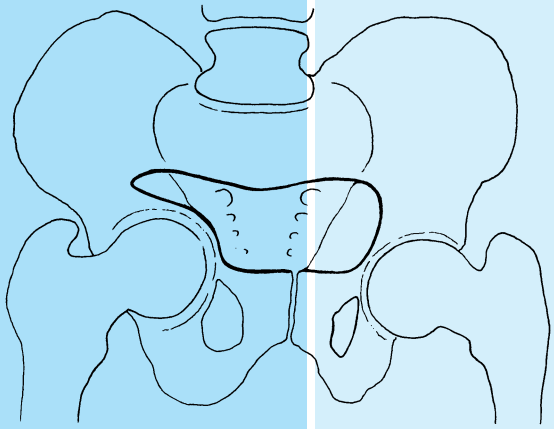	Acquired softening of bone (e.g., Paget's disease, osteomalacia) Congenital syndromes (e.g., achondroplasia, Down's syndrome, mucopolysaccharidosis, hereditary onycho-osteodysplasia) Posttraumatic Rheumatoid arthritis
Protrusio acetabuli 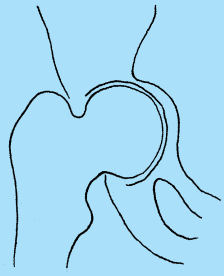	Acquired softening of bone (osteomalacia or rickets, hyperparathyroidism, Paget's disease, irradiation) Congenital or idiopathic (coxa vara with retroversion of the femoral neck, Otto pelvis) Degenerative joint disease, primary or secondary (including hemophilia, pseudogout, hemochromatosis, ochronosis) Infectious arthritis Osteogenesis imperfecta Traumatic (medial dislocation of the hip) Rheumatoid arthritis Rheumatoid variants (especially ankylosing spondylitis)
Widening of the pubic symphysis 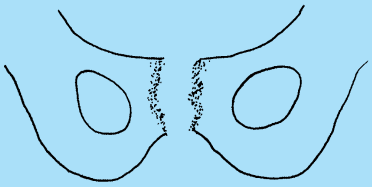	Ankylosing spondylitis Congenital (bladder extrophy, epispadia, hypospadia, anal atresia, prune belly syndrome, cleidocranial dysplasia, pubic hypoplasia, spondyloepiphyseal dysplasia) Hyperparathyroidism Massive osteolysis Neurogenic osteolysis (paraplegia) Osteitis pubis and other infections (pyogenic, tuberculous, luetic) Pregnancy (common) Pubic osteonecrosis Rheumatoid arthritis Traumatic dislocation Tumor destruction
Bridging of the pubic symphysis 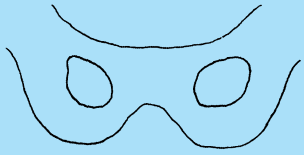	Ankylosing spondylitis Fluorosis Hyperparathyroidism (healed) idiopathic Healed infection Ochronosis Osteoarthritis Posttraumatic Postradiation therapy Rheumatoid arthritis Surgical fusion

(continues on page 261)

Table 12.2 (Cont.) Some Radiographic Changes Characteristic of the Pelvis and Their Differential Diagnosis

Radiographic Finding	An alphabetical List of Causes	Usual Appearance
Sacroiliac joint disease (erosion, widening, sclerosis and/or fusion)	Agenesis (caudal dysplasia)	Bilateral symmetric
	Ankylosing spondylitis	Bilateral symmetric
	Crohn's disease	Bilateral symmetric
	Enteropathic arthritis	Bilateral symmetric
	Familial Mediterranean fever	Bilateral asymmetric
	Gout	Bilateral asymmetric
	Hyperparathyroidism	Bilateral symmetric
	Infection (pyogenic or tuberculous)	Unilateral
	Multicentric reticulo histiocytosis	Bilateral symmetric
	Neoplastic destruction (primary, metastatic)	Unilateral
	Osteitis condensans ilii	Bilateral symmetric
	Osteoarthritis	Bilateral asymmetric
	Paraplegia	Unilateral
	Psoriatic arthritis	Bilateral asymmetric
	Reiter's disease	Bilateral asymmetric
	Relapsing polychondritis	Bilateral asymmetric
	Rheumatoid arthritis	Bilateral asymmetric
	Sacroiliitis circumscripta	

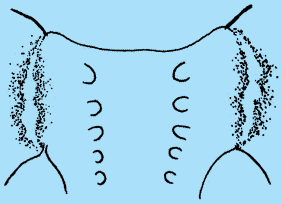

a) Erosion, widening

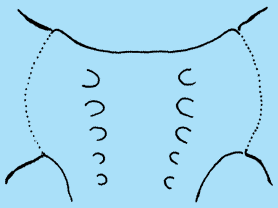

b) Fusion

Table 12.3 Differential Diagnosis of Cervicobasilar Abnormalities (Occiput, C1, C2)

Disease	Radiographic Findings	Comments
Anomalies of the occipital bone:		
Manifestations of occipital vertebra 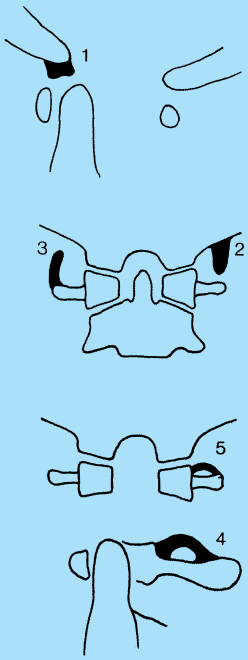	May appear in various forms and combinations: *Tertiary condyle* (1): A midline bony process at the anterior edge of foramen magnum. A joint between tertiary condyle and odontoid may be present. Seen in the lateral view. *Basilary process*: Bilateral, often asymmetric small protuberances at the anterior margin of the foramen magnum. Often too small to be appreciated. *Paracondylic* (2) and *epitransversary processes* (3). Bony protuberances lateral to the occipital condyles. When connected to the occipital bone, they are called paracondylic. The name epitransversary refers to their connection with the transverse process of the atlas. Best seen in AP and Stenver's views. *Posterior* (4) or *lateral* (5) ponticles refer to bony rings in the arch and transverse process of the atlas, respectively. The posterior ponticle is seen in the lateral view, whereas the lateral ponticle may be visible in anteroposterior projection.	Relatively uncommon (less than 1 %). May limit the mobility of the atlanto-occipital joint. Commonly present (12 %). No clinical significance as such. Relatively uncommon (less than 1 %). May cause a special form of atlantooccipital fusion. The posterior ponticle (Kimmerle's anomaly) is present in approximately 3 %. They have no clinical significance.
Basilar impression 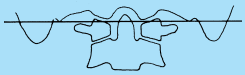	*Anterior* basilar impression results from platybasia and short clivus, evident on lateral skull film. *Medial* basilar impression results from elevation of the hypoplastic occipital bone and associated condyles. It may be unilateral and associated with tilting of the head. The dens is used as a reference.	The frequency of primary basilar impression is approximately 1 %. Platybasia: Angle between the clivus and a line connecting the nasion and the superior wall of the sphenoid sinus exceeds 150 degrees. For the measurement of basilar impression see Chapter 8. Anterior basilar impression can be measured from lateral skull films. Medial basilar impression can be reliably measured only from AP projection (digastric line).
Occipital condylar hypoplasia 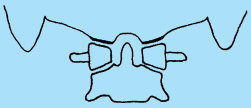	Hypoplasia of the occipital condyle without basilar impression results in a relatively high position of the atlas and axis. The odontoid seldom extends into the foramen magnum. The digastric line is the key to detect this abnormality.	Usually asymptomatic, but can be symptomatic if associated with altered size of the foramen magnum. It may also limit the mobility of of the atlanto-occipital joint (functional atlanto-occipital fusion). Elevation of the odontoid may occur in severe rheumatoid arthritis.
Anomalies of the atlas and the axis:		
Atlanto-occipital fusion (atlasassimilation) 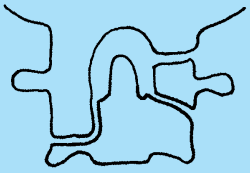	The atlas is either completely or partially fused into the occipital bone. If unilateral, may cause tilting of head.	Frequency approximately 0.25 %. Often associated with other anomalies like Klippel-Feil syndrome, spina bifida of the atlas or basilar impression. Clinical significance usually depends on associated anomalies. May cause atlantoaxial subluxation (in 50 % of cases).

(continues on page 263)

Table 12.3 (Cont.) Differential Diagnosis of Cervicobasilar Abnormalities (Occiput, C1, C2)

Disease	Radiographic Findings	Comments
Anomalies of the arch of the atlas	The dorsal arch may be totally absent or may have variable defects or clefts most commonly in the dorsal midline.	Dorsal cleft of the arch of the atlas is present in 4% of population. Arch defects are clinically asymptomatic.
Atlantoaxial fusion or malsegmentation 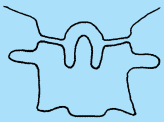	The lateral masses of the atlas and the body of the axis form a butterfly-looking complex in AP film. The dens and the anterior arch of the axis may be hypoplastic or totally missing. Various partial coalitions of the two bones may be present as a sign of abnormal segmentation.	These anomalies may be symptom-free or cause reduced mobility at the craniovertebral junction.
Odontoid bone (separate odontoid) (hypoplastic dens) (Figs. 12.1 and 12.2)	The dens of the axis is hypoplastic, seen as a protuberance at the site of the normal dens. The rounded odontoid bone is located either at the site of normal dens or higher up and anterior, maybe fused with clivus. The posterior arch of the axis is often absent. Atlas is usually ventrally subluxated.	In case of pseudoarthrosis of a fractured dens, the size and form of the odontoid process is normal. A small ossification center at the V-shaped tip of the dens is called ossiculum terminate Bergman. It has no clinical significance since it is not associated with atlantoaxial subluxation.

(continues on page 264)

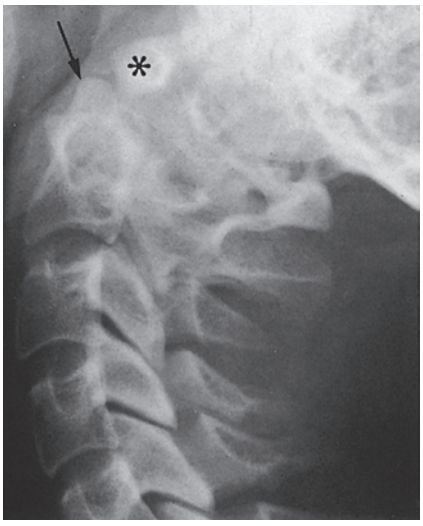

a **b**

Fig. 12.**1 a, b** **Hypoplastic dens** (arrow) as seen **a** in AP and **b** lateral in projection. The atlas (asterisk) is posteriorly displaced.

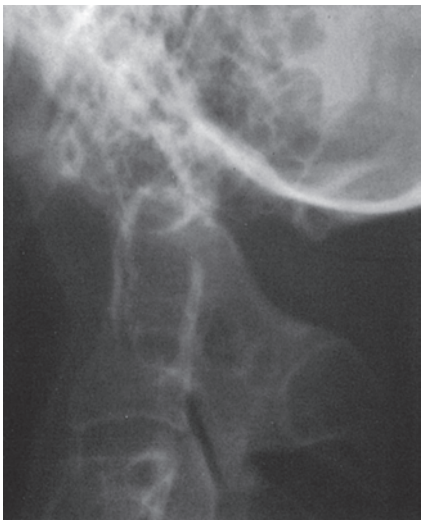

Fig. 12.**2** Hypoplastic dens, fusion of C2 and C3 and anterior displacement of the atlas. The posterior arch of the atlas is lacking **(Klippel-Feil anomaly, Type I).**

Table 12.3 (Cont.) Differential Diagnosis of Cervicobasilar Abnormalities (Occiput, C1, C2)

Disease	Radiographic Findings	Comments
Fractures: – **Jefferson fracture** 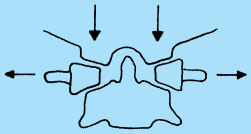 – **Fracture of the arch of the atlas** – **Fractures of the dens** – **Hangman's fracture (fracture of the arch of the atlas)** 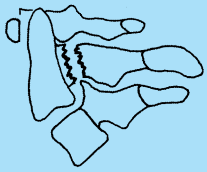	See Table 12.**4** and Chapter 4	See Table 12.**4** and Chapter 4

Table 12.4 Differential Diagnosis of Fractures and Dislocations of the Spine

	Radiographic Findings	Comments
Cervical spine		
Occipitocervical (atlanto-occipital) dislocation	The only sign of occipitocervical dislocation on radiographs may be widened prevertebral soft tissues. The distance between occipital condyles and C1 is increased. Distance from basion to odontoid in normal adult is less than 4–5 mm (in children less than 10 mm). On odontoid view increased distance between occipital condyles and C1.	Usually due to motor vehicle accident. Often fatal and therefore rare in hospitals. All major structures crossing occipitocervical junction are ruptured. Mechanism of the injury is complex or unknown.
Occipital condyle fracture 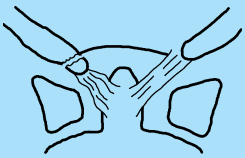	Usually conventional radiography fails demonstrate this fracture. Important to keep in mind when interpreting cervical radiographs (or CT).	Rare condition. CT is recommended method if occipital condyle fracture is suspected. Classification according to Anderson and Montesano: Type I: Occipital condyle impactation fracture caused by axial loading force like Jefferson fracture. Usually stable, if contralateral side intact. Type II: A component of basilar skull fracture. Usually stable. Type III: Avulsion of alar ligaments from occipital condyle. Potentially unstable.
Jefferson fracture (Fig 12.3) 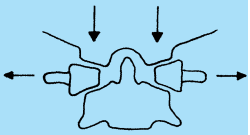	Best seen on open-mouth AP view. Lateral dislocation of one or both lateral masses of the atlas in anteroposterior projection. A small fragment may be seen medial to the lateral mass, representing an avulsion of the attachment of the transverse ligament. Additional lower level fractures in 25–50 % of cases.	Caused by an axial force (e.g., diving). Fracture lines are located posterior or anterior to the lateral mass in the arch of the axis. May be unstable or stable.
Fracture of the arch of the atlas (Fig. 12.4)	Unilateral fracture is often seen only in the oblique view. Bilateral may be seen in lateral view. In hyperflexion fracture the posterior fragment of the arch of the atlas is angulated and/or displaced downwards. In hyperextension fractures the posterior fragment of the atlas projects upwards.	Some patients have a lateral cleft in the arch of the axis, which should be differentiated from a fracture. Fractures of the anterior arch are rare except for in the combined fractures of the occipitovertebral region. Usually due to hyperextension trauma. Considered as stable. Fracture of the dens may be associated and therefore may be unstable (see below).

(continues on page 266)

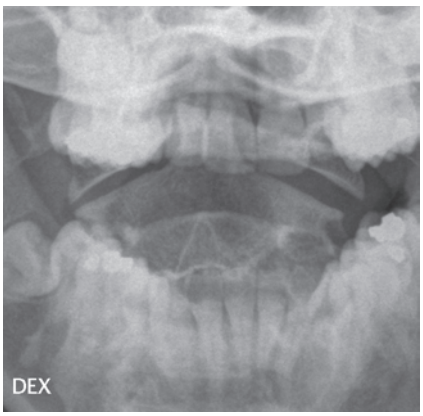

Fig. 12.3 **Jefferson fracture.** The space between left atlanto-axial facets has increased on AP view.

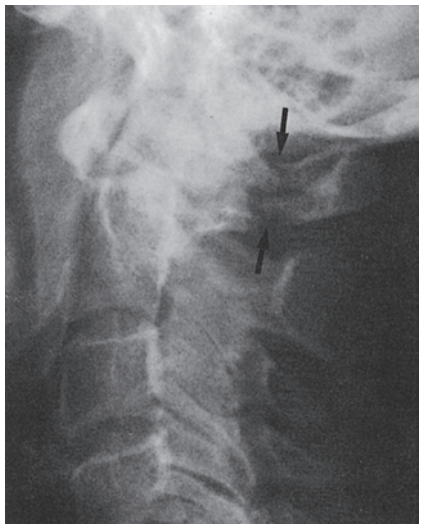

Fig. 12.4 **Hyperextension fracture** of the arch of the atlas (arrows). The posterior fragment of the atlas projects characteristically upwards.

Table 12.4 (Cont.) Differential Diagnosis of Fractures and Dislocations of the Spine

	Radiographic Findings	Comments
Fractures of the dens (Figs. 12.5 and 4.20) **Type I** 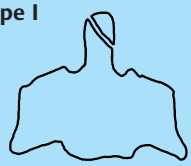 **Type II** 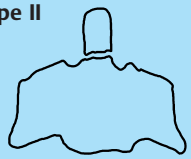 **Type III** 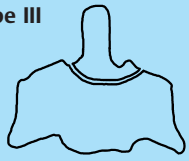	Lucent linear defect through C2 which may take place mainly at three levels: Type I: Fracture (usually oblique) cephalad to the base of the dens. Usually obliquely oriented. Type II: Transverse fracture at the base of the dens. Type III: Fracture extending from the base of the dens into the body of C2. On lateral view the normal ring shadow of the axis is disrupted. Hyperflexion fractures of the dens are often combined with anterior subluxation of the atlas and fracture of the posterior arch of the atlas. In typical hyperextension fractures both the dens and atlas are posteriorly displaced and the fractured posterior arch of the axis is displaced.	Over 10 % of fractures of the cervical spine involve dens. Isolated, nondisplaced fracture of the dens may not be detected until resorption of the fracture line. Type I: Usually stable Type II: Usually unstable Type III: Usually stable Unossified fracture or congenital nonunion of odontoid tip may result in odontoid bone (Figs. 12.**1, 2**). May be difficult to detect in elderly people with osteoporosis and degenerative changes. Multislice CT with coranal and sagittal reformats is recommended.
Hangman's fracture (fracture of the arch of the axis) (Fig. 12.6) (Fig. 4.21) **Type I** **Type II** **Type III** 	Best seen on lateral view. Bilateral fractures close to the body in the pedicles of C2 can be seen. Variable degree of anterior subluxation of C2.	Hyperextension injury of the axis presenting with bilateral pedicle fractures and varying degrees of anterior subluxation or frank dislocation of the body of C2. Nowadays most commonly found in automobile accidents when face strikes the windshield. Hangman's fracture is considered as unstable fracture. Three types are recognized: Type I: Fracture line close to the body in the pedicle without anterior displacement of the body. Type II: Concomitant disruption of intervertebral disk C2–3. Type III: This is type II fracture with associated C2–3 facet dislocation.

(continues on page 267)

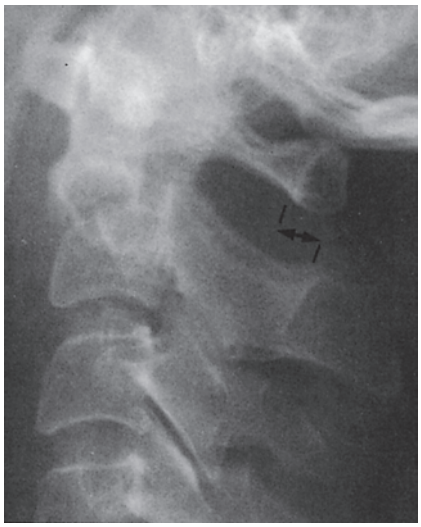

Fig. 12.**5** **Fracture of the dens** with anterior subluxation of the atlas and the dens.

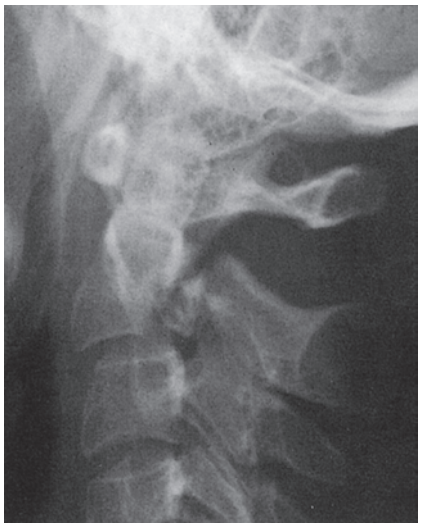

Fig. 12.**6** **Hangman's fracture** of the arch of the axis with anterior subluxation of the body of the axis.

Table 12.4 (Cont.) Differential Diagnosis of Fractures and Dislocations of the Spine

	Radiographic Findings	Comments
Burst fracture of C3–C7	On lateral view burst fracture is characterized by an anterior wedged deformity of vertebral body and retropulsion of a fragment from the posterior superior marging of vertebral body. On AP view widening of interpedicular distance may be seen.	Fracture mechanism is identical to Jefferson fracture, but fracture happens at the lower part of the cervical spine. Burst fracture is stable, if posterior ligaments are intact. Burst fracture becomes unstable if posterior ligaments disrupt. CT is recommended for evaluation of spinal canal.
Flexion tear drop fracture (Fig. 4.23)	Radiological features of flexion tear drop fractures include backward displacement of fractured vertebral body, posterior displacement of upper column, widening of interspinous spaces, and kyphotic deformity of the cervical spine on the lateral view. On AP view widening of interlaminar spaces, a sagittal split fracture through the vertebral body and one or both laminae is often seen.	The flexion tear drop fracture is a specific form of burst fracture. Usually accompanied by spinal cord injury. Flexion tear drop fracture is highly unstable. About 15% of all cervical fractures are flexion tear drop fractures.
Extension tear drop fracture (Fig 12.7)	Lateral view of the spine demonstrates the tear drop fracture of anterior inferior corner of vertebral body and there is no subluxation.	Extension tear drop fracture is usually stable, but may be unstable at the lower part of the cervical spine. The most common location is at the level of C2–3. Defect in the ossification of the endplate may simulate fracture.
Endplate compression fracture (Fig. 12.8) **Anterior** **Lateral** **Posterior**	Endplate compression fractures are usually hyperflexion injuries that leave the posterior height of the vertebral body normal while the anterior vertebral height decreases. In thoracic and lumbar vertebrae, an increased density or diameter and irregularities of the anterior margin of the vertebral body may be associated. Widening of the facet joint space may be present in acute trauma.	If the anterior vertebral height in the cervical spine is 3 mm less than the posterior height, a compression fracture is suspected. In thoracic and lumbar spine, this measurement is not valid because many diseases cause wedge-shaped or collapsed vertebrae (e.g., Scheuermann's disease). Compression fractures are common in the lower cervical spine and in the lower thoracic spine. Compression of the posterior inferior margin of the vertebral body is likely due to an extension injury.
Fractures of the pedicle, neural arch (Fig. 12.9), or articular process	May resemble simple dislocation in the lateral view. Fracture of the pedicle may be better appreciated in the frontal view.	Neural arch is the most common site of a fracture in cervical spine. The articular pillar is particularly vulnerable in fractures.
Clay-shoveler's fracture (Fig. 4.22)	Oblique or vertical avulsion fracture of the tip of the spinous process of C6 or C7 (occasionally Th1–Th3).	Caused by a repeated sudden load on the flexed spine. Must be differentiated from hyperflexion fracture, in which the fracture line is more horizontal.

(continues on page 268)

Fig. 12.7 **Tear drop fracture** of the anterior inferior margin of C4 resulting from extension injury. There is slight posterior dislocation of C4. Prevertebral soft tissue is thickened.

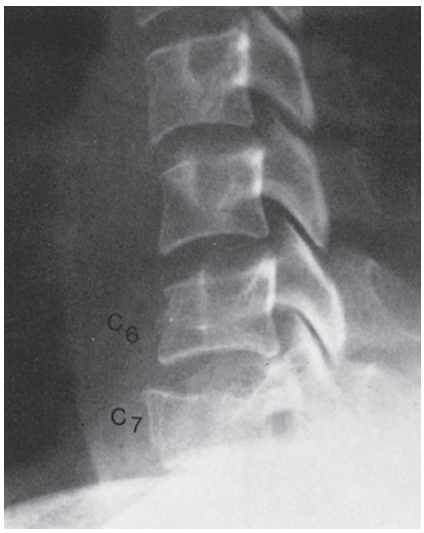

Fig. 12.8 **Compression fractures** of the anterior superior margins of C6 and C7. The height of the anterior C6 body is decreased, whereas C7 has a chip fracture. Prevertebral soft-tissue thickening is also observed.

Fig. 12.9 **Fracture through the neural arch** of C3 anterior dislocation of the body of C3.

Table 12.4 (Cont.) Differential Diagnosis of Fractures and Dislocations of the Spine

	Radiographic Findings	Comments
Locked facets **Unilateral (Fig. 12.10)** **Bilateral (Fig. 12.11)** 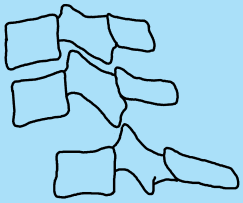	Lateral and oblique views are sufficient to demonstrate facet joint locking. On the lateral view inferior and superior articular processes are in apposition. Facet joints have changed configuration so that laminar cortices intersect at one point. On AP view mild rotation may be seen especially in unilateral facet locking.	A locking can be unilateral or bilateral. Unilateral locking is relatively stable. Bilateral locking is result of extreme flexion and is unstable condition. Relatively often missed on plain films.
Anterior subluxation	Kyphosis at the affected level on lateral view. The space between the inferior articular process of the upper vertebra and the upper process of lower vertebra shows of abnormal extent. The degree of subluxation may show milder than needed to rupture ligamentous complex due to regressed distortion.	Hyperflexion trauma, in which disruption of posterior ligamentous complex happens. Unstable.

(continues on page 269)

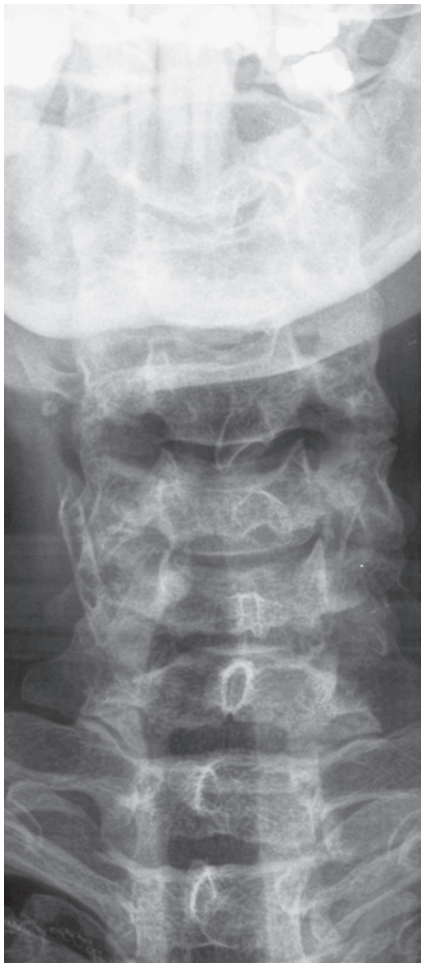

a

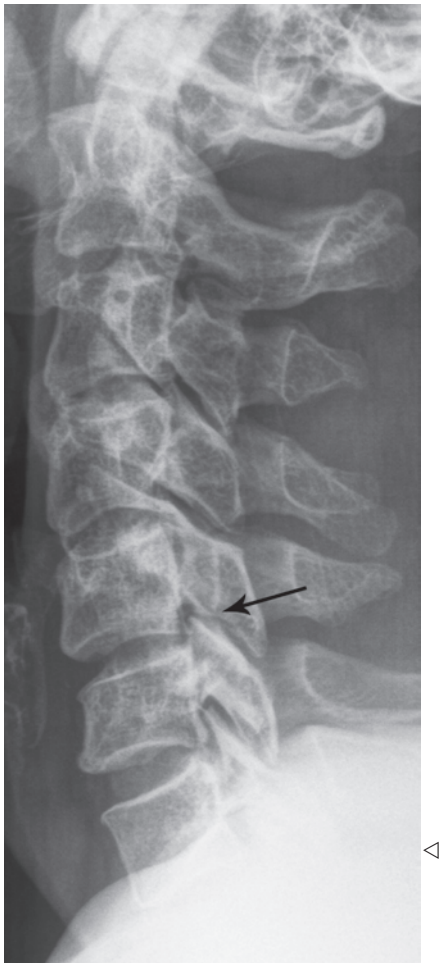

b

◁ Fig. 12.**10** **Unilateral locking of facet.** On AP view the spinous processes of lower cervical spine curve to the left. On lateral view unilateral locking of the facets between C5 and C6 can be seen (arrow).

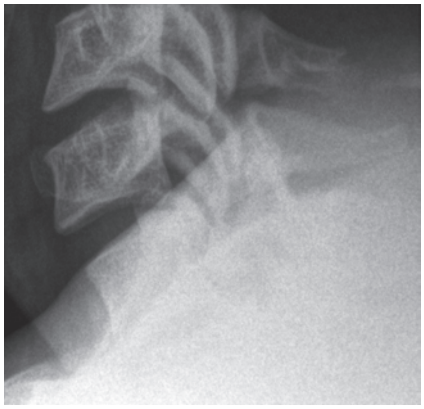

Fig. 12.**11** **Bilateral facet luxation.**

Table 12.4 (Cont.) Differential Diagnosis of Fractures and Dislocations of the Spine

	Radiographic Findings	Comments
Thoracolumbar spine		
Compression fractures: (Figs. 12.12a and 4.24) **anterior** **lateral**	Cortical bucking or wedging of anterior or less commonly lateral part of the vertebral body. Usually confined to the superior end plate. A zone of sclerosis is often present beneath the end plate. Note that posterior cortical line remains intact.	Flexion injury of the spine resulting in compression of the anterior column. In severe compression fractures posterior ligamentous distraction may be associated while middle column serves as the fulcrum. This is called as flexion-distraction fracture.
Flexion-distraction fracture	Cortical bucking or wedging of anterior part of the vertebral body. Posterior cortical line remains intact. Distinguished from a simple anterior compression fracture by horizontal fracture in the posterior elements e.g., pedicle. Widening of posterior bony elements of adjacent vertebrae.	This is a variant anterior compression fracture, in which middle column serves as a fulcrum and posterior column distracts leading to horizontal fractures of posterior bony elements or in the disruption of interspinosus ligaments.
Burst fractures (Figs. 12.12b and 44.24)	On lateral view increased sagittal diameter and moderate to marked anterior wedged deformity of the vertebral body. Retropulsion of a fragment from the posterior superior marging of vertebral body. On AP view widening of interpedicular distance may be seen.	Most commonly at thoracolumbal region. Caused by hyperflexion and axial load. Intervertebral disc usually herniated into the vertebral body. Retropulsion of osseous material into spinal canal often causes neurological symptoms. Burst fracture is considered as unstable.
Chance fracture (seat-belt injuries) (Figs. 12.12 c and 4.24)	The radiographic findings depend on whether the injury is predominantly osseous or ligamentous (see Fig. 4.**24**). Horizontal split of the vertebral body pedicles, lamina and spinous process in one level fracture. In two level chance fracture the fracture line passes through bone and ligaments.	Caused by hyperflexion of the spine resulting in distraction injuries of both the middle and posterior columns. Associated at times with anterior compression of the vertebral body. Most frequently at L1–3. Change fracture is considered unstable.
Fracture dislocations (Figs. 12.12 d and 44.24)	Intervertebral subluxation or dislocation. The loss of height of the vertebral body may be relatively small. Fragmentation of the injured vertebral bodies, dislocation of facet joints and fractures in the spinous processes and arches. Lateral plain films may show a wedge-formed vertebral body, kyphosis and distraction of the spinous processes. A small bony fragment arising from the anterior superior margin of the vertebrae below the dislocation. This may indicate an avulsion fracture created by the annulus.	Complete disruption of all three spinal columns. Usually mixed osseous–ligamentous injury.

(continues on page 271)

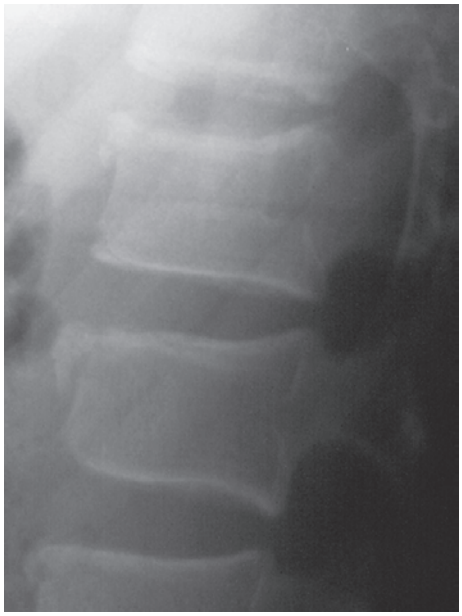

a

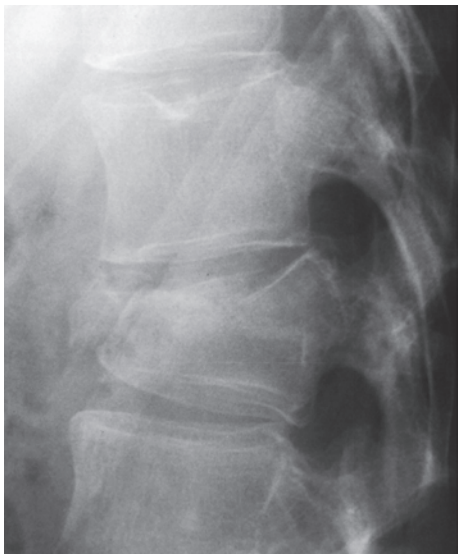

b

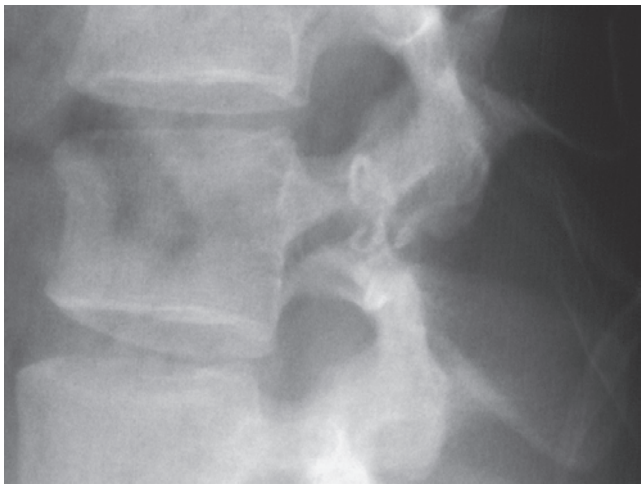

c

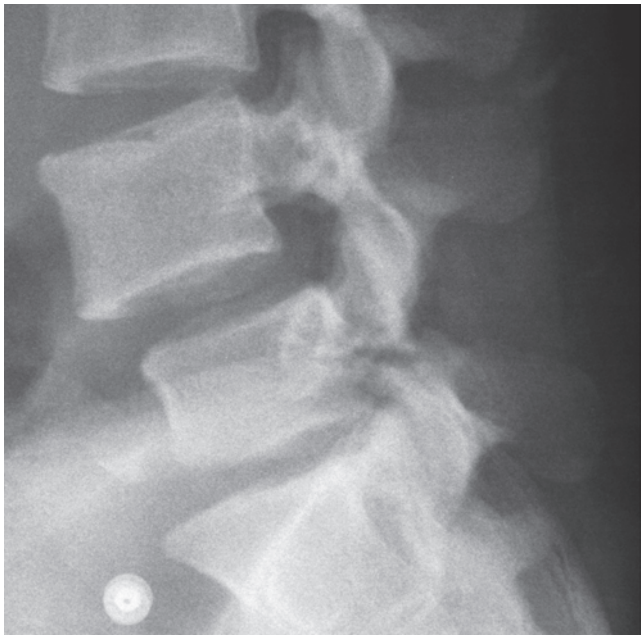

d

Fig. 12.**12** **a)** Anterior compression fracture of upper end plate. The fracture does not extent to posterior margin of the body. **b)** Burst fracture of L1. A bony fragment is seen protruding into the spinal canal from superior posterior aspect of the body. **c)** Chance fracture. Mild wedging of the body of L3. Fracture extends through pedicles and transverse processes. **d)** Fracture dislocation between L4 and L5. The space between processus spinosus of L4 and L5 has increased and processus interarticularis fracture of L5 is visible. L5 body is in mild retroposition. Anterior compression fracture on upper end plate of L4.

Table 12.4 (Cont.) Differential Diagnosis of Fractures and Dislocations of the Spine

	Radiographic Findings	Comments
Osteoporotic compression fractures (Figs. 12.13 a, b)	Wedge-shaped or biconcave vertebral body. Seen often on lateral view of chest X-ray. In acute fracture anterior wedge deformity usually involving the superior end plate with increase in bone density beneath the end plate. In old healed osteoporotic fracture a fine line of cortical bone is intact and there is no increased density of bone beneath the end plate. In an old fracture an anterior superior spur of an affected vertebra end plate is often present.	Determining whether the fracture is acute or not may be problematic. Previous images e.g., chest X-ray may be helpful.
Fractures of posterior spinal structures (spondylolysis)	See Table 12.**5**	Stress fractures, see spondylolysis in Table 12.**5**.
Pathologic fracture	See Table 12.**5** and Chapter 5.	

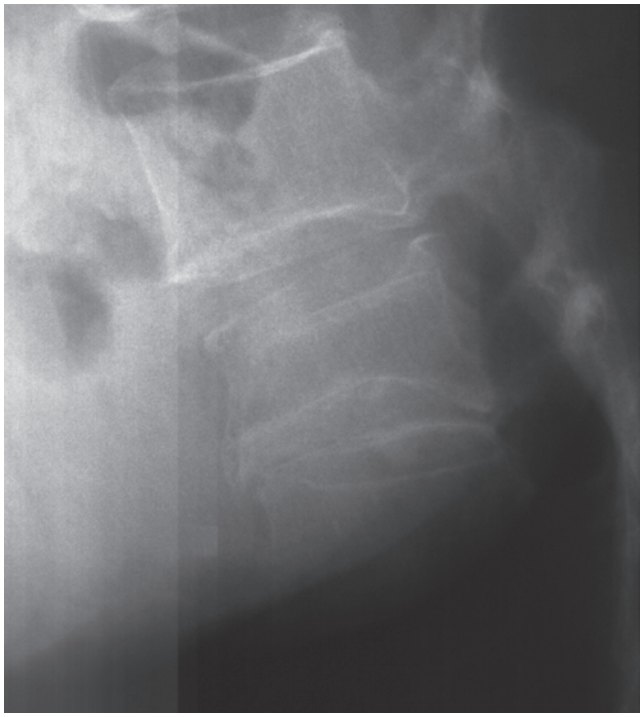

a

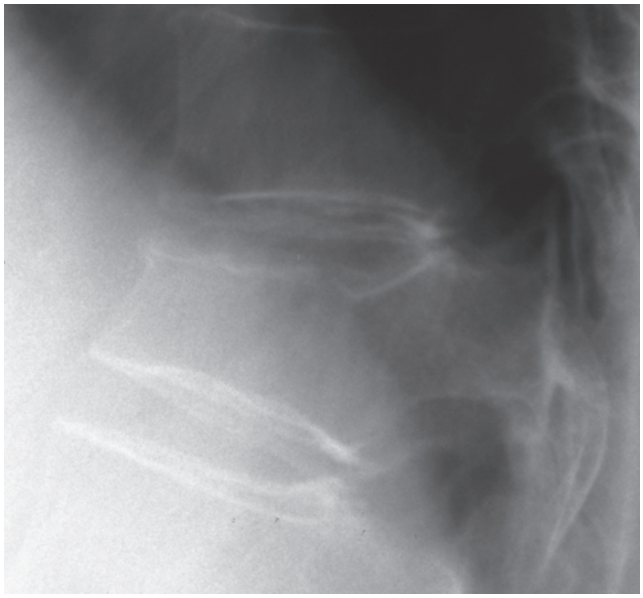

b

Fig. 12.**13** **a Biconcave** (Cod fish) **osteoporotic fracture. b** An old wedge-shaped osteoporotic fracture of T12.

Table 12.5 Differential Diagnosis of Anomalies of the Spine below the Axis

Disease	Radiographic Findings	Comments
Block vertebra (fusion of two or more vertebral bodies) (Figs. 12.14 and 12.15; see Figs. 12.16, 12.17, and 12.18 for comparison)	Variable grades of blocking from isolated hypoplasia of the intervertebral disk to complete fusion of bodies and even neural arches may be present. Decreased diameter of vertebrae at the site of segmentation defect, concavity of the anterior aspect of the block, and/or fusion of the neural arches are diagnostic of *congenital* block vertebra. Anterior blocking of several vertebral bodies is called *vertebral coalition*. It results in kyphosis due to asymmetric growth. *Klippel-Feil anomaly:* Type I: Short neck with block vertebrae, vertebrobasilar anomalies (including basilar impression), scoliosis, Sprengel's deformity, etc. Type II: Segmentation anomalies of one or two pairs of cervical vertebrae only. Type III; Thoracic or lumbar anomalies together with Type I or II.	Most common at C2–3. Somewhat similar changes in the spine may be produced by vertebral infection, rheumatoid spondylitis, and operative fusion. Several other disorders may occasionally lead to spinal block, e.g., vertebral hemangioma, fibrous dysplasia, Paget's disease, fracture, chondrosarcoma, and other primary neoplasms, achondroplasia, spinal stenosis. Multiple anterior blocks may occur secondary to Scheuermann's disease and senile kyphosis. Clinically short neck, low-lying hairline, and limited cervical motion. Type I is most common, Type II is rare. In addition to spinal anomalies, also genitourinary abnormalities, deafness, and synkinesia are common. Several other skeletal, cardiovascular, and neurological abnormalities occur.

(continues on page 274)

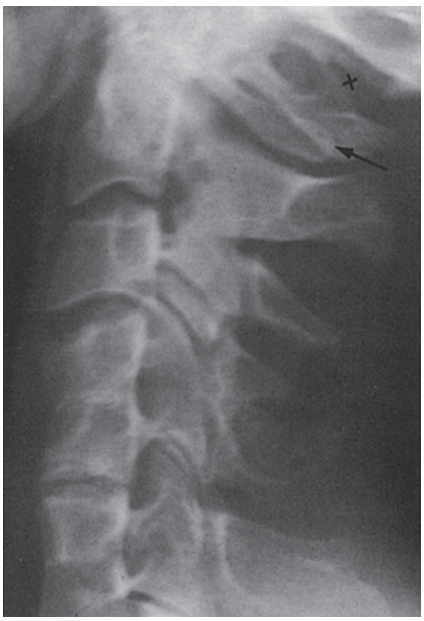

Fig. 12.**14** **Congenital block vertebrae** C4–5, C6–7, T1–2 (not shown), associated with posterior ponticle (foramen arcuale) (*) and a defect in the posterior arch of the atlas (arrow) (Klippel-Feil type III).

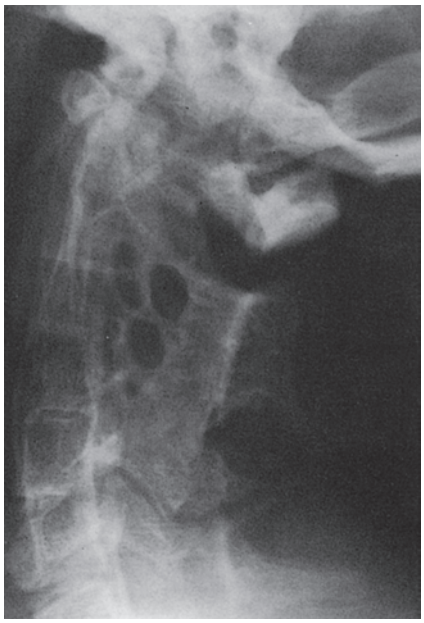

Fig. 12.**15** **Severe segmentation anomalies** of the vertebrobasilar junction and blocking of the cervical spine (Klippel-Feil type I).

Fig. 12.**16** **Tuberculous spondylitis** of the cervical spine resulted in multiple block vertebrae, which resemble Klippel-Feil anomaly.

Fig. 12.**17** **Tuberculous block vertebra** (T10 and T11) associated with a gibbus.

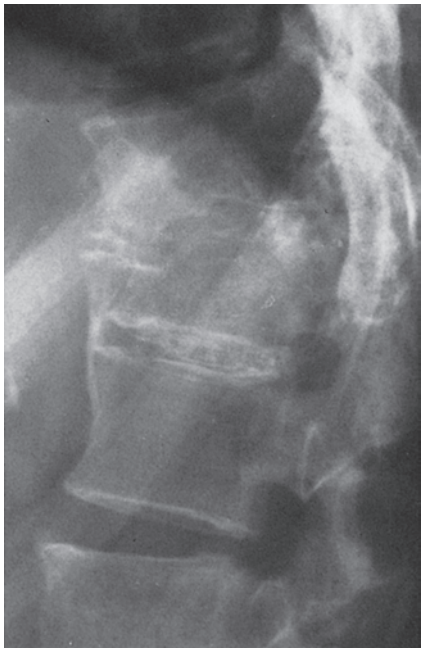

Fig. 12.**18** **Posttraumatic block** T11, T12, and partially L1.

Table 12.5 (Cont.) Differential Diagnosis of Anomalies of the Spine below the Axis

Disease	Radiographic Findings	Comments
Spondylolysis (Fig. 12.19)	Anterior slipping of one vertebral body on its subjacent neighbor while the posterior portions stay behind; is usually secondary to bilateral defects of pars interarticularis, called *spondylolysis*. Spondylolysis is best demonstrated in oblique films. Most common locations of spondylolysis are L5 and L4, rarely higher lumbar vertebrae or C6.	*Spondylolysis* may be a congenital failure of ossification or more likely traumatic, either an acute or a fatigue fracture. It is seen in 5% of the white population. When the facet joints are deformed or malpositioned, being more sagittal than coronal, the whole vertebra, including the posterior portion, slides forward. This results in dislocation, called *pseudospondylolisthesis* or degenerative spondylolisthesis with an intact neural arch. Hypertrophic osteoarthritis of the apophyseal joints is a basic finding. Spondylolisthesis should be differentiated from traumatic ventral luxation of vertebra without fracture. On perfectly positioned lateral films of the lumbar spine, an apparent defect of the pars interarticularis of L2 or L3 may resemble spondylolysis. This is a superimposition artifact (pseudospondylolysis), located slightly more superiorly on the pars than are true defects.
Spondylolisthesis (Figs. 12.20 and 12.21)	Spondylolisthesis does occur secondary to congenital elongation of posterior elements without fracture (interarticular dysplasia). Spondylolysis is often present without spondylolisthesis. Rarely an arch cleft is retrosomatic (in the pedicle) or retroisthmic (in the lamina). Isolated lateral deviation and rotation of a spinous process seen in anteroposterior radiographs of the lumbar spine are associated with inequality in the length of pars interarticularis. The spinous process deviates toward the side of the intact side or smaller defect. Unilateral spondylolysis may produce hypertrophy and sclerosis of the contralateral pedicle (see Fig. 12.**39b**). A posteriorly wedged, slightly hypoplastic L5 is often present.	
Pseudospondylolisthesis (Fig. 12.33) 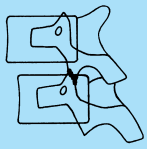		

(continues on page 276)

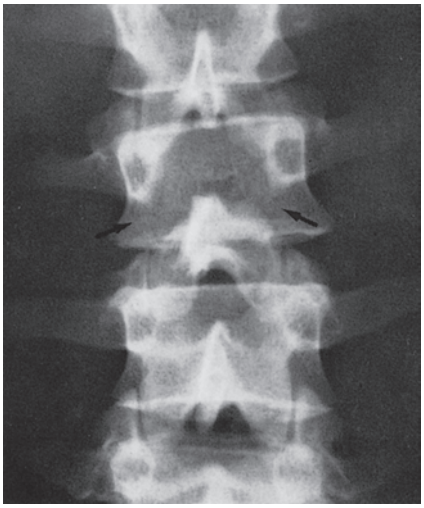

a

b

Fig. 12.**19 a, b** **Spondylolysis** with minimal Spondylolisthesis of L3. Bilateral defect in the pars interarticularis is well seen in both AP (**a**) and lateral (**b**) views.

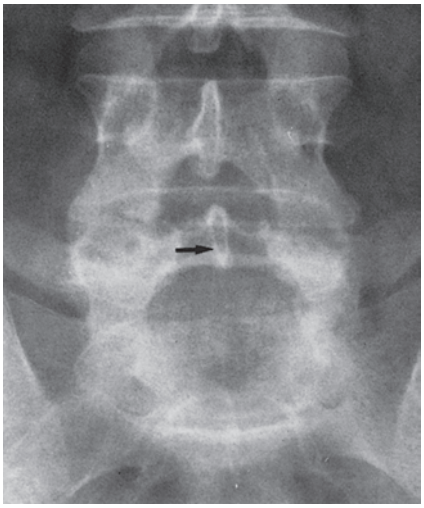

a

b

Fig. 12.**20 a, b** **Spondylolisthesis. a** The spinous process deviates slightly to the left (arrow) indicating shorter left pars interarticularis. **b** Anterior displacement of the characteristically wedge-shaped L5 on the lateral film.

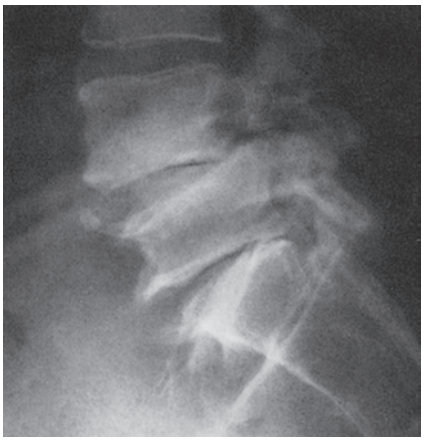

a

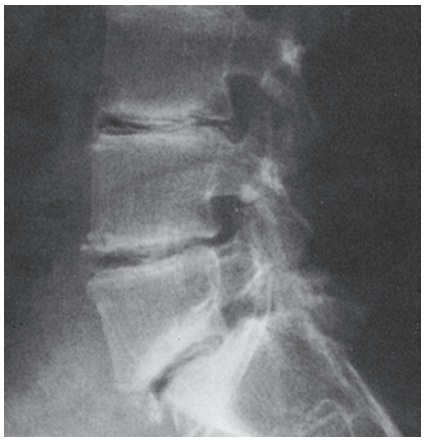

b

Fig. 12.**21 a, b** **Spondylolisthesis.** **a** Anterior slipping of L4 with disk degeneration and osteophytes both in spaces L4–L5 and L5–S1. **b** Spondylolisthesis of L5 in a patient with multiple calcified disk degenerations due to ochronosis.

Table 12.5 (Cont.) Differential Diagnosis of Anomalies of the Spine below the Axis

Disease	Radiographic Findings	Comments
Open dysraphisms ***Myelomenigocele*** ***Myelocele*** ***Hemimyelomeningocele*** ***Hemimyeocele*** **Closed spinal dysraphisms** ***Lipomyelocele*** ***Lipomyelomeningocele*** ***Meningocele*** **(Figs. 12.22–23)** ***Myelocystocele*** ***Spina bifida*** **(Fig. 12.24)** ***Tight filum terminale***	Occasionally one of the posterior neural arches will remain permanently open. This is commonly seen at S1 or L5, but may occur in any area. The cleft may be only 1 to 2 mm wide and vertical or oblique in orientation. Such a defect, if unassociated with other deformity, is called occult spina bifida. If multiple or associated with widened spinal canal (broad interpedicular distance or posterior scalloping of the vertebral body), they are likely due to a significant abnormality.	In open dysraphisms the placode is exposed to the environment. In closed spinal dysraphisms skin or other cutaneus appendage covers spinal structures. Advanced imaging modalities are suggested. MRI shows the depth of defect. CT may be needed for evaluating bony structures. Subtle neurologic deficits such as gait disturbance, foot deformity, or impaired sphincter control may occur in diastematomyelia. Syringomyelia, meningomyelocele, or an intraspinal tumor may also cause broad interpedicular distance. Posterior scalloping may also occur in neurofibromatosis, achondroplasia, increased intraspinal pressure, and tumors of the spinal canal.
Vertebral hypoplasia and asymmetry (Figs. 12.25–26)	A wide spectrum of anomalies involving focal hypoplasia of part or all of a vertebral element occurs. Hypoplastic lesions may involve more than one level (Fig. 12.**25**). Lateral hemivertebra (Figs. 12.**25** and 12.**26**) results in scoliosis. Posterior hemivertebra in kyphosis or gibbus. Posterior hemivertebra is usually displaced approximately 3 mm posteriorly from the neighboring vertebral bodies. Hypoplasia or absence of a pedicle or lamina may also cause scoliosis.	A hemivertebra may cause encroachment of the neural canal. Unlike fractures, hemivertebrae are outlined by a cortical margin. Absent pedicle (usually cervical) may simulate an expanding mass in the intervertebral canal or metastatic destruction of the pedicle. Hemivertebra or “butterfly” vertebra of the thoracic or lower cervical region may be part of a neurenteric canal anomaly (fistula, sinus or enteric cyst) or more rarely associated with pulmonary or cardiac anomalies. Severe forms of sacral hypoplasia may be associated with major anomalies of the gastrointestinal and genitourinary tracts. Narrowing of the arch associated with enlargement of the neural foramen is usually due to a neurinoma (Fig. 12.**27**) or neurofibroma (Fig. 12.**28**).

(continues on page 278)

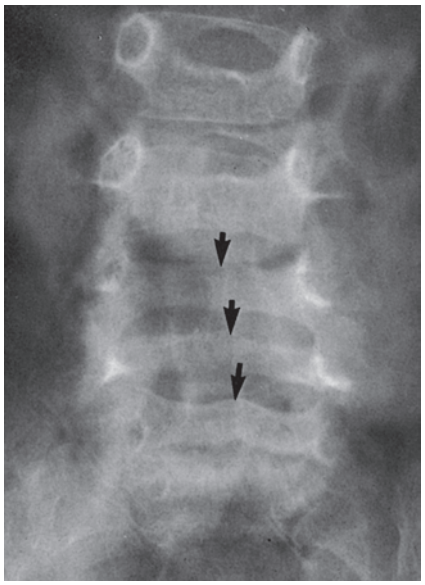

Fig. 12.**22** **Multiple clefts** in the posterior neural arches (arrows) and widening of the spinal canal due to meningocele.

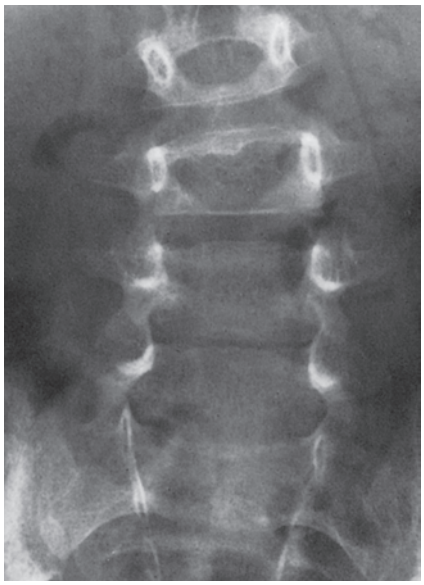

Fig. 12.**23** **Meningocele.** Defects in the neural arches are wide and involve three lumbar and all sacral segments.

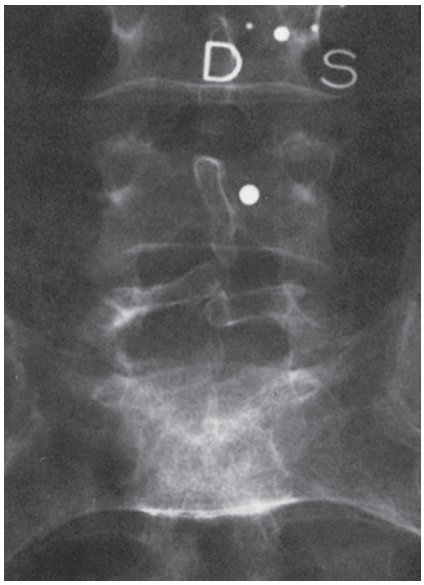

Fig. 12.**24** **Spina bifida** occulta of L5.

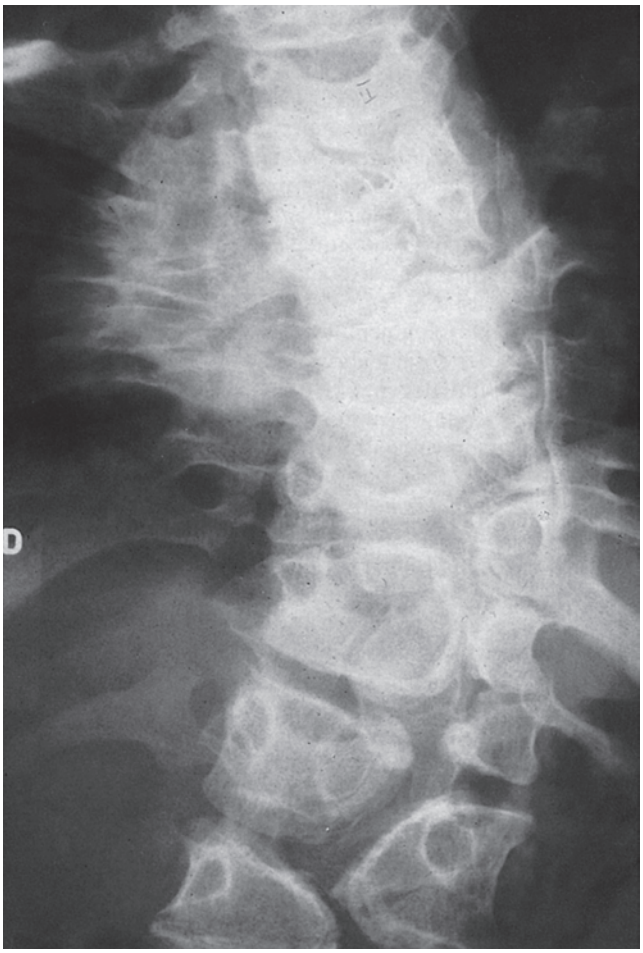

Fig. 12.**25** **Multiple segmentation anomalies** throughout the spinal column. Not a single normal vertebral body is present. Rib fusions are an associated finding.

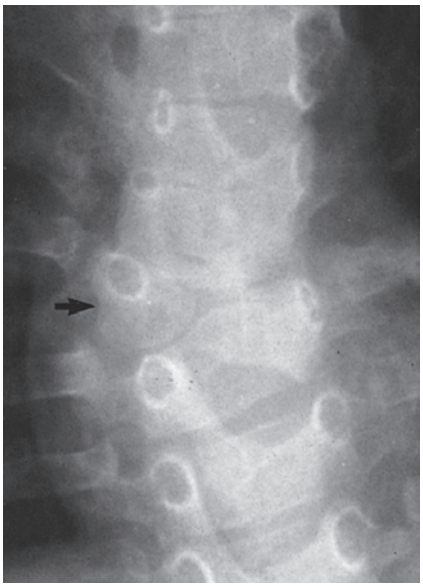

Fig. 12.**26** **Lateral hemivertebra** with scoliosis (arrow).

Fig. 12.**27** Narrowing and erosion of the arch of the axis and atlas due to neurinoma (arrows).

Fig. 12.**28** **Neurofibroma.** The neural foramen C6–C7 is enlarged (arrow). A dorsal cleft in the arch of the atlas is seen as an incidental finding.

Table 12.5 (Cont.) Differential Diagnosis of Anomalies of the Spine below the Axis

Disease	Radiographic Findings	Comments
Spinal stenosis (Figs. 12.29–30)	The decreased diameter of the spinal canal is due to short, heavy pedicles and enlarged apophyseal joints. (Stenosis at the level of Cl is due to craniovertebral anomalies, basilar impression, manifestations of occipital vertebrae, and atlantoaxial subluxation.) The normal sagittal diameter of the midcervical and lumbar canal is 15 mm or more; values below 13 mm may indicate stenosis. Congenital spinal stenosis may involve lumbar and, less frequently, cervical spine. Intervertebral foramina have a figure-of-eight configuration (Fig. 12.**30 b**) and lumbar lordosis is increased. In developmental lumbar and/or cervical spinal stenosis, the plain radiographic changes are less striking. The pedicles tend to be short and the lamina convergent, intervertebral foramina moderately narrowed in anteroposterior direction and elongated axially. Plain films may be deceptive in younger patients. In older patients the pattern is superimposed by spondylarthritic changes.	The most common cause of congenital spinal stenosis is achondroplasia. Abnormal enchondral bone formation and premature fusion of the cartilaginous synchondroses result in broad, squat vertebrae with concave dorsal surfaces and prominent intervertebral disks. Developmental stenosis is not associated with vertebral malformations and is asymptomatic until degenerative changes in the spine precipitate symptoms of neurogenic claudication or myelopathy. Except for high cervical stenosis, localized spinal stenosis is usually acquired, commonly involves midcervical or lower lumbar segments, and is associated with spondylotic and spondylarthritic changes. Lateral recess stenosis can occur in a canal with a normal sagittal diameter. Spinal stenosis is not adequately seen on plain films. CT or preferentially MRI should be available for assessment.

(continues on page 279)

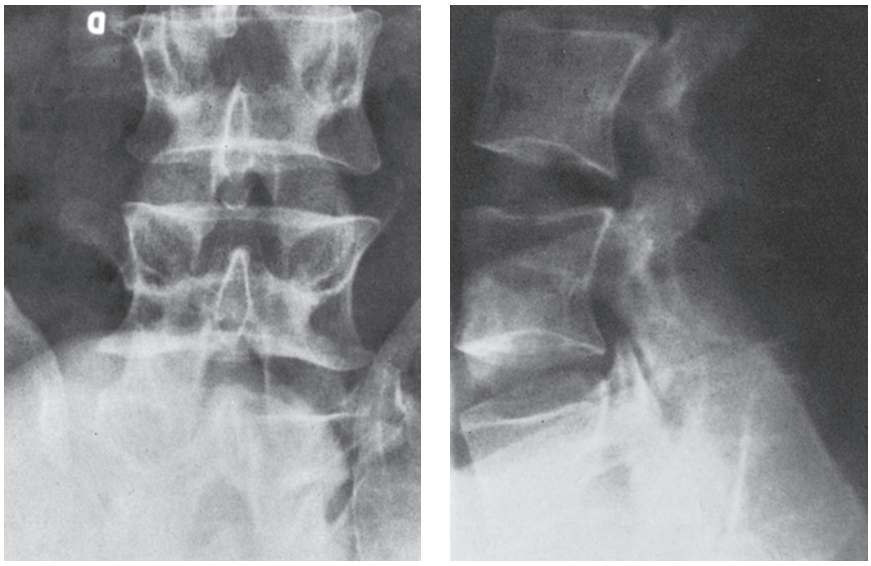

Fig. 12.**29 a, b** **Spinal stenosis in achondroplasia. a** Anteroposterior film demonstrates lateral narrowing of the spinal canal in L4 and 5. Hypoplastic sacrum is also obvious. **b** Lateral film of another patient demonstrates narrow sagittal diameter of the spinal canal and posterior scalloping of the vertebral bodies.

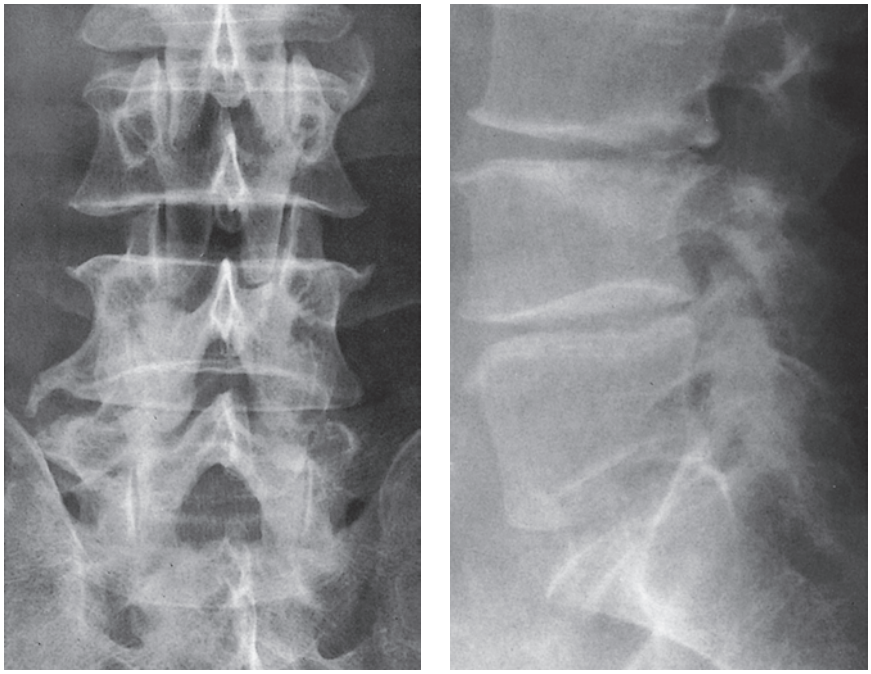

Fig. 12.**30 a, b** **Acquired spinal stenosis. a** The lamina are convergent and the articular processes hypertrophic with superimposed spondylarthritis. **b** Short pedicles and decreased sagittal diameter of the spinal canal associated with narrowed disk spaces L3–L4 and L4–L5.

Table 12.5 (Cont.) Differential Diagnosis of Anomalies of the Spine below the Axis

Disease	Radiographic Findings	Comments
Inflammatory lesions Pyogenic vertebral spondylitis (Figs. 12.31 and 12.32)	The radiographic changes follow a certain pattern, but may take weeks or months to become apparent, depending on the aggressiveness of the process. 1 Disk space narrowing 2 Loss of the normally sharp adjacent subchondral plates 3 Areas of cortical demineralization 4 Destruction of the vertebral body, possibly collapse 5 Sclerotic new bone formation, sometimes spontaneous fusion. The process more commonly involves the anterior two-thirds of the vertebral body than the posterior part. Changes are usually seen in one disk space and two adjacent vertebral bodies. Destruction of only one end plate is very rare. Involvement of multiple levels and soft-tissue abscesses occur in approximately 20 % each.	Pyogenic spondylitis refers to two distinct entities: 1. *Infectious diskitis*: occurs in children and adolescents, who have vascularized disks (Fig. 12.**32**). 2. *Blood-borne osteomyelitis* of the vertebral bodies in adults begins under the vertebral end plate and involves the disk secondarily, because the disk is avascular. In adults, primary infection of the disk is possible after surgery, needling, or trauma. Staphylococcus aureus is the infectious agent in approximately 90 %. A history of recent primary infection, surgery, or urogenital instrumentation is common. Drug abusers have increased incidence of gram-negative infections and cervical involvement that is otherwise rare.

(continues on page 280)

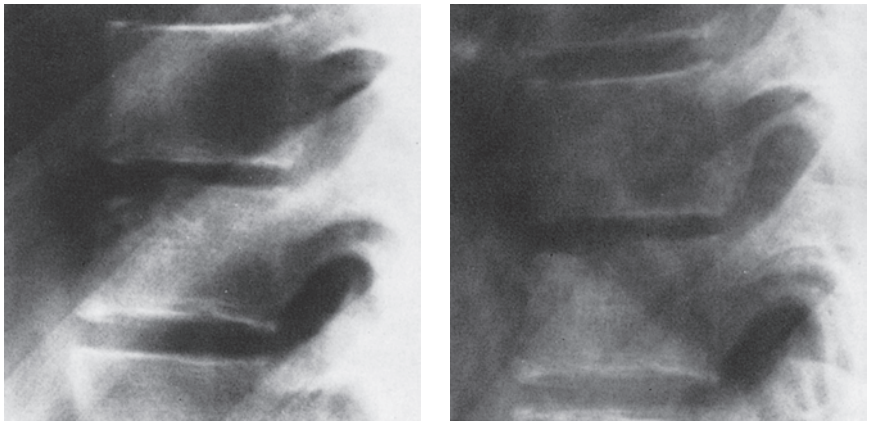

Fig. 12.**31 a, b** **Pyogenic spondylitis.** **a** There is disk space narrowing, destruction of the anterior portion of two adjacent vertebral bodies, more so in the inferior. **b** Three months later, sclerotic new bone formation is seen as a sign of healing.

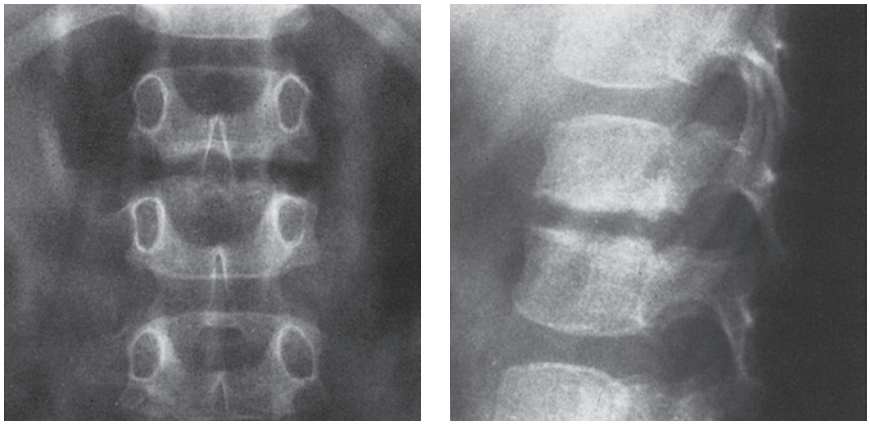

Fig. 12.**32 a, b** **Infectious diskitis** in a child. Narrowing of the disk space with erosion and sclerosis of the adjacent end plates.

Table 12.5 (Cont.) Differential Diagnosis of Anomalies of the Spine below the Axis

Disease	Radiographic Findings	Comments
Spinal tuberculosis (Fig. 12.33)	Characteristic findings are: involvement of the thoracolumbar or midthoracic spine, osteoporosis, large paravertebral abscess relative to the amount of bone destruction, narrowing of one or more disk spaces after erosion of endplates, anterior compression of adjacent vertebra. Reactive sclerosis is not a rule. A pedicle may rarely be the primary focus. Roentgen findings that favor spinal tuberculosis are: involvement of three or more vertebral bodies, skip lesions in the spine, a large or calcified paraspinal mass, and the rare involvement of neural arches.	Secondary to hematogenous spread from primary pulmonary tuberculosis. Neurological symptoms are common due to extradural compression of the cord by paravertebral abscess, even before gibbus appears. Distinction of spinal tuberculosis from pyogenic vertebral osteomyelitis is often impossible. Subligamentous spread of spinal tuberculosis with anterior irregularities (anterior gouge defects) resembles lymphoma. If only one vertebra is involved it mimics metastasis. Spinal brucellosis is rare. Its roentgen appearance is distinguishable from spinal tuberculosis.
Fungal infections: **Actinomycosis** **Coccidioidomycosis** **Blastomycosis** **Cryptococcosis** **Aspergillosis**	All mimic spinal tuberculosis, and diagnosis depends on biopsy and culture of the organism. Involvement of the posterior arch and ribs is common in actinomycosis, coccidioidomycosis, blastomycosis, and cryptococcosis. Absence of vertebral collapse and sparing of the disk is typical of actinomycosis and coccidioidomycosis. Aspergillosis is virtually indistinguishable from spinal tuberculosis.	All are rare. Actinomycosis spreading from the retropharyngeal space affects the cervical spine. Presence of draining sinus tracts is common in actinomycosis, Coccidioidomycosis, and blastomycosis.
Fractures of the vertebral body (Figs. 12.7–8)	See Table 12.**4**	See Table 12.**4**
Fractures of the pedicle, neural arch, or articular process (Fig. 12.9)	See Table 12.**4**	See Table 12.**4**
Neuropathic spine (Fig. 12.34)	Neuropathic changes are usually limited to one to three contiguous vertebral bodies. Sclerosis or destruction together with fragmentation and altered alignment are typical.	The progression of roentgen changes is relatively rapid and osteophyte formation is florid, involving also the posterior elements, which is not a feature in infectious spondylitis. Unlike metastases, disk spaces are involved.

(continues on page 282)

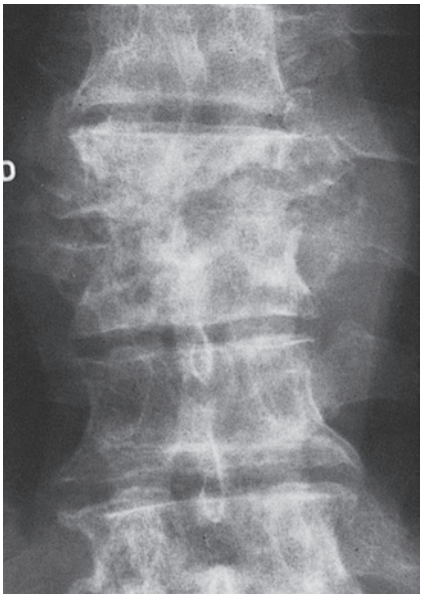

a

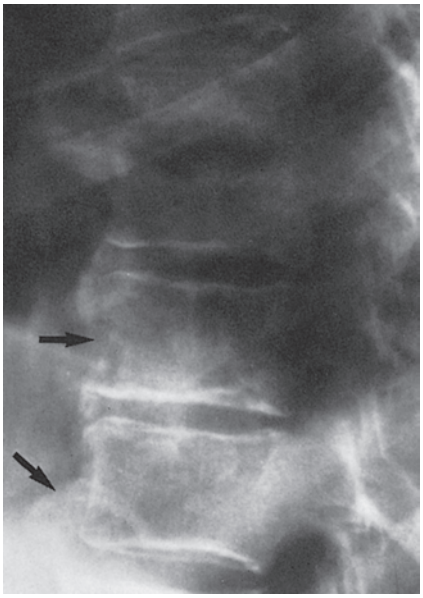

b

Fig. 12.**33 a, b** **Tuberculous spondylitis.** Paravertebral abscess is demonstrated in the AP view. Extensive destruction of two adjacent vertebral bodies with surrounding sclerosis. Anterior defects are seen in two lower vertebral bodies (arrows).

Fig. 12.**34** **Neuropathic spine.** There is sclerosis, destruction, fragmentation and altered alignment, as well as spondylosis.

Table 12.5 (Cont.) Differential Diagnosis of Anomalies of the Spine below the Axis

Disease	Radiographic Findings	Comments
Scheuermann's disease (adolescent kyphosis) (Figs. 12.35)	Commonly involves thoracic vertebrae (T4-T12). The radiographic findings include: 1 Slightly wedge-shaped vertebral bodies (kyphosis), with possibly narrowing of the anterior disk space 2 irregular but sharply demarcated endplates 3 increased sagittal diameter of involved bodies 4 Schmorl nodes 5 compensatory growth of a neighboring vertebra towards a Schmorl node 6 rarely fatigue fracture of the spinous process.	The most common disease of the spine in adolescents and young adults, considered as an aseptic necrosis of the vertebral endplate. May be painful or asymptomatic. At least 3 vertebral bodies should be involved to allow the diagnosis. Apophyseal separations may be incorrectly attributed to an acute injury.

(continues on page 283)

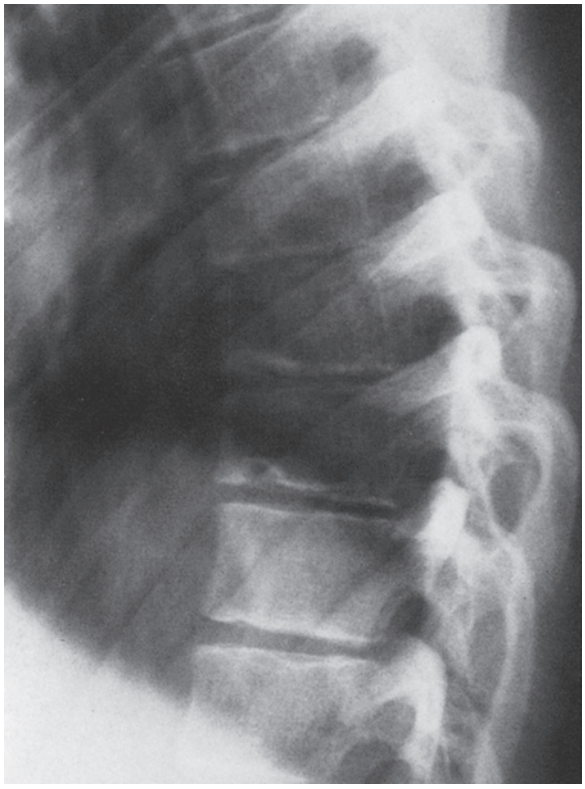

a

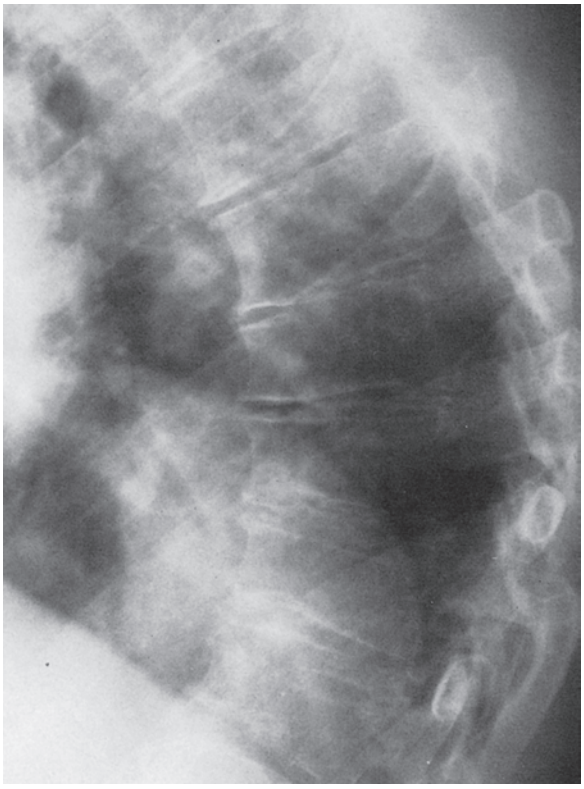

b

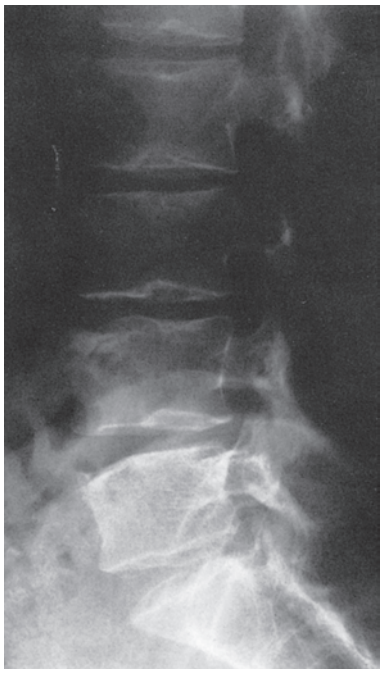

c

Fig. 12.**35 a–c** **Scheuermann's disease.** Irregular endplates, increased sagittal diameter of the vertebral bodies, and Schmorl nodes are observed, **a** Age 18, **b** age 41. Increased kyphosis due to wedge-shaped thoracic vertebral bodies, **c** Changes in the lumbar spine. Several endplates contain Schmorl nodes. Apophyseal separations in the upper anterior corners of L4 and L5 simulate fractures.

Table 12.5 (Cont.) Differential Diagnosis of Anomalies of the Spine below the Axis

Disease	Radiographic Findings	Comments
Disk degeneration (Figs. 12.36–38)	The disk space is narrower than usual. Later the adjacent endplates may become sclerotic and osteophytes develop. A streak of gas within the disk space is indicative of disk degeneration. Degeneration may induce de- creased or increased motility of the neighboring vertebrae. A “sciatic hook” is a secondary osteophyte projecting posteriorly and indicates old disk herniation. Disk degeneration together with lumbar hyperlordosis predisposes to false joint formation between spinous processes (Baastrup syndrome (Fig. 12.**37b**).	Most common between L4/L5 and L5/S1. Osteophytes developing around a not narrowed disk space is called spondylosis anterior. Small osteophytes throughout the thoracic spine, associated with increased kyphosis and osteoporosis is typical of senile kyphosis. The anterior portions of the disks are narrowed. Occasionally the vertebral bodies may even fuse together. Calcification of disks is common in a thoracic spine with spondylosis. Multiple disk degenerations associated with disk calcifications are characteristic of ochronosis (alkaptonuria) (Fig. 12.**38**).

(continues on page 284)

Fig. 12.**36 Disk degeneration** between L4/L5. The disk space is narrow and contains gas.

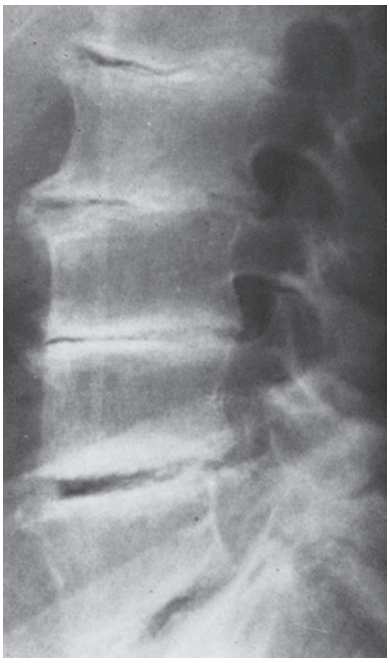

Fig. 12.**38 Multiple disk degenerations** and calcification of disk spaces secondary to ochronosis. There is anteposition of L5 relative to S1 (pseudolisthesis)

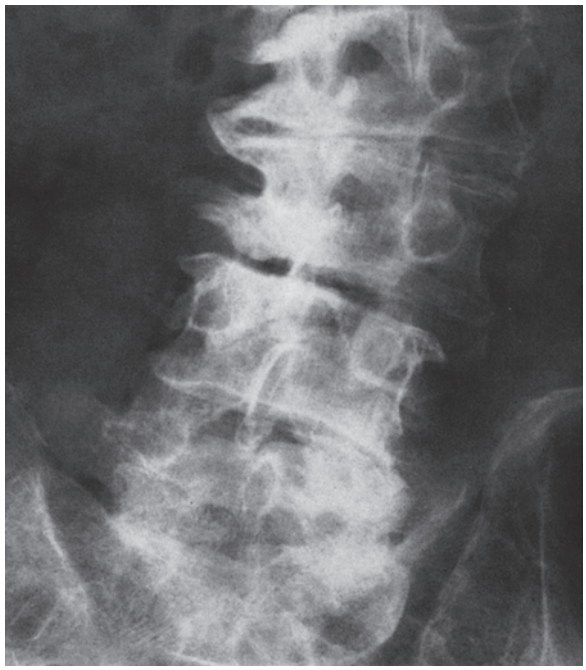

a

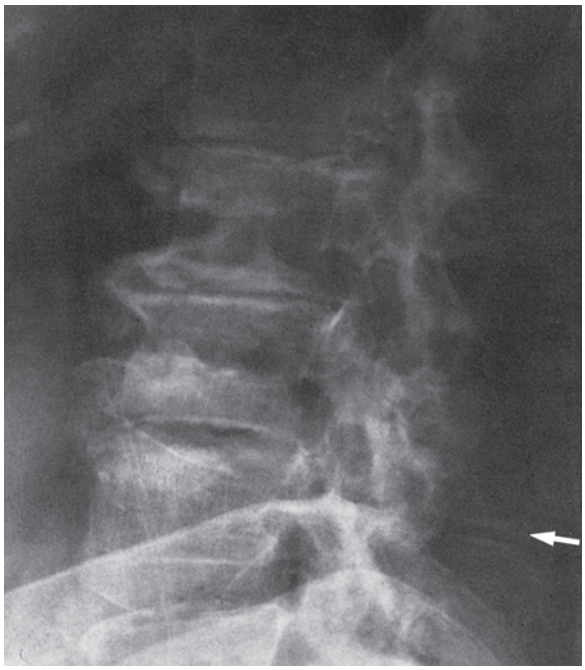

b

Fig. 12.**37 a, b Multiple disk degenerations** with scoliosis and extensive osteophytes. In the lateral view the osteophytes appear as sclerotic lines overlaying the vertebral bodies. Sclerosis in the adjacent spinous processes (arrow) indicates early Baastrup syndrome.

Table 12.5 (Cont.) Differential Diagnosis of Anomalies of the Spine below the Axis

Disease	Radiographic Findings	Comments
DISH (Diffuse idiopathic skeletal hyperostosis, ankylosing hyperostosis, Forestier's disease) (Fig. 12.39)	Flowing calcification and ossification along the anterolateral aspects of 4 or more contiguous vertebral bodies. The disk height in the involved segment is preserved, and apophyseal and sacroiliac joint manifestations are absent. Most commonly affects the thoracic and lumbar spine.	Additional findings include bony profile ration at sites of ligament and tendon attachments, calcification of iliolumbal and sacrotuberous and even other ligaments, and para-articular osteophytes. Etiology is unknown, but the condition often accompanies arthropathies, seronegative rheumatoid arthritis, diabetes, and other diseases. The only constant association is older age, generally over 50.
Paget's disease (Osteitis deformans) (Figs. 12.40 and 12.41)	Both vertebral body and arch are enlarged, having a rim of thickened cortex (a picture frame appearance), coarse trabeculae. Ivory appearance or squaring of the anterior margin are other presentations. Pathologic fractures may occur. May involve one or several vertebrae.	Involvement of the neural arch and spinous processes helps to differentiate Paget's disease from carcinoma metastases. Thickened cortex is not a feature of vertebral hemangioma. Squaring of the anterior margin helps to differentiate Paget's disease from osteoblastic metastases and Hodgkin's disease.
Nondiscogenic sclerosis (Fig. 12.42)	Homogeneously dense areas involving large segments of one or two vertebral bodies. They are usually continuous with the cortex or endplate and there is no narrowing of the disk space.	An asymptomatic localized, stable, benign, nonneoplastic form of vertebral body osteosclerosis of unknown etiology. It should be differentiated from bone island or sclerosis secondary to disk degeneration (discogenic sclerosis).

a

b

Fig. 12.**39 a, b** **DISH.** Extensive ankylosing osteophytes and calcification of disks, but the disk spaces are not narrowed.

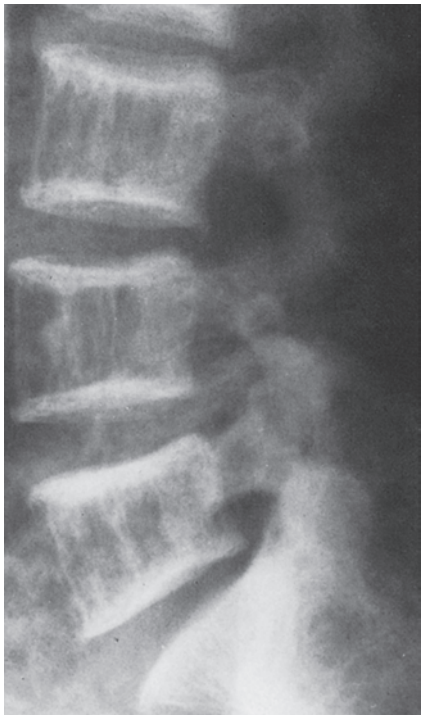

Fig. 12.**40** **Paget's disease.** Squared vertebral bodies have a framed appearance and coarse trabeculae. The process also involves the neural arches.

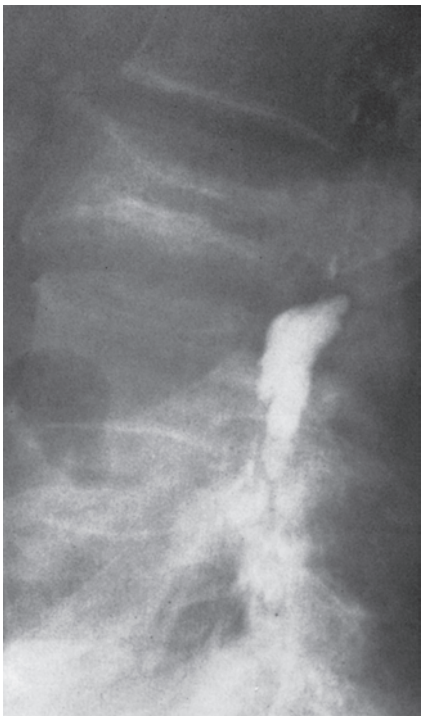

Fig. 12.**41** **Paget's disease.** Enlarged diameter of a partially collapsed vertebral body. Dural sac contains oily myelograph contrast media.

Fig. 12.**42** **Non-discogenic sclerosis.** A homogeneous density associated with the upper endplate of L4 without other abnormalities. Two disk degenerations (L4 and L5) are also seen.

Table 12.6 Differential Diagnosis of Bone Tumors in the Spine and Pelvis

Disease	Radiographic Findings	Comments
Benign bone tumors		
Aneurysmal bone cyst (Fig. 5.15c)	Lytic expansile lesion covered by a thin shell of bone. Involves primarily the posterior elements and possibly the body of the vertebra. May cross a vertebral interspace and involve adjacent vertebrae, a feature not often seen in other tumors, with the exception of chordoma.	Approximately 20% of aneurysmal bone cysts appear in the spine and another 15–20% in the pelvis. Rare after 25 years of age. The second most common benign spinal tumor.
Hemangioma (Figs. 12.43 and 5.20)	Vertebral lesions in the thoracic and lumbar areas with prominent or thickened vertical trabeculae are generally called hemangiomas, but some may only represent telangiectasia or varicosity of osseous veins. A true hemangioma may also present as an expansile or lucent lesion in the vertebral body.	Approximately 15% of true hemangiomas appear in the spine. Small hemangiomas are very common in spine (incidence over 10%), but they cannot be seen in roentgenograms.
Osteoid osteoma (Fig. 12.44a) **Osteoblastoma (Fig. 12.45)**	Located almost always in the posterior elements and seen as a "dense pedicle." Lesions less than 1.5 cm in diameter are called osteoid osteomas and those greater than 1.5 cm are called osteoblastomas. Expansion of the bone is common in bigger lesions. Scoliosis is common and the tumor is usually at the apex of the concavity. Another presentation of osteoblastoma is a lytic lesion with occasionally sclerotic margin, which is useful in differentiating it from an aneurysmal bone cyst.	Approximately 40% of osteoblastomas and 5% of osteoid osteomas appear in the spine, rarely in pelvis. Over 15% of benign spinal tumors belong to this category. Unilateral spondylolysis or hypoplasia of the posterior elements may induce localized hypertrophy and sclerosis in the contralateral pedicle and pars interarticularis, mimicking an osteoid osteoma (Fig. 12.**44b**).
Giant cell tumor	A radiolucent lesion with well-defined margins without sclerosis of adjacent bone. Expansile in the sacrum and pelvis. Rarely crosses the sacroiliac joint.	Over 10% of giant cell tumors occur in the spinal column, mostly in the sacrum. The most common benign tumor of the spine. Pelvis is almost as commonly affected.
Other spinal lesions		
Eosinophilic granuloma (Fig. 12.46)	The destructive phase with spotty radiolucen-cies in the centrum of the vertebra is followed by vertebral collapse and a residual vertebra plana. The disk spaces are preserved.	The majority of eosinophilic granulomas occur in children under 10 years of age. More common in pelvis (above acetabulum) than in spine. Reactive sclerosis along the margin of a destructive pelvic lesion is typical.

(continues on page 288)

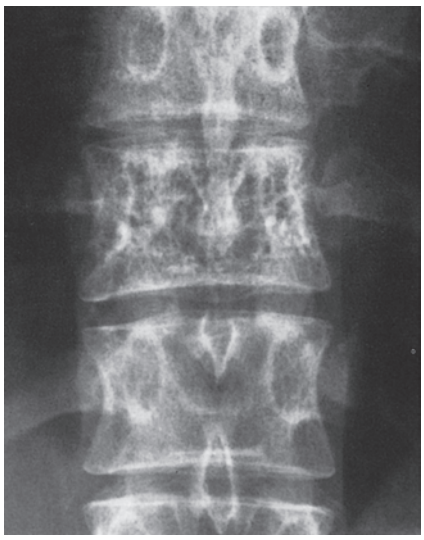

Fig. 12.**43** **Hemangioma** of T11.

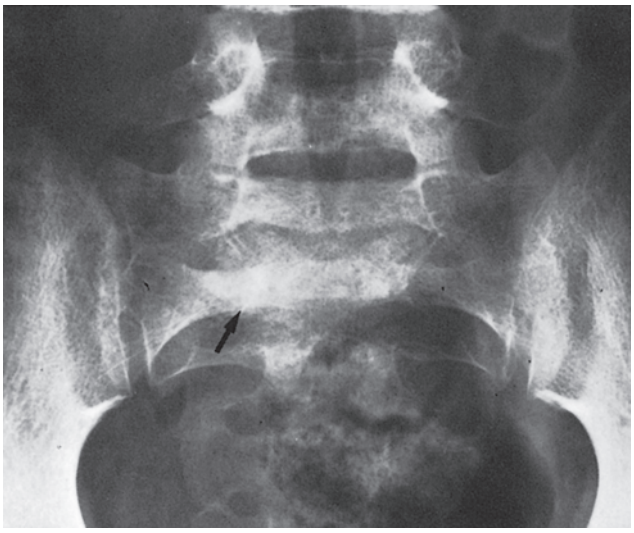

Fig. 12.**44 a** **Osteoid osteoma** of sacrum seen as a sclerotic area (arrow).

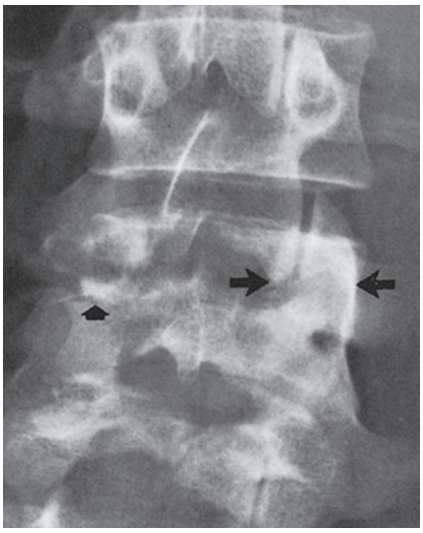

Fig. 12.**44 b** **Unilateral spondylolysis** with sclerosis of the contralateral pedicle mimicking osteoid osteoma. Spondylolysis of the right pars interarticularis (short arrow) of L4 is associated with a hypertrophic sclerotic left pedicle (arrows) in the same vertebra.

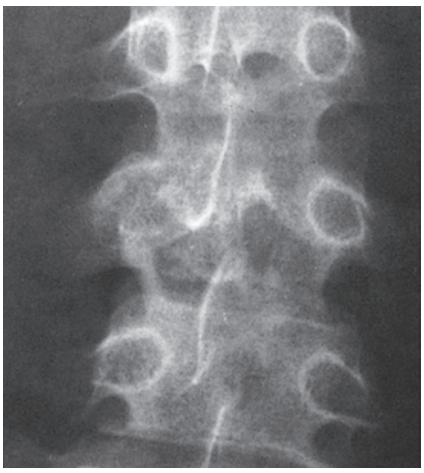

Fig. 12.**45** **Osteoblastoma.** An expansile lytic lesion surrounded by some sclerosis, also involving the pedicle of L3.

Fig. 12.**46** **Eosinophilic granuloma.** Collapse of the body of C3.

Table 12.6 (Cont.) Differential Diagnosis of Bone Tumors in the Spine and Pelvis

Disease	Radiographic Findings	Comments
Malignant bone tumors		
Chordoma (Fig. 12.47 and Fig. 5.25)	A lytic, expanding lesion in the sacrum, coccyx or less commonly C2 or elsewhere in the cervical spine, with stippled calcifications in approximately 30% of cases. It may expand to adjacent vertebrae and soft tissues.	About 50% occur in the sacrococcygeal area, where it is characteristically associated with a presacral soft-tissue mass, 30% in the clivus, and the remaining 20% in cervical or lumbar areas.
Sacrococcygeal teratoma	A soft-tissue mass in the sacrococcygeal area with irregular calcification or ossification.	Teratomas are composed of mixed tissues, often containing bone and cartilage. Less than 40% are malignant, presenting as a large soft-tissue mass.
Fibrosarcoma (Fig. 12.48)	Medullary fibrosarcoma is more frequent and appears as a poorly marginated or even permeative osteolytic lesion. Periosteal fibrosarcoma causes cortical erosion and minimal periosteal reaction.	Fibrosarcoma appears relatively often in the pelvis and sacrum, rarely in the upper spinal columns. Malignant fibrous histiocytoma may have identical appearance.
Osteosarcoma	See Table 5.**3**.	Rare in the spine, relatively common in the pelvis.
Plasmocytoma	A lytic, often expansile lesion of the vertebral body or pelvic bone. Sclerotic margin is rare.	A precursor of multiple myeloma.
Ewing's tumor (Ewing's sarcoma) (Figs. 12.49, 12.50)	The lesion in the spine is either sclerotic or lytic and may resemble osteosarcoma. A large paraspinal soft-tissue mass is frequently associated.	Primary Ewing's tumor of the spine is rare, but it is relatively common in sacrum. Pelvis is the second most common location. Metastatic involvement of the spine is frequent.

(continues on page 290)

Fig. 12.**47** **Chordoma.** Expansile destruction of C4, including enlargement of the neural foramen.

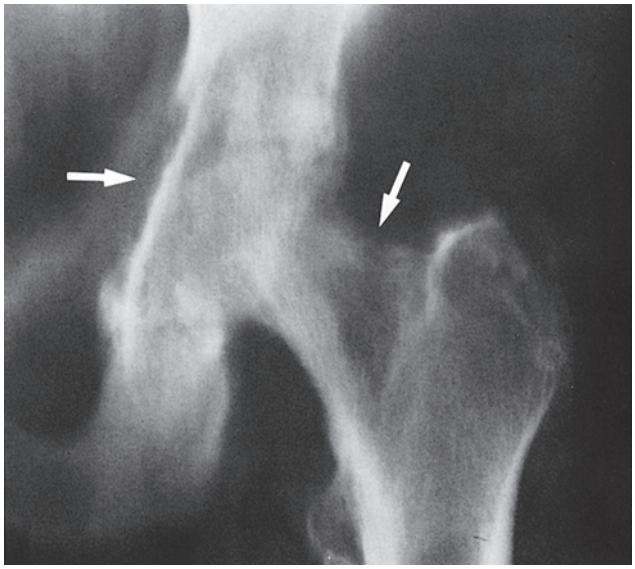

Fig. 12.**48** **Fibrosarcoma.** Tomography reveals poorly marginated destruction of the acetabulum and the femoral neck (arrows).

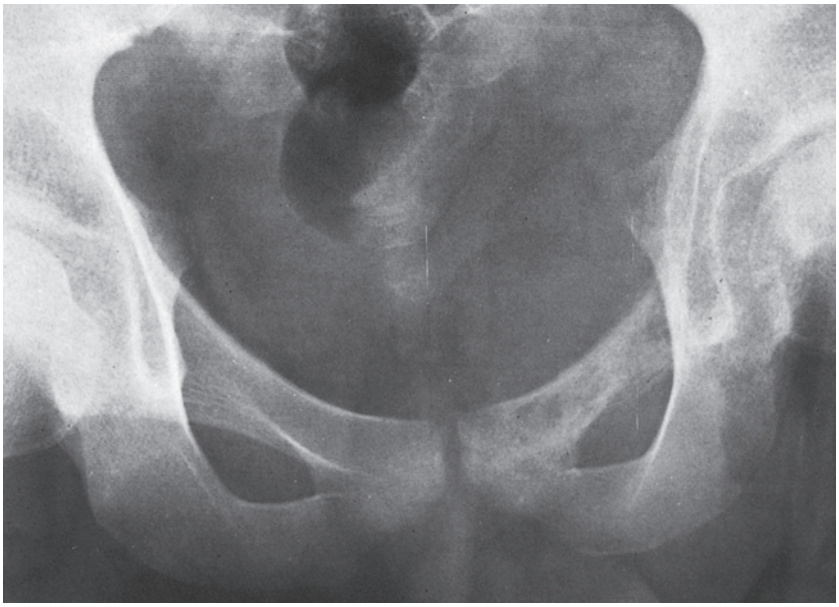

Fig. 12.**49** **Ewing's tumor.** Permeative destruction of the left acetabulum, ischium, and pubic bone. Lamellated periosteal reaction is seen in the pubic bone.

Fig. 12.**50** **Mixed lytic and sclerotic destruction** of the left ilium and sacrum by a tumor with histological characteristics of Ewing's tumor.

Table 12.6 (Cont.) Differential Diagnosis of Bone Tumors in the Spine and Pelvis

Disease	Radiographic Findings	Comments
Lymphomas (Figs. 12.51–53)	Spinal lymphoma is osteolytic in the majority of cases, but osteosclerosis and periosteal reaction occur. In Hodgkin's disease, marginal erosion of the vertebral bodies by lymph nodes is sometimes seen. The ivory type of sclerotic vertebra is more common in Hodgkin's than non-Hodgkin's lymphoma.	Extranodal disease including spinal and pelvic involvement is more common in non-Hodgkin's lymphomas than in Hodgkin's disease.
Chondrosarcoma (Figs. 12.54, 12.55 and 5.26a)	See Table 5.**3**	Pelvis is the most common location.
Hemangiopericytoma	Osteolytic, poorly marginated lesion. May affect either entire vertebra or a part of it.	A poorly understood, rare vascular neoplasm encountered in middle-aged patients, usually in the spine or pelvis. Differentiation from malignant fibrous tumors or metastasis is difficult.
Metastasis (Fig. 12.56)	Either lytic, mixed or sclerotic destruction of the vertebral body and pedicle is characteristic (see Chapter 5).	Primary malignancies are rare as compared with the high incidence of metastases. If several vertebrae are affected, metastases or multiple myeloma are likely.
Multiple myeloma (Fig. 12.57)	Loss of bone density and accentuation of trabecular pattern in spine and diffuse osteolytic lesions in pelvis are the most common patterns. (For other features, see Chapter 5)	Sparing of pedicles in the presence of osteolytic destruction of vertebral bodies differentiates multiple myeloma from typical osteolytic metastases.

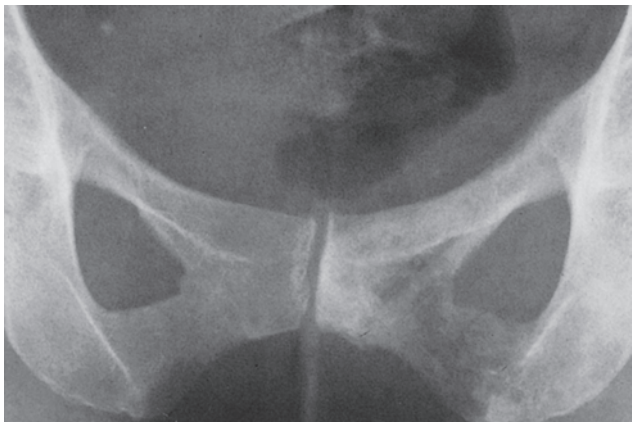

Fig. 12.**51** **Mixed lytic and sclerotic destruction** of the left pubic area by a non-Hodgkin's lymphoma of bone.

a

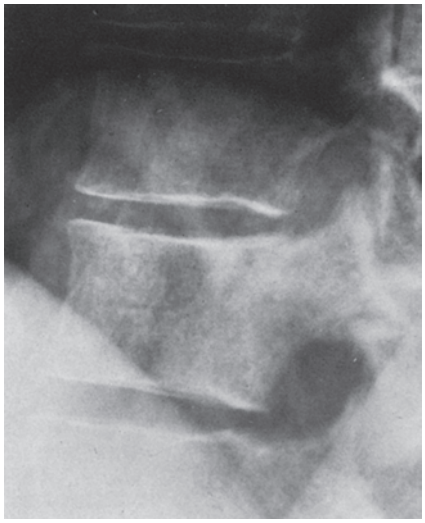

b

Fig. 12.**52 a, b** **Non-Hodgkin's lymphoma** of T11 causing mostly sclerotic destruction of the vertebral body and pedicle.

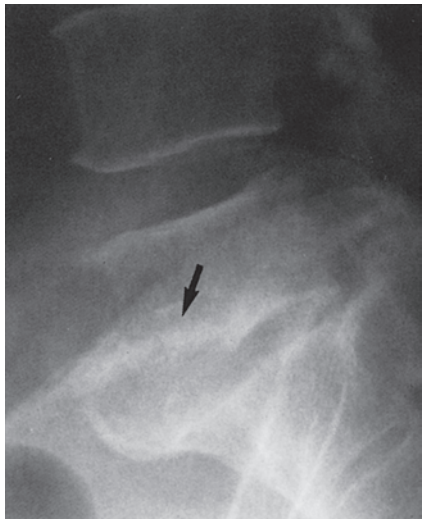

Fig. 12.**53** **Non-Hodgkin's lymphoma** that erodes the inferior endplate of L5 and its marginal spur (arrow).

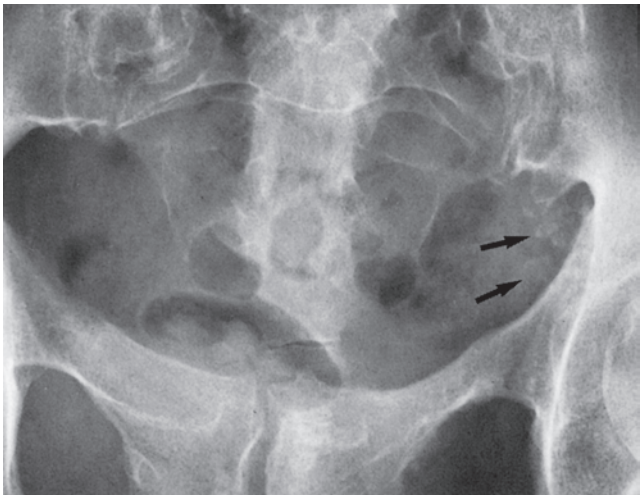

Fig. 12.**54** **Chondrosarcoma** of pelvis that started from a preexisting exostosis in the inferior aspect of the iliac bone. Typical tumor calcification is seen near the apex of the exostosis (arrows).

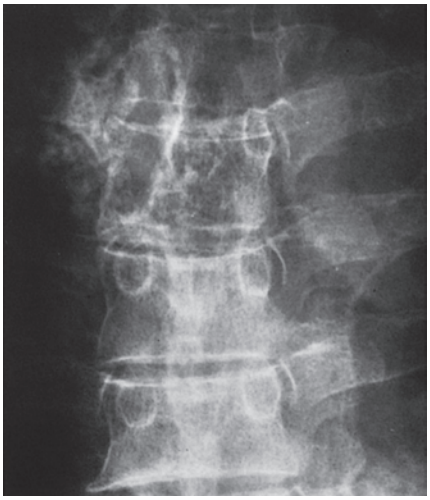

Fig. 12.**55** **Chondrosarcoma** of the thoracic spine involving two adjacent vertebrae as an osteolytic lesion with sclerotic margins and tumor calcification.

a **b** **c**

Fig. 12.**56 a–c** **Metastatic lesions** of the spine.
a Osteosclerotic metastases from breast carcinoma involving both the body and pedicle, **b** Osteolytic metastasis from renal adenocarcinoma with destruction of the pedicle, **c** "Ivory" vertebra due to metastatic carcinoma of the prostate, uncharacteristically only involving the body.

Fig. 12.**57** **Multiple myeloma.** Patchy demineralization of spinal bodies. One vertebral body has collapsed superiorly.

Table 12.7 Differential Diagnosis of Localized Lesions of the Pelvis

Disease	Radiographic Findings	Comments
Caudal hypoplasia	Absence or hypoplasia of the sacral segments and sacroiliac joints. Hypoplasia and deformity of pelvic bones.	Often a baby of a diabetic mother. Associated with urogenital, gastrointestinal, and neural anomalies. Widening of pubic symphysis and other anomalies often are associated with urogenital anomalies.
Cleidocranial dysostosis	Most constant radiologic findings are in the skull, clavicles, and pelvis. There is separation of pubic symphysis, defective ossification of the ischia, pubis, hypoplasia of iliac wings, and hypoplastic sacrum.	A congenital dysostosis with faulty intramembranous bone formation which results in large head relative to small facial bones, narrow chest, and ragging shoulders. Hypoplastic changes are present in facial bones and clavicles. Spine may show fusion defects.
Hereditary onychoosteodysplasia	Osteocartilagineous exostoses extending posteriorly from the iliac wings (iliac horns) are characteristic. The patella may show subluxation, hypoplasia, or aplasia. Radial head may also be hypoplastic.	An autosomal dominant disorder of ectodermal and mesodermal tissues, mainly manifesting dysplastic changes in nails, pelvis, knees and elbows. Iliac horns without associated abnormalities are called Fong's disease (Fig. 12.**58**).
Down's syndrome (Trisomy 21–22)	Flaring of the iliac wings, flattening of the roofs of the acetabula, and ischial tapering are characteristic radiological findings. Atlantoaxial subluxation is common.	Upward slanting eyes and characteristic face are detectable at birth. In trisomy 17–18 syndrome, the pelvis has an "antimongoloid" configuration.
Paget's disease (Osteitis deformans) (Fig. 12.59)	Cortical thickening, particularly of the pelvic rim, enlargement of the pubis and ischium, and coarse trabecular pattern are characteristic.	Pelvis is commonly involved, showing usually mixed lytic and sclerotic changes,
Osteitis condensans ilii (hyperostosis triangularis ilii) (Fig. 12.60)	Bilateral sclerosis of the iliac bones with normal sacroiliac joints. Triangular sclerosis is limited to the anterior aspect of the lower two thirds of the height of the sacroiliac joint.	Common among women of childbearing age. The bilateral triangular pattern distinguishes this condition from unilateral sclerotic conditions like a bone island, blastic metastases, sacroilitis circumscripta, or Paget's disease.
Sacroiliitis circumscripta (Fig. 12.61)	A circular or polycyclic, well-delineated area of sclerosis involving both sacral and iliac sides of the sacroiliac joint, with minimal erosion of the joint surfaces.	A rare inflammation of unknown etiology. Should be differentiated from osteitis condensans ilii, in which sacrum is not involved. Capsular calcifications of the sacroiliac joint (joint surfaces unaffected).

(continues on page 294)

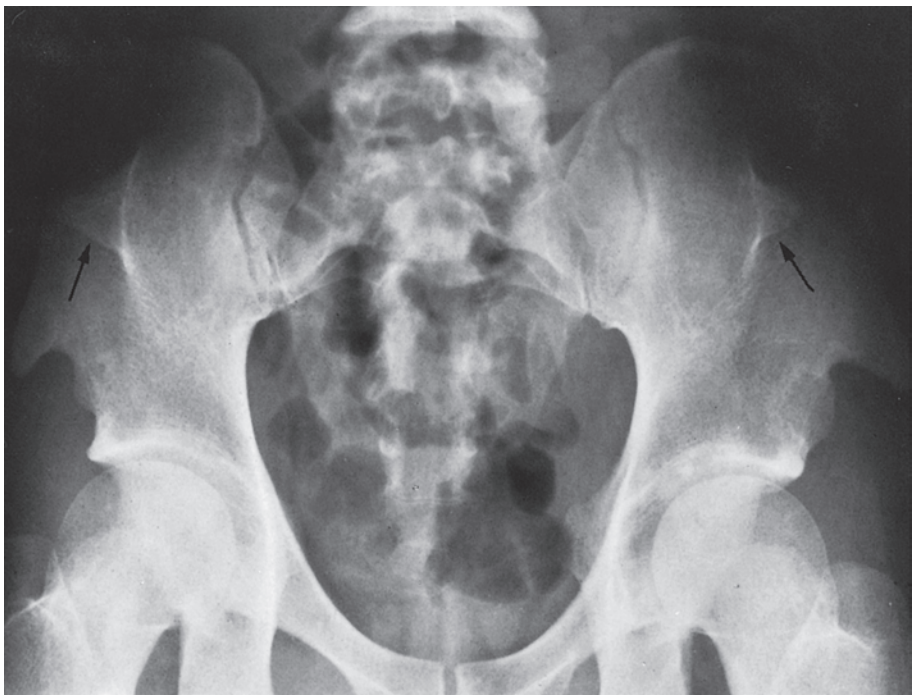

Fig. 12.**58** **Iliac horns** (arrows), Fong's disease.

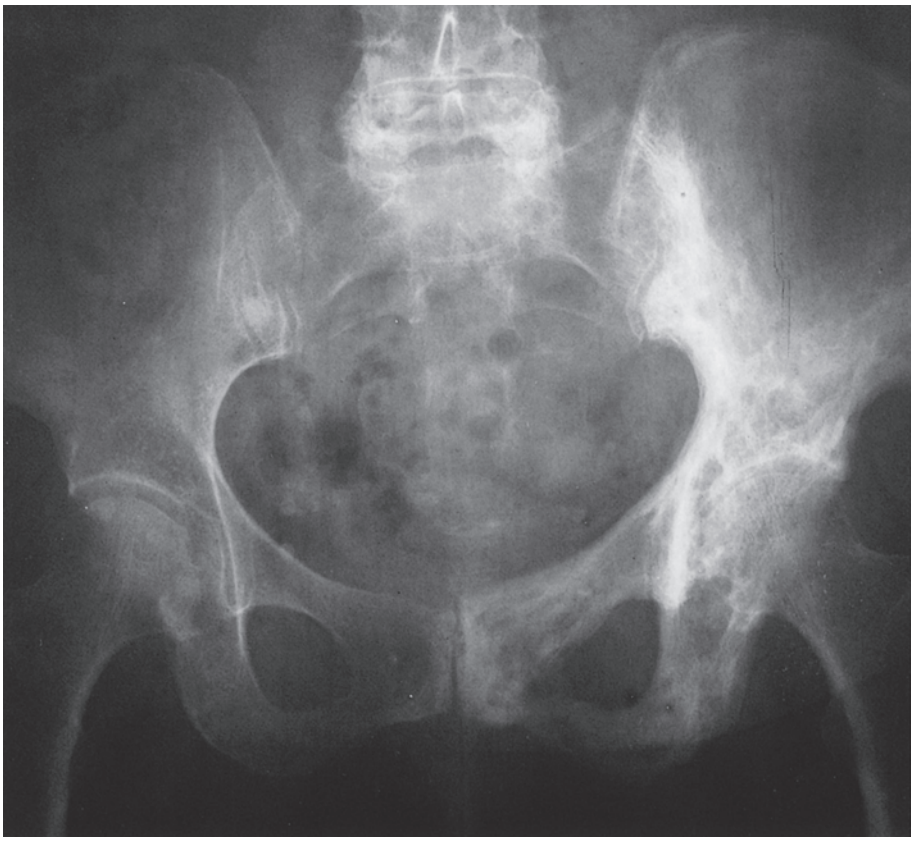

Fig. 12.**59** **Paget's disease** in the left pelvic bones. Enlargement of pubis and ischium and coarse trabecular pattern:

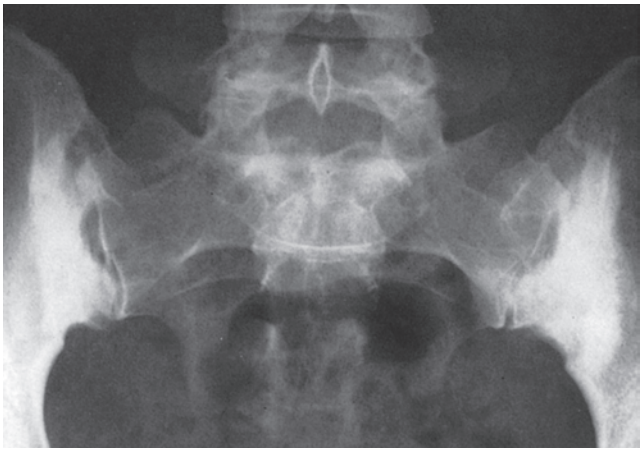

Fig. 12.**60** **Osteitis condensans ilii.** Bilateral triangular sclerosis of the iliac bones, normal sacroiliac joints.

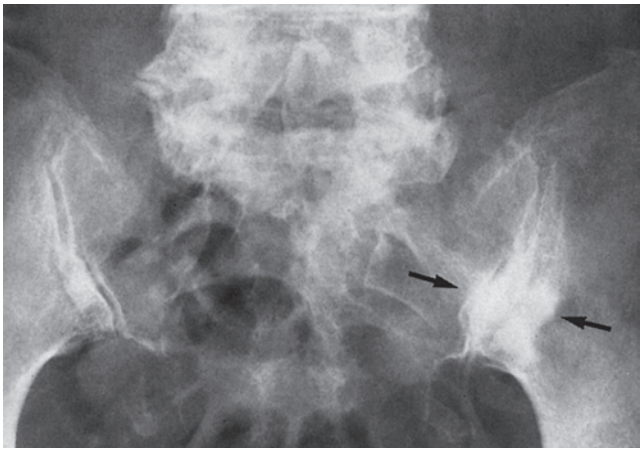

Fig. 12.**61** **Sacroiliitis circumscripta.** Polycyclic sclerosis on both sides of the sacroiliac joint. Tomography revealed minimal erosion.

Table 12.7 (Cont.) Differential Diagnosis of Localized Lesions of the Pelvis

Disease	Radiographic Findings	Comments
Pyogenic or tuberculous sacroilitis (Fig. 12.62)	Usually unilateral destruction of sacroiliac joint. May be surrounded by sclerosis and soft tissue calcification. Old sacroilitis may be seen as fusion of the joint.	Destruction of the sacroiliac joint cartilage is rare in relapsing polychondritis.
Osteochondrosis sacri	Sclerotic fragmentation of the lateral sacral apophyses with normal outline of the iliac joint contour.	A rare aseptic necrosis of the sacral apophyses. Occurs at the age of 16 to 20. Absence of erosions differentiates from juvenile ankylosing spondylitis and infection.
Osteolysis syndromes	Regional loss of bone around the sacroiliac joint (or elsewhere).	Very rare conditions, which may be associated with angiomatosis or lymphangiomatosis of bone in a child (massive osteolysis Gorham-Stout) or osteolysis secondary to paraplegia.
Osteonecrosis pubis	Erosion and/or sclerosis of the inferior and/or middle portion of the pubic symphysis (the attachment of the gracilis, adductor longus, and adductor brevis muscles).	A painful bone reaction similar to fatigue fractures. Usually occurs in young athletes, with pain in the pubic area.
Osteitis pubis (Fig. 12.63)	Demineralization, erosion, sclerosis of the pubic symphysis. Bridging of the pubic symphysis may result when healing,	Bacterial or aseptic inflammation of the pubic synchondrosis. Usually occurs 4 to 12 weeks after prostatectomy or other urogenital operation. Pregnancy, ankylosing spondylitis and other arthritides are more common causes of widening and/or erosion of the pubic symphysis.

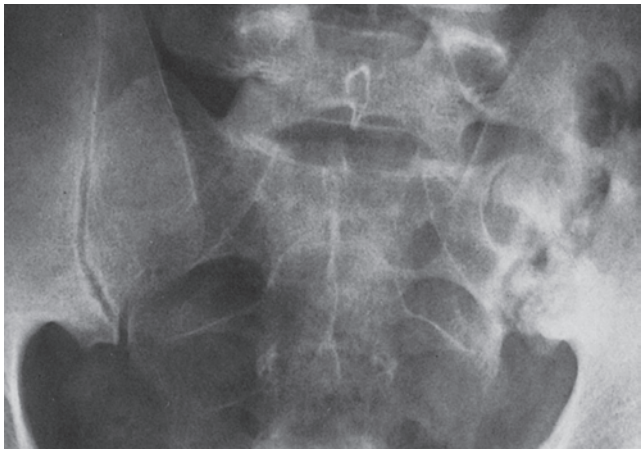

Fig. 12.**62** **Tuberculous sacroiliitis** with deep localized bone destruction, surrounding sclerosis, and calcification of soft tissue.

Fig. 12.**63** **Osteitis pubis** (aseptic). Widening of the symphysis, erosion of bone, and periosteal reaction at the pelvic rim (arrows).

Table 12.8 Differential Diagnosis of Disease with Generalized Involvement of Both Spine and Pelvis

Disease	Radiographic Findings	Comments
Achondroplasia (Fig. 12.64)	At birth, the spine shows flattened vertebral bodies and an increased height of the intervertebral spaces. The spinal canal is narrow, Hypoplasia of upper lumbar vertebra with kyphosis, partial beaking of lumbar vertebral bodies, and posterior scalloping may be present, The pelvis is smaller than normal due to short iliac bones and narrow sacrum. Milder forms exist. (See also spinal stenosis Fig. 12.**29**)	A hereditary bone dysplasia with a defect in enchondral bone formation.
Hurler's syndrome (mucopolysaccharidosis I) (gargoylism) (Figs. 12.65)	The vertebral bodies are oval with an anterior inferior beak. A hypoplastic "sail" vertebra may be present in the upper lumbar region causing angular kyphosis.	An autosomal recessive disease with dwarfism, retardation, and coarse facial features. The patients excrete heparan sulfate and dermatan sulfate in urine. Bone changes are seen after 2 years of age. The spinal changes may suggest an intraspinal mass.

(continues on page 296)

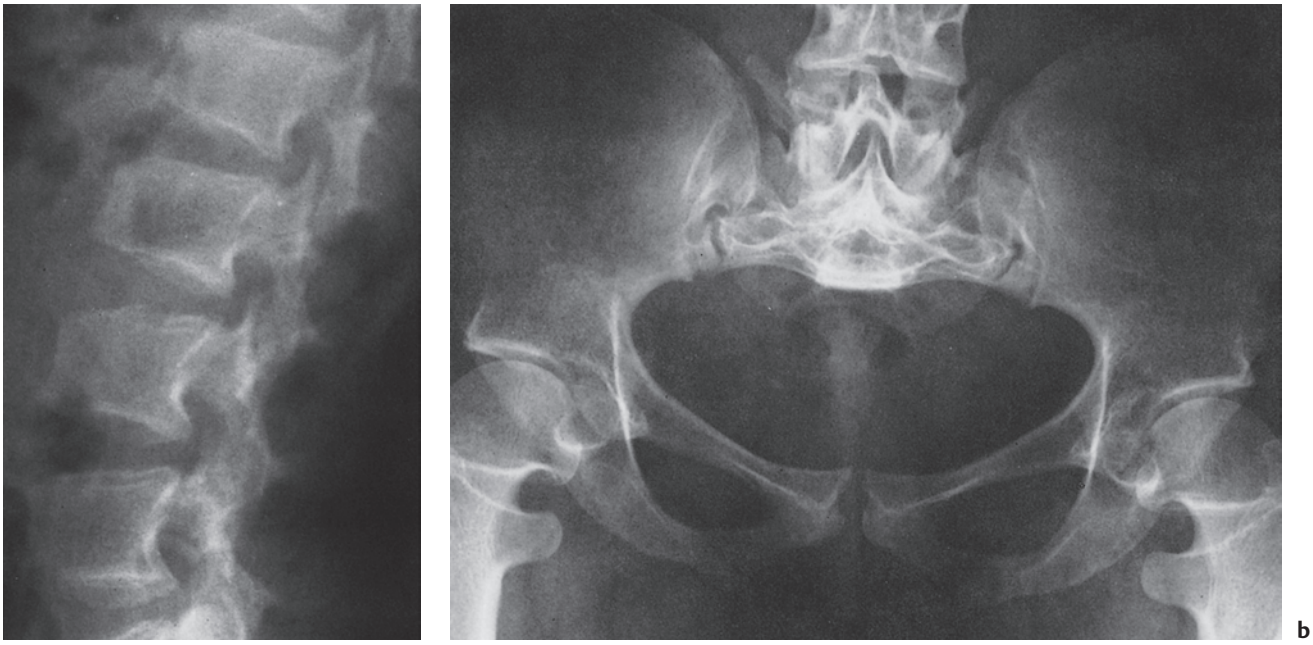

a b

Fig. 12.**64 a, b** **Achondroplasia. a** Abnormal vertebral bodies with partial beaking and posterior scalloping of vertebral bodies, **b** Hypoplastic sacrum, abnormal shape of pelvis and hip joints.

Fig. 12.**65** **Hurler's syndrome.** Oval vertebral bodies with an anterior inferior beak.

Table 12.8 (Cont.) Differential Diagnosis of Disease with Generalized Involvement of Both Spine and Pelvis

Disease	Radiographic Findings	Comments
Hunter's syndrome (mucopolysaccharidosis II) Fig. 12.66)	Hypoplasia of the pedicles and widening of the interpediculate spaces with posterior vertebral scalloping may be present.	The inferior beaking of ovoid bodies distinguish this condition from Morquio's syndrome. Hunter's syndrome is radiologically similar to Hurler's syndrome, but has a slower rate of progression.
Morquio's syndrome (mucopolysaccharidosis IV) (Fig. 12.67)	Universal vertebra plana show a central anterior beak in contrast to the inferior anterior beak seen in Hurler's syndrome. Other spinal findings include hypoplastic dens with atlantoaxial instability, dorsolumbar rotary kyphoscoliosis, and increased interpediculate distance as well as small sacrum with a narrow ovoid pelvic inlet and wide acetabula.	Manifests clinically during the second year of life. The patients excrete keratan sulfate in the urine. The trunk is short, whereas extremities are relatively normal. There is usually no mental retardation, but multiple deformities of the extremities and pigeon breast are present. Spondyloepiphyseal dysplasia congenita can be differentiated from Morquio's syndrome by absence of corneal clouding and mucopolysaccharidurie and by manifestations present at birth, although spinal changes are similar in these two conditions.
Progeria	The vertebral bodies retain their infantile central notching. Bilateral coxa valga is constantly present.	A rare disease of unkown etiology characterized by dwarfism and premature aging. Beaked nose, receded chin, and baldness are typical.
Arachnodactyly (Marfan's syndrome)	Lumbar vertebrae may be abnormally tall, ilium may be vertical with wide pelvic cavity. Widening of the spinal canal and posterior scalloping of vertebral bodies are noted. Scoliosis is common.	An autosomal dominant growth disturbance caused by failure to produce normal collagen. Long slender metatarsals, metacarpals, and phalanges are characteristic.
Homocystinuria	Flattening and biconcavity of osteoporotic vertebral bodies are a distinctive difference to Marfan's syndrome.	A hereditary, somewhat heterogeneous condition, usually a lack of enzyme cystathionine beta synthetase. One third of patients show changes similar to those seen in Marfan's syndrome.
Neurofibromatosis I (von Recklinghausen's disease) (Fig. 12.68)	Radiographic findings in the spine are multiple. Kyphoscoliosis with dysplastic vertebral bodies, erosion of intervertebral foramina due to "dumbbell" neurofibromas and posterior scalloping of the vertebral bodies with or without meningoceles are commonly observed. Several other spinal or pelvic anomalies are encountered, but they are not diagnostic of this disease.	A hereditary disturbance of mesodermal and neuroectodermal tissues. Neurofibromas, smooth marginated cafe-au-lait spots on the skin, and bone deformities are characteristic findings.

(continues on page 298)

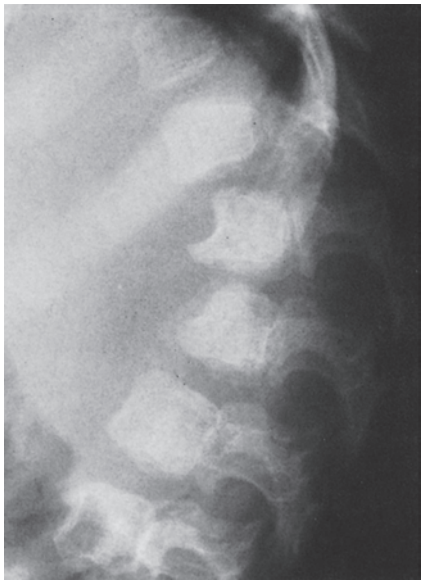

Fig. 12.**66** **Hunter's syndrome.** A hypoplastic vertebra with characteristic inferior beak and kyfosis is seen.

Fig. 12.**67** **Morquio's syndrome.** Universally flat vertebrae have a central anterior beak.

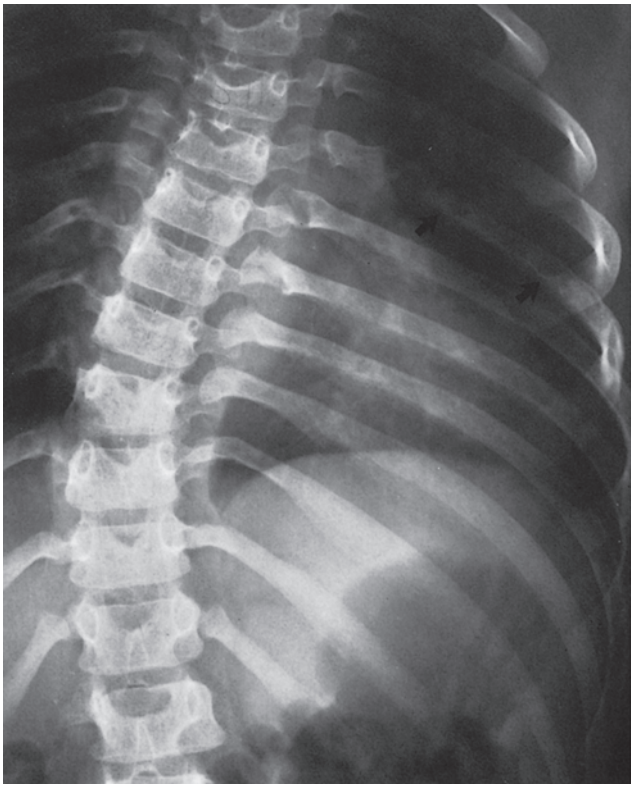

a

b

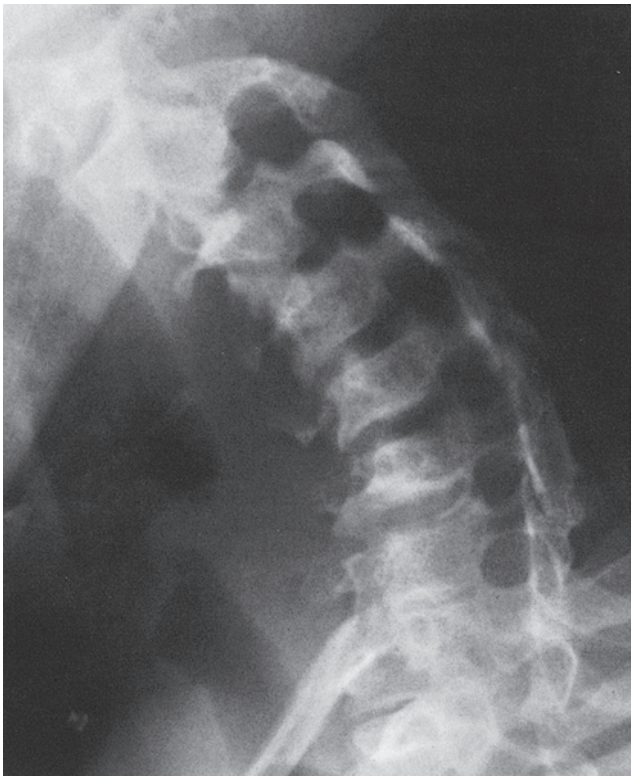

c

Fig. 12.**68 a, b, c** **Neurofibromatosis.** **a** AP projection shows scoliosis and rib abnormalities (arrows), **b** Lateral projection demonstrates posterior scalloping of vertebral bodies. Slightly enlarged neural foramina at the thoracolumbar region. **c** Oblique view of the cervical spine demonstrates dysplastic cervical vertebrae with scoliosis and wide neural foramina.

Table 12.8 (Cont.) Differential Diagnosis of Disease with Generalized Involvement of Both Spine and Pelvis

Disease	Radiographic Findings	Comments
Osteogenesis imperfecta (Fig. 12.69)	The vertebral bodies are osteoporotic and have a nonuniform biconcave configuration. Scoliosis and protrusio acetabuli are common.	An inherited autosomal dominant connective tissue disorder. The congenital form is present at birth; the tarda form may manifest in puberty or adulthood. Osteoporosis, multiple fractures, bowing of the long bones and blue sclera are characteristic.
Sickle-cell anemia (Fig. 12.70)	The spine is radiolucent even in young adults. The trabecular pattern is coarse, producing areas of increased and decreased bone density. Vertebral bodies tend to be biconcave. A cuplike depression involving the central three-fifths of both upper and lower endplates of several vertebral bodies is typical. In children, the anterior vertebral notch may be exaggerated.	A condition in which the red blood cells assume a sickled configuration at reduced oxygen tension. An abnormal hemoglobin S is Genetically transmitted. The signs and symptoms of sickle-cell disease are due to anemia, e.g., rapid destruction of abnormal erythrocytes.
Thalassemia	Biconcavity of vertebral bodies is not a feature of thalassemia, but loss of density and coarse trabecular pattern may be seen in spine and pelvis.	A heterogeneous group of microcytic anemias based on a decreased rate of synthesis of one or more hemoglobin polypeptide chains. Heterozygotes are mildly affected. The radiographic changes in bones result from erythroid hyperplasia of the marrow.
Cretinism (congenital hypothyroidism)	Kyphosis, flattened vertebral bodies, and increased width of intervertebral spaces. An upper lumbar vertebra may have a wedge or hook configuration (sail vertebra).	The changes are not present at birth. Sail vertebrae occur also in achondroplasia, Hurler's syndrome and Morquio's syndrome.
Osteopetrosis (Albers-Schönberg disease) (Fig. 12.71)	All bones may be involved, with loss of distinction between cortex and medulla, The vertebrae and pelvis may be uniformly dense or there may be a "bone-within-a-bone" appearance of the vertebral bodies. Increased density of endplates may give rise to "sandwich vertebrae." Similar alternating. bands occur in pelvis, too.	Hereditary failure of absorption of primary spongiosa. The congenital form is inherited as an autosomal recessive and is manifest at birth. The tarda form is dominantly inherited, clinically benign and asymptomatic in 50 %. Anemia is a common clinical symptom. Somewhat similar, osteosclerosis, but without bone-within-a-bone and without anemia, is seen in a rare hereditary condition called pycnodysostosis. In osteopoikilosis, the sclerotic patches tend to occur around acetabula but not in the spine, whereas osteopathia striata may involve both pelvis and spine.

(continues on page 300)

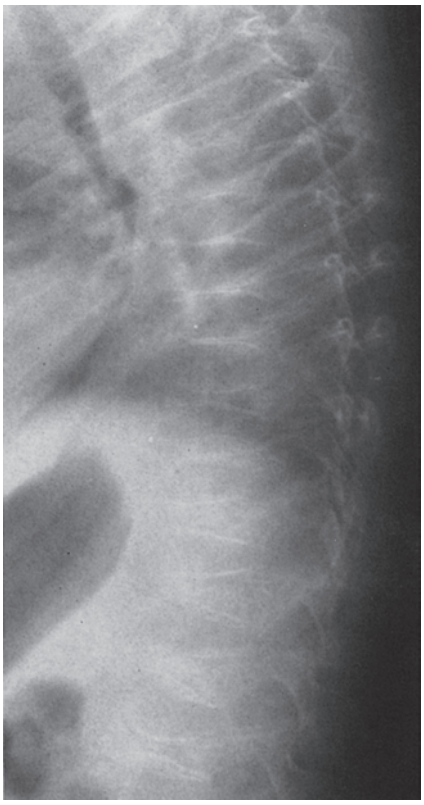

Fig. 12.**69 Osteogenesis Imperfecta** Radiolucent spine, biconcave lumbar vertebral bodies.

Fig. 12.**70 Sickle-cell anemia.** Cup-like depressions in the central endplates are clearest in the thoracolumbar region.

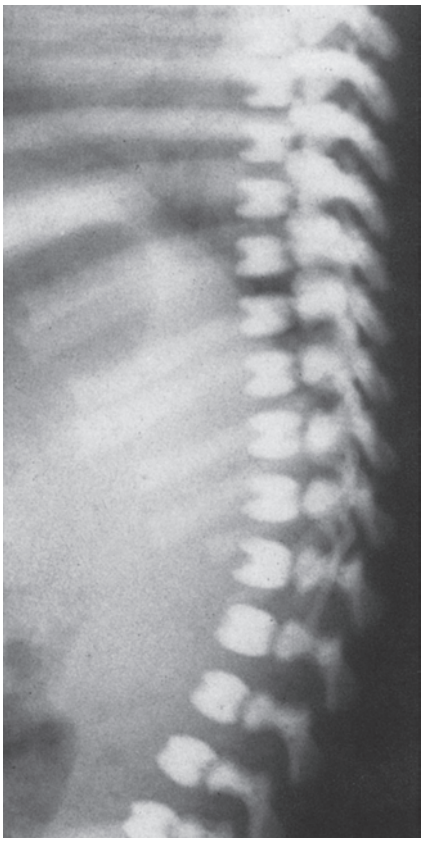

a

b

Fig. 12.**71 a, b Osteopetrosis. a** Uniformly dense vertebrae and ribs in a child, **b** "Sandwich vertebrae," increased density of the endplates.

Table 12.8 (Cont.) Differential Diagnosis of Disease with Generalized Involvement of Both Spine and Pelvis

Disease	Radiographic Findings	Comments
Myelofibrosis (myelosclerosis) (Fig. 12.72)	Variable degrees of osteosclerosis are seen in 50% of patients. The spine and pelvis are often involved. The increase of bone density may have either trabecular or "ground glass" pattern and it may be patchy.	Progressive fibrosis of the bone marrow with a leukemoid blood picture (splenomegaly) and osteosclerosis, usually in patients over 50. The condition is often preceded by polycytemia vera.
Mastocytosis (urticaria pigmentosa) (Fig. 12.73)	Spine and pelvis are commonly affected, showing a mixture of sclerosis (either diffuse or trabecular) and osteoporosis of the cancellous bone.	Abnormal number of mast cells in skin, resulting in umbilicated papules. Anemia is common. Bone marrow involvement results in sclerosis.
Tuberous sclerosis (Fig. 12.74)	Irregular patches of osteosclerosis without bone enlargement or coarsening of trabeculation. Lesions in the ilium are centrally located; pelvis and lumbar spine are involved in 40%.	A familial defect of ectodermal development. Adenoma sebaceum of the face, epilepsy, mental deficiency, hamartomas of the kidney, and small scattered intracranial calcifications are common.
Hypervitaminosis D	Vertebral bodies show dense endplates and a subcortical radiolucency.	Excessive intake of vitamin D. Metastatic calcifications are common (Chapter 7). Idiopathic hypercalcemia in a chronic form may also cause peripheral cortical sclerosis of vertebral bodies.
Fluorosis (Fig. 12.75)	Thickening of the trabecular pattern of the vertebral bodies and pelvis (also ribs and clavicles) is followed by dense, uniform, symmetrical sclerosis. Osteophytes are characteristically large and sclerotic. Bones may be widened. Calcification of the iliolumbal and sacral ligaments is common.	Excessive intake of fluoride, which inhibits normal bone resorption.

(continues on page 302)

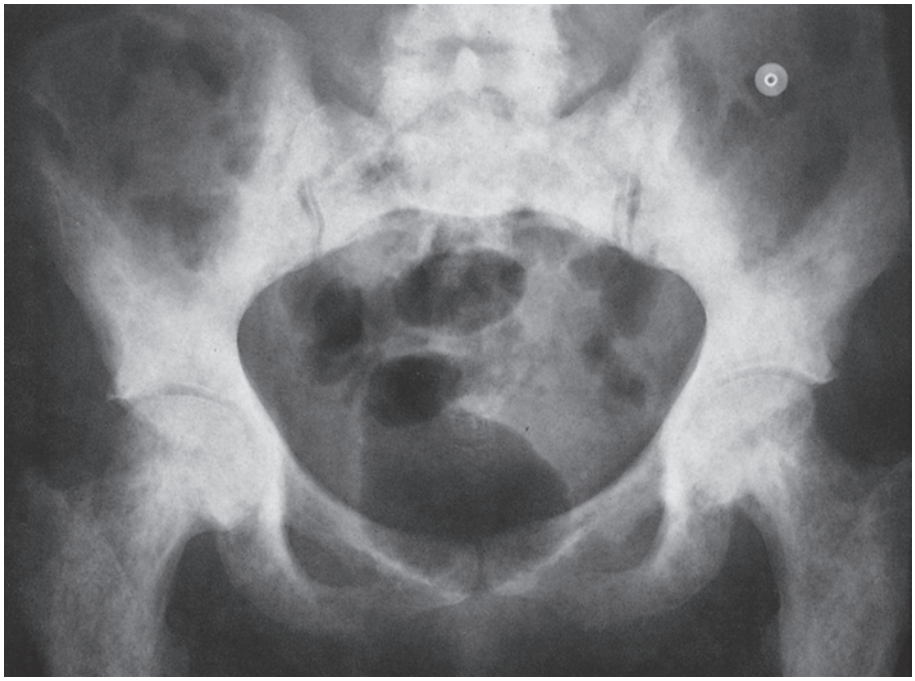

Fig. 12.**72** **Myelofibrosis.** Patchy sclerosis of the pelvis, lower lumbar spine, and upper femora. The pattern mimics widespread osteosclerotic metastases (e.g., carcinoma of prostate).

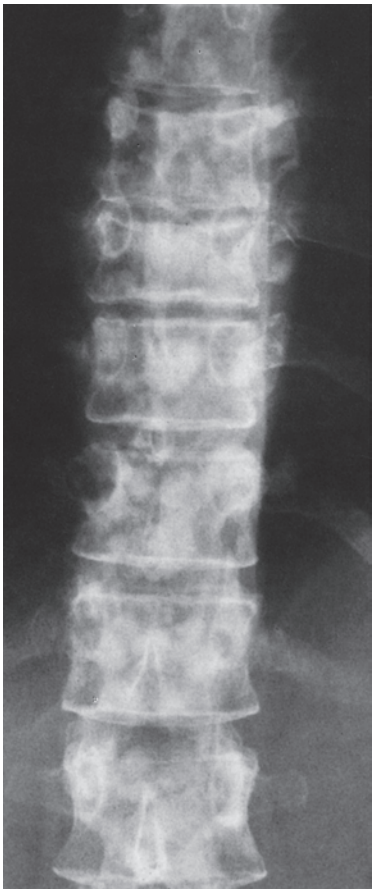

Fig. 12.**73** **Mastocytosis.** The vertebral bodies show patchy sclerosis

Fig. 12.**74** **Tuberous sclerosis.** Irregular patches of sclerosis are present around the pelvic rim, sacroiliac joints, and in the sacrum and lumbar spine. A scoliosis is an associated finding in this case.

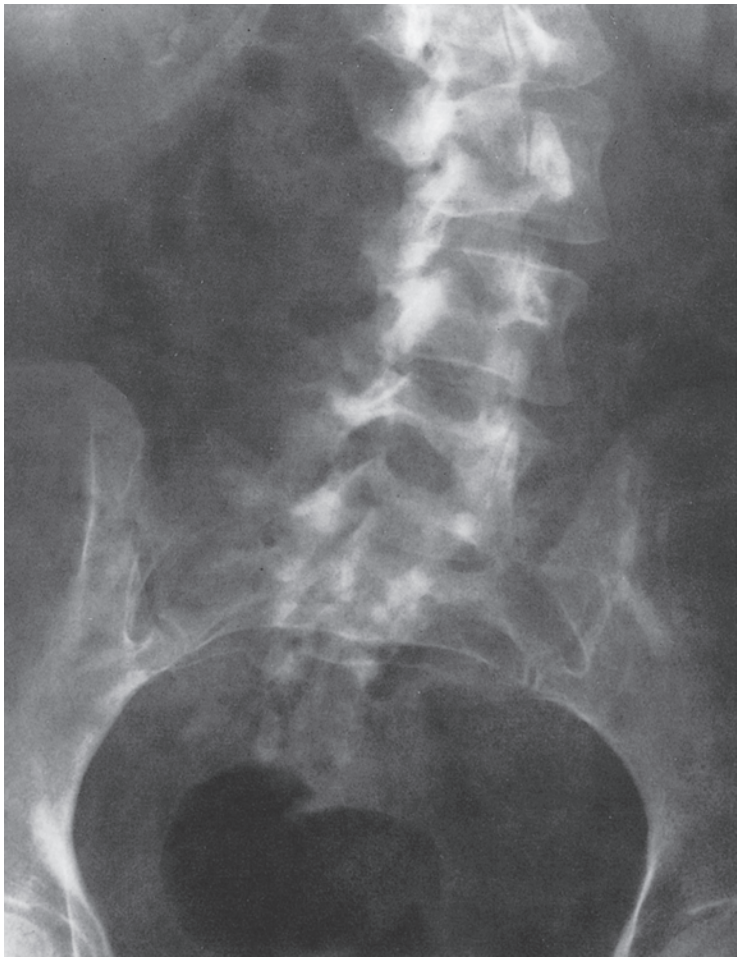

Fig. 12.**75** **Fluorosis.** Dense, uniform sclerosis of the lumbar spine.

Table 12.8 (Cont.) Differential Diagnosis of Disease with Generalized Involvement of Both Spine and Pelvis

Disease	Radiographic Findings	Comments
Hyperparathyroidism (primary or secondary) (Fig. 12.76)	Initially there is loss of bone density, subperiosteal and endosteal resorption of bone. Resorption is particularly prominent in symphysis pubis, ischia, and sacroiliac joints. Expanding focal bone lesions occur in pelvis. They are brown tumors or true cysts. Fractures and deformities of the pelvis follow. Generalized sclerosis of vertebral bodies or sclerotic bands adjacent to the endplates ("rugger jersey" spine) may be present.	"Rugger jersey" spine is more common in secondary hyperparathyroidism (renal osteodystrophy) than in primary hyperparathyroidism. A cyst will not heal after parathyroidectomy, but a brown tumor accumulates dense bone and may persist as a dense focus for years.

(continues on page 303)

a

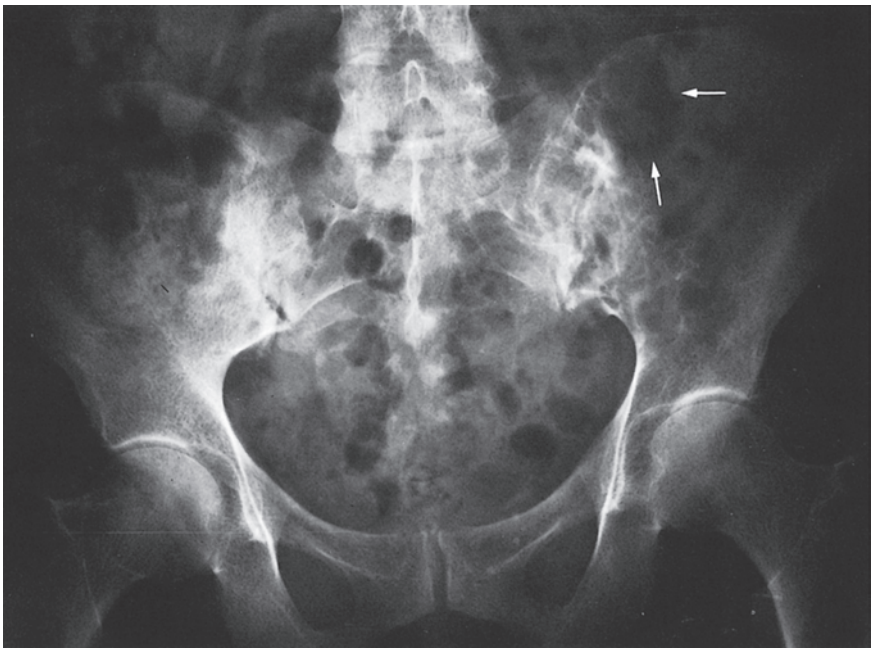

b

c

d

Fig. 12.**76 a–d** **Hyperparathyroidism** a Sclerotic bands adjacent to the vertebral endplates in renal osteodystrophy. **b** Large loculated cystic lesion in the left iliac bone (arrows) in primary hyperparathyroidism. **c** Erosion and sclerosis of the pubic symphysis (primary hyperparathyroidism). **d** Protrusio acetabuli and widespread cystic lesions in the pelvis and femur. Primary hyperparathyroidism.

Table 12.8 (Cont.) Differential Diagnosis of Disease with Generalized Involvement of Both Spine and Pelvis

Disease	Radiographic Findings	Comments
Arthritides and arthritislike conditions involving spine and pelvis (Figs. 12.77–80)	For general radiographic findings and differential diagnostic aspects see Table 6.**2**.	

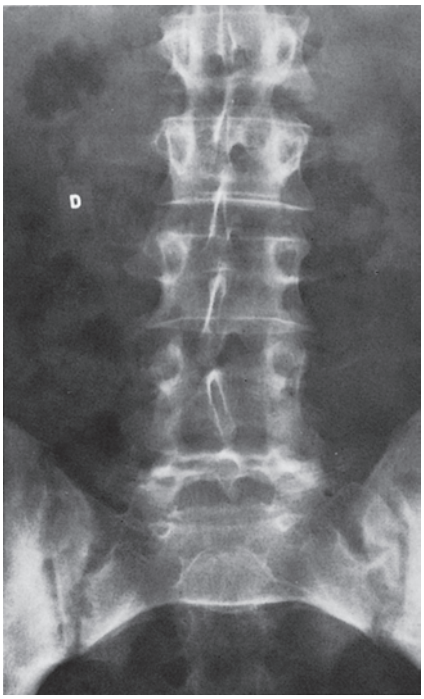

Fig. 12.**77** **Ankylosing spondylitis.** Erosion and sclerosis of both sacroiliac joints. Narrowing and erosion of the apophyseal joints, no recognizable syndesmophytes.

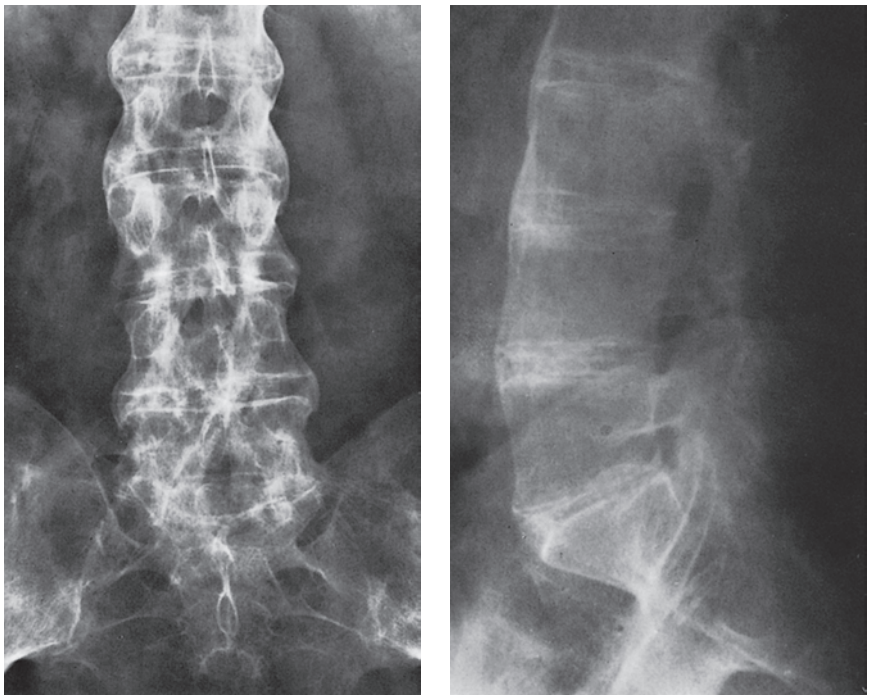

a **b**

Fig. 12.**78 a, b** **Advanced ankylosing spondylitis.** Bamboo spine with syndesmophytes, squaring of vertebral bodies, fusion of sacroiliac and apophyseal joints, and narrow calcified disk spaces.

Fig. 12.**79** **Ankylosing spondylitis.** Fusion of the apophyseal joints, squaring of vertebral bodies, and subluxation of the atlantoaxial joint (arrow).

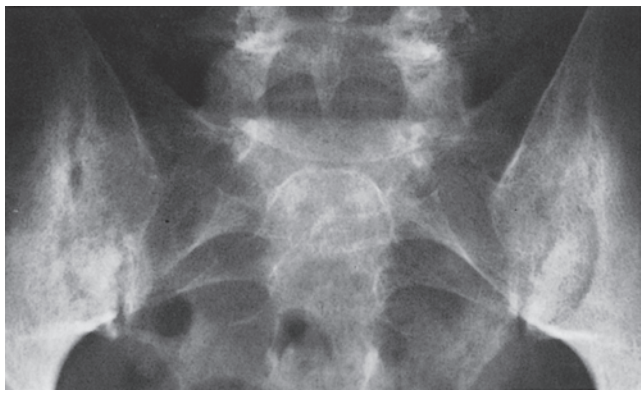

Fig. 12.**80** **Psoriatic arthritis.** Bilateral, asymmetric erosion and sclerosis of the sacroiliac joints.

13 Clavicles, Ribs, and Sternum

Clavicles, ribs, and sternum are usually seen on the same plain films and will therefore be dealt with in the same chapter, although anatomically clavicles are part of the upper extremity. Many of the roentgenographic findings are incidental, seen in chest roentgenograms. In these high KV_p exposures, bone details in the ribs and sternum are poorly visualized. Special views with lower KV_p and better contrast are taken in the presence of local pain, a history of trauma, or a palpable lesion. The costal cartilage is not visualized unless calcification has taken place. Costal cartilage calcification is more common in females and tends to be central, whereas peripheral calcifications predominate in males.

Rib Anomalies

Rib deformities occur in 2.8% of the population. The so-called *cervical rib* may be a supernumerary rib *originating from the lowermost cervical segment*. An asymmetrically developed *hypoplastic first thoracic rib may mimic a cervical rib*. A true cervical rib is usually an asymptomatic incidental finding. It may occasionally compress the subclavian artery or brachial plexus. Congenitally *bifid*, *spurred*, *widened*, or *fused* ribs are relatively common variants (Fig. 13.**1**). It may be a manifestation of the rare *basal cell nevus syndrome (Gorlin's syndrome)*, which consists of a combination of multiple basal cell epitheliomas, odontogenic cysts, brachydactyly, rib anomalies, scoliosis with vertebral anomalies, extensive calcification of the falx cerebri, and multiple calcified mesenteric cysts.

Thin or Small Ribs

Hypoplasia or *absence* of a rib is relatively common at Tl or T12. Eleven pairs of ribs are more common among females than males, and frequent among *Down's syndrome*.

A *regenerated rib* after resection (if periosteum is leaved intact) is usually thinner, shorter, and not as smoothly outlined as the original. In *neurofibromatosis*, ribs may be thin due to hypoplasia. Intercostal neurofibromas cause superior and inferior erosions (ribbon rib; Fig. 13.**3**). Thinned or "ribbon" ribs may be a feature in *hyperparathyroidism*, due to sub-periosteal bone resorption, *osteogenesis imperfecta*, *severe osteoporosis*, long-standing *paraplegia* (poliomyelitis), *rheumatoid arthritis*, *scleroderma*, *trisomy 12–15* and *trisomy 17–18* syndromes, as well as in a number of rare *osteochondrodysplasias*.

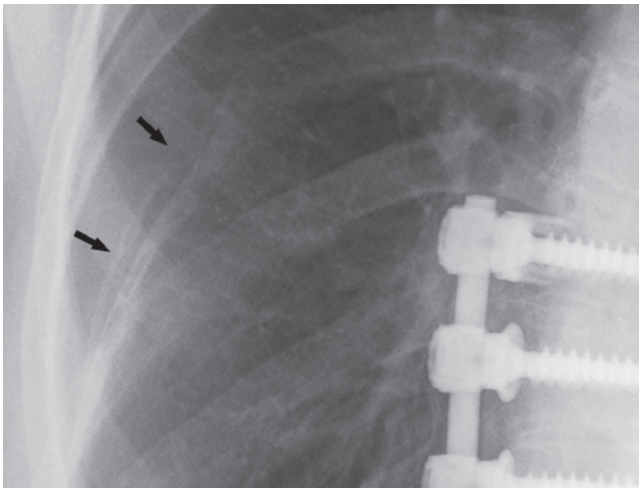

Fig. 13.**2** **Regenerated rib.** 7th rib on the right was removed because of skoliosis treatment. A regenerated rib is present two years after operation.

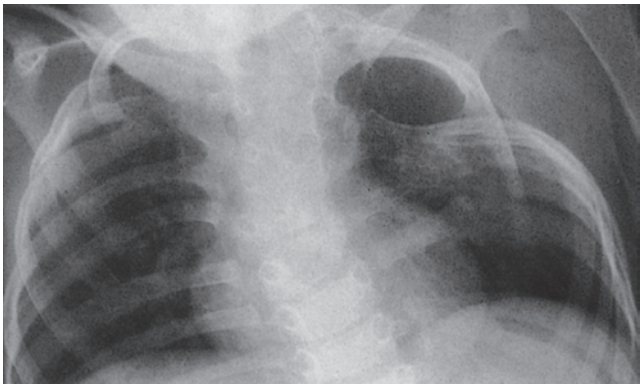

Fig. 13.**1** **Bilateral rib fusions** and vertebral anomalies cause severe deformity of the chest.

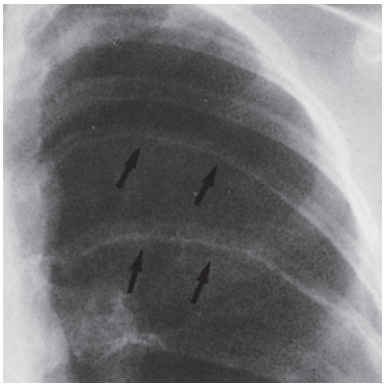

Fig. 13.**3** **Neurofibromatosis.** Hypoplastic ribs 5 and 6 on the left show inferior erosions (arrows). They are caused by intercostal neurinomas.

Wide Ribs

Several congenital conditions cause rib deformities as a reflection of generalized bone involvement.

In *achondroplasia* (Fig. 13.**4**), the ribs are *wide*, markedly *shortened*, and they do not extend normally around the chest. Among the *mucopolysaccharidoses*, rib widening is common (Fig. 13.**5**). In type IV (*Morquio's syndrome*), the ribs may have thinned posterior portions (Fig. 13.**6**). Rib changes similar to mucopolysaccharidoses are present also in various *mucolipidoses* (a congenital group of disorders in which excess material is stored in lysosomes and the clinical and radiologic findings resemble mucopolysaccharidoses). Patchy osteoporosis mimicking metastatic disease combined with rib widening may be present in *Gaucher's disease* and *Niemann-Pick disease*. Rib widening may be a feature in several other rare osteochondrodysplasias as well.

In *osteopetrosis* (Albers-Schonberg disease), the ribs and clavicles are uniformly dense (Fig. 12.**71a**). The sternal ends may be widened. Uniformly dense ribs are commonly caused by osteoblastic metastases, myelofibrosis, or Hodgkin lymphoma (see Chapter 2).

Anterior bulbous widenings and a coarse trabecular pattern are characteristic rib changes in *thalassemia*. Coarse trabeculation with cortical widening may also be seen in *sickle cell anemia* and *polycythemia*.

Cupping and widening of the sternal ends of ribs are characteristic of *rickets* (Fig. 13.**7**). Bulging, somewhat widened costochondral junctions are also seen in *scurvy*. In *Caffey's infantile cortical hyperostosis*, periosteal thickening and subperiosteal new bone formation are most frequently found in clavicles and ribs. The condition is accompanied by fever, soft-tissue swelling, and generalized symptoms of inflammation. Periosteal new bone formation in ribs also occurs in *leukemia*, especially in childhood.

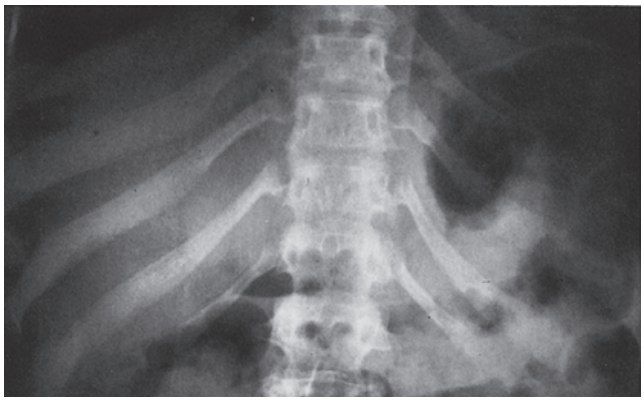

Fig. 13.**4** **Achondroplasia.** The ribs are wide and short.

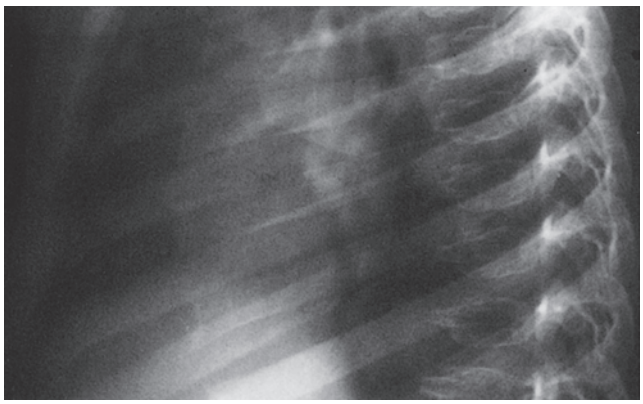

Fig. 13.**6** **Morquio's syndrome.** Characteristic vertebral bodies and wide ribs laterally and anteriorly.

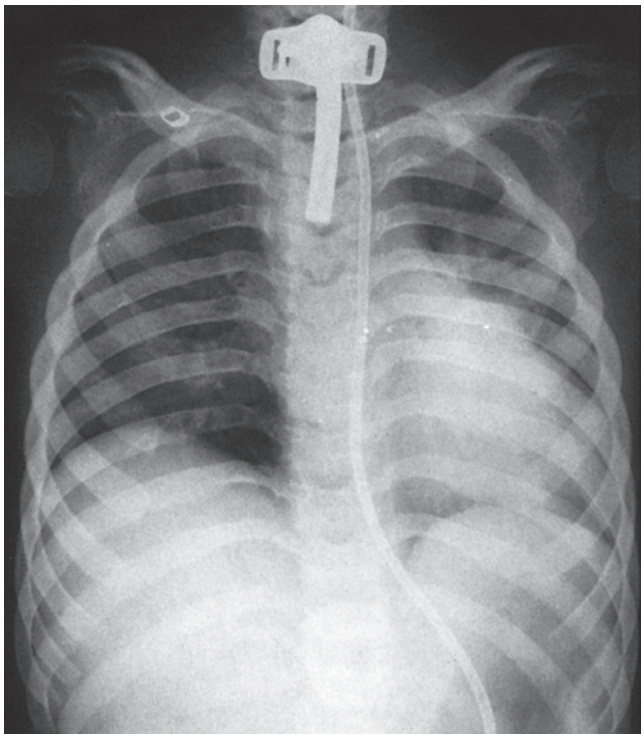

Fig. 13.**5** **Hurler's syndrome.** The ribs are abnormally wide. The glenoid fossa and humeral epiphysis are also abnormal.

Fig. 13.**7** **Rickets.** Wide sternal ends of the ribs, "rachitic rosary".

Localized Rib Lesions

Localized expansile lesions of the ribs occur most frequently due to *fibrocystic lesions*, e.g., *fibrous dysplasia* (Fig. 13.**8**), *bone cyst* (Fig. 13.**9**) or *nonossifying fibroma* (see Chapter 5). Expansion may also be due to *enchondroma* (Fig. 13.**10**), *osteochondroma* (exostosis) (Fig. 13.**11**), *expansile metastasis*, *myeloma* (Fig. 13.**12**), other neoplastic diseases, as well as a brown tumor of *hyperparathyroidism*, Langerhans cell histiocytosis (*eosinophilic granuloma*), *fracture* with extensive callus, and *osteomyelitis* (see Chapter 5). Cartilaginous expansion in *Tietze's syndrome* may occasionally cause expansion of the anterior end of the rib, but usually there is no associated bone abnormality. Long (>6 cm) solitary expansile lesions are encountered in sarcomatous tumors (*osteosarcoma, chondrosarcoma, Ewing's sarcoma*, Askin tumor is uncommon tumor of intercostals nerve.), *fibrous dysplasia*, *metastases*, and *plasmocytoma* or *myeloma*, but rarely in other bone tumors or in *Paget's disease*.

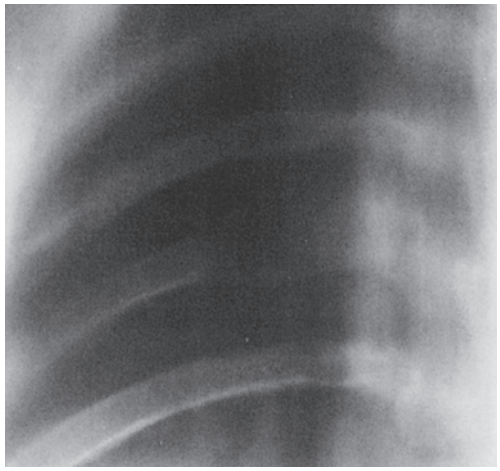

Fig. 13.**8** **Fibrous dysplasia** of a rib, seen as a local expansion in the posterior part of the rib.

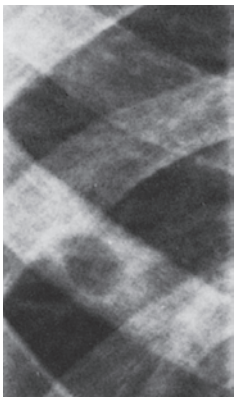

Fig. 13.**9** A small **unilocular bone cyst** of a rib. Eosinophilic granuloma or osteoid osteoma could have similar appearance.

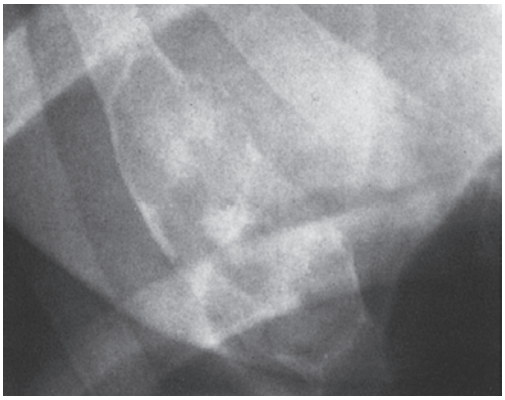

Fig. 13.**10** **Enchondroma.** An expansile lesion with ground glass appearance. Fibrous dysplasia could have similar appearance.

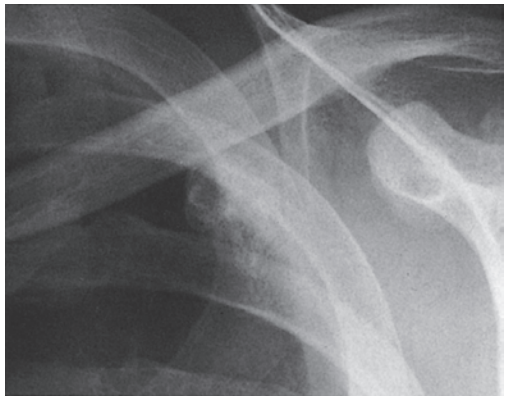

Fig. 13.**11** **Osteochondroma** of a rib.

Fig. 13.**12** **Multiple myeloma** presenting as a lytic rib lesion.

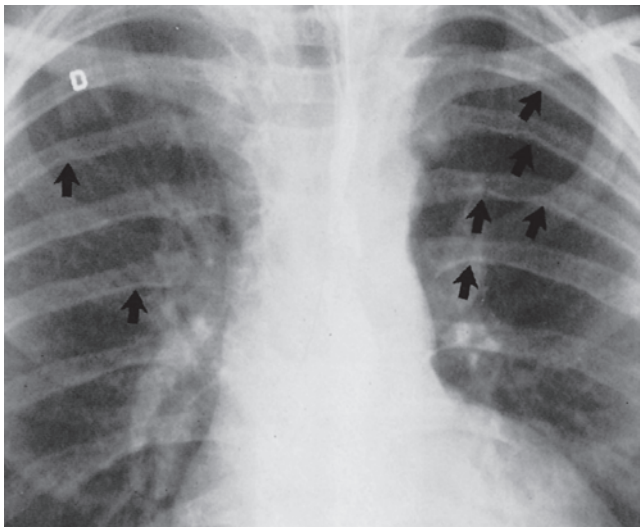

Fig. 13.**13** **Coarctation of the aorta** in a 6-year-old child. Multiple rib notches (arrows) and abnormal configuration of the left heart border.

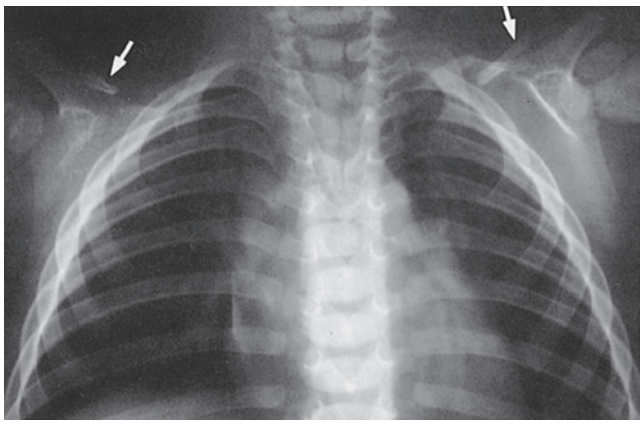

Fig. 13.**14** **Cleidocranial dysplasia.** Severe hypoplasia of clavicles (arrows), multiple spina bifidas, cone-shaped chest with relatively short ribs (long cartilaginous segments), relatively small scapulae.

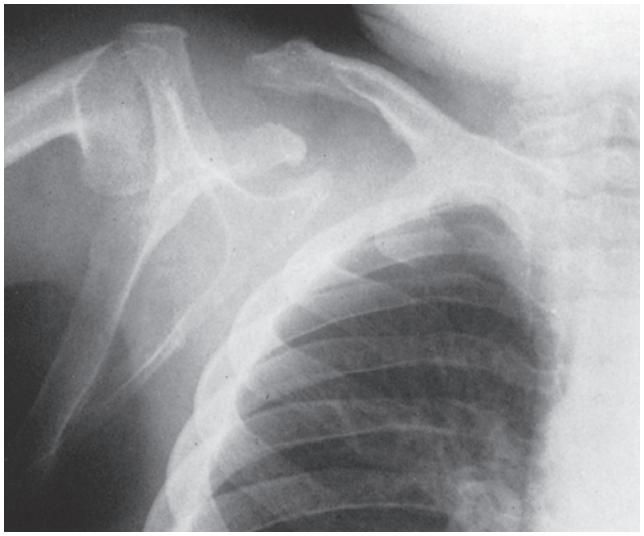

Fig. 13.**15** **Hurler's syndrome.** The clavicle is short and thick, the ribs are wide, and there is deformity of the scapula and humeral epiphysis.

Rib Notching

Rib notches (localized erosions of ribs) are considered characteristic of *coarctation of the aorta* (seen in 80% of cases). Rib notching due to coarctation occurs in ribs 3 to 9 (Fig. 13.**13**). The notches are usually located in the inferior margin of the ribs unless tortuous intercostal arteries are large enough to erode the superior surface of the adjacent rib. Rib erosions due to coarctation commonly appear after 6 to 12 years of age. Unilateral right-sided notching indicates coarctation proximal to the left subclavian artery and left-sided notching points to an anomalous origin of the right subclavian artery (take-off below coarctation). Several other conditions may cause rib notching, as follows:

- *obstruction of the abdominal aorta (thrombosis)*
- obstruction of the subclavian artery (*Blalock-Taussig procedure* for Fallot's tetralogy, *Takayasu's arteritis*, *arteriosclerosis obliterans*)
- pulmonary oligemia (*tetralogy of Fallot, absent pulmonary artery* or *pulmonary atresia* or *stenosis*, *pseudotruncus arteriosus*, *Ebstein's anomaly*, *pulmonary emphysema*)
- pulmonary or intercostal *arteriovenous malformation*
- *obstructions of the superior vena cava* or *subclavian vein*
- *neurofibromatosis* or intercostal neurinoma (Fig. 13.**3**)
- periosteal irregularities mimicking rib notches occur in *hyperparathyroidism*, *tuberous sclerosis*, *thalassemia*, *collagen diseases*, and sometimes without any known reason (idiopathic notching).

Notching of superior surface of ribs may occur in certain connective tissue diseases, such as rheumatoid arthritis, systemic lupus erythematosus, scleroderma and Sjögren's syndrome. Superior surface notching may occur in hyperparathyroidism, neurofibromatosis, restrictive lung disease, poliomyelitis, Marfan's syndrome, osteogenesis imperfecta and progeria.

Abnormal Clavicle

The clavicle is formed from three separate ossification centers. If one or more of them is absent, hypoplasia or absence of the clavicle occurs. This is a characteristic finding in *cleidocranial dysostosis* (hypoplasia or absence of clavicles, defective ossification of the calvarium, spina bifida, hypoplastic pelvic bones with separation of pubic symphysis). The chest may be cone-shaped and ribs may be short but otherwise normal in cleidocranial dysostosis (Fig. 13.**14**). Clavicular hypoplasia also occurs in *focal dermal hypoplasia* (*Goltz's syndrome*). In this condition, hypoplastic clavicles and ribs are associated with syndactyly, dental anomalies, and skin atrophy and pigmentations. *Holt-Oram syndrome* is characterized by finger-like or absent thumb and shoulder anomalies, including hypoplastic clavicles. Shortening and thickening of clavicles is a manifestation of *Hurler's syndrome* (Fig. 13.**15**), a more characteristic sign being hypoplasia of L2 and inferior beaking of the anterior margin of one or more vertebral bodies (see Chapter 12, Table 12.7). Thinning of clavicles and ribs occurs in *progeria*. In *trisomy 13/18*, tapering of the distal clavicle is one of the multiple anomalies. Unilaterally small clavicle and other shoulder bones may be caused by *brachial plexus damage at birth* (Fig. 13.**16**).

The most common *localized intraosseous lesions* of the clavicles are *osteomyelitis* (Fig. 13.**17**) and *trauma*. In patients

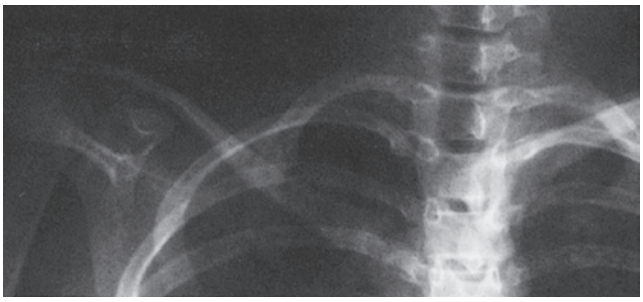

Fig. 13.**16** **Birth trauma** to brachial plexus. Unilateral thinning of right clavicle and small shoulder bones, but the structure of bones is normal. There is also a healing fracture of the right first rib and upward dislocation of the sternal end of the left clavicle.

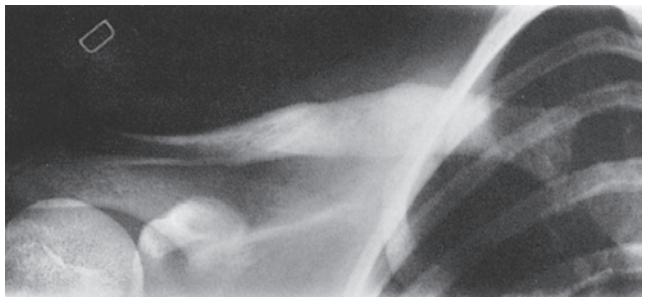

Fig. 13.**17** **Chronic osteomyelitis** of the right clavicle. No destruction is seen, but there is slowly progressing sclerosis and thickening of bone.

with so called SAPHO (Fig. 13.**18**) (synovitis, acne, pustulosis, hyperostosis and osteomyelitis) syndrome there is hyperostosis in the medial end of the clavicle which mimics osteomyelitis. Other possibilities exist, and the differential diagnostic list of such a lesion is essentially the same as with a localized lesion in a rib.

Erosion and destruction of the outer end of the clavicle is most commonly caused by *rheumatoid arthritis* (see Chapter 6), *hyperparathyroidism* (Fig. 13.**19**) (see Chapter 1), *myeloma* (Fig. 13.**20**), and *rickets*. Other conditions to be considered as causes of bone erosion or defects in the lateral end of the clavicle include *scleroderma* and *gout* (intra-articular or periarticular calcium deposits occur in both), *lipoid dermatoarthritis* (reticulohistiocytoma), and a number of other conditions that rarely cause localized lesions in ribs and clavicles such as *posttraumatic osteolysis*, *metastasis*, *Ewing's sarcoma*, *amyloidosis*, *osteomalacia*, *progeria*, *pycnodysostosis*, *massive osteolysis* (*Gorham-Stout*), and *neurogenic osteolysis*.

Erosive changes in the medial end of the clavicle and the sternoclavicular joint are usually due to *rheumatoid* or, more rarely, *pyogenic arthritis*. A notch at the attachment of the costoclavicular ligament (inferior surface) or the sternocleidomastoid muscle (superior surface) should be distinguished from inflammatory erosion.

Widespread *sclerosis* of the clavicle may be due to *chronic osteomyelitis* (Fig. 13.**17**) or *Paget's disease*. Widespread sclerosis and even fusion of the clavicles with the sternum occurs in the rare, painful *sternocostoclavicular hyperostosis*, which may mimic sclerosing osteomyelitis Garre (see Table 5.4). Painful sclerosis of the clavicle may also be due to *osteoid osteoma*. Sclerosis of the sternal end of the clavicle, often associated with pain, can be due *to osteitis condensans claviculae*. *Avascular necrosis (Friedrich's disease}* involves only the caudal half of the sternal end of the clavicle. In small children, the middle portion of the clavicle may be seen "end-on" due to normal curvature and may mimic a sclerotic process or healed fracture.

Luxation or subluxation of the acromioclavicular joint (Fig. 13.**21**) usually produces downward and lateral displacement of the acromion in weight bearing. *Luxation of the sternoclavicular joint* (Fig. 13.**16**) is usually post-traumatic, but is also common after radical neck dissection.

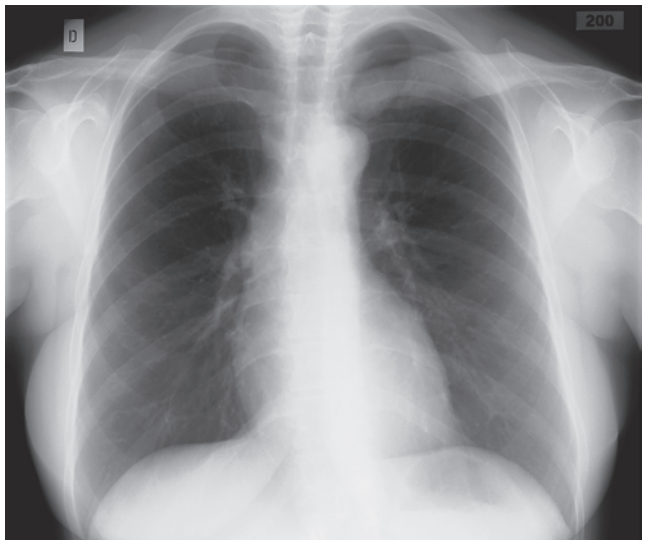

Fig. 13.**18** **SAPHO syndrome.** 35-year-old female with bilateral thickening and sclerosis of medial halves of clavicles.

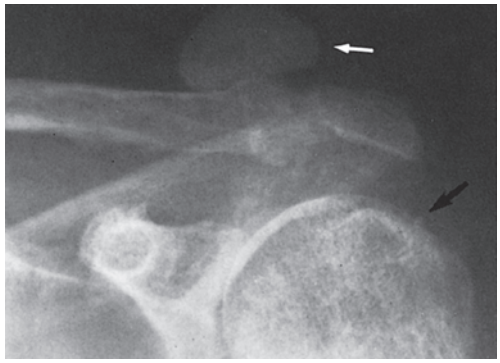

Fig. 13.**19** **Secondary hyperparathyroidism**/renal osteodystrophy). There is erosion of the distal end of the clavicle and endosteal thinning of the cortex. Soft-tissue calcification (arrows) is also seen.

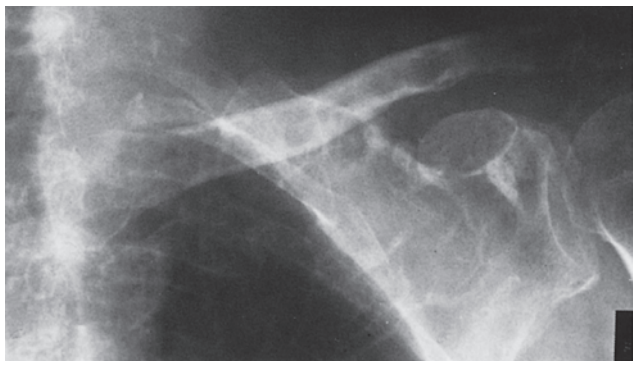

Fig. 13.**20** **Multiple myeloma.** Multiple osteolytic lesions in the distal clavicle and in scapula, the head of the hurnerus, and ribs. ▷

Abnormal Sternum

The sternum is visualized on lateral plain films, but is usually poorly shown in anteroposterior or oblique views. Fusion anomalies of the sternal segments (Fig. 13.**22**) are common and are sometimes seen in association with other anomalies, including congenital heart disease.

The most common anomaly is *fusion* of the *manubriosternal* synchondrosis, with or without a synchondrosis between the first and second segment of the body of the sternum. Fusion of the manubriosternal synchondrosis may also be the end result of *ankylosing spondylitis*, *rheumatoid arthritis*, *psoriatic arthritis*, *Reiter's syndrome*, *enteropathic arthritis*, healed *hyperparathyroidism*, *degenerative joint disease, trauma* or *surgery*, *pyogenic infection*, *fluorosis*, or, rarely, *relapsing polychondritis*. The same conditions may cause erosion and sclerosis of the sternal synchondrosis (Fig. 13.**23**). However, one should note that some irregularities of the joint surfaces are a normal finding.

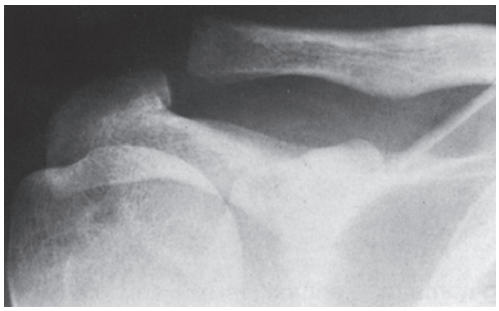

Fig. 13.**21** **Subluxation** of the acromioclavicular joint in weight bearing.

A defect in the body of the sternum may represent a fusion anomaly if the hole has smooth cortical margins. Sclerosis and blurring of the margins of a sternal defect point to *osteomyelitis* (pyogenic or tuberculous) or to *metastatic* destruction. Infectious lesions tend to have sclerotic margins (Fig. 13.**24**), whereas the pattern of metastases (Fig. 13.**25**) and primary tumors (Figs. 13.**26** and 13.**27**) are similar to those in any other flat bone.

The xiphoid process is often radiolucent or contains only some calcified cartilage instead of bone. It is therefore usually poorly visualized.

Undue depression of the sternum, called *pectus excavatum*, is usually idiopathic without abnormalities other than an asthenic habitus. There are two major types of pectus excavatum: (1) a deep deformity in the central and distal parts of the sternum, while the manubrium is in a normal position and (2) a broad, flat deformity that also may involve the manubrium. The second type may interfere with cardiac function. Both types may show a shift or enlargement of the cardiac silhouette in the frontal view. Pectus excavatum can be associated with *congenital heart disease*, *homocystinuria*, *Marfan's syndrome* (Fig. 13.**28**), the *systolic click-late systolic murmur syndrome*, *congenital bowing of tibia*, *idiopathic mitral valve prolapse*, *Ehlers–Danlos syndrome* and *osteogenesis imperfecta*. Coexistent sternomanubrial protrusion may be present. Deformities may have a traumatic origin (Fig. 13.**29**).

Pectus carinatum, "pigeon breast," or undue prominence of the sternum is less common than pectus excavatum. This anomaly may be seen associated with *congenital heart disease, mucopolysaccharidosis IV (Morquio's syndrome), Noonan's syndrome* (Turner's phenotype with normal karyotype), and *spondyloepiphyseal dysplasia congenita*.

Cleft sternum is usually clinically obvious. The cleft may be located in the superior or inferior portion of the sternum or even be complete. Inferior and complete sternal clefts are often associated with other anomalies (defects in the ventral abdominal wall, diaphragm, pericardium, and heart).

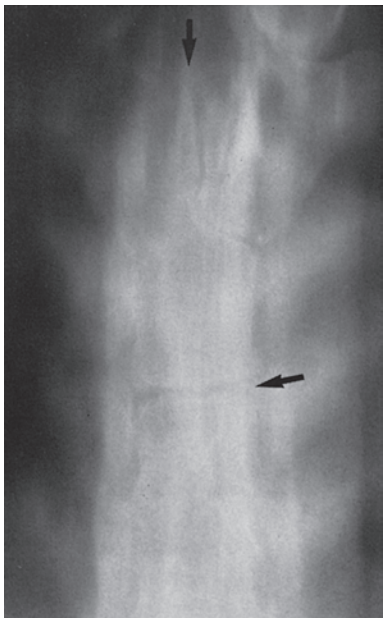

Fig. 13.**22** **Segmentation anomalies** of the sternum. There is a vertical cleft in the middle of the manubrium and a horizontal cleft between the first and second segments of the body (arrows).

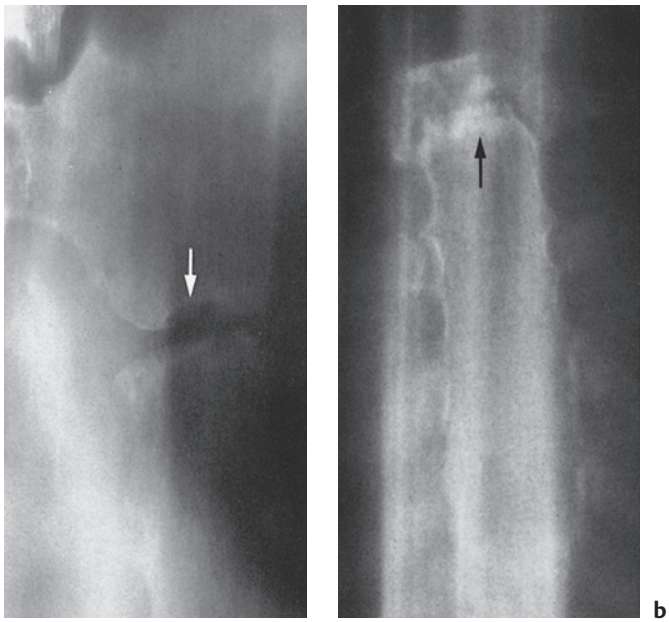

a b

Fig. 13.**23 a, b** **Psoriatic arthritis** with, predominantly, a erosive and b sclerotic changes in the manubriosternal synchondrosis (arrows). Identical changes occur in ankylosing spondylitis, and rarely in rheumatoid arthritis.

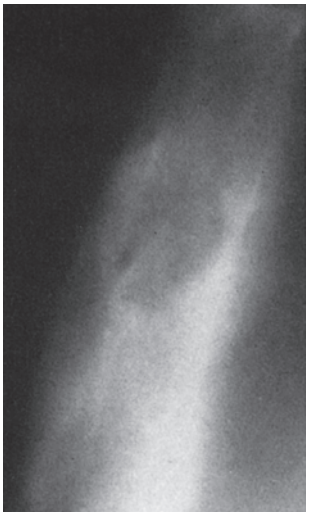

Fig. 13.**24** **Sternal tuberculosis** (healed). A slightly expansile osteolytic lesion surrounded by sclerosis.

Fig. 13.**25** **Metastatic adenocarcinoma** of the kidney. An expansile osteolytic lesion in the upper body of the sternum.

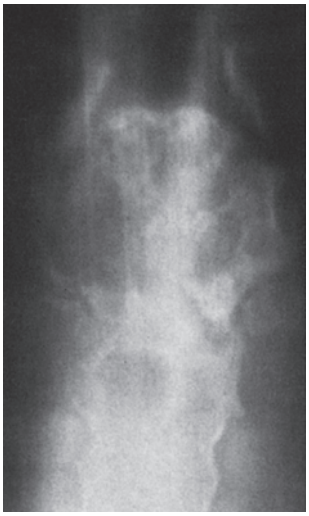

Fig. 13.**26** **Non-Hodgkin's lymphoma.** Predominantly osteolytic, poorly marginated destruction of the manubrium with involvement of manubriosternal synchondrosis.

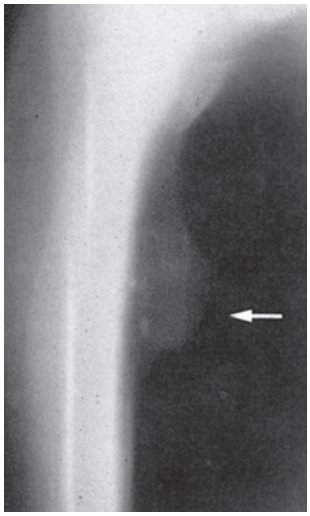

Fig. 13.**27** **Benign osteochondroma** of sternum. A soft tissue mass projecting toward the mediastinum (arrow). The finding is radiographically nonspecific.

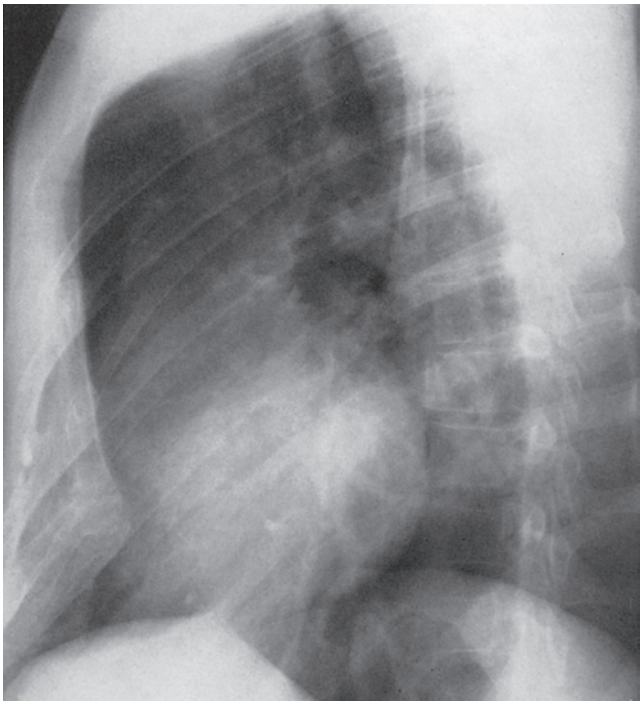

Fig. 13.**28** **Pectus excavatum** associated with Marfan's syndrome. The patient also has an aneurysm of the ascending aorta.

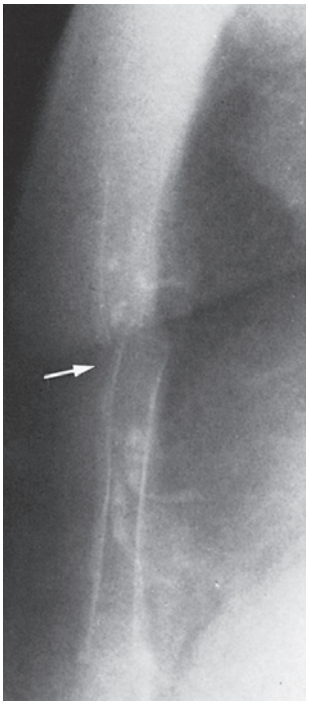

Fig. 13.**29** **Fracture of the body** of the sternum (arrow).

14 Extremities

Deformities of the long bones are either developmental, that is, caused by abnormal or asymmetric growth, or they may be the sequelae of fractures or associated with a disease that causes bone softening. In the latter case, the weight-bearing lower extremities are usually more affected than the upper extremities. The differential diagnosis of long bone deformities is discussed in Table 14.**1**.

Normally, the ends of long bones are wider than their diaphyses, and there is a progressive concentric decrease in the caliber of the shaft as one passes from the end toward the middle of a long bone. Abnormal modeling of the long bones can result from a variety of diseases affecting the growing bone and the end result is usually still evident in the adult. Less commonly, abnormal modeling of the long bones may only develop in adulthood. Such conditions are either associated with new periosteal bone formation (e.g. *Paget's disease* or healing *fractures* and *infections*) or caused by expansile nondestructive mass lesions within the bone. A widening of the bone shaft is termed *underconstriction* or *undertubulation*. Widening or splaying of the metaphyses may be associated with underconstriction of the shaft or may present as an isolated finding. A splayed distal femur metaphysis often assumes the shape of an Erlenmeyer flask and is accordingly termed "*Erlenmeyer flask*" *deformity* (Fig. 14.**1**). Conditions characterized by "Erlenmeyer flask" deformity include Gaucher's disease, Niemann-Pick disease, thalassemia, craniometaphyseal dysplasia, Pyle's disease, enchrondromatosis, hereditary multiple exstoses, osteogenesis imperfecta, osteopetrosis and lead poisoning. These disorders, as well as all other diseases with a more generalized, widened diametaphysis, are discussed in Table 14.**2**.

Overconstriction (or *overtubulation*) is the reverse of underconstriction. As one passes from the end of a long bone toward the middle, there is excessive concentric narrowing of the shaft. Overconstriction is usually the cause of a chronic disease affecting the growing bone. It is only rarely acquired in adulthood by marked periosteal resorption of the cortex, since abnormal cortical resorption in the adult occurs predominantly on the endosteal margins, this does not lead to overconstriction. Table 14.**3** deals with the differential diagnosis of overconstricted long bones.

Transverse radiolucent and *sclerotic bands* or *lines* in the metaphyses are commonly found in the growing bones and do not necessarily indicate a pathologic process. They may persist into adult life. The differential diagnosis of radiolucent and sclerotic transverse bands is summarized in Tables 14.**4** and 14.**5**, respectively.

Long tubular bones continue to increase in length until fusion of the epiphyseal plates. *Generalized elongation* or *overgrowth* of long bones is uncommon. The usual cause of overgrowth in association with normal length-width relationships is *gigantism*, either of hypothalamic or pituitary origin. Elongation of bones with narrow diametaphysis (overconstriction, overtubulation) is seen in *Marfan's syndrome* and *homocystinuria*. There are many individual variations in the width of bones, and it may be difficult to assess whether otherwise normal-looking bones are thin due to constitutional reasons or to a specific pathologic entity. If deformation of bone is an associated finding, as in *neurofibromatosis*, other clinical or radiographic signs are usually present to suggest a specific diagnosis. *Generalized* or *localized shortening* of a tubular bone is more likely to occur, since a number of congenital or acquired diseases or their treatment will interfere with the growth of bone.

In Table 14.**6**, some conditions associated with generalized or localized shortening, hypoplasia, or deformity of the long bones of the extremities are presented. The majority of congenital bone dysplasias will not be mentioned here, since their differential diagnosis is more likely to be successful when based on the appearance of the hands and feet and the spine.

The metaphyses of the long bones, especially the knee, hip, and shoulder regions, are favored sites of several malignant bone tumors. Also, benign bone tumors and tumor-like processes are common in the extremities. The general description of these diseases in Chapter 5 is based on their appearance in typical locations and will not be repeated here. Similarly, inflammatory lesions of bone such as bone infection, arthritis, and associated calcifications have been presented in a systematic fashion above. The femoral head is the most important site of fragmentation or deformation for traumatic, inflammatory, vascular, metabolic, or unknown reasons. Therefore, the causes of an abnormal proximal femur are presented in Tables 14.**10**–14.**12**, although some overlapping with other chapters unavoidably occurs. Many

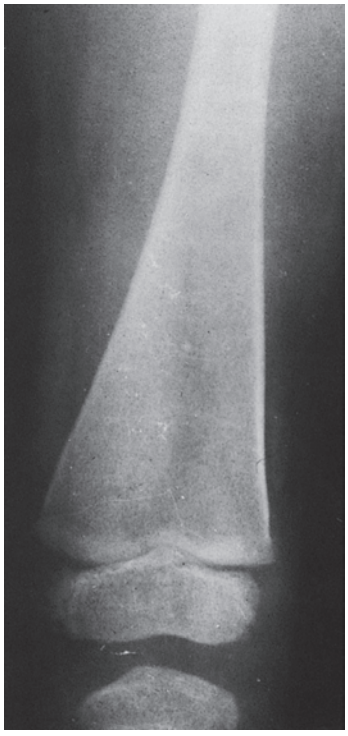

Fig. 14.**1** **"Erlenmeyer flask" deformity.** The splayed distal tibia metaphysis assumes the shape of an Erlenmeyer flask (Pyle's disease).

of the changes and diseases presented as typical of the femoral head also occur in other joints, especially in the shoulder.

Alignment of Joints of Extremities

Abnormalities of the alignment of the joints of the extremities may be the only sign of trauma, e.g., a dislocation without fracture. Malalignment may also be the result of a localized disease process characteristically seen in the knee joints. Since the alignment of the joint can be measured, it may be an objective starting point for a differential diagnostic approach, although it often represents a secondary phenomenon. Certain important facts concerning the alignment of the joints, and some terminological definitions, must be known in order to evaluate radiographs of the extremities appropriately and use Tables 14.**7**–14.**13** properly. These will be presented here briefly.

It is difficult to judge abnormalities of alignment in the *shoulder* (Table 14.**7**) because of its very wide range of normal motion. Shoulder dislocations are best detected from the axillary view (see Fig. 4.**33**). In *anterior dislocation*, the humeral head is displaced medially and inferiorly (superimposed over scapula, Fig. 14.**2**). A defect called *Hill-Sachs deformity* (Fig. 14.**3**), a compression fracture of the humeral head, is best seen when the arm is abducted and internally rotated 60 degrees. Fracture of the anterior inferior rim of the glenoid, known as the *Bankart lesion*, is less commonly seen. Bankart lesion may affect cartilaginous labrum only. Then the diagnosis can be made by MRI or by CT arthrography. *Posterior dislocation* of the humeral head is less common than anterior dislocation. It is difficult to recognize on a routine view. An abnormal appearance of the humeral head because of rotation may be the only sign of abnormality. In the axillary view the humeral head is superimposed on the acromion and does not articulate with the glenoid fossa. A compression fracture of the humeral head may be present. A *fracture of the lesser tuberosity* is so commonly associated with a posterior dislocation that its discovery on a routine view of the shoulder necessitates an axillary projection to determine its actual alignment. If the patient is capable of eversion of the humerus, the posterior dislocation is excluded. *Dislocation inferiorly*, towards the axilla, is rare and may be associated with a fracture of the greater tuberosity.

Normally, the *forearm* makes an angle of approximately 170 degrees with the humerus, deviating laterally. Medial deviation (*cubitus varus*) and lateral deviation (*cubitus valgus*) of the forearm may result from *trauma, connective tissue diseases, infections, neurotrophic diseases,* and *Turner's syndrome*.

The most common malalignment in the hip (Table 14.**12**) is an abnormal angle between the shaft of the femur and its neck. Normally this angle is between 120 and 130 degrees in an adult. In children before puberty, values between 130 and 140 degrees are encountered. An increase in an adult above 130 degrees is called *valgus deformity (coxa valga)*; a decrease below 120 degrees is a *varus deformity (coxa vara)*. Valgus deformities are often related to congenital defects, while varus deformities may result from bone softening, such as osteomalacia or Paget's disease. A simple method of determining if varus or valgus deformity is present is shown in Fig. 14.**4**. Normally there is anterior angulation (anteversion) of the femoral neck between 10 and 15 degrees in the adult, as compared with the line tangential to the distal femoral condyles. This angle is as high as 35 degrees in an infant and decreases towards adulthood. Without inversion of the inferior extremities (approximately 20 degrees), the angle of the femoral neck may not be correctly measurable in anteroposterior films of the hip. Various lines used for the determination of the congenital dislocation of the hip in a neonate are presented in Figure 14.**5**.

When the tibia is angled laterally, too close approximation of the distal thighs results in *knock knees (genu valgum)*. The

Fig. 14.**2** **Anterior dislocation of the humeral head** with characteristic medial and inferior displacement.

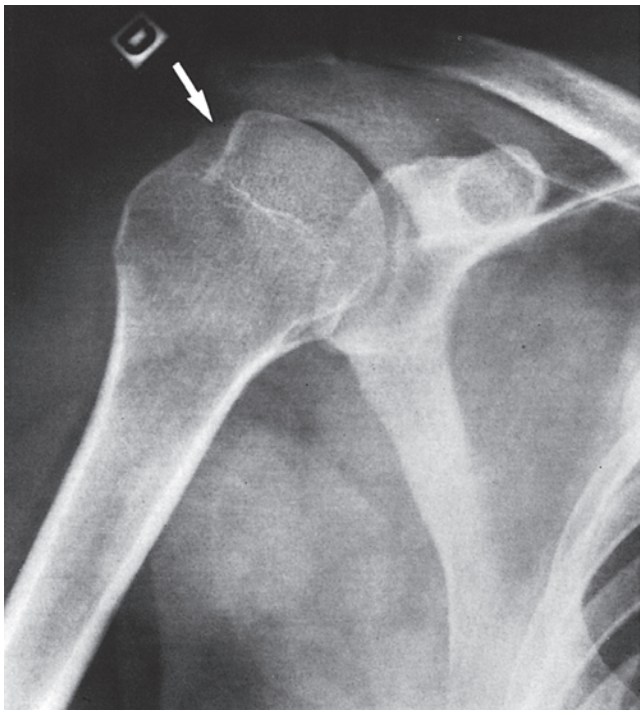

Fig. 14.**3** **Compression fracture of the humeral head** after dislocation (Hill-Sachs defect, arrow).

opposite condition, separation of the distal thighs, is called *bowlegs (genu varum)*. These deviations cause excessive stress on the knee and lead to degenerative changes. Medial displacement of the distal femur is called *genu laxum*. One measurement used to determine the position of the patella in a lateral view at flexion between 20 to 70 degrees is presented in Fig. 14.**6**. The ratio of maximal length of the patella to the distance from the distal tip of the patella to the tuberosity of the tibia is normally between 0.8 and 1.2. *Patella alta* (high patella) may be associated with *recurrent subluxation, chondromalacia of the patella, rupture of the patellar ligament, osteomyelitis* of the femur, *poliomyelitis, avascular necrosis of the tibial tuberosity (Osgood–Schlatter disease)*, or the inferior ossification center of the patella (*Sinding–Larsen–Johansson disease*), and *cerebral palsy*. *Patella profunda* or *baja* (low patella) may occur as an inborn condition, as in *achondroplasia*, secondary to *rupture of the quadriceps muscle tendon*, or surgical *transposition of the tibial tuberosity*. It may also be secondary to *juvenile rheumatoid arthritis* or to paresis of the quadriceps muscle in *poliomyelitis*. *Incongruity of patellar motion*, e. g. lateral dislocation and tilting are more common and important abnormalities. Their demonstration is best done with cross sectional images using CT or MRI at flexion less than 30 degrees, since plain films are insensitive.

The patella may be absent or hypoplastic. This is usually due to *hereditary onycho-osteodysplasia* or nail patella syndrome (Fig. 14.**7**), which is characterized by iliac horns and several other abnormalities. Hypoplasia of the patella is occasionally reported in association with acrocephalosyndactyly, and aplasia of the patella in association with *bird-headed dwarfism*, *neurofibromatosis* and *popliteal pterygium syndrome*.

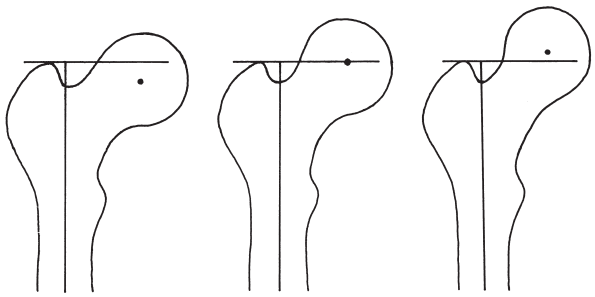

Fig. 14.**4 a–c** **Evaluation of the angle of the femoral neck**, **a** Coxa vara, **b** normal, and **c** coxa valga.

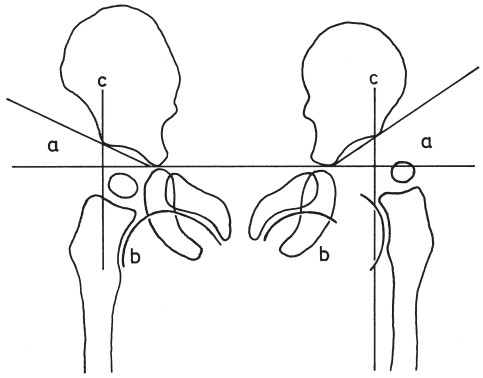

Fig. 14.**5** **Determination of congenital dislocation of the hip in a neonate.** The left side of the diagram represents normal relationships and the right side congenital dislocation, (**a**) Acetabular angle, (**b**) Shenton's line, and (**c**) Ombredanne line.

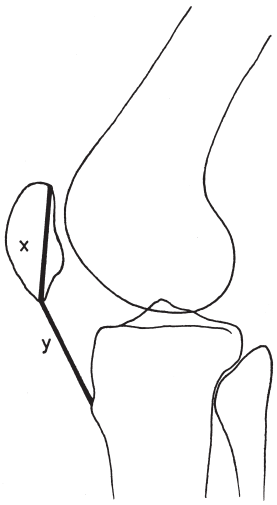

Fig. 14.**6** **Determination of the position of patella.** The measurements should be done at flexion between 20 to 70 degrees, y/x is normally between 0.8 and 1.2. Patella alta = y/x > 1.2., patella profunda = y/x < 0.8.

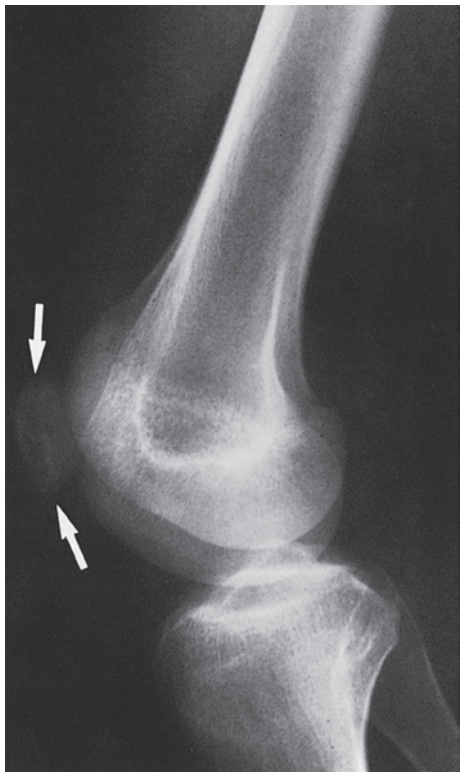

Fig. 14.**7** **Hereditary onycho-osteodysplasia.** Hypoplastic patella (arrows). ▷

Table 14.1 Bowed or Deformed Long Bones

Disease	Radiographic Findings	Comments
Congenital bowing	Bowlegs: Lateral and usually some anterior bowing of the proximal two-thirds of the tibias and/or the distal segments of the femora. Spurring of the medial aspect of the proximal tibia shaft or the posterior aspect of the distal femur shaft may also be present.	Idiopathic bowlegs of infancy disappear spontaneously after 2 to 3 years. Bowed limbs at birth may also be found in different forms of dwarfisms (e.g., *achondroplasia* and *camptomelic* and *thanatophoric* dwarfism).
Osteodysplasty (Melnick-Needles syndrome)	Lateral bowing of the tibia characteristic. Sclerosis of the base of the skull and mastoids, tall vertebrae, ribbon-like appearance of the ribs, and metaphyseal flaring of short and long bones may also be evident.	Found only in females with small face, large ears, protruding eyes, micrognathia, malaligned teeth and short upper arms.
Infantile cortical hyperostosis (Caffey's disease)	Occasional sequelae of the disease in adulthood include bowing of the limbs, mandibular asymmetry and osseous bridging between adjacent bones.	The disease becomes evident in infants of less than 5 months of age. Usually the clinical and radiographic features subside slowly within a few months to a few years.
Osteogenesis imperfecta (Fig. 14.8)	Bowing deformities in slender overconstricted and osteoporotic long bones with tendency to fracture characteristic.	Inherited connective tissue disorder.
Hypophosphatasia	Bowing deformities and increased bone fragility are characteristically present both in the most severe form (seen in infants) and in the mildest form (seen in adults). In infancy, the disease resembles rickets (cupping and fraying of metaphyses), whereas in the adult the long bones are shortened and often demonstrate cortical thickening and pseudofractures.	Hypophosphatasia is a genetically determined metaphyseal dysplasia with failure to form primary spongiosa. Low serum alkaline phosphatase levels are characteristic.
Vitamin D resistent rickets (x-linked hypophosphatemia) (Fig. 14.9a)	Bowing deformities occur in the long bones of the lower extremities. Pseudofractures (Looser's zones) may be associated and progress to complete fractures.	Extensive enteropathy and a general increase in bone density (especially in the axial skeleton) are characteristic features in adulthood. In the spine the disease may simulate ankylosing spondylitis without sacro-iliac joint involvement or DISH.
Madelung's deformity (dyschondrosteosis)	Radius is bowed and short and its distal articular surface demonstrates ulnar and volar angulation. The distal ulna is deformed and subluxed dorsally. The carpal bones are wedged between the deformed radius and ulna and assume a triangular configuration with the lunate at the apex. May be associated with short and bowed tibia, short fibula, and valgus deformity of the knee.	Rare hereditary mesomelic bone dysplasia with female preponderance. Process usually begins in adolescence with premature fusion of the medial aspect of the distal radial epiphysis resulting in asymmetrical growth. In the majority of cases, the patients are of short stature and the deformities are bilateral.
Blount's disease (tibia vara)	Medial tibia condyle is enlarged and deformed with an irregular, beak-like extension originating from the media! metaphysis and projecting medially and posteriorly. Medial aspect of proximal tibia epiphysis may also be deformed.	Osteochondrosis of the medial tibia metaphysis resulting in bowlegs. An infantile type (usually bilateral) is differentiated from an adolescent type (usually unilateral).
Weismann-Netter syndrome (Fig. 14.9b)	Bilateral and symmetrical anterior and medial bowing of the tibia and fibula, producing a "sabreshin" deformity. The fibula shaft is typically thickened ("tibialization" of the fibula).	Congenital nonprogressive condition that has also been reported in the elderly.
Enchondromatosis (Ollier's disease)	Deformity and shortening of tubular bones containing round, often expansile lesions or alternating columnar radiolucent and radiodense streaks. Enchondromas may contain punctate or stippled calcifications. Disease may be relatively localized, unilateral, or generalized.	Disease is usually diagnosed in the first decade of life. May be associated with multiple hemangiomas containing phleboliths (*Maffucci's syndrome*). In *hereditary multiple exostoses* bowing deformities typically are found in the radius and ulna.

(continues on page 318)

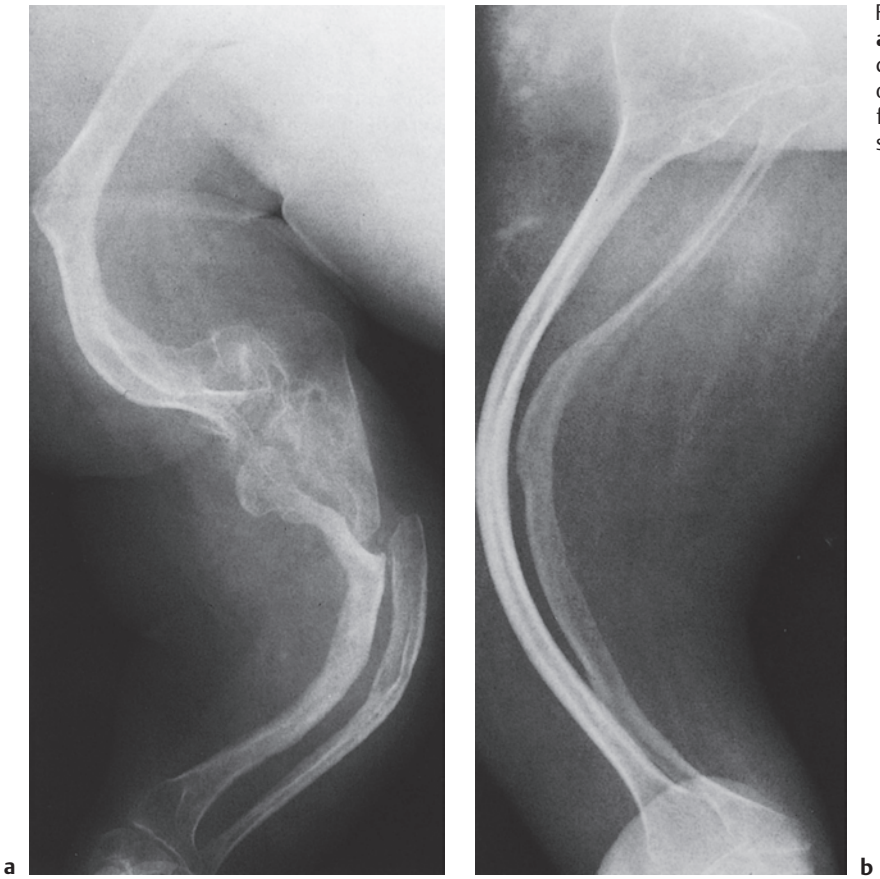

Fig. 14.8 a, b **Osteogenesis imperfecta.** **a** Upper extremity; **b** lower extremity. Bowing deformities in slender over-constricted and osteoporotic long bones are associated with fractures, pseudarthrosis (proximal ulna) and splayed metaphyses.

Fig. 14.9 a **Vitamin D resistent rickets (x-linked hypophosphatemia).** Increased bone density is seen in this adult with lateral bowing of the femur and a pseudofracture (arrow) in the lateral cortex.

Fig. 14.9 b **Weismann–Netter syndrome.** Anterior bowing of the tibia and fibula producing a "sabre-shin" deformity is seen. Note also the characteristic underconstriction of the fibula ("tibialization" of the fibula).

Table 14.1 (Cont.) Bowed or Deformed Long Bones

Disease	Radiographic Findings	Comments
Osteomyelitis (Fig. 14.10)	Severe osteomyelitis may result in a deformed or bowed sclerotic tubular bone, particularly in the leg. Anterior bowing and cortical thickening of the tibia produces a "sabre-shin" appearance, characteristically found as late sequelae of both congenital and acquired *syphilis* and *yaws*. Bowing deformities confined to the distal half of the tibia associated with localized cortical thickening and solid periosteal reaction can be found in *tropical ulcer*.	*Echinococcus* rarely involves bones. Besides the spine, pelvis, and sacrum, the long bones may be affected with multiloculated cystic lesions, resulting occasionally in bone deformities.
Bowing fracture	Anteroposterior or lateral bending of radius, ulna or fibula. A fracture in the neighboring bone (e.g. radius or tibia) might be associated.	Usually in young children.
Fracture (healed)	Common cause of bone deformity usually associated with locally increased sclerosis.	All ages may be affected. Bowlegs in infancy are occasionally secondary to trauma.
Paralysis during growth	Bowed long tubular bones with narrowed, overconstricted shaft diameter due to decreased medullary cavity while the width of the cortex is relatively little affected.	In longstanding paralytic and pseudoparalytic conditions such as *old poliomyelitis*, *muscular dystrophy,* and *juvenile rheumatoid arthritis*.
Osteomalacia (Fig. 14.11)	Bowing deformities occur, besides in the pelvis, spine, and thorax, particularly in the lower extremities. The cortex is thinned as in osteoporosis, but bone deformities, pseudofractures and poor definition of the inner cortical margin and trabeculae help to differentiate osteomalacia from osteoporosis.	Bowing deformities are also a common feature in *rickets* of any etiology.
Hyperparathyroidism	Bone deformities similar to osteomalacia occur in an advanced stage.	In *renal osteodystrophy* (secondary hyperparathyroidism) bone deformities may be secondary to both osteomalacia and hyperparathyroidism.
Paget's disease (Fig. 14.12)	Bone deformities are common in the lower extremities involved by combined (sclerotic and lytic) phase of the disease. This results characteristically in coxa vara ("shepherd's crook" deformity of the upper femur) and anterior bowing of the tibia. In this stage, the involved long bones are widened, and both cortex and disorganized-looking trabeculae are thickened.	Common cause of bone deformities in the elderly patient. *Hereditary hyperphosphatasia* ("juvenile Paget's disease"), which occurs in children, presents characteristically with bowing and thickening of all long bones in the upper and lower extremities.
Fibrous dysplasia (Fig. 14.13)	Marked deformities of the long bones occur, particularly in the polyostotic form, where the bone involvement is generally more extensive. "Shepherd's crook" deformity (upper femur), cortical thickening, widening of the bone, and accentuated or abnormal trabeculation may be present, similar to Paget's disease. The presence of radiolucent or cyst-like lesions or "ground-glass" appearance of the involved bone are useful in differentiating fibrous dysplasia from Paget's disease.	In contrast to Paget's disease, fibrous dysplasia is usually diagnosed in children and young adults. Skin pigmentations ("café-au-lait" spots with irregular outline) and sexual prematurity in females may be present in the polyostotic form (*Albright's syndrome*).
Neurofibromatosis (Fig. 14.14)	Overgrowth of the long bones may result in bowed appearance. The fibula frequently is slender (overconstricted). Pseudarthrosis (especially of the tibia) is common with this presentation. Bowed long bones may occasionally also demonstrate cortical thickening and increased sclerosis.	Hereditary disease often associated with skin neurofibromas and smoothly marginated "café-au-lait" spots. *Congenital pseudarthrosis* of the radius and ulna may also be associated with bowing, but this condition is not related to neurofibromatosis.

Fig. 14.**10** **Osteomyelitis (yaws).** Cortical thickening and symmetrical anterior bowing of both legs produces "sabre-shin" appearance of both tibias as sequelae of the disease.

Fig. 14.**11** **Healed rickets.** Late sequelae of severe rickets are seen in this adult with symmetrical bowing deformities of both legs including anterior and lateral bowing of the tibia and fibula and lateral bowing of the femur. Only lateral view of the right lower leg is shown.

14.12

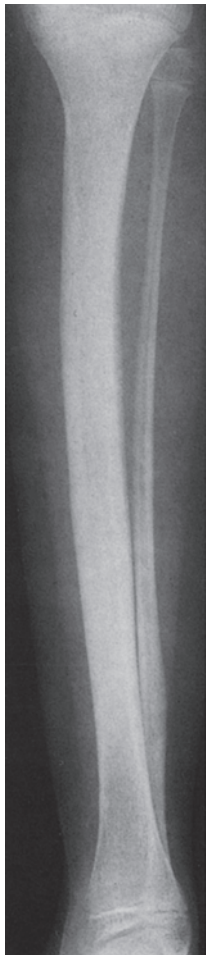

14.13

14.14

Fig. 14.**12** **Paget's disease.** Anterior bowing of tibia that is markedly widened, sclerotic, and irregularly trabeculated in its proximal two-thirds is seen.

Fig. 14.**13** **Fibrous dysplasia.** "Shepherd's crook" deformity of the femur that is widened in its proximal half. Characteristic "ground-glass" appearance is also evident beside sclerotic changes and ovoid radiolucencies.

Fig. 14.**14** **Neurofibromatosis.** Long slender (overconstricted) tibia and fibula with thickened cortex and slight medial bowing are present.

Table 14.2 Wide Diametaphyses (Underconstriction or Undertubulation)

Disease	Radiographic Findings	Comments
Biliary atresia	Undertubulation and "Erlenmeyer flask" deformities combined with signs of osteoporosis and rickets are seen.	Congenital malformation resulting in progressive obstructive jaundice. Usually fatal within 2 years unless corrected surgically.
Rubella embryopathy	Undertubulation of the long bones with alternating radiolucent and sclerotic longitudinal streaks ("celery-stick pattern") and irregular metaphyses with radiolucent bands.	Osseous changes regress in those infants who grow normally, but may persist in those who fail to thrive.
Infantile cortical hyperostosis (Caffey's disease) (Fig. 14.15)	Periosteal new bone formation, cortical thickening and widening, primarily of the mandible, scapulae, clavicles, ribs and ulnae, are characteristic.	Disease develops in the first 5 months of life. Fever of abrupt onset, hyperirritability, and tender soft-tissue swelling over the affected bones are characteristic. The radiographic changes tend to regress spontaneously within one year.
Progressive diaphyseal dysplasia (Engelmann-Camurati disease) (Fig. 14.16)	Symmetrical involvement of the long bones with undertubulation and cortical thickening of the midshaft resulting in a spindle-shaped appearing bone.	Rare hereditary disease associated with progressive midshaft cortical thickening and neuromuscular dystrophy. Usually diagnosed between 4 and 12 years, causing a wide-based, waddling gate.
Mucopolysaccharidosis (Fig. 14.17)	Thickened undertubulated shafts, often with irregular wavy contours, are common findings. Metaphyseal flaring can be seen with Morquio's disease, whereas tapering of the small tubular bones suggests Hurler's disease.	Clinical and radiographic findings of different mucopolysaccharidoses and *mucolipidoses* are similar. A large dolichocephalic skull with J-shaped sella turcica, oval or hook-shaped vertebral bodies with gibbus formation in the thoracolumbar region, underdevelopment of the supra-acetabular region resulting in a widened acetabular roof, and coxa valga deformities with widened femoral necks, are characteristic.
Metatropic dwarfism	Long tubular bones are shortened and have "dumbbell" appearance that is caused by the markedly enlarged metaphyses at both ends.	Short-limb dwarfism, which is normal at birth with progressive kyphoscoliosis, finally resembling Morquio's disease. Flaring of the metaphyses with very short limbs are also seen in *thanatophoric dwarfism*, but this condition results in stillbirth or death in the neonatal period.
Pseudoachondroplasia (Fig. 14.18)	Initially the epiphyses are small and flattened and the metaphyses wide with dense, mushroom-shaped provisional zones of calcifications. In the adults the tubular bones are short and expanded at their end.	*Spondyloepimetaphyseal dysplasias* and *epimetaphyseal dysplasias* consist of a heterogeneous group of conditions that have metaphyseal flaring in common.
Osteogenesis imperfecta (Fig. 14.19)	Metaphyses of the long bones are often markedly widened and may contain irregular calcifications while the shaft is overconstricted and may show severe bending deformities and multiple fractures of different ages. Osteopenia is usually a dominant feature.	Radiographic findings are more severe in the congenital than tarda form of osteogenesis imperfecta.
Homocystinuria	Widened metaphyses and epiphyses with usually severe osteopenia and prominent growth lines are seen. In addition, Marfan-like changes (e.g., arachnodactyly) may be present.	Inborn error of the methionine metabolism.
Pyle's disease (familial metaphyseal dysplasia) (Fig, 14.20)	"Erlenmeyer flask" deformity or paddle-shapped enlargement of the metaphyses and, to a lesser degree, undertubulation of the long bones associated with cortical thinning and osteoporosis are characteristic. Thickened ribs and symmetrically enlarged proximal portions of the clavicles may be associated.	Rare hereditary disorder that can be differentiated from craniometaphyseal dysplasia by the lack of skull changes.
Craniometaphyseal dysplasia (Fig. 14.21)	Undertubulation and "Erlenmeyer flask" deformities characteristic and usually most pronounced in the distal femur, radius, and ulna. Osteoporosis may be associated. Skull may show sclerosis of the base and calvarium, lack of aeration of paranasal sinuses and mastoids, and thickening and sclerosis of the mandible.	Rare congenital and familial bone dysplasia. Clinical features include hypertelorism, a broad flat nose, and defective dentition.

(continues on page 322)

Fig. 14.**15** **Infantile cortical hyperostosis** (Caffey's disease). Periosteal reactions progressing to cortical thickening are evident in the diaphyses of the long bones of the upper extremity, resulting in considerable widening especially of the ulna.

Fig. 14.**16** **Progressive diaphyseal dysplasia** (Engelmann-Camurati disease). Spindle-shaped widening and sclerosis of the diaphyses of the long bones are characteristic.

Fig. 14.**17** **Mucopolysaccharidosis (Morquio).** Widened femoral neck and mild coxa valga deformity associated with a widened acetabular roof, are characteristic.

Fig. 14.**18** **Pseudoachondroplasia.** Metaphyseal flaring and irregular epiphyses are seen.

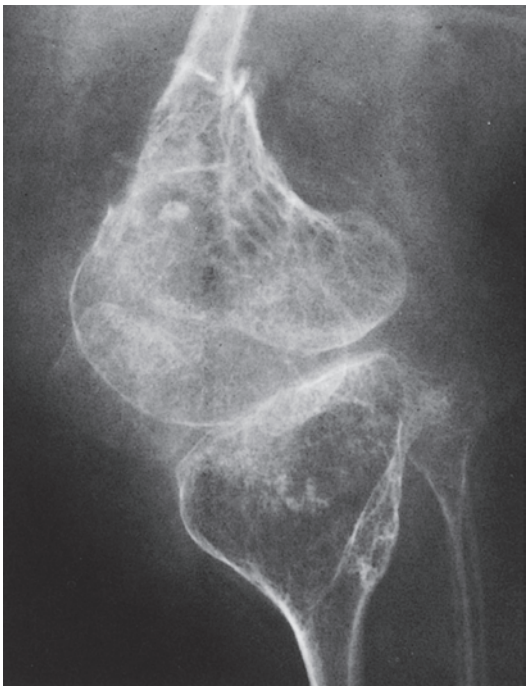

Fig. 14.**19** **Osteogenesis imperfecta.** Markedly widened metaphyses containing small ("popcorn") calcifications are connected to overconstricted shafts. Severe osteopenia and a fracture in the distal femur are also present.

Fig. 14.**20** **Pyle's disease.** Considerable widening of both proximal and distal ends of the tibia, and to a lesser degree of the fibula, is associated with a slight bowing deformity of the midshafts.

a b

Fig. 14.**21 a, b** **Craniometaphyseal dysplasia. a** Humerus; **b** radius and ulna. Undertubulation of the shafts with gradually splayed metaphyses and gowing deformities are seen.

Table 14.2 (Cont.) Wide Diametaphyses (Underconstriction or Undertubulation)

Disease	Radiographic Findings	Comments
Hereditary multiple exostosis (diaphyseal aclasis) (Fig. 14.22)	Undertubulation and often bowing of the long bones of both upper and lower extremities with multiple osteochrondromas in the metaphyseal regions, but usually sparing the elbow, are characteristic. Shortening of ulna and fibula is often present, Shortening of the ulna may result in congenital dislocation of the radial head, false articulation between the distal ulna and radius, and ulnar deviation of the carpus.	The inherited disease is usually diagnosed in the first decade of life. Transformation to chondrosarcoma occurs in approximately 5% of cases, although higher malignant transformation rates have been described.
Enchondromatosis (Ollier's disease) (Fig. 14.23)	Undertubulation, deformity, and shortening of the involved bones are common. Longitudinal radiolucent streaks interspersed with normal to sclerotic-appearing streaks may extend from the metaphysis into the shaft, or expansile radiolucent lesions with or without stippled calcifications may be seen. The metaphyses are usually most severly involved and often show "Erlenmeyer flask" deformities.	The generalized form of the disease is usually discovered in the first decade of life. The disease may also be unilateral or present only with a few enchondromas, characteristically located near a joint. Malignant degeneration in this nonhereditary disease is reported in 5–25% of cases.
Bone cysts and benign tumors	Localized widening usually near the end of long bones is caused by a variety of benign expansile mass lesions.	For further differentiation, see Chapter 5.
Chronic osteomyelitis (Fig. 14.24a)	Marked thickening of the involved area with scattered radiolucent, destructive lesions, solid periosteal new bone formation and sclerosis is characteristic.	In chronic *sclerosing osteomyelitis (Garré)*, diffuse uniform sclerosis of the involved bone may be seen (Fig. 14.**24b**).
Healed fracture	Localized to generalized widening of the shaft often associated with a bone deformity. Elevated solid periosteal reaction may initially simulate a double cortex or even "bone-within-bone" appearance during the healing phase, particularly in infants and children, but will disappear with further bone remodeling. Cortex may be thickened by periosteal bone formation, but may become normal or even thinned at a later stage. A metaphyseal injury may result in an "Erlenmeyer flask" deformity.	Common cause of localized undertubulation and deformity of a long bone.
Thalassemia	Thinned cortices and a uniform reticular to cystic trabecular pattern in the widened diametaphyses with "Erlenmeyer flask" deformities characteristic, especially in the young patient.	A group of different hereditary hypochromic microcytic anemias, caused by the synthesis of abnormal hemoglobin polypeptide chains. Usually found in "Mediterranean" people and their descendants. Bone changes are caused by erythroid hyperplasia and are most pronounced in thalassemia major. Initially, all bones may be involved. With the conversion of red to yellow marrow in the tubular bones later in life the lesions may regress at these locations.
Sickle-cell anemia	Cortical thinning and coarsening of the trabecular pattern due to bone marrow hyperplasia occur, but are less pronounced than in thalassemia. Changes in the long bones are caused by osteomyelitis and/or infarction and include destructive changes and new bone formation that may result in irregular diametaphyseal widening. Cortical infarcts may result in cortical thickening or "splitting of the cortex." Layering of new bone along the inner cortex may produce a "bone-within-bone" appearance.	Sickle-cell anemia is a hereditary disorder limited almost exclusively to blacks, and caused by an abnormal hemoglobin HbS, where in position 6 of the β-globin chain, valine is substituted for glutamic acid.

(continues on page 324)

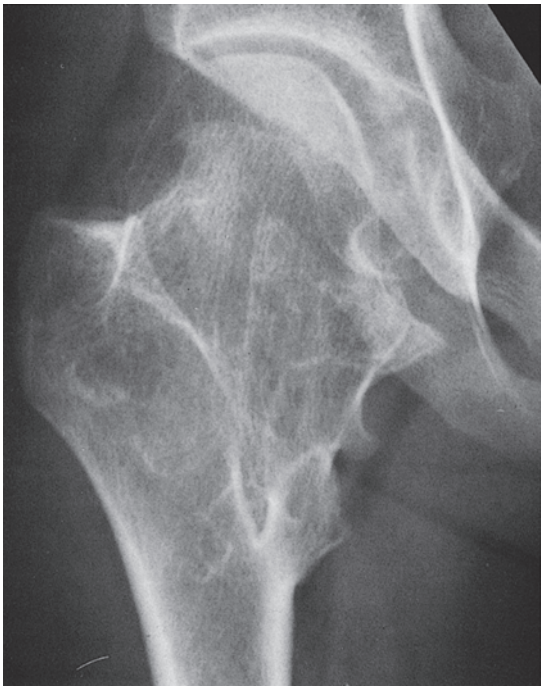

Fig. 14.**22** **Hereditary multiple exostoses.** Deformed proximal femur with widened femoral neck containing several osteochondromas is characteristic.

Fig. 14.**23** **Enchondromatosis.** Undertubulation of the shortened and slightly bent long bones, and widened metaphyses containing longitudinal streaks of calcifications, are characteristic.

Fig. 14.**24 a** **Congenital syphilis.** Widening of the humeral shaft and flaring of the metaphyses are caused by periosteal new bone formation. A destructive lesion is also present in the distal metaphysis.

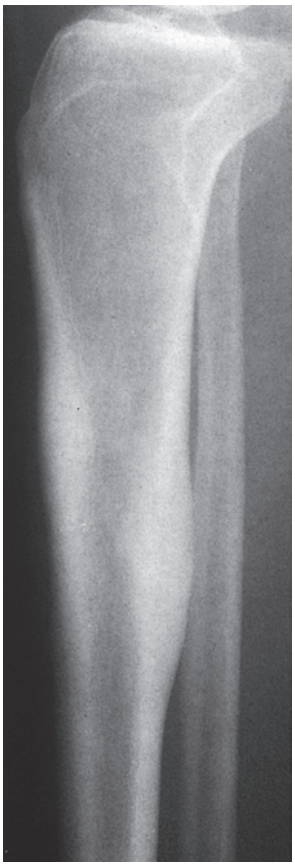

Fig. 14.**24 b** **Sclerosing osteomyelitis Garre.** Circumferential localized cortical thickening and widening of the proximal tibia shaft is seen.

Table 14.2 (Cont.) Wide Diametaphyses (Underconstriction or Undertubulation)

Disease	Radiographic Findings	Comments
Gaucher's disease (Fig. 14.25 a, b)	Lower extremities are involved more often. Characteristic is the combination of avascular necrosis of the femoral head and an "Erlenmeyer flask" deformity at the distal femur. The shaft of the long bones may be locally expanded. Bone resorption and reparation may result in generalized osteopenia, lytic lesions of varying sizes simulating metastases, and patchy areas of sclerosis. Similarly, the cortex may be thinned, with a scalloped inner margin, or thickened and "split." An inner layer of new bone formation may produce "bone-within-bone" appearance. Solid or lace-like periosteal reaction can occur, probably secondary to infarction.	Hereditary metabolic disease characterized by the accumulation of cerebrosides in the reticuloendothelial cells, resulting in hepatosplenomegaly. There is no sex predilection. The most common "adult" type occurs in Ashkenazic Jews, with the earliest manifestations appearing in childhood and progressing in the second and third decade of life. The acute type of Gaucher's disease is a rare, fatal neurodegenerative disorder with no ethnic predilection, that usually becomes manifest shortly after birth and has an average survival time of one year.
Niemann-Pick disease (Fig. 14.26)	Widening of the diametaphyses (undertubulation) and osteopenia with thinned cortices and coarsening of the trabecular pattern characteristic. Coxa valga occurs commonly. An "Erlenmeyer flask" deformity in the distal femur may simulate Gaucher's disease.	Hereditary metabolic disorder characterized by the accumulation of phospholipids (sphingomyelins) in the reticuloendothelial cells. Niemann-Pick disease can be differentiated radiographically from Gaucher's disease by the usual absence of avascular epiphyseal necroses, bone infarcts, and well-circumscribed radiolucent lesions.
Langerhans cell histiocytosis (histiocytosis X)	Expansile lytic lesion and periosteal new bone formation may produce irregular localized widening of the long bones.	The bone manifestations may be monostotic or disseminated.
Fibrous dysplasia (Fig. 14.27)	Localized widening by expansile lesion, usually at the metaphysis, or expansion of the entire shaft may occur. Lesions may be radiolucent, trabeculated, or have a "ground-glass" appearance and occasionally contain dense linear or irregular calcifications. The cortex is intact and can be thickened, but usually does not show periosteal new bone formation unless a fracture or pseudofracture has occurred. Marked deformities and pseudoarthrosis may be associated.	Fibrous dysplasia may be monostotic, monomelic or polyostotic. In the latter case, it is often unilateral and associated with irregular ("coast of Maine") "cafe-au-lait" spots in approximately one-third of the cases. Endocrine anomalies such as sexual precocity (almost exclusively in females), hyperthyroidism, acromegaly, Cushing's syndrome, gynecomastia, and parathyroid enlargement may be associated.
Paget's disease	Considerable widening of the involved bone with thickened cortex and coarse disorganized-appearing trabeculation. Bowing deformities, pathologic fractures, or pseudofractures may be associated.	The long bones are most commonly involved in the combined (sclerotic and lytic) phase. Localized expansion may occasionally also be seen in the much less common lytic phase.
Osteopetrosis (Fig. 14.28)	Besides a marked, uniform, and symmetrical increase in bone density "Erlenmeyer flask" deformities and widened proximal and distal diaphyses are commonly present. Occasionally, alternating transverse dense bands and lucent lines are found in widened diametaphyses.	*Pycnodysostosis*, a rare hereditary disorder, is also characterized by generalized osteosclerosis, but can be differentiated from osteopetrosis by the absence of "Erlenmeyer flask" deformities, no "bone-within-bone" appearance, and hypoplasia of the mandible.
Hypophosphatasia	"Erlenmeyer flask" deformity and cortical thickening of the long bones often with multiple fractures or pseudofractures and bowing deformities (especially femora) are characteristic for hypophosphatasia in adults.	Bony changes of hypophosphatasia in infants and childhood are more severe and similar to rickets.
Rickets (Fig. 14.29)	Irregular "frayed" metaphyses, which become widened and cupped with progression of the disease, are characteristic for the florid stage of the disease. "Erlenmeyer flask" deformities and undertubulation may be seen with healing.	Findings are similar in *vitamin D resistent rickets.*

(continues on page 326)

a

b

Fig. 14.**25 a, b** **Gaucher's disease. a** Proximal femur: Avascular necrosis of the femoral head and increased patchy sclerotic areas in the proximal femur are seen. **b** Distal femur: "Erlenmeyer flask" deformity of the distal femur and osteolytic lesions in the distal femur and proximal tibia are seen. Irregular sclerosis in the proximal tibia metaphysis is caused by old bone infarcts.

Fig. 14.**26** **Niemann-Pick disease.** Generalized osteopenia and flaring of the distal femur resulting in "Erlenmeyer flask" deformity are evident.

Fig. 14.**27** **Fibrous dysplasia.** Widening (undertubulation) of the humerus shaft with thinned cortices and "ground-glass" appearancec is seen.

Fig. 14.**28** **Osteopetrosis.** Splayed metaphyses are associated with a uniform dense osteosclerosis.

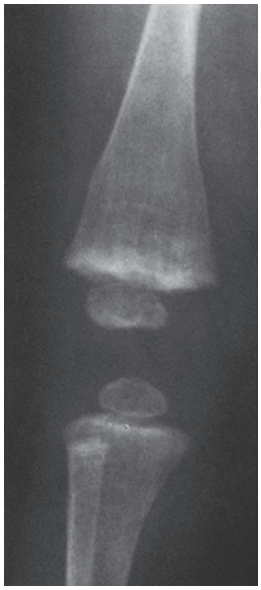

Fig. 14.**29** **Healing rickets.** Splayed metaphyses with irregular sclerotic ends best seen in the distal femur are found in the healing stage of the disease.

Table 14.2 (Cont.) Wide Diametaphyses (Underconstriction or Undertubulation)

Disease	Radiographic Findings	Comments
Scurvy (healing)	Wide diametaphyses with cortical thickening that may persist for many years result from healing subperiosteal hemorrhages, which calcify and subsequently ossify.	
Lead poisoning (Fig. 14.30)	Besides the dense metaphyseal bands, "Erlenmeyer flask" deformities and, at a more advanced stage, undertubulation of the shaft may occur.	Mortality rate of chronic lead poisoning in children under 2 years of age may be as high as 25%.
Idiopathic hypercalcemia of infancy (Williams syndrome)	Osteosclerosis (particularly in the metaphyses) and "Erlenmeyer flask" deformities occur in the distal femora. Dense metaphyseal bands and cortical thickening are frequently associated. Soft tissue calcifications may also be present.	Clinical manifestations include an elfin face, mental and physical retardation and neonatal hypercalcemia. Supravalvular aortic stenosis and hypoplasia of major vessels are frequently associated. *Hypervitaminosis D* may produce a similar radiographic and clinical picture.

Fig. 14.**30** **Lead poisoning.** Splaying of the metaphyses is associated with dense transverse metaphyseal bands.

Table 14.3 Narrow Diametaphyses (Overconstriction or Overtubulation)

Disease	Radiographic Findings	Comments
Hypopituitarism	Proportional dwarfism often with overconstricted tubular bones and delayed epiphyseal closure.	Hypogonadism and other endocrinological disturbances may concur.
Tubular stenosis (Kenny-Caffey disease)	Overconstricted tubular bones show symmetrical endosteal thickening and narrowed medulla. Sclerosis of the calvarium and coxa valga may be associated.	Proportional dwarfism. Tetany in early infancy from hypocalcemia.
Progeria	Excessive constriction of the long bones and generalized osteoporosis are common. Associated features include thin calvarium with wormian bone formation, small facial bones and small mandible, progressive resorption of tufts, clavicles and, occasionally, ribs, coxa valga, prominent knees and enlargement of the head of the radius and capitulum.	Progeria is characterized by dwarfism, cardiomegaly secondary to hypertension, coronary artery disease, and premature aging, with death occurring usually in the second or third decade. Onset of disease occurs at the end of first year of life.
Osteogenesis imperfecta (Fig. 14.31)	Long bones are slender and overconstricted. Bowing and fracture deformities are common. Osteoporosis with thinning of the cortex is characteristically present.	The hallmark of the disease is a marked susceptibility to fracture from minimal trauma. Blue sclera and a white ring surrounding the cornea (“Saturn’s ring”) are often present.
Marfan’s syndrome	Elongation and thinning of all tubular bones, but most pronounced in the hands and feet (arachnodactyly). Bone mineralization is normal. Scoliosis and pectus deformity are common. Lumbar vertebra may be abnormally tall and demonstrate posterior scalloping.	Autosomal dominant growth disturbance caused by failure to produce normal collagen. Patients are tall, measuring usually over 6 feet in height. Laxity of ligaments leads to hyperextensible joints with recurrent dislocations. Bilateral subluxed lenses occur in over 50% of cases. Aortic aneurysm or dissection is the most serious complication.
Homocystinuria	Marfan-like features including slender shafts of the tubular bones. In contrast to Marfan’s syndrome, the long tubular bones have widened metaphyses and epiphyses and osteopenia is commonly present, resulting in biconcavity or compression fractures of the vertebral bodies.	Inborn error of metabolism resulting in high homocystine serum levels and homocystinuria.

(continues on page 328)

Fig. 14.**31** **Osteogenesis imperfecta.** Markedly narrowed (overconstricted) and bowed shaft of the radius and to a lesser degree of the ulna, with only moderate osteoporosis is evident.

Table 14.3 (Cont.) Narrow Diametaphyses (Overconstriction or Overtubulation)

Disease	Radiographic Findings	Comments
Neurofibromatosis (Fig. 14.32)	Overtubulation may result in an extremely slender shaft (especially fibula) and is often associated with bowing deformities. Localized bony overgrowth and pseudarthroses are other characteristic features of neurofibromatosis, whereas shortening of the long bones is rare. Subperiosteal hematomas, cortical thickening, and intraosseous neurofibromas presenting as expansile cyst-like lesions are occasionally seen.	Approximately 50 % of patients have bone involvement ranging from minimal to extensive and generalized.
Epidermolysis bullosa	Overconstriction of the shaft of the long bones occasionally associated with flexion contractures and subluxations. Resorption of terminal phalanges also occurs.	Rare hereditary disease characterized by skin blisters formation occurring either spontaneously or following minimal trauma. Flexion contractures and webbing between fingers may produce a claw-like hand. Healing of esophageal mucosal lesions may progress to stenotic webs.
Disuse atrophy	Osteoporosis with thin cortices and a decrease in size and number of trabeculae in the spongiosa are the hallmark of disuse atrophy. Concentric constriction of the shaft is commonly associated in children, but rarely seen in adults.	Found after disuse of the involved part of the skeleton for a long time. May be localized or generalized.
Juvenile rheumatoid arthritis	Overconstricted long tubular bones with narrow medullary cavity and osteopenia may be seen besides the more characteristic arthritic changes. Epiphyses, especially of large affected joints, are enlarged and appear ballooned.	See Chapter 6 for additional information.
Paralysis (infancy and childhood) (Fig. 14.33)	Paralysis in the growing bone results commonly in overconstriction of the shafts at the expense of the medullary cavity, whereas the cortex seems relatively little affected.	E.g., in *poliomyelitis*, *birth palsies*, *congenital malformations of the spinal cord* and *brain*.
Muscular dystrophy (Fig, 14.34)	Overconstriction of the diaphyses similar to paralysis (narrowed medullary cavity with relatively little affected cortices). Atrophic muscle bundles separated by increased fat layers and hypertrophy of the subcutaneous fat are often radiographically recognizable in these conditions.	E.g., *arthrogryposis multiplex congenita, amyotonia congenita (Oppenheim's disease)*, *infantile muscular atrophy (Werdnig-Hoffmann disease)*, and others.

Fig. 14.**32** **Neurofibromatosis.** A very slender fibula shaft is usually present in the disease. Osteopenia with chronic fractures in the distal tibia and fibula shafts resulting in bony deformities and pseudarthroses are also quite characteristic.

Fig. 14.**33** **Poliomyelitis.** Markedly narrowed (overconstricted) shafts of both tibia and fibula at the expense of the medulla are seen, whereas the cortex is affected relatively little.

a

b

Fig. 14.**34 a, b** **Muscular dystrophy** (Werdnig-Hoffmann). **a** Femur; **b** tibia and fibula. Overconstriction of the shafts, coxa valga deformity, atrophic muscles separated by thick layers of adipose tissue, and hypertrophy of the subcutaneous fat are recognizable.

Table 14.4 Radiolucent Transverse Bands in the Metaphyses

Disease	Radiographic Findings	Comments
Normal variant in neonates	Striated appearance of metaphyses is not unusual.	Found in apparently healthy infants.
Osteogenesis imperfecta	Radiolucent metaphyses are part of the generalized osteopenia. Characteristic are slender long bones with thin cortices and bowing deformities.	Secondary shortening and thickening of the long bones may be secondary to "telescoping" fractures and subsequent excessive callus formation.
Leukemia (Fig. 14.35)	Transverse radiolucent bands are usually the earliest radiographic manifestation in childhood leukemia, whereas they are uncommon in adults. Scattered lytic and, rarely, sclerotic areas and periosteal reactions are found in more advanced cases.	Bony involvement in leukemia occurs in over 50% of cases in childhood and up to 10% in adults.
Metastases (especially from neuroblastoma)	Transverse radiolucent bands and other findings are indistinguishable from leukemia.	Approximately 80% of neuroblastomas are found in children under $2^1/_2$ years of age. Presence of urinary vanillylmandelic acid and vanilphenylethylamine is diagnostic.
Juvenile rheumatoid arthritis	Osteopenia with transverse radiolucent bands. In contrast to adult rheumatoid arthritis, periostitis and joint fusions are common, and both joint space narrowing and erosions are late manifestations.	Occurs usually in children over 10 years of age with female predominance.
Prenatal infections (e.g., rubella, cytomegalic inclusion disease)	Transverse radiolucent metaphyseal bands may develop after neonatal period. Metaphyses are irregular but not cupped. Alternating longitudinal sclerotic and lucent streaks and coarse trabeculation are often seen in the diaphyses of the long bones.	Radiolucent metaphyseal bands can also be seen with other severe prenatal and postnatal infections and systemic diseases.
Osteoporosis in neonates and during childhood	Osteoporosis of any etiology developing in utero, infancy and early childhood is most pronounced in the metaphyses and may assume a striped appearance.	E.g. in neuromuscular disorders and paralysis, juvenile rheumatoid arthritis and malnutrition.
Scurvy	A radiolucent band (Trümmerfeld zone) is characteristically seen beneath the widened and sclerotic-appearing zone of provisional calcification in the metaphyses.	Radiographic signs of scurvy are summarized in Chapter 1.
Cushing's syndrome	Rare cause of band-like metaphyseal radiolucencies as part of generalized osteoporosis in the growing bone.	Caused by abnormally high (exogenous or endogenous) steroid blood levels. Endogenous overproduction of steroids in children is caused in over half of the cases by *adrenal carcinoma*.

Fig. 14.**35** **Leukemia in childhood.** A transverse radiolucent band in the metaphyses of both the radius and ulna is seen.

Table 14.5 Sclerotic Transverse Bands or Lines in the Metaphyses

Disease	Radiographic Findings	Comments
Normal variant in young children	Relatively dense metaphyseal ends of long tubular bones, equal to the cortical density of the same bone, are commonly present.	In active children of less than 4 years of age.
Growth arrest lines (Fig. 14.36)	Single or multiple, sharply defined, fine sclerotic lines running across the metaphyses. Occur in infants and children, but may persist and remain recognizable in adults.	Normal finding, but may be related to malnutrition or severe disease during growth. Appear particularly prominent when associated with osteopenia. DD: *Reinforcement lines (bone bars)* developing in chronic osteopenia of adults as response to chronically weakened bone.
Osteopetrosis (Fig. 14.37)	Multiple transverse or longitudinal metaphyseal striations occur. At a more advanced stage, "bone-within-bone" appearance may result. "Erlenmeyer flask" deformity is commonly associated.	Hereditary disorder characterized by symmetrical generalized increase in bone density and failure of tubulation.
Cretinism (hypothyroidism)	Dense, transverse metaphyseal bands associated with shortened slender shafts, endosteal thickening, and irregular, fragmented epiphyses are characteristic.	Delayed appearance and fusion of all epiphyses (delayed bone age) is a hallmark of the disease.
Hypoparathyroidism and pseudohypoparathyroidism	Transverse sclerotic bands are found in the metaphyses of long bones. A slight generalized increase in bone density, ossification of tendinous and ligamentous insertions mimicking exostoses, and subcutaneous calcifications, are often also present.	Other associated findings may include marginal sclerosis of the iliac crests and vertebral bodies. In the skull, calvarial thickening, basal ganglia calcifications, and defective dentition, are characteristic. In pseudohypoparathyroidism, short metacarpals and metatarsals are also present.
Metaphyseal chondrodysplasia (Fig. 14.38)	Cupping and irregular mineralization of the metaphyses, which may demonstrate irregular sclerotic bands with radiolucent streaks. Diaphyses and epiphyses are normal, but the ossification of the latter may be delayed.	Several different and probably unrelated cartilage dysplasias with similar radiographic features are comprised in this rare entity (e.g. Schmid, Jansen, McKusick, and Schwachmann-Diamond types). Metaphyseal changes may resemble rickets but, in contrast to the latter, epiphyses are normal.

(continues on page 332)

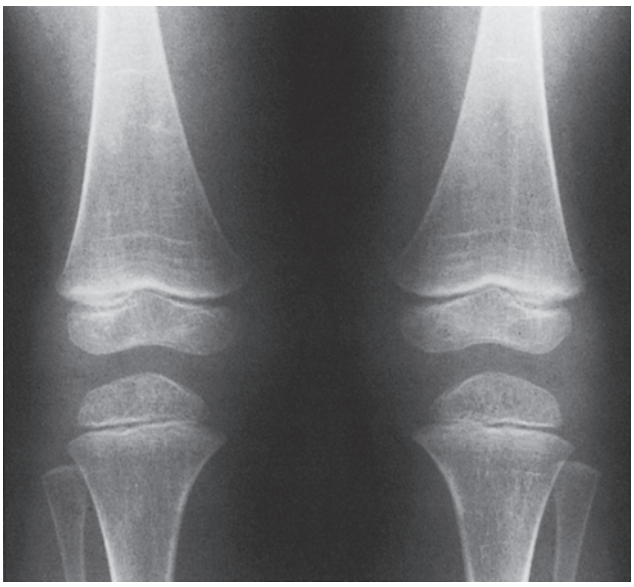

Fig. 14.**36** **Growth lines.** Several fine and symmetric transverse lines in the distal femora are seen bilaterally. Osteopenia is also evident, caused by homocystinuria in this case.

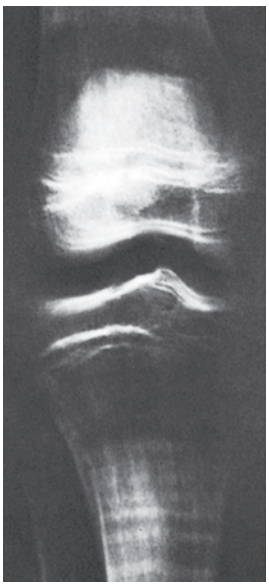

Fig. 14.**37** **Osteopetrosis.** Multiple broad transverse striations are seen in the undertubulated distal femur and proximal tibia, both demonstrating "Erlenmeyer flask" deformities.

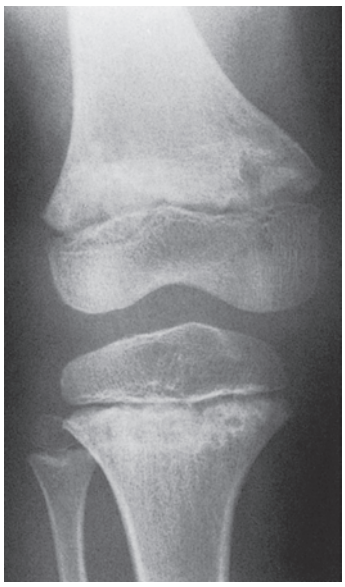

Fig. 14.**38** **Metaphyseal chondrodysplasia** (McKusick). Irregular sclerotic and widened metaphyses are seen.

Table 14.5 (Cont.) Sclerotic Transverse Bands or Lines in the Metaphyses

Disease	Radiographic Findings	Comments
Idiopathic hypercalcemia of infancy (Williams syndrome) (Fig. 14.39)	Dense metaphyseal bands are characteristic of the severe, chronic form, often associated with cortical thickening and an overall increase in bone density. Sclerosis of the orbital rim and sphenoids may produce a striking "spectacle" appearance.	The severe chronic form of idiopathic hypercalcemia is associated with the triad of azotemia, mental and physical retardation, and osteosclerosis. Idiopathic hypercalcemia may result from hypersensitivity to vitamin D or an inborn error in the cholesterol metabolism. *Hypervitaminosis D* may produce identical findings.
Congenital syphilis (Fig. 14.40)	Transverse metaphyseal striping (sclerotic and lucent bands) may be the earliest finding. Destructive metaphyseal changes may be seen in more advanced cases, most characteristically located in the medial aspect of the proximal tibia metaphysis (Wimberger's sign).	Transverse striping of the metaphysis in infancy is not diagnostic for syphilis and can be seen with other severe diseases during the fetal period (e.g., *toxoplasmosis*, *rubella*, and *cytomegalic inclusion disease*), as well as with the administration of bismuth to the mother during pregnancy.
Erythroblastosis fetalis	Transverse metaphyseal bands and diffuse sclerosis of the diaphyses may be present.	Congenital hemolytic anemia resulting from Rhesus factor incompatibility.
Thalassemia Sickle-cell anemia	Transverse metaphyseal bands may occur.	More characteristic changes in thalassemia include splaying of the metaphysis ("Erlenmeyer flask" deformities), thinning of the cortices, and accentuated trabeculation. In sickle-cell anemia, bone changes are primarily caused by infarction and osteomyelitis and may result in "bone-within-bone" appearance, "cortical splitting," and new periosteal bone formation.
Radiation osteitis	A dense metaphyseal band can develop in the growing bone as a manifestation of repair.	Radiation-induced changes in the growing metaphyses include irregularities, fraying and sclerosis, and may superficially resemble rickets.
Healed radiolucent metaphyseal bands of different etiologies (e.g., treated rickets, renal osteodystrophy, scurvy, and leukemia) (Fig. 14.41)	Original disease characteristically produces radiolucent metaphyseal bands that may become dense under proper therapy.	Occasionally alternating radiolucent and sclerotic metaphyseal bands may already be seen in childhood leukemia before treatment.
Stress fractures (Fig. 14.42)	A band-like focal sclerosis is seen at the end of tubular bones (e.g. femoral neck and tibia plateau).	Present clinically with activity- related pain that is relieved by rest. *Fatigue fractures* resulting from abnormal stress in normal bone can be differentiated from *insufficiency fractures* resulting form normal stress in osteopenic bone.
Lead poisoning (Fig. 14.43 a)	Dense metaphyseal bands exceeding the cortical density of the same bone, found in the growing skeleton. Interference with normal modeling may result in splaying of the involved metaphysis ("Erlenmeyer flask" deformity). Separation of the cranial sutures and lead particles seen in the gastrointestinal tract support the diagnosis.	Bone changes become radiographically evident approximately 3 months after chronic lead poisoning. *Bismuth, phosphorus*, and *mercury poisoning* as well as *vitamin D intoxication* may also produce one or several dense bands in the metaphysis similar to lead poisoning. Occasionally, dense metaphyses are seen in an apparently healthy child under the age of 4.
Drug or hormone therapy (Fig. 14.43 b)	Rare cause of transverse sclerotic bands.	E.g., with high dosages of steroids, parathormone, methotrexate, and other drugs.

14.39

14.40

14.41

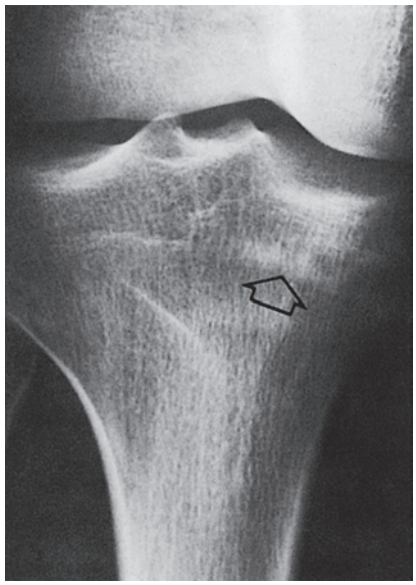

14.42

Fig. 14.**39** **Idiopathic hypercalcemia of infancy** (Williams syndrome). Transverse metaphyseal bands are seen in the distal radius and ulna. Cortical thickening and a marked generalized osteosclerosis is also present.

Fig. 14.**40** **Congenital syphilis.** Irregular transverse metaphyseal striping is associated with destructive metaphyseal lesions.

Fig. 14.**41** **Leukemia.** Sclerotic metaphyseal bands are seen in this child already prior to the initiation of proper treatment.

Fig. 14.**42** **Stress fracture.** A band-like focal sclerosis (arrow) is seen in the proximal tibia.

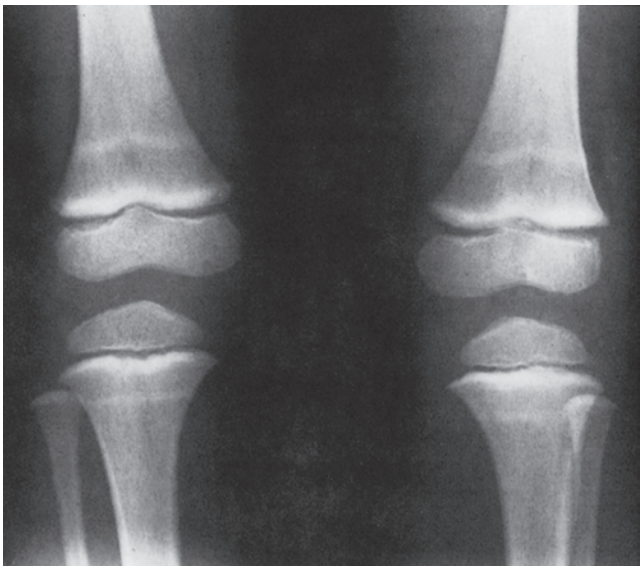

Fig. 14.**43 a** **Lead poisoning.** Dense and symmetrical metaphyseal bands in the metaphyses of both the distal femora and the proximal tibias are seen.

Fig. 14.**43 b** **Methotrexate therapy in acute lymphoblastic leukemia.** Dense metaphyseal bands only developped after initiation of therapy. Note also the sclerotic outline of the epiphyses and the “Erlenmeyer flask” deformity of the distal femur.

Table 14.6 Short Bone in Extremities

Abnormality	Usual Causes	Comments
Symmetrically short limbs	*Achondroplasia* (most common) (Fig. 14.**44**) Other *short limb dwarfism syndromes*. Syndromes with *growth disturbance of bone*.	For differential diagnosis, analyze various portions of bone and eventual associated findings.
Localized shortening of bone (resulting from an insult to a growing bone)	*Osteomyelitis*	Epiphyseal damage causes shortening and may produce a "ball-and-socket" metaphyseal deformity.
	Trauma	Shortening is due to impacted fracture or epiphyseal damage in a growing bone.
	Scurvy	In severe scurvy, a fracture through a radiolucent Trummerfeld zone may cause premature fusion.
	Hypervitaminosis A	May rarely cause asymmetric shortenings due to premature fusion of the ossification centers. Splayed metaphyses.
	Rickets (all etiologies)	Infantile or juvenile rickets may leave shortening and deformation of long bones after healing.
	Enchondromatosis (Ollier's disease)	Rounded expansile radiolucencies in the metaphyses may be associated with deformities and shortening of bone.
	Radiation therapy	Sufficient dosages cause an arrest of bone growth in infants and children. More important sequelae tend to occur in spine and pelvis, mimicking achondroplasia or osteochondrodystrophy.
	Bone infarcts (e.g., sickle-cell anemia)	The majority of infarcts occur in HbSS genotype, and are located between the shaft and metaphysis of femur, proximal tibia, and distal humerus. The radiographic pattern is indistinguishable from osteomyelitis, which may be superimposed.
	Neoplasm	Bone tumor like *Ewing's sarcoma* may invade the growth plate.
	Hereditary multiple exostoses (Fig. 14.**55**)	

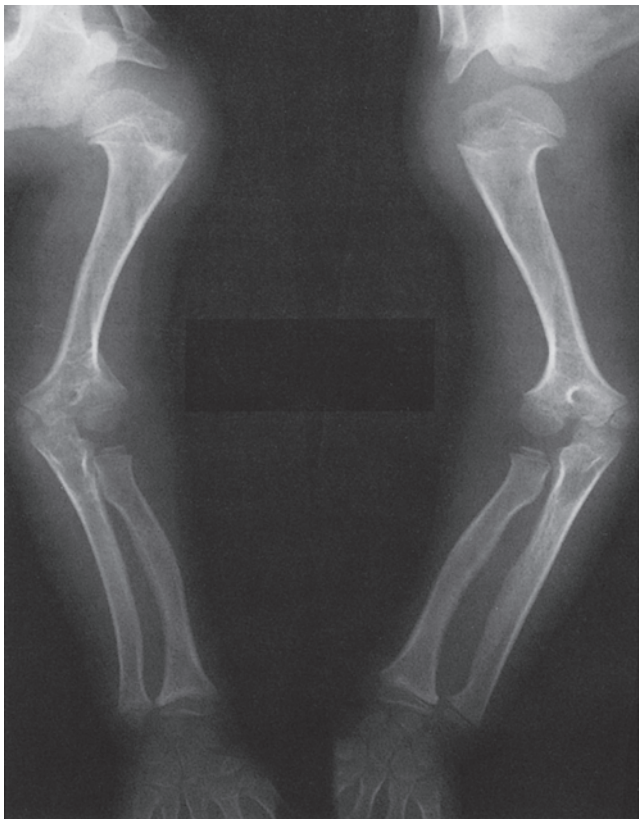

Fig. 14.**44** **Achondroplasia.** Bilaterally short, deformed upper extremities.

Table 14.7 Abnormal Scapula

Abnormality	Usual Causes	Comments
Hypoplasia	*Achondroplasia*	Hypoplastic scapula may be a feature in several bone dysplasias but other radiographic characteristics are more diagnostic.
	Nail-patella syndrome	Hypoplastic scapula and thickening of the glenoid rim may be associated with this condition.
Malposition	*Sprengel's deformity* (Fig. 14.**45**)	Elevation of scapula. Scapula is connected to the cervical spine by an *omovertebral bone* in one third of cases. In the absence of an omovartebral bone, a fibrous fascial shealt extends from the superior angle of the scapula to the spinous process, the lamina or the transverse process of 1 or more lower cervical vertebrae. The scapula may be hypoplastic.
	Brachial plexus damage (Fig. 14.**46**)	Winging of scapula, downward subluxation of the humerus, and various secondary deformities may occur. The radiographic pattern depends on the site and number of nerve roots involved.

(continues on page 336)

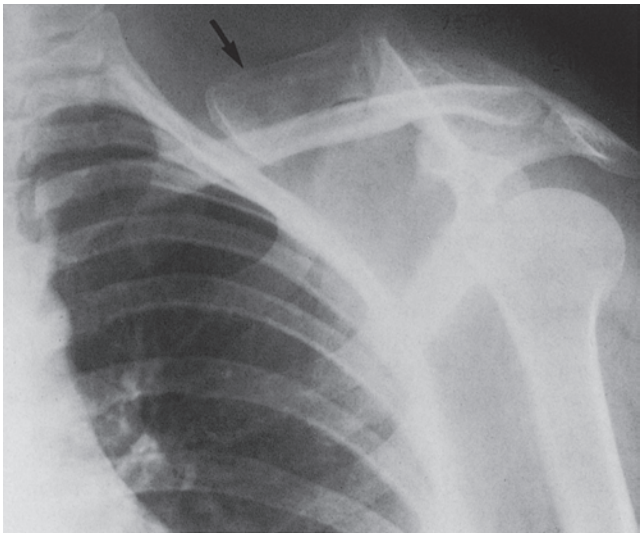

Fig. 14.**45** **Sprengel's deformity.** An anomalous omovertebral bone on the left (arrow) is connected to the scapula. The scapula is elevated and hypoplastic.

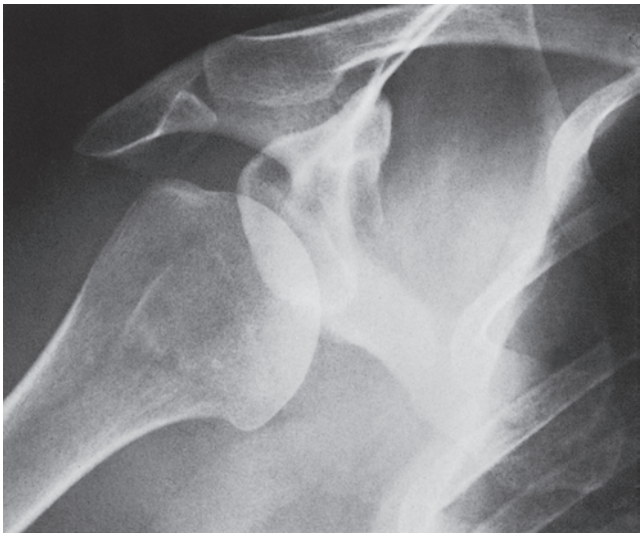

Fig. 14.**46** **Brachial plexus (C5 root) damage.** Winging of the scapula and depression of the shoulder joint secondary to posttraumatic paralysis of the rhomboideus muscle.

Table 14.7 (Cont.) Abnormal Scapula

Abnormality	Usual Causes	Comments
Deformation	*Glenohumeral dysplasia* (Fig. 14.**48**)	Deformation or absence of the rim of the glenoid fossa Flattening of the humeral head Deformation of the humeral head is more obvious than deformity of the scapula. Hurler's syndrome: see Fig. 13.**15**
	Arthritis *Syringomyelia*	Severe deformation of these structures may be seen in several *arthritides* and in *syringomyelia* (neurotrophic joint), but changes in the humeral head are more characteristic (see Table 14.**8**).
	Benign bone tumors (Fig. 14.**47**)	*Osteochondroma* or *enchondroma* may cause deformation. (Destructive lesion of scapula is likely due to *eosinophilic granuloma*, *metastasis*, *Ewing's sarcoma*, or *osteomyelitis*, but they are rare) .
	Fracture	

Fig. 14.**47** **Osteochondroma** of the scapula which has an appearance somewhat similar to Sprengel's deformity (Fig. 14.**45**).

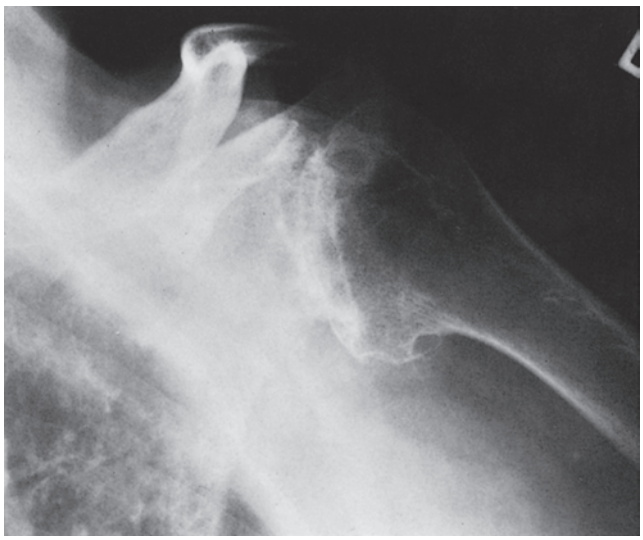

Fig. 14.**48** **Glenohumeral dysplasia** with absence of the glenoid rim and flattening of the humeral head. Secondary osteoarthritis is also present.

Table 14.8 Humeral Head Deformity

Etiology	Abnormality	Comments
Congenital	*Glenohumeral dysplasia* (Fig. 14.**48**)	Usually bilateral and asymptomatic.
Traumatic	*Fracture of greater tuberosity*	A displaced fracture of the greater tuberosity is an obvious cause of a grooved defect. *Fracture of the lesser tuberosity* is usually associated with a posterior dislocation of the head of the humerus.
	Hill-Sachs deformity (repeated dislocation) (Fig. 14.**3**)	An irregularity and/or area of condensed bone on the *posterior superior* border of the articular surface, best seen in an abducted and internally rotated humerus. It is a compression fracture caused by (repeated) anterior dislocations.
Arthritis	*Rotator cuff tear* (Fig. 14.**49**)	Upward subluxation of the humeral head indicates rotator cuff (supraspinatus tendon) tear. Longstanding elevation may erode the inferior surface of the acromion.
	Periarthrosis humeroscapularis (periarthritis humeroscapularis, bursitis calcarea)	Deposition of calcium in the wall of the subdeltoid bursa.
	Rheumatoid arthritis *Ankylosing spondylitis*	Erosions and grooves appear first *near the attachment of the joint capsule*. Often associated with erosion of the distal clavicle and inferior acromion, upward subluxation of the humerus, subchrondral cysts, and distention of the subdeltoid bursa.
	Gout	Grooved defects have sclerotic margins. Otherwise similar to rheumatoid arthritis, unless gout tophi are calcified.
	Multicentric reticulohistiocytosis	Rheumatoid arthritis-like erosions associated with cutaneous xanthomas.
	Infectious arthritis	May mimic rheumatoid arthritis, but changes occur much more rapidly.
Tumor	*Pigmented villonodular synovitis*	Erosions are near the capsular attachment, as in rheumatoid arthritis, but no osteoporosis or narrowing of the joint space is present. May contain hemosiderin and therefore appears calcified.
	Other tumors, see Chapter 5.	

(continues on page 338)

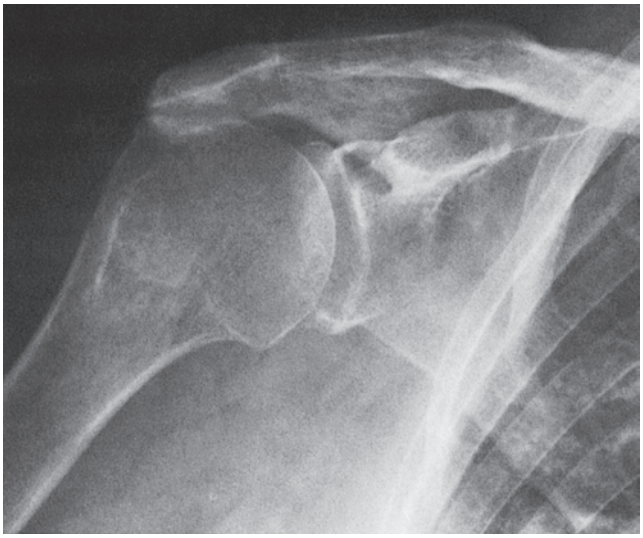

Fig. 14.**49** **Rotator cuff tear.** Narrowing of the space between the humeral head and the acromion with erosion on adjacent bone surfaces. Osteoarthritic spurs and a cyst (geode) in the glenoid fossa are present as additional findings.

Table 14.8 (Cont.) Humeral Head Deformity

Etiology	Abnormality	Comments
Vascular	*Aseptic necrosis* (Fig. 14.**50**) (most common causes: sickle cell disease, steroid therapy) (see also hip, Fig. 14.**63**)	Beginning in the center of the articular surface, cortical breaks, rarefaction, and sclerosis continue until the humeral head is flattened and deformed. The glenoid fossa is intact, which indicates a primary epiphyseal disturbance.
	Hemophilia	Mimics Hill-Sachs deformity, but radiolucent defects also occur in the glenoid fossa.
Neurotrophic	*Syringomyelia* (Figs. 14.**51**–**52**)	Fragmentation of articular surface without reactive changes and intra-articular scattered bone fragments are a typical finding in Charcot joint. Bone fragments may migrate to midhumerus along dissection of chronically distended joint capsule.

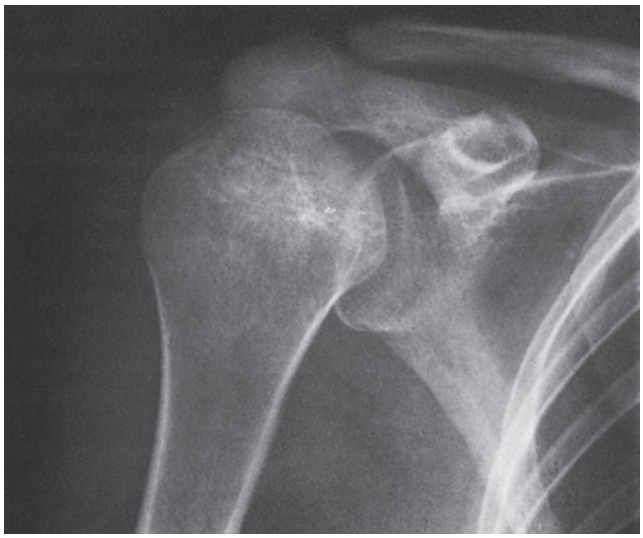

a

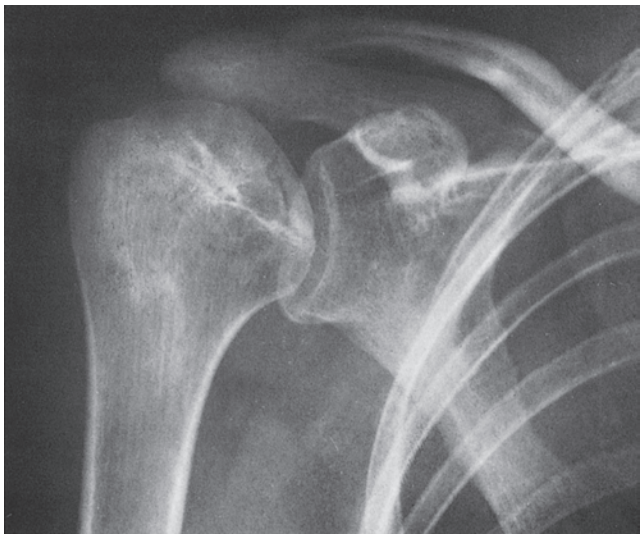

b

Fig. 14.**50 a, b** **The course of avascular necrosis** of the humeral head due to steroid therapy, **a** Subchondral resorption of bone and small depressed fractures of the articular surface (arrows), **b** Sclerosis of the humeral head with an obvious fracture line. Flattening of the articular surface.

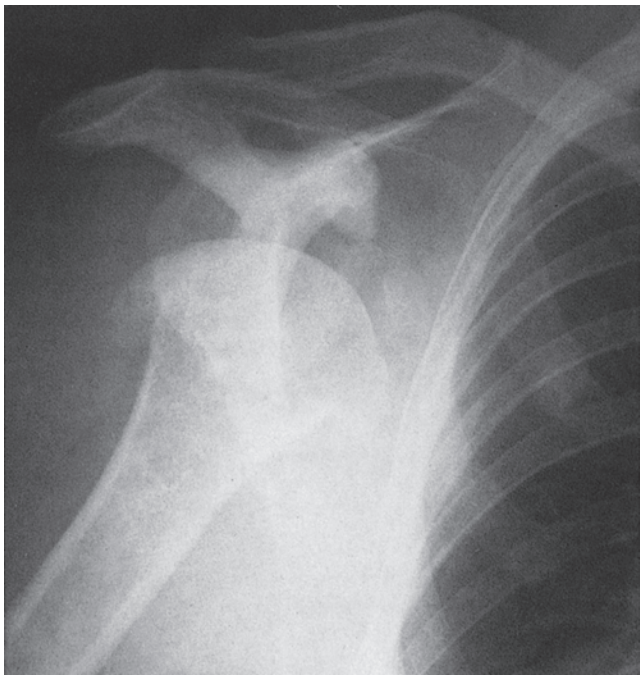

Fig. 14.**51** **Syringomyelia.** The humeral head is deformed and subluxed downwards. No obvious bone fragmentation is seen in this case.

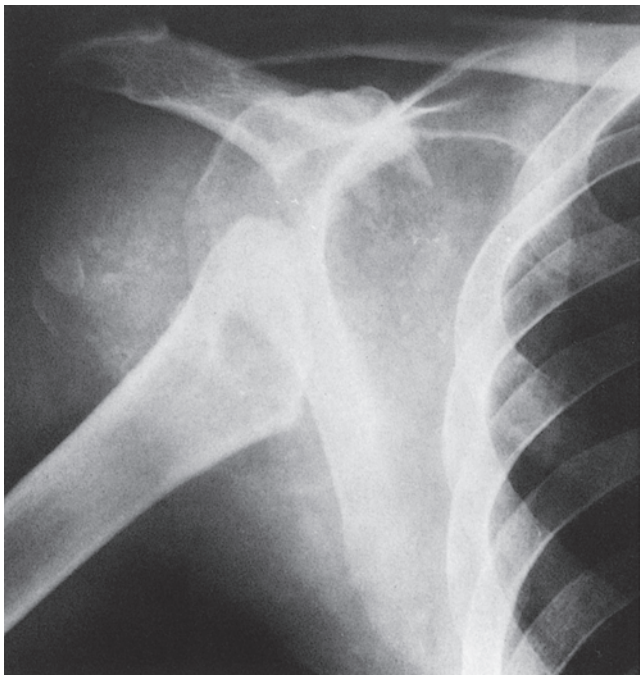

Fig. 14.**52** **Syringomyelia.** The whole humeral head is destroyed. Bone fragments are present in the joint capsule.

Table 14.9 Forearm Deformity

Deformity	Usual Causes	Comments
Proximal radioulnar dislocation	Traumatic *Chassaignac subluxation* ("nursemaid's elbow", occurs in children under 6 years of age). *Traumatic dislocation of radial head* without fracture (occurs in children over 6).	The head of the radius should be in direct relation to the capitellum no matter what position the elbow is in, A "nursemaid's elbow" is usually a result of jerking upward on a child's arm. Dislocation may be partial and not detectable radiologically.
	Fracture of the ulna with dislocation of the head of the radius usually in anterolateral direction (*Monteggia fracture*) (Fig. 14.**53**).	A fracture through ulna with significant foreshortening of the forearm is always accompanied by either a fracture or dislocation of the radius.
Deformity or hypoplasia of radius or ulna	Syndromes with hypoplastic radius (see Table 14.**1**) or aplasia of radius (Fig. 14.**54**).	Hypoplasia of the radial head predisposes to dislocation.
	Enchondromatosis (Ollier's disease)	Shortening of ulna secondary to enchondromas.

(continues on page 340)

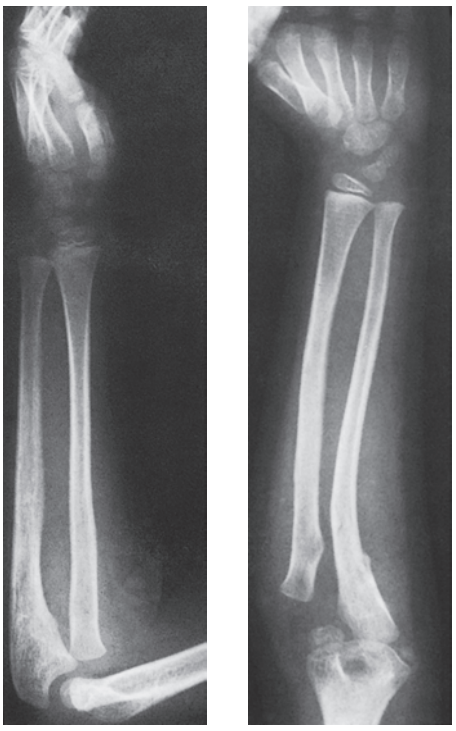

a b

Fig. 14.**53 a, b** **Monteggia fracture.** Fracture of the ulna with anterolateral dislocation of the radius.

Fig. 14.**54** **Fanconi's anemia.** Absence of radius, short and deformed ulna, carpal bone fusion, and the absence of the first metacarpal and the thumb.

Table 14.9 (Cont.) Forearm Deformity

Deformity	Usual Causes	Comments
	Hereditary multiple exostoses (diaphyseal aclasis) (Fig. 14.**55**)	There is a characteristic *shortening of the ulna* and fibula. Ulnar shortening causes curvature of the radius and often dislocation of the radial head, see Table 14.**6**.
	Osteogenesis imperfecta (Fig. 14.**31**)	Secondary to bowing of bones.
	Madelung's deformity (Fig. 14.**56**)	Premature fusion of the ulnar part of the epiphysis of radius, manifest at adolescence as a characteristic deformity: 1 ulnar and volar angulation of the distal radial articular surface; 2 decreased carpal angle; and 3 dorsal subluxation of the distal ulna. May occur as an isolated unilateral or bilateral anomaly. When associated with other anomalies such as a short, curved tibia, short fibula, and valgus deformity of the knee, the condition is called *dyschondrosteosis*. Juvenile trauma may produce a similar deformity in the wrist called *pseudo-Madelung*. A somewhat similar deformity may be present in *mucopolysaccharidosis I (Hurler's syndrome)*.
	Congenital radioulnar fusion (Fig. 14.**57**)	A rare anomaly which results in relative hypoplasia of the involved bones secondary to a lack of muscular stress.
	Isolated anomaly	Hypoplasia or aplasia of the radius may be also associated with other anomalies, including *nail-patella syndrome*.
	Generalized growth disturbance of bones (Fig. 14.**58**)	

Fig. 14.**55 a, b** **Hereditary multiple exostoses.** Shortening of the ulna with exostoses. Bowing of the radius but no dislocation of the radial head.

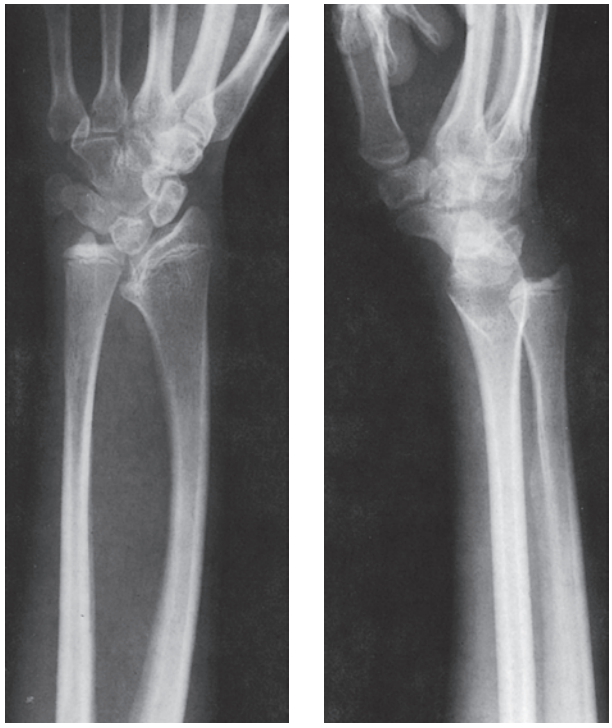

Fig. 14.**56 a, b** **Madelung's deformity.** Ulnar and volar angulation of the distal radial articular surface, decreased (v-shaped) carpal angle, and dorsal subluxation of the distal ulna.

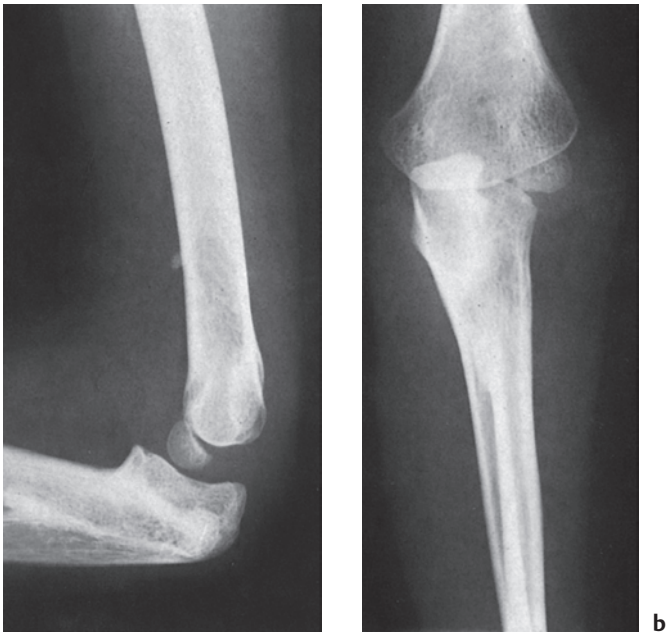

Fig. 14.**57 a, b** **Proximal radioulnar fusion** in a 4-year-old girl. The radial head has grown together with the olecranon. Both radial and ulnar shafts are thin.

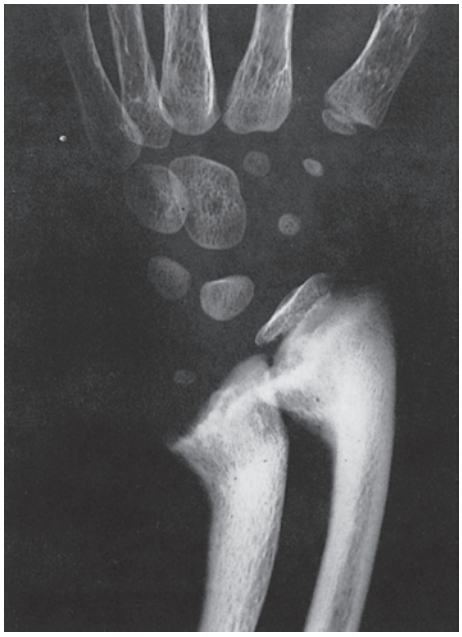

Fig. 14.**58** **Severe deformity, sclerosis,** and ulnar deviation of distal radius and ulna in a child with renal osteodystrophy (renal rickets).

Table 14.10 Abnormal Femoral Epiphysis in a Child or Adolescent

Disease	Radiographic Findings	Comments
Legg-Perthes disease (osteochondrosis of the femoral epiphysis, avascular necrosis of the femoral head) (Fig. 14.59)	Changes in order of appearance: 1. slight widening of the joint space and lateral displacement of the femur, epiphyseal ossification center may be smaller than that of the other side; 2. subchrondral fracture, subcortical radiolucent crescent; 3. flattening of the femoral head; 4. sclerosis of the epiphysis; 5. radiolucent metaphyseal defects; and 6. reossification and remodeling resulting in either a spherical or deformed shape.	Peak age of 4 to 8 years, male : female ratio is 4 : 1 Bilateral in 10 % to 15 % of cases. MRI allows earlier detection than plain films of the presence and extent of the process of avascular necrosis.
Congenital dislocation of hip ("Perthes' luxation")	Untreated dislocation results in a deformed, dislocated femoral head and coxa valga.	Avascular necrosis of the femoral head is unusually frequent in children with congenital dislocation of the hip, either secondary to treatment or on a constitutional basis.
Hemophilia	Epiphyseal changes are similar to Perthe's disease, but no metaphyseal changes occur.	Probably due to increased pressure from intra-articular hemorrhages.
Infection Arthritis	See Chapter 6	Increased intra-articular pressure may cause avascular necrosis of the femoral head.
Slipped capital femoral epiphysis (epiphysiolysis capitis femoris) (Fig. 14.60)	Salter-Harris type 1 fracture through the proximal epiphyseal cartilage plate. The direction of slipping depends on the angulation between the shaft of the femur and its neck. The most common combination is an angulation of 140 degrees (coxa valga) and slipping toward the posteroinferior direction. Avascular necrosis of the epiphysis may complicate slipping (with or without operative treatment).	Usually occurs between ages 9 and 17, bilateral in 20 % to 30 %. Is either *idiopathic* or *secondary* to *trauma*, *renal osteodystrophy*, or *rickets*. Rare causes: *scurvy*, *lues*, *metaphyseal dysostosis*, *hyperparathyroidism*, *congenital coxa vara*, *pseudohypoparathyroidism*, *hemophilia* and *Gaucher's disease*.
Osteochondritis dissecans (osteochondrosis dissecans, Segmental avascular necrosis)	A small, dense segment of bone with its articular cartilage lies in depression in the joint surface, demarcated by a crescenting radiolucent zone. It usually occurs in the uppermost (weight-bearing) region of the femoral head. Secondary osteoarthrosis may occur in older age.	MRI is helpful in defining the lesion and the viability of the fragment.
Chondrodysplasia punctata (chondrodystrophia calcificans congenita, Conradi's syndrome)	Multiple discrete punctate areas of calcification in the epiphyses of hips, knees, shoulders, and wrists, which may disappear at the age of three years.	For other anomalies in this rare entity see Table 15.**1**
Multiple epiphyseal dysplasia (Fairbank's disease)	The epiphyseal ossification centers of hips, knees, and ankles are mottled and irregular.	May be a tarda form of chondrodysplasia punctata, which manifests usually between 5 and 14 years of age. A number of other anomalies occur (see Table 15.**1**). Rare.
Mucopolysaccharidosis (especially Morquio's syndrome) (Fig. 14.61)	Defective, irregular ossification of the femoral capital epiphyses. Femoral neck is short and thick.	Spinal changes are more characteristic (Table 12.**7**)
Diastrophic dysplasia (dwarfism)	Bone ends are enlarged. The femoral heads may be larger than acetabula.	
Cretinism (congenital hypothyroidism) (Fig. 14.62)	Delayed and spotty ossification of epiphyses, which may be nonhomogeneous, stippled, or fragmented. The femoral neck is shortened and there is coxa vara.	
Rickets (all etiologies)	Irregularity of the provisional zone of calcification and widening of the epiphyseal plate.	Residual deformity of the femoral head and other epiphyses may persist after treatment.

Fig. 14.**59** **Legg-Perthes disease,** left hip, age 8. Widening of the joint space; smaller femoral epiphysis with flattening, fragmentation, and sclerosis.

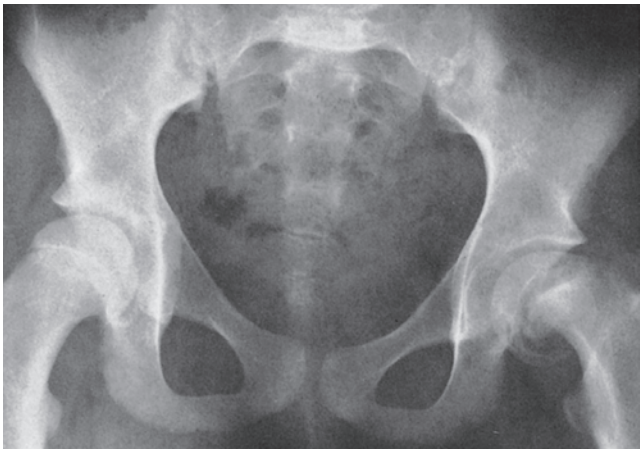

Fig. 14.**60** **Slipped capital femoral epiphysis** on the left with posteroinferior slipping. There is also coxa valga of the right side.

Fig. 14.**61** **Morquio's syndrome,** age 7. Fragmented, irregular femoral capital epiphyses with short and thick femoral necks. Deformed acetabula.

Fig. 14.**62** **Cretinism,** age 20. Unfused, slightly deformed femoral epiphyses and generalized delay of ossification. The femoral neck angles are within normal limits in this case.

Table 14.11 Abnormal Femoral Head in Adult

Disease	Radiographic Findings	Comments
Trauma	Fragmented or irregular femoral head after intracapsular femoral neck fracture, traumatic dislocation of the femoral head, or surgical correction of slipped femoral epiphysis	Avascular necrosis follows if the blood supply from the femoral neck or the ligamentum teres is inadequate.
Sickle-cell disease	Radiographic evidence of avascular necrosis of the femoral head in up to 60% of patients.	Sludging of sickled erythrocytes results in functional vascular occlusion.
Necrosis of femoral head, vide variety of causes such as: **Steroid therapy** **Cushing's disease** **Atherosclerosis** **Thromboembolic disease Pancreatitis** **Fat embolism (alcoholism)** **Collagen disease** **Dysbaric osteonecrosis (Caisson disease)** **Gaucher's disease** **Gout** **Radiation therapy (Fig. 14.63)**	Radiographic changes of avascular necrosis of the femoral head include cortical breaks and rarefaction of bone followed by sclerosis, flattening and deformation. No late remodeling occurs in adult avascular necrosis (cf. Legg-Perthes). MRI allows early detection of avascular necrosis of bone .	Underlying mechanism is unclear, and may be similar in most conditions. May be due to microscopic emboli in end-arteries, steroid-induced osteoporosis, with microfractures or compression of the vascular bed by an increase in the marrow fat cell mass. Avascular necrosis of the femoral head has also been reported in association *adult myxedema, sarcoidosis, amyloidosis, histiocytosis* and *polyvinylpyrrolidone therapy*, as well as during *pregnancy*.
Osteoarthritis, primary or secondary	(See Ch. 6)	The most common cause of hip joint abnormality in the elderly.
Neurotrophic joint	(See Ch. 6)	

Fig. 14.**63** **Bilateral avascular necrosis** of the femoral head following therapy of Hodgkin's disease. There is subchondral demineralization of the joint surface, flattening, fragmentation, and sclerosis of the femoral head.

Table 14.12 Abnormal Angle of the Femoral Neck

Disease	Radiographic Findings	Comments
Primary congenital coxa vara	1 Decreased angle of the femoral neck; 2 epiphyseal plate almost vertical, with inferior metaphyseal fragmentation; 3 short and thick neck of femur; and 4 delayed ossification, dysplastic acetabulum and other deformities may occur.	A deformity that is sometimes associated with aplasia of fibula.
Secondary congenital coxa vara (Figs. 14.64–65)	As above.	Associated with various *osteochondrodysplasias*.
Osteogenesis imperfecta (Fig. 14.78)	Coxa vara with bowing, overconstricted long bones, and fractures.	
Osteopetrosis	Coxa vara with marble bones. Fractures are common.	
Cretinism (Fig. 14.66)	Coxa vara with short femoral neck.	
Rickets, renal osteodystrophy	Coxa vara with other signs characteristic of hyperparathyroidism (see Chapter 12, Table 12.**7**).	Softening of bone and metaphyseal disturbance cause deformity.
Old Legg-Perthes Old slipped capital femoral epiphysis (Fig. 14.67)	Unilateral coxa vara associated with deformity of the femoral head	
Fibrous dysplasia (Fig. 14.13)	Upper femur is commonly involved. Expanding, trabeculated, lucent or ground-glass lesion. The “shepherd’s crook” deformity of the proximal femur occurs in polyostotic fibrous dysplasia. Pathologic fractures may be present.	

Fig. 14.**64** **Achondroplasia with bilateral coxa vara,** short and thick neck of femur and small sacrum.

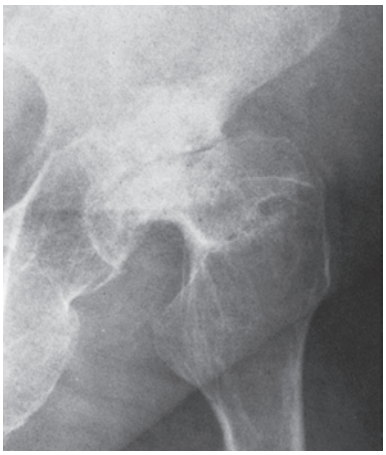

Fig. 14.**65** **Achondroplasia.** Coxa vara with almost complete destruction of the femoral head and hypoplastic acetabulum. Severe secondary osteoarthritic changes. Age 38.

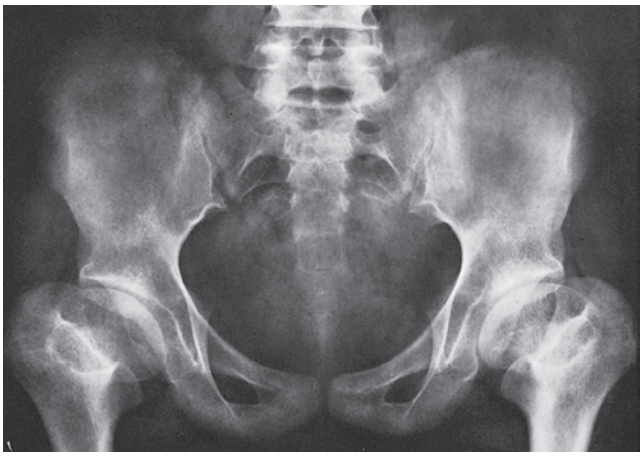

Fig. 14.**66** **Cretinism with bilateral coxa vara.** Iliac apophyses are still unfused. Age 31.

Fig. 14.**67** **Coxa vara after slipped capital femoral epiphysis.** Growth disturbance has resulted in a short femoral neck. Secondary osteoarthritis. Age 51.

Table 14.12 Abnormal Angle of the Femoral Neck

Disease	Radiographic Findings	Comments
Malunited fracture **Osteomyelitis of the femoral neck** **Paget's disease**	May cause "shepherd's crook" deformity of the upper femur.	
Rheumatoid arthritis	Usually unilateral coxa valga. Severe erosion of the superior aspect of the femoral head may give a coxa vara appearance. Protrusio acetabuli may be present.	
Juvenile rheumatoid arthritis (Fig. 14.68)	Bilateral coxa valga, with or without deformity of the femoral head. Protrusio acetabuli may be present.	
Bilateral paralytic disorders (meningomyelocele, muscular dystrophy, poliomyelitis) (Fig. 14.69)	Bilateral coxa valga, often associated with obvious mineral loss from bones or hypoplastic bones.	Lack of muscular force. In unilateral paralytic disorders, coxa valga may be unilateral.
Rare congenital syndromes or idiopathic (Fig. 14.70)	Bilateral coxa valga and often other more diagnostic radiographic findings.	Bilateral coxa valga is a constant finding in *progeria*.
Congenital dislocation of hip	Untreated dislocated hip will assume a coax valga configuration.	

Fig. 14.**68** **Juvenile rheumatoid arthritis,** age 12. Bilateral destruction of the femoral head and acetabulum, coxa valga and protrusio acetabuli.

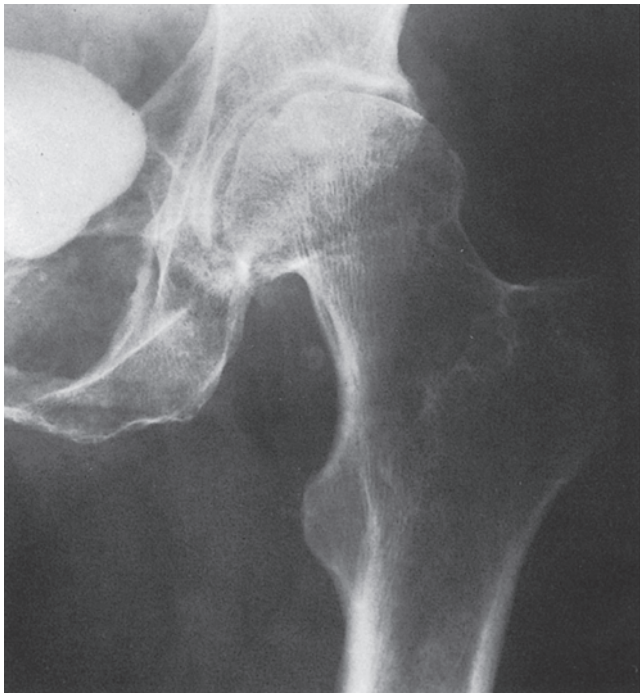

Fig. 14.**69** **Bilateral coxa valga** in a patient with meningomyelocele.

◁ Fig. 14.**70** **Coxa valga** (bilateral) in a patient with acromegaly, an incidental finding. There are also osteoarthritic changes in the hip joint.

Table 14.13 Abnormal Angulation of the Knee

Abnormality	Usual Causes	Comments
Genu varum (bow legs) bilateral	Idiopathic or physiologic *prenatal bowing* (Fig. 14.**71**)	No obvious pathology. May straighten without treatment.
	Tibia vara (Blount's disease) (Fig. 14.**72**)	Aseptic necrosis of the medial tibial metaphysis. The infantile type is usually bilateral. It may also occur at adolescence and be unilateral. The medial metaphysis is irregular. A beak-like projection from the metaphyseal plate pointing medially and distally is characteristic.

(continues on page 348)

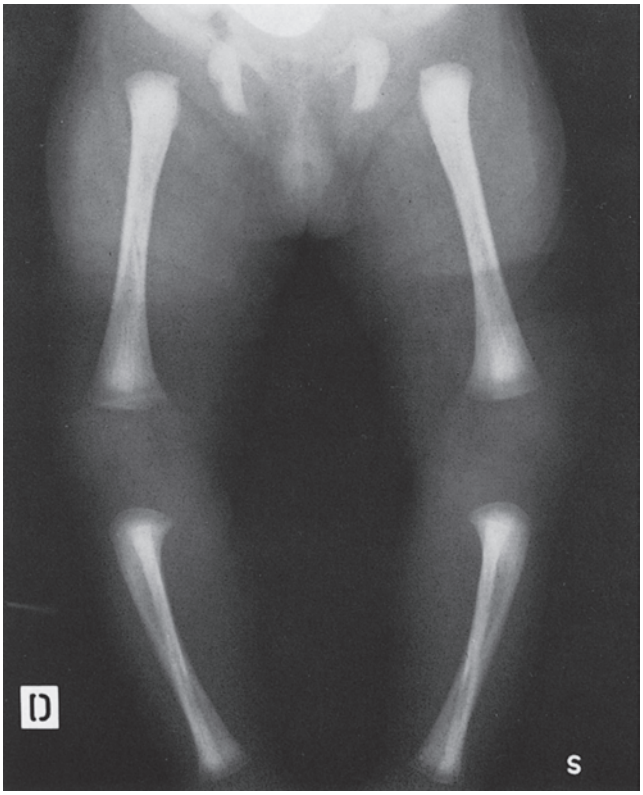

Fig. 14.**71** **Prenatal bowing of knees** (physiologic) in a patient with congenital hypothyroidism. Delayed ossification of femoral epiphyses.

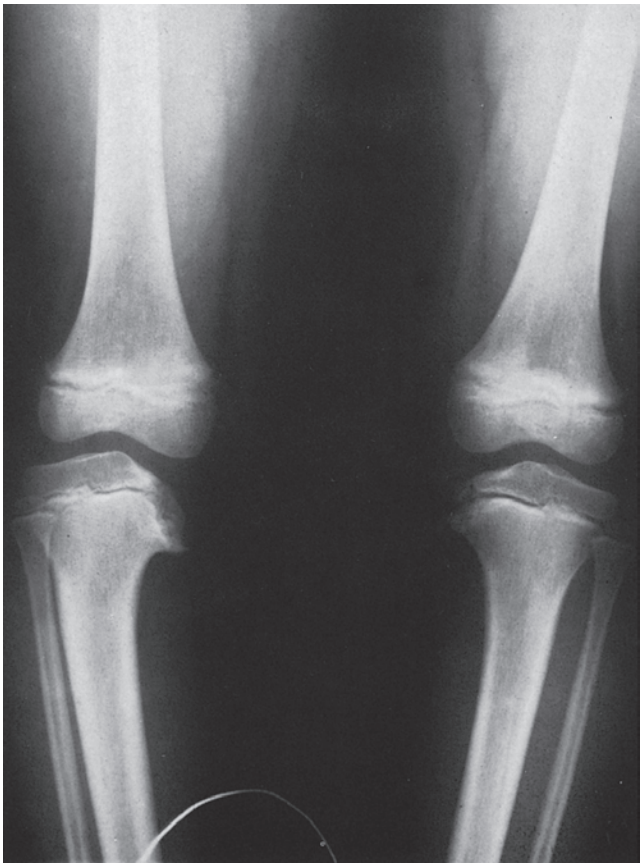

Fig. 14.**72** **Bilateral Blount's disease** (tibia vara), age 6. The medial tibial metaphysis of both knees is irregular and shows a characteristic beak.

Table 14.13 (Cont.) Abnormal Angulation of the Knee

Abnormality	Usual Causes	Comments
bilateral	*Rickets* (all causes) (Fig. 14.**73**)	Bowing of legs with typical changes of rickets. Deformity may remain after treatment of the disease.
	Turner's syndrome (Fig. 14.**74**)	Depression of the medial tibial plateau is the most common skeletal sign in this disorder. Medial tibial exostoses or overgrowth of medial tibial condyles may be present.
	(*Campomelic dysplasia* [dwarfism], *metaphyseal dysplasia*, *dyschondrosteosis*, and *spondyloepiphyseal dysplasia* are rare causes of bilateral genu varum.)	

(continues on page 349)

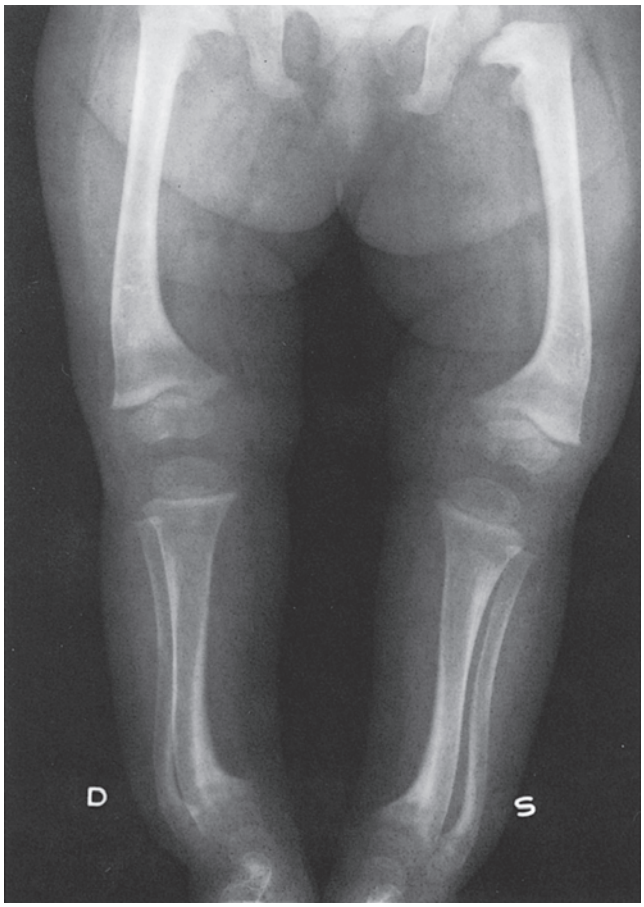

Fig. 14.**73** **Rickets,** age 2. A mixed pattern of genu valgum and genu varum is produced by severe bowing of distal femora. Bowing and characteristic metaphyseal changes are also seen at ankles. There is bilateral coxa vara.

Fig. 14.**74** **Turner's syndrome,** age 20, Depression of the medial tibial plateau and medial tibial (and fibular) exostoses are characteristic.

Table 14.13 (Cont.) Abnormal Angulation of the Knee

Abnormality	Usual Causes	Comments
Genu varum, genu laxum unilateral	*Trauma* *Osteoarthritis*, primary or secondary *Neurotrophic knee* (Fig. 14.**75**, 14.**77**) *Achondroplasia* (Fig. 14.**76**)	Fracture of the medial condyle of femur or tibia. Osteoarthritis of the knee predominantly affects the medial compartment and the patellofemoral joint and results in a genu varum deformity, often associated with medial displacement of the femur (genu laxum).
	Dysplasia epiphysealis hemimelica (Trevor's disease)	A rare, unilateral overgrowth of the epiphysis, usually in the knee or ankle. A single osteochondroma may rarely have a similar effect. If the overgrowth appears on the lateral side, the end result is genu varum; if it appears on the medial aspect, genu valgum results.

(continues on page 350)

Fig. 14.**75** **Neurotrophic knee, diabetes.** Depression of the medial tibial plateau due to bone destruction. A mild genu varum deformity.

Fig. 14.**76** **Achondroplasia,** age 38. Severe depression of the medial tibial plateau and medial displacement of the femur (genu laxum).

Fig. 14.**77** **Genu laxum in a severely deformed neurotrophic knee.** Medial displacement of the deformed distal femur and destruction of the proximal tibia and loose bodies.

Table 14.13 (Cont.) Abnormal Angulation of the Knee

Abnormality	Usual Causes	Comments
Genu valgum (knock knee)	*Physiologic* or due to regional muscular weakness or bowing bones (Fig. 14.**78**)	Due to the wide pelvis, a certain degree of genu valgum is physiologic in women.
	Flatfeet	Malalignment of the tarsus may produce genu valgum as a secondary, compensatory phenomenon.
	Rickets	Instead of bow knees, a knock-knee deformity may arise secondary to rickets.
	Hereditary osteo-onychodysplasia (nail-patella syndrome)	The lateral femoral condyle is small and results in genu valgum and lateral subluxation of the hypoplastic patella.
	Dysplasia epiphysealis hemimelica (Trevor's disease)	
	Juvenile rheumatoid arthritis (Fig. 14.**79**)	Asymmetric growth of the epiphyses may result in knock knees.
	Secondary osteoarthritis confined to the lateral compartment of the knee joint (Fig. 14.**80**)	Common causes include *rupture of the lateral meniscus* and *rheumatoid arthritis*.

Fig. 14.**78** **Osteogenesis imperfecta.** There is bilateral coxa vara and left-sided genu valgum. The bones are slender and bowed and the metaphyses widened ("Erlenmeyer flask" deformity).

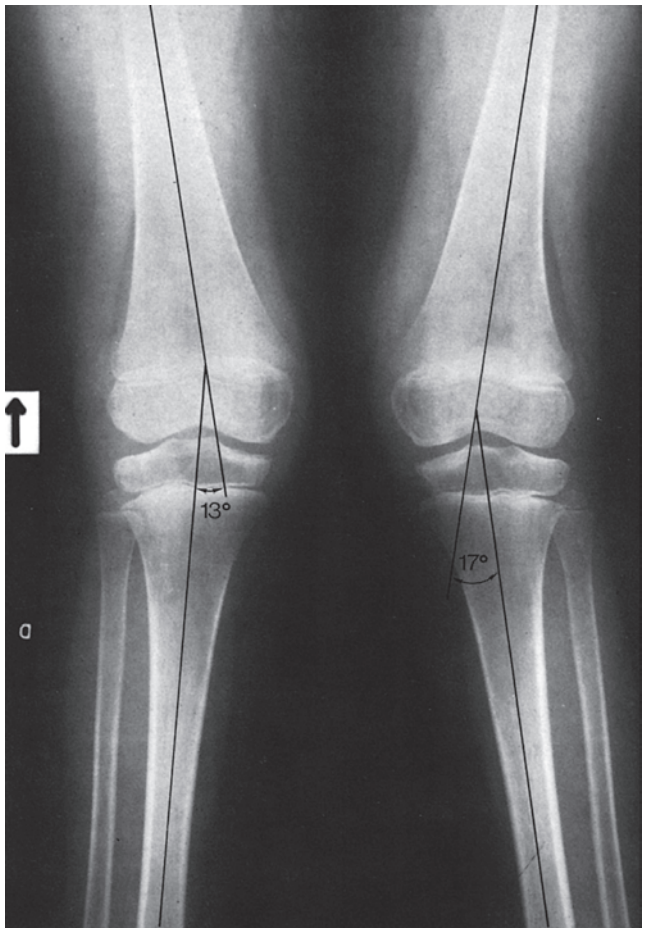

Fig. 14.**79** **Juvenile rheumatoid arthritis** with bilateral genu valgum deformity.

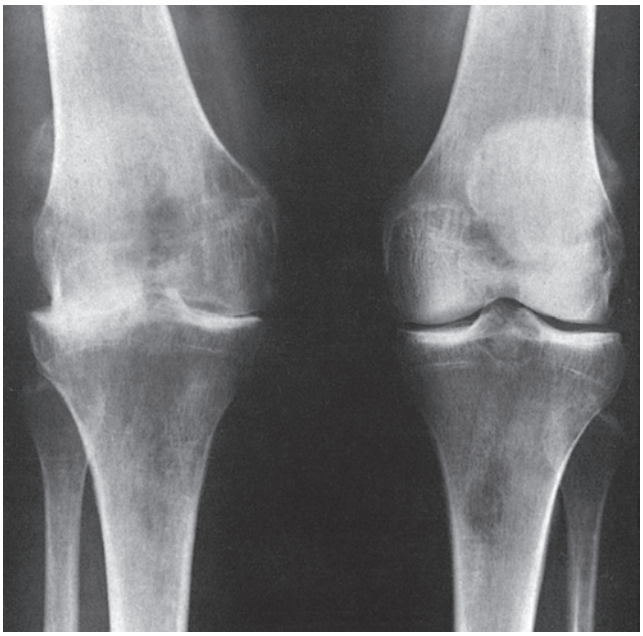

Fig. 14.**80** **Rheumatoid arthritis** with secondary osteoarthritis of the right knee. The lateral compartment is more affected and results in genu valgum deformity on the right side.

15 Hands and Feet

There are 106 bones in the hands and feet, which is more than 50% of the total number of bones (206) in the entire skeleton. These bones, therefore, reflect fairly accurately both normal skeletal development and congenital or acquired disorders of the peripheral skeleton. Minor changes are better visualized in the hands and feet than in the more central skeleton. These provide early diagnostic sign in generalized arthritic and metabolic diseases.

Several measurements are useful in the examination of the radiograph of the hand and wrist: (1) *Metacarpal sign:* A line tangential to the heads of the fourth and fifth metacarpals normally extends distal to the head of the third metacarpal. A positive metacarpal sign is present when the line passes through the head of the third metacarpal (Fig. 15.**1**). Positive metacarpal sign occurs in such disorders as *pseudo- and pseudopseudohypoparathyroidism* (Figs. 15.**2** and 15.**8**), gonadal dysgenesis *(Turner's syndrome), basal cell nevus syndrome, multiple epiphyseal dysplasia, Beckwith-Wiedemann syndrome, juvenile rheumatoid arthritis, sickle-cell anemia with infarction, trauma, and neonatal hyperthyroidism.*

(2) *Metacarpal index:* The ratio of the length to width at midshaft of metacarpals two to five varies from 5.4 to 7.9. In *arachnodactyly (Marfan's syndrome),* it is more than eight (Fig. 15.**3**). (3) *Carpal angle:* The angle between two lines: the first tangent to the proximal surfaces of the scaphoid and lunate, the second tangent to the proximal margins of the triquetrum and lunate (Fig. 15.**4**) in a normal white population, it ranges from 120 to 150 degrees. It may be abnormal in several congenital syndromes.

Congenital Anomalies

Many anomalies of the hands and feet are isolated without any association with a syndrome, but when detected, a possible constitutional condition should be sought. A detailed discussion of various bone dysplasias of infancy is beyond the scope of this text. Radiographs of the hand have such an important role in the differential diagnosis of many constitutional conditions that it was felt imperative to in-

Fig. 15.**1** **Positive metacarpal** sign in Turner's syndrome. The terminal tufts have a drumstick appearance.

Fig. 15.**2** **Pseudopseudohypoparathyroidism.** Short metacarpals and phalanges, with strongly positive metacarpal sign due to very short metacarpals 4 and 5.

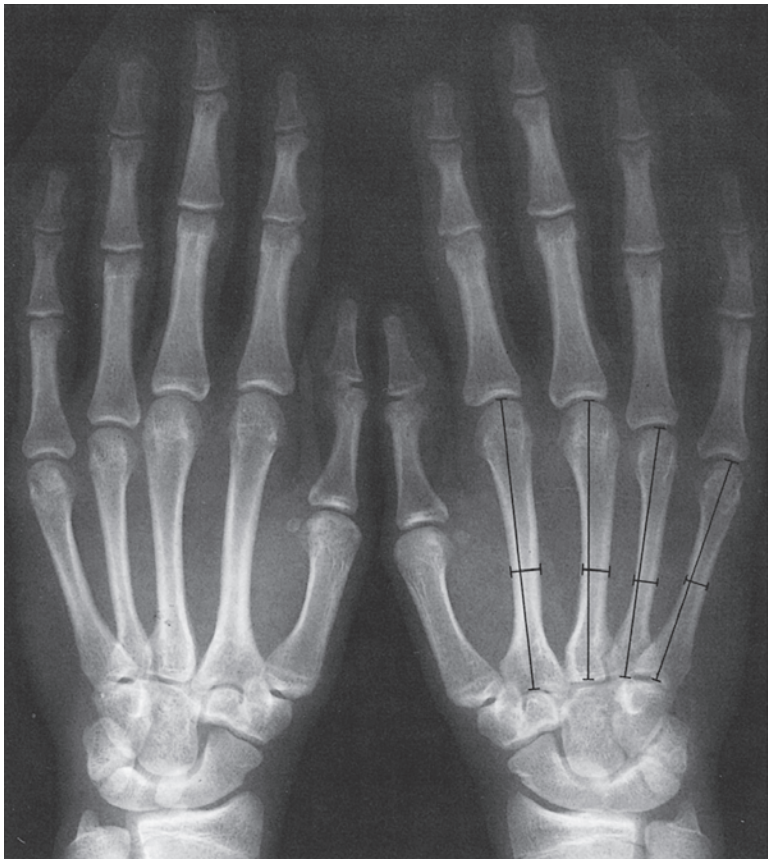

Fig. 15.**3** **Metacarpal index** over eight in arachnodactyly.

Fig. 15.**4** **Normal carpal angle.**

clude a short summary of hand, wrist and foot anomalies and associated conditions (Tables 15.**1** and 15.**2**). For the proper understanding of Tables 15.**1** and 15.**2**, less common terms used are explained here*:

Brachydactyly	=	shortening of phalanx or phalanges (Figs. 15.**5** and 15.**6**)
Brachymetacarpaly	=	shortening of metacarpal(s) (Fig. 15.**7**)
Camptodactyly	=	permanent flexion of finger(s) (Fig. 15.**13** and 15.**14**)
Clinodactyly	=	curvature of (usually fifth) finger in a mediolateral plane (Figs. 15.**9** and 15.**10**)
Diastrophic	=	twisted
Dysplasia	=	intrinsic growth disturbance
Polydactyly	=	supernumerary digits (Fig. 15.**11**)
Symphalangism	=	end-to-end fusion of contiguous phalanges (absent joint)
Syndactyly	=	soft-tissue or bony union between adjacent digits (Fig. 15.**9**)

The foot, as much as the hand, may yield useful information in the study of generalized congenital disorders. In certain conditions, the radiographic finding may be most characteristic in the foot. Many congenital syndromes involve some foot abnormality, but Table 15.**2** is limited to those disorders in which the foot findings are an important part of the syndrome or are unique or unusual.

* Some other features mentioned in Tables 15.**1** and 15.**2** are further illustrated in Figs. 15.**12–15**.

Fig. 15.**5** **Achondroplasia.** Short metacarpals and phalanges with wide epiphyses.

Fig. 15.**6** **Cretinism.** Short metacarpals and slightly shortened phalanges. Fusion of epiphyseal plates at the age of 26.

Fig. 15.**7** **Brachymetacarpaly.** Short metacarpals IV and V on the right and IV on the left. Incidental finding without constitutional abnormalities.

Fig. 15.**8** **Pseudohypoparathyroidism.** Short metacarpals 4 and 5, as well as short distal phalanges and abnormally shaped carpal bones.

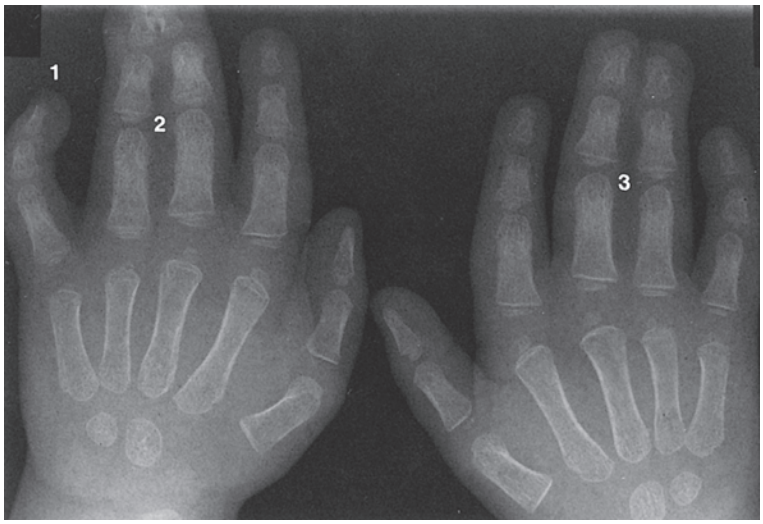

Fig. 15.**9** **Multiple anomalies** in the hands of a 2-year-old child: 1 clinodactyly, 2 syndactyly with bony fusion of distal phalanges of fingers 3 and 4, 3 syndactyly with only soft-tissue fusion of fingers 3 and 4.

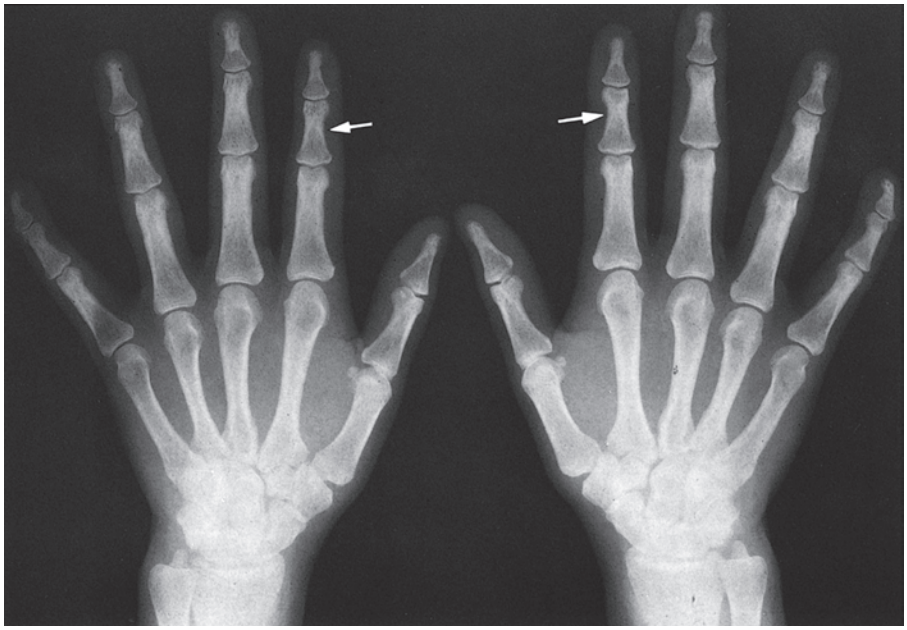

Fig. 15.**10** **Kirner's deformity** in the distal phalanges of both 5th fingers. This produces a distal medial curvature like clinodactyly. Incidentally the patient also has hyperparathyroidism with subperiosteal tunneling and frank erosion of the radial side of the second phalanx of the index fingers (arrows).

Fig. 15.**11** **Polydactyly.** A supernumerary, rudimentary 6th finger.

Fig. 15.**12** **Aplasia** of 1st metacarpal and thumb. A case of **Fanconi's anemia.**

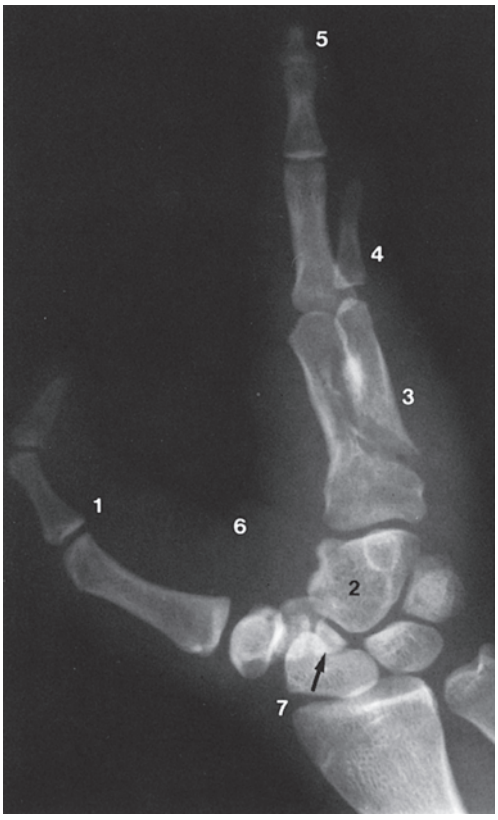

Fig. 15.**13** **Severe anomalies in a cleft hand:** 1 Camptodactyly of the thumb. 2 abnormal shape of capitate with fusion of capitate and hamate, 3 partial fusion of two metacarpals with fracture of the union, 4 uniphalangeal hypoplastic finger, 5 short distsal phalanx, 6 aplasia of two metacarpals and fingers, and 7 os centrale (arrow)

Fig. 15.**14** **Anomalies in the hand bones.** 1 Camptodactyly of the index finger, 2 hypertrophic finger with wide proximal phalanx articulating with two adjacent metacarpals, one of which has an abnormal, cone-shaped epiphysis (3), and 4 short distal phalanx of the thumb with a cone-shaped epiphysis.

Table 15.**1** Hand and Wrist Anomalies and Associated Dysplasias

| | | | Syndromes usually evident at birth | | | | | | | | | | | | | | | | | | | | | | | | | | | | | | | | | | | | | | | May manifest later | | | | | | | | | | | | | | | | | | |

Table 15.**2** Foot Anomalies in Some Congenital Bone Dysplasias

		Syndromes usually manifest at birth																				May manifest later					
+ = Frequent occurrence ○ = Occasional occurrence		Acrocephalosyndactyly (Apert's syndrome)	Acrocephalopolysyndactyly (Carpenter's syndrome)	Arthrogryposis multiplex congenita	Chondrodysplasia punctata	Chondroectodermal dysplasia (Ellis-van Creveld syndrome)	Cornelia de Lange syndrome	Diastrophic dysplasia (dwarf)	Down's syndrome (Trisomy 21)	Fanconi's anemia	Focal dermal hypoplasia (Goltz's syndrome)	Hand-foot-uterus syndrome	Laurence–Moon–Biedl syndrome	Oculodento-osseous syndrome	Otopalatodigital syndrome	Prader–Willi syndrome	Rubinstein–Taybi syndrome	Russell–Silver syndrome	Trisomy 13–15	Trisomy 18	Symphalangism-surdity syndrome	Dyschondrosteosis	Myositis ossificans progressiva	Pseudohypoparathyreoidism	Pseudopseudohypoparathyreoidism	Turner's syndrome
Metatarsal and toes	Cone-shaped epiphyses											○			○							○					
	Hemihypertrophy																	+									
	Hypoplasia metatarsal (III, IV and/or II)																					○		+	+		○
	Polydactyly		+		○	+					○		+				+	+									
	Symphalangism											+		+							+						
	Syndactyly	+	+		○		○		○	○	○	○		○	○	○	○											
Great to	Short metatarsal	+	+									+			+					+			+				
	Short proximal phalanx						+								+								+				
	Short distal phalanx						+					+			+					+							
	Broad distal phalanx																+										
	Uniphalangeal great toe	+																					+				
Tarsus	Short calcaneus											+															
	Tarsal fusion (including cuneiform)	+	+	+	○							+			+						+						+
	Clubfoot			+		○	○	+											○	+							
	Small feet											+															

Compiled from AK Poznanski, Foot manifestations of the congenital malformation syndromes. Semin Roentgenol 1970;5:354–66.

Terminal Phalanx Pattern

(Revised after SN Jones, DJ Stoker, Radiology at your fingertips: lesions of the terminal phalanx. Clin Radiol 1988;39: 478–85).

The distal ends of the toes are usually poorly delineated in ordinary radiographs, but the distal phalanges of fingers are well visualized. A variety of acquired and congenital diseases, as well as localized lesions, cause changes in the radiographic appearance of the terminal phalanges. The radiographic changes around the distal interphalangeal joints are similar to elsewhere in the skeleton and joints, but the pattern may be different in the terminal tufts. A list of various patterns of distal phalangeal abnormalities with their common or typical causes is presented in Table 15.**3**.

a

b

Fig. 15.**15 a, b** **Otopalatodigital syndrome. a** The distal row of carpal bones and the scaphoid are fused. Metacarpal bones 2–4 have narrow diaphyses, while the fifth has an abnormally wide diaphysis but normal length. Finger bones show no gross abnormality. **b** The foot shows fusion of the navicular with the first cuneiform and of the cuboid with the third cuneiform. The first metatarsal is short relative to the others. The great toe has an abnormal shape (clinodactyly).

Table 15.3 Differential Diagnosis of Abnormal Terminal Phalanx

Type of Change	Common or Typical Causes
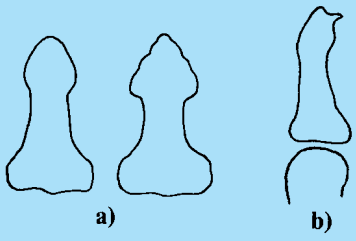	a) Normal variants b) Subungual exostosis (Fig. 15.**16a**)
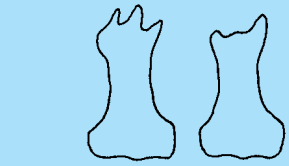	Causes of clubbing of the fingers (bronchogenic carcinoma, cirrhosis of liver, congenital heart disease, pulmonary hypertrophic osteoarthropathy, pachydermoperiostosis, pulmonary interstitial fibrosis)
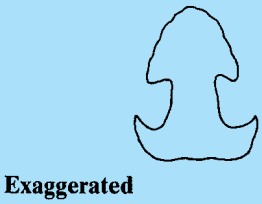	Acromegaly (Fig. 15.**16b**) Basal cell nevus syndrome

(continues on page 362)

a

b

Fig. 15.**16a** **Subungual** exostosis projects characteristically from the distal and dorsomedial aspects of the terminal phalanx of the great toe.

Fig. 15.**16b** **Acromegaly** with exaggerated terminal phalangeal tufts, wide metacarpophalangeal joint spaces, increased soft tissue, and premature osteoarthritis.

Table 15.3 (Cont.) Differential Diagnosis of Abnormal Terminal Phalanx

Type of Change	Common or Typical Causes
Acro-osteosclerosis	Idiopathic Rheumatoid arthritis (and other connective tissue disorders) (Fig. 15.**17**) Chronic active hepatitis Sarcoidosis (Osteopetrosis, melorheostosis, osteopoikilosis, Figs. 15.**18** and 15.**19**)
Smoothly delineated lytic lesion	Epidermoid inclusion cyst Enchondroma Glomus tumor Sarcoidosis Bone cyst Arthritis Cystic osteomyelitis Tuberous sclerosis Osteoid osteoma
Poorly defined lytic lesion at phalangeal tuft	Osteomyelitis (panaritium ossale) (Fig. 15.**20**) Leprotic osteomyelitis (rare) Aneurysmal bone cyst (rare)
Poorly defined lytic lesion, including the base	Metastasis (especially bronchogenic carcinoma, Fig. 15.**21**) Carcinoma of nail bed Subungual sarcoma Psoriatic arthropathy Giant cell tumor (rare) Myeloma (rare) Sarcoidosis (rare) Fibrous dysplasia

(continues on page 364)

15.17

15.18

15.19

15.20a

15.20b

15.21

Fig. 15.**17** **Acro-osteosclerosis** of the distal phalanges. Incidentally, small erosions (arrows) due to early rheumatoid arthritis are also present.

Fig. 15.**18** **Melorheostosis** involving fingers, including terminal phalanges.

Fig. 15.**19** **Osteopoikilosis** with acro-osteosclerosis.

Fig. 15.**20 a, b** **Osteomyelitis** with swelling of soft-tissue and destruction of the terminal phalanx.

Fig. 15.**21** **Metastasis of bronchogenic carcinoma** in the distal phalanx. A relatively well-demarcated osteolytic lesion and soft-tissue swelling is seen.

Table 15.3 (Cont.) Differential Diagnosis of Abnormal Terminal Phalanx

Type of Change	Common or Typical Causes
"Morning star"	Psoriatic arthritis (Fig. 15.**23**) Hyperparathyroidism (Fig. 15.**24**) Sjogren's syndrome
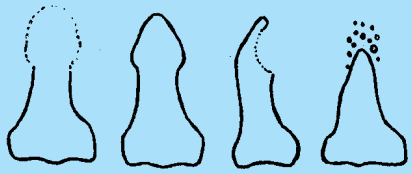 Acro-osteolysis (*with possible soft-tissue calcification)	Collagen vascular disease* (especially scleroderma and dermatomyositis) (Fig. 15.**25**) Sjogren's syndrome Hyperparathyroidism* (Fig. 15.**22**) Arteriosclerosis obliterans Diabetic gangrene Buerger's disease Burn, frostbite, radiation (Fig. 15.**26**) Pachydermoperiostosis Neurotrophic disease (syringomyelia, leprosy) (Fig. 15.**27**) Epidermolysis bullosa* Psoriatic arthritis Pycnodysostosis Familial acro-osteolysis Progeria Pseudoxanthoma elasticum Congenital indifference to pain* Porphyria Vinylchloride exposure Lesch-Nyhan syndrome Multicentric reticulohistiocytosis Rothmund's syndrome*

(continues on page 366)

Fig. 15.**23** **Psoriatic arthritis.** "Morning star" erosion of terminal phalangeal tuft of the 4th finger (arrow).

Fig. 15.**22** **Secondary hyperparathyroidism** (renal osteodystrophy). Rarefaction of terminal tufts and subperiosteal erosion in phalanges (arrows).

15.24

15.26

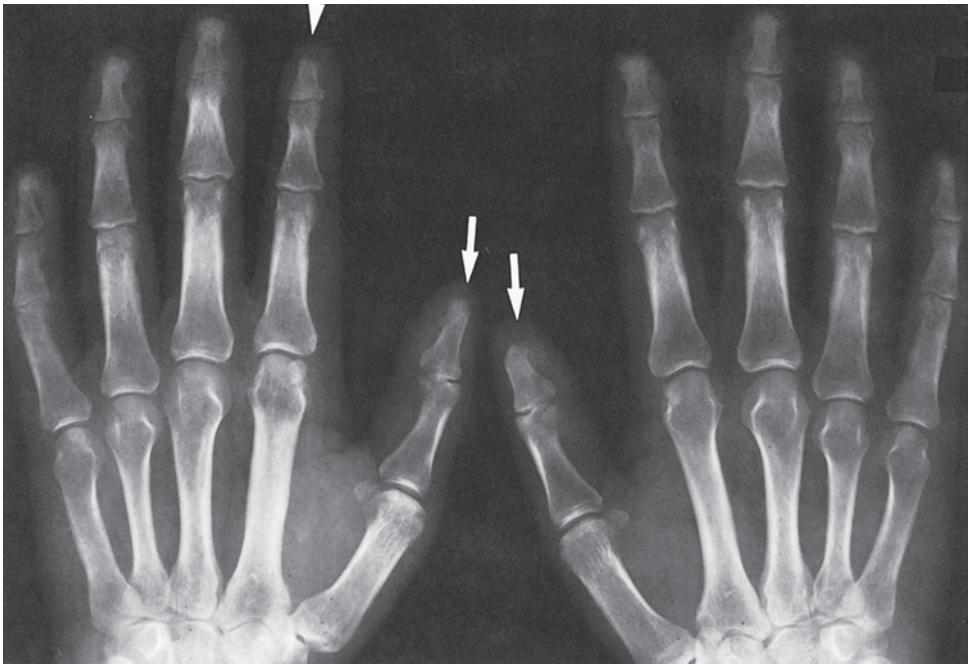

15.25

15.27

Fig. 15.**24** **Hyperparathyroidism.** Erosion in the index finger has a "morning star" pattern, but unlike psoriatic arthritis, there is widespread demineralization and subperiosteal erosion elsewhere in the fingers. The other tufts only show rarefaction.

Fig. 15.**25** **Scleroderma.** Acro-osteolysis and soft-tissue atrophy in some fingers (arrows), but no other obvious bone changes.

Fig. 15.**26** **Frostbite.** Localized acro-osteolysis in the great toe with a large soft-tissue ulcer (arrows).

Fig. 15.**27** **Leprosy.** Acro-osteolysis in distal phalanges of the second, fourth and fifth fingers.

Table 15.3 (Cont.) Differential Diagnosis of Abnormal Terminal Phalanx

Type of Change	Common or Typical Causes
Short distal phalanges (absent tufts) Brachy-telephalangy	Several congenital syndromes with short phalanges (see Table 15.**1**) Associated with hypoplastic nails Maternal use of anticonvulsants (phenytoin) Frostbite Trauma
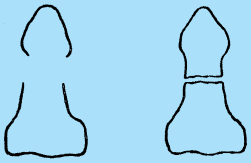 **Midtuft erosion** **Pseudoepiphysis in small distal phalanges**	Chemical acro-osteolysis (vinyl chloride exposure) Hyperparathyroidism (primary or secondary) (Fig. 15.**28**) Hajdu-Cheney syndrome (congenital acro-osteolysis) Juvenile rheumatoid arthritis (Fig. 15.**29**) Cleidocranial dysostosis
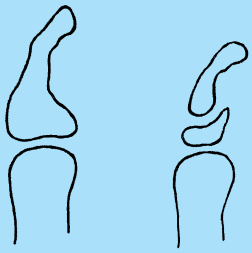 **adult** **juvenile** **Kirner's deformity**	Isolated anomaly (Fig. 15.**10**) or in congenital syndromes (Russell-Silver syndrome, Cornelia de Lange syndrome)
Drumstick (rounded, broad tuft)	Turner's syndrome (Fig. 15.**30**)

Fig. 15.**28** **Renal osteodystrophy** with midtuft erosions and subperiosteal erosions in the phalanges.

Fig. 15.**30** **Tuner's syndrome.** Drumstick tufts and positive metacarpal sign.

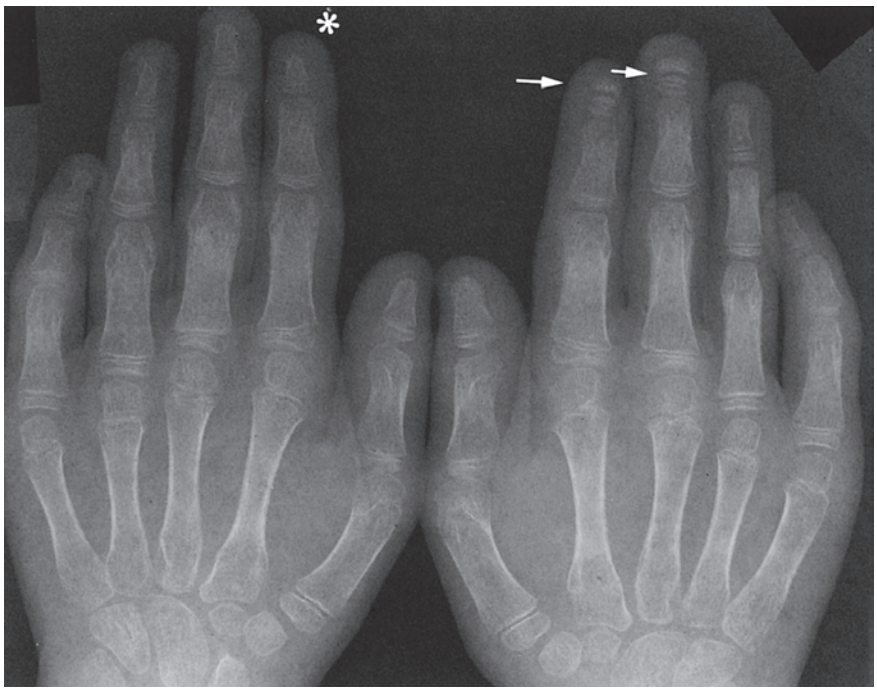

Fig. 15.**29** **Juvenile rheumatoid arthritis.** Midtuft erosions are seen in the 2nd and 3rd fingers on the right (arrows). There is acro-osteolysis in the left index finger (asterisk).

Orthopedic Foot Problems

The feet are subject to a number of deformations or painful conditions, not necessarily as a result of the congenital syndromes listed in Tables 15.**1** and 15.**2**.

In the analysis of a deformed foot, one should be aware of a number of important lines and angles of the foot. Some useful lines and angles that should be evaluated from the weight-supporting dorsoplantar and lateral views are presented here (Fig. 15.**31**).

The *midtarsal joint line* (A-A) is a continuous line along the anterior margin of the talus and calcaneus on the lateral view and talus and cuboid on the anteroposterior view. A lack of continuity indicates a mobile talus, altered position of the talus and calcaneus relative to the navicular and cuboid at the midtarsal joint, e.g., a *midtarsal fault*.

The *calcaneal pitch* (B) is an index of the height of the foot framework; low: 10 to 20 degrees; medium: 20 to 30 degrees; and high, over 30 degrees. Low pitch is indicative of a change in the position of the calcaneus and talus at the ankle joint, e.g., a *hindfoot fault* as seen in flatfoot.

Böhler's angle of the calcaneus (C, normal: 20 to 40 degrees) indicates the integrity of the plantar arch of the calcaneus. It is decreased by a *calcaneal fracture*.

The diagonal axis of the talus (D-D) is a fair indicator of the proper relation of the talus to the calcaneus, normally nearly horizontal. It is not horizontal in most foot deformities.

The *talocalcaneal angle* in the dorsoplantar view (E) ranges from 20 degrees to 50 degrees in infants and young children and from 15 degrees to 30 degrees from age five on. A line through the axis of the talus points to the head of the first metatarsal bone. The axial line of the calcaneus points to the fourth metatarsal bone. The talocalcaneal angle is increased in *flatfoot* and is reduced or reversed in *clubfoot*.

The *midtalar* and *midcalcaneal* lines from the lateral view meet near the anterior margin of the cuboid, forming an angle of 25 to 50 degrees (F). The *midtalar/ midcalcaneal angle* is reduced in *clubfoot* or *rockerbottom deformity* and increased in *flatfoot* and *pes cavus*. The angle formed by lines along the inferior margin of the calcaneus and the fifth metatarsal bone (G) ranges from 150 degrees to 175 degrees and is unaffected by age. The apex of this angle faces downward in *flatfoot* and *rockerbottom deformity*.

In order to give a meaningful roentgenographic report on a deformed foot, the radiologist must also know the orthopedic terminology:

1. Valgus (eversion, pronation) = bent outward from the midline of the body, distal to the point or joint of reference
2. Varus (inversion, supination) = bent inward toward midline of the body, distal to the point or joint of the reference
3. Adduction = displacement on a transverse plane toward the axis of the body
4. Abduction = displacement on a transverse plane away from the axis of the body
5. Heel valgus (Fig. 15.**32 b**) = the outward slant of the heel, as seen from the rear, is increased above 10 degrees (associated with an increased talocalcaneal angle from the dorsoplantar view)
6. Heel varus (Fig. 15.**32 c**) = the normal valgus angle (5 to 10 degrees) is decreased or the heel slants inward (associated with a decreased talocalcaneal angle in the dorsoplantar view)
7. Equinus = fixed plantar flexion of the hindfoot (anterior end of calcaneus down). From the lateral view, the calcaneus makes an angle of more than 90 degrees anteriorly with the tibia

Heel valgus or varus cannot be determined directly from the routine AP and lateral radiographs, but can be inferred from the talocalcaneal angle on the AP view. Table 15.**4** lists the more common foot deformities, with their diagnostic and differential diagnostic criteria. The overall appearances of various congenital foot deformities are presented diagrammatically in Fig. 15.**33 a–g**.

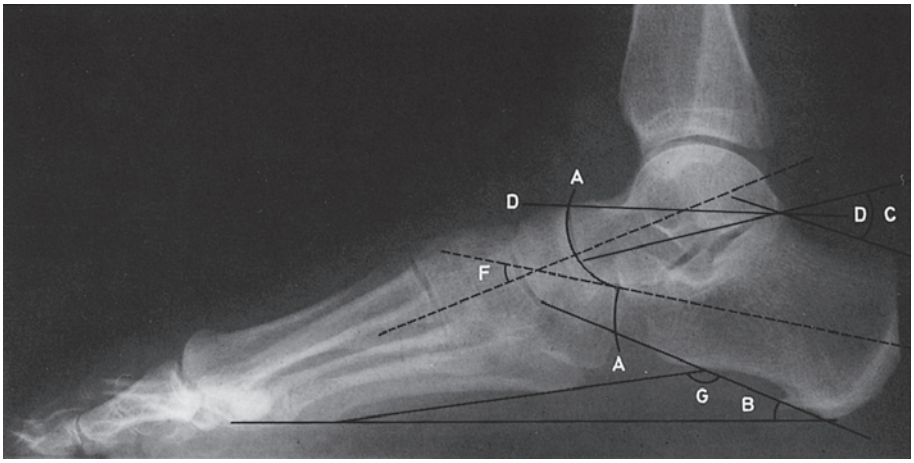

a

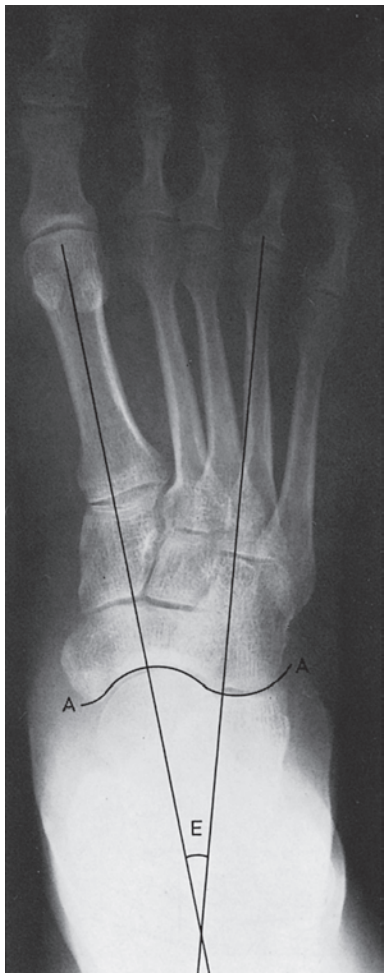

b

Fig. 15.**31 a, b** **Some useful lines and angles in the evaluation of an orthopedic foot problem.** A–A = midtarsal joint line, B = calcaneal pitch, C = Böhler's angle of the calcaneus. D = diagonal axis of the talus, E = talocalcaneal angle, F = midtalar-midcalcaneal angle, and G = inferior cortex of calcaneus-fifth metatarsal angle.

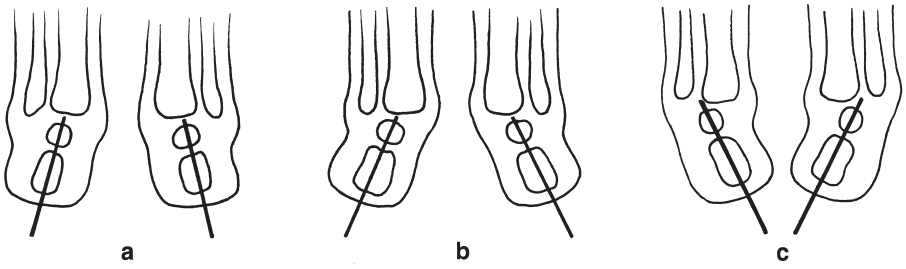

Fig. 15.**32 a–c** **a** Normal heel position (as seen from the rear); **b** Heel valgus, seen in metatarsus varus (adductus). **c** Heel varus, seen in clubfoot.

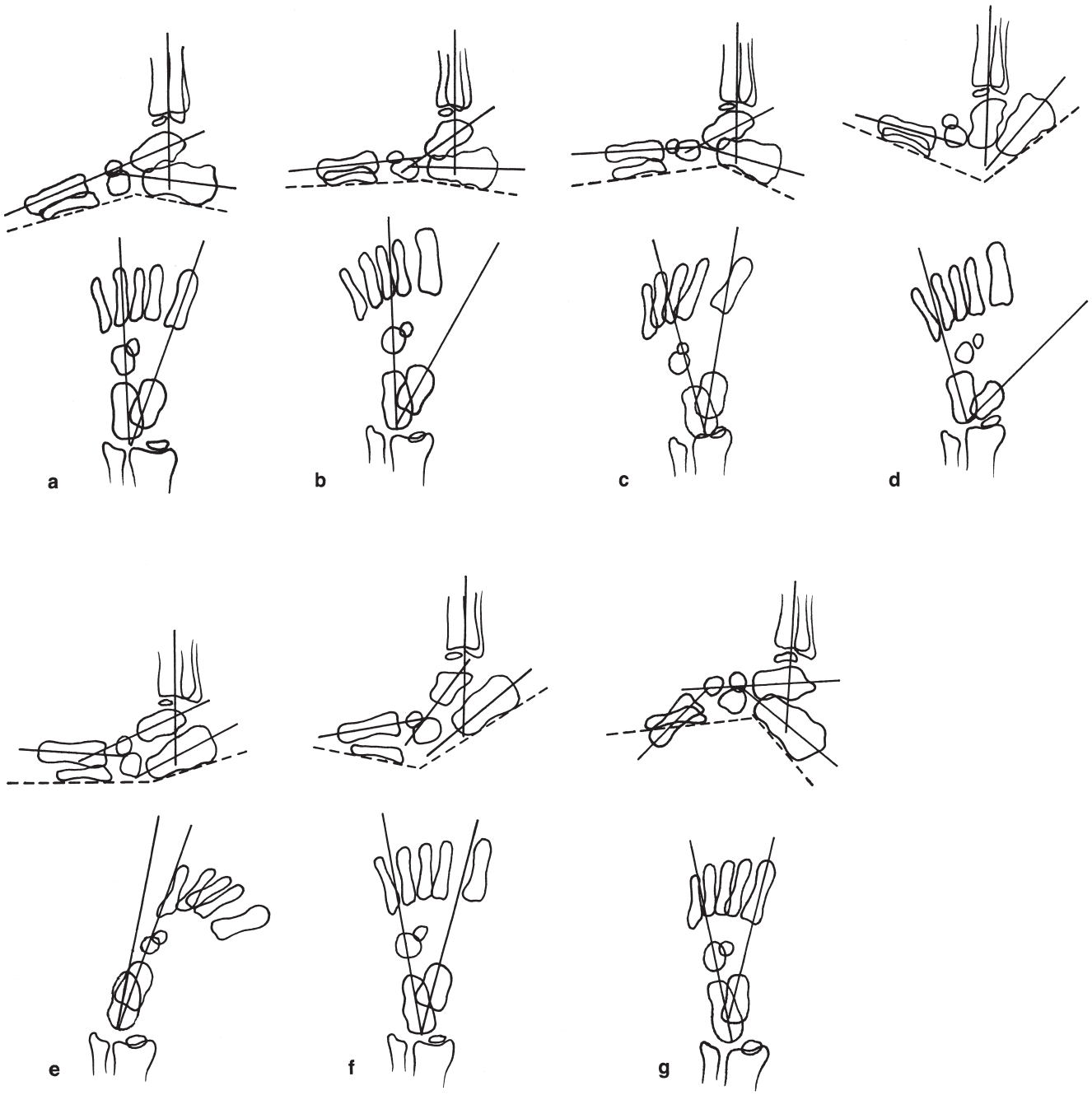

Fig. 15.**33 a–g** **The appearance of various congenital foot deformities** with special reference to the midtalar-midcalcaneal angle (AP, normally 15°–30°, infants 30°–50° and lateral 25°–50°), the inferior cortex of calcaneus-fifth metatarsal angle (lateral, normally 150°–175°) and the orientation of the metatarsals. **a** Normal foot, **b** flatfoot, **c** metatarsus varus (adductus), **d** congenital vertical talus (rockerbottom deformity), **e** clubfoot, **f** overcorrected clubfoot, and **g** pes cavus

Table 15.4 Differential Diagnosis of a Deformed Foot

Deformity	Radiographic Characteristics	Comments
Hallux valgus (hallux abductus valgus) (Figs. 15.34, 15.35)	1 Abduction of the hallux (angle between the first metatarsal and great toe 10 degrees to 20 degrees = mild; 20 degrees to 30 degrees = moderate; 30 degrees to 45 degrees = severe) with valgus rotation of the hallux. 2 Deviation or subluxation of the metatarsophalangeal joint. 3 Medial prominence and cratering of the medial epicondyle of the first metatarsal head. 4 Adduction of the first metatarsal, intermetatarsal angle (between metatarsal I and II) over 10 degrees. 5 Relative lateral displacement of sesamoid bones. Adduction of the first metatarsal bone may be structural (abnormal metatarsal base called *congenital metatarsus primus adductus*: abnormal, elongated anterodistal margin of the cuneiform) or positional (hypermobile gap of the first metatarsal segment of the adducted forefoot).	The most common foot deformity: Diversion of the big toe into abduction followed by inflammatory reaction over the medial epicondyle of the metatarsal head. Associated with shoe incompatibility and/or predisposing foot anatomy. The valgus (eversion) component of the deformity occurs due to the rotating effect of imbalanced muscle action on the proximal phalanx. Progressive deformity is more likely to occur in positional abnormalities. Hallux valgus may be a feature of *rheumatoid arthritis* and of *Ehlers-Danlos syndrome* (joint laxity, subcutaneous calcifications). In the absence of soft-tissue calcification (in gout), the erosions and degenerative changes of the first metatarsal head due to hallux valgus alone and in connection with gout may be similar.
Morton's metatarsus atavicus (Morton's syndrome)	The first metatarsal is short and the second is broad.	Also called Dudley Joy Morton. Causes pain while walking usually bilateral.
Morton's neuroma	Plain film findings are usually normal.	A neuralgia most often in the region of either the head of the fourth metatarsal, since the third and fourth or the fourth and fifth metatarsal bones are too close together and compress the plantar nerve. MRI or ultrasound are suggested for diagnosis.

(continues on page 372)

a b

Fig. 15.**34 a, b** **Mild hallux valgus** with lateral displacement of sesamoid bones, medial prominence, and cratering of the medial epicondyle of the first metatarsal head, best seen in the oblique projection, and structural adduction of the first metatarsal.

15.35

Fig. 15.**35** **Severe hallux valgus.** Incidentally, renal osteodystrophy is also present.

Table 15.4 (Cont.) Differential Diagnosis of a Deformed Foot

Deformity	Radiographic Characteristics	Comments
Flatfoot (Pes planus) (Figs. 15.37, 15.38)	Dorsoplantar view: 1 talocalcaneal angle is increased; 2 forefoot is abducted; 3 the heel is valgus: the long axis of the talus runs medial to the first metatarsal while the long axis of the calcaneus remains near the fourth metatarsal base. Lateral view: 1 the foot dorsiflexes to normal angle (or even more); 2 the talocalcaneal angle is increased due to plantar flexion of the talus; 3 the long axes of the talus and the fifth metatarsal angulate toward the plantar.	*Acquired flatfoot* can be differentiated from *congenital flatfoot* through a careful study of the position and shape of the calcaneus and an evaluation of the midtarsal joint: 1 In acquired foot collapse the calcaneal pitch is 10 degrees or more, in congenital it is less. 2 In acquired flatfoot the calcaneus has a downwards concave form, in congenital it is downward convex or flat. 3 In acquired flatfoot the midtarsal joint line is altered (talus juts forward), in congenital pes planus the joint line is pseudonormal, although the talus is displaced medially. In *rigid flatfoot*, pronation and supination are limited and the condition is painful, unlike flexible flatfoot.

(continues on page 374)

Fig. 15.**36** **Diabetic arthropathy** (neurotrophic foot) with an acquired rockerbottom deformity due to destruction and malposition of bones.

a

b

Fig. 15.**37 a, b** **Acquired flatfoot. a** The calcaneal pitch is low and the midtarsal joint line is slightly discontinuous. **b** Flattening of the transverse arch is seen as an increased distance between metatarsal heads in dorsoplantar projection.

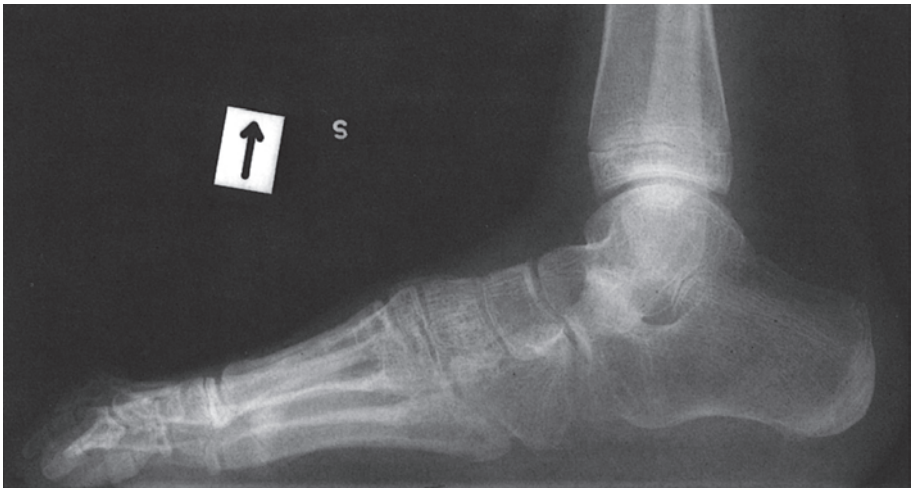

a

b

Fig. 15.**38 a, b** **Congenital left flatfoot** in a 13-year-old with scleroderma and bone deformities in the left foot. The calcaneal pitch is less than 10 degrees, calcaneus is convex downwards, and the midtarsal joint line appears normal in the lateral view, although the talus is displaced medially in the dorsoplantar view.

Table 15.4 (Cont.) Differential Diagnosis of a Deformed Foot

Deformity	Radiographic Characteristics	Comments
Metatarsus varus (adductus) (Fig. 15.39)	Dorsoplantar view: 1 the heel is in normal position or in valgus (long axis of talus either near the base of the first metatarsal or medial to it) ; 2 forefoot is adducted and in varus (overlapping metatarsals). Lateral view; 1 normal or greater than normal dorsiflexion of the foot; 2 the talocalcaneal angle is normal or slightly increased; 3 the first metatarsal is higher than the fifth.	A congenital foot type in which the forefoot is adducted. Often overlooked in infancy.
Congenital vertical talus (Fig. 15.40)	Dorsoplantar view: Severe heel valgus (increased talocalcaneal angle, the talar axis falls far medial to the first metatarsal). Lateral view: 1 the heel is in the equinus position (plantar flexed, calcaneus tilted front end down); 2 talus is in extreme plantar flexion the talocalcaneal angle is increased; 3 the forefoot dorsiflexes at midtarsal level, producing a convex plantar surface (rockerbottom deformity); 4 dorsal dislocation of the navicular (becomes visible after its ossification center has appeared).	*Severe flatfoot* also has vertical talus but no heel equinus. *Treated clubfoot* has persistent heel equinus but not a plantar flexed talus. In *triple arthrodesis* reduction of plantar flexion is often attemted by placing the anterior talus into the inferior aspect of the navicular, thus the navicular projects dorsal to the talus. A *neurotrophic foot* in an adult may show a rockerbottom deformity due to bone destruction and malposition (Fig. 15.**36**).
Clubfoot (Talipes equinovarus) (Fig. 15.41)	Dorsoplantar view: 1 the talocalcaneal angle is markedly reduced, the talus and calcaneus may be parallel; 2 the forefoot is in varus and adducted. The bases of metatarsals may be overlapping or appear in lateral profile if varus is severe. Lateral view: 1 the heel is in the equinus position; 2 the forefoot is plantar flexed (cavus), more than hindfoot, even in forced dorsiflexion; 3 long axes of the talus and calcaneus are parallel.	*Flat-top talus* is a late complication of clubfoot, causing incongruity of the ankle joint.

(continues on page 376)

a

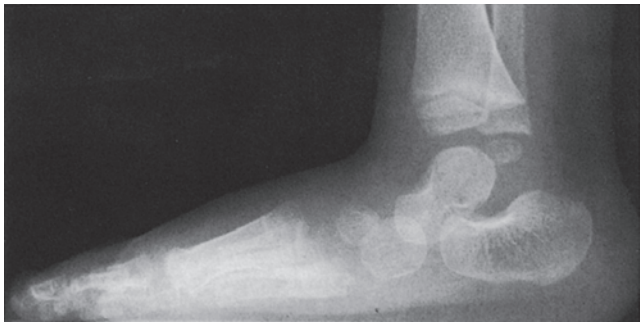

b

Fig. 15.**39 a, b** **Metatarsus varus** in a 2-year-old, left more than right. a The long axis of the talus is medial to the first metatarsal (heel valgus) and the metatarsals are overlapping in the dorsoplantar view. b Lateral view shows a slightly increased talocalcaneal angle. The first metatarsal is much higher than the fifth.

a

c

b

Fig. 15.**40 a–c** **Congenital vertical talus. a** Dorsoplantar view at the age of 4 months. The talus is adducted and the talocalcaneal angle is very wide. **b** Lateral view at the age of 6 years. The talus is tilted front end down and the talocalcaneal angle is increased. Calcaneus is in relatively normal position due to treatment and consequently there is no more rockerbottom deformity left. **c** An untreated case with rockerbottom deformity.

a

b

Fig. 15.**41 a, b** **Clubfoot,** age 27. **a** Dorsoplantar view: markedly reduced talocalcaneal angle and overlapping metatarsals. **b** Lateral view: plantar flexion of the forefoot, and the long axes of the talus and calcaneus are parallel. The top of the talus is flat, a late complication.

Table 15.4 (Cont.) Differential Diagnosis of a Deformed Foot

Deformity	Radiographic Characteristics	Comments
Pes cavus (cavus deformity) (Fig. 15.42)	Dorsoplantar view: normal findings unless associated with other abnormalities. Lateral view: 1 increased talocalcaneal angle; 2 midtalar -first metatarsal lines form an angle, apex upward; 3 heel varus, heel valgus, equinus or calcaneus deformity may be present.	Abnormally high longitudinal arch of the foot, often associated with neuromuscular disease.
Tarsal coalition (Figs. 15.43–46)	*Calcaneonavicular coalition* may not become visible until ossified, then seen as fusion or abnormal articulation between the anterior process of the calcaneus and the navicular, best seen in a 45 degree medial oblique view of the foot. *Talocalcaneal coalition* usually takes place at the sustentaculum tali joint or near the os trigonum posteriorly. Sustentacular talar coalition is best seen from the tangential view of the heel (Harris view) with varying angles of the central beam parallel to the articular surfaces of the sustentaculum tali joint. A common secondary sign of talocalcaneal coalition is an osseous excrescence at the dorsal aspect of the talus, called talar beak.	Bony, cartilaginous or fibrous bridging of either the calcaneus and navicular or the calcaneus and talus, are common causes of *peroneal spastic flatfoot.* Tarsal coalition may not be seen before age 10 because tarsal ossification centers are small and coalition is still cartilaginous. Tarsal coalition in many multiple malformation syndromes involves the cuneiforms. Fusion of tarsal (and carpal) bones may be secondary to *rheumatoid arthritis* or an *inflammatory lesion*. Talar beak may be also secondary to degenerative changes in the talonavicular joint, or a plain anatomical variant once considered to be secondary to wearing high heeled shoes (Fig. 15.**46**).

Fig. 15.**42** **Pes cavus type deformity** in an 8-year-old with meningomyelocele.

Fig. 15.**43** **Bilateral coalition** of tarsal navicular and cuneiform. There is also calcinosis circumscripta in the toes. ▷

15.44a

15.44b

15.45a

15.45b

15.46

Fig. 15.**44 a, b** **Tarsal coalition** in a foot with multiple malformations. The coalition involves calcaneus, cuboideum, cuneiforms and several metatarsals.

Fig. 15.**45 a** **Midtarsal fusion** and **b talocalcaneal fusion** secondary to rheumatoid arthritis.

Fig. 15.**46** **"Talar beak"** without associated abnormality.

Tumors and Infections

Tumors involving hands and feet have radiographic characteristics not dissimilar to the general descriptions given in Chapter 5 and will not be discussed in detail here. The most common *benign bone tumor* of the small tubular bones of the hand is an *enchondroma*. It is also frequent in the foot. Whereas solitary enchondromas are usually seen between the ages of 10 and 50, *enchondromatosis* (Fig. 15.**47**) is already present in the very young. An epidermoid inclusion cyst may mimic enchondroma (Fig. 15.**9**). The most common tumor in the foot is an *osteochondroma*. A *subungual exostosis* arises from the distal phalanx beneath the nail bed, usually on the medial aspect of the big toe. *Solitary bone cysts* appear frequently in the lateral aspect of the anteroinferior portion of the calcaneus (Fig. 15.**48 a**). A pseudocystic radiolucency in this location may mimic a true cyst (Fig. 15.**48 b**). A calcified fleck in the cystic cavity is considered to be characteristic of *lipoma of the calcaneus* (Fig. 15.**48 c**). Malignant primary or metastatic bone tumors are rare in hands and feet. Also, soft-tissue tumors are rare. A *hemangioma* may be identified due to associated phleboliths and it may cause gigantism of the involved area. *Neurofibromatosis* may cause elephantoid-like soft-tissue changes and bone deformation. *Villonodular synovitis* may present as bone erosion and soft-tissue tumor.

Arthritides and inflammatory lesions of the bones are discussed in Chapter 6. Many of the characteristic features are seen in hands and feet, and are not repeated here.

Local trauma is the most common cause of *osteomyelitis* of the hands and feet, more common than hematogeneous (Fig. 15.**49**). In children, the calcaneus is an important site of primary hematogeneous osteomyelitis. It is relatively common (8.8 % of all hematogeneous infections), but may run an indolent course. *Osteomyelitis* in a diabetic (Fig. 15.**50**) and *neurotrophic (diabetic)* arthropathy with extensive demineralization may have identical patterns in the foot. *Tuberculosis* of the small tubular bones also causes pronounced demineralization, followed by bone destruction, minimal sclerosis, but no sequestra (Fig. 15.**51**). It is more common in fingers *(spina ventosa)* than in toes. Disseminated *fungal infections* may involve hands and feet. Their radiographic features are nonspecific and may mimic tuberculosis, pyogenic osteomyelitis, or a malignant neoplasm. Localized cyst-like rarefactions and sclerosis may also be present in noninflammatory conditions such as *tuberous sclerosis*, which especially affects the distal phalanges. The rare *granulomatous disease of childhood* occurs predominantly in hands and feet. It lacks local inflammatory signs, causing bone destruction without either sclerosis, abscess, or sequestra. *Sarcoidosis* can cause a variable spectrum of bone changes in hands and feet including cyst-like defects, acroosteolysis or acroosteosclerosis, periosteal reaction, and abnormal trabecular pattern of the small tubular bones.

Several infectious diseases that are rare in temperate regions are endemic and common in tropical areas. Many of them cause destructive changes in the underlying bone, although they primarily affect the skin and soft tissues. Often they are inoculated through the hands or feet. Since tropical diseases are rarely considered as a major differential diagnostic possibility in temperate or cold climates. They often involve the hands and feet and are summarized in Table 15.**5**.

Fig. 15.**47** **Enchondromatosis of the hand.** Multiple, expansile radiolucent lesions cause marked deformity of the bones. Faint calcifications are seen within the tumors.

a **b** **c**

Fig. 15.**48 a–c** **a Calcaneal cyst. b** A **pseudocystic** lucency mimicking calcaneal cyst. **c Lipoma** of the calcaneus.

a

b

Fig. 15.**49 a, b** **Pyogenic osteomyelitis** complicating an osteoarthritic first metatarsophalangeal joint. **a** Periarticular soft-tissue swelling and early destructive changes are seen in the sclerotic head of the first metatarsal, three weeks after penetrating trauma. **b** Extensive destruction of the joint and adjacent bone eight months later.

Fig. 15.**50** **Diabetic foot.** Extensive bone destruction in toes and metatarsophalangeal joints due to osteomyelitis.

Fig. 15.**51** **Tuberculous osteomyelitis** of the middle phalanx of the fourth finger. Radiolucent bone destruction and some sclerosis, but no sequestra.

Table 15.5 Tropical Diseases Involving Hands and Feet

Disease	Radiographic Findings	Comments
Yaws (Figs. 15.52, 15.53)	*Primary yaws:* skin eruption , no bone lesions. *Secondary yaws:* a sequence of osteoporosis, small, coalescent foci of bone rarefaction and florid periosteal reaction. *Tertiary yaws:* like secondary yaws but larger foci of destruction, some sclerosis and more ragged periostitis. Growth disturbances occur in children.	A nonvenereal infection caused by *Treponema pertenue*. Enters through skin abrasion, usually in childhood, and causes osteoperiostitis of feet, hands, legs, and forearms. Bone changes are seen in about one-sixth of the cases.
Leprosy (Fig. 15.54)	Three types of bone changes: 1 *Osteitis leprosum*, a localized cortical or subperiosteal bone destruction within the phalanges, especially the fingers. 2 *Nonspecific osteitis* modified by neurotrophic and vascular factors in patients with sensory loss: erosion of subungual tufts due to infection or acute osteitis. The phalanges in fingers and distal metatarsal bones may be eroded, fragmented or completely dissolved. 3 *Disuse osteoporosis*.	A *Mycobacterium leprae* infection. Disability is due primarily to involvement of peripheral nerves, which is minimal in the *tuberculoid* type, but extensive in the more virulent *lepromatous* type. About 15% of cases have bone changes. *Mimics diabetic neuropathy, congenital indifference to pain, syringomyelia, scleroderma, psoriasis, Raynaud's disease and frostbite.* May affect tarsal bones and result in Charcot-type joint.
Tropical ulcer	About 20% develop a nonspecific periosteal reaction of the underlying anterior tibia. A malignant change may occur in chronic cases.	A chronic ulcer, caused by the *fusiform bacilli* and *Vincent's spirochetes*, usually in mid-or lower leg.
Smallpox (variola) osteomyelitis	Within 10 days tubular bones show a transverse band of metaphyseal destruction with possible sequestration of the epiphysis. Periosteal new bone appears along the shaft. Original shaft may appear sequestered after 2 to 3 weeks, but becomes incorporated in the slowly remodeling involucrum. Growth disturbances, ankyloses, and secondary osteoarthritis are common,	Occurs in about 5% of young children with smallpox, 1–6 weeks after the onset of the disease. Metaphysitis of elbows, hands, wrists, ankles, and feet causes tenderness and swelling.
Mycetoma (Madura foot)	*Superficial:* Soft-tissue swelling in the confines of the plantar aponeurosis. *Deep:* Bone changes develop after several months: 1 endosteal cavitation, no sequestration; 2 parosteal erosion; 3 periosteal new bone; 4 amorphous expansion of bone. Usually affects tarsal and metatarsal bones, which appear moth-eaten,	Direct inoculation of fungus (actinomyces or maduromyces) via a thorn prick into the bare foot, causing either a superficial or deep plantar mycetoma. Sinus tracts discharge grains. Endemic in thorny, semidesert areas.
Filariasis	Enormous soft-tissue swelling. No underlying bone involvement; calcified coils of worms are rarely seen in soft tissues of extremities.	Infection of lymphatics by *Wuchereria bancrofti* worms. Lymphangitis and granulomatous or allergic reaction results in subcutaneous edema followed by lymphedema.

(continues on page 382)

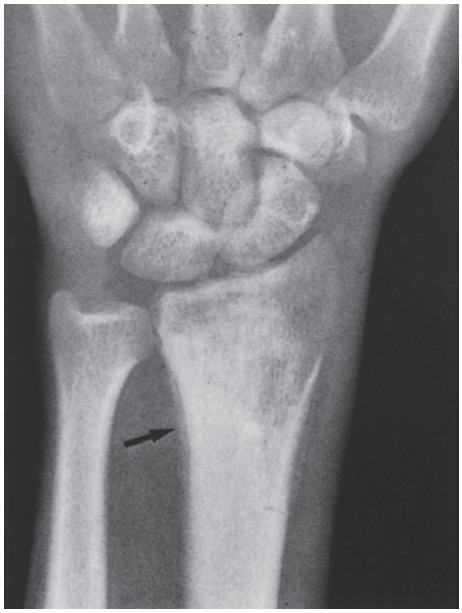

Fig. 15.**52** **Secondary yaws** in distal radius seen as a bone rarefaction and periosteal reaction (arrow).

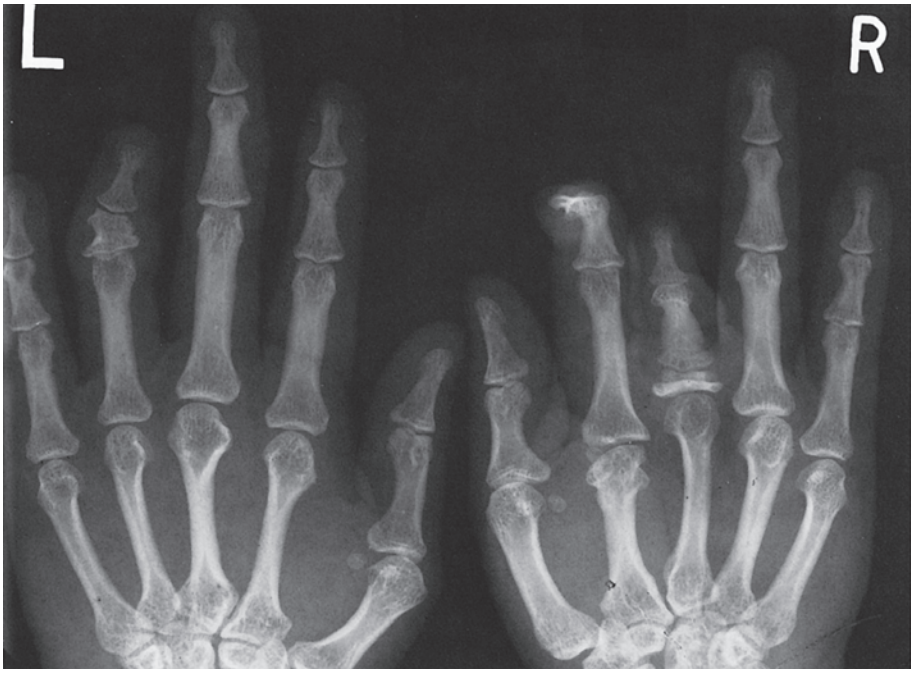

Fig. 15.**53** **Tertiary yaws.** Growth disturbances have resulted in short middle phalanx of the left fourth finger and rudimentary proximal phalanx of the right middle finger. There is flexion contracture of the distal interphalangeal joint in the right index finger.

Fig. 15.**54** **Leprosy.** Bone destruction in fingers (non-specific osteitis).

Table 15.5 (Cont.) Tropical Diseases Involving Hands and Feet

Disease	Radiographic Findings	Comments
Guinea worm (dracunuliasis)	Serpiginous, coiled calcifications in subcutaneous tissues of the feet and ankles, also elsewhere.	The worm, *Dracunculus medinensis*, may cause an inflammatory reaction. Dead worms may calcify.
Loiasis	Fine, coiled, lacelike or filamentous calcifications between metacarpal and metatarsal bones.	Loa-loa infection is characterized by hot erythematous swellings, especially in upper limbs.
Kaposi's sarcoma	Soft-tissue nodules, osteoporosis of underlying bones, cortical erosions and small bone cysts. No new bone production or periosteal reaction.	A low-grade chronic malignancy, primarily affecting the skin as bluish-red, rubbery, highly vascular nodules. Feet, legs, hands, and arms usually affected. Common in equatorial regions and South Africa. High incidence in AIDS *(acquired immune deficiency syndrome).*
Ainhum (Fig. 15.55)	Constriction of soft tissue between proximal and middle phalanx of the fifth toe. Pressure may cause erosion, fracture, or dissolution of the underlying bone.	A nonspecific concentric inflammation of the deep fascial layers of the fifth toe. Affects African blacks and their descendants, mainly elderly men.
Sickle cell dactylitis (hand-foot syndrome) Fig. 15.56)	Bone destruction followed by periosteal new bone formation (bone within bone) secondary to bone infarction of the metacarpal, metatarsals, and/or phalanges.	Affects infants and young children with sickle-cell anemia. Hands and feet are tender and swollen. May be complicated by (salmonella) osteomyelitis. Osteomyelitis by itself may produce an identical picture.

Fig. 15.**55** **Ainhum.** Dissolution of bone due to soft-tissue constriction of the middle phalanx of the fifth toe.

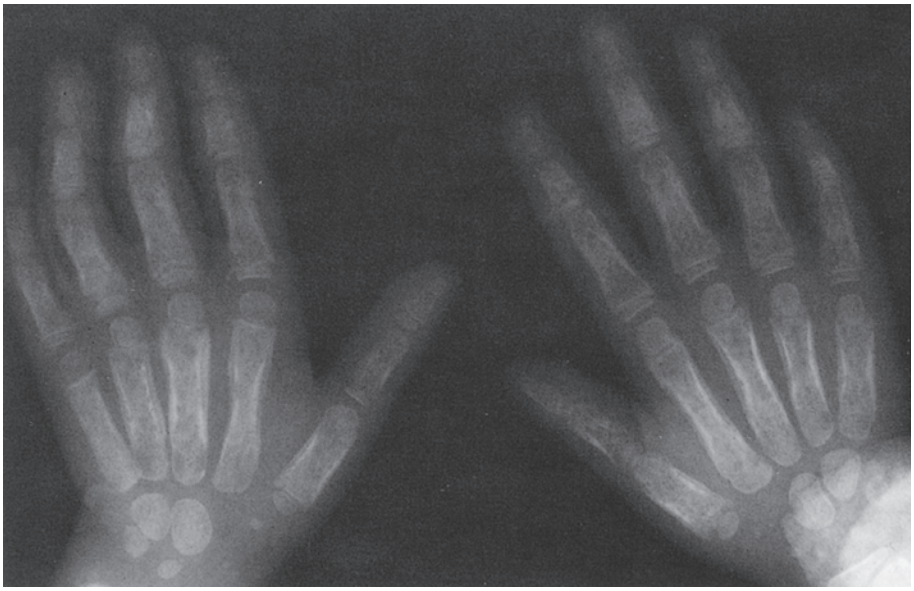

a

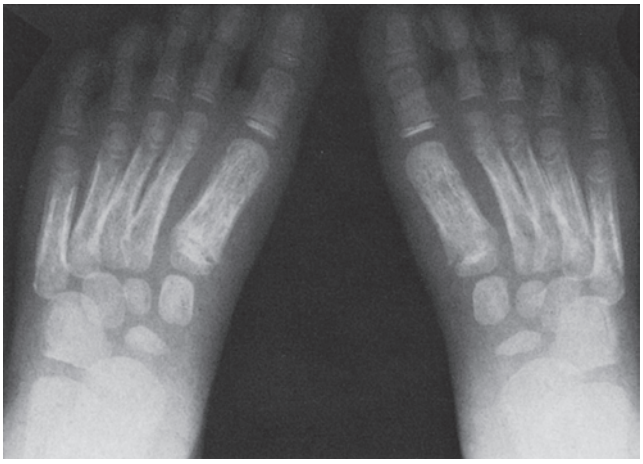

b

Fig. 15.**56 a, b** **Sickle-cell dactylitis.** Bone destruction and periosteal reaction in both hands and feet. Radiographic changes are similar to osteomyelitis but occur symmetrically in multiple bones.

Traumatic Lesions

Fractures and other traumatic lesions of the hands and feet are an everyday problem. The most common location in the upper extremity is the wrist, and in the lower extremity, the ankle. The multiplicity of bones in hands and feet creates a wide variety of different lesions.

The alignment abnormalities of a lunate or perilunate dislocation should not remain unrecognized, since severe osteoarthrosis and permanent limitation of motion will ensue in untreated cases.

In a *perilunate dislocation*, the lunate maintains a normal relationship with the distal radius, and the surrounding carpal bones dislocate dorsally (Fig. 15.**57**). It is often associated with fractures of the ulnar styloid, the scaphoid bone, and the triquetrum. The lateral view shows dislocation that might be overlooked on an anteroposterior projection.

Lunate dislocation involves volar displacement of the lunate. The distal carpal row moves toward the radius to fill the space left by the lunate. This type of dislocation is clearly identified on the lateral projection (Fig. 15.**58**). *Scaphoid subluxation* may be a residual deformity from an incomplete reduction of a carpal dislocation, or it may result from a localized rupture of the lunate-scaphoid ligament. On an anteroposterior view, the scaphoid appears shortened, and there is a gap of more than 2 mm between lunate and scaphoid.

The epiphyses in the hands and feet may be duplicated, stippled, fragmented, or remain divided without fracture. In juvenile patients it is advisable to make a comparison with the opposite extremity in case of uncertainty. Among accessory ossicles of the wrists the os centrale (Fig. 15.**13**) and os triangulare (accessory ossicle between ulna and carpal bones) are of interest, since they are common in certain congenital malformation syndromes. Ossicles should not be confused with fractures. Fusion of the carpal bones can be a congenital anomaly. The most common is fusion of the lunate and the triquetrum (Figs. 15.**59**, 15.**63 b**). In the foot, major fractures and dislocations are usually not a problem to detect if one pays attention to the normal lines of alignment and the structural integrity of the bones. *Avulsion* fractures are generally thin and easily overlooked. They are usually seen only in tangential projection. Chip fractures of the foot should be sought at the site of clinical symptoms. Small avulsion fractures between the major bones are common. Sesamoids and accessory ossicles may have similar locations, but they are smooth in outline and frequently symmetrical (Fig. 15.**60**).

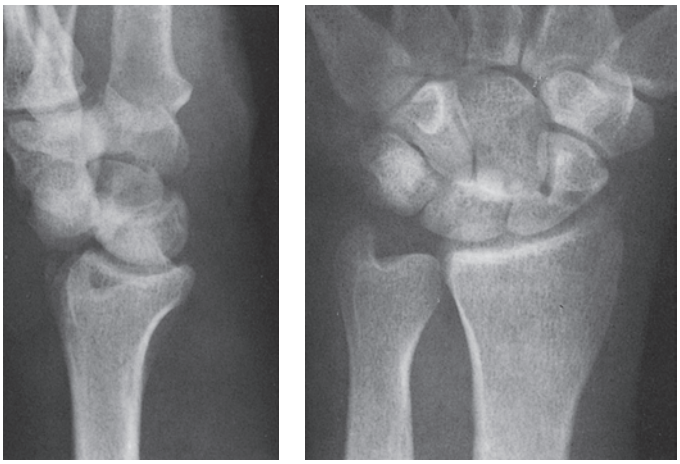

a **b**

Fig. 15.**57 a, b** **Perilunate dislocation** of the wrist with the lunate in normal relationship with the distal radius. Navicular fracture is associated (perilunate transschaphoid dislocation).

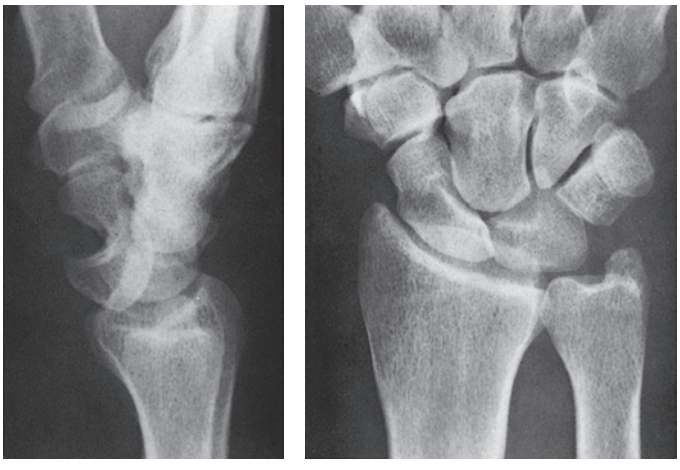

a **b**

Fig. 15.**58 a, b** **Lunate dislocation** with volar displacement of the lunate. **a** The shape of the lunate is abnormal in the AP projection, whereas the lateral view **b** shows abnormal location and alignment of the lunate.

Fig. 15.**59** **Fusion anomaly** of the lunate and triquetrum.

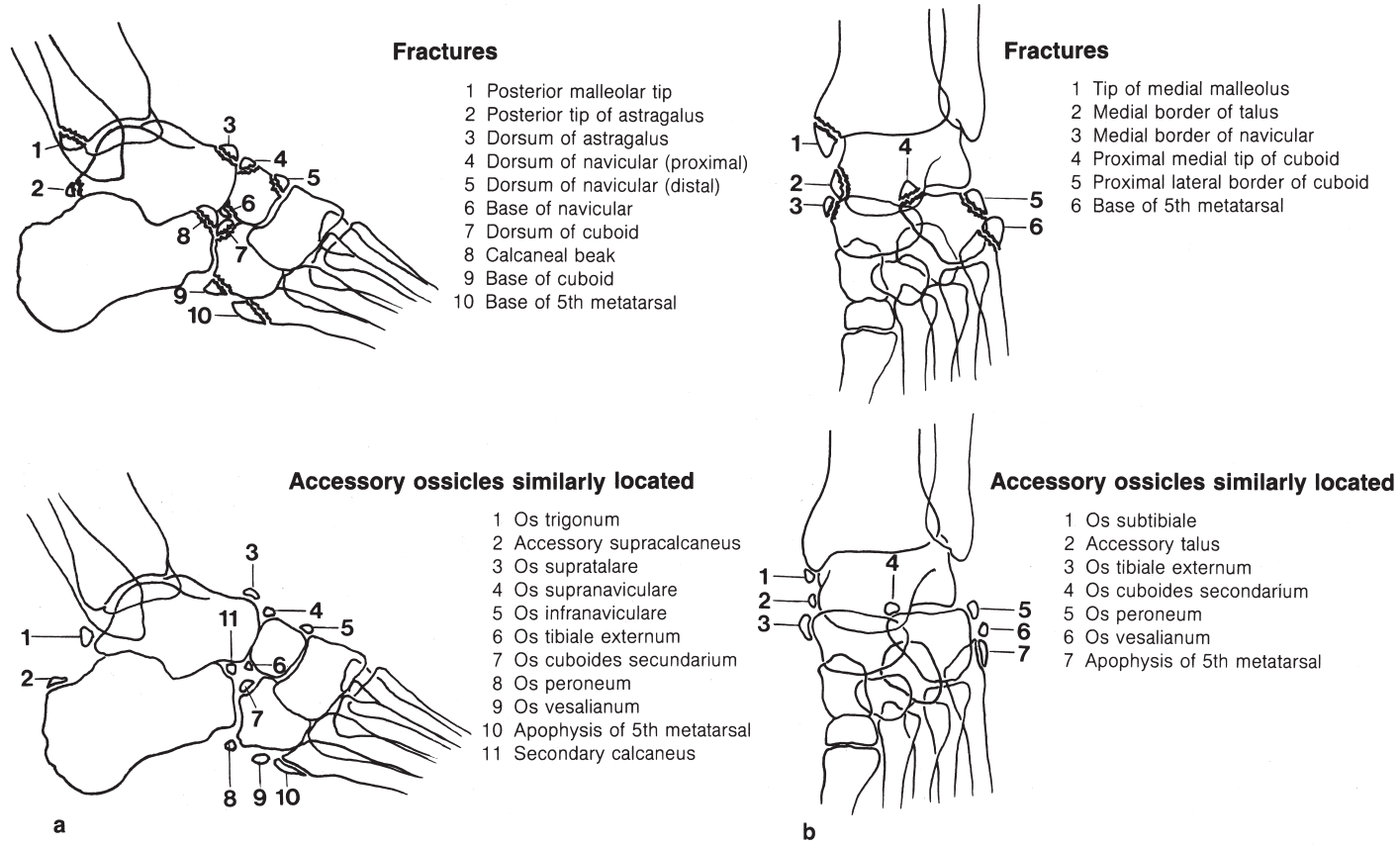

Fig. 15.**60 a, b** **Differential diagnosis** between common avulsion fractures and accessory ossicles **a** in lateral view and **b** in dorsplantar view.

Secondary Osteoarthritis

When *osteoarthritis* involves a nontypical joint of the hand or foot, one should look for an underlying factor. Any condition that limits normal motion results in exaggerated stress and predisposes to secondary osteoarthritis. In the wrist it is often an *old fracture*, especially of the scaphoid. In the foot, primary osteoarthritis usually involves only the first metatarsophalangeal, the first tarsometatarsal and the talonavicular joints. *Osteoarthrosis of one of the metatarsophalangeal joints* other than the first is likely to be secondary to trauma or avascular necrosis (*Freiberg's disease*, Fig. 15.**61**). Avascular necroses occur relatively frequently in the lunate (*Kienböck*, Fig. 15.**62**), scaphoid (*Preiser*, Fig. 15.**63**), and the tarsal navicular (*Köhler*, Fig. 15.**64**). If all metatarsophalangeal joints are involved, *epiphyseal dysplasia* may be the underlying cause. Extensive osteoarthritis of the talonavicular joint points to abnormal subtalar motion (due to *tarsal coalition* or *subtalar arthritis*). Dramatic progression of denegerative changes with destruction in the ankle, tarsal joints, or, occasionally, in metatarsophalangeal joints is suggestive of a *neurotrophic process* (Charcot joint, Fig. 15.**36**). Neurotrophic changes in the hands are most commonly due to *syringomyelia*.

a b

Fig. 15.**61 a Avascular necrosis** of the third metatarsal head, incidentally associated with a fracture of the diaphysis of the third metatarsal. **b** Early avascular necrosis of the third metatarsal in a 7-year-old associated with epiphyseal destruction and periosteal reaction. Later a typical appearance of Freiberg's disease developed.

Fig. 15.**62 Avascular necrosis** of the lunate, evident as dense sclerosis of this bone.

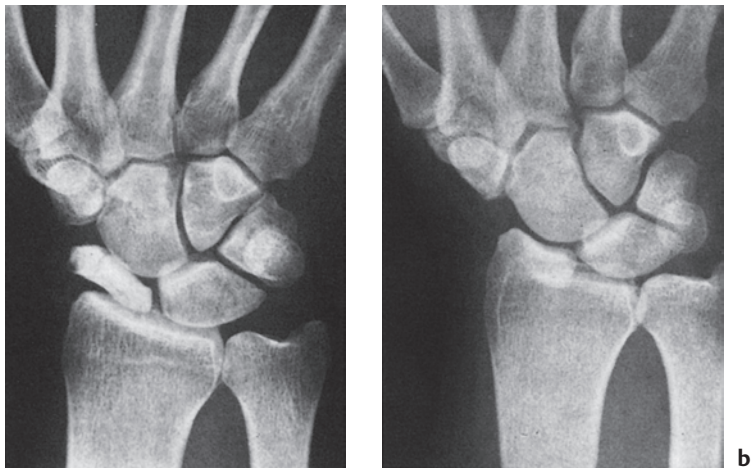

a b

Fig. 15.**63 a, b a Avascular necrosis** of the scaphoid. **b** fusion of the scaphoid into the radius with abnormal alignment of the carpus. An unusual anomaly, somewhat mimicking avascular necrosis.

Soft-Tissue Changes

In a small percentage of films the definitive clue to diagnosis lies in the soft tissues. Often, careful analysis of the soft-tissue densities of the radiographs gives important supplementary information and helps in the differential diagnosis. Ultrasound examination using a high-frequency transducer is often helpful. At certain sites the information may be important enough to warrant a special soft-tissue exposure. The various causes of soft-tissue calcification have been presented in Chapter 7.

Apart from edema due to systemic diseases such as cardiac, renal, or hepatic failure, myxedema and malignancy, a *generalized increase of soft tissue in hands and feet* may represent overgrowth due to *acromegaly* (Fig. 15.**65**) or infiltration of the skin by edema and fibrous tissue in *idiopathic osteoarthropathy (pachydermoperiostosis).*

In the absence of edema, myxedema, local infection, and the rare condition of pachydermoperiostosis, any increase in the heel pad thickness is a reliable indicator of acromegaly. Heel pad thickness of less than 21 mm in men and 18 mm in women in non-weight bearing practically excludes acromegaly. On the other hand, heel pad thickness of over 25 mm with a body weight of 60 kg and 30 mm with a body weight of 120 kg almost certainly indicates acromegaly.

A diffuse increase in soft tissue, usually due to edema, of the whole hand or foot may be due to *venous or lymphatic obstruction, Sudeck's atrophy, shoulder-hand syndrome, neurotrophic disorder* (in the hand, most likely syringomyelia, in the foot, diabetic neuropathy), or *myxedema* (Fig. 15.**66**). Transient edema may follow a *cerebrovascular accident*.

A *generalized decrease* of soft-tissue thickness in hands and feet is most commonly due to *collagen vascular diseases* (Fig. 15.**67**), *epidermolysis bullosa*, disuse from *muscle or neurologic abnormalities*, and, rarely, *lipodystrophy*.

Clubbing of Fingers

Bulbous configurations of the ends of fingers, called finger clubbing, is most commonly due to *bronchogenic carcinoma, cirrhosis of the liver, congenital heart disease, pulmonary hypertrophic osteoarthropathy, or pulmonary interstitial fibrosis* with or without *pneumoconiosis*. Several uncommon causes of finger clubbing include *pachydermoperiostosis, polycythemia*, and some *chronic infections*. It may rarely be idiopathic.

Fig. 15.**64** **Avascular necrosis** of the navicular, which is shrunken and sclerotic.

Fig. 15.**65** **Acromegaly.** Generalized incerase of soft tissues of the foot, best seen as increased thickness of the heel pad. Calcaneal "spur" is also demonstrated (arrow).

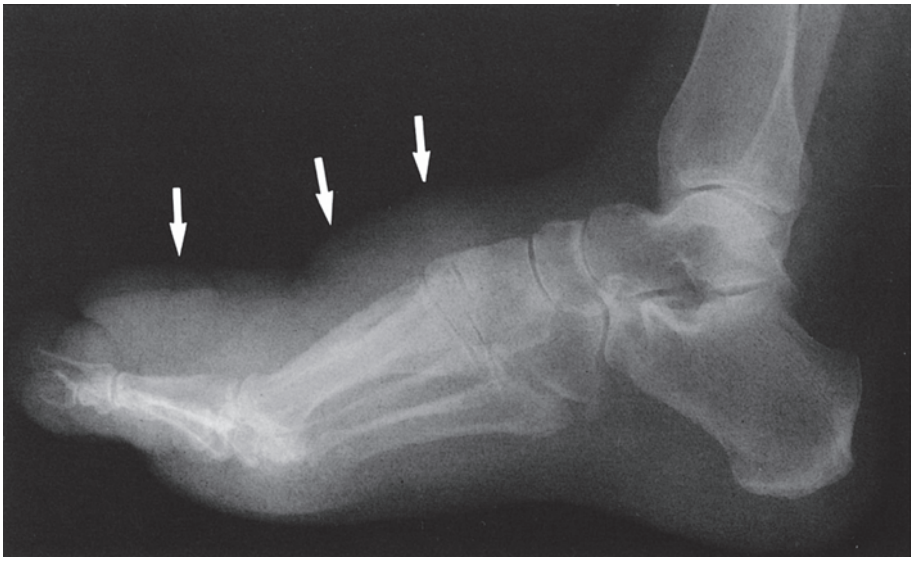

Fig. 15.**66** **Localized myxedema** of the dorsum of the foot seen as increased soft-tissue thickness without bone lesions (arrows).

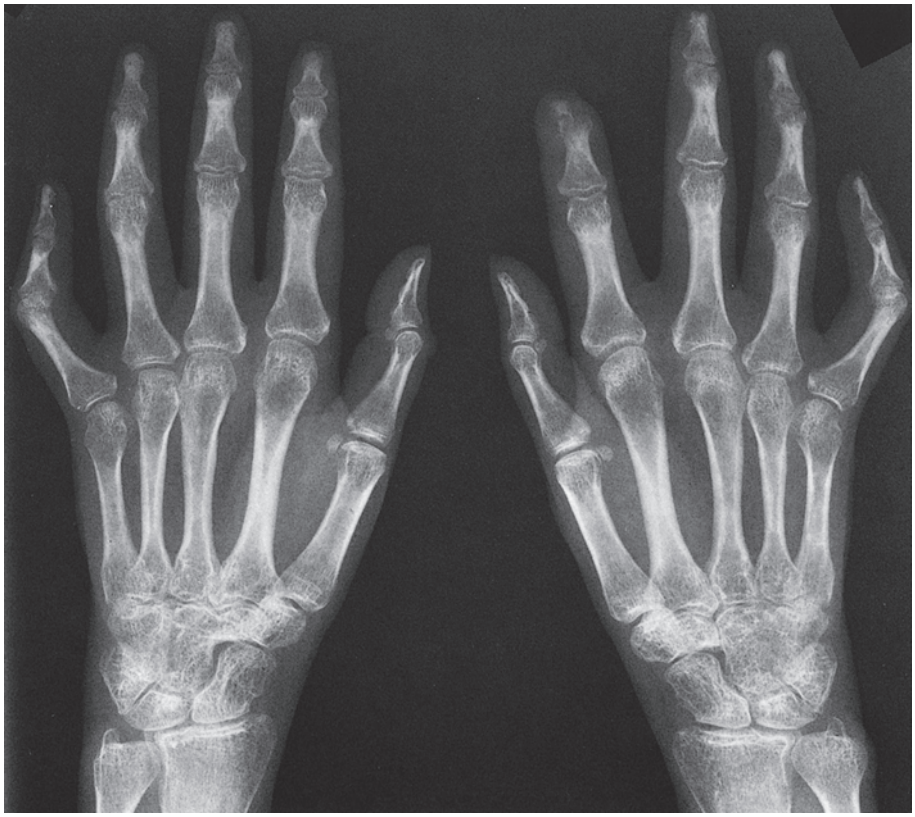

Fig. 15.**67** **Scleroderma.** Generalized soft-tissue atrophy associated, incidentally, with acrosclerosis of the fingers.

Soft-Tissue Masses

An isolated soft-tissue mass in the hand or foot may represent a benign or malignant *soft-tissue tumor* or an underlying arthritis. Subcutaneous nodules in *rheumatoid arthritis* are more common in the extensor surface of the forearms, but may occur in hands. *Tuberculosis* (cold abscess) may rarely cause a localized mass in a digit, whereas other granulomatous diseases (e.g., sarcoidosis and leprosy) tend to cause more generalized swelling of a digit. Metabolic arthritides *gout*, Figs. 6.**63**–6.**69**, p. 157, 158, *amyloidosis, lipoid dermatoarthritis*, and *hyperlipidemia* may produce discrete soft-tissue masses. These should be distinguished from soft-tissue masses and mucoid cysts adjacent to the joint margins in *osteoarthrosis*, commonly seen in the distal interphalangeal joints of fingers. Localized swelling of soft tissue may also be due to inflammation of the subcutaneous tissues, called *cellulitis*. Radiolucent areas in a localized subcutaneous swelling indicate either gas-forming organisms such as *Clostridia (gas gangrene)* or access of air into tissues through an open wound (subcutaneous emphysema).

Articular effusions cause expansion and/or increased density of the soft tissues of the joint involved. *Rheumatoid arthritis, viral infections* (particularly viral hepatitis), *sarcoidosis*, and several *gastrointestinal disorders* (Whipple's disease, ulcerative colitis, Crohn's disease, Henoch-Schonlein purpura, and small-bowel bypass surgery) may develop monoarticular or polyarticular effusions without bone lesions. Other causes of monoarticular effusions are gout, fungal infections, tuberculosis, hemophilia, and villonodular synovitis. Secondary erosion of underlying bone often follows. Unlike rheumatoid arthritis, *psoriatic arthritis* and *Reiter's syndrome* affect joints in a random fashion, involving tendons as well as joint capsules. The entire finger may become swollen (sausage finger). Overgrowth or other causes of enlargement of digits involving both soft tissues and possibly also osseous structures is called localized gigantism. Causes of localized gigantism are presented in Table 15.**6**.

Table 15.6 Localized Gigantism in Hands or Feet

Disease	Radiographic Findings	Comments
Macrodystrophia lipomatosa (Fig. 15.68)	Overgrowth of both soft tissues and osseous structures; second and third digits of either hand or foot are most frequently involved. Soft-tissue overgrowth is most marked along the volar aspect. The phalanges are long, broad and often splayed. Changes are most severe at the distal ends of the digits.	A rare form of congenital localized gigantism. The condition may be static or progressive, but growth ceases with puberty. Polydactyly or syndactyly is often associated, clinodactyly is almost invariable.
Maffucci's syndrome	Multiple enchondromas in the bones of hands and feet, with the addition of hemangiomas seen as phleboliths, and soft-tissue masses.	Radiographic features are similar to those of Ollier's disease (multiple enchondromas), with the addition of soft-tissue masses.
Klippel-Trenaunay-Weber syndrome	Localized gigantism with both soft-tissue and osseous overgrowth. May affect an entire extremity or only the distal digits. Other osseous anomalies are common.	A triad of cutaneous capillary hemangiomas, varicose veins and localized gigantism. Arteriovenous malformations are common.
Neurofibromatosis	Enlarged digits may be bilateral, not necessarily involving contiguous digits. Distal phalanges are not most severely affected. Premature fusion of the growth plates may occur.	Macrodactyly resulting from plexiform neurofibromas combined with mesodermal dysplasia.
Hemangioma Lymphangioma	Soft-tissue enlargement in the involved region.	Phleboliths may be present in a hemangioma.
Ollier's disease	Multiple enchondromas	Large enchondromas may cause an appearance of localized gigantism even in the absence of soft-tissue tumor.
Dactylitis (Fig. 15.69)	Soft-tissue mass in a digit secondary to infection, infarction gout, sarcoidosis, or Still's disease.	See Chapter 6.

(continues on page 390)

Fig. 15.**68** **Macrodystraphia lipomatosa** involving the soft tissues and bones of the thumb, first metacarpal and greater multangulum.

Fig. 15.**69** **Dactylitis in sarcoidosis.** The index finger is swollen, and the proximal phalanx contains coarse, expansile bone lesions.

Table 15.6 Localized Gigantism in Hands or Feet

Disease	Radiographic Findings	Comments
Osteoid osteoma	Bone changes in metatarsals, metacarpals or phalanges are variable, depending on the location of the tumor. Soft-tissue swelling may be prominent.	See Chapter 5.
Melorrheostosis (Fig. 15.70)	Characteristic osseous excrescences along the length of the involved bone simulate candle wax flowing down the side of a lit candle.	Growth disturbance may cause increased circumference and inequality of limb length. Soft-tissue changes include tense, erythematous skin and subcutaneous edema.
Localized myxedema (Fig. 15.66)	Soft-tissue swelling without bone involvement.	A rare cause of localized enlargement of a limb.

Fig. 15.**70** **Melorrheostosis.** The first, fourth, and fifth metacarpals and finger bones are thickened. The sclerotic changes follow the length of the bones. There is also soft-tissue swelling.

Tendons, Capsules, and Bursae

A properly exposed radiograph is able to delineate some tendon sheaths and joint capsules. Inflammation in these locations manifests itself as either an increased density or an increased width. Ultrasound examination is more sensitive and will show decreased echogenicity and/or expansion due to edema, effusion and inflammation.

Tenosynovitis of the *extensor pollicis brevis* and the *abductor pollicis longus* can cause obliteration of tissue planes in the radial aspect of the wrist.

In rheumatoid arthritis the *extensor carpi ulnaris* tendon is frequently involved and recognized by swelling of the ulnar side of the wrist in anteroposterior projection. Distension of the capsules of interphalangeal and metacarphophalangeal joints may further document synovitis.

The anatomy of the Achilles tendon is sharply defined on a lateral projection of the ankle due to a triangular fat pad anterior to it (Kager's triangle). The normal diameter of the Achilles tendon is 9 mm or less. Any cause of *tendinitis, edema,* or *hemorrhage* results in an increased diameter of the Achilles tendon, with or without loss of sharpness of the posterior margin of Kager's triangle. Causes of an increased diameter of the Achilles tendon include hemorrhage due to *rupture*, *stress tendinitis*, edema due to *venous stasis*, *infection* of adjacent tissues, or *inflammation* (rheumatoid arthritis, ankylosing spondylitis, Reiter's syndrome, and gout). Inflammation of the retrocalcaneal bursa between the bone and the Achilles tendon may cause an erosion of the posterior calcaneus. This is characteristic for an inflammatory arthritis. Any of the *metabolic arthritides* (gout, amyloidosis, lipoid dermatoarthritis and hyperlipidemia) may increase the diameter of the Achilles tendon or produce localized swelling. In asymptomatic hypercholesterolemic patients, increased thickness (over 9 mm) of the Achilles tendon is virtually diagnostic of familial hypercholesterolemia (Fig. 15.**71**), since nonfamilial hypercholesterolemia does not produce xanthomatous thickening of the Achilles tendon.

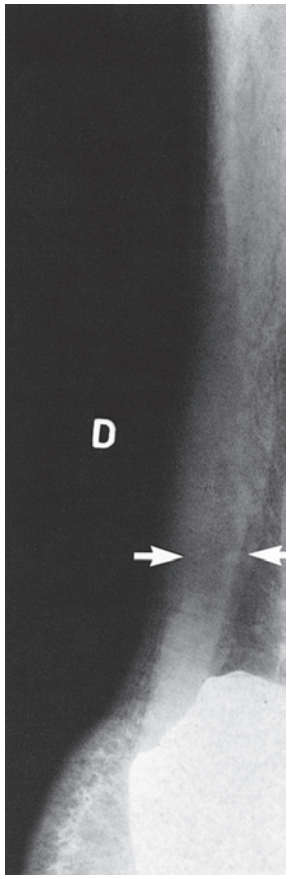

Fig. 15.**71** **Thickening of the Achilles tendon** measuring 13 mm in diameter in familial type IIA hypercholesterolemia.

The extent of tendon involvement is dependent on the patient's age and serum cholesterol concentration. Ultrasound examination is more sensitive than radiography in detecting subtle xanthomas in the Achilles tendon of a patient with familial hypercholesterolemia.

References

Browner B. Skeletal trauma. Philadelphia: Elsevier Science. 2003.
Burgener FA, Kormano M. Differential diagnosis in cumputed tomography. Stuttgart: Thieme, 1996.
Burgener FA, Meyers SP, Tan RK, Zaunbauer W. Differential diagnosis in magnetic resonance imaging. Stuttgart: Thieme, 2002.
Dähnert W. Radiology review manual. 5th ed. Baltimore: Williams and Wilkins, 2003.
Damjanov I, ed. Anderson's pathology. 8th ed. St Louis: Mosby, 1996.
Ebel K-D, Blickmann H. Differential diagnosis in pediatric radiology. Stuttgart: Thieme, 1999.
Federle MP, Megibow AJ, Naidich DP. Radiology of AIDS. New York: Raven Press, 1988.
Freyschmidt J et al. Borderlands of Normal and Early Pathological Findings in Skeletal Radiography. Stuttgart: Thieme, 2003.
Goldman L. Cecil's textbook of medicine. 22nd ed. Philadelphia: Saunders, 2003.
Gray HL, Bannister LH, Williams PL. Gray's anatomy. ed. Edinburgh: Churchill Livingstone, 2004.
Greenspan A, Duprey L. Orthopedic imaging: A practical approach. Philadelphia: Lippincott, 2004.
Kaspar D. Harrison's Principles of Internal Medicine. 16th Ed. New York: Mc Graw-Hill Co. 2004.
Keats TE, Lusted LB. Atlas of roentgenographic measurement. 7th Ed. Chicago: Year Book Medical 2001.
Keats TE. Atlas of normal roentgen variant that may simulate disease. 7th ed. St Louis: Mosby. 2001.
Kreel L. Outline of radiology. London: Heinemann Medical, 1992.
Kuhn J, ed. Caffey's pediatric Diagnostic Imaging Chicago: Year Book Medical, 2003.
Kumar V, Cotran RS, Collins T. Robbins and Cotran pathalogic basis of disease. Rev Philadelphia: Saunders. 2004.
Meschan I. Analysis of roentgen signs in general radiology. Philadelphia: Saunders, 1973. 2 vol set
Mims C. Medical microbiology. London: Elsevier Science. 2004
Reeder MM. Reeder and Felson's gamuts in radiology. New York: Springer, 2003.
Reeders JW, Mathieson JR. Imaging in AIDS. Philadelphia: Saunders, 1998.
Robbins SL. Pathologic basis of disease. Philadelphia: Saunders, 1974.
Schinz HR. Lehrbuch der Röntgendiagnostik. Stuttgart: Thieme, 1989.
Stoller D et al. Diagnostic Imaging Orthopaedics. Salt Lake City: Amirsys, 2004.
Sutton D. A textbook of radiology and imaging. 7th ed. Edinburgh: Churchill Livingstone, 2002.
Swischuk LE. Imgaing of the newborn, infant and young child. 5th. Ed. Baltimore: Williams and Wilkins, 2003.
Taybi H, Lachmann RS. Radiology of syndromes, metabolic disorders. 4th ed. Chicago: Mosby, 1997.
Townsend C. Sabiston textbook of surgery: the biological basis of modern surgical practice. 16th ed. Philadelphia: Saunders, 2000.

Index

Page numbers in **bold type** refer to illustrations

A

abscess
  brain 209
  Brodie's 20, **22**, 80, 120, **121**
  paravertebral **280**
  periapical 247
  periodontal 246, 247
  retropharyngeal, in child 256
abused child syndrome 64–65, **65**
accessory bones **72**, 384, **385**
acetabular angle **315**
Achilles tendon thickening 391, **391**
achondroplasia
  hand anomalies **355**
  knee angulation 349, **349**
  long bone anomalies 316, 334, **334**, **345**
  rib anomalies 306, **306**
  scapula anomalies 335
  spine/pelvis 256–258, 260, 272, 276, 295, **295**
    spinal stenosis 278, **278**
aclasis, diaphyseal 18, 322, 340
acoustic neuroma 231, **231**
acromegaly 164, 192, **346**
  foot anomalies **131**, **165**, **387**
  hand anomalies **192**, **361**
  paranasal sinuses and 237
  skull 216–217, **217**
  soft-tissue overgrowth 387, **387**
  spinal changes 256, 258, 259
acromioclavicular joint
  degeneration 132
  subluxation 309, **310**
  widened 133, **133**
acro-osteolysis 122, **364**, **365**, 366, **367**
  chemical 366
  familial 364
  sarcoidosis **187**
  scleroderma 154
acro-osteosclerosis 26, 362, **363**
actinomycosis 240, 280
adamantimoma 81, 98, **99**, 249
adanoameloblastoma 249, **249**
Addison's disease 8
adenocarcinoma 227
  kidney **311**
adenoma
  basophil 227
  chromophobe 227, **228**, 235
  eosinophil 227
  parathyroid 10
  pituitary 207, **228**
adrenal carcinoma 330
Ahlbäck's disease 24, 38, **39**, 183, **184**
AIDS 178, **179**, 382
  septic arthritis **180**
  tuberculous arthritis **180**
ainhum 382, **382**
air-fluid level, paranasal sinuses 237, **237**
Albers-Schönberg disease 30, 298, 306
Albright's syndrome 319
alcoholism 344
alkaptonuria 162, 192, 194, 259
ameloblastic fibroma 249
ameloblastic odontoma 250, **250**
ameloblastoma 98, **99**, **246**, 249, **249**
amyloidosis 114, **115**, 165, **165**
  in chronic renal failure **165**
  primary 114, 164
  secondary 114, 164
amyotonia congenita 328
anal atresia 260
anemia 6, 32, 212, 217–218
  acquired 217
  Fanconi's 10, **339**, **357**
  hemolytic 217
  sickle cell *see* sickle cell anemia
aneurysm
  aorta 257
  calcifications 205, **205**
    vein of Galen 205
  internal carotid artery 232, 235
  ophthalmic artery 235
  orbital 233, 235
  vertebral artery 258
aneurysmal bone cyst **78**, **79**, 80, 82, **83**
  hand 362
  jaw 251
  Paget's disease **124**
  secondary 82
  spine 256, 258, 286
  with teleangiectatic osteosarcoma **104**
angiofibroma, juvenile 239
angioma 208, 233
angiomatosis
  cystic 86, **87**
  meningofacial 205
angiosarcoma 106, **107**
ankle
  accessory bones **72**, **385**
  effusions **139**, **143**
  fractures 60, **60**
ankylosing hyperostosis 284
ankylosing spondylitis 131–132, **131**, 145, **145–148**, 192
  humoral head deformity 337
  juvenile-onset 144
  pelvic changes 260, 261
  periosteal reactions 42, **42**
  spinal changes 256, 257, 259, **303**
annulus fibrosus
  calcification 258
  ossification 259
aorta
  aneurysm 257
  coarctation 308, **308**
arachnodactyly 256, 258, 296, 327
  metacarpal index 353
arachnoid cyst 222
arachnoid granulations 210, 221
  calcified 204, **205**
Armillifer armillatus 196
Arnold-Chiari malformation 228
arteriosclerosis obliterans 364
arteriosclerotic calcifications 204
arteriovenous malformations 211, 235
  calcifications 205–208, **205**, 233
artery
  internal carotid
    aneurysm 232, 235
    calcification 204, **204**, **205**
  meningeal **211**
  nutrient 74, **74**
  ophthalmic, aneurysm 235
  sclerosis 201, **201**
  supraorbital 211, **211**
  temporal 211, **211**
  vertebral, aneurysm 258
arthritis
  enteropathic 150, **151**, **153**, 261
  fungal **132**, 178, **179**
  hand anomalies 362
  humoral head deformity 337
  Jaccoud's 152, **153**
  joint deformities **137**
  monoarticular 129
  polyarticular 129–130
    distribution patterns 130–132
  scapula deformation 336
  septic (pyogenic) 67, 129, 176, **176–177**
    in AIDS **180**
  silicone-induced **187**
  viral 178
  see also osteoarthritis; psoriatic arthritis; rheumatoid arthritis; tuberculous arthritis
arthrodesis, triple 374
arthrogryposis multiplex congenita 328
articular disorders *see* joint diseases
articular surface fragmentation **134**, 135, **135**
Askin tumor 307
aspergillosis 240, **241**, 280
astrocytoma 206
atheromatous calcifications **200**, 201
atherosclerosis 344
atlantoaxial fusion 262, 263
atlantoaxial subluxation **143**, 256, 262, **303**
atlanto-occipital dislocation 265
atlanto-occipital fusion 262
atlas anomalies 262–264
  arch defects 263, 264
    fracture 264, 265, **265**
atrophy
  cerebral 216
  disuse 6, 12, 328
  infantile muscular 328
  Sudeck's 12
avascular necrosis 24, **25**, 67, 116, 129
  capitulum of the humerus **37**
  clavicle 309
  differential diagnosis 37–39, 185
  femoral head 342, 344, **344**
  foot **386–387**
    lunate **25**, 386, **386**
    navicular **39**, 386, **387**
    scaphoid 386, **386**
  Gaucher's disease 32, **33**, 50, 324, **324**
  humeral head **37**, **338**
  joints 183, **183–184**
  metatarsal **39**
  secondary 183
  segmental 342
  subchondral cyst **135**
avulsion fracture **53**, 70–71, **71**, 384, **385**
axis fracture 266, **266**

B

Baastrup syndrome 170, **171**, 283, **283**
ball-in-cup deformity **137**, 147
bamboo spine 145, **146**, **303**
Bankart lesion 314
barotrauma 242
Barton fracture 55, **56**
basal angle **229**
basal cell nevus syndrome 200, 204, 305
basal ganglia calcifications 204, **204**, 210
basilar invagination (impression) 5, 228, **229**, 262
  anterior 262
  medial 262
  radiologic assessment **229**
battered child syndrome 50, 71
Behçet's syndrome 154, **155**
bejel 48
Bennett fracture 57, **58**
Bertolotti's syndrome 170, **171**
biliary atresia 320

birth anoxia 210
bismuth intoxication 34, 332
bizarre parosteal osteochondromatous proliferation (BPOP) 90, **91**
bladder extrophy 260
blastomycosis 240, 280
blind loop syndromes 8
block vertebra 256, 272, **273**
  congenital 272, **273**
  post-traumatic **273**
  tuberculous **273**
Blount's disease 38, 317, 347, **347**
blow-out lesion **111**, 237, **237**, 242
Böhler's angle 368, **369**
bone
  accessory **72**, **385**
  hemorrhage 12
  heterotopic formation 71
  infarct 12, **15**, 23, **23**, 50, 116, **117**
    long bone changes 334
    matrix calcification **77**
  islands 15, **15**, 16, **16**, 94, **94**
    intramedullary ossification **77**
    spine 257
  lesions *see* bone lesions
  marble 30
  resorption *see* bone resorption
  rider's 71
  sequestrum 78–79, **78**
  wormian 211, **212**
  see also fracture; *specific bones*
bone bars 70, **70**
bone cyst **79**, 80, 82, **83**
  calcaneal 378, **378**
  hand 362
  long bones 322
  rib 307, **307**
  see also aneurysmal bone cyst
bone lesions
  cortical 81, **81**
    benign fibrous cortical defects 92
  diametaphyseal 80
  epiphyseal 80
  expansile 79, **79**, 80, **84**, **107**
    skull vault **220**
  geographic 75, **75**
  healed 20, **22**
  juxtacortical 81, **81**
  localized 75–127
    differential diagnosis 82–127
  metaphyseal 80
  moth-eaten 75, **75**
  orbits 233–236
  permeative 75, **76**
  skull 219–220, 221–226
  see also fracture
bone resorption
  hyperparathyroidism **11**
  osteopenia 3–5
bone-within-bone appearance
  healed fracture 323
  osteopetrosis 30, **30**
  sickle-cell anemia 323, 332
Bouchard's nodes 139, 169
boutonnière deformity **137**, **142**
bowing fracture 62, **63**, 318
bowlegs 315, 316–319, 347–348, **347**
boxer's fracture 57
brachial plexus damage 335, **335**
  birth trauma 308, **309**
brachydactyly 354, **355**
brachymetacarpaly 354, **355**
brachytelephalangy 366
Brailsford's disease 37
brain abscess 209
brain stone 205, **205**
brain tumors 206–208
breast carcinoma metastases **15**, 20, **110**
  paranasal sinuses **238**
  periosteal reactions 46, **47**
  skull **213**
  spine **291**
Brodie's abscess 20, **22**, 80, 120, **121**
bronchogenic carcinoma metastases **81**, **110**, **111**, **363**
  jaw **251**
  skull **223**
brown tumor in hyperparathyroidism **11**, 114, **115**, 226, 307
brucellosis, spinal 280
Buchman's disease 37
bucket handle fracture **59**, **65**
buckling fracture 62, **64**
Buerger's disease 364
Burkitt's lymphoma 112, **251**
burns 12, 50, 364
Burn's disease 37
burr holes 225
bursitis
  calcarea 337
  trochanteric **161**
burst fracture 62, **63**, 267, 269, **269**
butterfly vertebra 256, 276
button sequestrum 220, **220**, **224**
buttressing
  aneurysmal bone cyst 79, **79**, 82
  avascular necrosis **135**
  chondroma **91**
  osteoarthritis **167**

C

cadmium poisoning 10
Caffey's disease 28, **29**, 37, 38
  long bone anomalies 316, 320, **321**
  periosteal reactions 43, **43**
  rib anomalies 306
Caisson disease 344
calcaneal cyst **378**
calcaneal fractures 61
calcaneal pitch 368, **369**, **372**, **373**
calcaneal spur **387**
  degenerative **131**
  inflammatory **131**
calcaneonavicular coalition 376
calcific tendinitis **138**
calcification 189
  acromegaly **192**
  amorphous 71
  aneurysms 205
  ankylosing spondylitis **146**
  arteriosclerotic 204
  arteriovenous malformations 205–208
  atheromatous **200**, 201
  basal ganglia 204, **204**, 210
  bone infarct **15**, **23**, **77**
  brain tumors 206–208
  chondroblastoma **91**
  chondrodysplasia punctata **17**
  chondrosarcoma **101**, **102**, **103**, **291**
  chordoma **98**
  cysticercosis **197**
  dentate nucleus 204, **204**, 210
  dermatomyositis **155**, **194**, **197**, **200**
  differential diagnosis 190–201
  DISH **284**
  dystrophic 189
  eggshell 71, **105**
  enchondroma **15**, **23**, **77**, **89**
  fibrous dysplasia **126**
  gout **117**
  hemophilic pseudotumor **116**
  hyperparathyroidism **186**, **193**
  hypoparathyroidism **210**
  internal carotid artery 204, **204**, **205**
  intervertebral disks 138, **160**, 170, 192, 258
  intracranial hemorrhages 205, 209
  jaws 245
  ligaments 71, **198**, **204**
  lipoma **85**, **199**
  liposarcoma **199**
  matrix 77, **77**, **91**, **98**, **101–103**
  metastatic 189
  myositis ossificans 71, **73**
    post-traumatic **105**
  ochronosis 162, **163**
  orbits 233
  osteoarthritis **167**
  osteogenesis imperfecta **321**
  osteoid osteoma **95**
  periosteal 198, **198**
    chondroma **91**
  pineal gland 203, **204**
  pituitary 204, **204**
  polymyositis **194**
  postoperative 198
  post-traumatic 195, **195**, 198
  radiation osteonecrosis **117**
  rickets **44**
  sacroiliitis **294**
  salivary glands 245, **245**
  scleroderma **138**, 154, **155**, **193**
  scurvy **44**
  skull 203–210
    artifacts **203**
    pathologic 204–210
    physiologic 203–204
  soft tissue 189, **189**
    periarticular 137, 138, 193–195
  synovial osteochondromatosis **181**
  tumor, intra-articular 190
  vascular 201
calcinosis 189
  circumscripta **376**
  idiopathic universal 196
  interstitial 200
    universal **194**
  pseudotumoral 195
calcium deficiency 8
calcium hydroxyapatite deposition disease (HADD) 132, 161, **161**, 194, **194**
calcium malabsorption 8
calcium pyrophosphate dihydrate deposition disease (CPPD) 67, **68**
  chondrocalcinosis 137, **138**
  distribution patterns 130–132
  joints 129, 130, 159, **160**, 192, **192**
  with gout 157, **158**
calculus, salivary gland 245, **245**
callus formation 20
  excessive, following fracture 71–73
  periosteal **55**
calvarium thickness 216–219
Calvé-Kümmel-Verneuil disease 37
camptodactyly 354, **357**
carbon monoxide poisoning 196, 210
carcinoma
  adrenal 330
  breast *see* breast carcinoma metastases
  bronchogenic *see* bronchogenic carcinoma metastases
  epidermoid 120
  ethmoid sinus **238**
  mastoids 232
  maxillary antrum **238**
  nail bed 362
  nasopharynx 232, 234, 239, **239**
  paranasal sinus 232, 234
  parathyroid 10
  prostate *see* prostate carcinoma metastases
  renal 20, **71**, **111**, **291**
  skull base sclerosis and 229
  sphenoid sinus **228**, 235, 239, **239**
  thyroid 20, **223**
  see also metastases
carcinomatosis 6
caries sicca 195
carotid cavernous fistula 232
carpal angle 353, **354**
carpal bones
  fractures 55–57
  fusion 384, **385**
  ligamentous injuries 57
cataracts 233
caudal hypoplasia 292
cavernous hemangioma 233
celery-stick appearance **27**, 320
celiac disease 8
cellulitis 388
cement synovitis **187**

cementoma 250, **250**
cephalohematoma, ossified 212, **214**
cerebral atrophy 216
cervical rib 305
cervical spine
  degenerative disease **171**
  fractures 61–62, 265–268
  see also spine; vertebra
cervicobasilar anomalies 262–264
Chance fracture 62, **63**, 269, **269**
Charcot joint 174, 386
Charcot spine 256
Chassaignac subluxation 339
chauffeur's fracture 55, **56**
cherubism 253
chip fracture **53**
chloroma 112, **113**
cholesteatoma 231–232, **231**
  primary 231
  secondary 231–232
chondroblastoma 80, 90, **91**
chondrocalcinosis
  CPPD 137, **138**, 159, **160**, 192
  post-traumatic osteoarthritis **168**
chondrodysplasia
  metaphyseal 331, **331**
  punctata 16, **17**, 342
chondrodystrophia calcificans congenita 342
chondroma
  intra-capsular 190
  paranasal sinuses 238
  periosteal (juxtacortical) **81**, 90, **91**, **96**
chondrometaplasia, synovial 67, 180
chondromyxoid fibroma 80
chondrosarcoma 18, 46, 198, 208
  central 100, **101**
  clear cell 80, 102, **102**
  cortical **101**
  dedifferentiated 102, **102**
  jaw 251
  mesenchymal 103, **103**
  pelvis 290, **291**
  periosteal (juxtacortical) 100
  peripheral 100, **101**
  rib 307
  spine 257, 272, **291**
Chopart fracture-dislocation 61
chordoma 98, **98**, **205**, 208, **208**, 232, **232**
  chondroid 98
  orbital 235
  spine 258, 288, **288**
choroid plexus
  calcification 203–204, **204**
  papilloma 206
chronic recurrent multifocal osteomyelitis (CRMO) 20
clavicle anomalies 308–309
claw toe 137
clay-shoveler's fracture 62, **62**, 267
cleft sternum 310
cleidocranial dysostosis 237, 366
  clavicle 308
  pelvis 292
  skull 211, 228
cleidocranial dysplasia 260, **308**
clinodactyly 354, **356**, **360**
clubbing of fingers **361**, 387
clubfoot 368, **370**, 374, **375**
  overcorrected **370**
coalition
  tarsal 376, **376–377**, 386
  vertebral 272
coarctation of the aorta 308, **308**
coast of California appearance 55
coast of Maine appearance 34, 55, 325
coccidioidomycosis **121**, 209, 240, 280
coccyx 255
cock-up toe 137
cod fish fracture 271
Codman's triangle 41, **42**, **47**, 103, 104
collagen disease 344, 364, 387
collateral ligament, Pallegrini-Stieda lesion 71, **73**
Colles fracture 55, **56**
comminuted fracture **53**
compound fracture 53
compression fracture **53**
  cervical spine 267, **267**
  humoral head **314**
  osteoporotic 271, **271**
  thoracolumbar spine 62, **63**, 269, **269**, **270**, **271**
congenital cytomegalic inclusion disease 209
congenital heart disease, cyanotic 217
congenital indifference to pain 174, **175**, 364
congenital syphilis 27, **27**, 43, **43**, **323**, 332, **333**
congenital toxoplasmosis **205**, 209, **209**
congenital vertical talus 374, **375**
connective tissue disease 6, 233
Conradi's syndrome 342
cookie-bite sign 110
corduroy appearance 86, **86**, **109**
Cornelia de Lange syndrome 366
corpus callosum lipoma **205**, **208**
cortical destruction 79, **79**, 80
cortical tunneling **33**, **106**
costovertebral osteoarthritis 170
cotton wool appearance **124**, 212, 217, **218**
coxa valga **144**, 314, **315**, **321**, 324, **329**, 346, **346**
coxa vara **126**, **144**, 260, 314, **315**, 319, **345**
  primary congenital 345
  secondary congenital 345
CPPD *see* calcium pyrophosphate dihydrate deposition disease
craniolacunia 221
craniometaphyseal dysplasia 28, **230**, **236**, 320, **321**
craniopharyngioma **205**, 206, **207**, 227, **228**
  orbital 235
craniotomies 225
cranium bifidum 221
crescent sign 116, 183, **183**, **184**
cretinism 16, 185, 211, 256
  hand anomalies **355**
  long bone changes 331, 342, **343**, 345, **345**
  spinal changes 298
Crohn's disease 8, **151**, **153**, 261
cross-over toe 137
CRST syndrome 193
cruciate ligament injuries 58
cryoglobulinemia 154
cryptococcosis 209, **209**, 240, 280
cubitus valgus 314
cubitus varus 314
cuff tear arthropathy 161
cup-in-saucer deformity **137**, 147
curly toe 137
Cushing's syndrome 3, 8, 330, 344
cyst 46, 240
  apical 247
  arachnoid 222
  bone **79**, 80, 82, **83**
    solitary, of the mandible 248, **248**
    see also aneurysmal bone cyst
  calcaneal **378**
  carpal
    amyloidosis **165**
    chronic overuse osteoarthritis **168**
  dental 247
  dentigerous **246**, 247, **247**
  echinococcal (hydatid) 82
  epidermoid (inclusion) 84, **84**, 362
  eruptive 247
  fissural 248
  follicular 247
  hemorrhagic 226
  periodontal **246**, 247, **247**
  post-traumatic (leptomeningeal) 226, **226**
  primordial **246**, 248, **248**
  radicular 247
  residual 247, **247**
  retention 240, **241**
  sarcoidosis **187**
  subchondral *see* subchondral cyst
  traumatic 82, 248, **248**
cystic angiomatosis 86, **87**
cystic lymphangiomatosis 86
cystic rheumatoid arthritis 141, **143**
cystic tuberculosis 118
cysticercosis 196, **197**, 209
cystinosis 10
cytomegalic inclusion disease 27, **205**
  congenital 209, 330, 332

D

dactylitis 389, **389**
  sickle cell 382, **383**
  tuberculous 118, **120**
dagger sign 145, **146**
De Toni-Debre-Fanconi syndrome 10
degenerative disease
  intervertebral disks 170, **170–171**, 192, 258, 283, **283**
  joints 67
    temporomandibular joint **245**
    with detached spur 190
    see also osteoarthritis
  spine 170, **170–171**
dens
  fractures 61, **61**, 264, 266, **266**
  hypoplastic 263, **263**
dental cyst 247
dentate nucleus calcifications 204, **204**, 210
dentigerous cyst **246**, 247, **247**
dentinoma 250, **250**
dermatomyositis 154, **155**
  calcifications 193, **194**, 196, **197**, 200, **200**
  hand 364
dermoid 221, 233
  cerebral 207
  orbital 233
  paranasal sinuses 238
  spine 258
desmoid, periosteal (juxtacortical) 92, **92**
diabetes mellitus 8
  osteomyelitis and 48, **49**, **119**
diabetic foot **119**, 174, **175**, 378, **379**
diabetic gangrene 364
diaphyseal aclasis 18, 322, 340
diastematomyelia 258, 276
Diaz's disease 38
Dietrich's disease 37
diffuse idiopathic skeletal hyperostosis (DISH) 42, **42**, 50, **52**, 172, **173**
  enthesopathy **136**
  spinal changes 259, 284, **284**
diploic lakes 210, 221
diploic veins 210–211, 221
disk *see* intervertebral disk
diskitis 176, **177**
  infectious 279, **279**
dislocation 65, 137
  atlanto-occipital 265
  hip, congenital 314, **315**, 342, 346
  leprosy **175**
  lunate 57, **57**, 384, **384**
  midcarpal 57
  occipitocervical 265
  pelvic **59**
  pericarpal 57
  perilunate 57, **57**, 384, **384**
  radial head 339
  radioulnar 339
  rheumatoid arthritis **142**
  shoulder **66**, 314
    anterior 314, **314**
    posterior 314
  see also fracture-dislocation
dissociation, scapholunate 57, **57**
disuse atrophy 6, 12, 328
dorsum sella 227
double-floor sella 220–227, **227**
doughnut lesion 220, **221**
Down's syndrome 256, 260, 292
  rib anomalies 305
Dracunculus medinensis 196, 382
drooping shoulder 132–133, **133**, 138
Dupuytren fracture 60
dura, calcification 204, **204**

dwarfism 316, 327, 334, 342
  campomelic 316, 348
  metatropic 320
  thanatophoric 316, 320
dyschondrosteosis 317, 340, 348
dysosteosclerosis 30
dysostosis, cleidocranial 237, 366
  clavicle 308
  pelvis 292
  skull 211, 228
dysplasia
  campomelic 348
  cleidocranial 260, **308**
  craniodiaphyseal 28, **29**, 320, **321**
  craniometaphyseal 28, **230**, **236**
  diaphyseal, progressive 28, **29**, 213, 320, **321**
  diastrophic 342
  epimetaphyseal 320
  epiphyseal 185, 386
    multiple 342
  familial metaphyseal 320
  fibrous *see* fibrous dysplasia
  glenohumoral 336, **336**, 337
  metaphyseal 348
  Meyer's 185
  osteofibrous 24, **25**, 125, **126**
  spondyloepimetaphyseal 320
  spondyloepiphyseal 185, **185**, 260, 296, 348
dysplasia epiphysealis hemimelica 88, **89**, 349, 350
dysproteinemia 44
dysraphism 256
  closed 276
  open 276
dystrophy
  mixed sclerosing bone 30, **31**
  muscular 318, 328, **329**, 346
  reflex sympathetic (RSD) 12, **17**

E

echinococcal cyst 82, 196, 209
  spine 256
effusions, joints *see* joint diseases
eggshell calcification 71, **105**
Ehlers-Danlos syndrome 194, 200, 371
elbow
  effusions **139**
  fractures 55
  nursemaid's 339
electrical injuries 50
emphysema, orbital 233, **233**, 237
empty box sign 3, **110**
empty orbit sign 234, **234**
empty sella syndrome 227, **228**
enchondroma **15**, 18, **23**, 88, **89**, **155**
  hand 362, 378
  location 80
  Maffucci's syndrome **91**
  matrix calcification **77**
  rib 307, **307**
  scapula 336
  skull 208
enchondromatosis 18, 88, **90**
  hand 378, **378**
  long bone anomalies 317, 322, **322**, 334, 339
endosteal scalloping 76, **76**
  ameloblastoma **99**
  amyloidosis **115**
  chondrosarcoma **101**
  fibrosarcoma **99**
  fibrous dysplasia **125**
  osteomyelitis **119**
  sarcoidosis 127, **127**
Engelmann-Camurati disease 28, **29**, 213, 320, **321**
enostoma 16, **16**
enostosis 16, **77**, 94, **94**
enteropathic arthritis 150, **151**, **153**, 261
enthesopathy 136, **136**, 166
enthesophyte
  degenerative **131**
  inflammatory **131**
eosinophilic granuloma 50, 80, 114, **115**
  jaw 253, **253**
  rib 307
  skull **220**, 224, **224**
  spine 257, 258, 286, **287**
ependymoma 206, **206**, 258
epidermoid 221, **222**
  orbital 233
epidermoid carcinoma 120
epidermoid cyst 84, **84**
epidermolysis bullosa 328, 364, 387
epimetaphyseal dysplasia 320
epiphyseal dysplasia 185, 385
  multiple 342
epiphyseolysis capitis femoris 342
epispadia 260
equinus 368
Erdheim-Chester disease 34, **35**
Erlenmeyer flask deformity 313, **313**, **333**
  biliary atresia 320
  craniometaphyseal dysplasia 28, 320
  enchondromatosis 322
  Gaucher's disease 32, 50, 324, **324**
  healed fracture 323
  hypophosphatasia 325
  idiopathic hypercalcemia of infancy 326
  lead poisoning 326, 332
  Niemann-Pick disease 324, **324**
  osteogenesis imperfecta **351**
  osteopetrosis 325, **331**
  Pyle's disease 320
  rickets 325
  thalassemia 323, 332
erosions 133–134
  ankylosing spondylitis **148**
  Behçet's syndrome **155**
  clavicles 309, **309**
  enteropathic arthritis **153**
  gout 157, **157–158**
  hemophilia **156**
  hyperparathyroidism **186**, **302**, **309**
  osteoarthritis 169, **169**
  psoriatic arthritis **148–149**, **303**
  Reiter's syndrome **151**
  relapsing polychondritis **155**
  rheumatoid arthritis **142–143**
    juvenile **144**
  ribs **305**
  sacroiliac joint 261, **303**
  sternum **310**
  tuberculous arthritis **179**
  vertebral pedicle 258
erythema nodosum 154, 240
erythroblastosis fetalis 27, 332
Essex-Lopresti fracture 55
ethmoid sinus carcinoma **238**
Ewing's sarcoma 18, **19**, 106, **106–107**
  age at presentation 81
  jaw 251
  location 80
  long bone changes 334
  metastases 20
  pelvis 288, **289**
  periosteal reactions 46, **46–47**
  permeative lesion **76**
  rib 307
  spine 257, 288
exostosis
  hereditary multiple 18, 86, **88**, **101**
    long bone changes 317, 322, **322**, 334, 340, **341**
  rib 307
  subungual 86, **87**, **361**, 378
  turret 86

F

facet joints, locked 268
  bilateral **268**
  unilateral **268**
Fahr's disease 210
Fairbank's disease 342
fallen fragment sign 82, **83**
falx, calcification 204, **204**, **205**
familial acro-osteolysis 364
familial Mediterranean fever 154, **155**, 261
familial metaphyseal dysplasia 320
Fanconi's anemia 10, **339**, **357**
Farber's disease 122
fat embolism 344
fat necrosis **199**
  post-injection/traumatic 200
fatigue fracture 20, 68, 332
feet *see* foot
Felty syndrome 141
femoral epiphysis
  anomalies 342–343
  osteochondrosis 342
  slipped 64, **65**, 342, **343**, 345, **345**
    avascular necrosis 38, **39**
femoral head
  anomalies 344
  avascular necrosis 342
femoral neck angle **315**
  anomalies 345–346
femur fractures
  distal 58
  proximal 58, **59**
fibrogenesis imperfecta ossium 10
fibroma 198
  ameloblastic 249
  chondromyxoid 80, 92, **92**
  desmoplastic 92, **93**
  nonossifying **75**, 80, 92, **93**
    rib 307
  ossifying 24, 125, 239
    jaw 252, **252**
fibromatosis 122, **122**
fibromyxoma 250, **250**
fibrosarcoma 46, 98, **99**, 198
  jaw 251
  pelvis 288, **288**
fibrosing osteitis 226
fibrous dysplasia 14, **14**, 24, **78**, 125, **125–126**
  hand anomalies 362
  jaw 246, 252, **252**
    hereditary (cherubism) 253
  location 80
  long bone anomalies 319, **319**, 325, **325**, 345
  orbits **236**
  paranasal sinuses 239, **240**
  polyostotic form 34, **35**, **126**
  pseudarthrosis 55
  pseudofractures 74
  rib anomalies 307, **307**
  skull 212, 217, **217**, 225, **225**, 230, **230**
  spine 256, 272
fibular fractures 60, 62
Filaria loa loa 196
filariasis 380
filum terminale, tight 276
fish vertebra **3**, 256
fissural cyst 248
fistula
  carotid cavernous 232
  small bowel 8
flatfoot 350, 368, **370**, 372, 374
  acquired **372**
  congenital 372, **373**
  peroneal spastic 376
  rigid 372
floating face **243**
floating maxilla **243**
floating palate **243**
floating teeth 114, 245, 246, **246**, 253, **253**
fluorosis 34, **36**, 42, 50, 198
  pelvic changes 260
  skull 218–219
  spinal changes 257, 259, 300, **301**
Fong's disease 292, **292**
foot 353
  accessory bones **72**, **385**
  congenital anomalies 354, 359
  diabetic **119**, 174, **175**, 378, **379**

gigantism 389–390
infections 378–379
joint disease 130–131
Madura 178, 380
neurotrophic **372**, 374, 378
orthopedic problems 368
differential diagnosis 371–377
secondary osteoarthritis 386
soft-tissue changes 387
soft-tissue masses 388
trauma 384–385
tropical diseases 380–383
tumors 378
foramen
intervertebral, enlargement 258
parietal 221, **221**
foreign body
granuloma 127, **127**
intraorbital 233
synovitis 186, **186**
Forestier's disease *see* diffuse idiopathic skeletal hyperostosis (DISH)
fracture 53–64
ankle 60, **60**
atlas 264, 265, **265**
avulsion **53**, 70–71, **71**, 384, **385**
axis 266, **266**
Barton 55, **56**
Bennett 57, **58**
blow-out, of the orbit 237, **237**, 242
bowing 62, **63**, 318
boxer's 57
bucket handle **59**
buckling 62, **64**
burst 62, **63**, 267, 269, **269**
butterfly fragment **53**
calcaneal 61
Chance 62, **63**, 269, **269**
chauffeur's 55, **56**
children 62–64
chip **53**
Chopart 61
classification **53**
Neer four-segment classification 55
clay-shoveler's 62, **62**, 267
cod fish 271
Colles 55, **56**
comminuted **53**
compound 53
compression **53**, 256
cervical spine 267, **267**
humoral head **314**
osteoporotic 271, **271**
thoracolumbar spine 62, **63**, 269, **269**, **270**, **271**
delayed union 53
dens 61, **61**, 264, 266, **266**
Dupuytren 60
elbow 55
Essex-Lopresti 55
fatigue 20, 68, 332
femur 58, **59**
flexion-distraction 269
foot 384, **385**
Galeazzi 55, **56**
greenstick 62, **63**
hand 384, **385**
hangman's 61–62, **61**, 264, 266, **266**
healed **22**, **54**, **55**, **78**, 118, **118**, 318, 323
healing **51**, 53, 55, **69**, **117**, 118, **118**
abused child syndrome **65**
diabetic foot **175**
hip, subcapital 116
humerus 55
Hutchinson 55, **56**
impacted **53**
insufficiency 20, **22**, 68, 332
intra-articular 73, **74**
Jefferson 61, 264, 265, **265**
Jones 61
juvenile Tillaux 62, **64**
knee 58
Lefort 242, **243**
longitudinal **53**
Maisonneuve 60, **60**
Malgaigne **59**
malunion 53, 346
Monteggia 55, **56**, 339, **339**
nonunion 53–54, **54**, **55**
atrophic 54, **54**
hypertrophic 54, **54**
oligotrophic **54**
oblique **53**
osteochondral 182, **182**
paranasal sinuses 237, 242
pathologic 70, **71**, 271
pelvis 58
stable **58**
unstable **59**
periosteal reactions 50, **51**
pilon 60
Pott 60
rib 307
Rolando 57
segmental **53**
Segond 58–60
skull 211, **212**
Smith 55, **56**
spine 255, 257, 265–271, 280
cervical 61–62, 265–268
thoracolumbar 62, **63**, 269–271
spiral **53**
sternum **311**
straddle **59**
stress *see* stress fracture
T-shaped **53**
talus 60–61
tear drop 62, **62**, 267, **267**
torus 62, **64**
transverse **53**
triplane 62–64, **65**
tripod 242, **242**
V-shaped **53**
vertebra 280
with avulsed fragment in joint 190
Y-shaped **53**
fracture-dislocation
Chopart 61
Lisfranc 61, **61**
thoracolumbar spine 62, **63**, 270, **270**
Frankel, white line of **6**
Freiberg's disease 38, **39**, 386
Friedrich's disease 37, 309
frontal sinus
metastases **238**
mucocele **242**
see also paranasal sinuses
frostbite 12, **134**, 364, **365**, 366
fungal arthritis **132**, 178, **179**
fungal osteomyelitis 118, **121**

G

Galeazzi fracture 55, **56**
gamekeeper's thumb 57–58, **58**
ganglion, intraosseous 80, 82, **82**
gangrene
diabetic 364
gas 388
Gardner's syndrome 18, 50, 94
gargoylism 295
gas gangrene 388
gastric resection 8
Gaucher's disease 6, 32, **33**, 50, 116, 256
long bone anomalies 324, **324**, 344
rib anomalies 306
genu laxum 315, 349, **349**
genu valgum 314, **348**, 349, **349**, 350, **351**
genu varum 315, 347, **347**, **348**
geographic lesions 75, **75**
geographic skull 114, **115**, 224, **224**
giant cell arteritis 154
giant cell tumor **79**, 80, 81, 96, **97**
hand 362
jaw 251
malignant 96
spine 256, 258, 286
gibbus deformity **179**
gigantism 313
hands and feet 389–390
glanders 240
glenohymeral dysplasia 336, **336**, 337
glioma **205**, 206, 233, 234
optic chiasm 227, **227**
optic nerve 234, **234**, 235
glomus tumor 84, 232, 362
gnathic osteosarcoma 103, 251, **251**
Goltz's syndrome 308
Gorham's disease 122, **122**
Gorlin's syndrome 248, 305
gout 129, 130, 157, **157–158**, 192, 194, 344
clavicle anomalies 309
CPPD and 157, **158**
distribution patterns 130–131
erosions 134, **134**
humoral head deformity 337
pelvic changes 261
saturnine 157
secondary 157
tophus 116, **117**, 157, **158**
granuloma
dental **246**
eosinophilic *see* eosinophilic granuloma
foreign body 127, **127**
giant cell (reparative) 96, **97**
intracerebral **205**
midline 239
periapical 247
plasma cell 20, **21**
granulomatous disease of childhood 378
greenstick fracture 62, **63**
ground glass appearance 78, **78**
fibrous dysplasia 14, **14**, **35**, **78**, **125**, **126**, **230**, **319**, **325**
myelofibrosis 300
osteomalacia 3, **3**
growth arrest lines 331, **331**
Guinea worm disease 196, 382
gumma, syphilitic 209

H

habenula, calcified 203, **204**
Haglund's syndrome 38, 131, **131**
Hajdu-Cheney syndrome 366
hallux rigidus **168**
hallux valgus 137, 371, **371**
hamartoma 208
hammer toe 137
hand 353
accessory bones **72**, **385**
congenital anomalies 353–358
deformities **137**
gigantism 389–390
infections 378–379
joint disease 130
secondary osteoarthritis 386
soft-tissue changes 387
soft-tissue masses 388
terminal phalanx pattern 359, **361**
differential diagnosis 361–367
trauma 384–385
tropical diseases 380–383
tumors 378
hand-foot syndrome 50, 382
Hand-Schüller-Christian disease 114, **115**, 224, **224**
hangman's fracture 61–62, **61**, 264, 266, **266**
Hass's disease 37
hatchet sign 132, **132**, 145
Heberden's nodes 139, 169
heel valgus 368, **369**, **374**
heel varus 368, **369**
hemangioendothelioma 106
hemangioma 86, **86–87**, **215**, 225, 378
cavernous 233
hand/foot 389
jaw 251
Maffucci's syndrome **91**
orbital 234
paranasal sinuses 238
spine 256, 257, 272, 286, **286**
synovial 180

hemangiopericytoma 106, 258, 290
hemarthrosis 73, **73**
hematoma **198**
  calcified 116, **195**, 205, 209, 233
  epidural 209
  intracerebral 205, 209
  subdural 209, 212
hemimyelocele 276
hemimyelomeningocele 276
hemivertebra 256, 276, **277**
hemochromatosis 162, **163**, 192
  pelvic changes 260
  primary 162
  secondary 162
  spinal changes 258
hemodialysis, chronic 193
hemophilia 50, 156, **156**, 260, 338, 342
hemophilic pseudotumor 116
hemorrhage
  bone 12
  epidural **205**, 209
  intracerebral 205, **205**, 209
  paranasal sinuses 237
  subdural **205**, 209
  subperiosteal **6**, **44**, 50
hemorrhagic cyst 226
Henoch-Schönlein purpura 154
heparin, osteoporosis induction 8
hepatitis 362
hepatolenticular degeneration 159
hereditary fibrous dysplasia of the jaw 253
hereditary hyperphosphatasia 28, 74, 319
hereditary multiple exostoses 18, 86, **88**, **101**
  long bone changes 317, 322, **322**, 334, 340, **341**
hereditary onycho-osteodysplasia 292, **315**, 350
hereditary spherocytosis 256
herniation pit 82, **83**
herpes 209
Hill-Sachs deformity 314, **314**, 337
hindfoot fault 368
hip
  dislocation, congenital 314, **315**, 342, 346
  joint disease 131–132
  malalignment 314
  rapidly destructive osteoarthritis 166, **168**
hip prosthesis, myositis officans and **189**
histiocytoma
  benign fibrous 92, **93**
  malignant fibrous 100, **100**
histiocytosis 6
  Langerhans cell *see* Langerhans cell histiocytosis
  multicentric reticulo 261
histiocytosis X *see* Langerhans cell histiocytosis
histoplasmosis 240
hitchhiker's thumb **137**, **142**, **153**
HIV infection 178, **179**
Hodgkin's disease 20, **21**, 112, **113**, 257
  spine 290
Holt-Oram syndrome 308
homocystinuria 6, 256, 296, 313, 320, 327
  growth lines **331**
housemaid's knee **161**
humerus
  distal fractures 55
  proximal fractures 55
  supracondylar process 86, **88**
humoral head
  anterior dislocation **314**
  compression fracture **314**
  deformity 337–338
  posterior dislocation 314
Hunter's syndrome 296, **296**
Hurler's syndrome 227, 258, 295, **295**
  clavicle anomalies 308, **308**
  long bone anomalies 340
  rib anomalies **306**
Hutchinson fracture 55, **56**
hydatid cyst 82, 196
  spine 256
hydrocephalus 227
hydroxyapatite deposition disease (HADD) 132, 161, **161**, 194, **194**
hypercalcemia 233
  idiopathic 213, 215, 257
    of infancy 34, 326, 332, **333**
hypercemetosis 250, **250**
hypercholesterolemia, familial **391**
hyperlipoproteinemia 6
hyperostosis
  ankylosing 284
  frontalis interna 212, **214**
  generalized cortical 28, **29**, 213, **216**
  infantile cortical *see* infantile cortical hyperostosis
  interna generalisata 212
  sternocostoclavicular 309
  triangularis ilii 292
hyperparathyroidism **3**, 4–5, **4**, **11**, 186, **186**, 218
  basilar invagination 228
  brown tumor **11**, 114, **115**, 226, 307
  calcification **186**, 192, 193, **193**
  clavicle anomalies 309, **309**
  differential diagnosis 10–11
  hand anomalies 364, **364**, **365**, 366
  lamina dura resorption 245, 253
  long bone anomalies 319
  pelvic changes 260, 261, 302, **302**
  primary **3**, **4**, 5, 10, **22**, **219**, 302
  renal osteodystrophy and 50
  rib anomalies 305
  secondary **3**, **4**, 5, 10, **133**, 186, **186**
    see also renal osteodystrophy
  spinal changes 257, 258, 302, **302**
  tertiary 10
  treatment effects 219
hyperphosphatasia 213
  hereditary 28, 74, 319
hyperthyroidism 8
hypertrophic osteoarthropathy
  primary 44, **45**
  secondary 44, **45**
hypervitaminosis A 43, 334
hypervitaminosis D 34, **36**, 192, 213, 219, 326
  spinal changes 258, 300
hypocalcemia 28
hypogonadism 8
hypoparathyroidism 28, 42, 193, 213
  long bone changes 331, 342
  spinal changes 259
  spontaneous origin 210, **210**
hypophosphatasia 10, **10**, 192, 211, 316, 325
hypophosphatemia, x-linked 8, **9**, 317, **317**
hypopituitarism 327
hypoplasia
  caudal 292
  clavicle 308
  occipital condylar 262
  paranasal sinuses 237
  patella 315, **315**
  pubic 260
  radius 339
  rib 305, **305**
  sacrum **278**, **295**
  scapula 335
  ulna 339
  vertebrae 256, 276
hypoplastic dens 263, **263**
hypospadia 260
hypothyroidism 211, 298, 331

I

idiopathic hypercalcemia 213, 215, 257
  of infancy 34, 326, 332, **333**
idiopathic osteoarthritis 166, 192
idiopathic universal calcinosis 196
iliac horns 292, **292**
iliac spine avulsion **58**
iliac wing fracture **58**
impacted fracture **53**
impingement syndrome **168**
inclusion cyst 84, **84**
infantile cortical hyperostosis 28, **29**
  long bone anomalies 316, 320, **321**
  periosteal reactions 43, **43**
  rib anomalies 306
infantile muscular atrophy 328
infarct
  bone 12, **15**, 23, **23**, 50, 116, **117**
    long bone changes 334
    matrix calcification **77**
  cerebral 209
infectious diskitis 279, **279**
insufficiency fracture 20, **22**, 68, 332
interclinoid ligament calcification 204, **204**
internal carotid artery
  aneurysm 232, 235
  calcification 204, **204**, **205**
intervertebral disk
  calcification 138, **160**, 170, 192, 258
  degeneration 170, **170–171**, 192, 258, 283, **283**
  displacement 170
  infection 176
intervertebral foramen enlargement 258
intra-articular bodies
  differential diagnosis 66–67
  fragmentation 135
intra-articular fracture 73, **74**
intracranial pressure 216, 227, 235
intramedullary ossification 77, **77**
intramedullary rod removal 23
intraspinal pressure 258, 276
iron deficiency 6, 217
Iselin's disease 38
ivory hand **49**
ivory vertebra **21**, 24, 106, 110, 112, **113**, 123, **124**, 257, **291**

J

J-shaped sella 227, **227**
Jaccoud's arthritis 152, **153**
Jaffe-Campanacci syndrome 92
jaws 245–253
  calcifications 245
  lytic lesions 247–251
Jefferson fracture 61, 264, 265, **265**
joint alignment 314–315
joint diseases
  deformities 137
  degenerative 67
    with detached spur 190
    see also osteoarthritis
  differential diagnosis 141–187
  effusions 73, **73**, 137–139, **139**, 388
    hemophilia 156
    pyogenic (septic) arthritis **176**
    rheumatoid arthritis **143**
  erosions 133–134
  monoarticular 129
  polyarticular 129–130
    distribution patterns 130–132
  see also specific diseases
joint space width 132–133
  loss of **131**, **132**
Jones fracture 61
juvenile angiofibroma 239
juvenile osteoporosis 6, 330
juvenile rheumatoid arthritis (JRA) 48, 144, **144**, 185, 318
  chronic 144
  femoral neck anomalies 346, **346**
  hand anomalies 366
  knock knees 350, **351**
  long bone anomalies 328, 330
  spinal changes 256
juvenile Tillaux fracture 62, **64**

K

Kaposi's sarcoma 382
Kayser-Fleischer ring 10
Kenny-Caffey disease 327
keratocyst 248, **248**

Kienböck's disease 24, **25**, 37, 183, **184**
Kimmerle's anomaly 262
Kirner's deformity **356**, 366
kissing spines 170, **171**
Klebsiella rhinoscleromatis 240
Klippel-Feil deformity 228, **263**, 272, **273**
Klippel-Trenaunay-Weber syndrome 389
knee
  abnormal angulation 347–351
  effusions **139**
  fractures 58
  housemaid's **161**
  joint disease 131
  neuropathic 349, **349**
  spontaneous osteonecrosis (SONC) 24, 38, **39**, 183, **184**
knock knees 314, 350, **351**
Köhler's disease 38
Kummel-Verneuil's syndrome 257
kwashiorkor 6
kyphoscoliosis 5, 256
kyphosis **179**, 255, 256, 268, 276
  adolescent 256, 282
  block vertebra and 272

L

lacrimal gland tumors 233–234, **233**
lacunar skull 221, **222**
lamina dura, resorption 245–246
Langerhans cell histiocytosis (histiocytosis X) 114, **114–115**
  jaw 253, **253**
  long bone anomalies 324
  orbits 235, **236**
  periosteal reactions 50
  skull 224, **224**, **228**, 231, 232, **232**
lead poisoning 10, 34, 210, 326, **326**, 332, **333**
Lefort fracture 242, **243**
Legg-Calvé-Perthes disease 38, **39**, 185
Legg-Perthes disease 342, **343**, 345
leontiasis ossea 239, 252
leprosy 48, 174, **175**, 198, 240
  hand anomalies 364, **365**, 380, **381**
leptomeningeal cyst 226, **226**
Lesch-Nyhan syndrome 157, 364
Letterer-Siwe disease 114
leukemia 20, 32, **33**, 46, 112, **113**
  long bone anomalies 330, **330**, 332, **333**
  methotrexate therapy effects **333**
  osteopenia and 6
  rib anomalies 306
  skull anomalies 224
licked candy stick appearance 174, **175**
Liffert-Arkin disease 38
ligament
  calcifications 71, 198, **198**
    interclinoid ligament 204, **204**
    petroclinoid ligament 204, **204**
  carpal bone, injuries 57
  collateral, Pellegrini-Stieda lesion 71, **73**
  cruciate, injuries 58
  ossifications 71, **73**
    posterior longitudinal ligament (OPLL) 172, **173**
lipid granulomatosis 34
lipocalcinogranulomatosis 195
lipodystrophy 387
  membranous 123, **123**
lipohemarthrosis **74**
lipoid dermatoarthritis 164, 309
lipoma 80, 84, **85**, 198, **199**, 208
  calcaneus 378, **378**
  corpus callosum **205**, **208**
  paranasal sinuses 238
  spine 258
lipoma arborescens 180
lipomyelocele 276
lipomyelomeningocele 276
liposarcoma 84, 198, **199**
Lisfranc fracture-dislocation 61, **61**
listeriosis 240
loiasis 196, 382
long bone anomalies 313, 316–319
Looser's zones 3, 73, **74**, 317
lordosis 255
Lückenschädel 221
lumbar spine *see* thoracolumbar spine
lunate dislocation 57, **57**, 384, **384**
lupus erythematosus 116
  systemic 152, **153**, **184**, 193
luxation
  acromioclavicular joint 309
  facet joints **268**
  Perthes' 342
  sternoclavicular joint 309
  see also subluxation
lymphangioma 389
lymphangiomatosis, cystic 86
lymphoepithelioma 229
lymphoma 112, **112–113**, 224
  age at presentation 81
  Burkitt's 112, **251**
  histiocytic 20, 112, **112**, **113**
  Hodgkin's disease 20, **21**, 112, **113**, 257
  jaw 251
  location 80
  non-Hodgkin **75**, 112, **112**, **113**, **290**
    paranasal sinuses 239
    sternum anomalies **311**
  orbital 234
  primary bone 46
  spine 257, 258, 290, **290**

M

McCune-Albright syndrome 125
macrodystrophia lipomatosa 389, **389**
Madelung's deformity 317, 340, **341**
Madura foot 178, 380
Maffucci's syndrome 88, **91**, 201, 317, 389
main en lorgnette **137**
Maisonneuve fracture 60, **60**
malabsorption 6, 8
Malgaigne fracture **59**
malignant reticulosis 224
mallet toe 137
malnutrition 6
mandible
  lesions 246–247, **246**
  solitary bone cyst 248, **248**
Mandl's disease 38
manubriosternal synchondrosis fusion 310
marble bones 30
Marfan's syndrome 296, **311**
  hand anomalies 353
  long bone anomalies 313, 327
mastocytosis 24, **25**, 34, 212
  spinal changes 257, 300, **301**
mastoiditis **231**
matrix
  calcification 77, **77**, **91**
  septation 78, **78**
maxillary antrum
  carcinoma **238**
  fibrous dysplasia **240**
  non-Hodgkin's lymphoma **239**
  retention cyst **241**
  sinusitis **241**
  Wegener's granulomatosis **240**
medulloblastoma 206
melanoma 234
Melnick-Needles syndrome 316
melorheostosis 18, **18**, 30, **31**, 213
  hand anomalies 362, **363**, 390, **390**
melting snow appearance 178
membranous lipodystrophy 123, **123**
meningioma **205**, 206, **207**
  base of skull 229, **230**, 232
  orbital 233, 234, 235, **236**
  skull vault 212, **215**
  spine 258
  vascular markings 211
meningocele 221, 276, **276**
  lateral 258
meningoencephalocele 221, **222**
meningofacial angiomatosis 205
meningomyelocele 258, 276, 346, **346**, **376**
mercury poisoning 332
mesenchymoma, fibrocartilagenous 92
metacarpal fractures 57–58
metacarpal index 353, **354**
metacarpal sign 353, **353**, **367**
metachondromatosis 86, **89**
metaphyseal chondrodysplasia 331, **331**
metaphyseal dysplasia 348
metastases 32, 46, 110, **110–111**, 198
  age at presentation 81
  breast carcinoma *see* breast carcinoma metastases
  bronchogenic carcinoma *see* bronchogenic carcinoma metastases
  hand 362
  Hodgkin's disease **21**
  intracranial 208, 210
  jaw 251, **251**
  location 80
  long bone anomalies 330
  neuroblastoma **47**, 330
  orbital 234, 235
  osteoblastic 15, **15**, 20, **21**, 110, **110–111**
  osteolytic 12, 110, **110**, **111**
  prostate carcinoma *see* prostate carcinoma metastases
  renal cell carcinoma 20, **71**, **111**, **291**
  rib 307, **307**
  skull 212, **213**, 222, **223**
  spine 257, 258, 290, **291**
  sternum 310, **311**
  thyroid carcinoma **223**
metatarsus varus **370**, 374, **374**
methotrexate therapy effects, leukemia **333**
methylmethacrylate cement 16, **16**
Meyer's dysplasia 185
midcalcaneal line 368
midtalar line 368
midtalar/midcalcaneal angle 368, **369**, **370**
midtarsal fault 368
midtarsal joint line 368, **369**
Milch's disease 37
milk-alkali syndrome 193
Milkman's syndrome 3, 73
Milwaukee shoulder syndrome 132, **132**, 161, **161**
mixed calcium phosphate deposition disease 161
mixed sclerosing bone dystrophy 30, **31**
Monckeberg's medial sclerosis 201
Monteggia fracture 55, **56**, 339, **339**
morning star erosion **364**, **365**
Morquio's syndrome 256, 258, 296, **296**
  long bone anomalies **321**, 342, **343**
  rib anomalies 306, **306**
Morton's metatarsus atavicus 371
moth-eaten lesion 75, **75**, 112, **112**, 222, **223**
mucocele 233, 234, **234**, 242
  frontal sinus **242**
  sphenoid sinus 235
mucolipidoses 306, 320
mucopolysaccharidosis 185, 256, 257, 258, 260
  long bone anomalies 320, **321**, 340, 342
  rib anomalies 306
  type I 295, 340
  type II 296
  type IV 296
mucormycosis 240
Mueller-Weiss disease 38
multicentric reticulohistiocytosis 164, **165**, 337, 364
multiple myeloma 6, **7**, 12, **13**, 108, **108–109**, **309**
  age at presentation 81
  amyloidosis **115**
  endosteal scalloping **76**
  Fanconi's syndrome and 10
  geographic lesions **75**
  location 108
  orbits 234
  osteosclerosis 20, 32
  rib **307**
  skull 224, **224**
  spine 258, 290, **291**

muscular dystrophy 318, 328, **329**, 346
mycetoma 380
Mycobacterium leprae 380
mycosis fungoides 112
myelocele 258, 276
myelocystocele 276
myelofibrosis 32, **33**, 300, **300**
myeloid metaplasia 32
myeloma 257, 307, 309
  hand 362
  multiple *see* multiple myeloma
myelomeningocele 276
myelosclerosis 32, 257, 300
myositis ossificans 71, **73**, 189, **189**
  after total hip prosthesis **189**
  localisata 195, **195**
  post-traumatic 104, **105**
  progressiva 196, **197**
myxedema, localized 390
  foot **387**
myxofibroma, liposclerosing 84, **85**

N

nail-patella syndrome 335, 340, 350
nasopharyngeal carcinoma 232, 234
  sphenoid sinus invasion 239, **239**
necrosis
  aseptic 257, 338, **338**
  avascular *see* avascular necrosis
  fat **199**
    postinjection/traumatic 200
  femoral head 344
  ischemic 212
Neer four-segment classification, proximal humerus fractures 55
nephrosis 6
neural arch fracture 267, **267**, 280
neurinoma 258, 276, **277**
  intercostal **305**
neuroblastoma 20, 258
  metastasis 46, **47**, 330
neurofibroma 208, 251
  spine 258, 276, **277**
neurofibromatosis 125, 234, **234**, 378
  hand/foot anomalies 389
  jaw 252, **252**
  long bone anomalies 313, 319, **319**, 328, **329**
  orbits 235
  paranasal sinuses 240, **241**
  periosteal reactions 50
  pseudarthrosis 55, **55**
  rib anomalies 305, **305**
  skull 210, 212, 225, **225**, 231, **231**
  spinal changes 256, 258, 276, 296, **297**
neuroma, acoustic 231, **231**
neuropathic arthropathy 67, **68**, 131, 190
neuropathic knee 349, **349**
neuropathic osteoarthropathy 130, 174, **174–175**
  axial 174
neuropathic spine 281, **281**
neurotrophic foot **372**, 374, 378
neurotrophic spine 256
Nieman-Pick disease 6, 306, 324, **324**
non-Hodgkin lymphoma **75**, 112, **112**, **113**
  histiocytic type 112, **112**, **113**
  paranasal sinuses 239, **239**
  spine/pelvis **290**
  sternum anomalies **311**
nucleus pulposus calcification 170, 258
nursemaid's elbow 339

O

occipital bone anomalies 262
occipital condyle
  fracture 265
  hypoplasia 262
occipitocervical dislocation 265
occipitovertebral junction 255
ochronosis 162, **163**, 192, 194
  pelvic changes 260
  spinal changes 258, 259, **275**, **283**
odontogenic lesions 239, 245–253
odontoid bone 263
odontoma **246**, 247, 250, **250**
  ameloblastic 250, **250**
  complex 250, **250**
oligodendroglioma 206, **206**
Ollier's disease 18, 88, **90**, 317, 322, 334, 339, 389
Ombredanne line **315**
omovertebral bone 335
onion skin appearance **42**
  Ewing's sarcoma 106, **106**
onycho-osteodysplasia, hereditary 292, **315**, 350
opera-glass deformity **137**
ophthalmic artery aneurysm 235
Oppenheim's disease 328
optic canal diameter 235
optic nerve glioma 227, **227**, 234, **234**
orbital emphysema 233, **233**, 237
orbital fissure, superior 235
orbital varix 235
orbits
  blow-out fracture 237, **237**, 242
  bony defects 233–236
  calcification 233
os centrale **357**, 384
os triangulare 384
Osgood-Schlatter disease 38
ossiculum terminate Bergman 263
ossification 189
  differential diagnosis 190–201
  intramedullary 77, **77**
  ligaments 71, **73**
    posterior longitudinal ligament (OPLL) 172, **173**
  paravertebral 259
  soft tissues 189
    tumoral 189
  spinal 259
  see also myositis ossificans
ossifying fibroma 24, 125, 239
  jaw 252, **252**
osteitis
  condensans claviculae 309
  condensans ilii 261, 292, **293**
  deformans *see* Paget's disease
  fibrosing 226
  leprosy 380, **381**
  pubis 260, 294, **294**
  radiation 332
osteoarthritis 129, 130, 166, **167–168**
  chronic overuse **168**
  costovertebral 170
  distribution patterns 130
  erosive 169, **169**
  femoral head 344
  fragmentation **135**
  idiopathic 166, 192
  joint space loss **132**
  knee angulation and 349, 350, **351**
  osteophytosis **136**
  pelvic changes 260, 261
  post-traumatic **168**
  primary 166, 192
  rapidly destructive, of the hip 166, **168**
  sacroiliac joints 166, **168**
  sclerosis 135–136
  secondary 129, 166, 192, **336**, 386
osteoarthropathy
  hypertrophic
    primary 44, **45**
    secondary 44, **45**
  idiopathic 387
  neuropathic 130, 174, **174–175**
    axial 174
osteoblastoma 18, 96, **96–97**
  aggressive (malignant) 96
  location 80, 96
  spine 256, 257, 286, **287**
osteochondritis dissecans 37, 38, **39**, 66, **66**, 342
  differential diagnosis 66, 182, **182**
osteochondroma 18, 80, 86, **87**, 208, 212
  foot 378
  hereditary multiple exostoses **322**
  malignant transformation **101**
  rib 307, **307**
  scapula 336, **336**
  sternum **311**
osteochondromatosis 66, **67**
  synovial 180, **181**, 190, **190**
osteochondrosis 170, **171**, 317
  dissecans 190, **191**, 342
  femoral epiphysis 342
  sacri 294
osteodysplasty 316
osteodystrophy *see* renal osteodystrophy
osteofibrous dysplasia 24, **25**, 125, **126**
osteogenesis imperfecta 6, **7**, 211, 345
  basilar invagination 228
  congenita 6
  fracture healing 55, 73
  knee **351**
  long bone anomalies 316, **316**, 320, **321**, 327, **327**, 330, 340
  pelvic changes 260
  rib anomalies 305
  spinal changes 256, 257, 298, **298**
  tarda 6
osteolysis 260, 294
  neurogenic 260
osteoma 18, **19**, 94, **95**, 208, 212, 247
  osteoid 18, 46, **47**, 94, **95**
    clavicle 309
    hand/foot 362, 390
    intra-articular **96**
    location 80, 94
    spine 256, 286, **287**
  paranasal sinuses 238
osteomalacia 3–4, **3**, **4**, **9**
  axial 10
  basilar invagination 228
  differential diagnosis 8–10
  drug-induced 10
  lamina dura loss 246
  long bone anomalies 318
  pelvic changes 260
  spinal changes 257
osteomyelitis 12, 68, 118, **119**
  acute
    hematogenous 46, **47**, 118, **119**
    skull 225, **226**
  BCG 48
  blood-borne 279
  chronic 20, 48, **49**, **78**, 120, **121**, 323
    recurrent multifocal 120, **121**
    skull 212, **213**
  clavicle anomalies 308, **309**
  cystic 362
  foot 378, **379**
  from contiguous infective source 48, **49**, 118
  fungal 118, **121**
  hand 362, **363**, 378
  in diabetes mellitus **49**, **119**
  leprotic 362
  long bone anomalies 318, **318**, 323, 334, 346
  pyogenic 118, **379**
  rib anomalies 307
  sclerosing, of Garré 20, **21**, 120, **121**, 323, **323**
  smallpox 380
  spinal changes 257
  sternum 310
  tuberculous 48, **49**, 118, **120**
osteonecrosis 116, **117**, 183
  dysbaric 344
  hemophilia 156
  pubis 260, 294
  radiation 12, **13**, 24, **25**, 116, **117**
    skull 212, **213**, 226
  spontaneous, of the knee (SONC) 24, 38, **39**, 183, **184**
osteopathia striata 16, **17**, **31**, 213, **216**

osteopenia 3–14
  differential diagnosis 6–14, 70, **70**
    generalized osteopenia 6–11
    localized osteopenia 12–14
  spinal changes 256
osteopetrosis 30, **30–31**, 213, **215**
  hand anomalies 362
  long bone anomalies 325, **325**, 331, **331**, 345
  rib anomalies 306
  spinal changes 257, 298, **299**
osteophytes 259, **283**
osteophytosis 136
  neuropathic osteoarthropathy **174**
  osteoarthritis **136**, 166, **167**, **168**
  rheumatoid arthritis **143**
  spine **170**, **171**
osteopoikilosis 16, **17**, **31**, 94, 298
  hand anomalies 362, **363**
osteoporosis 3, **3**, **4**, 136–137
  differential diagnosis 6–8
  drug-induced 8, **8**
  insufficiency fractures and 70
  juvenile (idiopathic) 6, 330
  lamina dura loss 246
  leprosy 380
  neonates 330
  regional transitory 12
  rib anomalies 305
  senile/postmenopausal 6, **219**
  spinal changes 256, 257
osteoporosis circumscripta 14, 225, **226**
osteosarcoma 18, **19**, 103, **103–104**
  age at presentation 81
  calcification 198
  conventional 103
  cortical penetration **77**
  gnathic 103, 251, **251**
  intracortical 103
  intraosseous 103
  location 80
  osteolytic **45**
  Paget's disease 123, **124**
  parosteal 80, **81**, 104, **105**
  pelvis 288
  periosteal 80, 104, **104**
  periosteal reactions 44, **44–45**
  rib 307
  skull 212
  small cell 103
  spine 257, 288
  surface high-grade 104
  teleangiectatic 103, **104**
osteosarcomatosis 18, 103
osteosclerosis 15–39
  differential diagnosis 16–36
    generalized diffuse osteosclerosis 27–36
    solitary or multiple scattered lesions 16–26
  physiologic, of newborn 27
otopalatodigital syndrome **360**
otosclerosis 229
Otto pelvis 260
overconstriction (overtabulation) 313, 327–329
oxalosis 34, **36**

P

Pacchionian granulations 210, 221
  calcified 204, **205**
pachydermoperiostosis 44, **45**, 364, 387
Paget's disease 14, **14**, 24, **25**, 34, **35**, 123, **123–124**
  aneurysmal bone cyst **124**
  clavicle anomalies 309
  jaw **246**, 253
  juvenile 28, 74, 319
  long bone anomalies 319, **319**, 325, 346
  osteosarcoma **124**
  paranasal sinuses 240, **241**
  pelvic changes 260, 292, **293**
  pseudarthrosis and **54**
  pseudofractures 74, **74**
  skull 212, 217, **218**, 225, **226**, 230, **230**
    basilar invagination 228, **229**
  spinal changes 256, 257, 272, 284, **284–285**
panaritium ossale 362
pancreatitis 344
Panner's disease 37, **37**
papilloma, choroid plexus 206
paragonimiasis 209
paralysis during growth 318, 328
paranasal sinuses 237–243
  air-fluid level 237, **237**
  carcinoma 232, 234
  fractures 237, 242
  hypoplasia 237
paraplegia 198, 260, 261, 305
parietal foramina 221, **221**
parietal thinning 221, **221**
patella alta 315, **315**
patella profunda/baja 315, **315**
patellar hypoplasia 315, **315**
pectus
  carinatum 310
  excavatum 310, **311**
Pelkan's spur **6**
Pellegrini-Stieda lesion 71, **73**, **168**, **195**
pelvis 255, 260–261
  dislocation **59**
  fractures 58
    stable 58, **58**
    unstable 58, **59**
  localized lesions 292–294
  Otto 260
  tumors 286–291
pencil-in-cup deformity **137**, 147, 178
per anserinus spur 86
periapical abscess 247
periapical granuloma 247
periarthrosis humeroscapularis 337
perilunate dislocation 57, **57**, 384, **384**
periodontal anomalies 245–246
  abscess 246, 247
  cyst **246**, 247, **247**
periodontal membrane space width 246
periodontitis 246, 247
periodontosis 246
periosteal reactions 41–52
  differential diagnosis 43–52
  Ewing's sarcoma **106**, **289**
  infantile cortical hyperostosis **321**
  interrupted 41, **42**
  osteitis pubis **294**
  osteoblastoma **96**
  osteomyelitis 118, **119**
  osteosarcoma **103**
  rickets **9**
  solid 41, **41**
  yaws **380**
periostitis 41–42, 136
  lymphoma and 112
  physiological, infants 43, **43**
  pyogenic (septic) arthritis **177**
  Reiter's syndrome **151**
  see also periosteal reactions
Perthes' luxation 342
pes cavus 368, **370**, 376, **376**
pes planus 372
petroclinoid ligament calcification 204, **204**
Phemister's triad 178
phenytoin exposure 218, 366
phlebolith 201, 233
phosphorus intoxication 34, 332
phosphorus malabsorption 8
phthysis bulbi 233
picture frame vertebra 123, **124**
Pierson disease 37
pigeon breast 310
pigmented villonodular synovitis (PVNS) 118, **119**, 180, **181**, 195, 337
pilon fracture 60
Pindborg tumor 249, **249**
pineal gland
  calcification 203, **204**
  teratoma **207**
pinealoma **205**, 207
pituitary gland
  calcification 204, **204**
  tumor 227
    adenoma 207, **228**
plasma cell granuloma 20, **21**
plasmacytoma **78**, 106, **107–108**, 224
  jaw 251
  rib 307
  spine/pelvis 288
platybasia 228, **229**, 262
pneumatocyst 82
pneumocephalus 237
pneumohemarthrosis 138
pneumolipohemarthrosis 138
POEMS syndrome 20
poliomyelitis 258, 305, 318, 328, **329**, 346
polyarteritis nodosa 48, 154, 193
polychondritis, relapsing 154, **155**, 261, 294
polycystic lipomembranous osteodysplasia 123
polycythemia 306
polydactyly 354, **357**
polymyalgia rheumatica 154
polymyositis 193, **194**
polyp 240
porphyria 364
Pott fracture 60
Preiser's disease 37
primitive neuroectodermal tumors (PNET) 106, **107**
primordial cyst **246**, 248, **248**
progeria 194, 211, 296, 308, 327, 346
  hand anomalies 364
progressive diaphyseal dysplasia 28, **29**, 213, 320, **321**
prostaglandin, hypervitaminosis A and 43
prostate carcinoma metastases 20, **21**, **32**, **111**
  periosteal reactions 46
  spine **291**
protein deficiency 6
protrusio acetabuli 132, 260, **302**, 346
proximal femoral focal deficiency (PFFD) 122, **122**
prune belly syndrome 260
pseudarthrosis 54–55, **54**, **55**, 319
  congenital 55, 319
pseudoachondroplasia 320, **321**
pseudoepiphysis 366
pseudofracture 73–74, **74**
  hereditary hyperphosphatasia 28
  osteomalacia 3–4, **9**
  vitamin D resistant rickets 317, **317**
pseudogout 159, 192
  pelvic changes 260
  spinal changes 256, 258
  see also calcium pyrophosphate dihydrate deposition disease (CPPD)
pseudohypoparathyroidism 28, 210, 213, 331
  hand anomalies 353, **356**
pseudo-Madelung deformity 340
Pseudomonas mallei 240
pseudopseudohypoparathyroidism 28
  hand anomalies 353, **353**
pseudospondylolisthesis 274
pseudospondylolysis 274
pseudotumor
  hemophilic 116, **116**, 156
  orbital 234, 235
pseudotumoral calcinosis 195
pseudoxanthoma elasticum 200, 204, 364
psoriasis 42
psoriatic arthritis 48, **49**, 147, **148–149**
  erosions 134, **134**
  hand anomalies 362, 364, **364**
  pelvic changes 261, **303**
  spinal changes 257, 259
  sternum anomalies **310**
pubic hypoplasia 260
pubic ramus fracture **58**, **59**
pubic symphysis
  bridging 260
  widening 260

punched-out lesions
  gout 157
  multiple myeloma 108, **108**, 224, **224**
  osteolytic metastases **223**
  sarcoidosis 26, 127
pycnodysostosis 30, 213, 298, 325, 364
Pyle's disease 320, **321**
pyogenic osteomyelitis 118, **379**
pyogenic (septic) arthritis 67, 129, 176, **176–177**
  clavicle anomalies 309
  in AIDS **180**
  sequestrum 190
pyogenic spondylitis 279, **279**
pyrophosphate arthropathy **192**
  see also calcium pyrophosphate dihydrate deposition disease (CPPD)

R

rachischisis 256
rachitic rosary 8, **306**
radial fractures 55, **56**, 62, **63–64**
radiation osteitis 332
radiation osteonecrosis 12, **13**, 24, **25**, 116, **117**
  skull 212, **213**, 226
radiation therapy **111**
  long bone changes 334, 344, **344**
  pelvic changes 260
  spinal changes 257
radioulnar dislocation 339
radioulnar fusion 340, **341**
radius deformity 339
rapidly destructive osteoarthritis of the hip 166, **168**
Raynaud's syndrome 193, **194**
reactive bony changes 135–136
  excrescence 86
  see also periosteal reactions
reflex sympathetic dystrophy (RSD) 12, **17**
regenerated rib 305
reinforcement lines 70, **70**, 331
Reiter's syndrome 42, 48, **49**, **131**
  joint anomalies 150, **151**
  pelvic changes 261
  spinal changes 257, 259
relapsing polychondritis 154, **155**, 261, 294
renal carcinoma metastases 20, **71**, **111**, **291**
renal failure, chronic **165**
renal osteodystrophy 3, 10, 34, **35**, 50, **51**, 186
  calcification 192, 193
  clavicle anomalies **309**
  foot anomalies **371**
  hand anomalies **364**, **367**
  long bone anomalies 319, 332, **341**, 345
  pseudofractures 74
  spinal changes 256, 257, 302
renal tubular acidosis 10, **10**
residual cyst 247, **247**
retention cyst 240, **241**
reticulohistiocytoma 309
reticulohistiocytosis, multicentric 164, **165**, 337, 364
reticulosis, malignant 224
retinoblastoma 233, 234, 235
retinoids, hypervitaminosis A and 43
retrolental fibroplasia 233, **233**
rheumatic fever 152
rheumatoid arthritis 6, 12, 129, 141, **142–143**, 193
  clavicle anomalies 309
  cystic 141, **143**
  distribution patterns 130–132
  elbow **142**
  erosions 133–134, **133**
  femoral neck anomalies 346
  foot anomalies 141, 371, 376
  hand anomalies **137**, 141, **142**, 362, **363**, 388
  humoral head deformity 337
  insufficiency fractures and 70
  joint deformities 137, **137**
  juvenile *see* juvenile rheumatoid arthritis (JRA)
  knee **351**
  pelvic changes 260, 261
  rib anomalies 305
  shoulder **142**
  soft tissue anomalies 139, **140**
  spinal changes 256, 257
  wrist 141, **142**
rhinolith 238, **238**
rhinoscleroderma 240
rhinosporidiosis 240
rib anomalies 305–308
  absence 305
  fusions 305, **305**
  hypoplasia 305, **305**
  localized lesions 307
  notching 308
  regenerated rib 305
Ribbing's disease 28, 120
rickets 8, **9**, 211, 348, **348**
  clavicle anomalies 309
  healed **318**
  healing 44, **44**, **325**
  knock knees 350
  long bone anomalies 317, **317**, 325, **325**, 332, 334, 342, 345
  pelvic changes 260
  rib anomalies 306, **306**
  treatment effects 219
  vitamin D-resistant 8, **12**, 42, 317, **317**
rider's bone 71
rockerbottom deformity 368, **370**, **375**
Rolando fracture 57
rotator cuff tear 337, **337**
Rothmund's syndrome 364
rubella 209, 330, 332
  embryopathy 27, **27**, 320
rugger jersey spine
  hyperparathyroidism **3**, **4**, 5, 302
  renal osteodystrophy 34, **35**
Russel-Silver syndrome 366

S

sabre-shin deformity 317, **317**, 318, **318**
sacral fracture **58**
sacrococcygeal teratoma 288
sacroiliac joint 255
  disease 261
  infection 176
  osteoarthritis 166, **168**
sacroiliitis **145**
  circumscripta 261, 292, **293**
  pyogenic/tuberculous 294, **294**
sacrum 255
  hypoplastic **278**, **295**
sail vertebra 295, 298
salivary gland calcifications 245, **245**
salt and pepper appearance
  glomus tumor 84
  skull 5, 218, **219**, 226
Salter-Harris classification, growth plate injuries 62–64, **64**
sandwich vertebra 298, **299**
SAPHO syndrome 20, 120, 309, **309**
sarcoidosis 26, **26**, 34, 127, **127**, 193
  articular lesions 186, **187**
  hand/foot anomalies 362, 378, **389**
  sinusitis and 240
  skull lesions 225
  spinal changes 257
sarcoma 46
  Ewing's *see* Ewing's sarcoma
  granulocytic 112, **113**
  Kaposi's 382
  location 80
  osteogenic 71
  paranasal sinuses 239
  parosteal **19**, 44, **73**, 81
  periosteal 44
  reticulum cell 20, 46
  spine 257
  subungual 362
  synovial 190, 195, **196**, 198
Saturn's ring 327
scalloping
  endosteal *see* endosteal scalloping
  vertebral body **278**
    anterior 257
    posterior 258, **295**, **297**
scaphoid
  fractures 55–57, **56**
  subluxation 57, 384
scapholunate advanced collapse (SLAC) 159, **160**
scapula anomalies 335–336
Scheuermann's disease 37, 256, 257, 282, **282**
schistosomiasis 196
Schmorl's nodes 3, 170, **282**
sciatic hook 283
scleroderma 8, 154, **155**, 196
  clavicle anomalies 309
  foot anomalies **373**
  hand anomalies 364, **365**, **388**
  periodontal membrane space widening 246
  rib anomalies 305
  soft tissue calcification **138**, 193, **193**
sclerosing osteomyelitis 246
  of Garré 20, **21**, 120, **121**, **247**
sclerosis
  adamantinoma **99**
  amyloidosis **165**
  ankylosing spondylosis **303**
  arteries 201, **201**
  Brodie's abscess **121**
  clavicle 309, **309**
  CPPD **160**
  craniometaphyseal dysplasia **236**
  cystic angiomatosis **87**
  diskitis **177**
  Ewing's sarcoma **289**
  fibrous dysplasia **125**, 217, **225**, 230, **230**, **236**, **240**, **252**
  fluorosis **301**
  foreign body granuloma **127**
  fungal arthritis **179**
  gout **158**
  hemangioma **86**, **215**
  hemophilia **156**
  hyperparathyroidism **186**, 302, **302**
  Langerhans cell histiocytosis **236**
  mastocytosis **301**
  meningioma **230**, **236**
  Monckeberg's medial 201
  myelofibrosis **300**
  neuropathic osteoarthropathy **174–175**
  non-discogenic 285, **285**
  non-Hodgkin's lymphoma **290**
  osteitis condensans ilii **293**
  osteoarthritis **132**, 135–136, 166, **167**, **168**
  osteoblastoma **287**
  osteomyelitis **121**, **213**, **309**
  osteopathia striata **216**
  osteopetrosis **215**
  Paget's disease **124**, 217, **218**, **230**, **241**
  periosteal desmoid **92**
  pigmented villonodular synovitis **119**
  psoriatic arthritis **303**
  renal osteodystrophy **51**, **341**
  sacroiliitis **293**, **294**
  septic arthritis **180**
  skull
    base 229–231
    diffuse 213–219
    localized 212
  spinal changes 257, **281**
  sternum **310**, **311**
  tuberous *see* tuberous sclerosis
scoliosis 255, 256, 258, 276, **283**, **297**
  tuberous sclerosis **301**
scurvy **6**, 306
  healing 44, **44**, 326
  long bone anomalies 330, 332, 334
seat-belt injuries 62, 269
segmental fracture **53**

segmentation anomalies **273**
multiple **277**
sternum **310**
Segond fracture 58–60
sella turcica anomalies 220–228
dorsum sella 227
double-floor sella 220–227, **227**
empty sella syndrome 227, **228**
J-shaped sella 227, **227**
small sella 220
septation 78, **78**
septic arthritis *see* pyogenic (septic) arthritis
sequestrum 78–79, **78**, 190
button 220, **220**, **224**
sesamoids **72**
Sever's disease 38
Shenton's line **315**
shepherd's crook **126**, 319, **319**, 345, 346
shiny corner sign 145
shoulder
dislocation **66**, 314
anterior 314, **314**
posterior 314
drooping 132–133, **133**, 138
joint disease 132
malalignment 314
Milwaukee 132, **132**, 161, **161**
shoulder-hand syndrome 12, **13**, 387
sickle cell anemia 6, 32, **33**, 116, 217
bone infarcts **23**, 50
long bone anomalies 323, 332, 334, 344
rib anomalies 306
spinal changes 256, 257, 298, **299**
sickle cell dactylitis 382, **383**
signet ring sign 57
silicone-induced arthritis **187**
Sinding-Larsen disease 38
sinusitis 234
acute 237, 240, **241**
chronic granulomatous 240, **241**
Sjogren's syndrome 141, 364
skier's thumb 57–58, **58**
skull
basilar impression 5
bone defects 219–220, 221–226
calcifications 203–210
artifacts **203**
pathologic 204–210
physiologic 203–204
fractures 211, **212**
geographic 114, **115**, 224, **224**
lacunar 221, **222**
osteoporosis circumscripta 14
salt and pepper appearance 5, 218, **219**
sclerosis
diffuse 213–219
localized 212
skull base 229–231
sutures 211, **212**
vascular structures 210–211, **210**, 221
slipped femoral epiphysis 64, **65**, 342, **343**, 345, **345**
avascular necrosis 38, **39**
small bowel
bypass surgery 8
fistula 8
resection 8
smallpox 178, 380
Smith fracture 55, **56**
soap bubble appearance
aneurysmal bone cyst 82, **83**, **104**
giant cell tumor 96, **97**
plasmacytoma **108**
soft tissue
calcification 137, 138
para-articular anomalies 139, 140
sphenoid sinus
carcinoma **228**, 235, 239, **239**
infection 229
mucocele 235
see also paranasal sinuses
spherocytosis, hereditary 256
spina bifida 276, **276**
spina ventosa 118, **120**, 378
spinal stenosis 278, **278**
acquired **278**
spinal tuberculosis 280, **280**
spine 255, 256–259
bamboo 145, **146**, **303**
degenerative disease 170, **170–171**
cervical **171**
lumbar **170–171**
fractures 255, 257, 265–271
neuropathic 281, **281**
neurotrophic 256
rugger jersey
hyperparathyroidism **3**, **4**, 5, 302
renal osteodystrophy 34, **35**
thoracolumbar fractures 62, **63**
tumors 286–291
see also vertebra
spondylarthropathy **278**
seronegative 129–130
spondylarthrosis 170, **171**
spondylitis 256
ankylosing *see* ankylosing spondylitis
psoriatic 256
pyogenic 279, **279**
tuberculous **120**, 178, **179**, **273**, **280**
spondyloepimetaphyseal dysplasia 320
spondyloepiphyseal dysplasia 185, **185**, 260, 296, 348
spondylolisthesis 255, 274, **275**
spondylolysis 271, 274, **275**
unilateral 286, **287**
spondylosis 259, **281**
spondylosis deformans 170, **170**
spondylysis, unilateral 94
spontaneous osteonecrosis about the knee (SONC) 24, 38, **39**, 183, **184**
sporotrichosis 240
Sprengel's deformity 272, 335, **335**
sprue 8
spur 42, **42**
calcaneal **387**
degenerative **131**
inflammatory **131**
pes anserinus 86
post-traumatic 86
traction 259
Stafne's mandibular defect 251, **251**
stenosis
spinal 278, **278**
acquired **278**
tubular 327
stepladder appearance 159
sternoclavicular joint luxation 309
sternocostoclavicular hyperostosis 309
sternum anomalies 310
fracture **311**
steroids
avascular necrosis induction 24, 344
osteoporosis induction 8, **8**
Still's disease 144
straddle fracture **59**
stress fracture 20, 50, 68–70, **68–70**, 332, **333**
healed 118, **118**
healing **51**, 118
Sturge-Weber syndrome 205, **205**, **209**
subchondral cyst 82, **82**, 116, **118**, 134, 135
avascular necrosis **135**
gout **158**
hemophilia **156**
osteoarthritis **132**, **167**, **168**
rheumatoid arthritis **143**
subluxation 65, 137
acromioclavicular joint 309, **310**
Chassaignac 339
leprosy **175**
osteoarthritis **167**
rheumatoid arthritis **142**, **143**
scaphoid 57, 384
vertebral
anterior 268
atlantoaxial **143**, 256, 262, **303**
submandibular gland calculus **245**
subungual exostosis 86, **87**, **361**
subungual sarcoma 362
Sudeck's atrophy 12, 387
sunburst appearance **42**
Ewing's sarcoma 106
skull vault 212, 217
diffuse sunburst spiculations 212, **215**
superior orbital fissure 235
sutures, skull 211
diastasis **212**
metopic **212**
swan-neck deformity **137**, **142**
symphalangism 354
syndactyly 354, **356**
syndesmophytes 259
synovial chondrometaplasia 67, 180
synovial hemangioma 180
synovial osteochondromatosis 180, **181**, 190, **190**
synovial sarcoma 190, 195, **196**, 198
synovitis
foreign body 186, **187**
pigmented villonodular (PVNS) 118, **119**, 180, **181**, 195, 337
villonodular 378
syphilis 48, 225, 240
acquired (tertiary) 120, 318
congenital 27, **27**, 43, **43**, **323**, 332, **333**
gumma 209
syringomyelia 174, **174–175**, **191**, 258, 276
hand anomalies 364, 386
humoral head deformity 338, **338**
scapula deformity 336
systemic lupus erythematosus 152, **153**, **184**, 193, 196

T

tabes dorsalis 174, **175**
Taenia solium 196
talar beak 376, **377**
talipes equinovarus 374
talocalcaneal angle 368, **369**, **375**
talocalcaneal coalition 376, **377**
talus
diagonal axis of 368, **369**
flat-top 374
vertical, congenital 374, **375**
talus fractures 60–61
tarsal coalition 376, **376–377**, 386
calcaneonavicular 376
talocalcaneal 376
tear drop fracture 62, **62**, **267**
extension 267
flexion 267
teeth
anomalies 245–246
floating 114, 245, 246, **246**, 253, **253**
habitual clenching 246
molar, anatomy **246**
telescoping deformity **137**
temporal arteritis 154
temporomandibular joint dysfunction 245
tendinitis 391
calcific **138**
tenosynovitis 391
tentorium, calcification 204, **204**, **205**
teratoma **205**, 206
pineal **207**
sacrococcygeal 288
Terry Thomas sign 57, **57**
thalassemia 6, 217–218, **218**
long bone anomalies 323, 332
major **7**, 256
rib anomalies 306
spinal changes 298
thermal injuries 12, 50
Thibierge-Weissenbach syndrome 193
Thiemann's disease 37, 38
thoracolumbar spine
degenerative disease **170–171**
fracture-dislocations 62, **63**, 270, **270**
fractures 62, **63**, 269–271
see also spine; vertebra

thromboembolic disease 308, 344
  calcified thrombus 201
  venous thrombosis 200
thyroid acropachy 50, **51**
thyroid carcinoma metastases 20, **223**
tibia vara 317, 347, **347**
tibial fractures 58–60
Tietze's syndrome 307
tight filum terminale 276
tooth *see* teeth
torus fracture 62, **64**
torus mandibularis 247
torus palatinus 247
toxoplasmosis 27
  congenital **205**, 209, **209**, 332
traction spur 259
trauma
  birth, brachial plexus 308, **309**
  bone shortening 334
  calcification and 192
  clavicle 308
  cyst 82
  femoral head 344
  foot 384–385
  hand 384–385
  see also fracture
Treponema pertenue 380
Trevor's disease 88, **89**, 349, 350
Trichinella spiralis 196
trichinosis 196, 209
triplane fracture 62–64, **65**
tripod fracture 242, **242**
trochanteric bursitis **161**
trolley-track sign 145
tropical ulcer 20, 48, 318, 380
Trümmerfeld zone **6**, 330
tuberculosis 12, 209, 225, 240, 388
  cystic 118
  hand 378
  spinal 280, **280**
    radiographic changes 257, 258
  sternal **311**
tuberculous arthritis 67, 129, 178, **179**
  healed 195, **196**
  in AIDS **180**
  sequestrum 190
tuberculous block vertebra **273**
tuberculous dactylitis 118, **120**
tuberculous osteomyelitis 48, **49**, 118, **120**
  hand **379**
tuberculous sacroiliitis 294, **294**
tuberculous spondylitis **120**, 178, **179**, **273**, **280**
tuberous sclerosis 26, **26**, 34, 94, 212
  hand anomalies 362
  intracranial calcifications **205**, 210
  periosteal reactions 50
  spinal changes 257, 300, **301**
tubular stenosis 327
tug lesions 86
tumors 12, 18, 46, 222
  brain 206–208
  hands and feet 378
  lacrimal gland 233–234, **233**
  orbital 234–235
  paranasal sinuses 238
  pelvis 286–291
  spinal canal 258
  spine 286–291
  see also specific tumors
tunneling of the cortex 4
Turner's syndrome 8, 348, **348**
  hand anomalies **353**, 365, **367**
type 1 glycogen storage disease 157

U

ulcer, tropical 20, 48, 318, 380
ulna deformity 339
ulnar fractures 55, 62, **63**
underconstriction (undertabulation) 313, 320–326
urticaria pigmentosa 300

V

vacuum phenomenon 139, **139**, **163**, 170
van Buchem's disease 28, **29**, 213, **216**
van Neck's disease 37
vanishing bone disease 122, **122**
varicose veins 200, **201**
varicosis **51**
variola 178
vasculitides 154
vein of Galen, calcified aneurysm 205
venous lakes 210, **211**
venous malformations 233
venous stasis **51**
venous thrombosis 200
vertebra
  alignment 255
  biconcave 256
  block 256, 272, **273**
  butterfly 256, 276
  collapse 257
  dense 257
  diameter 256
  fish **3**, 256
  fractures 280
  fused 256, 272, **273**
  height 256
  hypoplasia 256, 276
  ivory **21**, 24, 106, 110, 112, **113**, 123, **124**, 257, **291**
  occipital 262
  pedicle erosion/destruction 258
  picture frame 123, **124**
  pyogenic spondylitis 279, **279**
  sail 295, 298
  sandwich 298, **299**
  scalloping **278**
    anterior 257
    posterior 258, **295**, **297**
  squared 257
  steplike endplate depression 256
  see also spine
vertebral coalition 272
villonodular synovitis 378
vinylchloride exposure 364, 366
viral arthritis 178
vitamin C deficiency 6
vitamin D deficiency 8, 73
vitamin D intoxication 193, 332
von Hippel-Lindau disease 208, 233
von Recklinghausen's disease 258, 296

W

Waldenström's macroglobulinemia 108
Wegener's granulomatosis 239, **240**
  limited form 239
Weismann-Netter syndrome 317, **317**
Werdnig-Hoffmann disease 328, **329**
Werner's syndrome 194
whiskering appearance
  DISH 172, **173**
  periosteal reactions 41–42, **42**, **49**, 50, **52**
Williams syndrome 34, 213, 215, 326, 332, **333**
Wilson's disease 10, 159, 192
Wimberger's line **6**
Wimberger's sign 27
Winchester's syndrome 122
wormian bones 211, **212**
Worth's syndrome 28
wrist
  accessory bones **72**, **385**
  congenital anomalies 358
  effusions **139**
  joint disease 130
Wuchereria bancrofti 380

X

x-linked hypophosphatemia 8, **9**, 317, **317**

Y

yaws 48, 240, 318, **318**, 380, **380–381**
  primary 380
  secondary 380, **380**
  tertiary 380, **381**

Z

Zellweger's cerebrohepatorenal syndrome 16